frontiers | Research Topics

The immune system and inflammation in musculoskeletal health, aging, and disease

Edited by
Matthew William Grol and Gurpreet S. Baht

Published in
Frontiers in Immunology

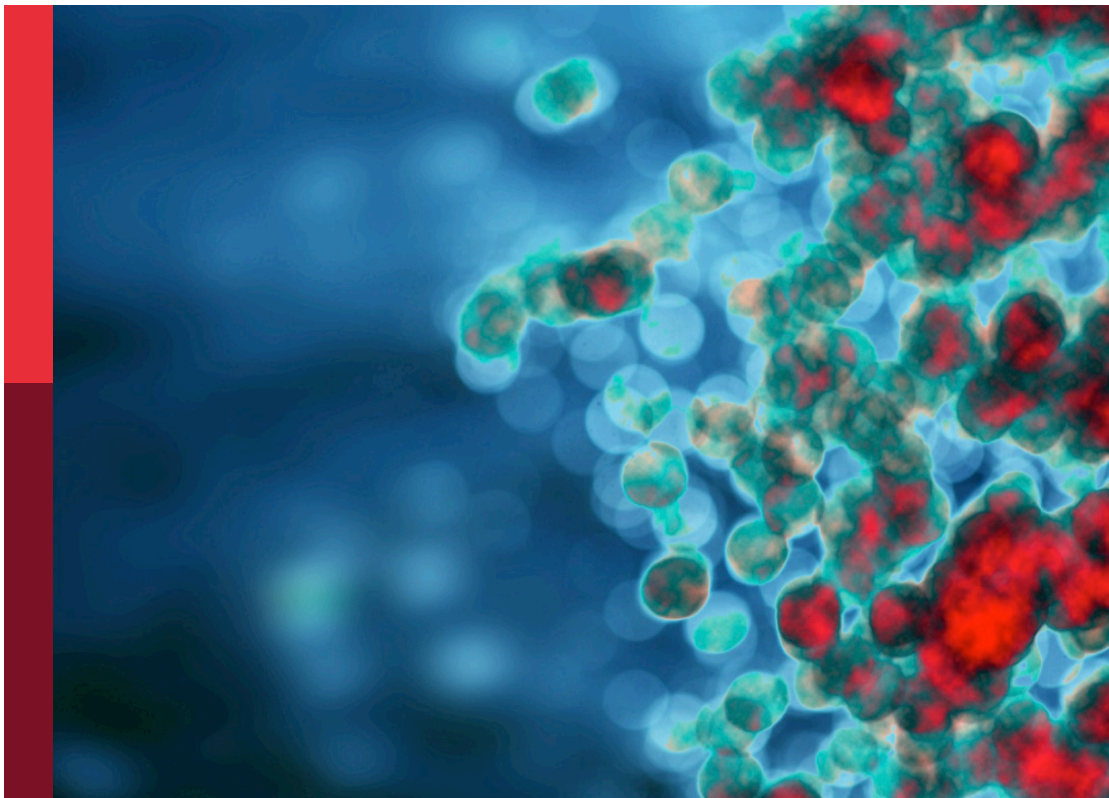

ISSN 1664-8714
ISBN 978-2-8325-2449-7
DOI 10.3389/978-2-8325-2449-7

About Frontiers

Frontiers is more than just an open access publisher of scholarly articles: it is a pioneering approach to the world of academia, radically improving the way scholarly research is managed. The grand vision of Frontiers is a world where all people have an equal opportunity to seek, share and generate knowledge. Frontiers provides immediate and permanent online open access to all its publications, but this alone is not enough to realize our grand goals.

Frontiers journal series

The Frontiers journal series is a multi-tier and interdisciplinary set of open-access, online journals, promising a paradigm shift from the current review, selection and dissemination processes in academic publishing. All Frontiers journals are driven by researchers for researchers; therefore, they constitute a service to the scholarly community. At the same time, the *Frontiers journal series* operates on a revolutionary invention, the tiered publishing system, initially addressing specific communities of scholars, and gradually climbing up to broader public understanding, thus serving the interests of the lay society, too.

Dedication to quality

Each Frontiers article is a landmark of the highest quality, thanks to genuinely collaborative interactions between authors and review editors, who include some of the world's best academicians. Research must be certified by peers before entering a stream of knowledge that may eventually reach the public - and shape society; therefore, Frontiers only applies the most rigorous and unbiased reviews. Frontiers revolutionizes research publishing by freely delivering the most outstanding research, evaluated with no bias from both the academic and social point of view. By applying the most advanced information technologies, Frontiers is catapulting scholarly publishing into a new generation.

What are Frontiers Research Topics?

Frontiers Research Topics are very popular trademarks of the *Frontiers journals series*: they are collections of at least ten articles, all centered on a particular subject. With their unique mix of varied contributions from Original Research to Review Articles, Frontiers Research Topics unify the most influential researchers, the latest key findings and historical advances in a hot research area.

Find out more on how to host your own Frontiers Research Topic or contribute to one as an author by contacting the Frontiers editorial office: frontiersin.org/about/contact

The immune system and inflammation in musculoskeletal health, aging, and disease

Topic editors

Matthew William Grol — Western University, Canada

Gurpreet S. Baht — Duke University, United States

Citation

Grol, M. W., Baht, G. S., eds. (2023). *The immune system and inflammation in musculoskeletal health, aging, and disease*. Lausanne: Frontiers Media SA.

doi: 10.3389/978-2-8325-2449-7

Table of contents

frontiers | Frontiers in Immunology

TYPE Editorial
PUBLISHED 18 May 2023
DOI 10.3389/fimmu.2023.1218118

OPEN ACCESS

EDITED AND REVIEWED BY
Pietro Ghezzi,
University of Urbino Carlo Bo, Italy

*CORRESPONDENCE
Gurpreet S. Baht
gurpreet.baht@duke.edu
Matthew W. Grol
mgrol2@uwo.ca

RECEIVED 06 May 2023
ACCEPTED 09 May 2023
PUBLISHED 18 May 2023

CITATION
Baht GS and Grol MW (2023) Editorial: The immune system and inflammation in musculoskeletal health, aging, and disease. *Front. Immunol.* 14:1218118. doi: 10.3389/fimmu.2023.1218118

Editorial: The immune system and inflammation in musculoskeletal health, aging, and disease

Gurpreet S. Baht[1]* and Matthew W. Grol[2]*

[1]Department of Orthopaedic Surgery, Duke Molecular Physiology Institute, Duke University, Durham, NC, United States, [2]Department of Physiology and Pharmacology, Schulich School of Medicine & Dentistry, University of Western Ontario, London, ON, Canada

KEYWORDS

inflammation, immune system, musculoskeletal disorders, musculoskeletal system, osteoarthritis, rheumatoid arthritis, intervertebral disc degeneration, dental implants

Editorial on the Research Topic
The immune system and inflammation in musculoskeletal health, aging, and disease

The musculoskeletal and immune systems are intricately linked in anatomical space and function, with crosstalk between immune cells and musculoskeletal tissues, including bone, cartilage, muscle, and tendons, being essential for normal development and homeostasis (1–4). Such a relationship is also critical during injury and repair, with inflammation and immune cells being necessary for initiating and resolving injury-induced tissue responses and altered extracellular matrix composition and turnover, likewise regulating immune cell engagement (5–9). Over the last decade, growing evidence has demonstrated that alterations to immune cell populations caused by aging and metabolic dysfunction underly the impaired tissue repair responses seen in chronic musculoskeletal diseases and acute injuries, including those affecting synovial joints (e.g., osteoarthritis), bones (e.g., osteoporosis, fracture healing), muscles (e.g., sarcopenia), and tendons/ligaments (e.g., tendinopathy, rupture).

The burden from musculoskeletal conditions continues to rise globally, impacting patients' quality of life, independence, and health, social and economic systems due to increasing care costs and work loss. Over 1.7 billion people globally live with musculoskeletal conditions, according to the World Health Organization (10) and findings from the Lancet's Global Burden of Disease Study 2019 (11–13). Low back pain is the main contributor to this overall burden, while osteoarthritis (OA) shows the most rapid increase of these conditions. While advances have been made in treating osteoporosis in the past decade, intervertebral disc degeneration (IVDD), OA, and many others where disease pathogenesis is less understood lack disease-modifying therapeutics. Progress in understanding how diseases such as IVDD and OA progress has revealed an essential role for inflammatory dysregulation in these conditions; however, several important questions must be resolved before this can be mobilized as a therapeutic strategy. In this Frontiers of Immunology – Inflammation Section Research Topic; The Immune System and Inflammation in Musculoskeletal Health, Aging, and Disease; we present a collection of

articles focused on the aging skeleton and aim to shed light on age-associated dysregulation of inflammatory processes that lead to musculoskeletal morbidity with the hope of identifying targets for future disease-modifying therapeutics (Figure 1).

OA is a multifactorial disease affecting synovial joints and one of the most common musculoskeletal diseases worldwide (14, 15). The disease is characterized by progressive loss of articular cartilage, subchondral bone and peri-articular bone remodeling, and intra-articular inflammation with synovitis, culminating in chronic pain and reduced mobility. The role of immune cells in OA progression was long recognized but remains poorly understood. In this Research Topic, Haubruck et al. outline the role of monocytic cells in post-traumatic OA (PTOA) and discuss therapeutic interventions to potentially improve disease outcomes. In addition to modifying disease outcomes, improved metrics for classifying OA severity are required to better manage the disease and for the development of disease-modifying drugs. In this regard, the search for biomarkers that can identify the stage of OA progression and distinguish between OA at different anatomical sites has become increasingly important. In this Research Topic, Zhang et al. identify extracellular vesicle sub-species that are more prevalent in patients with knee OA and carry a pro-inflammatory cargo, including tumor necrosis factor-alpha (TNF-α). In a second study in this Research Topic, Ratneswaran et al. investigated patients with hand OA and identified that circulating cytokines could distinguish OA severity of the trapeziometacarpal joint. Specifically, interleukin-7 (IL-7) was identified as a marker capable of differentiating disease severity with higher levels associated with a decreased likelihood of trapeziometacarpel joint OA needing surgical intervention. In terms of targeting inflammation to treat OA, Vachhani et al. investigated whether CD200R1 agonists could delay the progression of PTOA; however, neither the protein therapeutic CD200Fc nor the synthetic DNA aptamer CCS13 were able to attenuate cartilage degeneration or synovitis, despite their ability to blunt inflammatory response in the knee. This study points to the complexities of targeting inflammation in complex diseases such as OA.

In recent years, synoviocytes and resident immune cells within the synovium have emerged as key players in the progression of OA and other joint diseases (16, 17). In this Research Topic, Jones et al. used ChIP-seq to assay fibroblast-like synoviocytes and identified that SOX4 and RELA physically interact on chromatin, with TNF-responsive genes being the primary targets of this transcriptional complex. Sodhi et al. identified sex-dependent differences between complement and synovial microvascular pathology in patients, with higher synovial fluid C5 levels being associated with increased complement activation and decreased synovial vascularization in males but not in females with OA. Farina et al. identified that the binding of pro-nerve growth factor to p75NTR on synoviocytes elicits an inflammatory response, resulting in the release of IL-1β, IL-6 and TNF-α. Inhibition of this binding prevented this inflammatory response and represents a novel therapeutic approach in chronic arthritis. Finally, the role of Hippo pathway targets, the mechanoresponsive Yap/Taz transcription factors, was

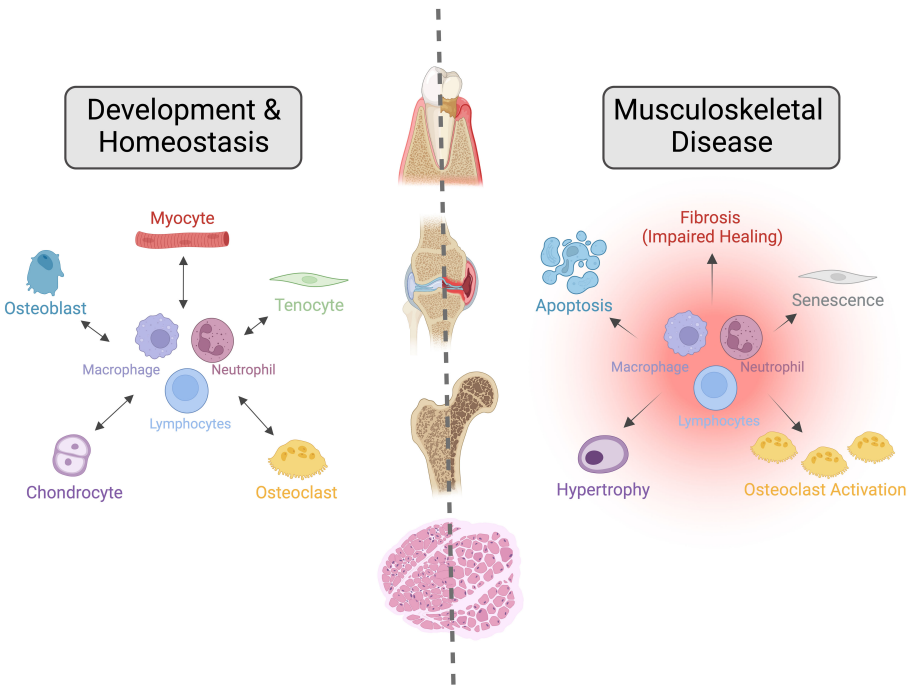

FIGURE 1
The Importance of Crosstalk between the Immune and Musculoskeletal Systems during Development, Homeostasis, and Disease. Interactions between the immune and musculoskeletal systems are critical for their development and homeostasis. Alterations to these interactions caused by aging, metabolic dysfunction, or genetic mutations lead to impaired repair responses and dysregulated tissue homeostasis, resulting in various musculoskeletal diseases such as osteoarthritis, osteoporosis, sarcopenia, periodontal disease and dental implant loosening, and intervertebral disc degeneration. In this Frontiers of Immunology – Inflammation Section research topic, we present a collection of articles that aim to shed light on age-associated dysregulation of inflammatory processes that lead to musculoskeletal morbidity. Image created with BioRender.com under Academic License.

investigated in the context of rheumatoid arthritis (RA) by Caire et al., where the authors demonstrated that RA activates Yap/Taz within synoviocytes. Treatment with a Yap/Taz inhibitor reversed the RA phenotype indicating their transcriptional inhibition could be relevant to treat inflammatory-related diseases.

Aging also affects other tissues of the skeleton. The effect of oxidative stress on IVDD was studied by Cao et al. Specifically, this group found that *Ccnb1* and *Pkd1* help to regulate oxidative stress during intervertebral disc degeneration and lead to CD8+ T cell infiltration. This work presents *Ccnb1* & *Pkd1* as potential targets for treatment in IVDD. A lesser-considered modality of the aging skeleton is dental health. Schluessel et al. investigated the loosening of dental implants and related gene expression profiles with the loosening of orthopedic implants. Using co-culture systems, disparate and overlapping gene profiles were established, identifying potential therapeutic targets for improving and maintaining the integration of dental and orthopedic implants. Ma et al. investigated the ratio of pro-inflammatory and anti-inflammatory macrophages within the infrapatellar fat pad and subcutaneous fat tissue of patients receiving total knee arthroplasties. The macrophage ratio differed between infrapatellar and subcutaneous fat, with the infrapatellar environment presenting a more inflammatory niche that could be targeted for therapeutic intervention in joint disease.

The works within this collection shed light on the importance of immune cell populations and signaling mechanisms in musculoskeletal disease progression; however, more work is certainly needed before therapeutics targeting these mechanisms can be developed to modify complex diseases such as OA and IVDD.

In conclusion, we thank the contributing authors for sharing their findings and insights in these critical areas. Musculoskeletal diseases have long presented a challenge to the medical and scientific communities. However, with an improved understanding of how the immune and musculoskeletal systems interact, better and more selective therapies could be on the horizon.

Author contributions

All authors listed have made equal substantial, direct, and intellectual contributions to the work and approved it for publication.

Funding

G.S.B. was supported by a Borden Scholars award, Duke Claude D. Pepper Older Americans Independence Center Pilot Award (P30AG028716), and by the NIH/NIA (R21AG067245). M.W.G. was supported by funding from the Canada Research Chairs Program and the Canadian Institutes of Health Research.

Conflict of interest

The authors declare that the research was conducted in the absence of any commercial or financial relationships that could be construed as a potential conflict of interest.

Publisher's note

References

1. Guder C, Gravius S, Burger C, Wirtz DC, Schildberg FA. Osteoimmunology: a current update of the interplay between bone and the immune system. *Front Immunol* (2020) 11:58. doi: 10.3389/fimmu.2020.00058

2. Longoni A, Knezevic L, Schepers K, Weinans H, Rosenberg A, Gawlitta D. The impact of immune response on endochondral bone regeneration. *NPJ Regener Med* (2018) 3:22. doi: 10.1038/s41536-018-0060-5

3. Sun Z, Liu B, Luo ZJ. The immune privilege of the intervertebral disc: implications for intervertebral disc degeneration treatment. *Int J Med Sci* (2020) 17:685–92. doi: 10.7150/ijms.42238

4. Tidball JG. Regulation of muscle growth and regeneration by the immune system. *Nat Rev Immunol* (2017) 17:165–78. doi: 10.1038/nri.2016.150

5. Baht GS, Vi L, Alman BA. The role of the immune cells in fracture healing. *Curr Osteoporos Rep* (2018) 16:138–45. doi: 10.1007/s11914-018-0423-2

6. Crosio G, Huang AH. Innate and adaptive immune system cells implicated in tendon healing and disease. *Eur Cell Mater* (2022) 43:39–52. doi: 10.22203/eCM.v043a05

7. Woodell-May JE, Sommerfeld SD. Role of inflammation and the immune system in the progression of osteoarthritis. *J Orthop Res* (2020) 38:253–7. doi: 10.1002/jor.24457

8. Xiong Y, Mi BB, Lin Z, Hu YQ, Yu L, Zha KK, et al. The role of the immune microenvironment in bone, cartilage, and soft tissue regeneration: from mechanism to therapeutic opportunity. *Mil Med Res* (2022) 9:65. doi: 10.1186/s40779-022-00426-8

9. Ye F, Lyu FJ, Wang H, Zheng Z. The involvement of immune system in intervertebral disc herniation and degeneration. *JOR Spine* (2022) 5:e1196. doi: 10.1002/jsp2.1196

10. Organization WH. Musculoskeletal health (2022).

11. Diseases GBD, Injuries C. Global burden of 369 diseases and injuries in 204 countries and territories, 1990-2019: a systematic analysis for the global burden of disease study 2019. *Lancet* (2020) 396:1204–22. doi: 10.1016/S0140-6736(20)30925-9

12. Liu S, Wang B, Fan S, Wang Y, Zhan Y, Ye D. Global burden of musculoskeletal disorders and attributable factors in 204 countries and territories: a secondary analysis of the global burden of disease 2019 study. *BMJ Open* (2022) 12:e062183. doi: 10.1136/bmjopen-2022-062183

13. Sebbag E, Felten R, Sagez F, Sibilia J, Devilliers H, Arnaud L. The world-wide burden of musculoskeletal diseases: a systematic analysis of the world health organization burden of diseases database. *Ann Rheum Dis* (2019) 78:844–8. doi: 10.1136/annrheumdis-2019-215142

14. Loeser RF, Goldring SR, Scanzello CR, Goldring MB. Osteoarthritis: a disease of the joint as an organ. *Arthritis Rheum* (2012) 64:1697–707. doi: 10.1002/art.34453

15. Martel-Pelletier J, Barr AJ, Cicuttini FM, Conaghan PG, Cooper C, Goldring MB, et al. Osteoarthritis. *Nat Rev Dis Primers* (2016) 2:16072. doi: 10.1038/nrdp.2016.72

16. Mathiessen A, Conaghan PG. Synovitis in osteoarthritis: current understanding with therapeutic implications. *Arthritis Res Ther* (2017) 19:18. doi: 10.1186/s13075-017-1229-9

17. Yoshitomi H. Regulation of immune responses and chronic inflammation by fibroblast-like synoviocytes. *Front Immunol* (2019) 10:1395. doi: 10.3389/fimmu.2019.01395

frontiers in Immunology

ORIGINAL RESEARCH
published: 06 October 2021
doi: 10.3389/fimmu.2021.758386

TNF-α Carried by Plasma Extracellular Vesicles Predicts Knee Osteoarthritis Progression

Xin Zhang[1,2*], *Ming-Feng Hsueh*[1,2], *Janet L. Huebner*[1] *and Virginia B. Kraus*[1,2,3]

[1] *Duke Molecular Physiology Institute, Duke University School of Medicine, Duke University, Durham, NC, United States,*
[2] *Department of Orthopaedic Surgery, Duke University School of Medicine, Duke University, Durham, NC, United States,*
[3] *Department of Medicine, Duke University School of Medicine, Duke University, Durham, NC, United States*

OPEN ACCESS

Edited by:
Matthew William Grol,
Western University, Canada

Reviewed by:
Ahuva Nissim,
Queen Mary University of London, United Kingdom
Mark Hamrick,
Augusta University, United States

****Correspondence:***
Xin Zhang
xin.zhang193@duke.edu

Specialty section:
This article was submitted to Inflammation, a section of the journal Frontiers in Immunology

Received: *13 August 2021*
Accepted: *21 September 2021*
Published: *06 October 2021*

Citation:
Zhang X, Hsueh M-F, Huebner JL and Kraus VB (2021) TNF-α Carried by Plasma Extracellular Vesicles Predicts Knee Osteoarthritis Progression. Front. Immunol. 12:758386. doi: 10.3389/fimmu.2021.758386

Objectives: To identify plasma extracellular vesicles (EVs) associated with radiographic knee osteoarthritis (OA) progression.

Methods: EVs of small (SEV), medium (MEV) and large (LEV) sizes from plasma of OA participants (n=30) and healthy controls (HCs, n=22) were profiled for surface markers and cytokine cargo by high-resolution flow cytometry. The concentrations of cytokines within (endo-) and outside (exo-) EVs were quantified by multiplex ELISA. EV associations with knee radiographic OA (rOA) progression were assessed by multivariable linear regression (adjusted for baseline clinical variables of age, gender, BMI and OA severity) and receiver operating characteristic (ROC) curve analysis.

Results: Based on integrated mean fluorescence intensity (iMFI), baseline plasma MEVs carrying CD56 (corresponding to natural killer cells) predicted rOA progression with highest area under the ROC curve (AUC) 0.714 among surface markers. Baseline iMFI of TNF-α in LEVs, MEVs and SEVs, and the total endo-EV TNF-α concentration, predicted rOA progression with AUCs 0.688, 0.821, 0.821, 0.665, respectively. In contrast, baseline plasma exo-EV TNF-α (the concentration in the same unit of plasma after EV depletion) did not predict rOA progression (AUC 0.478). Baseline endo-EV IFN-γ and exo-EV IL-6 concentrations were also associated with rOA progression, but had low discriminant capacity (AUCs 0.558 and 0.518, respectively).

Conclusions: Plasma EVs carry pro-inflammatory cargo that predict risk of knee rOA progression. These findings suggest that EV-associated TNF-α may be pathogenic in OA. The sequestration of pathogenic TNF-α within EVs may provide an explanation for the lack of success of systemic TNF-α inhibitors in OA trials to date.

Keywords: extracellular vesicles, knee osteoarthritis progression, immune cells, cytokines, TNF-α

INTRODUCTION

Extracellular vesicles (EVs) are released by almost all mammalian cells. Due to their cargo (cytoplasmic proteins, DNA, mRNA, miRNA, small non-coding RNAs, mitochondria, and cytokines), EVs are believed to be able to act as mediators of cell-to-cell communication and as paracrine effectors (1–4). Studies in OA have focused on the beneficial effects of mesenchymal stem cell (MSC)-derived EVs (5, 6), the detrimental effects of subchondral bone osteoblast-derived small EVs (SEVs) (7), and the surface markers and cytokine cargo of SEVs (also known as exosomes) in OA synovial fluid (SF) (8, 9). SEVs from knee OA SF carry surface markers CD9, CD81 and CD63 and cytokines (IL-1β, IL-2, IL-4, IL-5, IL-6, IL-13, IL-17, TNF-α and IFN-γ (8–10), and are associated with OA disease severity (8). SEVs from OA SF induce the release of pro-inflammatory cytokines (IL-1β, IL-6 and TNF-α), chemokines and metalloproteases *in vitro* by M1 macrophages (9), enhance chemotaxis of peripheral blood mononuclear cells, promote inflammatory responses, and inhibit chondrocyte proliferation (10). SEVs from IL-1β stimulated human synovial fibroblasts significantly up-regulate articular chondrocyte expression of MMP-13 and ADAMTS-5 (11). Taken together, these studies suggest a pathogenic role of SF-derived EVs in OA.

Despite the evidence for a role of EVs in the pathogenesis of OA, to our knowledge, there have been no previous studies evaluating the role of EV subpopulations in OA progression. To fill this important knowledge gap, we profiled OA and healthy control (HC) plasma for EV surface markers, 'endo-EV' (within EV) cytokine cargo, and exo-EV cytokine concentrations (in EV-depleted supernatant after ExoQuick precipitation of EVs from the unit of plasma), to evaluate and compare their associations with knee radiographic (r)OA severity and progression.

METHODS

Study Participants

Sixty plasma specimens were analyzed including: (1) healthy controls (HCs, n=16), non-progressive OA (OA-NP, n=16) and progressive OA (OA-P, n=14) from the completed Genetics of Generalized Osteoarthritis (GOGO) study (12); and (2) additional HC samples (n=6) from the commercial vendor (Zenbio). The samples were matched for gender, race and decade of age (**Table 1**). Samples were stored at -80°C until analysis. All samples and data were acquired with informed consent under IRB approval of Duke University or the commercial vendor (Zenbio).

Radiographic Procedures and Grading

Knee radiographic imaging was performed as reported previously for the GOGO study (12) and scored for Kellgren and Lawrence (K/L) grade (0–4) (12–14). K/L scores from both knees of a participant were summed yielding scores with range 0-8. HCs from GOGO were defined as participants having knee K/L grade 0 bilaterally. Participants having knee OA was defined as having summed K/L grade ≥1 at baseline. The change of K/L scores from both knees of a participant were summed yielding scores with range 0-6. Radiographic knee OA progression was defined as K/L grade increase ≥1 unit in at least one knee during follow-up (mean 3.8 years, range 1.1-8.6 years) (**Table 1**). HCs from Zenbio were defined as no self-reported diseases or medical conditions.

EV Separation From Plasma Samples

EV isolation required 50 µl plasma for each marker panel as previously reported (4, 15). Blood samples were centrifuged at 3000 rpm for 15 min at 4 °C to separate plasma from cells and debris; plasma samples were aliquoted and frozen at – 80 °C until analysis. Frozen plasma samples were thawed followed by centrifugation at 2000 g for 10 minutes at 4°C to remove remaining debris. EVs in plasma were separated by ExoQuick (System Biosciences) following the manufacturer's instructions (4, 15, 16). As described below, EVs were profiled for surface markers and cytokines; endo-EV and exo-EV cytokine concentrations were also measured.

Profiling EV-Carried Surface Markers and Cytokines by High Resolution Multicolor Flow Cytometry

As previously described (4, 15), EVs were profiled for the following surface markers to identify EV subpopulations by cell of origin (**Supplementary Table 1**) (4, 15, 17–25): CD81, CD9, CD29, CD63, CD8, CD68, CD14, CD56, CD15, CD235a, CD41a, CD34, CD31, major histocompatibility complex (MHC)-class I antigens HLA-A, HLA-B and HLA-C (HLA-ABC), MHC-class II antigens HLA-DR, -DP and -DQ (HLA-DRDPDQ) (BD Biosciences), CD4, CD19 and MHC-class I antigen HLA-G (ThermoFisher Scientific). We also profiled endo-EV cytokines IL-1β, TNF-α, IFN-γ (BD Biosciences), and IL-6 (ThermoFisher

TABLE 1 | Demographic information of the study participants.

	HC*	HC	OA-NP	OA-P
Sample number	n=6	n=16	n=16	n=14
Mean (SD) age at enrollment (years)	55.5 (11)	68.4 (8)	68.7 (8)	69.3 (8)
Gender (Female) %	50%	50%	50%	57%
Mean (SD) BMI at enrollment (kg/m^2)	28 (8)	27 (3)	32 (8)	29 (5)
Median (range) Summed Baseline K/L grade	N/A	0 (0)	2 (1-6)	2 (1-6)
Median (range) Summed Change in K/L grade	N/A	0 (0)	0 (0)	3 (1-6)

*HC, healthy control; *obtained from Zenbio; OA-P, radiographic knee osteoarthritis progressor; OA-NP, radiographic knee osteoarthritis non-progressor; SD: standard deviation; BMI, body mass index; K/L grade, Kellgren and Lawrence grade; N/A, not applicable.*

Scientific). The percentages (%) and geometric mean fluorescence intensity (MFI) of EVs carrying each tested marker were determined using a high-resolution multicolor BD LSR Fortessa X-20 Flow Cytometer with the BD FACSDiVa software (BD Biosciences). The integrated MFI (iMFI) of surface markers and cytokines was calculated by multiplying percentage of positive population with the MFI of that population (15, 26, 27).

Multiplex ELISA for Cytokine Quantification

To confirm the efficiency of the EV precipitation, the concentration and size distribution of particles (in the ExoQuick precipitate of EVs and the remaining EV-depleted supernatants) derived from 50 µl plasma were measured by nanoparticle tracking analysis and dynamic light scattering as previously reported (4, 15) (**Supplementary Figure 1**). As previously described (15), EV pellets were lysed in NP40 lysis buffer (Thermo Fisher Scientific) in the same volume as the EV-depleted supernatants. The concentrations of endo-EV and exo-EV (remaining EV-depleted supernatant after ExoQuick precipitation) cytokines were measured by multiplex ELISA using the Custom Pro-inflammatory Panel (IL-1β, IL-6, TNF-α, IFN-γ, Meso Scale Diagnostics) following the manufacturer's instructions (15, 28, 29).

Receiver Operating Characteristic (ROC) Curve Analysis

Multivariable logistic regression and ROC curve analyses (30, 31) were performed to evaluate the discriminant ability of baseline EV-related variables for knee OA progression, defined as change in knee K/L grade (summed across knees). Model stabilities were validated using a 2,500 non-parametric bootstrap resampling approach; 95% bias-corrected confidence intervals (CIs) for area under the ROC curve (AUC) are reported. Likelihood ratio (32) test was used to assess model fit; the R-square value (RSq) (33), corrected Akaike's Information Criterion (AICs) (34) and the Bayesian Information Criterion (BIC) (35) are reported. Rsq closer to 1 indicates a better fit to the data; while for AIC and BIC, the model having the smaller value is considered better. Specificity was determined at sensitivity 80%. The analyses were performed using JMP Pro 15 (SAS). AUC is interpreted as follows: AUC ≤0.5 indicates no better than a random classifier; AUC >0.5 is considered validated; AUC >0.65 is considered a moderate discriminant capability.

Statistical Analyses

Data in this study were not normally distributed based on D'Agostino-Pearson omnibus normality test; therefore, nonparametric analyses were performed. Comparisons between HC, OA-NP and OA-P were performed using Kruskal-Wallis test. Comparisons of endo-EV and exo-EV cytokines were performed using Wilcoxon matched-pairs signed rank test. Comparisons between the tested cytokines in each participant group were performed using Friedman test. False Discovery Rate (FDR) was generated using the Benjamini and Yekutieli method with significant results defined by FDR (q value) <0.05. Multivariable linear regression modeling was performed with adjustment for baseline clinical variables (age, gender, body mass index [BMI] and summed knee OA K/L score) to identify associations of endo-EV and exo-EV biomarkers with knee rOA progression, defined by change in summed K/L score from baseline to follow-up. A p value <0.05 was considered statistically significant. GraphPad Prism 8.0 software (GraphPad) and JMP Pro 15 software were used for statistical analyses.

RESULTS

Multiple Immune Cell-Related LEVs and MEVs Were Associated With Knee rOA Progression

There are currently no specific markers for different EV subtypes (36). Following the recommendations from the International Society for Extracellular Vesicles (36), we used operational terms (range of sizes along with descriptions of cell of origin defined by their surface markers) to describe EV subsets as in our previous work (4, 15). With our newly developed high-resolution multicolor flow cytometry-based methodology, we identified three major subsets of plasma EVs in human HCs: large EVs (LEVs), 1000-6000 nm; medium sized EVs (MEVs), 100-1000 nm; and SEVs, <100 nm; these major subsets based on size were confirmed using dynamic light scattering (4, 15). In this study, these three major subsets of plasma EVs were also identified in plasma of participants with knee OA. Plasma EVs from HC and OA participants all carried surface markers of human stem cells and progenitor cells, immune cells, activated pro-inflammatory fibroblasts, epithelial and endothelial cells indicative of their cell origins (**Supplementary Figure 2** and **Supplementary Table 1**) (4, 15, 17–25).

Baseline iMFI of multiple plasma EV subpopulations were associated with baseline clinical variables including age, gender, BMI and summed knee OA K/L score (**Supplementary Figure 3**). Adjusting for these baseline clinical variables, baseline iMFI of multiple plasma LEVs and MEVs were statistically significantly associated with knee rOA progression. LEV subpopulations associated with rOA progression included the following: $CD29^+$, $CD63^+$, $CD8^+$, $CD15^+$, $CD14^+$, $CD19^+$, and ratio of CD15/CD8 (reflecting neutrophil-EV to T cell-EV ratio) (**Figure 1A**). MEV subpopulations associated with rOA progression included the following: $CD81^+$, $CD9^+$, $CD31^+$, $CD29^+$, $CD63^+$, $CD56^+$, $CD68^+$, and $HLA\text{-}DRDPDQ^+$ (**Figure 1B**). No SEV subpopulations based on EV surface markers were associated with knee rOA progression. These LEV and MEV surface markers yielded AUCs >0.5 (**Figures 1C, D**); $CD56^+$ MEVs (AUC 0.714), corresponding to NK cell-EVs, yielded the highest AUC (**Figure 1D**).

Endo-EV TNF-EV TNF-α in Plasma Associated With Knee OA Progression

TNF-α is a classical pro-inflammatory cytokine playing critical roles in OA pathogenesis (29, 37–41). Recently, we found that

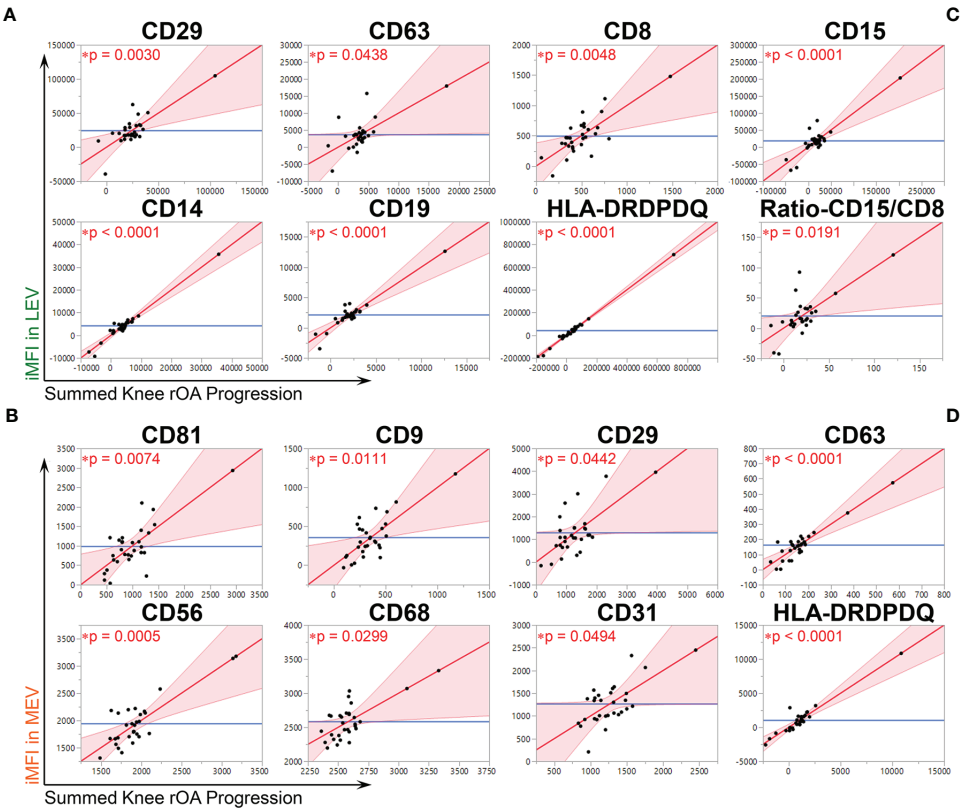

C

LEVs

Surface Markers	AUC	95% CI Lower	95% CI Upper
CD29	0.504	0.387	0.556
CD63	0.527	0.417	0.603
CD8	0.536	0.391	0.638
CD15	0.518	0.315	0.592
CD14	0.536	0.333	0.693
CD19	0.576	0.385	0.799
HLA-DRDPDQ	0.506	0.335	0.582
Ratio-CD15/CD8	0.506	0.335	0.582

D

MEVs

Surface Markers	AUC	95% CI Lower	95% CI Upper
CD81	0.571	0.452	0.732
CD9	0.629	0.487	0.818
CD29	**0.665**	0.472	0.838
CD63	0.625	0.481	0.810
CD56	**0.714**	0.500	0.890
CD68	0.571	0.385	0.742
CD31	0.594	0.440	0.772
HLA-DRDPDQ	0.552	0.401	0.692

FIGURE 1 | Multiple immune cell-associated LEVs and MEVs at baseline were associated with knee radiographic (r)OA progression. Plasma EVs from OA participants (n = 30, 53% OA-NP and 47% OA-P) at baseline were profiled with the indicated surface markers by high resolution multicolor flow cytometry. **(A, B)** Multivariable linear regression modeling was performed with adjustment for the baseline clinical variables (age, gender, BMI and summed knee OA K/L score) to identify the associations of the knee OA radiographic severity changes from baseline to follow-up with the baseline iMFI of each surface marker in gated LEVs, MEVs or SEVs. The Leverage Plots represent plots of leverage of summed knee rOA progression (x axis, scaled in units of the response) vs the baseline iMFI (y axis) of the indicated surface markers in LEVs **(A)** and MEVs **(B)** with an asterisks indicate the $p < 0.05$. No SEV subpopulations based on EV surface markers were associated with knee rOA progression. **(C, D)** Multivariable logistic regression and ROC curve analysis were used to assess AUC of the knee rOA progression-associated surface markers in LEVs **(C)** and MEVs **(D)** to predict progression of radiographic knee OA. Since all tested surface markers in SEVs were not significantly associated with knee rOA progression, they were excluded from ROC analysis. AUC > 0.5 was considered validated and AUC > 0.65 (red font) was considered a moderate discriminant capability. 95% bias-corrected confidence intervals (CIs) for AUCs are reported. LEVs, large EVs; MEVs, medium EVs; iMFI, integrated mean fluorescence intensity. *$p < 0.05$.

endo-EV concentrations of TNF-α (in lysates of EV pellets) were significantly higher than the exo-EV concentrations (in EV-depleted supernatants) in the same unit volume of plasma from OA participants, suggesting that EVs are a major source of systemic TNF-α(15). Here, we report, the concentration of endo-EV TNF-α was significantly higher in OA-P than HC participants, while exo-EV TNF-α concentrations did not differ among the study groups (**Figure 2A**). Adjusting for baseline clinical variables, the baseline concentration of endo-EV TNF-α was statistically significantly associated with knee rOA progression (**Figure 2B**). In addition, the baseline concentration of endo-EV TNF-α predicted knee rOA progression with moderate discriminant ability (AUC 0.665, **Figure 2C**). In contrast, exo-EV TNF-α was neither associated with nor predictive of knee rOA progression (**Figures 2B, C**). In addition to EVs being a major source of systemic TNF-α, this suggests that plasma endo-EV TNF-α represents a promising systemic biomarker for predicting risk of knee rOA progression.

Plasma EVs from HCs, OA-NP and OA-P participants were assessed by flow cytometry for an array of cytokines including TNF-α. TNF-α was present in all sizes of plasma EVs and was the most abundant endo-EV cytokine of the four analyzed and the most abundant cytokine in all three participant groups based on mean percentage of TNF-α^+ LEVs, MEVs and SEVs (**Supplementary Figure 4**). Baseline iMFI of TNF-α in LEVs was significantly higher in OA-P than HCs (**Figure 3A**), which is consistent with the differential concentration of endo-EV TNF-α observed between these two groups by ELISA based analyses (**Figure 2A**). Moreover, baseline iMFI of TNF-α in MEVs and SEVs was significantly higher in OA-P than OA-NP (**Figure 3A**). With adjustment for baseline clinical variables, baseline iMFI of TNF-α in EVs of all sizes was associated with knee rOA

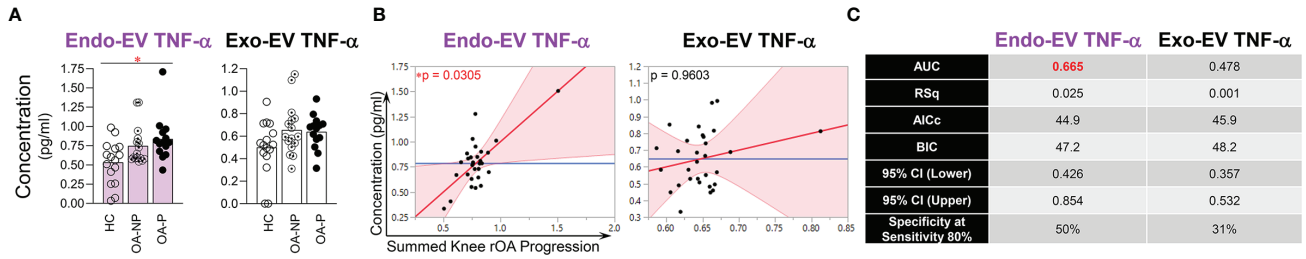

FIGURE 2 | The concentration of endo-EV TNF-α at baseline was associated with knee rOA progression. The concentrations of exo-EV and endo-EV TNF-α in plasma from HC (n = 16), OA-NP (n = 16) and OA-P (n = 14) participants at baseline were measured by multiplex immunoassay. **(A)** The graphs represent the differential concentrations of endo-EV and exo-EV TNF-α between HC, OA-NP and OA-P. Comparisons between HC, OA-NP and OA-P were performed using Kruskal-Wallis test with significant results defined by FDR q< 0.05; asterisks indicate the p value as * <0.05. **(B)** Multivariable linear regression modeling was performed with adjustment for the baseline clinical variables to identify the associations of summed knee rOA progression with baseline concentrations of TNF-α in OA participants (n = 30, 53% OA-NP and 47% OA-P). The Leverage Plots represent plots of leverage of summed knee rOA progression (x axis) vs the baseline concentrations (y axis) of endo-EV and exo-EV TNF-α. **(C)** Multivariable logistic regression and ROC curve analysis were used to assess AUC and specificity (at sensitivity 80%) of endo-EV and exo-EV TNF-α in OA participants (n = 30, 53% OA-NP and 47% OA-P) to predict progression of radiographic knee OA. Rsq, AICs, and BICs were based on likelihood ratio test. 95% bias-corrected confidence intervals (CIs) for AUCs are reported. Endo-EV, within EV; Exo-EV, outside EV; HC, healthy control; OA-P, radiographic knee osteoarthritis progressor; OA-NP, radiographic knee osteoarthritis non-progressor.

progression (P<0.1); this was statistically significant for TNF-α in MEVs (**Figure 3B**). Although the baseline iMFI of TNF-α in EVs of all sizes predicted knee rOA progression, MEVs and SEVs had higher AUCs and specificity (both AUC 0.821 and specificity 81% at sensitivity 80%) than LEVs (AUC 0.688 and specificity 63% at sensitivity 80%) (**Figure 3C**).

Other Pro-Inflammatory Cytokines Associated With Knee rOA Progression

Endo-EV IFN-γ concentrations were significantly higher in OA-P than both OA-NP and HC participants; exo-EV IFN-γ concentrations did not differ among the study groups (**Figure 4A**). In contrast, exo-EV IL-6 concentrations were significantly higher in OA-P than both OA-NP and HC participants; endo-EV IL-6 concentrations did not differ among the study groups (**Figure 4B**). There were no statistically significant differences between the study groups based on concentrations of endo-EV or exo-EV IL-1β, or iMFIs of IL-1β, IL-6 or IFN-γ in EVs of all sizes (data not shown). Adjusting for baseline clinical variables, baseline concentrations of endo-EV IFN-γ (**Figure 4C**) and exo-EV IL-6 (**Figure 4D**) were statistically significantly associated with knee rOA progression and yielded validated AUCs of 0.558, and 0.518, respectively.

DISCUSSION

All major types of immune cells (neutrophils, macrophages, NK cells, T cells, B cells, dendritic cells, and granulocytes) actively infiltrate OA synovial tissues, releasing cytokines and EVs into the joint that may contribute to structural progression of OA (11, 42–45). In this study, we identified plasma EVs from OA participants carrying surface markers indicative of multiple cell origins including human stem cells and progenitor cells, all major types of immune cells, activated pro-inflammatory fibroblasts, epithelial and endothelial cells (4, 15, 17–25). We identified plasma EVs in OA that carry the major pro-inflammatory cytokines, TNF-α, IFN-γ, IL-6 and IL-1β, demonstrating their pro-inflammatory phenotype. We found that the concentration of endo-EV TNF-α and the iMFI of TNF-α in EV subsets in OA plasma were associated with and strong predictors of knee rOA progression, while plasma exo-EV TNF-α was neither associated with nor predictive of knee rOA progression. Based on this prior work, we know that these TNF-α^+ EVs are present and abundant in OA synovial fluid (15). This suggests that EV associated TNF-α may play a role in OA progression.

TNF-α is a classical pro-inflammatory cytokine produced by a broad variety of cell types, including, but not limited to, macrophages, monocytes, T cells, B cells, NK cells, mast cells, keratinocytes, astrocytes, microglial cells, muscle cells, intestinal paneth cells, tumor cells, synoviocytes and articular chondrocytes (46–48). Based on human *in vitro* data, TNF-α may play a critical role in the pathogenesis of OA (38, 40, 49). Previous human studies reported that serum TNF-α concentrations predicted knee rOA progression (50), and were associated with joint space narrowing (51). SF TNF-α concentrations were associated with knee pain (29). In addition, TNF-α polymorphisms were associated with susceptibility to OA in a Korean population (52).

Although in an animal study, TNF-α inhibition significantly decreased pro-inflammatory cytokines (IL-1β, IL-17a and IL-8), MMP-3 and MMP-9, inflammatory cell infiltration and bone destruction in joints and cartilage of rats with OA (53), the reported human trials of TNF-α inhibitors for OA are limited to three and all have been negative. These three trials (n=60 hand OA, n=84 hand OA, and n=20 knee OA) all used human TNF antibody, adalimumab (54). Only a single case report indicated that neutralizing TNF-α using adalimumab (40 mg subcutaneously every other week) decreased pain and improved joint function, visibly decreased synovial effusion and synovitis and bone marrow edema, and dramatically decreased nocturnal pain and improved

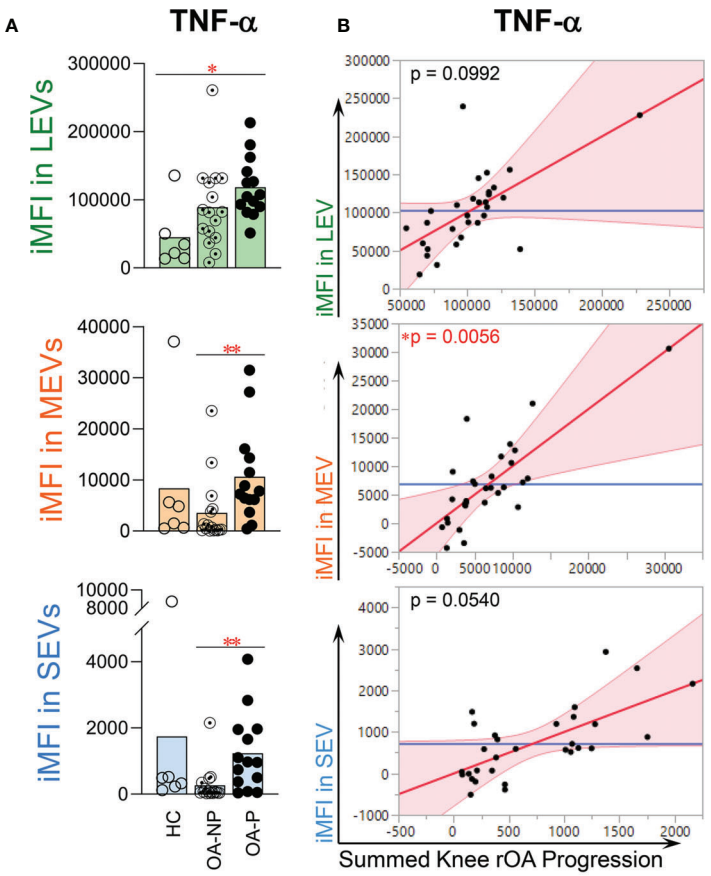

C

TNF-α

	LEVs	MEVs	SEVs
AUC	0.688	0.821	0.821
RSq	0.055	0.274	0.267
AICc	43.6	34.5	34.8
BIC	46.0	36.9	37.2
95% CI (Lower)	0.458	0.643	0.611
95% CI (Upper)	0.864	0.952	0.957
Specificity at Sensitivity 80%	63%	81%	81%

FIGURE 3 | The iMFI of endo-EV TNF-α at baseline was associated with knee rOA progression. Plasma EVs from HC (n = 6), OA-NP (n = 16) and OA-P (n = 14) participants at baseline were profiled for intra-vesicle TNF-α by high-resolution multicolor flow cytometry. **(A)** The graphs represent the iMFI of TNF-α in gated LEVs, MEVs and SEVs between HC, OA-NP and OA-P. Comparisons between HC, OA-NP and OA-P were performed using Kruskal-Wallis test with significant results defined by FDR q< 0.05; asterisks indicate the p value as * <0.05 and ** <0.01. **(B)** Multivariable linear regression modeling was performed with adjustment for the baseline clinical variables to identify the associations of the knee OA radiographic severity changes from baseline to follow-up with the baseline iMFI of TNF-α in OA participants (n = 30, 53% OA-NP and 47% OA-P). The Leverage Plots represent plots of leverage of summed knee rOA progression (x axis) vs the baseline iMFI (y axis) of TNF-α in LEVs, MEVs and SEVs. **(C)** Multivariable logistic regression and ROC curve analysis were used to assess AUC and specificity (at sensitivity 80%) of TNF-α in LEVs, MEVs and SEVs in OA participants (n = 30, 53% OA-NP and 47% OA-P). Rsq, AICs, and BICs were based on likelihood ratio test. 95% bias-corrected CIs for AUCs are reported. LEVs, large EVs; MEVs, medium EVs; SEVs, small EVs; iMFI, integrated mean fluorescence intensity. HC, healthy control obtained from Zenbio; OA-P, radiographic knee osteoarthritis progressor; OA-NP, radiographic knee osteoarthritis non-progressor.

walking distance (48). One possible explanation for these conflicting results is that TNF-α binds to two types of receptors with opposing functions — TNFRI mediating pro-inflammatory signals, and TNFRII mediating anti-inflammatory signals. Therefore, neutralization of TNF-α could result in a mixed clinical response, similar to prior observations resulting from treatments targeting both receptors: inhibiting signaling of both TNFRI and TNFRII reduced collagen-induced arthritis, but increased pro-inflammatory

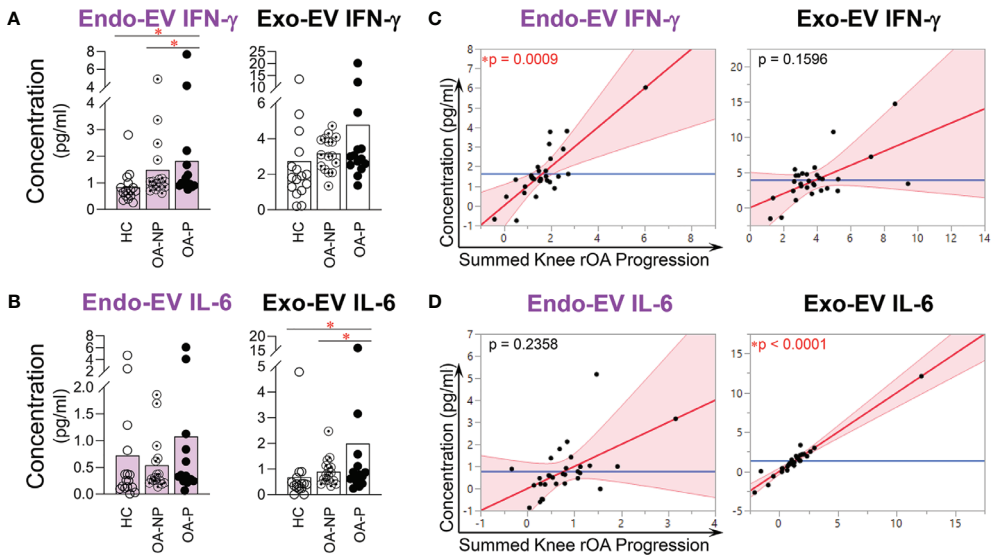

FIGURE 4 | The concentrations of endo-EV IFN-γ and exo-EV IL-6 at baseline were associated with knee rOA progression. The concentrations of exo-EV and endo-EV IFN-γ and IL-6 in plasma from HC (n = 16), OA-NP (n = 16) and OA-P (n = 14) participants at baseline were measured by multiplex immunoassay. **(A, B)** The graphs represent the differential concentrations of endo-EV and exo-EV IFN-γ **(A)** and IL-6 **(B)** between HC, OA-NP and OA-P. Comparisons between HC, OA-NP and OA-P were performed using Kruskal-Wallis test with significant results defined by FDR q < 0.05; asterisks indicate the p value as * < 0.05. **(C, D)** Multivariable linear regression modeling was performed with adjustment for the baseline clinical variables to identify the associations of summed knee rOA progression from baseline to follow-up with the baseline concentrations of IFN-γ and IL-6 in OA participants (n = 30, 53% OA-NP and 47% OA-P). The Leverage Plots represent plots of leverage of summed knee rOA progression (x axis) *vs* the baseline concentrations (y axis) of endo-EV and exo-EV IFN-γ **(C)** and IL-6 **(D)**. Endo-EV, within EV; Exo-EV, outside EV; HC, healthy control; OA-P, radiographic knee osteoarthritis progressor; OA-NP, radiographic knee osteoarthritis non-progressor.

cytokine levels and reduced Treg cell activity. In contrast, selective blockade of TNFRI signaling reduced collagen-induced arthritis without the major side effects observed with both TNFRI and TNFRII blockade (55, 56). Another possible explanation is that TNF-α carried by EVs is sequestered from systemic anti-TNF-α. For flow cytometric quantification of intra-vesicular cytokines including TNF-α, it is necessary to fix and permeabilize the EVs; thus, permeability to antibodies is not expected to be a property of circulating EVs *in vivo*. We observed that the concentration of endo-EV TNF-α was higher than the matched exo-EV TNF-α in the same unit volume of OA plasma. Therefore, neutralizing soluble TNF-α in blood may not be sufficient when a large amount of pathogenic TNF-α is sequestered in EVs and potentially inaccessible to the neutralizing antibody. Nevertheless, these EVs would be expected to be able to fuse their membrane to the plasma membrane of specific target cells, followed by discharge of their luminal cargo [e.g. TNF-α) to the cytoplasm of their target cell (57)]. Given the dual biological functions of TNF-α in arthritis mediated by TNFRI and TNFRII, and potential technical difficulties depleting EV-carried TNF-α *in vivo*, neutralizing TNF-α with biologics may not be an ideal therapeutic approach for treating OA. Instead, it may be important to lower the production of TNF-α^+ EVs. Monitoring of TNF-α^+ EVs in plasma could also be a promising companion diagnostic for OA.

Similar to TNF-α, the concentration of endo-EV, but not exo-EV, IFN-γ was significantly associated with knee OA progression, although it was not as strong a predictor of knee OA progression. In contrast, the concentration of exo-EV, but not endo-EV, IL-6 was significantly associated with knee OA progression. These findings suggest that endo-EV and exo-EV pro-inflammatory cytokines may play different roles in the pathogenesis and worsening of OA and represent different biological processes in OA progression.

Among the test surface markers, $CD56^+$ MEVs, related to NK cells, were the strongest predictor of knee rOA progression with the highest AUC. NK cells are one of the principal leukocyte subsets that infiltrate OA synovia (58); NK cells in both peripherial blood and SF of patients with OA produce pro-inflammatory cytokines,TNF-α, IL-6, and IFN-γ. The frequency of NK cells producing these pro-inflammatory cytokines is significantly higher in OA SF than plasma (59). *In vivo* antibody-mediated depletion of NK cells ameliorates disease in experimental OA, demonstrating their pathogenicity, which is likely mediated by their ability to promote inflammation and bone destruction (60).

The neutrophil to lymphocyte ratio (NLR) in peripheral blood is already a non-invasive and cost-effective biomarker of various systemic diseases, including cancers, cardiovascular diseases and rheumatologic diseases, and has been shown to be associated with OA severity (61–63). Recently, we found that the ratios of neutrophil EVs to lymphocyte EVs (from T cells, B cells and NK cells), and to T cell EVs, were highly correlated between SF and plasma in OA (15). Here we show that the ratio of neutrophil EVs to T cell EVs was associated with knee OA progression (with a validated AUC). These data taken together suggest that these NLR ratios, based on EV quantification, could

serve as systemic biomarkers of OA joint pathology and possibly other comorbidities, such as cardiovascular disease. The breakthrough advantage of determining NLR ratio based on EVs is the ability to use frozen archival samples in contrast to the current method requiring fresh cells.

The first limitation of this exploratory study was the limited number of available samples related to difficulties collecting human specimens of matched gender, race, decade of age, and diversity of OA disease severity and progression. The second limitation was the lack of fresh cells, so we could not directly link EV profiles to the inflammatory phenotype of their parent cells. In addition, OA is often associated with comorbidities that might increase the prevalence of pro-inflammatory EVs. Given the sample sizes, assessing effects of comorbidities was outside the scope of these analyses. However, the GOGO study recruited cognitively intact, ambulatory older adults. In this regard, there is potential selection bias for individuals without major comorbidities other than OA. Although these limitations exist, this study identified several potential new knee OA progression-associated EV biomarkers and predictors worthy of further study as new systemic predictors of knee OA progression. This study also provides insights to optimize therapies targeting TNF-α pathways in OA. Our findings would encourage more studies to explore the roles of these EV biomarkers in OA pathogenesis and disease development.

In summary, we identified several immune cell- and pro-inflammatory cytokine-associated EV subpopulations that were significant independent predictors of knee rOA progression. Among these EV biomarkers, baseline iMFI of TNF-α in MEVs and SEVs was significantly higher in plasma of OA-Progressors than OA-Non-progressors, and the best predictor of knee rOA progression with highest AUC and specificity. Interestingly, baseline iMFI of TNF-α in EVs of all sizes, and total concentration of endo-EV TNF-α all predicted rOA progression. In contrast, baseline exo-EV TNF-α concentration was not associated with nor predictive of rOA progression. These data suggest that EV-associated TNF-α may be pathogenic in OA. Sequestration of large amounts of TNF-α in plasma EVs of OA patients, as shown here, may explain the disappointing results to date of TNF-α inhibitors in OA disease modifying trials.

DATA AVAILABILITY STATEMENT

The original contributions presented in the study are included in the article/**Supplementary Material**. Further inquiries can be directed to the corresponding author.

ETHICS STATEMENT

The plasma samples used for this study were acquired under approval of Duke University (n=46) or acquired through a commercial entity, ZenBio (n=6) who provided an assurance, as indicated on their website (https://www.zen-bio.com/products/cells/), that all samples are acquired under donor consent and IRB approval. The patients/participants provided their written informed consent to participate in this study.

AUTHOR CONTRIBUTIONS

XZ and VK designed the study. XZ and JH performed the experiments and analyzed the data. M-FH performed ROC analyses. VK performed data analyses for radiographic procedures and grading. XZ and VK drafted the manuscript. All authors contributed to the article and approved the submitted version.

FUNDING

This research was funded by the National Institute on Aging at National Institutes of Health, grant numbers R56AG060895 (VK and XZ), R01AG070146 (VK, XZ, and JH) and P30AG028716 (VK and JH).

ACKNOWLEDGMENTS

The authors wish to acknowledge all participants who donated specimens for this study; the Duke Cancer Institute Flow Cytometry Shared Resource for providing access to the LSR Fortessa X-20 Flow Cytometer; and the Duke Human Vaccine Institute Research Flow Cytometry Shared Resource Facility for providing the FCS Express 5 software. Nanoparticle tracking analyses were performed by Marina Sokolsky-Papkov at the Nanomedicines Characterization Core Facility, Center of Nanotechnology in Drug Delivery, UNC School of Pharmacy.

SUPPLEMENTARY MATERIAL

The Supplementary Material for this article can be found online at: https://www.frontiersin.org/articles/10.3389/fimmu.2021.758386/full#supplementary-material

REFERENCES

1. Samanta S, Rajasingh S, Drosos N, Zhou Z, Dawn B, Rajasingh J. Exosomes: New Molecular Targets of Diseases. *Acta Pharmacol Sin* (2018) 39(4):501–13. doi: 10.1038/aps.2017.162
2. Thery C, Ostrowski M, Segura E. Membrane Vesicles as Conveyors of Immune Responses. *Nat Rev Immunol* (2009) 9(8):581–93. doi: 10.1038/nri2567
3. Phinney DG, Di Giuseppe M, Njah J, Sala E, Shiva S, St Croix CM, et al. Mesenchymal Stem Cells Use Extracellular Vesicles to Outsource Mitophagy and Shuttle microRNAs. *Nat Commun* (2015) 6:8472. doi: 10.1038/ncomms9472
4. Zhang X, Hubal MJ, Kraus VB. Immune Cell Extracellular Vesicles and Their Mitochondrial Content Decline With Ageing. *Immun Ageing* (2020) 17(1):1. doi: 10.1186/s12979-019-0172-9
5. D'Arrigo D, Roffi A, Cucchiarini M, Moretti M, Candrian C, Filardo G. Secretome and Extracellular Vesicles as New Biological Therapies for Knee

Osteoarthritis: A Systematic Review. *J Clin Med* (2019) 8(11):1867. doi: 10.3390/jcm8111867
6. Wu X, Wang Y, Xiao Y, Crawford R, Mao X, Prasadam I. Extracellular Vesicles: Potential Role in Osteoarthritis Regenerative Medicine. *J Orthop Translat* (2020) 21:73–80. doi: 10.1016/j.jot.2019.10.012
7. Wu X, Crawford R, Xiao Y, Mao X, Prasadam I. Osteoarthritic Subchondral Bone Release Exosomes That Promote Cartilage Degeneration. *Cells* (2021) 10 (2):251. doi: 10.3390/cells10020251
8. Gao K, Zhu W, Li H, Ma D, Liu W, Yu W, et al. Association Between Cytokines and Exosomes in Synovial Fluid of Individuals With Knee Osteoarthritis. *Mod Rheumatol* (2020) 30(4):758–64. doi: 10.1080/14397595.2019.1651445
9. Domenis R, Zanutel R, Caponnetto F, Toffoletto B, Cifu A, Pistis C, et al. Characterization of the Proinflammatory Profile of Synovial Fluid-Derived Exosomes of Patients With Osteoarthritis. *Mediators Inflammation* (2017) 2017:4814987. doi: 10.1155/2017/4814987
10. Li Z, Li M, Xu P, Ma J, Zhang R. Compositional Variation and Functional Mechanism of Exosomes in the Articular Microenvironment in Knee Osteoarthritis. *Cell Transplant* (2020) 29:963689720968495. doi: 10.1177/0963689720968495
11. Kato T, Miyaki S, Ishitobi H, Nakamura Y, Nakasa T, Lotz MK, et al. Exosomes From IL-1beta Stimulated Synovial Fibroblasts Induce Osteoarthritic Changes in Articular Chondrocytes. *Arthritis Res Ther* (2014) 16(4):R163. doi: 10.1186/ar4679
12. Kraus VB, Jordan JM, Doherty M, Wilson AG, Moskowitz R, Hochberg M, et al. The Genetics of Generalized Osteoarthritis (GOGO) Study: Study Design and Evaluation of Osteoarthritis Phenotypes. *Osteoarthritis Cartilage* (2007) 15(2):120–7. doi: 10.1016/j.joca.2006.10.002
13. Zuo X, Luciano A, Pieper CF, Bain JR, Kraus VB, Kraus WE, et al. Combined Inflammation and Metabolism Biomarker Indices of Robust and Impaired Physical Function in Older Adults. *J Am Geriatr Soc* (2018) 66(7):1353–9. doi: 10.1111/jgs.15393
14. Daghestani HN, Pieper CF, Kraus VB. Soluble Macrophage Biomarkers Indicate Inflammatory Phenotypes in Patients With Knee Osteoarthritis. *Arthritis Rheumatol* (2015) 67(4):956–65. doi: 10.1002/art.39006
15. Zhang X, Huebner JL, Kraus VB. Extracellular Vesicles as Biological Indicators and Potential Sources of Autologous Therapeutics in Osteoarthritis. *Int J Mol Sci* (2021) 22(15):8351. doi: 10.3390/ijms22158351
16. Eitan E, Green J, Bodogai M, Mode NA, Baek R, Jorgensen MM, et al. Age-Related Changes in Plasma Extracellular Vesicle Characteristics and Internalization by Leukocytes. *Sci Rep* (2017) 7(1):1342. doi: 10.1038/s41598-017-01386-z
17. Chou CH, Jain V, Gibson J, Attarian DE, Haraden CA, Yohn CB, et al. Synovial Cell Cross-Talk With Cartilage Plays a Major Role in the Pathogenesis of Osteoarthritis. *Sci Rep* (2020) 10(1):10868. doi: 10.1038/s41598-020-67730-y
18. Wright MD, Moseley GW, van Spriel AB. Tetraspanin Microdomains in Immune Cell Signalling and Malignant Disease. *Tissue Antigens* (2004) 64 (5):533–42. doi: 10.1111/j.1399-0039.2004.00321.x
19. Park KR, Inoue T, Ueda M, Hirano T, Higuchi T, Maeda M, et al. CD9 Is Expressed on Human Endometrial Epithelial Cells in Association With Integrins Alpha(6), Alpha(3) and Beta(1). *Mol Hum Reprod* (2000) 6 (3):252–7. doi: 10.1093/molehr/6.3.252
20. Lin KK, Rossi L, Boles NC, Hall BE, George TC, Goodell MA. CD81 Is Essential for the Re-Entry of Hematopoietic Stem Cells to Quiescence Following Stress-Induced Proliferation *via* Deactivation of the Akt Pathway. *PloS Biol* (2011) 9(9):e1001148. doi: 10.1371/journal.pbio.1001148
21. Iwasaki T, Takeda Y, Maruyama K, Yokosaki Y, Tsujino K, Tetsumoto S, et al. Deletion of Tetraspanin CD9 Diminishes Lymphangiogenesis *In Vivo* and *In Vitro*. *J Biol Chem* (2013) 288(4):2118–31. doi: 10.1074/jbc.M112.424291
22. Jin Y, Takeda Y, Kondo Y, Tripathi LP, Kang S, Takeshita H, et al. Double Deletion of Tetraspanins CD9 and CD81 in Mice Leads to a Syndrome Resembling Accelerated Aging. *Sci Rep* (2018) 8(1):5145. doi: 10.1038/s41598-018-23338-x
23. Privratsky JR, Newman PJ. PECAM-1: Regulator of Endothelial Junctional Integrity. *Cell Tissue Res* (2014) 355(3):607–19. doi: 10.1007/s00441-013-1779-3
24. Sarangi PP, Hyun YM, Lerman YV, Pietropaoli AP, Kim M. Role of Beta1 Integrin in Tissue Homing of Neutrophils During Sepsis. *Shock* (2012) 38 (3):281–7. doi: 10.1097/SHK.0b013e31826136f8
25. Togarrati PP, Dinglasan N, Desai S, Ryan WR, Muench MO. CD29 Is Highly Expressed on Epithelial, Myoepithelial, and Mesenchymal Stromal Cells of Human Salivary Glands. *Oral Dis* (2018) 24(4):561–72. doi: 10.1111/odi.12812
26. Shooshtari P, Fortuno ES3rd, Blimkie D, Yu M, Gupta A, Kollmann TR, et al. Correlation Analysis of Intracellular and Secreted Cytokines *via* the Generalized Integrated Mean Fluorescence Intensity. *Cytomet A* (2010) 77 (9):873–80. doi: 10.1002/cyto.a.20943
27. Brummelman J, Mazza EMC, Alvisi G, Colombo FS, Grilli A, Mikulak J, et al. High-Dimensional Single Cell Analysis Identifies Stem-Like Cytotoxic CD8 (+) T Cells Infiltrating Human Tumors. *J Exp Med* (2018) 215(10):2520–35. doi: 10.1084/jem.20180684
28. Hsueh MF, Zhang X, Wellman SS, Bolognesi MP, Kraus VB. Synergistic Roles of Macrophages and Neutrophils in Osteoarthritis Progression. *Arthritis Rheumatol* (2020) 73(1):89–99. doi: 10.1002/art.41486
29. Leung YY, Huebner JL, Haaland B, Wong SBS, Kraus VB. Synovial Fluid Pro-Inflammatory Profile Differs According to the Characteristics of Knee Pain. *Osteoarthritis Cartilage* (2017) 25(9):1420–7. doi: 10.1016/j.joca.2017.04.001
30. Zweig MH, Campbell G. Receiver-Operating Characteristic (ROC) Plots: A Fundamental Evaluation Tool in Clinical Medicine. *Clin Chem* (1993) 39 (4):561–77. doi: 10.1093/clinchem/39.4.561
31. Kraus VB, Feng S, Wang S, White S, Ainslie M, Brett A, et al. Trabecular Morphometry by Fractal Signature Analysis Is a Novel Marker of Osteoarthritis Progression. *Arthritis Rheumatol* (2009) 60(12):3711–22. doi: 10.1002/art.25012
32. Wilks SS. The Large-Sample Distribution of the Likelihood Ratio for Testing Composite Hypotheses. *Ann Math Statist* (1938) 9(1):60–2. doi: 10.1214/aoms/1177732360
33. McFadden D. *Conditional Logit Analysis of Qualitative Choice Behavior*. Berkeley, Calif: Univ. of California (1973).
34. Akaike H. A New Look at the Statistical Model Identification. *IEEE Trans Automatic Control* (1974) 19(6):716–23. doi: 10.1109/TAC.1974.1100705
35. Burnham KP, Anderson DR. Multimodel Inference : Understanding AIC and BIC in Model Selection. *Sociologic Methods Res* (2004) 33(2):261–304. doi: 10.1177/0049124104268644
36. Thery C, Witwer KW, Aikawa E, Alcaraz MJ, Anderson JD, Andriantsitohaina R, et al. Minimal Information for Studies of Extracellular Vesicles 2018 (MISEV2018): A Position Statement of the International Society for Extracellular Vesicles and Update of the MISEV2014 Guidelines. *J Extracell Vesicles* (2018) 7(1):1535750. doi: 10.1080/20013078.2018.1535750
37. Westacott CI, Sharif M. Cytokines in Osteoarthritis: Mediators or Markers of Joint Destruction? *Semin Arthritis Rheum* (1996) 25(4):254–72. doi: 10.1016/s0049-0172(96)80036-9
38. Lopez-Armada MJ, Carames B, Lires-Dean M, Cillero-Pastor B, Ruiz-Romero C, Galdo F, et al. Cytokines, Tumor Necrosis Factor-Alpha and Interleukin-1beta, Differentially Regulate Apoptosis in Osteoarthritis Cultured Human Chondrocytes. *Osteoarthritis Cartilage* (2006) 14(7):660–9. doi: 10.1016/j.joca.2006.01.005
39. Kennedy MI, Whitney K, Evans T, LaPrade RF. Platelet-Rich Plasma and Cartilage Repair. *Curr Rev Musculoskelet Med* (2018) 11(4):573–82. doi: 10.1007/s12178-018-9516-x
40. Bondeson J, Wainwright SD, Lauder S, Amos N, Hughes CE. The Role of Synovial Macrophages and Macrophage-Produced Cytokines in Driving Aggrecanases, Matrix Metalloproteinases, and Other Destructive and Inflammatory Responses in Osteoarthritis. *Arthritis Res Ther* (2006) 8(6): R187. doi: 10.1186/ar2099
41. Wojdasiewicz P, Poniatowski LA, Szukiewicz D. The Role of Inflammatory and Anti-Inflammatory Cytokines in the Pathogenesis of Osteoarthritis. *Mediators Inflammation* (2014) 2014:561459. doi: 10.1155/2014/561459
42. Caruso S, Poon IKH. Apoptotic Cell-Derived Extracellular Vesicles: More Than Just Debris. *Front Immunol* (2018) 9:1486. doi: 10.3389/fimmu.2018.01486
43. de Lange-Brokaar BJ, Ioan-Facsinay A, van Osch GJ, Zuurmond AM, Schoones J, Toes RE, et al. Synovial Inflammation, Immune Cells and Their

Cytokines in Osteoarthritis: A Review. *Osteoarthritis Cartilage* (2012) 20 (12):1484–99. doi: 10.1016/j.joca.2012.08.027
44. Deligne C, Casulli S, Pigenet A, Bougault C, Campillo-Gimenez L, Nourissat G, et al. Differential Expression of Interleukin-17 and Interleukin-22 in Inflamed and non-Inflamed Synovium From Osteoarthritis Patients. *Osteoarthritis Cartilage* (2015) 23(11):1843–52. doi: 10.1016/j.joca.2014.12.007
45. Li YS, Luo W, Zhu SA, Lei GH. T Cells in Osteoarthritis: Alterations and Beyond. *Front Immunol* (2017) 8:356. doi: 10.3389/fimmu.2017.00356
46. Vassalli P. The Pathophysiology of Tumor Necrosis Factors. *Annu Rev Immunol* (1992) 10:411–52. doi: 10.1146/annurev.iy.10.040192.002211
47. Fernandes JC, Martel-Pelletier J, Pelletier JP. The Role of Cytokines in Osteoarthritis Pathophysiology. *Biorheology* (2002) 39(1-2):237–46.
48. Grunke M, Schulze-Koops H. Successful Treatment of Inflammatory Knee Osteoarthritis With Tumour Necrosis Factor Blockade. *Ann Rheum Dis* (2006) 65(4):555–6. doi: 10.1136/ard.2006.053272
49. Xue J, Wang J, Liu Q, Luo A. Tumor Necrosis Factor-Alpha Induces ADAMTS-4 Expression in Human Osteoarthritis Chondrocytes. *Mol Med Rep* (2013) 8(6):1755–60. doi: 10.3892/mmr.2013.1729
50. Bastick AN, Belo JN, Runhaar J, Bierma-Zeinstra SM. What Are the Prognostic Factors for Radiographic Progression of Knee Osteoarthritis? A Meta-Analysis. *Clin Orthop Relat Res* (2015) 473(9):2969–89. doi: 10.1007/s11999-015-4349-z
51. Stannus O, Jones G, Cicuttini F, Parameswaran V, Quinn S, Burgess J, et al. Circulating Levels of IL-6 and TNF-Alpha Are Associated With Knee Radiographic Osteoarthritis and Knee Cartilage Loss in Older Adults. *Osteoarthritis Cartilage* (2010) 18(11):1441–7. doi: 10.1016/j.joca.2010.08.016
52. Han L, Song JH, Yoon JH, Park YG, Lee SW, Choi YJ, et al. TNF-Alpha and TNF-Beta Polymorphisms Are Associated With Susceptibility to Osteoarthritis in a Korean Population. *Korean J Pathol* (2012) 46(1):30–7. doi: 10.4132/KoreanJPathol.2012.46.1.30
53. Li H, Xie S, Qi Y, Li H, Zhang R, Lian Y. TNF-Alpha Increases the Expression of Inflammatory Factors in Synovial Fibroblasts by Inhibiting the PI3K/AKT Pathway in a Rat Model of Monosodium Iodoacetate-Induced Osteoarthritis. *Exp Ther Med* (2018) 16(6):4737–44. doi: 10.3892/etm.2018.6770
54. Chevalier X, Eymard F, Richette P. Biologic Agents in Osteoarthritis: Hopes and Disappointments. *Nat Rev Rheumatol* (2013) 9(7):400–10. doi: 10.1038/nrrheum.2013.44
55. Bluml S, Binder NB, Niederreiter B, Polzer K, Hayer S, Tauber S, et al. Antiinflammatory Effects of Tumor Necrosis Factor on Hematopoietic Cells in a Murine Model of Erosive Arthritis. *Arthritis Rheumatol* (2010) 62 (6):1608–19. doi: 10.1002/art.27399
56. McCann FE, Perocheau DP, Ruspi G, Blazek K, Davies ML, Feldmann M, et al. Selective Tumor Necrosis Factor Receptor I Blockade Is Antiinflammatory and Reveals Immunoregulatory Role of Tumor Necrosis Factor Receptor II in Collagen-Induced Arthritis. *Arthritis Rheumatol* (2014) 66(10):2728–38. doi: 10.1002/art.38755
57. Prada I, Meldolesi J. Binding and Fusion of Extracellular Vesicles to the Plasma Membrane of Their Cell Targets. *Int J Mol Sci* (2016) 17(8):1296. doi: 10.3390/ijms17081296
58. Huss RS, Huddleston JI, Goodman SB, Butcher EC, Zabel BA. Synovial Tissue-Infiltrating Natural Killer Cells in Osteoarthritis and Periprosthetic Inflammation. *Arthritis Rheumatol* (2010) 62(12):3799–805. doi: 10.1002/art.27751
59. Jaime P, Garcia-Guerrero N, Estella R, Pardo J, Garcia-Alvarez F, Martinez-Lostao L. CD56(+)/CD16(-) Natural Killer Cells Expressing the Inflammatory Protease Granzyme A Are Enriched in Synovial Fluid From Patients With Osteoarthritis. *Osteoarthritis Cartilage* (2017) 25(10):1708–18. doi: 10.1016/j.joca.2017.06.007
60. Benigni G, Dimitrova P, Antonangeli F, Sanseviero E, Milanova V, Blom A, et al. CXCR3/CXCL10 Axis Regulates Neutrophil-NK Cell Cross-Talk Determining the Severity of Experimental Osteoarthritis. *J Immunol* (2017) 198(5):2115–24. doi: 10.4049/jimmunol.1601359
61. Tasoglu O, Boluk H, Sahin Onat S, Tasoglu I, Ozgirgin N. Is Blood Neutrophil-Lymphocyte Ratio an Independent Predictor of Knee Osteoarthritis Severity? *Clin Rheumatol* (2016) 35(6):1579–83. doi: 10.1007/s10067-016-3170-8
62. Galizia G, Lieto E, Zamboli A, De Vita F, Castellano P, Romano C, et al. Neutrophil to Lymphocyte Ratio Is a Strong Predictor of Tumor Recurrence in Early Colon Cancers: A Propensity Score-Matched Analysis. *Surgery* (2015) 158(1):112–20. doi: 10.1016/j.surg.2015.02.006
63. Adamstein NH, MacFadyen JG, Rose LM, Glynn RJ, Dey AK, Libby P, et al. The Neutrophil-Lymphocyte Ratio and Incident Atherosclerotic Events: Analyses From Five Contemporary Randomized Trials. *Eur Heart J* (2021) 42(9):896–903. doi: 10.1093/eurheartj/ehaa1034

Conflict of Interest: The authors declare that the research was conducted in the absence of any commercial or financial relationships that could be construed as a potential conflict of interest.

Publisher's Note: All claims expressed in this article are solely those of the authors and do not necessarily represent those of their affiliated organizations, or those of the publisher, the editors and the reviewers. Any product that may be evaluated in this article, or claim that may be made by its manufacturer, is not guaranteed or endorsed by the publisher.

frontiers in Immunology

REVIEW
published: 04 November 2021
doi: 10.3389/fimmu.2021.763702

Monocytes, Macrophages, and Their Potential Niches in Synovial Joints – Therapeutic Targets in Post-Traumatic Osteoarthritis?

Patrick Haubruck[1,2], Marlene Magalhaes Pinto[3], Babak Moradi[4†], Christopher B. Little[2†] and Rebecca Gentek[3†]*

[1] Centre for Orthopaedics, Trauma Surgery and Spinal Cord Injury, Trauma and Reconstructive Surgery, Heidelberg University Hospital, Heidelberg, Germany, [2] Raymond Purves Bone and Joint Research Laboratory, Kolling Institute, Institute of Bone and Joint Research, Faculty of Medicine and Health University of Sydney, Royal North Shore Hospital, St. Leonards, NSW, Australia, [3] Centre for Inflammation Research & Centre for Reproductive Health, University of Edinburgh, Edinburgh, United Kingdom, [4] Clinic of Orthopaedics and Trauma Surgery, University Clinic of Schleswig-Holstein, Kiel, Germany

OPEN ACCESS

Edited by:
Matthew William Grol, Western University, Canada

Reviewed by:
Oreste Gualillo, Servicio Gallego de Salud, Spain
Kyuho Kang, Chungbuk National University, South Korea

***Correspondence:**
Christopher B. Little
Christopher.little@sydney.edu.au

[†]These authors have contributed equally to this work

Specialty section:
This article was submitted to Inflammation, a section of the journal Frontiers in Immunology

Received: *24 August 2021*
Accepted: *18 October 2021*
Published: *04 November 2021*

Citation:
Haubruck P, Pinto MM, Moradi B, Little CB and Gentek R (2021) Monocytes, Macrophages, and Their Potential Niches in Synovial Joints – Therapeutic Targets in Post-Traumatic Osteoarthritis? Front. Immunol. 12:763702. doi: 10.3389/fimmu.2021.763702

Synovial joints are complex structures that enable normal locomotion. Following injury, they undergo a series of changes, including a prevalent inflammatory response. This increases the risk for development of osteoarthritis (OA), the most common joint disorder. In healthy joints, macrophages are the predominant immune cells. They regulate bone turnover, constantly scavenge debris from the joint cavity and, together with synovial fibroblasts, form a protective barrier. Macrophages thus work in concert with the non-hematopoietic stroma. In turn, the stroma provides a scaffold as well as molecular signals for macrophage survival and functional imprinting: "a macrophage niche". These intricate cellular interactions are susceptible to perturbations like those induced by joint injury. With this review, we explore how the concepts of local tissue niches apply to synovial joints. We introduce the joint micro-anatomy and cellular players, and discuss their potential interactions in healthy joints, with an emphasis on molecular cues underlying their crosstalk and relevance to joint functionality. We then consider how these interactions are perturbed by joint injury and how they may contribute to OA pathogenesis. We conclude by discussing how understanding these changes might help identify novel therapeutic avenues with the potential of restoring joint function and reducing post-traumatic OA risk.

Keywords: osteoarthritis, monocyte - macrophage, inflammation, niche, native immune functions, synovitis, immunomodulation

INTRODUCTION

Osteoarthritis (OA) is the most common joint disorder (1). Its prevalence is expected to increase further (2) due to rising societal levels of ageing, obesity and injury, key risk factors for OA. While the disease commonly affects knees, hips, hands and feet, OA of the knee accounts for more than 80% of the disease burden (1, 3). The knee is particularly susceptible to injury, with approximately

40% of patients that suffer a traumatic knee injury developing so-called "post-traumatic" (pt)OA, and surgical reconstruction and restoration of joint biomechanics insufficient to prevent its development (4). Treatment options for OA are very limited, and there is a particular need for effective preventive and disease modifying drugs (DMD). This is highlighted by clinical data showing comparable disease burden at diagnosis but significantly higher burden 6 months later in OA compared to rheumatoid arthritis (RA) patients (5). Owing to this paucity of treatment options and the high and rising prevalence, OA contributes substantially to the global burden of disease. In a 2015 survey, OA was identified as the second most prevalent cause for years lived with disability (2), highlighting the impact OA has on both individuals and society (2).

Although the name osteoarthritis implies an inherent inflammatory process (6), it was historically believed that OA had purely biomechanical causes (7). Indeed, OA was regarded a disease of the elderly, inevitably caused by years of "wear and tear". Breaking with this previously held view, we now know that OA development involves a complex active biological response with local interaction between joint tissues and their resident cells, and these with systemic mediators. This includes an inflammatory response (8) that is accompanied by complex metabolic changes, which contribute to cartilage degradation and activation of bone remodeling (9). Although innate immune cells, and monocytes and macrophages in particular have been implicated (7, 10, 11), the exact nature of the inflammatory response in OA, its underlying mechanisms and its relative contribution to onset or progression of structural pathology and symptoms remain incompletely resolved (12).

Much like OA etiology, our understanding of the complex development and functional heterogeneity of macrophages and monocytes as well as their interactions within local tissue "niches" has dramatically changed in recent years. It is now firmly established that the long-held paradigm of discrete, polarized monocyte and macrophage activation states is an oversimplification of what in reality is a spectrum of cell states. Likewise, it is now recognized that macrophages established from fetal progenitors can persist in adult tissues, and that many macrophages self-maintain independently of monocytes (13–16). Lastly, we are beginning to appreciate that macrophages engage in bidirectional crosstalk with other cell types within their local niches, interactions that are of mutual benefit and implicate macrophages as gatekeepers of tissue function (17, 18). While much remains to be learned and confirmed, these concepts developed in other organs and tissues appear to also apply to macrophages in joints (19, 20). Indeed, macrophages found in the healthy synovium are predominantly monocyte-independent, and they protect and contribute to joint homeostasis in several ways, including barrier formation, clearance of debris and even lubrication (20). Under inflammatory conditions, such as may occur with joint injury however, monocytes are recruited to the affected joint and can differentiate into macrophages, which retain a more inflammatory phenotype (21). These joint macrophage populations thus not only differ in their origins, but also exert distinct functions (22, 23).

Modifying the developmental, functional and *in situ* dynamics of joint macrophages and monocytes might therefore represent an attractive avenue for novel therapeutic approaches in OA. This may be particularly relevant in ptOA, where causal initiation and subsequent temporal changes in monocytes, macrophages and their activation with disease onset and progression may be targeted. This review aims to explore this notion, with a focus on the synovial rather than osseous joint tissue niche. We will summarize experimental and clinical studies on macrophages and monocytes in healthy and diseased joints and interpret these in the context of current paradigms of myeloid biology. Our emphasis in this review is on joint injury and ptOA, as this represents the major OA phenotype studied in pre-clinical research, and as noted above, it has the most well demarcated disease stages and thus potentially the broadest therapeutic opportunity. In doing so, we hope to bridge persisting gaps between bench and bedside and highlight research questions with the potential to pave the way towards better treatment options for ptOA, but also other OA phenotypes more broadly.

MACRO- AND MICROANATOMY OF THE KNEE JOINT

Synovial joints provide critical motion segments that allow low friction movement between rigid (osseous) skeletal components. They enable diverse and essential bio-mechanical functions ranging from fine movements of arms, hands and fingers through to walking, running and jumping. The knee represents an anatomically complex example of a joint (**Figure 1**) that enables locomotion in a variety of terrains, while minimizing muscular energy requirements and absorbing and redistributing forces that originate from the contact between the walking surface and the foot (24). Its main osseous components are the femur, tibia and patella, that articulate in two locations: the tibiofemoral and patellofemoral joints. The menisci, two C-shaped fibro-cartilaginous structures, absorb and distribute load between the femoral and tibial surfaces. Together with a multitude of extra- and intra-articular ligaments and the fibrous joint capsule, the menisci also provide stability in flexion/extension and rotation, enabling the unique biomechanical function of the knee (25). As in all joints, the osseous surfaces in the knee are covered by hyaline cartilage, a sparsely cellular, deformable connective tissue matrix with key components of collagen type II and highly hydrated proteoglycans. Cartilage is heterogenous and can be broadly divided into three zones based on depth from the surface. These have distinct composition, biomechanical properties and functions (26). Chondrocytes make up about 2% of the articular cartilage volume (27) and are responsible for the maintenance and repair of the cartilage extracellular matrix. They are highly specialized cells derived from mesenchymal stem cells that have limited potential for replication *in situ*, but can react to a plethora of mechanical and molecular stimuli (26). The knee also harbors several adipose tissues. These are located intra-articularly and extra-synovially,

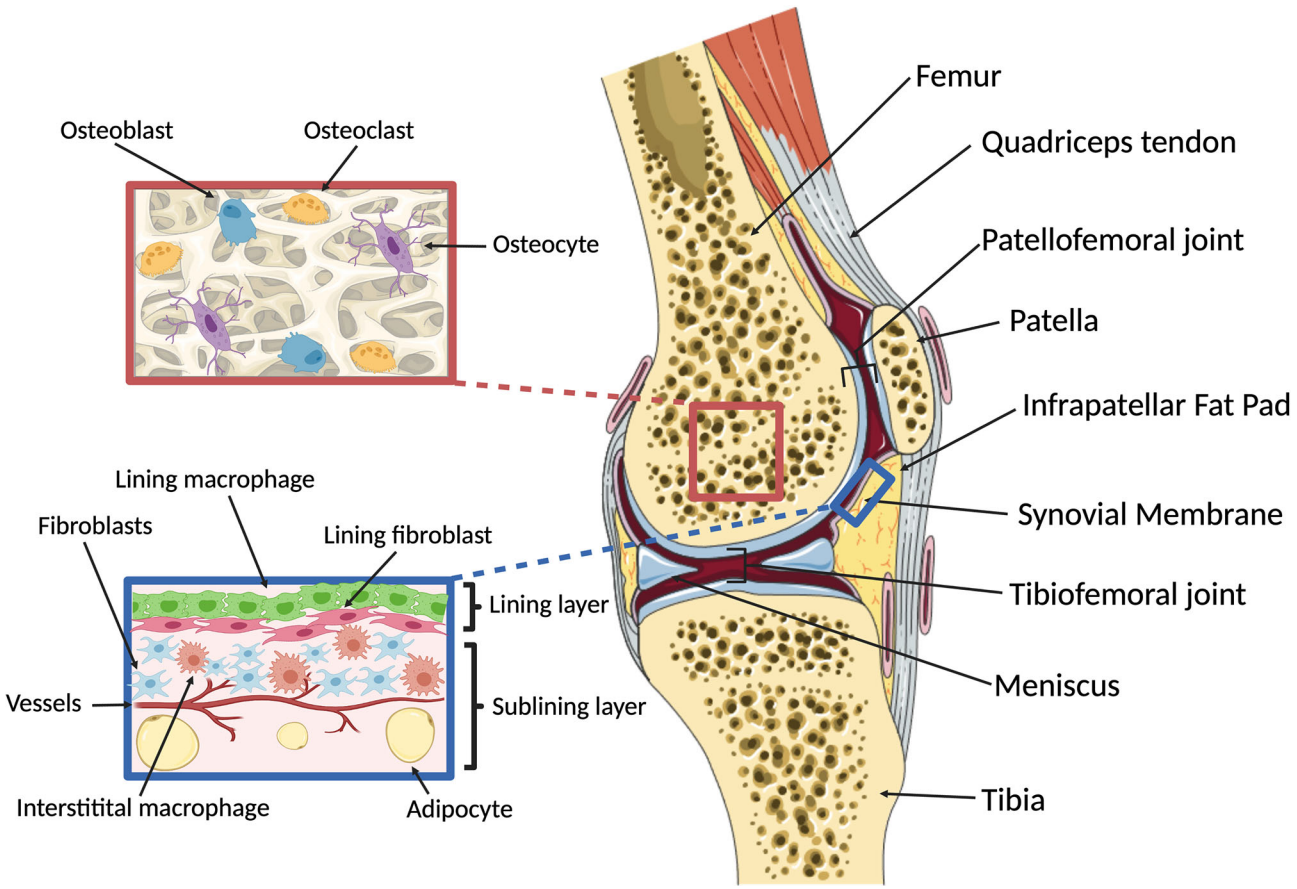

FIGURE 1 | Overview of knee macro- and microanatomy. (Right) Sagittal cut through a human knee. The femur and tibia articulate in the tibiofemoral joint, with two fibrocartilaginous menisci serving to provide rotational and anterior-posterior stability and load distribution. The patella is a hypomochlion (pivot point) for the quadriceps tendon that articulates with the femur in the patellofemoral joint. The intra-articular components of the osseous structures are covered by cartilage, enabling low-friction bearing. Joint function and stability are maintained by ligaments and the joint capsule. The inner surface of the joint capsule is lined with the synovial membrane, which is accompanied by adipose tissues located intra-articularly and extra-synovially, including the infrapatellar fat pad. (Left, top) Microanatomy of subchondral bone. The cellular components of bone include osteoblasts, osteoclasts and osteocytes that dynamically respond to changes in mechanical loading and potentially communicate with the overlying cartilage *via* soluble signals. (Left, bottom) Microanatomy of the synovial membrane. The synovium comprises three layers: the intimal lining layer which consists of macrophages and fibroblasts that together form a semi-permeable protective barrier; the vascularized subintimal or sublining layer which contains interstitial macrophages and fibroblasts as well as adipocytes; and an outer fibrous stromal layer forming the joint capsule (not shown). Created with BioRender.com and smart.servier.com.

and include the infrapatellar fat pad, which can be considered a highly specialized compartment in the sublining interstitial tissue [in humans known as Hoffa's fat pad (28)]. Beyond filling the space in the joint cavity and absorbing shock, adipose tissues also secrete cytokines and adipokines (29, 30) and are therefore potent immune-modulators. It is also believed that the infrapatellar fat pad engages in intimate crosstalk with the synovial membrane, a specialized connective tissue that lines the inner surface of the joint capsule (31). The synovial membrane consists of three layers: The intimal lining layer is found closest to the joint cavity and consists mainly of macrophages ("type A cells") and fibroblasts ("type B cells") that show low degrees of cell division (31). Beneath this is the vascularized subintimal layer, also referred to as sublining interstitial tissue, and finally a fibrous stromal layer forming the joint capsule. The synovial membrane maintains joint homeostasis by providing lubrication and nutrition to the cartilage. It also forms a semi-permeable protective barrier that controls the molecular traffic in and out of the joint (32) and renders the synovial cavity relatively immune-privileged (20). Because of its critical role in joint homeostasis, this review will largely focus on monocyte and macrophage biology of the synovial membrane, including its sublining interstitial layer.

A REVISED VIEW OF MONOCYTE AND MACROPHAGE BIOLOGY

Many historically held views of monocyte and macrophage biology have been overhauled in recent times, including their phenotypic

and functional heterogeneity, developmental dynamics as well as their crosstalk and functional interdependence with other cell types in the same tissue microenvironment.

Monocyte and Macrophage Development

It was previously believed that the key (if not sole) function of monocytes was to produce macrophages, and that in turn, all macrophages found in peripheral tissues originate exclusively from monocytes (33). Elegant studies exploiting genetic fate mapping have since shown that most tissue-resident macrophages are in fact of fetal origin and self-maintain in adult tissues independently of bone marrow (BM)-derived monocytes (33). Indeed, macrophages colonize tissues concomitantly with their development in what appears to be a demand-driven way. They are generated from successive, but overlapping waves of hematopoietic progenitors produced at distinct anatomical sites (34). The majority of fetal macrophages originate from erythro-myeloid progenitors (EMP) produced in the extra-embryonic yolk sac (15, 16). EMP are fetal-restricted progenitors that differentiate into macrophages either directly or *via* fetal liver intermediates, but as an uncommitted entity do not persist into adulthood.

This new paradigm of predominantly fetal origins of tissue macrophages notwithstanding, monocytes can still complement tissue phagocyte compartments on demand (33). While this applies to some tissues at homeostasis (e.g. skin and gastro-intestinal tract), it is particularly true and important in inflammatory conditions. Importantly, in both scenarios, monocytes themselves have a number of key effector functions (35).

Monocytes differentiate from BM hematopoietic stem cells (HSC) in a strictly hierarchical, tree-like maturation process (35). They share a common progenitor with dendritic cells (DCs) known as "monocyte-macrophage DC progenitor" (MDP) (36, 37), which gives rise to a monocyte-committed intermediate, designated the "common monocyte progenitor" (cMoP) (38). The downstream "transitional pre-monocytes" (TpMos) (38, 39) are believed to be the final intermediate stage in monocyte differentiation (39). They are capable of rapid proliferation and express high levels of C-X-C motif chemokine Receptors (CXCR) 4, which anchors them to the BM. Based on differential expression of Lymphocyte antigen 6C (Ly6C), CX3CR1 and C-Chemokine Receptor type 2 (CCR2) in mice (40) or Cluster of Differentiation (CD)14 and CD16 in humans (37), mature monocytes can be broadly classified into classical (mice: Ly6C^{high} CX3CR1^{low} CCR2^{high}; humans: CD14^{high} CD16^{-}) and non-classical monocytes (mice: Ly6C^{low} CX3CR1^{high} CCR2^{low}; humans: CD14^{low} CD16^{+}) (35, 41–44). This binary classification is now widely established (45) and has more recently been backed up by extensive high-dimensional studies, the latter also revealing a previously underappreciated heterogeneity (46). A third monocyte population with an intermediate phenotype is exclusive to humans (CD14^{+} CD16^{+}) (35). Classical and non-classical monocytes differ in a number of features, including their relative abundance and the regulatory mechanisms governing their retention in and egress from the BM (47). The mature monocyte compartment in the BM is vastly predominated by Ly6C^{high} monocytes, which downregulate CXCR4 (48, 49) and highly express CCR2 (50, 51), collectively enabling their egress from the BM. Ly6C^{low} monocytes, on the other hand, only express very low levels of CCR2, and while still under investigation, Sphingosine-1-Phosphate Receptor 5 (S1PR5) signaling has been implicated in orchestrating their BM egress (52).

Once released into the blood stream, classical Ly6C^{high} monocytes have a relatively short half-life lasting for a mere 20-24 hours in mice (53–55), whereas their non-classical counterparts are slightly longer-lived with a half-life of around 2 days in mice and 7 days in humans (53). The two populations are also developmentally connected: lineage tracing indicating that Ly6C^{low} monocytes originate from aging Ly6C^{high} monocytes (41, 53), a gradual conversion that is dependent on Nuclear Receptor subfamily 4 group A member 1 (NR4A1) signaling (56) and involves direct cellular contact with endothelial cells and Notch signaling (57, 58). Similar mechanisms appear to be at play in human monocytes (59, 60). At homeostasis, Ly6C^{low} monocytes do not normally extravasate but instead patrol the luminal side of the endothelium (61). They roll along the vascular endothelium, independent of the direction of the blood flow, *via* CX3CR1, β2 integrin (58, 62) and interactions between Lymphocyte Function-associated Antigen-1 (LFA-1) and IntraCellular Adhesion Molecule 1 (ICAM1) and ICAM2 (58, 62). They have thus been considered the "tissue-resident" macrophages of blood vessels. In non-homeostatic conditions, Ly6C^{low} monocytes are thought to promote resolution of inflammation, however, they can also contribute to autoimmunity and chronic inflammatory diseases (58), as we will discuss further below. Intriguingly, experiments using bleomycin-induced lung fibrosis in mice identified an alternative pathway to Ly6C^{low} monocytes, consisting of a separate progenitor referred to as a "Segregated-nucleus-containing atypical Monocyte (SatM)", whose production depends on the transcription factor C/EBPβ (63). Whether this pathway is relevant to other pathologies remains to be determined.

Unlike their non-classical counterparts, Ly6C^{high} monocytes do traffic into peripheral tissues even at steady state (64). In tissues that (partially) rely on homeostatic renewal from the BM, such as the skin and gastro-intestinal tract (65, 66), the majority of recruited Ly6C^{high} monocytes gradually differentiate into macrophages, a process phenotypically characterized as a "monocyte waterfall" (67). These macrophages are functionally imprinted in response to local cues that superpose tissue-specific identity onto a transcriptional core lineage program (68, 69). Provided monocytes encounter a homeostatic environment and are allowed sufficient time in the tissue, monocyte-derived macrophages are phenotypically, transcriptomically and epigenetically indistinguishable from pre-existing tissue-resident macrophages (70, 71). However, this is not the case following inflammation or other insults resulting in perturbed homeostasis, which might have important functional implications. Indeed, different and sometimes even opposing roles have been reported for developmentally distinct macrophages in conditions like cancer (72–74) and stroke (75), and this might also be the case in joint pathology, as we will discuss below.

Monocyte Effector Functions

In addition to representing an "on-demand" source for macrophages, monocytes also have important effector functions in their own right. Indeed, a fraction of classical monocytes recruited at steady state maintains their monocytic phenotype with minimal transcriptional changes (76). In the parenchyma of non-lymphoid organs like the skin, lung, and heart (43, 66), they contribute to immune surveillance. During sterile inflammatory responses, as would occur following closed traumatic knee injury, Ly6C^{high} and Ly6C^{low} monocytes are recruited in a highly orchestrated manner facilitated by differential chemokine release. Under such conditions, Ly6C^{low} monocytes have primarily been attributed beneficial, anti-inflammatory roles. In the ischemic heart and kidney for example, deficiency in Ly6C^{low} monocytes results in higher inflammatory levels and impaired restoration of organ function (77–79). In line with this, Ly6C^{low} monocytes predominantly produce anti-inflammatory mediators like Interleukin (IL)-10 (80, 81) as well as Vascular Endothelial Growth Factor (VEGF) and other pro-angiogenic factors (82), as observed during spinal cord injury and myocardial infarction (82), respectively.

Somewhat contradictory evidence exists regarding the role of Ly6C^{high} monocytes. Historically, these classical monocytes have been recognized as potent pro-inflammatory effector cells. Indeed, CCR2 knockout mice, which are largely deficient in classical monocytes in the periphery, show decreased levels of IL-1β and Tumor Necrosis Factor (TNF)-α and an increase in the anti-inflammatory cytokines IL-4, IL-5 and IL-13 at the site of inflammation during cerebral ischemia (83). Ly6C^{high} monocytes also show high levels of reactive oxygen species, TNF-α and IL-6 (84) in the context of liver ischemia reperfusion injury (84). In line with this pro-inflammatory phenotype, Ly6C^{high} monocytes mediate tissue damage in the ischemic liver as well as the heart following myocardial infarction, and contribute to progression of atherosclerosis (84–87). At the same time however, Ly6C^{high} monocytes have also been implicated in regression of atherosclerosis (88), although this may be attributable to anti-inflammatory effects of monocyte-derived macrophages, rather than a true monocyte effector function. Nonetheless, these findings collectively suggest that instead of being globally pro- and anti-inflammatory, classical and non-classical monocytes differentially shape the local inflammatory response *via* the tailored production of cytokines and other cellular mediators. Although similarities exist between tissues and insults, their exact trafficking patterns and effector functions appear to be context-dependent, and therefore need to be delineated specifically in the homeostatic, injured and OA joint.

Tissue Adaptation and Activation of Monocytes and Macrophages

Monocytes and macrophages dynamically respond to a variety of cues in their microenvironment, which shape their local tissue adaptation and activation state. Consequently, although they share a lineage-defining core transcriptomic signature, macrophages in different tissues are transcriptionally, phenotypically and functionally very diverse (70, 71, 89). The core macrophage program is initiated in committed fetal progenitors or BM-derived monocytes and driven by lineage-determining transcription factors (68–71).

Acquisition of tissue-specific identity and function is subsequently orchestrated by additional transcription factors in response to signals present in the local microenvironment (69). In the spleen, for example, heme from senescent red blood cells induces expression of the transcription factor SPI-C, which in turn activates a transcriptional program inducing differentiation of red pulp macrophages (90). Experimental data from adoptive transfer experiments demonstrate that exposure to different environments partially, though not fully, rewires the tissue-specific identity of macrophages, indicating a limited degree of plasticity even under such non-physiological conditions (70, 91).

At the same time, the activation state of terminally differentiated macrophages can vary as a function of microenvironmental signals, in particular cytokines. Historically, it has been thought that macrophages polarize into either classically activated, pro-inflammatory ("M1") or alternatively activated, anti-inflammatory ("M2") (92, 93) subtypes in response to cytokines associated respectively with type I or type II immunity (94, 95). However, it is now abundantly clear that this strict dichotomy is a drastic oversimplification of real-life *in vivo* physiology. Rather, these opposing polarization states represent extremes (94, 95) of a much wider and more fluid spectrum of activation states (96, 97). Understanding the different activation states of macrophages and monocytes in OA and the signals that drive them will be paramount in delineating their respective contribution to disease pathogenesis. Since circulating monocytes represent a modifiable source, they – and their relationship with macrophages found in the joints – are of particular translational relevance.

Macrophage Niches

The intricate developmental dynamics between monocytes and macrophages and their adaptation to tissue-derived signals illustrate that these cell types actively engage with each other and their immediate environment or "niche". Research into such niches represents a current focus in the field of myeloid cell biology. The niche concept postulates that macrophages are not only functionally imprinted by tissue-specific cues, but that their niches also provide them with a physical scaffold for anchoring and survival factors (17, 18). In turn, macrophages support appropriate functioning of their cellular partners. They thus form mutually beneficial cellular circuits (18) with their niches. In line with this, organ function is heavily impaired in mice lacking numerous tissue-resident macrophages owing to genetic deficiency in Colony Stimulating Factor (CSF)1, a key macrophage survival signal, or its receptor (98–100). Niches consist of macrophages and other, often non-hematopoietic stromal cell types, as well as the extracellular matrix surrounding them, and they can also "call" monocytes for replenishment. In the liver, for example, hepatocytes, endothelial and stellate cells together provide numerous signals to resident Kupffer cells and incoming monocytes, including CSF1, IL-34, CCL2 and Notch ligands (101), whereas in the red pulp of the spleen, macrophages depend on CSF1 produced by fibroblasts (102). In return, macrophages help facilitate tissue-specific functions and homeostasis. Beyond their

role in immune surveillance and protective immunity, macrophages have been implicated in diverse physiological processes ranging from haemoglobin recycling, intestinal motility, surfactant degradation in the lung, to cardiac conduction (64, 102–109). The circuits underlying some of these less-traditional macrophage effects are starting to be deciphered. For example, macrophages located in the interstitial space of the testis produce cholesterol, which stimulates steroidogenesis in Leydig cells (110–112).

Whilst their cellular partners, signaling circuitry and functions remain incompletely understood, it is highly conceivable that distinct macrophage niches also exist in the joint. In the following, we will thus discuss how the current concepts of monocyte and macrophage biology in other tissues and organs reviewed above, apply to synovial joints, with particular emphasis on molecular and cellular mechanisms bearing potential for translational exploitation in OA. By interpreting the dynamics between these pleiotropic cell types and their functions within their potential joint-associated niches, we aim to provide an integrative view of their contribution to joint health and disease.

MONOCYTES AND MACROPHAGES IN JOINT HOMEOSTASIS

Bone and Adipose Tissue

The bone-resident macrophages are known as osteoclasts, peculiar large and multinucleated cells whose primary function is bone resorption. They are essential for skeleton remodeling and maintenance of the hematopoietic environment in the BM. Consequently, defects in osteoclasts cause osteopetrosis and hematopoietic failure, while their overactivation leads to osteoporosis. Osteoclasts allow for homeostatic bone turnover in joint-associated subchondral bone in response to loading. Osteoclasts first colonize the ossification centers of developing bones in the fetus from EMP, where they form long-lived syncytia that are maintained throughout life by low-grade fusion with incoming monocytes (113, 114). Adding to this complexity, elegant recent intra-vital imaging has shown that osteoclasts do not necessarily undergo apoptosis following activation and bone resorption, but instead, can fission into daughter cells termed "osteomorphs" (115). These can be recycled by fusion with osteoclasts but remain transcriptionally distinct from both osteoclasts and other macrophages.

As in many other tissues, adipose tissue-resident macrophages are developmentally and functionally heterogeneous. In the healthy adipose tissue of lean mice and likely humans (116, 117), monocyte-derived macrophages co-exist with long lived, fetal yolk sac EMP-derived macrophages and regulate appropriate development of adipose tissues and lipid storage during homeostasis (116, 118). Of note, it is currently unclear whether the macrophage compartments within joint-specific adipose tissues, such as the infra-patellar fat pad, are developmentally and functionally equivalent to those in more commonly studied adipose depots, such as the subcutaneous or inguinal fat. The infrapatellar fat is highly vascularized and innervated, and thus more reminiscent of visceral than subcutaneous fat (Reviewed in Urban and Little 2018) (30). It is also interesting to note that although generally considered a type of white adipose tissue, the infrapatellar fat may not always behave like other adipose tissues, for example in conditions of obesity. Although the infrapatellar fat pad increases in volume, vascularization and adipocyte size in response to obesity like other adipose tissues, it may be more protected from obesity-induced inflammation (119–121). This suggests that infrapatellar fat may show features of both white and brown adipose tissue in response to obesity, and distinct responses to other white adipose deposits have also been observed in OA (122). In end-stage knee OA patients the infrapatellar fat pad had significantly less macrophages, toll-like receptor 4 expression and fibrosis compared with other peri-synovial adipose tissue. In these same patients both adipose tissues had increases in adipocyte size and haematopoietic and M2 macrophage cell infiltration correlated with body mass index. This complex interplay between systemic and local joint factors related to post-traumatic OA, and how these affect and are affected by infrapatellar fat pad macrophage polarization, has been demonstrated in mouse models (123). The infrapatellar fat has been implicated as a major player in sustaining and perpetuating inflammation in OA (29). While macrophage deregulation has been associated with pathological changes in other adipose depots, those in the infrapatellar fat can contribute directly or indirectly to OA pathogenesis and future research is needed to better characterize which macrophage features it shares with other adipose tissues and which are unique.

Synovial Membrane and Interstitial Connective Tissue

At homeostasis, macrophages are virtually the only immune cells in the synovial membrane (124, 125), and whilst the underlying interstitial connective tissue does harbor other lineages like mast cells and lymphocytes, macrophages predominate by far (126). Importantly, both the steady state synovial membrane and interstitium are largely devoid of monocytes. Healthy synovial tissue contains three populations of macrophages that are dynamically interconnected: lining macrophages gradually turn over from proliferating $MHCII^+$ macrophages found in the sub-lining connective tissue, which also generate a second population of interstitial macrophages characterized by expression of Hypoxia-Induced Mitogenic Factor (Resistin-like alpha; RELMa) (22). The exact sources from which synovial macrophages are originally established during development remain to be determined with appropriate additional fate mapping systems. However, chimeras and parabiosis have now firmly established that all three populations receive minimal if any monocyte input in the adult steady state (22).

Despite their developmental interdependence, the distinct populations of synovial macrophages are phenotypically and functionally highly specialized. In addition to being a source of other synovial macrophages, $MHCII^+$ sub-lining macrophages are particularly well-equipped for antigen presentation, while the $RELMa^+$ population shows a regulatory phenotype and

abundantly expresses scavenger receptors like CD206 and CD163 (22). Lining macrophages protect joint functionality and the immune privilege of the joint space through a multitude of mechanisms: they act as sentinels for molecular and cellular changes in the joint cavity (124) and facilitate clearance of cartilage and bone debris, highly immunogenic and hence dangerous signals that are constantly shed into the synovial fluid due to mechanical shear stress. In both mice and humans, lining macrophages express high levels of scavenger receptors, in particular Triggering Receptor Expressed on Myeloid Cells 2 (TREM2) and CD163 and are highly phagocytic and anti-inflammatory (22, 124, 127–129). Lining macrophages also actively participate in production of extracellular matrix (ECM) components and synovial fluid (22). Finally, sophisticated genetic and imaging approaches recently revealed that reminiscent of epithelial cells, lining macrophages form tight junctions with one another and thereby constitute a structural and immunological barrier (22). This barrier limits immune cell trafficking across the synovial membrane and thereby protects the avascular cavity from systemic threats. Conversely, it shelters the synovial connective tissue from immunogenic stimuli present in the joint space. Collectively, these features make synovial macrophages key regulators of joint homeostasis.

Potential Macrophage Niches and Signals in Healthy Joints

The exact cellular interactions and molecular signals comprising macrophage niches in healthy joint tissues remain to be deciphered with state-of-the-art approaches, however, fibroblasts are likely key players. This is the case for the spleen and peritoneal cavity (102, 130) and may also be particularly true for the synovial lining, where in the absence of a basement membrane they are in intimate contact with lining macrophages. Synovial fibroblasts and macrophages have been characterized individually in great detail over the last several years (22, 131, 132), and their potential interplay has been discussed in excellent recent reviews (133–135). Fibroblasts are ideally suited to provide anchorage to macrophages, and they are also a recognized source of key macrophage survival factors, such as CSF1 (**Figure 2**). Synovial lining macrophages are lacking in CSF1-deficient osteopetrotic ("op/op") mice (99) demonstrating their CSF1-dependence, at least during development. Intriguingly, systemic administration of CSF1 does not restore synovial macrophages, whereas transgenic overexpression of the full-length transmembrane protein does, suggesting they depend on the membrane-bound isoform of the growth factor and thus, local sources (99, 136). Whilst synovial lining macrophages express the receptor for CSF1 receptor (CSF1R) at steady state (22), it is currently unclear whether they also rely on CSF1 for their homeostatic maintenance and turnover.

Fibroblasts could also act to bring macrophages in proximity of tissue-specific cues that imprint their functional identity, although this process may be orchestrated by additional stromal cell types in the joint, such as adipocytes, endothelial cells and chondrocytes. Such complexity is seen in the liver, where incoming monocytes are functionally imprinted by a triad of hepatocytes, endothelial cells and stellate cells (101). Joint tissues are constantly exposed to shear stress and tensile forces that dynamically change with variations in joint loading. Mechanical stimuli are amongst the candidate cues that could play a particularly important role in instructing the specific identity of macrophages in joint tissues. Macrophages are in principle capable of sensing mechanical forces. Human BM-derived macrophages for example respond to substrates with different stiffness with changes in their shape, migration and proliferation (137). Mechanotransduction can also directly modulate their inflammatory cytokine production (138, 139). This latter effect is dependent on the NLRP3 (NOD-, LRR- and pyrin domain containing 3) inflammasome and can also involve signaling through TRPV1 and 4 (Transient receptor potential vanilloid-type 1 and 4) cation channels, which have been implicated in ptOA pathophysiology in mice (140–142). Transduction of mechanical signals through TRPV4 has also been implicated in the formation of multinucleated giant cells, inflammatory and destructive multinucleated macrophages (143). In addition to mechanical stress, normal ECM turnover products represent candidate signals that could imprint joint macrophage identities. Indeed, synovial lining macrophages appear to be highly phagocytic and constantly scavenge cartilage debris from the joint cavity (144–146). Joint biomechanics are altered during OA pathogenesis, and joint-tissue ECM degradation products more prevalent than at homeostasis, thus these pathways likely also impact macrophage identities and functions in arthritic joints.

MONOCYTE AND MACROPHAGE FUNCTIONS IN THE INJURED AND OSTEO-ARTHRITIC JOINT

Macrophage Functions in ptOA Pathogenesis

In addition to self-maintained lining and interstitial sub-lining macrophages already present at steady state, the arthritic synovium contains inflammatory monocyte-derived macrophages (147, 148). Similar changes also occur in other tissues within the joint (e.g. subchondral bone), regional (e.g. lymph node) and in remote tissues (e.g. spleen, peripheral blood). The necessity to delineate the specific roles of these distinct macrophage populations is highlighted by discrepant findings on the consequences of macrophage depletion depending on the experimental approach. Although the precise contribution of the various populations remains to be shown, systemic depletion of macrophages in mice in which apoptosis is induced in cells expressing CSF1R exacerbates experimental ptOA, whereas local clodronate liposome-mediate depletion within the joint is beneficial (149).

In RA, the respective functions of the distinct macrophage subsets have now been well explored, and macrophages originating from recruited monocytes appear to have overall disease-promoting functions (150, 151). Similarly, the majority of studies on OA-affected joints have identified inflammatory, monocyte-derived macrophages as the main culprit in

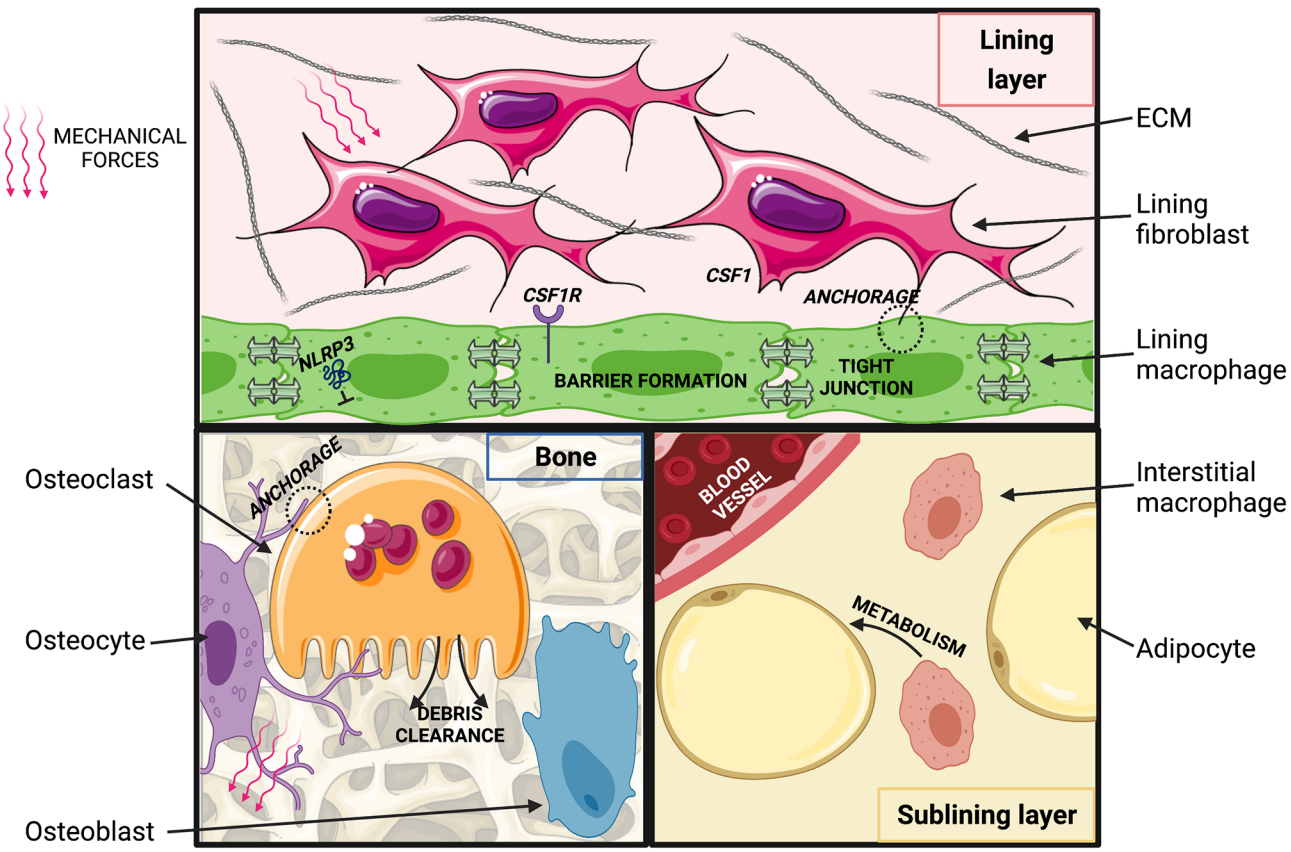

FIGURE 2 | Putative macrophage niches in the healthy joint. (Top) Synovial lining: macrophages are connected *via* tight junctions and are in close contact with fibroblasts. Fibroblasts may provide CSF1 and anchorage to macrophages, which may be imprinted by exposure to ECM degradation products. Movement-induced cyclic stretch may inhibit NLRP3 inflammasome activation. (Bottom, left) Osteoblasts lining the bone surface synthesize bone matrix in response to soluble mediators released by osteocytes that sense changes in mechanical loading and bone deformation. Osteoclasts resorb bone and thereby regulate balanced homeostatic bone turnover ("modelling") in response to anchorage and soluble signals from osteocytes and osteoblasts. (Bottom, right) In the synovial sub-lining, self-maintained interstitial macrophages may regulate adipose tissue metabolism and act as a reservoir to replenish synovial lining macrophages. Created with BioRender.com and smart.servier.com.

promoting and sustaining inflammation (124, 152). These cells produce pro-inflammatory cytokines and release additional signaling molecules associated with tissue-injury, which can attract lymphocytes that further propagate inflammation. However, exploiting these findings therapeutically is currently hindered by a lack of detailed understanding of the exact interplay between monocyte-derived macrophages and different types of lymphocytes, and how these change in the distinct stages of ptOA pathogenesis. Monocyte-derived macrophages also participate in cartilage destruction *via* production of IL-1β and TNF-α, which suppress synthesis of the ECM components aggrecan and collagen by chondrocytes and upregulate expression of catabolic enzymes like ADAMTS-4 and MMP-13 (153–155). Soluble matrix degradation products in turn can activate resident synovial macrophages *via* Toll-Like Receptors (TLRs) and other pattern-recognition receptors (156). As this example illustrates, different macrophage populations in the joint can be functionally interlinked.

Another effector by which macrophages might contribute to ptOA pathogenesis is B cell Activating Factor (BAFF), a member of the TNF superfamily. BAFF is a crucial B cell survival factor, but also exerts co-stimulatory effects on T cell activation *via* upregulation of B-cell lymphoma 2 (BCL-2) (157). Furthermore, BAFF promotes T-helper-cell (Th)1 and suppresses Th2 responses (158), and drives Th17 differentiation *via* Il-6 signaling (87, 158–161). BAFF levels are elevated in serum and synovial fluid from RA patients (162), and BAFF appears to have a pathogenic role in RA (163, 164). During established RA, BAFF promotes pro-inflammatory polarization of $CD4^+$ T cells, DC maturation as well as proliferation of inflammatory fibroblasts (163). In the inflamed joint, macrophages (165) are the main source of BAFF, although it is unclear if these are monocyte-derived or resident macrophages, or both. This compelling evidence led to the development of BAFF antagonists as DMDs for RA, which are currently being tested in early phase clinical trials (163). Whether BAFF production is also a

mechanism by which macrophages contribute to pathogenesis of OA has not been determined but elevated BAFF levels have been detected in OA synovial fluid (166).

Unlike their monocyte-derived counterparts, and some controversy notwithstanding, self-maintained resident synovial macrophages have largely been attributed protective roles in arthritis. The barrier generated by synovial lining macrophages is disrupted in both RA patients and experimental RA (22). In mice, this occurs rapidly upon induction of serum transfer-mediated arthritis, and thus constitutes an early event in disease development. In this model, barrier breakdown occurs following phagocytosis of immune complexes containing auto-antibodies, which activate lining macrophages and induce structural joint pathologic changes. Consequently, depletion of lining macrophages or specific disruption of their tight junctions worsens experimental RA. In turn, drug-mediated stabilization of tight junctions protects mice from RA (22), a finding that is translationally promising. Whilst the role of synovial lining macrophages has not yet been addressed specifically in OA pathogenesis, it is worthwhile noting that targeting lining macrophages or tight junctions not only exacerbates RA but may also result in spontaneous inflammation in the joint cavity in otherwise healthy animals (20, 22). With respect to ptOA, one could thus envision a scenario in which following injury, mechanical disruption of the synovial lining macrophage barrier enables rapid influx of inflammatory cells and hence, transition to the inflammatory phase of OA pathogenesis. Unlike in RA however, this barrier breach might be transient in nature, since the barrier appears more intact in patients with established OA compared to RA (22). This might be due to differences between immune complex-mediated and mechanical barrier-breakdown and could contribute to the, often considerable, lag phase between joint injury and ptOA onset.

Monocyte Functions in Joint Pathogenesis

Monocytes are critical players in OA pathogenesis, both as effector cells and a source of additional macrophages. As described earlier, it is widely accepted that Ly6C^{high} and Ly6C^{low} monocytes can differentiate into macrophages with distinct polarization profiles in response to the cytokine milieu encountered in the tissue microenvironment. Reflecting this complexity, the overall impact of classical and non-classical monocytes on joint disease pathogenesis remains unclear. On the one hand, adoptive transfer of Ly6C^{low} monocytes following pan monocyte depletion increases the development of serum-transfer induced arthritis (58, 167, 168). In this model, Ly6C^{low} monocytes are actively recruited to the joint, where they are critical for the initiation of sterile joint inflammation and differentiate into inflammatory macrophages (169). On the other hand, Ly6C^{low} monocytes were also found to limit excessive inflammation in arthritic mice *via* enhanced recruitment of regulatory T-cells (Tregs) (58, 170). This seemingly contradictory evidence regarding the role of Ly6C^{low} monocytes in RA underscores the need for further studies that improve the understanding of the complex role of monocytes in inflammatory arthritis, and similar considerations apply to OA. The diverse roles of monocytes and macrophages in ptOA pathogenesis will be discussed in more detail in the following section, focusing on molecular and cellular factors shaping their respective functions.

SIGNALS AND CELLULAR INTERACTIONS SHAPING MONOCYTES AND MACROPHAGES IN PTOA

Depending on severity, joint injury can induce marked mechanical, anatomical and immunological changes, initially resulting in recruitment of monocytes and other inflammatory cells. Pathological changes persist throughout ptOA development and in established disease, and impact both incoming monocytes and previously resident macrophages. This section discusses how the perturbed joint tissue environment might affect monocytes and macrophages (**Figure 3**). An overview of murine and human monocytes and macrophages found in the synovial tissue during homeostasis, rheumatoid arthritis and in as far as known osteoarthritis, can be found in **Table 1**.

Perturbations Following Joint Injury

Joint injury triggers a series of complex mechano-biological and immunological changes, which can be broadly separated into three successive phases. Immediately after injury, mechanical perturbation effects predominate. These are direct results of the injury (9, 171) and may include tissue disruption (e.g., subchondral bone (micro)fractures, ligament tearing), collagenous matrix disruption and cartilage swelling, blood-vessel injury and hemarthrosis i.e. the presence of blood in the synovial cavity. This immediate joint-tissue injury is followed by an acute inflammatory phase (172), which is characterized by abundant cell death and pro-inflammatory signaling involving both innate and adaptive lineages (173). The nature and duration of this inflammatory response have been identified as major determinants for the risk of developing ptOA post injury (9, 172, 173). While appropriate control and resolution of inflammation is essential for normal wound-healing and might prevent ptOA development, perpetuated inflammation leads to the chronic and final phase of OA pathogenesis, which is defined by fluctuating low-level synovitis (174) and continuous tissue remodeling processes that ultimately lead to destruction of the cartilage and joint failure (175). Delayed or failed resolution of inflammation can be due to a permanently disrupted equilibrium of pro- and anti-inflammatory factors (171) or inadequate post-injury inflammation control (172). In addition, biomechanical factors such as instability or recurring joint injuries (176) can result in continuous re-triggering of acute mechano-biological responses, which initiate an inflammatory vicious circle. These considerations identify the acute inflammatory phase as a potential target for ptOA DMDs and highlight the need for a better understanding of its cellular and molecular regulators.

Mechanisms Underlying Monocyte Recruitment During OA Pathogenesis

The exact nature of the inflammatory response subsequent to joint injury is still under investigation, and differences might

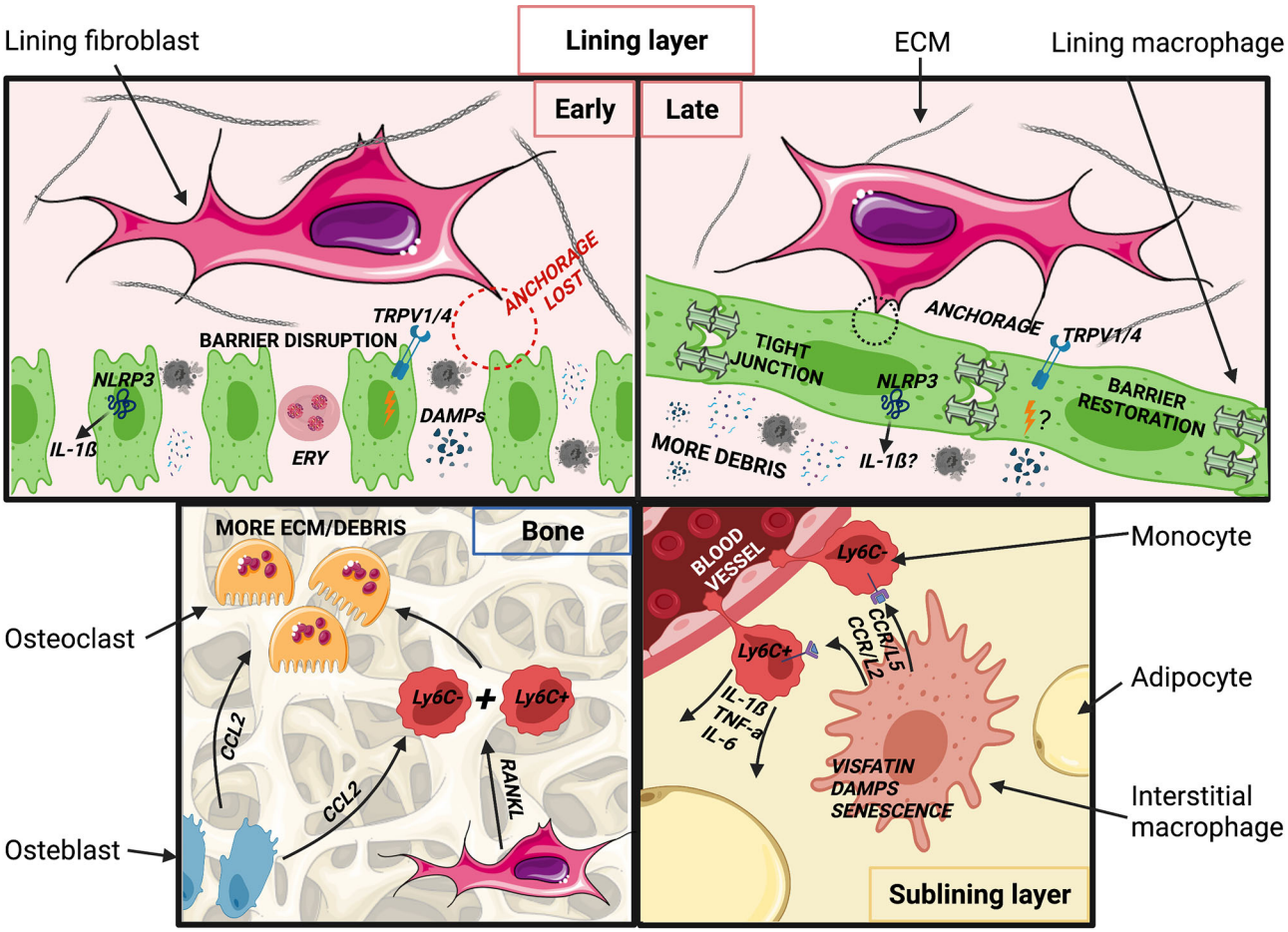

FIGURE 3 | Putative changes in joint tissues after injury and during post-traumatic OA development. (Top, left) Acutely following injury, synovial lining macrophages are spatially re-orientated and the barrier is disrupted. DAMPs, PAMPs and catabolic enzymes are released into the synovial cavity by chondrocytes and damaged tissues (ligament, meniscus). Extra-vascular erythrocytes and associated free heme from blood vessel injury may pathologically imprint synovial macrophages. Barrier disruption may impede cyclic stretching of lining macrophages, resulting in NLRP3 inflammasome activation and increased IL-1ß production, known to promote of OA. Altered mechanics may also promote joint inflammation through TRPV1/4 cation channels. (Top right) At later stages of ptOA pathogenesis, the synovial lining layer may be restored. Levels of IL-1ß remain elevated, though involvement of the NLRP3 inflammasome is unclear. TRPV1 activation may continue to promote OA pathogenesis, although likely *via* signals other than or in addition to mechanical stimuli. Cellular debris, DAMPs and PAMPs remain abundant in the synovial cavity and thus potentially imprint pathological macrophage phenotypes. (Bottom, left) Increased numbers and activation of osteoclasts contribute to accelerated bone turnover and remodeling in the arthritic joint. Osteoclastogenesis may be promoted by CCL2 produced by activated osteoblasts and inflammatory cells, potentially resulting in recruitment and fusion of Ly6C^{high} and Ly6C^{low} monocytes, a process that may be further stimulated by RANKL produced by lining fibroblasts. (Bottom, right) In the sublining layer, exposure to ECM degradation products may stimulate interstitial macrophages to produce CCL2 and CCL5, leading to recruitment of Ly6C^{high} and Ly6C^{low} monocytes. Ly6C^{high} monocytes produce IL-1ß, TNF-α and IL-6, potentially in response to the adipokine visfatin, a TLR4 receptor agonist, which also induces changes in the subchondral bone. Ly6C^{low} monocytes may supply the interstitial macrophage pool, but these macrophages may retain higher baseline NF-κB and IL-1ß activity than those in healthy joints. Created with BioRender.com and smart.servier.com.

exist depending on the type of injury and/or tissues injured, as we will discuss below. Overall, however, a growing body of evidence implicates chemokines and their receptors in monocyte recruitment during OA pathogenesis. As reported for other pathologies (177), classical and non-classical monocytes differentially depend on CCL2/CCR2 or CCL5/CCR5 and CX3CL1/CX3CR1. CCL2 (also known as MCP-1) is a key regulator of Ly6C^{high} monocyte egress from the BM and their recruitment to peripheral tissues (178). Following joint injury, release of ECM degradation products and complement factors temporally induces CCL2 production by chondrocytes, resident synovial macrophages (179) and endothelial cells (180). This occurs *via* a positive feedback loop, stimulated by increased IL-1β and TNF-α expression in synovial macrophages (181) and fibroblasts (182). In keeping with this, clinical studies have reported elevated levels of CCL2 in synovial fluid immediately after traumatic joint injury (183) and subsequent to meniscal tears (184), and concentrations correlate with severity of OA (185, 186). Its expression is also significantly elevated in the serum of OA patients (187), and CCL2 might also affect other

TABLE 1 | Markers, origin and putative function of monocytes and synovial macrophage subsets in mouse and human.

Population, location	Phenotype	Origin, maintenance	Functions at homeostasis	Functions in osteoarthritis
	Mouse: TREM2$^+$ CX3CR1^{high} MHCII$^-$	Long-lived, BM-independent, not proliferating[2],[3] replenished from sublining interstitial	Protective barrier[2]	Protective barrier,[2] limiting disease development (RA), immune regulation[3]
Macrophages, synovial lining	"mTOR activated M1 macrophages" iNOS^{+}[1]	Unknown	Unknown (low number)	Chondrocyte differentiation[1]
	Human: TREM2$^+$ CD68$^+$ MerTK$^+$ LYVE1$^+$ FOLR2^{+}[4,2]	Proliferation[4,5]	Protective barrier[2] Control local immune responses[4]	Protective barrier[2] Resolution of inflammation, induce reparative fibroblast
	CD14$^+$HLADR$^+$ FOLR2$^+$CD86^{+}[5] KI67^{high} ULK1$^+$	Proliferation[5]	Unknown	
	CD14$^+$HLADR$^+$ FOLR2$^+$CD86$^+$ KI67^{low} *HTRA1*+ (location uncertain)	Uncertain	Unknown	Cartilage remodelling[5]
Macrophages, synovial sublining/ interstitital	Mouse: RELMa$^+$ CD206$^+$ CD163$^+$	BM-independent[2]	Joint homeostasis	
	CX3CR1$^-$ MHCII$^+$ CSF1R$^+$	Proliferation, BM-independent (RA)[2] / BM (arthritis)[3]	Generate lining and sublining macrophages[2]	Generate lining and sublining macrophages[2], Inflammation
	Human TREM2$^-$ MerTK$^-$ CD206$^-$ CLEC10a^{+}[42]	Unknown	Unknown	Fibroblast inflammatory response[4]
Macrophages, synovial tissue of the "bare area"	Mouse: CX3CR1$^+$ MHCII$^+$ Ly6C^{int}F4/80$^+$	BM[6]	Absent	Osteoclastogenesis[6]
	Human: CX$_3$CR1$^+$ HLA-DR^{high} CD11c$^+$ CD80$^-$ CD86$^+$	Unknown	Unknown	Osteoclastogenesis[6]
Monocytes, synovial tissue	Mouse: Ly6C$^+$ CD64^{int}	BM[3]	Tissue patrolling	Generate Ly6C$^-$ monocytes
	Ly6C$^-$	BM[3]	Absent	Initiation of sterile joint inflammation[3] Generate MHCII$^+$ macrophages[3]
	Human: CD14$^+$ CD11c$^+$ CD38$^+$ IL1B$^+$ IFN-activated SPP1+[7]		Unknown	Pro-inflammatory[7]
	CD14$^+$ CD11c^{-}[7] *NUPR1*$^{+}$[7]		Joint homeostasis[7]	Inversely correlated with tissue inflammation, bone remodelling[7]

TREM2, triggering receptor expressed on myeloid cells 2; CXCR1, C-X3-C Motif Chemokine Receptor 1; MHCII, major histocompatibility complex class II; mTOR, mammalian target of rapamycin; iNOS, inducible nitric oxide synthase; BM, bone marrow; RA, rheumatoid arthritis; MerTK, MER Proto-Oncogene, Tyrosine Kinase; LYVE1, Lymphatic Vessel Endothelial Hyaluronan Receptor 1; FOLR2, Folate Receptor Beta; CD, cluster of differentiation; HLADR, Human Leukocyte Antigen – DR isotype; ULK1, Unc-51 Like Autophagy Activating Kinase 1; HTRA1, HtrA Serine Peptidase 1; RELMa, Resistin-like molecule a; CSF1R, colony-stimulating factor 1 receptor; CLEC10a, C-type lectin domain family 10; Ly6, lymphocyte antigen 6; IL, interleukin; IFN, interferon; SPP1, Secreted phosphoprotein 1; NUPR1, Nuclear Protein 1.

[1]Zhang, H. et al. Synovial macrophage M1 polarisation exacerbates experimental osteoarthritis partially through R-spondin-2. Ann. Rheum. Dis. 77, 1524–1534 (2018).

[2]Culemann, S. et al. Locally renewing resident synovial macrophages provide a protective barrier for the joint. Nature 572, 670–675 (2019).

[3]Misharin, A. V. et al. Nonclassical Ly6C- monocytes drive the development of inflammatory arthritis in mice. Cell Rep. 9, 591–604 (2014).

[4]Alivernini, S. et al. Distinct synovial tissue macrophage subsets regulate inflammation and remission in rheumatoid arthritis. Nat. Med. 26, 1295–1306 (2020).

[5]Wood, M. J. et al. Macrophage proliferation distinguishes 2 subgroups of knee osteoarthritis patients. JCI Insight 4, (2019).

[6]Hasegawa, T. et al. Identification of a novel arthritis-associated osteoclast precursor macrophage regulated by FoxM1. Nat. Immunol. 20, 1631–1643 (2019).

[7]Zhang, F. et al. Defining inflammatory cell states in rheumatoid arthritis joint synovial tissues by integrating single-cell transcriptomics and mass cytometry. Nat. Immunol. 20, 928–942 (2019).

cells relevant to OA pathogenesis. In chondrocytes, for example, CCL2 increases expression of the catabolic enzymes MMP3 and MMP13 (179) and inhibits proliferation and enhances apoptosis. CCL2 might thus promote OA pathogenesis *via* attracting monocytes to the joint, but also by directly promoting cartilage destruction (179).

Unlike CCL2, which is found mainly in the intimal lining of the synovium, CCL5 [also known as RANTES (Regulated on Activation, Normal T Cell Expressed and Secreted)] is distributed more diffusely throughout the synovial tissue (188). Conflicting evidence exists regarding the role of CCL5 and its receptor CCR5, which possess strong chemo-attractive properties for Ly6C^{low} monocytes. In line with a disease-promoting role of Ly6C^{low} monocytes, CCR5$^{-/-}$ mice were initially reported to exhibit reduced cartilage destruction (189), however, a recent study by Raghu and colleagues found that neither deficiency in CCL5, nor CCR5 protects mice from ptOA (21). This was further corroborated by a clinical study of synovial biopsy specimens, which found significantly higher levels of CCL5 in RA compared to OA patients, whilst expression of all other chemokines and receptors is comparable (188). This may suggest that the inflammatory responses underlying these different arthritides have some unique molecular signatures or phenotypes. Considering its role in attracting Ly6C^{low} monocytes, which are known to promote pathogenesis of inflammatory arthritis, it seems surprising that depletion of CCR5 has no protective function in ptOA (21). However, CX3CL1/CX3CR1 signaling also participates in recruitment of non-classical monocytes, and elevated levels of CX3CL1 have been found in peripheral blood (190) and synovial fluid (186) of OA patients. Functional experiments revealed that in addition to its chemo-attractive properties, CX3CL1 also stimulates inflammation specifically at

the early stages of OA (190). Finally, soluble CX3CL1 induces production of the pro-inflammatory cytokines IL-1β, IL-6 and TNF-α in recently recruited monocytes (191). Taken together these data indicate that the CX3CL1/CX3CR1 axis predominates in recruitment and pro-inflammatory activation of Ly6C^{low} monocytes in the context of OA initiation. Ly6C^{high} monocytes recruited and activated *via* CCL2/CCR2, on the other hand, might help sustain inflammation at later stages (192). Temporal changes in chemokine expression and associated monocyte sub-population recruitment and accumulation, may in part explain the recently described loss with time post-injury, of an initially protective/anabolic effect of injured synovium on chondrocytes (193).

Osteoclasts have been implicated in progressive joint destruction. Osteoclastogenesis is controlled by RANK (Receptor Activator of Nuclear factor Kappa B (NF-κB) (194). Its ligand (RANKL) is expressed by fibroblast-like synoviocytes and Th17 cells, and expression is regulated by pro-inflammatory cytokines secreted by monocytes and macrophages (IL-1β, IL-6, IL-17 and TNF-α) (195). A particularly interesting mechanism by which monocytes could contribute to increased osteoclastogenesis in the context of arthritis was proposed by Hirose *et al.* They postulated that CCL2 secreted by osteoblasts leads to fusion of Ly6C^{high} with Ly6C^{low} monocytes stimulated by RANKL, resulting in mature, multinucleated osteoclasts (195). In addition to osteoblasts, activated inflammatory cells produce large amounts of CCL2 and this might explain the accelerated osteoclastogenesis and joint destruction in an inflammatory setting (195).

Signals Governing Monocyte Differentiation, Activation, and Functions in OA

Following their recruitment to the tissue, monocyte functions can be shaped by a variety of signals present in the non-homeostatic joint. Calcium binding proteins can act as damage- or pathogen-associated molecular patterns (DAMPs and PAMPs, respectively) and have multi-faceted effects on OA pathogenesis. Damage to the cartilage leads to increased levels of S100A8 and its binding partner S100A9 specifically in synovial pro-inflammatory macrophages, but not fibroblasts (196). Secretion of these factors induces the production of pro-inflammatory cytokines in these macrophages in an autocrine manner (196). In addition, in a murine collagenase-induced OA model, which has a more inflammatory phenotype than surgically-induced disease, release of S100A8/9 elicits influx of Ly6C^{high} monocytes *via* upregulation of CCL2 (197) and increased egress of Ly6C^{high} monocytes from the BM (197). In turn, activated monocytes are a major source for S100A8/9, which might thus constitute a positive feedback loop. Finally, S100A8/9 might also be derived from chondrocytes and directly contribute to cartilage disruption in OA by inducing production of ADAMTS-4 and -5, MMP-1, -3, -9 and -13 and the pro-inflammatory cytokines IL-6, IL-8 and CCL2 in chondrocytes in a TLR4-dependent manner (198, 199). Interestingly, chondrocyte-derived S100A8/9 may play a predominant role in the acute post-injury phase, as expression and protein levels in cartilage decrease with post-traumatic OA disease progression while levels are maintained in immune-mediate inflammatory arthropathy (199). S100A8/9 thus fuel the initial pro-inflammatory microenvironment in the joint, provide chemotactic cues for Ly6C^{high} monocytes and exert direct catabolic effects within the cartilage, processes which are further amplified by several feedback loops. Another class of OA-associated DAMPs are basic calcium phosphate (BCP) crystals. Whilst *in vivo* data on their relevance to OA are currently lacking, *in vitro* exposure of monocyte-derived macrophages to BCP crystals leads to a classically activated, pro-inflammatory phenotype, a bioenergetic switch towards glycolysis and increased expression of S100A8 (200). Promisingly, both BCP-induced phenotypic polarization and S100A8 expression are inhibited by a glycolytic inhibitor (2DG) indicating that metabolic reprogramming might be underlying these effects (200).

The Janus Kinase/Signal Transducer and Activator of Transcription (JAK/STAT), Mitogen-Activated Protein Kinase (MAPK) and NF-κB pathways are involved in differentiation of monocytes into macrophages and their functional polarization. The latter depends on interferon regulatory factors (IRFs) (201). IRF5 is a also downstream target of Granulocyte-Macrophage Colony-Stimulating Factor Receptor (GM-CSFR), and plays a critical role in pro-inflammatory macrophage polarization (202). A recent clinical study investigated the role of IRF5 in OA and found it to be overexpressed in synovial macrophages, but not circulating monocytes (203). However, exposure to synovial fluid from OA patients induced expression of IRF5 and IL-12 (via the individual subunits IL-12p35 and IL-12p40) in monocytes, in turn making them potent inducers of a Th1 response characterized by expression of IFN-γ and Tbx21 in co-cultured naïve CD4$^+$ T-cells (203). This suggests that patient synovial fluid contains soluble factors capable of inducing IRF5 in monocytes, thus contributing towards a Th1 inflammatory response.

TLR 4 is a receptor for PAMPs and DAMPs expressed on monocytes that plays an important role in the activation of innate immunity (204), and has been implicated in the inflammatory reaction associated with OA (205). The adipokine visfatin was recently identified as a TLR4 receptor agonist capable of evoking inflammatory responses (206). In addition, visfatin stimulates production of IL-1β, TNF-α and IL-6 by monocytes (207), and the resulting inflammatory environment displays higher levels of circulating visfatin, thus constituting a positive feedback loop (208, 209). Visfatin is also involved in inter-tissue joint communication underlying changes in the subchondral bone (210). These have long been described in OA, but the exact mechanisms of this remodeling and pathways of its activation has remained elusive. Emerging evidence now points towards direct communication between the subchondral bone and cartilage *via* diffusion (211). Laiguillon *et al.* found that visfatin is produced in cartilage, synovium and subchondral bone and exerts an enzymatic effector function selectively inducing a pro-inflammatory phenotype in chondrocytes, osteoblasts and synoviocytes, characterized by increased secretion of IL-6 and CCL2 (210, 212–214). Because of its contribution to the inflammatory response and tissue remodeling, inhibition of visfatin might be a promising DMD approach.

The gene expression profiles of monocytes and monocyte-derived macrophages, and hence, their functional polarization,

might also be shaped by microRNAs expressed in response to environmental stimuli. A recent study identified miR-155 as a potential genomic switch in monocyte-derived macrophages generated *in vitro*, which regulates their inflammatory profile (215). Intriguingly, this phenomenon is partially reversed by treatment with monoclonal anti-TNF antibodies, but not a soluble TNF receptor (Etanercept) (215). MiRNAs expressed by monocytes and their macrophage progeny, such as miR-155, might therefore represent promising candidate DMD targets.

While we have focused primarily on joint injury and ptOA, monocytes and macrophages in the arthritic joint might also be affected by age and cellular senescence, as has been demonstrated for RA. In this context, an elegant mouse study from Misharin *et al.* is of note, where the role of different monocyte subsets in RA pathogenesis using serum-transfer induced arthritis was investigated. Ly6C^{low} monocytes are recruited to the joint and initially develop into classically activated macrophages, but the macrophage compartment gradually undergoes a switch towards a more alternatively activated phenotype (169). The initial highly pro-inflammatory nature of the Ly6C^{low} monocytes could be caused by a senescence-associated secretory phenotype, which is associated with high baseline NF-κB and IL-1α activity (216). In addition, accumulation of Ly6C^{low} monocytes is found in the elderly. These findings suggest that senescence might correlate with increased numbers and pro-inflammatory skewing of Ly6C^{low} monocytes, which might further exaggerate the inflammatory response unfolding during RA progression. Whether similar mechanisms might be at play in ptOA requires evaluation, but it is interesting to note the accelerated disease progression, increased expression of inflammatory genes and inhibitory effects of MIF ablation following medial meniscal destabilization in older versus younger mice (217, 218).

Immunogenic and Imprinting Signals in the Injured Joint

As introduced, the synovial membrane plays a key role in maintaining joint homeostasis as it guarantees the relative immune privilege of the synovial cavity. However, while the joint space itself is not vascularized, the synovial membrane also features a vascular net located just below the intima. This comprises capillaries, venules, arterioles and lymphatics (219) through which systemic and local inflammatory stimuli can be sensed (125, 220). Hemarthrosis and cartilage damage are direct consequences of joint trauma, which affect the joint not only macroscopically, but also on a cellular and molecular level (176). Of note, the presence of blood in synovial fluid is an independent predictor or poorer 2-year outcome following joint injury (221). It is tempting to speculate that heme could be a cellular cue shaping macrophages in the early stages of ptOA pathogenesis, but unlike in the homeostatic spleen, it may instruct more inflammatory cell states (222). Moreover, hemarthrosis directly activates the complement system, leading to production of complement anaphylatoxins (C3a and C5a) and formation of the membrane attack complex (223). Intriguingly, genetic deficiency for individual components of the complement system in mice leads to either attenuated [C5 and C6 (224)] or aggravated [CD59, also known as protectin (224)] ptOA joint damage following injury.

As discussed above, mechanical forces may directly shape macrophage functions in the homeostatic joint. It is therefore plausible that the mechanical changes following joint injury, impact on resident and recruited macrophages. This appears to be the case at least in experimental RA, where the extent of mechanical loading determines the local distribution of inflammation and degree of damage (225). Mechanical damage to the cartilage also leads to substantial ECM degradation. Collagen fibers fail to contract (226, 227) and ECM degradation is further enhanced by the lack of maintenance and repair (228) following chondrocyte death. ECM-derived tissue fragments are widely recognized as pro-inflammatory and immunogenic (229, 230). These fragments and the complement anaphylatoxin C5a can act as effective chemo-attractants for innate and adaptive immune cells (231, 232) and directly activate macrophages *via* NF-kB signaling (233). Released cartilage destruction products such as matrilin-3 (229, 234), tenascin-C (235), fragmented biglycan (236) and fibronectin (237) can also potently activate resident synovial macrophages. Finally, cartilage and other joint tissue degradation can induce release of additional DAMPs (238) capable of activating innate immune cells *via* TLR2 and 4 (239) and NF-kB signaling. The mechano-biological damage induced by injury thus generates an inflammatory microenvironment in the joint space, which is characterized by an increase in soluble inflammatory mediators and chemo-attractants that might induce transition to the acute inflammatory phase, and importantly shape subsequent responses of both recruited monocytes and resident macrophages.

T Cell-Mediated Monocyte and Macrophage Activation in OA?

Other immune cells may provide signals amplifying the effects of monocytes and macrophages. In the context of joint injury, recruitment and activation of lymphocytes have traditionally been thought of as secondary events that follow monocyte influx and changes in macrophages (11). However, T cells are found in synovium at higher levels in early versus late OA (240) and might actively contribute to monocyte and macrophage activation *via* co-stimulatory pathways. One such pathway relies on interactions between CD40, a member of the TNF receptor family found primarily on antigen-presenting cells and monocytes, and its ligand CD40L (CD154), which is almost exclusively expressed by activated CD4$^+$ T cells (241, 242). CD40/CD40L interactions elicit a broad pro-inflammatory response (243) that involves B cell differentiation (244) and macrophage activation. In turn, activated macrophages and other antigen-presenting cells enhance immunoglobulin antigen affinity (241), activate cytotoxic T cells and promote a Th1 immune response (245). This co-stimulatory pathway therefore has the potential to initiate a powerful amplification loop that propagates joint inflammation. In keeping with this notion, exaggerated CD40/CD40L signaling contributes to autoimmunity (246), including RA. Multiple studies have

shown overexpression of both CD40L (247–249) and CD40 (246) in RA, and levels of CD40L are associated with disease activity (248) and perpetuation (247). Based on these findings, biological treatments targeting this axis in RA have been developed, which are currently undergoing early phase clinical trials (250). Despite differences in the pathogenesis and mechanisms involved in the development of RA and OA, shared elements in the underlying inflammatory response seem plausible (251). The effects of targeting the CD40/CD40L axis in OA remain to be determined, however we have found that CD40L mRNA levels are elevated exclusively in the synovium immediately after ACL rupture and during early onset of OA development (252). These preliminary findings support the notion that CD40/CD40L may be an early driver of T cell-mediated synovial macrophage activation and warrant future research into the CD40/CD40L axis specifically in ptOA.

Additional Candidate Pathways and Mechanisms Leading to Macrophage Dysregulation During OA Pathogenesis

In addition to the factors discussed above, obesity is a well-established risk factor contributing to OA development (253), through increased mechanical loading but also *via* dysregulated secretion of adipokines and other metabolic factors (254). In mice, high-fat diet (HFD) results in elevated leptin-induced levels of lysophosphatidylcholine (lysoPC), which in turn increases MMP13 production by chondrocytes. As a consequence, obese mice show an earlier onset and progressive course of spontaneous OA (254). Direct links between obesity and OA have also been shown in mouse models of ptOA. HFD was associated with inflammation in the infrapatellar fat pad, characterized by macrophage crown-like structures, which may have a priming effect on the fat pad leading to a metabolic state of progressive OA following injury (123). HFD was also shown to aggravate inflammation of the synovial membrane post-injury, which was marked by increased macrophage infiltration (255). These findings are in line with the notion that obesity contributes to aberrant macrophage activation in OA pathogenesis. Intriguingly, these detrimental effects of HFD on OA persisted even after a normal diet was resumed (254), indicating long-lasting effects and potential windows or particular susceptibility. Some of these effects may even be programmed in early life and transmitted across generations. Indeed, increased higher susceptibility to experimental ptOA has been reported in the first and second generation offspring of mice fed a HFD during breeding (256). Immune cells have been implicated as mediators of such programming and transgenerational effects of obesity in offspring (256), and epigenetic dysregulation has been postulated as a central mechanism.

While some epigenetic modifications are stable and passed on across generations, others are more dynamic and responsive to environmental stimuli (257). These are believed to play a significant role in OA development. Of the studies that have investigated epigenetic changes in OA development, most have focused on epigenetic mechanisms modulating chondrocyte biology and inflammatory mediators (258). Evidence for epigenetic modifications of macrophage remains scarce in the context of OA. In principle, epigenetic processes govern various aspects of macrophage biology, including their development, differentiation, and activation, as well as the specification of their tissue identity (259–261). For example, active DNA demethylation occurs during monocyte to macrophage differentiation *in vitro* (262) and the identity of tissue-resident macrophages is shaped by unique enhancer landscapes in response to microenvironmental cues (70, 71). They also activate genes governing embryonic stem cell-like self-renewal through macrophage-specific enhancers (263). Fully differentiated macrophages are maintained in a "balanced" state through a combination of activating (such as PU.1, H3K4me1 and open chromatin) (264) and repressive (such as H3K9me3, H3K27me3 and H4K20me3) (265) epigenetic marks and regulators (262). These repressive marks are removed upon stimulation of macrophages through TLR, and specifically TLR4, ultimately resulting in the production of inflammatory cytokines such as IL-1β, CXCL10, IL-6 and TNF (262). TLR4 signaling has also been implicated in low-grade inflammation mediated by plasma proteins present in the synovial fluid of OA patients (266). Whether epigenetic changes in macrophages contribute to this remains to be formally shown, however.

Activation *via* TLR4 also initiates metabolic reprogramming of macrophages, and distinct metabolic states have been linked to functional differences in macrophage subsets. For example, metabolic reprogramming towards increased glycolysis promotes pro-inflammatory polarization (267). In OA, increased glucose uptake correlates with disease progression, and the hypoxic environment in the OA synovium may enhance osteoclastogenesis (267, 268). Osteoclastogenesis appears to also be promoted by metabolic syndrome through NF-κB activation and advanced glycation end products (269). A bioenergetic switch towards glycolysis is also induced in macrophages by basic calcium phosphate crystals, which are specifically found in OA (220), further supporting the notion that macrophages may undergo metabolic reprogramming during OA pathogenesis.

Finally, epigenetic and immunometabolic changes are also hallmarks of "trained immunity". This recently coined concept (270) acknowledges that innate immune cells, including macrophages, show increased responsiveness to secondary stimuli following "training" by primary exposures. Whilst trained immunity has not specifically been studied in the context of OA, many of the cellular signals that impact on macrophages during OA pathogenesis – or even preceding disease onset - could mediate long-term effects through inducing this type of innate memory in macrophages. Thus, obesity/HFD may be primary exposures that train heightened or specific OA inducing immune responses to a secondary stimulus such as injury (123, 256). It is interesting to speculate that this may also be relevant in the context of prior even minor joint injuries increasing the risk and/or severity of ptOA following a critical/destabilizing injury such as anterior cruciate ligament (ACL) rupture (see Blaker et al., 2021 and references therein) (271).

HARNESSING MONOCYTE AND MACROPHAGE BIOLOGY FOR OA RISK STRATIFICATION, DIAGNOSIS, AND THERAPY?

It is now well recognized that ptOA development features an early inflammatory response. This involves systemic processes resulting in monocyte recruitment, as well as a local disbalance within the immune "niches" of the affected joint, whose immune privilege is therefore compromised. This recognition has several implications that in the future could be exploited for prognostic, diagnostic and therapeutic benefit, examples of which we discuss below.

Monocytes and Macrophages as Biomarkers for OA

To this day, OA diagnosis largely depends on clinical presentation/symptoms and conventional imaging methods like x-ray, computerized tomography (CT) scans or magnetic resonance imaging (MRI) (272). Diagnostic biomarkers are currently missing, as are reliable predictive markers. Access to synovial fluid and hence, the search for useful biomarkers, is limited by the invasive nature of the acquisition procedure. Nonetheless, advances have been made recently in the search for cellular and molecular biomarkers with diagnostic and/or predictive potential (221, 273), using synovial fluid where available, or peripheral blood, which can be more readily obtained.

On the cellular level, a growing body of data implicates monocytes and monocyte-derived macrophages in OA pathogenesis, as discussed in this review. Several recent clinical studies therefore investigated the prognostic value of peripheral immune cell ratios. While the exact ratios differ between studies, monocytes represent a common denominator. In particular, the neutrophil to monocyte ratio is independently and inversely associated with OA severity as classified using the Kellgren-Lawrence scale (274). Similarly, the monocyte to lymphocyte ratio reliably predicts OA progression (275). MicroRNA analysis of peripheral blood mononuclear cells (PBMCs) from OA patients showed elevated expression of miRNA-146a and miRNA-155 (276), which influence inflammatory cell signaling *via* the NF-κB pathway (277, 278). Moreover, transcriptomic analysis of PBMCs from OA patients identified more than 1000 differently expressed genes, pathway analysis of which implicated inhibition of chondrocyte differentiation, increased osteoclastogenesis and MAPK activation (279). These data collectively indicate that peripheral blood monocytes of OA patients differ from healthy controls both quantitatively and qualitatively. It is tempting to speculate that specific OA-primed inflammatory monocytes exist in the peripheral blood during disease progression, and even potentially prior to onset. This notion is corroborated by data from Loukov and colleagues, who demonstrated that following *in vitro* exposure to DAMPs, peripheral blood monocytes from women with knee OA produced higher levels of the pro-inflammatory cytokines IL-1β and TNF-α than monocytes from healthy controls (280). The same group also demonstrated significantly higher levels of CD14 expression on monocytes of OA patients, further implicating non-classical activated monocytes.

Within the synovial fluid of knee OA patients, monocytes and macrophages constitute the second most abundant cell population after T cells, and a large proportion of these are $CD16^-$, thus further implicating non-classical monocytes (281). Liu et al. investigated the relative abundance of phenotypically distinct macrophages in synovial fluid of knee OA patients and found an increased ratio of "classically" compared to "alternatively" activated macrophages (282). This ratio further correlated with disease severity, suggesting that despite the limitations of this simplistic dichotomy, such analyses can yield clinically relevant data.

A wealth of experimental and clinical studies has analysed inflammatory parameters and markers in synovial fluid for their potential to serve as biomarkers. These studies have shown that levels of CCL2, IL-6 and IL-8 accurately distinguish OA from normal joints (283–285) and inflammatory markers can even predict the outcome of ACL reconstruction. Similarly, the presence and severity of synovitis following meniscal injury are associated with the risk of progressive cartilage damage, even if inflammation subsequently resolves (286). Elevated levels of several additional synovial fluid biomarkers associate not only with radiographic OA severity (sVCAM-1, sICAM-1, TIMP-1 and VEGF) and OA symptoms (VEGF, MMP-3, TIMP-1, sVCAM-1, sICAM-1 and MCP-1) but are also highly correlated with levels of neutrophil elastase (287). This highlights a potential role for neutrophil activation in the onset of OA. These initial findings were further corroborated by a recent study indicating that expression levels of TGF-ß1 and elastase were associated with radiographic severity scores and predictive of knee OA progression (288).

Based on such findings, Jayadev *et al.* used a novel machine learning approach to develop a "cytokine fingerprint" for end-stage OA. Using a panel of eight biomarkers (PIIANP, TIMP-1, ADAMTS-4, CCL2, IP-10 and TGF-β3), this model distinguishes between OA, knee injury and inflammatory knee arthritis (i.e. RA or psoriatic arthritis) with almost 100% efficacy (289). Interestingly, knee/hip arthroplasty further increases the levels of angiogenic and pro-inflammatory cytokines, but leaves anti-inflammatory cytokines unaffected, suggesting underlying changes specifically in pro-inflammatory pathways, which might be further exacerbated with surgical treatment (290).

In summary, biomarker research has both leveraged and fueled the notion that monocytes contribute to OA pathogenesis, and that OA-primed non-classical monocytes might exist. Although this progress is encouraging, the majority of recently identified biomarkers are associated with disease progression, rather than onset. There remains thus a pressing, unmet clinical need for biomarkers instrumental in diagnosis and stratification of individuals at risk of developing ptOA following knee injury.

Disease Modifying Drugs for OA: Where Are We on the Clinical and Pre-Clinical Level?

To target the early inflammatory phase that follows joint injury and initiates OA pathogenesis, adjuvant DMDs are urgently

needed. A variety of agents with the potential to serve as DMDs are currently being tested, but unfortunately, with limited success (291). Some studies on local inhibition of IL-1 in animal models showed promising results. In particular after closed articular fracture, intra-articular injection of an antagonist for IL-1 receptor (IL-1Ra) reduces post-traumatic OA, cartilage degeneration and synovitis (292–294). However, the clinical efficacy of this approach remains controversial. While an early clinical study found that intra-articular administration of IL-1Ra performed within 1 month of severe knee injury led to reduced knee pain and improved function over a 2-week follow-up period (295), other clinical studies using either IL-1Ra (Anakira) or a dual variable domain immunoglobulin that simultaneously inhibits IL-1α and IL-1β (Lutikizumab) have yielded no benefit in OA patients compared to placebo controls (291). Interestingly, retrospective secondary analysis of a large-scale clinical trial of a monoclonal antibody targeting IL-1β for cardiovascular disease found reduced incidence of hip and knee replacement in patients with high C-reactive protein, suggesting a potential effect on OA progression in an inflammatory setting (296).

It is noteworthy, that the OA-specific studies of DMD candidates described above were tested mostly in patients with advanced OA with the intention of reducing established clinical and radiological disease progression. In line with the current difficulties in risk stratification and early diagnosis outlined above, to date, no drugs have been advanced to the clinical stage that target the inflammatory response at the onset or early stages of disease. Experimentally, however, attempts to advance in this direction have been made recently. One study explored the role of incretin hormone receptors *in vitro*. It found that an analogue for the human Glucagon-Like Peptide-1 (GLP-1), liraglutide, reduced production of reactive oxygen species, IL-6 and CCL2, reduced collagen and aggrecan degradation and inhibited inflammation *via* deactivation of NF-kB signaling (297). Similarly, administration of dexamethasone, rapamycin or BMP-7 results in a more anti-inflammatory macrophage phenotype *in vitro*. Whilst these findings await *in vivo* confirmation, these drugs might hold potential of modulating synovial inflammation in patients (298).

One of the few *in vivo* studies investigating the impact of anti-inflammatory therapy immediately after joint injury utilized a porcine model. Here, the authors induced OA *via* transection of the anterior cruciate ligament (ACL) and immediately provided corticosteroids by intraarticular injection, which resulted in mitigated collagen degradation, reduced monocyte recruitment and a less inflammatory macrophage profile/phenotype (299). Our group has investigated the respective effects of intraarticular administration of hyaluronan or BM-derived mesenchymal stem cells in a murine OA model. We found that hyaluronan therapy increased anti-fibrotic macrophages and decreased pain sensitization, while treatment with MSCs did not impact pain, but led to long-term chondroprotection (300). Along similar lines, another recent study demonstrated that administration of Alpha defensin-1 renders macrophages less inflammatory and attenuates OA in a surgical model (301). Collectively, these data suggest that specific anti-inflammatory treatment immediately after knee injury might represent a promising future therapeutic approach, and thus, justify additional experimental and ultimately clinical studies.

CONCLUDING REMARKS, OPEN QUESTIONS, AND FUTURE DIRECTIONS

Distinct Inflammatory Responses in Different Joint Injuries?

Post-traumatic OA accounts for nearly 12% of all cases of symptomatic OA (302) and a recent longitudinal cohort study showed that the risk of developing OA is almost sixfold increased by knee injury at a young age (303). Further stratification of these data revealed distinct risks for different injury types: ACL injury, meniscal tears and articular fractures of the tibia (risk difference (RD) of 19.5%, 10.5% and 6.6%, respectively) were associated with the highest risk (303). In trying to identify possible reasons for these differences, the simplest explanation of variable biomechanical aberration is insufficient, as an abundance of data has shown that restoration of biomechanics alone does not prevent ptOA development (4). An alternative hypothesis is that phenotypic differences exist in the pathogenesis of ptOA depending on the type of tissue affected by injury. Thus, metabolic and immunobiological differences may determine the individual risk of developing ptOA. Although comprehensive studies investigating the tissue- and phenotype-specific immune response after joint injury are missing, existing evidence supports an immunological role for the meniscus (304), which engages in a pro-inflammatory crosstalk with the synovium in OA (305). Furthermore, synovial fluid, cartilage tissue and isolated cartilage cells display distinct pro-inflammatory cytokine profiles depending on the type of pathology, further supporting the notion that a phenotype-specific cytokine topography exists in the joint (306). Future studies should therefore be designed to examine the inflammatory reaction associated with different types of joint injury.

Could Restoring Joint Immune Homeostasis Hold the Key to OA?

Owing to decades of research, we have come to understand that OA cannot simply be attributed to "wear and tear" resulting from biomechanical changes. Rather, OA results from a complex biological response of different cells in multiple joint tissues, with "inflammation" playing a crucial role this process. Monocytes and macrophages are emerging as key players in the inflammatory process associated with OA. Circulating monocytes are particularly attractive as druggable targets, but selective targeting of tissue-resident macrophages might be equally feasible, for example using antibody-conjugated lipid nanoparticles (72). It is tempting to speculate that dysregulated dynamics between monocytes, macrophages and other cell types they cross-react with in the joint not only fuels pathology, but in fact represents an underlying cause of OA. To harness these intricate cellular interactions for diagnostic and therapeutic

purposes, we need to further improve our understanding of monocyte and macrophage biology in both healthy and arthritic joints. Deciphering their developmental and functional dynamics harbours the potential of one day being able to restore synovial immune homeostasis and thus, finally provide a causative treatment for this debilitating disease.

Can Findings From ptOA Be Translated to Other OA Phenotypes?

A wide range of small and large animal models for OA have been developed, and these have recently been reviewed (307). Far and away the most commonly used models are those induced by joint injury. They share a comparably rapid onset and highly standardized disease progression, and allow investigation of underlying molecular and cellular mechanisms, as well as evaluation of potential treatments at different stages of disease progression. However, the translation of findings made in these models to clinical settings has remained challenging (308). One explanation is the current discrepancy between preclinical research predominantly using ptOA models and clinical studies, the majority of which investigate late-stage "primary OA" which occurs in the absence of prior trauma or disease (309). There is emerging evidence that the pathophysiologic mechanisms of structural and symptomatic OA differs depending on the key initiating factors or disease phenotype (310, 311). How different the complex cellular inflammatory response is in different OA phenotypes remains to be resolved. In a first attempt to overcome this issue, findings from preclinical ptOA studies should be tested in preclinical models of primary OA, such as spontaneous age-associated and metabolic/obesity-induced disease. Whilst the associated immune response may be different in strength and spatio-temporal patterns, it is likely that at least some aspects of monocyte and macrophage biology relevant to ptOA apply to other OA phenotypes, such as their roles in ECM degradation and chondrocyte death, which are universal OA disease features. Likewise, some molecular signals identified in ptOA models as regulators of macrophage activation and polarization, such as specific cytokines and chemokines, and are also present in multiple OA phenotypes (312).

Open Questions and Future Directions for Research

- Does the initial inflammatory response following joint injury pathologically imprint monocytes, macrophages and their stromal niche in the joint?
- Do disease-specific, "imprinted" populations of monocytes and macrophages emerge prior to disease onset? Do they mediate (or: propagate) OA pathogenesis?
- Are monocyte and macrophage dynamics permanently altered following joint injury?
- Can these populations be targeted therapeutically?
- Is there an optimal ratio between pro- and anti-inflammatory monocyte/macrophage subsets that mitigates the risk of OA after joint injury?
- Can a threshold be determined that governs the future direction of either resolution of inflammation and restoration of joint function or ongoing inflammation that contributes towards development of OA?
- Do similar considerations also apply to non-traumatic forms of OA?

Addressing these questions will provide the critical scientific understanding necessary to improve diagnosis, risk prognosis, and underpin development of specific targeted therapies to prevent OA onset and/or slow its progression following joint injury. Recognizing that the targets may differ depending on injury and change with time and being able to identify these therapeutic stages/windows, will be key to providing effective individualized patient management.

AUTHOR CONTRIBUTIONS

Conception and design of study: PH, CL, BM, and RG. Acquisition of data: PH, RG, CL, and MP. Drafting of article: PH, RG, MP, CL, and BM. Revising it critically for important intellectual content: PH, RG, MP, CL, and BM. All authors have approved the final version of the manuscript.

FUNDING

The authors acknowledge salary support from the following agencies: Raymond E Purves Foundation PhD Scholarship (PH), University of Edinburgh and the Kennedy Trust for Rheumatology Research (RG, MP). The funding bodies had no input into the design, drafting, editing or content of the manuscript.

ACKNOWLEDGMENTS

We would like to acknowledge the general contribution of colleagues, institutions, and agencies that have aided the research efforts of the authors in areas related to the topic of this review.

REFERENCES

1. Spitaels D, Mamouris P, Vaes B, Smeets M, Luyten F, Hermens R, et al. Epidemiology of Knee Osteoarthritis in General Practice: A Registry-Based Study. *BMJ Open* (2020) 10(1):e031734. doi: 10.1136/bmjopen-2019-031734
2. Kloppenburg M, Berenbaum F. Osteoarthritis Year in Review 2019: Epidemiology and Therapy. *Osteoarthritis Cartilage* (2020) 28(3):242–8. doi: 10.1016/j.joca.2020.01.002
3. Vos T, Flaxman AD, Naghavi M, Lozano R, Michaud C, Ezzati M, et al. Years Lived With Disability (YLDs) for 1160 Sequelae of 289 Diseases and Injuries 1990-2010: A Systematic Analysis for the Global Burden of Disease

Study 2010. *Lancet* (2012) 380(9859):2163–96. doi: 10.1016/S0140-6736(12)61729-2
4. Barton KI, Shekarforoush M, Heard BJ, Sevick JL, Vakil P, Atarod M, et al. Use of Pre-Clinical Surgically Induced Models to Understand Biomechanical and Biological Consequences of PTOA Development. *J Orthop Res* (2017) 35(3):454–65. doi: 10.1002/jor.23322
5. Chua JR, Jamal S, Riad M, Castrejon I, Malfait AM, Block JA, et al. Disease Burden in Osteoarthritis Is Similar to That of Rheumatoid Arthritis at Initial Rheumatology Visit and Significantly Greater Six Months Later. *Arthritis Rheumatol* (2019) 71(8):1276–84. doi: 10.1002/art.40869
6. Dequeker J, Luyten FP. The History of Osteoarthritis-Osteoarthrosis. *Ann Rheum Dis* (2008) 67(1):5–10. doi: 10.1136/ard.2007.079764
7. Orlowsky EW, Kraus VB. The Role of Innate Immunity in Osteoarthritis: When Our First Line of Defense Goes on the Offensive. *J Rheumatol* (2015) 42(3):363–71. doi: 10.3899/jrheum.140382
8. Sokolove J, Lepus CM. Role of Inflammation in the Pathogenesis of Osteoarthritis: Latest Findings and Interpretations. *Ther Adv Musculoskelet Dis* (2013) 5(2):77–94. doi: 10.1177/1759720X12467868
9. Punzi L, Galozzi P, Luisetto R, Favero M, Ramonda R, Oliviero F, et al. Post-Traumatic Arthritis: Overview on Pathogenic Mechanisms and Role of Inflammation. *RMD Open* (2016) 2(2):e000279. doi: 10.1136/rmdopen-2016-000279
10. Berenbaum F. Osteoarthritis as an Inflammatory Disease (Osteoarthritis is Not Osteoarthrosis!). *Osteoarthritis Cartilage* (2013) 21(1):16–21. doi: 10.1016/j.joca.2012.11.012
11. Woodell-May JE, Sommerfeld SD. Role of Inflammation and the Immune System in the Progression of Osteoarthritis. *J Orthop Res* (2020) 38(2):253–7. doi: 10.1002/jor.24457
12. Mora JC, Przkora R, Cruz-Almeida Y. Knee Osteoarthritis: Pathophysiology and Current Treatment Modalities. *J Pain Res* (2018) 11:2189–96. doi: 10.2147/JPR.S154002
13. Schulz C, Gomez Perdiguero E, Chorro L, Szabo-Rogers H, Cagnard N, Kierdorf K, et al. A Lineage of Myeloid Cells Independent of Myb and Hematopoietic Stem Cells. *Science* (2012) 336(6077):86–90. doi: 10.1126/science.1219179
14. Hashimoto D, Chow A, Noizat C, Teo P, Beasley MB, Leboeuf M, et al. Tissue-Resident Macrophages Self-Maintain Locally Throughout Adult Life With Minimal Contribution From Circulating Monocytes. *Immunity* (2013) 38(4):792–804. doi: 10.1016/j.immuni.2013.04.004
15. Gomez Perdiguero E, Klapproth K, Schulz C, Busch K, Azzoni E, Crozet L, et al. Tissue-Resident Macrophages Originate From Yolk-Sac-Derived Erythro-Myeloid Progenitors. *Nature* (2015) 518(7540):547–51. doi: 10.1038/nature13989
16. Hoeffel G, Chen J, Lavin Y, Low D, Almeida FF, See P, et al. C-Myb(+) Erythro-Myeloid Progenitor-Derived Fetal Monocytes Give Rise to Adult Tissue-Resident Macrophages. *Immunity* (2015) 42(4):665–78. doi: 10.1016/j.immuni.2015.03.011
17. Guilliams M, Scott CL. Does Niche Competition Determine the Origin of Tissue-Resident Macrophages? *Nat Rev Immunol* (2017) 17(7):451–60. doi: 10.1038/nri.2017.42
18. Guilliams M, Thierry GR, Bonnardel J, Bajenoff M. Establishment and Maintenance of the Macrophage Niche. *Immunity* (2020) 52(3):434–51. doi: 10.1016/j.immuni.2020.02.015
19. Ginhoux F, Guilliams M. Tissue-Resident Macrophage Ontogeny and Homeostasis. *Immunity* (2016) 44(3):439–49. doi: 10.1016/j.immuni.2016.02.024
20. Culemann S, Gruneboom A, Kronke G. Origin and Function of Synovial Macrophage Subsets During Inflammatory Joint Disease. *Adv Immunol* (2019) 143:75–98. doi: 10.1016/bs.ai.2019.08.006
21. Raghu H, Lepus CM, Wang Q, Wong HH, Lingampalli N, Oliviero F, et al. CCL2/CCR2, But Not CCL5/CCR5, Mediates Monocyte Recruitment, Inflammation and Cartilage Destruction in Osteoarthritis. *Ann Rheum Dis* (2017) 76(5):914–22. doi: 10.1136/annrheumdis-2016-210426
22. Culemann S, Gruneboom A, Nicolas-Avila JA, Weidner D, Lammle KF, Rothe T, et al. Locally Renewing Resident Synovial Macrophages Provide a Protective Barrier for the Joint. *Nature* (2019) 572(7771):670–5. doi: 10.1038/s41586-019-1471-1
23. Boersema GSA, Utomo L, Bayon Y, Kops N, van der Harst E, Lange JF, et al. Monocyte Subsets in Blood Correlate With Obesity Related Response of Macrophages to Biomaterials. *Vitro Biomater* (2016) 109:32–9. doi: 10.1016/j.biomaterials.2016.09.009
24. Masouros SD, Bull AMJ. Amis AA.(i) Biomechanics of the Knee Joint. *Orthopaedics Trauma* (2010) 24(2):84–91. doi: 10.1016/j.mporth.2010.03.005
25. Blackburn TA, Craig E. Knee Anatomy: A Brief Review. *Phys Ther* (1980) 60(12):1556–60. doi: 10.1093/ptj/60.12.1556
26. Sophia Fox AJ, Bedi A, Rodeo SA. The Basic Science of Articular Cartilage: Structure, Composition, and Function. *Sports Health* (2009) 1(6):461–8. doi: 10.1177/1941738109350438
27. Alford JW, Cole BJ. Cartilage Restoration, Part 1: Basic Science, Historical Perspective, Patient Evaluation, and Treatment Options. *Am J Sports Med* (2005) 33(2):295–306. doi: 10.1177/0363546504273510
28. Hoffa A. The Influence Of The Adipose Tissue With Regard To The Pathology Of The Knee Joint. *J Am Med Assoc* (1904) XLIII(12):795–6. doi: 10.1001/jama.1904.92500120002h
29. Jiang LF, Fang JH, Wu LD. Role of Infrapatellar Fat Pad in Pathological Process of Knee Osteoarthritis: Future Applications in Treatment. *World J Clin cases* (2019) 7(16):2134–42. doi: 10.12998/wjcc.v7.i16.2134
30. Urban H, Little CB. The Role of Fat and Inflammation in the Pathogenesis and Management of Osteoarthritis. *Rheumatol (Oxford)* (2018) 57(suppl_4):iv10–21. doi: 10.1093/rheumatology/kex399
31. Kung MS, Markantonis J, Nelson SD, Campbell P. The Synovial Lining and Synovial Fluid Properties After Joint Arthroplasty. *Lubricants* (2015) 3(2):394–412. doi: 10.3390/lubricants3020394
32. Scanzello CR, Goldring SR. The Role of Synovitis in Osteoarthritis Pathogenesis. *Bone* (2012) 51(2):249–57. doi: 10.1016/j.bone.2012.02.012
33. Varol C, Mildner A, Jung S. Macrophages: Development and Tissue Specialization. *Annu Rev Immunol* (2015) 33:643–75. doi: 10.1146/annurev-immunol-032414-112220
34. Mass E, Gentek R. Fetal-Derived Immune Cells at the Roots of Lifelong Pathophysiology. *Front Cell Dev Biol* (2021) 9:648313. doi: 10.3389/fcell.2021.648313
35. Guilliams M, Mildner A, Yona S. Developmental and Functional Heterogeneity of Monocytes. *Immunity* (2018) 49(4):595–613. doi: 10.1016/j.immuni.2018.10.005
36. Fogg DK, Sibon C, Miled C, Jung S, Aucouturier P, Littman DR, et al. A Clonogenic Bone Marrow Progenitor Specific for Macrophages and Dendritic Cells. *Science* (2006) 311(5757):83–7. doi: 10.1126/science.1117729
37. Auffray C, Fogg DK, Narni-Mancinelli E, Senechal B, Trouillet C, Saederup N, et al. CX3CR1+ CD115+ CD135+ Common Macrophage/DC Precursors and the Role of CX3CR1 in Their Response to Inflammation. *J Exp Med* (2009) 206(3):595–606. doi: 10.1084/jem.20081385
38. Hettinger J, Richards DM, Hansson J, Barra MM, Joschko AC, Krijgsveld J, et al. Origin of Monocytes and Macrophages in a Committed Progenitor. *Nat Immunol* (2013) 14(8):821–30. doi: 10.1038/ni.2638
39. Chong SZ, Evrard M, Devi S, Chen J, Lim JY, See P, et al. CXCR4 Identifies Transitional Bone Marrow Premonocytes That Replenish the Mature Monocyte Pool for Peripheral Responses. *J Exp Med* (2016) 213(11):2293–314. doi: 10.1084/jem.20160800
40. Geissmann F, Jung S, Littman DR. Blood Monocytes Consist of Two Principal Subsets With Distinct Migratory Properties. *Immunity* (2003) 19(1):71–82. doi: 10.1016/s1074-7613(03)00174-2
41. Teh YC, Ding JL, Ng LG, Chong SZ. Capturing the Fantastic Voyage of Monocytes Through Time and Space. *Front Immunol* (2019) 10:834. doi: 10.3389/fimmu.2019.00834
42. Ginhoux F, Jung S. Monocytes and Macrophages: Developmental Pathways and Tissue Homeostasis. *Nat Rev Immunol* (2014) 14(6):392–404. doi: 10.1038/nri3671
43. Jakubzick C, Gautier EL, Gibbings SL, Sojka DK, Schlitzer A, Johnson TE, et al. Minimal Differentiation of Classical Monocytes as They Survey Steady-State Tissues and Transport Antigen to Lymph Nodes. *Immunity* (2013) 39(3):599–610. doi: 10.1016/j.immuni.2013.08.007
44. Jung S, Aliberti J, Graemmel P, Sunshine MJ, Kreutzberg GW, Sher A, et al. Analysis of Fractalkine Receptor CX(3)CR1 Function by Targeted Deletion and Green Fluorescent Protein Reporter Gene Insertion. *Mol Cell Biol* (2000) 20(11):4106–14. doi: 10.1128/mcb.20.11.4106-4114.2000
45. Kratofil RM, Kubes P, Deniset JF. Monocyte Conversion During Inflammation and Injury. *Arterioscler Thromb Vasc Biol* (2017) 37(1):35–42. doi: 10.1161/ATVBAHA.116.308198

46. Zhao M, Tuo H, Wang S, Zhao L. The Roles of Monocyte and Monocyte-Derived Macrophages in Common Brain Disorders. *BioMed Res Int* (2020) 2020:9396021. doi: 10.1155/2020/9396021
47. Carlin LM, Stamatiades EG, Auffray C, Hanna RN, Glover L, Vizcay-Barrena G, et al. Nr4a1-Dependent Ly6C(low) Monocytes Monitor Endothelial Cells and Orchestrate Their Disposal. *Cell* (2013) 153(2):362–75. doi: 10.1016/j.cell.2013.03.010
48. Jung H, Mithal DS, Park JE, Miller RJ. Localized CCR2 Activation in the Bone Marrow Niche Mobilizes Monocytes by Desensitizing Cxcr4. *PloS One* (2015) 10(6):e0128387. doi: 10.1371/journal.pone.0128387
49. Liu Q, Li Z, Gao JL, Wan W, Ganesan S, McDermott DH, et al. CXCR4 Antagonist AMD3100 Redistributes Leukocytes From Primary Immune Organs to Secondary Immune Organs, Lung, and Blood in Mice. *Eur J Immunol* (2015) 45(6):1855–67. doi: 10.1002/eji.201445245
50. Tsou CL, Peters W, Si Y, Slaymaker S, Aslanian AM, Weisberg SP, et al. Critical Roles for CCR2 and MCP-3 in Monocyte Mobilization From Bone Marrow and Recruitment to Inflammatory Sites. *J Clin Invest* (2007) 117 (4):902–9. doi: 10.1172/JCI29919
51. Serbina NV, Pamer EG. Monocyte Emigration From Bone Marrow During Bacterial Infection Requires Signals Mediated by Chemokine Receptor CCR2. *Nat Immunol* (2006) 7(3):311–7. doi: 10.1038/ni1309
52. Debien E, Mayol K, Biajoux V, Daussy C, De Aguero MG, Taillardet M, et al. S1PR5 is Pivotal for the Homeostasis of Patrolling Monocytes. *Eur J Immunol* (2013) 43(6):1667–75. doi: 10.1002/eji.201343312
53. Yona S, Kim KW, Wolf Y, Mildner A, Varol D, Breker M, et al. Fate Mapping Reveals Origins and Dynamics of Monocytes and Tissue Macrophages Under Homeostasis. *Immunity* (2013) 38(1):79–91. doi: 10.1016/j.immuni.2012.12.001
54. Scott CL, Zheng F, De Baetselier P, Martens L, Saeys Y, De Prijck S, et al. Bone Marrow-Derived Monocytes Give Rise to Self-Renewing and Fully Differentiated Kupffer Cells. *Nat Commun* (2016) 7:10321. doi: 10.1038/ncomms10321
55. Varol C, Landsman L, Fogg DK, Greenshtein L, Gildor B, Margalit R, et al. Monocytes Give Rise to Mucosal, But Not Splenic, Conventional Dendritic Cells. *J Exp Med* (2007) 204(1):171–80. doi: 10.1084/jem.20061011
56. Hanna RN, Carlin LM, Hubbeling HG, Nackiewicz D, Green AM, Punt JA, et al. The Transcription Factor NR4A1 (Nur77) Controls Bone Marrow Differentiation and the Survival of Ly6C- Monocytes. *Nat Immunol* (2011) 12(8):778–85. doi: 10.1038/ni.2063
57. Gamrekelashvili J, Giagnorio R, Jussofie J, Soehnlein O, Duchene J, Briseno CG, et al. Regulation of Monocyte Cell Fate by Blood Vessels Mediated by Notch Signalling. *Nat Commun* (2016) 7:12597. doi: 10.1038/ncomms12597
58. Narasimhan PB, Marcovecchio P, Hamers AAJ, Hedrick CC. Nonclassical Monocytes in Health and Disease. *Annu Rev Immunol* (2019) 37:439–56. doi: 10.1146/annurev-immunol-042617-053119
59. Schmidl C, Renner K, Peter K, Eder R, Lassmann T, Balwierz PJ, et al. Transcription and Enhancer Profiling in Human Monocyte Subsets. *Blood* (2014) 123(17):e90–9. doi: 10.1182/blood-2013-02-484188
60. Buenrostro JD, Corces MR, Lareau CA, Wu B, Schep AN, Aryee MJ, et al. Integrated Single-Cell Analysis Maps the Continuous Regulatory Landscape of Human Hematopoietic Differentiation. *Cell* (2018) 173(6):1535–48 e16. doi: 10.1016/j.cell.2018.03.074
61. Quintar A, McArdle S, Wolf D, Marki A, Ehinger E, Vassallo M, et al. Endothelial Protective Monocyte Patrolling in Large Arteries Intensified by Western Diet and Atherosclerosis. *Circ Res* (2017) 120(11):1789–99. doi: 10.1161/CIRCRESAHA.117.310739
62. Thomas G, Tacke R, Hedrick CC, Hanna RN. Nonclassical Patrolling Monocyte Function in the Vasculature. *Arterioscler Thromb Vasc Biol* (2015) 35(6):1306–16. doi: 10.1161/ATVBAHA.114.304650
63. Satoh T, Nakagawa K, Sugihara F, Kuwahara R, Ashihara M, Yamane F, et al. Identification of an Atypical Monocyte and Committed Progenitor Involved in Fibrosis. *Nature* (2017) 541(7635):96–101. doi: 10.1038/nature20611
64. Epelman S, Lavine KJ, Beaudin AE, Sojka DK, Carrero JA, Calderon B, et al. Embryonic and Adult-Derived Resident Cardiac Macrophages are Maintained Through Distinct Mechanisms at Steady State and During Inflammation. *Immunity* (2014) 40(1):91–104. doi: 10.1016/j.immuni.2013.11.019
65. Bain CC, Bravo-Blas A, Scott CL, Perdiguero EG, Geissmann F, Henri S, et al. Constant Replenishment From Circulating Monocytes Maintains the Macrophage Pool in the Intestine of Adult Mice. *Nat Immunol* (2014) 15 (10):929–37. doi: 10.1038/ni.2967
66. Tamoutounour S, Guilliams M, Montanana Sanchis F, Liu H, Terhorst D, Malosse C, et al. Origins and Functional Specialization of Macrophages and of Conventional and Monocyte-Derived Dendritic Cells in Mouse Skin. *Immunity* (2013) 39(5):925–38. doi: 10.1016/j.immuni.2013.10.004
67. Tamoutounour S, Henri S, Lelouard H, de Bovis B, de Haar C, van der Woude CJ, et al. CD64 Distinguishes Macrophages From Dendritic Cells in the Gut and Reveals the Th1-Inducing Role of Mesenteric Lymph Node Macrophages During Colitis. *Eur J Immunol* (2012) 42(12):3150–66. doi: 10.1002/eji.201242847
68. Mass E, Ballesteros I, Farlik M, Halbritter F, Gunther P, Crozet L, et al. Specification of Tissue-Resident Macrophages During Organogenesis. *Science* (2016) 353(6304):353–85. doi: 10.1126/science.aaf4238
69. T'Jonck W, Guilliams M, Bonnardel J. Niche Signals and Transcription Factors Involved in Tissue-Resident Macrophage Development. *Cell Immunol* (2018) 330:43–53. doi: 10.1016/j.cellimm.2018.02.005
70. Lavin Y, Winter D, Blecher-Gonen R, David E, Keren-Shaul H, Merad M, et al. Tissue-Resident Macrophage Enhancer Landscapes are Shaped by the Local Microenvironment. *Cell* (2014) 159(6):1312–26. doi: 10.1016/j.cell.2014.11.018
71. Gosselin D, Link VM, Romanoski CE, Fonseca GJ, Eichenfield DZ, Spann NJ, et al. Environment Drives Selection and Function of Enhancers Controlling Tissue-Specific Macrophage Identities. *Cell* (2014) 159(6):1327–40. doi: 10.1016/j.cell.2014.11.023
72. Etzerodt A, Tsalkitzi K, Maniecki M, Damsky W, Delfini M, Baudoin E, et al. Specific Targeting of CD163(+) TAMs Mobilizes Inflammatory Monocytes and Promotes T Cell-Mediated Tumor Regression. *J Exp Med* (2019) 216 (10):2394–411. doi: 10.1084/jem.20182124
73. Zhu Y, Herndon JM, Sojka DK, Kim KW, Knolhoff BL, Zuo C, et al. Tissue-Resident Macrophages in Pancreatic Ductal Adenocarcinoma Originate From Embryonic Hematopoiesis and Promote Tumor Progression. *Immunity* (2017) 47(3):597. doi: 10.1016/j.immuni.2017.08.018
74. Loyher PL, Hamon P, Laviron M, Meghraoui-Kheddar A, Goncalves E, Deng Z, et al. Macrophages of Distinct Origins Contribute to Tumor Development in the Lung. *J Exp Med* (2018) 215(10):2536–53. doi: 10.1084/jem.20180534
75. Werner Y, Mass E, Ashok Kumar P, Ulas T, Handler K, Horne A, et al. Cxcr4 Distinguishes HSC-Derived Monocytes From Microglia and Reveals Monocyte Immune Responses to Experimental Stroke. *Nat Neurosci* (2020) 23(3):351–62. doi: 10.1038/s41593-020-0585-y
76. Swirski FK, Nahrendorf M, Etzrodt M, Wildgruber M, Cortez-Retamozo V, Panizzi P, et al. Identification of Splenic Reservoir Monocytes and Their Deployment to Inflammatory Sites. *Science* (2009) 325(5940):612–6. doi: 10.1126/science.1175202
77. Li L, Huang L, Sung SS, Vergis AL, Rosin DL, Rose CEJr., et al. The Chemokine Receptors CCR2 and CX3CR1 Mediate Monocyte/Macrophage Trafficking in Kidney Ischemia-Reperfusion Injury. *Kidney Int* (2008) 74 (12):1526–37. doi: 10.1038/ki.2008.500
78. Huen SC, Cantley LG. Macrophages in Renal Injury and Repair. *Annu Rev Physiol* (2017) 79:449–69. doi: 10.1146/annurev-physiol-022516-034219
79. Furuichi K, Wada T, Iwata Y, Kitagawa K, Kobayashi K, Hashimoto H, et al. CCR2 Signaling Contributes to Ischemia-Reperfusion Injury in Kidney. *J Am Soc Nephrol* (2003) 14(10):2503–15. doi: 10.1097/01.asn.0000089563.63641.a8
80. Shechter R, Raposo C, London A, Sagi I, Schwartz M. The Glial Scar-Monocyte Interplay: A Pivotal Resolution Phase in Spinal Cord Repair. *PloS One* (2011) 6(12):e27969. doi: 10.1371/journal.pone.0027969
81. Shechter R, London A, Varol C, Raposo C, Cusimano M, Yovel G, et al. Infiltrating Blood-Derived Macrophages are Vital Cells Playing an Anti-Inflammatory Role in Recovery From Spinal Cord Injury in Mice. *PloS Med* (2009) 6(7):e1000113. doi: 10.1371/journal.pmed.1000113
82. Nahrendorf M, Swirski FK, Aikawa E, Stangenberg L, Wurdinger T, Figueiredo JL, et al. The Healing Myocardium Sequentially Mobilizes Two Monocyte Subsets With Divergent and Complementary Functions. *J Exp Med* (2007) 204(12):3037–47. doi: 10.1084/jem.20070885
83. Dimitrijevic OB, Stamatovic SM, Keep RF, Andjelkovic AV. Absence of the Chemokine Receptor CCR2 Protects Against Cerebral Ischemia/Reperfusion Injury in Mice. *Stroke* (2007) 38(4):1345–53. doi: 10.1161/01.STR.0000259709.16654.8f

84. Bamboat ZM, Ocuin LM, Balachandran VP, Obaid H, Plitas G, DeMatteo RP. Conventional DCs Reduce Liver Ischemia/Reperfusion Injury in Mice. *Via IL-10 Secretion J Clin Invest* (2010) 120(2):559–69. doi: 10.1172/JCI40008
85. Spahn JH, Kreisel D. Monocytes in Sterile Inflammation: Recruitment and Functional Consequences. *Arch Immunol Ther Exp (Warsz)* (2014) 62(3):187–94. doi: 10.1007/s00005-013-0267-5
86. Robbins CS, Chudnovskiy A, Rauch PJ, Figueiredo JL, Iwamoto Y, Gorbatov R, et al. Extramedullary Hematopoiesis Generates Ly-6C(High) Monocytes That Infiltrate Atherosclerotic Lesions. *Circulation* (2012) 125(2):364–74. doi: 10.1161/CIRCULATIONAHA.111.061986
87. Zhou X, Liu XL, Ji WJ, Liu JX, Guo ZZ, Ren D, et al. The Kinetics of Circulating Monocyte Subsets and Monocyte-Platelet Aggregates in the Acute Phase of ST-Elevation Myocardial Infarction: Associations With 2-Year Cardiovascular Events. *Med (Baltimore)* (2016) 95(18):e3466. doi: 10.1097/MD.0000000000003466
88. Rahman K, Vengrenyuk Y, Ramsey SA, Vila NR, Girgis NM, Liu J, et al. Inflammatory Ly6Chi Monocytes and Their Conversion to M2 Macrophages Drive Atherosclerosis Regression. *J Clin Invest* (2017) 127(8):2904–15. doi: 10.1172/JCI75005
89. Gautier EL, Shay T, Miller J, Greter M, Jakubzick C, Ivanov S, et al. Gene-Expression Profiles and Transcriptional Regulatory Pathways That Underlie the Identity and Diversity of Mouse Tissue Macrophages. *Nat Immunol* (2012) 13(11):1118–28. doi: 10.1038/ni.2419
90. Haldar M, Kohyama M, So AY, Kc W, Wu X, Briseno CG, et al. Heme-Mediated SPI-C Induction Promotes Monocyte Differentiation Into Iron-Recycling Macrophages. *Cell* (2014) 156(6):1223–34. doi: 10.1016/j.cell.2014.01.069
91. van de Laar L, Saelens W, De Prijck S, Martens L, Scott CL, Van Isterdael G, et al. Yolk Sac Macrophages, Fetal Liver, and Adult Monocytes Can Colonize an Empty Niche and Develop Into Functional Tissue-Resident Macrophages. *Immunity* (2016) 44(4):755–68. doi: 10.1016/j.immuni.2016.02.017
92. Gordon S, Martinez FO. Alternative Activation of Macrophages: Mechanism and Functions. *Immunity* (2010) 32(5):593–604. doi: 10.1016/j.immuni.2010.05.007
93. Sica A, Mantovani A. Macrophage Plasticity and Polarization: *In Vivo* Veritas. *J Clin Invest* (2012) 122(3):787–95. doi: 10.1172/JCI59643
94. Hume DA. The Many Alternative Faces of Macrophage Activation. *Front Immunol* (2015) 6:370. doi: 10.3389/fimmu.2015.00370
95. Murray PJ. Macrophage Polarization. *Annu Rev Physiol* (2017) 79:541–66. doi: 10.1146/annurev-physiol-022516-034339
96. Martinez FO, Gordon S. The M1 and M2 Paradigm of Macrophage Activation: Time for Reassessment. *F1000Prime Rep* (2014) 6:13. doi: 10.12703/P6-13
97. Xue J, Schmidt SV, Sander J, Draffehn A, Krebs W, Quester I, et al. Transcriptome-Based Network Analysis Reveals a Spectrum Model of Human Macrophage Activation. *Immunity* (2014) 40(2):274–88. doi: 10.1016/j.immuni.2014.01.006
98. Wiktor-Jedrzejczak W, Bartocci A, Ferrante AWJr., Ahmed-Ansari A, Sell KW, Pollard JW, et al. Total Absence of Colony-Stimulating Factor 1 in the Macrophage-Deficient Osteopetrotic (Op/Op) Mouse. *Proc Natl Acad Sci U.S.A.* (1990) 87(12):4828–32. doi: 10.1073/pnas.87.12.4828
99. Cecchini MG, Dominguez MG, Mocci S, Wetterwald A, Felix R, Fleisch H, et al. Role of Colony Stimulating Factor-1 in the Establishment and Regulation of Tissue Macrophages During Postnatal Development of the Mouse. *Development* (1994) 120(6):1357–72. doi: 10.1242/dev.120.6.1357
100. Dai XM, Ryan GR, Hapel AJ, Dominguez MG, Russell RG, Kapp S, et al. Targeted Disruption of the Mouse Colony-Stimulating Factor 1 Receptor Gene Results in Osteopetrosis, Mononuclear Phagocyte Deficiency, Increased Primitive Progenitor Cell Frequencies, and Reproductive Defects. *Blood* (2002) 99(1):111–20. doi: 10.1182/blood.v99.1.111
101. Bonnardel J, T'Jonck W, Gaublomme D, Browaeys R, Scott CL, Martens L, et al. Stellate Cells, Hepatocytes, and Endothelial Cells Imprint the Kupffer Cell Identity on Monocytes Colonizing the Liver Macrophage Niche. *Immunity* (2019) 51(4):638–54 e9. doi: 10.1016/j.immuni.2019.08.017
102. Bellomo A, Mondor I, Spinelli L, Lagueyrie M, Stewart BJ, Brouilly N, et al. Reticular Fibroblasts Expressing the Transcription Factor WT1 Define a Stromal Niche That Maintains and Replenishes Splenic Red Pulp Macrophages. *Immunity* (2020) 53(1):127–42 e7. doi: 10.1016/j.immuni.2020.06.008
103. Mortha A, Chudnovskiy A, Hashimoto D, Bogunovic M, Spencer SP, Belkaid Y, et al. Microbiota-Dependent Crosstalk Between Macrophages and ILC3 Promotes Intestinal Homeostasis. *Science* (2014) 343(6178):1249288. doi: 10.1126/science.1249288
104. Kana V, Desland FA, Casanova-Acebes M, Ayata P, Badimon A, Nabel E, et al. CSF-1 Controls Cerebellar Microglia and is Required for Motor Function and Social Interaction. *J Exp Med* (2019) 216(10):2265–81. doi: 10.1084/jem.20182037
105. Muller PA, Koscso B, Rajani GM, Stevanovic K, Berres ML, Hashimoto D, et al. Crosstalk Between Muscularis Macrophages and Enteric Neurons Regulates Gastrointestinal Motility. *Cell* (2014) 158(2):300–13. doi: 10.1016/j.cell.2014.04.050
106. Yoshida M, Ikegami M, Reed JA, Chroneos ZC, Whitsett JA. GM-CSF Regulates Protein and Lipid Catabolism by Alveolar Macrophages. *Am J Physiol Lung Cell Mol Physiol* (2001) 280(3):L379–86. doi: 10.1152/ajplung.2001.280.3.L379
107. Guilliams M, De Kleer I, Henri S, Post S, Vanhoutte L, De Prijck S, et al. Alveolar Macrophages Develop From Fetal Monocytes That Differentiate Into Long-Lived Cells in the First Week of Life *via* GM-CSF. *J Exp Med* (2013) 210(10):1977–92. doi: 10.1084/jem.20131199
108. De Schepper S, Verheijden S, Aguilera-Lizarraga J, Viola MF, Boesmans W, Stakenborg N, et al. Self-Maintaining Gut Macrophages Are Essential for Intestinal Homeostasis. *Cell* (2018) 175(2):400–15.e13. doi: 10.1016/j.cell.2018.07.048
109. Hulsmans M, Clauss S, Xiao L, Aguirre AD, King KR, Hanley A, et al. Macrophages Facilitate Electrical Conduction in the Heart. *Cell* (2017) 169(3):510–22 e20. doi: 10.1016/j.cell.2017.03.050
110. Bergh A, Damber JE, van Rooijen N. Liposome-Mediated Macrophage Depletion: An Experimental Approach to Study the Role of Testicular Macrophages in the Rat. *J Endocrinol* (1993) 136(3):407–13. doi: 10.1677/joe.0.1360407
111. Hutson JC, Garner CW, Doris PA. Purification and Characterization of a Lipophilic Factor From Testicular Macrophages That Stimulates Testosterone Production by Leydig Cells. *J Androl* (1996) 17(5):502–8.
112. Lukyanenko YO, Chen JJ, Hutson JC. Production of 25-Hydroxycholesterol by Testicular Macrophages and its Effects on Leydig Cells. *Biol Reprod* (2001) 64(3):790–6. doi: 10.1095/biolreprod64.3.790
113. Yahara Y, Barrientos T, Tang YJ, Puviindran V, Nadesan P, Zhang H, et al. Erythromyeloid Progenitors Give Rise to a Population of Osteoclasts That Contribute to Bone Homeostasis and Repair. *Nat Cell Biol* (2020) 22(1):49–59. doi: 10.1038/s41556-019-0437-8
114. Jacome-Galarza CE, Percin GI, Muller JT, Mass E, Lazarov T, Eitler J, et al. Developmental Origin, Functional Maintenance and Genetic Rescue of Osteoclasts. *Nature* (2019) 568(7753):541–5. doi: 10.1038/s41586-019-1105-7
115. McDonald MM, Khoo WH, Ng PY, Xiao Y, Zamerli J, Thatcher P, et al. Osteoclasts Recycle *via* Osteomorphs During RANKL-Stimulated Bone Resorption. *Cell* (2021) 184(5):1330–47 e13. doi: 10.1016/j.cell.2021.02.002
116. Cox N, Geissmann F. Macrophage Ontogeny in the Control of Adipose Tissue Biology. *Curr Opin Immunol* (2020) 62:1–8. doi: 10.1016/j.coi.2019.08.002
117. Zeyda M, Farmer D, Todoric J, Aszmann O, Speiser M, Gyori G, et al. Human Adipose Tissue Macrophages are of an Anti-Inflammatory Phenotype But Capable of Excessive Pro-Inflammatory Mediator Production. *Int J Obes (Lond)* (2007) 31(9):1420–8. doi: 10.1038/sj.ijo.0803632
118. Cox N, Crozet L, Holtman IR, Loyher PL, Lazarov T, White JB, et al. Diet-Regulated Production of PDGFcc by Macrophages Controls Energy Storage. *bioRxiv* (2021) 373(6550):eabe9383. doi: 10.1126/science.abe9383
119. Barboza E, Hudson J, Chang WP, Kovats S, Towner RA, Silasi-Mansat R, et al. Profibrotic Infrapatellar Fat Pad Remodeling Without M1 Macrophage Polarization Precedes Knee Osteoarthritis in Mice With Diet-Induced Obesity. *Arthritis Rheumatol* (2017) 69(6):1221–32. doi: 10.1002/art.40056
120. Fujisaka S, Usui I, Bukhari A, Ikutani M, Oya T, Kanatani Y, et al. Regulatory Mechanisms for Adipose Tissue M1 and M2 Macrophages in Diet-Induced Obese Mice. *Diabetes* (2009) 58(11):2574–82. doi: 10.2337/db08-1475
121. Iwata M, Ochi H, Hara Y, Tagawa M, Koga D, Okawa A, et al. Initial Responses of Articular Tissues in a Murine High-Fat Diet-Induced

Osteoarthritis Model: Pivotal Role of the IPFP as a Cytokine Fountain. *PloS One* (2013) 8(4):e60706. doi: 10.1371/journal.pone.0060706
122. Harasymowicz NS, Clement ND, Azfer A, Burnett R, Salter DM, Simpson A. Regional Differences Between Perisynovial and Infrapatellar Adipose Tissue Depots and Their Response to Class II and Class III Obesity in Patients With Osteoarthritis. *Arthritis Rheumatol* (2017) 69(7):1396–406. doi: 10.1002/art.40102
123. Warmink K, Kozijn AE, Bobeldijk I, Stoop R, Weinans H, Korthagen NM. High-Fat Feeding Primes the Mouse Knee Joint to Develop Osteoarthritis and Pathologic Infrapatellar Fat Pad Changes After Surgically Induced Injury. *Osteoarthritis Cartilage* (2020) 28(5):593–602. doi: 10.1016/j.joca.2020.03.008
124. Kurowska-Stolarska M, Alivernini S. Synovial Tissue Macrophages: Friend or Foe? *RMD Open* (2017) 3(2):e000527. doi: 10.1136/rmdopen-2017-000527
125. de Lange-Brokaar BJE, Ioan-Facsinay A, van Osch GJVM, Zuurmond AM, Schoones J, Toes REM, et al. Synovial Inflammation, Immune Cells and Their Cytokines in Osteoarthritis: A Review. *Osteoarthritis Cartilage* (2012) 20(12):1484–99. doi: 10.1016/j.joca.2012.08.027
126. Buckley CD, Ospelt C, Gay S, Midwood KS. Location, Location, Location: How the Tissue Microenvironment Affects Inflammation in RA. *Nat Rev Rheumatol* (2021) 17(4):195–212. doi: 10.1038/s41584-020-00570-2
127. Ambarus CA, Noordenbos T, de Hair MJ, Tak PP, Baeten DL. Intimal Lining Layer Macrophages But Not Synovial Sublining Macrophages Display an IL-10 Polarized-Like Phenotype in Chronic Synovitis. *Arthritis Res Ther* (2012) 14(2):R74. doi: 10.1186/ar3796
128. Fonseca JE, Edwards JC, Blades S, Goulding NJ. Macrophage Subpopulations in Rheumatoid Synovium: Reduced CD163 Expression in CD4+ T Lymphocyte-Rich Microenvironments. *Arthritis Rheum* (2002) 46 (5):1210–6. doi: 10.1002/art.10207
129. Smith MD, Barg E, Weedon H, Papengelis V, Smeets T, Tak PP, et al. Microarchitecture and Protective Mechanisms in Synovial Tissue From Clinically and Arthroscopically Normal Knee Joints. *Ann Rheum Dis* (2003) 62(4):303–7. doi: 10.1136/ard.62.4.303
130. Buechler MB, Kim KW, Onufer EJ, Williams JW, Little CC, Dominguez CX, et al. A Stromal Niche Defined by Expression of the Transcription Factor WT1 Mediates Programming and Homeostasis of Cavity-Resident Macrophages. *Immunity* (2019) 51(1):119–30 e5. doi: 10.1016/j.immuni.2019.05.010
131. Alivernini S, MacDonald L, Elmesmari A, Finlay S, Tolusso B, Gigante MR, et al. Distinct Synovial Tissue Macrophage Subsets Regulate Inflammation and Remission in Rheumatoid Arthritis. *Nat Med* (2020) 26(8):1295–306. doi: 10.1038/s41591-020-0939-8
132. Croft AP, Campos J, Jansen K, Turner JD, Marshall J, Attar M, et al. Distinct Fibroblast Subsets Drive Inflammation and Damage in Arthritis. *Nature* (2019) 570(7760):246–51. doi: 10.1038/s41586-019-1263-7
133. Schuster R, Rockel JS, Kapoor M, Hinz B. The Inflammatory Speech of Fibroblasts. *Immunol Rev* (2021) 302:126–46. doi: 10.1111/imr.12971
134. Hannemann N, Apparailly F, Courties G. Synovial Macrophages: From Ordinary Eaters to Extraordinary Multitaskers. *Trends Immunol* (2021) 42 (5):368–71. doi: 10.1016/j.it.2021.03.002
135. Franklin RA. Fibroblasts and Macrophages: Collaborators in Tissue Homeostasis. *Immunol Rev* (2021) 302:86–103. doi: 10.1111/imr.12989
136. Ryan GR, Dai X-M, Dominguez MG, Tong W, Chuan F, Chisholm O, et al. Rescue of the Colony-Stimulating Factor 1 (CSF-1)–Nullizygous Mouse (Csf1op/Csf1op) Phenotype With a CSF-1 Transgene and Identification of Sites of Local CSF-1 Synthesis. *Blood* (2001) 98(1):74–84. doi: 10.1182/blood.V98.1.74
137. Adlerz KM, Aranda-Espinoza H, Hayenga HN. Substrate Elasticity Regulates the Behavior of Human Monocyte-Derived Macrophages. *Eur Biophys J* (2016) 45(4):301–9. doi: 10.1007/s00249-015-1096-8
138. Escolano JC, Taubenberger AV, Abuhattum S, Schweitzer C, Farrukh A, Del Campo A, et al. Compliant Substrates Enhance Macrophage Cytokine Release and NLRP3 Inflammasome Formation During Their Pro-Inflammatory Response. *Front Cell Dev Biol* (2021) 9:639815. doi: 10.3389/fcell.2021.639815
139. Maruyama K, Nemoto E, Yamada S. Mechanical Regulation of Macrophage Function - Cyclic Tensile Force Inhibits NLRP3 Inflammasome-Dependent IL-1beta Secretion in Murine Macrophages. *Inflamm Regener* (2019) 39:3. doi: 10.1186/s41232-019-0092-2
140. O'Conor CJ, Ramalingam S, Zelenski NA, Benefield HC, Rigo I, Little D, et al. Cartilage-Specific Knockout of the Mechanosensory Ion Channel TRPV4 Decreases Age-Related Osteoarthritis. *Sci Rep* (2016) 6(1):29053. doi: 10.1038/srep29053
141. Lv Z, Xu X, Sun Z, Yang YX, Guo H, Li J, et al. TRPV1 Alleviates Osteoarthritis by Inhibiting M1 Macrophage Polarization *via* Ca2+/CaMKII/Nrf2 Signaling Pathway. *Cell Death Dis* (2021) 12(6):504. doi: 10.1038/s41419-021-03792-8
142. Michalick L, Kuebler WM. Trpv4—A Missing Link Between Mechanosensation and Immunity. *Front Immunol* (2020) 11:413(413). doi: 10.3389/fimmu.2020.00413
143. Arya RK, Goswami R, Rahaman SO. Mechanotransduction via a TRPV4-Rac1 Signaling Axis Plays a Role in Multinucleated Giant Cell Formation. *J Biol Chem* (2020) 296:100–29. doi: 10.1074/jbc.RA120.014597
144. Bhattaram P, Chandrasekharan U. The Joint Synovium: A Critical Determinant of Articular Cartilage Fate in Inflammatory Joint Diseases. *Semin Cell Dev Biol* (2017) 62:86–93. doi: 10.1016/j.semcdb.2016.05.009
145. Kennedy A, Fearon U, Veale DJ, Godson C. Macrophages in Synovial Inflammation. *Front Immunol* (2011) 2:52. doi: 10.3389/fimmu.2011.00052
146. van Lent PL, Licht R, Dijkman H, Holthuysen AE, Berden JH, van den Berg WB. Uptake of Apoptotic Leukocytes by Synovial Lining Macrophages Inhibits Immune Complex-Mediated Arthritis. *J Leukoc Biol* (2001) 70 (5):708–14.
147. Goldring MB, Otero M. Inflammation in Osteoarthritis. *Curr Opin Rheumatol* (2011) 23(5):471–8. doi: 10.1097/BOR.0b013e328349c2b1
148. Mills CD, Kincaid K, Alt JM, Heilman MJ. Hill AM. M-1/M-2 Macrophages and the Th1/Th2 Paradigm. *J Immunol* (2000) 164(12):6166–73. doi: 10.4049/jimmunol.164.12.6166
149. Wu CL, McNeill J, Goon K, Little D, Kimmerling K, Huebner J, et al. Conditional Macrophage Depletion Increases Inflammation and Does Not Inhibit the Development of Osteoarthritis in Obese Macrophage Fas-Induced Apoptosis-Transgenic Mice. *Arthritis Rheumatol* (2017) 69 (9):1772–83. doi: 10.1002/art.40161
150. Tu J, Wang X, Gong X, Hong W, Han D, Fang Y, et al. Synovial Macrophages in Rheumatoid Arthritis: The Past, Present, and Future. *Mediators Inflammation* (2020) 2020:1583647–. doi: 10.1155/2020/1583647
151. Udalova IA, Mantovani A, Feldmann M. Macrophage Heterogeneity in the Context of Rheumatoid Arthritis. *Nat Rev Rheumatol* (2016) 12(8):472–85. doi: 10.1038/nrrheum.2016.91
152. Shi C, Pamer EG. Monocyte Recruitment During Infection and Inflammation. *Nat Rev Immunol* (2011) 11(11):762–74. doi: 10.1038/nri3070
153. Fernandes JC, Martel-Pelletier J, Pelletier JP. The Role of Cytokines in Osteoarthritis Pathophysiology. *Biorheology* (2002) 39(1-2):237–46.
154. Schlaak JF, Pfers I, Meyer Zum Buschenfelde KH, Marker-Hermann E. Different Cytokine Profiles in the Synovial Fluid of Patients With Osteoarthritis, Rheumatoid Arthritis and Seronegative Spondylarthropathies. *Clin Exp Rheumatol* (1996) 14(2):155–62.
155. Blom AB, van der Kraan PM, van den Berg WB. Cytokine Targeting in Osteoarthritis. *Curr Drug Targets* (2007) 8(2):283–92. doi: 10.2174/138945007779940179
156. Cui J, Chen Y, Wang HY, Wang RF. Mechanisms and Pathways of Innate Immune Activation and Regulation in Health and Cancer. *Hum Vaccin Immunother* (2014) 10(11):3270–85. doi: 10.4161/21645515.2014.979640
157. Huard B, Schneider P, Mauri D, Tschopp J, French LE. T Cell Costimulation by the TNF Ligand BAFF. *J Immunol* (2001) 167(11):6225–31. doi: 10.4049/jimmunol.167.11.6225
158. Chen M, Lin X, Liu Y, Li Q, Deng Y, Liu Z, et al. The Function of BAFF on T Helper Cells in Autoimmunity. *Cytokine Growth Factor Rev* (2014) 25 (3):301–5. doi: 10.1016/j.cytogfr.2013.12.011
159. Lai Kwan Lam Q, King Hung Ko O, Zheng BJ, Lu L. Local BAFF Gene Silencing Suppresses Th17-Cell Generation and Ameliorates Autoimmune Arthritis. *Proc Natl Acad Sci U.S.A.* (2008) 105(39):14993–8. doi: 10.1073/pnas.0806044105
160. Zheng SG, Wang J, Horwitz DA. Cutting Edge: Foxp3+CD4+CD25+ Regulatory T Cells Induced by IL-2 and TGF-Beta are Resistant to Th17

Conversion by IL-6. *J Immunol* (2008) 180(11):7112–6. doi: 10.4049/jimmunol.180.11.7112
161. Serada S, Fujimoto M, Mihara M, Koike N, Ohsugi Y, Nomura S, et al. IL-6 Blockade Inhibits the Induction of Myelin Antigen-Specific Th17 Cells and Th1 Cells in Experimental Autoimmune Encephalomyelitis. *Proc Natl Acad Sci USA* (2008) 105(26):9041–6. doi: 10.1073/pnas.0802218105
162. Bosello S, Youinou P, Daridon C, Tolusso B, Bendaoud B, Pietrapertosa D, et al. Concentrations of BAFF Correlate With Autoantibody Levels, Clinical Disease Activity, and Response to Treatment in Early Rheumatoid Arthritis. *J Rheumatol* (2008) 35(7):1256–64.
163. Wei F, Chang Y, Wei W. The Role of BAFF in the Progression of Rheumatoid Arthritis. *Cytokine* (2015) 76(2):537–44. doi: 10.1016/j.cyto.2015.07.014
164. Weyand CM. Immunopathologic Aspects of Rheumatoid Arthritis: Who is the Conductor and Who Plays the Immunologic Instrument? *J Rheumatol Suppl* (2007) 79:9–14.
165. Seyler TM, Park YW, Takemura S, Bram RJ, Kurtin PJ, Goronzy JJ, et al. BLyS and APRIL in Rheumatoid Arthritis. *J Clin Invest* (2005) 115(11):3083–92. doi: 10.1172/JCI25265
166. Yang L, Chen Z, Guo H, Wang Z, Sun K, Yang X, et al. Extensive Cytokine Analysis in Synovial Fluid of Osteoarthritis Patients. *Cytokine* (2021) 143:155546. doi: 10.1016/j.cyto.2021.155546
167. Kouskoff V, Korganow AS, Duchatelle V, Degott C, Benoist C, Mathis D. Organ-Specific Disease Provoked by Systemic Autoimmunity. *Cell* (1996) 87(5):811–22. doi: 10.1016/s0092-8674(00)81989-3
168. Korganow AS, Ji H, Mangialaio S, Duchatelle V, Pelanda R, Martin T, et al. From Systemic T Cell Self-Reactivity to Organ-Specific Autoimmune Disease *via* Immunoglobulins. *Immunity* (1999) 10(4):451–61. doi: 10.1016/s1074-7613(00)80045-x
169. Misharin AV, Cuda CM, Saber R, Turner JD, Gierut AK, Haines GK3rd, et al. Nonclassical Ly6C(-) Monocytes Drive the Development of Inflammatory Arthritis in Mice. *Cell Rep* (2014) 9(2):591–604. doi: 10.1016/j.celrep.2014.09.032
170. Brunet A, LeBel M, Egarnes B, Paquet-Bouchard C, Lessard AJ, Brown JP, et al. NR4A1-Dependent Ly6C(low) Monocytes Contribute to Reducing Joint Inflammation in Arthritic Mice Through Treg Cells. *Eur J Immunol* (2016) 46(12):2789–800. doi: 10.1002/eji.201646406
171. Anderson DD, Chubinskaya S, Guilak F, Martin JA, Oegema TR, Olson SA, et al. Post-Traumatic Osteoarthritis: Improved Understanding and Opportunities for Early Intervention. *J Orthop Res* (2011) 29(6):802–9. doi: 10.1002/jor.21359
172. Lieberthal J, Sambamurthy N, Scanzello CR. Inflammation in Joint Injury and Post-Traumatic Osteoarthritis. *Osteoarthritis Cartilage* (2015) 23(11):1825–34. doi: 10.1016/j.joca.2015.08.015
173. Kandahari AM, Yang X, Dighe AS, Pan D, Cui Q. Recognition of Immune Response for the Early Diagnosis and Treatment of Osteoarthritis. *J Immunol Res* (2015) 2015:192415. doi: 10.1155/2015/192415
174. Jackson MT, Moradi B, Zaki S, Smith MM, McCracken S, Smith SM, et al. Depletion of Protease-Activated Receptor 2 But Not Protease-Activated Receptor 1 may Confer Protection Against Osteoarthritis in Mice Through Extracartilaginous Mechanisms. *Arthritis Rheumatol* (2014) 66(12):3337–48. doi: 10.1002/art.38876
175. Chen L, Zheng JJY, Li G, Yuan J, Ebert JR, Li H, et al. Pathogenesis and Clinical Management of Obesity-Related Knee Osteoarthritis: Impact of Mechanical Loading. *J Orthop Translat* (2020) 24:66–75. doi: 10.1016/j.jot.2020.05.001
176. Lotz MK, Kraus VB. New Developments in Osteoarthritis. Posttraumatic Osteoarthritis: Pathogenesis and Pharmacological Treatment Options. *Arthritis Res Ther* (2010) 12(3):211. doi: 10.1186/ar3046
177. Tacke F, Alvarez D, Kaplan TJ, Jakubzick C, Spanbroek R, Llodra J, et al. Monocyte Subsets Differentially Employ CCR2, CCR5, and CX3CR1 to Accumulate Within Atherosclerotic Plaques. *J Clin Invest* (2007) 117(1):185–94. doi: 10.1172/JCI28549
178. Conti P, DiGioacchino M. MCP-1 and RANTES are Mediators of Acute and Chronic Inflammation. *Allergy Asthma Proc* (2001) 22(3):133–7. doi: 10.2500/108854101778148737
179. Yuan GH, Masuko-Hongo K, Sakata M, Tsuruha J, Onuma H, Nakamura H, et al. The Role of C-C Chemokines and Their Receptors in Osteoarthritis. *Arthritis Rheum* (2001) 44(5):1056–70. doi: 10.1002/1529-0131(200105)44:5<1056::AID-ANR186>3.0.CO;2-U
180. Tong X, Zeng H, Gu P, Wang K, Zhang H, Lin X. Monocyte Chemoattractant Protein1 Promotes the Proliferation, Migration and Differentiation Potential of Fibroblastlike Synoviocytes *via* the PI3K/P38 Cellular Signaling Pathway. *Mol Med Rep* (2020) 21(3):1623–32. doi: 10.3892/mmr.2020.10969
181. Tu J, Hong W, Guo Y, Zhang P, Fang Y, Wang X, et al. Ontogeny of Synovial Macrophages and the Roles of Synovial Macrophages From Different Origins in Arthritis. *Front Immunol* (2019) 10:1146. doi: 10.3389/fimmu.2019.01146
182. Nadiv O, Beer Y, Goldberg M, Agar G, Loos M, Katz Y. Decreased Induction of IL-1beta in Fibroblast-Like Synoviocytes: A Possible Regulatory Mechanism Maintaining Joint Homeostasis. *Mol Immunol* (2007) 44(12):3147–54. doi: 10.1016/j.molimm.2007.02.001
183. Watt FE, Paterson E, Freidin A, Kenny M, Judge A, Saklatvala J, et al. Acute Molecular Changes in Synovial Fluid Following Human Knee Injury: Association With Early Clinical Outcomes. *Arthritis Rheumatol* (2016) 68(9):2129–40. doi: 10.1002/art.39677
184. Scanzello CR, McKeon B, Swaim BH, DiCarlo E, Asomugha EU, Kanda V, et al. Synovial Inflammation in Patients Undergoing Arthroscopic Meniscectomy: Molecular Characterization and Relationship to Symptoms. *Arthritis Rheum* (2011) 63(2):391–400. doi: 10.1002/art.30137
185. Li L, Jiang BE. Serum and Synovial Fluid Chemokine Ligand 2/Monocyte Chemoattractant Protein 1 Concentrations Correlates With Symptomatic Severity in Patients With Knee Osteoarthritis. *Ann Clin Biochem* (2015) 52(Pt 2):276–82. doi: 10.1177/0004563214545117
186. Endres M, Andreas K, Kalwitz G, Freymann U, Neumann K, Ringe J, et al. Chemokine Profile of Synovial Fluid From Normal, Osteoarthritis and Rheumatoid Arthritis Patients: CCL25, CXCL10 and XCL1 Recruit Human Subchondral Mesenchymal Progenitor Cells. *Osteoarthritis Cartilage* (2010) 18(11):1458–66. doi: 10.1016/j.joca.2010.08.003
187. Ni F, Zhang Y, Peng X, Li J. Correlation Between Osteoarthritis and Monocyte Chemotactic Protein-1 Expression: A Meta-Analysis. *J Orthop Surg Res* (2020) 15(1):516. doi: 10.1186/s13018-020-02045-2
188. Haringman JJ, Smeets TJ, Reinders-Blankert P, Tak PP. Chemokine and Chemokine Receptor Expression in Paired Peripheral Blood Mononuclear Cells and Synovial Tissue of Patients With Rheumatoid Arthritis, Osteoarthritis, and Reactive Arthritis. *Ann Rheum Dis* (2006) 65(3):294–300. doi: 10.1136/ard.2005.037176
189. Takebe K, Rai MF, Schmidt EJ, Sandell LJ. The Chemokine Receptor CCR5 Plays a Role in Post-Traumatic Cartilage Loss in Mice, But Does Not Affect Synovium and Bone. *Osteoarthritis Cartilage* (2015) 23(3):454–61. doi: 10.1016/j.joca.2014.12.002
190. Wojdasiewicz P, Poniatowski LA, Kotela A, Deszczynski J, Kotela I, Szukiewicz D. The Chemokine CX3CL1 (Fractalkine) and its Receptor CX3CR1: Occurrence and Potential Role in Osteoarthritis. *Arch Immunol Ther Exp (Warsz)* (2014) 62(5):395–403. doi: 10.1007/s00005-014-0275-0
191. Yano R, Yamamura M, Sunahori K, Takasugi K, Yamana J, Kawashima M, et al. Recruitment of CD16+ Monocytes Into Synovial Tissues is Mediated by Fractalkine and CX3CR1 in Rheumatoid Arthritis Patients. *Acta Med Okayama* (2007) 61(2):89–98. doi: 10.18926/AMO/32882
192. Yarmola EG, Shah YY, Lakes EH, Pacheco YC, Xie DF, Dobson J, et al. Use of Magnetic Capture to Identify Elevated Levels of CCL2 Following Intra-Articular Injection of Monoiodoacetate in Rats. *Connect Tissue Res* (2020) 61(5):485–97. doi: 10.1080/03008207.2019.1620223
193. Lai-Zhao Y, Pitchers KK, Appleton CT. Transient Anabolic Effects of Synovium in Early Post-Traumatic Osteoarthritis: A Novel Ex Vivo Joint Tissue Co-Culture System for Investigating Synovium-Chondrocyte Interactions. *Osteoarthritis Cartilage* (2021) 29(7):1060–70. doi: 10.1016/j.joca.2021.03.010
194. Takayanagi H. New Developments in Osteoimmunology. *Nat Rev Rheumatol* (2012) 8(11):684–9. doi: 10.1038/nrrheum.2012.167
195. Hirose S, Lin Q, Ohtsuji M, Nishimura H, Verbeek JS. Monocyte Subsets Involved in the Development of Systemic Lupus Erythematosus and Rheumatoid Arthritis. *Int Immunol* (2019) 31(11):687–96. doi: 10.1093/intimm/dxz036
196. van den Bosch MH, Blom AB, Schelbergen RF, Koenders MI, van de Loo FA, van den Berg WB, et al. Alarmin S100A9 Induces Proinflammatory and

Catabolic Effects Predominantly in the M1 Macrophages of Human Osteoarthritic Synovium. *J Rheumatol* (2016) 43(10):1874–84. doi: 10.3899/jrheum.160270
197. Cremers NAJ, van den Bosch MHJ, van Dalen S, Di Ceglie I, Ascone G, van de Loo F, et al. S100A8/A9 Increases the Mobilization of Pro-Inflammatory Ly6C(high) Monocytes to the Synovium During Experimental Osteoarthritis. *Arthritis Res Ther* (2017) 19(1):217. doi: 10.1186/s13075-017-1426-6
198. Schelbergen RF, Blom AB, van den Bosch MH, Sloetjes A, Abdollahi-Roodsaz S, Schreurs BW, et al. Alarmins S100A8 and S100A9 Elicit a Catabolic Effect in Human Osteoarthritic Chondrocytes That is Dependent on Toll-Like Receptor 4. *Arthritis Rheum* (2012) 64(5):1477–87. doi: 10.1002/art.33495
199. Zreiqat H, Belluoccio D, Smith MM, Wilson R, Rowley LA, Jones K, et al. S100A8 and S100A9 in Experimental Osteoarthritis. *Arthritis Res Ther* (2010) 12(1):R16. doi: 10.1186/ar2917
200. Mahon OR, Kelly DJ, McCarthy GM, Dunne A. Osteoarthritis-Associated Basic Calcium Phosphate Crystals Alter Immune Cell Metabolism and Promote M1 Macrophage Polarization. *Osteoarthritis Cartilage* (2020) 28 (5):603–12. doi: 10.1016/j.joca.2019.10.010
201. Schneider A, Weier M, Herderschee J, Perreau M, Calandra T, Roger T, et al. IRF5 Is a Key Regulator of Macrophage Response to Lipopolysaccharide in Newborns. *Front Immunol* (2018) 9:1597. doi: 10.3389/fimmu.2018.01597
202. Krausgruber T, Blazek K, Smallie T, Alzabin S, Lockstone H, Sahgal N, et al. IRF5 Promotes Inflammatory Macrophage Polarization and TH1-TH17 Responses. *Nat Immunol* (2011) 12(3):231–8. doi: 10.1038/ni.1990
203. Ni Z, Zhao X, Dai X, Zhao L, Xia J. The Role of Interferon Regulatory Factor 5 in Macrophage Inflammation During Osteoarthritis. *Inflammation* (2019) 42(5):1821–9. doi: 10.1007/s10753-019-01044-8
204. Alonso-Perez A, Franco-Trepat E, Guillan-Fresco M, Jorge-Mora A, Lopez V, Pino J, et al. Role of Toll-Like Receptor 4 on Osteoblast Metabolism and Function. *Front Physiol* (2018) 9:504. doi: 10.3389/fphys.2018.00504
205. Kalaitzoglou E, Lopes EBP, Fu Y, Herron JC, Flaming JM, Donovan EL, et al. TLR4 Promotes and DAP12 Limits Obesity-Induced Osteoarthritis in Aged Female Mice. *JBMR Plus* (2019) 3(4):e10079. doi: 10.1002/jbm4.10079
206. Franco-Trepat E, Guillan-Fresco M, Alonso-Perez A, Jorge-Mora A, Francisco V, Gualillo O, et al. Visfatin Connection: Present and Future in Osteoarthritis and Osteoporosis. *J Clin Med* (2019) 8(8). doi: 10.3390/jcm8081178
207. Moschen AR, Kaser A, Enrich B, Mosheimer B, Theurl M, Niederegger H, et al. Visfatin, an Adipocytokine With Proinflammatory and Immunomodulating Properties. *J Immunol* (2007) 178(3):1748–58. doi: 10.4049/jimmunol.178.3.1748
208. Dahl TB, Yndestad A, Skjelland M, Oie E, Dahl A, Michelsen A, et al. Increased Expression of Visfatin in Macrophages of Human Unstable Carotid and Coronary Atherosclerosis: Possible Role in Inflammation and Plaque Destabilization. *Circulation* (2007) 115(8):972–80. doi: 10.1161/CIRCULATIONAHA.106.665893
209. Hong EH, Yun HS, Kim J, Um HD, Lee KH, Kang CM, et al. Nicotinamide Phosphoribosyltransferase is Essential for Interleukin-1beta-Mediated Dedifferentiation of Articular Chondrocytes *via* SIRT1 and Extracellular Signal-Regulated Kinase (ERK) Complex Signaling. *J Biol Chem* (2011) 286 (32):28619–31. doi: 10.1074/jbc.M111.219832
210. Laiguillon MC, Houard X, Bougault C, Gosset M, Nourissat G, Sautet A, et al. Expression and Function of Visfatin (Nampt), an Adipokine-Enzyme Involved in Inflammatory Pathways of Osteoarthritis. *Arthritis Res Ther* (2014) 16(1):R38. doi: 10.1186/ar4467
211. Mahjoub M, Berenbaum F, Houard X. Why Subchondral Bone in Osteoarthritis? The Importance of the Cartilage Bone Interface in Osteoarthritis. *Osteoporos Int* (2012) 23 Suppl 8:S841–6. doi: 10.1007/s00198-012-2161-0
212. Brentano F, Schorr O, Ospelt C, Stanczyk J, Gay RE, Gay S, et al. Pre-B Cell Colony-Enhancing Factor/Visfatin, a New Marker of Inflammation in Rheumatoid Arthritis With Proinflammatory and Matrix-Degrading Activities. *Arthritis Rheum* (2007) 56(9):2829–39. doi: 10.1002/art.22833
213. Meier FM, Frommer KW, Peters MA, Brentano F, Lefevre S, Schroder D, et al. Visfatin/pre-B-Cell Colony-Enhancing Factor (PBEF), a Proinflammatory and Cell Motility-Changing Factor in Rheumatoid Arthritis. *J Biol Chem* (2012) 287(34):28378–85. doi: 10.1074/jbc.M111.312884
214. Evans L, Williams AS, Hayes AJ, Jones SA, Nowell M. Suppression of Leukocyte Infiltration and Cartilage Degradation by Selective Inhibition of Pre-B Cell Colony-Enhancing Factor/Visfatin/Nicotinamide Phosphoribosyltransferase: Apo866-Mediated Therapy in Human Fibroblasts and Murine Collagen-Induced Arthritis. *Arthritis Rheum* (2011) 63(7):1866–77. doi: 10.1002/art.30338
215. Paoletti A, Rohmer J, Ly B, Pascaud J, Riviere E, Seror R, et al. Monocyte/Macrophage Abnormalities Specific to Rheumatoid Arthritis Are Linked to miR-155 and Are Differentially Modulated by Different TNF Inhibitors. *J Immunol* (2019) 203(7):1766–75. doi: 10.4049/jimmunol.1900386
216. Ong SM, Hadadi E, Dang TM, Yeap WH, Tan CT, Ng TP, et al. The Pro-Inflammatory Phenotype of the Human non-Classical Monocyte Subset is Attributed to Senescence. *Cell Death Dis* (2018) 9(3):266. doi: 10.1038/s41419-018-0327-1
217. Loeser RF, Olex AL, McNulty MA, Carlson CS, Callahan MF, Ferguson CM, et al. Microarray Analysis Reveals Age-Related Differences in Gene Expression During the Development of Osteoarthritis in Mice. *Arthritis Rheum* (2012) 64(3):705–17. doi: 10.1002/art.33388
218. Rowe MA, Harper LR, McNulty MA, Lau AG, Carlson CS, Leng L, et al. Reduced Osteoarthritis Severity in Aged Mice With Deletion of Macrophage Migration Inhibitory Factor. *Arthritis Rheumatol* (2017) 69(2):352–61. doi: 10.1002/art.39844
219. Smith MD. The Normal Synovium. *Open Rheumatol J* (2011) 5:100–6. doi: 10.2174/1874312901105010100
220. Klein-Wieringa IR, de Lange-Brokaar BJ, Yusuf E, Andersen SN, Kwekkeboom JC, Kroon HM, et al. Inflammatory Cells in Patients With Endstage Knee Osteoarthritis: A Comparison Between the Synovium and the Infrapatellar Fat Pad. *J Rheumatol* (2016) 43(4):771–8. doi: 10.3899/jrheum.151068
221. Garriga C, Goff M, Paterson E, Hrusecka R, Hamid B, Alderson J, et al. Clinical and Molecular Associations With Outcomes at 2 Years After Acute Knee Injury: A Longitudinal Study in the Knee Injury Cohort at the Kennedy (KICK). *Lancet Rheumatol* (2021) 3:648–58. doi: 10.1016/S2665-9913(21)00116-8
222. Pradhan P, Vijayan V, Gueler F, Immenschuh S. Interplay of Heme With Macrophages in Homeostasis and Inflammation. *Int J Mol Sci* (2020) 21(3). doi: 10.3390/ijms21030740
223. Struglics A, Okroj M, Sward P, Frobell R, Saxne T, Lohmander LS, et al. The Complement System is Activated in Synovial Fluid From Subjects With Knee Injury and From Patients With Osteoarthritis. *Arthritis Res Ther* (2016) 18 (1):223. doi: 10.1186/s13075-016-1123-x
224. Wang Q, Rozelle AL, Lepus CM, Scanzello CR, Song JJ, Larsen DM, et al. Identification of a Central Role for Complement in Osteoarthritis. *Nat Med* (2011) 17(12):1674–9. doi: 10.1038/nm.2543
225. Cambre I, Gaublomme D, Burssens A, Jacques P, Schryvers N, De Muynck A, et al. Mechanical Strain Determines the Site-Specific Localization of Inflammation and Tissue Damage in Arthritis. *Nat Commun* (2018) 9 (1):4613. doi: 10.1038/s41467-018-06933-4
226. Otsuki S, Brinson DC, Creighton L, Kinoshita M, Sah RL, D'Lima D, et al. The Effect of Glycosaminoglycan Loss on Chondrocyte Viability: A Study on Porcine Cartilage Explants. *Arthritis Rheum* (2008) 58(4):1076–85. doi: 10.1002/art.23381
227. Quinn TM, Grodzinsky AJ, Hunziker EB, Sandy JD. Effects of Injurious Compression on Matrix Turnover Around Individual Cells in Calf Articular Cartilage Explants. *J Orthop Res* (1998) 16(4):490–9. doi: 10.1002/jor.1100160415
228. D'Lima DD, Hashimoto S, Chen PC, Colwell CWJr., Lotz MK. Impact of Mechanical Trauma on Matrix and Cells. *Clin Orthop Relat Res* (2001) 391 Suppl):S90–9. doi: 10.1097/00003086-200110001-00009
229. Maldonado M, Nam J. The Role of Changes in Extracellular Matrix of Cartilage in the Presence of Inflammation on the Pathology of Osteoarthritis. *BioMed Res Int* (2013) 2013:284873. doi: 10.1155/2013/284873
230. Adair-Kirk TL, Senior RM. Fragments of Extracellular Matrix as Mediators of Inflammation. *Int J Biochem Cell Biol* (2008) 40(6-7):1101–10. doi: 10.1016/j.biocel.2007.12.005
231. Senior RM, Hinek A, Griffin GL, Pipoly DJ, Crouch EC, Mecham RP. Neutrophils Show Chemotaxis to Type IV Collagen and its 7S Domain and

Contain a 67 kD Type IV Collagen Binding Protein With Lectin Properties. *Am J Respir Cell Mol Biol* (1989) 1(6):479–87. doi: 10.1165/ajrcmb/1.6.479
232. Duca L, Blanchevoye C, Cantarelli B, Ghoneim C, Dedieu S, Delacoux F, et al. The Elastin Receptor Complex Transduces Signals Through the Catalytic Activity of its Neu-1 Subunit. *J Biol Chem* (2007) 282(17):12484–91. doi: 10.1074/jbc.M609505200
233. Noble PW, McKee CM, Cowman M, Shin HS. Hyaluronan Fragments Activate an NF-Kappa B/I-Kappa B Alpha Autoregulatory Loop in Murine Macrophages. *J Exp Med* (1996) 183(5):2373–8. doi: 10.1084/jem.183.5.2373
234. Bonnans C, Chou J, Werb Z. Remodelling the Extracellular Matrix in Development and Disease. *Nat Rev Mol Cell Biol* (2014) 15(12):786–801. doi: 10.1038/nrm3904
235. Patel L, Sun W, Glasson SS, Morris EA, Flannery CR, Chockalingam PS. Tenascin-C Induces Inflammatory Mediators and Matrix Degradation in Osteoarthritic Cartilage. *BMC Musculoskelet Disord* (2011) 12:164. doi: 10.1186/1471-2474-12-164
236. Schaefer L, Babelova A, Kiss E, Hausser HJ, Baliova M, Krzyzankova M, et al. The Matrix Component Biglycan is Proinflammatory and Signals Through Toll-Like Receptors 4 and 2 in Macrophages. *J Clin Invest* (2005) 115 (8):2223–33. doi: 10.1172/JCI23755
237. Fan L, Wang Q, Liu R, Zong M, He D, Zhang H, et al. Citrullinated Fibronectin Inhibits Apoptosis and Promotes the Secretion of Pro-Inflammatory Cytokines in Fibroblast-Like Synoviocytes in Rheumatoid Arthritis. *Arthritis Res Ther* (2012) 14(6):R266. doi: 10.1186/ar4112
238. Newton K, Dixit VM. Signaling in Innate Immunity and Inflammation. *Cold Spring Harb Perspect Biol* (2012) 4(3). doi: 10.1101/cshperspect.a006049
239. Kim HA, Cho ML, Choi HY, Yoon CS, Jhun JY, Oh HJ, et al. The Catabolic Pathway Mediated by Toll-Like Receptors in Human Osteoarthritic Chondrocytes. *Arthritis Rheum* (2006) 54(7):2152–63. doi: 10.1002/art.21951
240. Benito MJ, Veale DJ, FitzGerald O, van den Berg WB, Bresnihan B. Synovial Tissue Inflammation in Early and Late Osteoarthritis. *Ann Rheum Dis* (2005) 64(9):1263–7. doi: 10.1136/ard.2004.025270
241. Elgueta R, Benson MJ, de Vries VC, Wasiuk A, Guo Y, Noelle RJ. Molecular Mechanism and Function of CD40/CD40L Engagement in the Immune System. *Immunol Rev* (2009) 229(1):152–72. doi: 10.1111/j.1600-065X.2009.00782.x
242. Graf D, Muller S, Korthauer U, van Kooten C, Weise C, Kroczek RA. A Soluble Form of TRAP (CD40 Ligand) is Rapidly Released After T Cell Activation. *Eur J Immunol* (1995) 25(6):1749–54. doi: 10.1002/eji.1830250639
243. Zirlik A, Maier C, Gerdes N, MacFarlane L, Soosairajah J, Bavendiek U, et al. CD40 Ligand Mediates Inflammation Independently of CD40 by Interaction With Mac-1. *Circulation* (2007) 115(12):1571–80. doi: 10.1161/CIRCULATIONAHA.106.683201
244. Perazzio SF, Soeiro-Pereira PV, Dos Santos VC, de Brito MV, Salu B, Oliva MLV, et al. Soluble CD40L is Associated With Increased Oxidative Burst and Neutrophil Extracellular Trap Release in Behcet's Disease. *Arthritis Res Ther* (2017) 19(1):235. doi: 10.1186/s13075-017-1443-5
245. Soong RS, Song L, Trieu J, Lee SY, He L, Tsai YC, et al. Direct T Cell Activation *via* CD40 Ligand Generates High Avidity CD8+ T Cells Capable of Breaking Immunological Tolerance for the Control of Tumors. *PloS One* (2014) 9(3):e93162. doi: 10.1371/journal.pone.0093162
246. Guo Y, Walsh AM, Fearon U, Smith MD, Wechalekar MD, Yin X, et al. CD40L-Dependent Pathway Is Active at Various Stages of Rheumatoid Arthritis Disease Progression. *J Immunol* (2017) 198(11):4490–501. doi: 10.4049/jimmunol.1601988
247. MacDonald KP, Nishioka Y, Lipsky PE, Thomas R. Functional CD40 Ligand is Expressed by T Cells in Rheumatoid Arthritis. *J Clin Invest* (1997) 100 (9):2404–14. doi: 10.1172/JCI119781
248. Roman-Fernandez IV, Garcia-Chagollan M, Cerpa-Cruz S, Jave-Suarez LF, Palafox-Sanchez CA, Garcia-Arellano S, et al. Assessment of CD40 and CD40L Expression in Rheumatoid Arthritis Patients, Association With Clinical Features and DAS28. *Clin Exp Med* (2019) 19(4):427–37. doi: 10.1007/s10238-019-00568-5
249. Liu MF, Chao SC, Wang CR, Lei HY. Expression of CD40 and CD40 Ligand Among Cell Populations Within Rheumatoid Synovial Compartment. *Autoimmunity* (2001) 34(2):107–13. doi: 10.3109/08916930109001958
250. Lai JH, Luo SF, Ho LJ. Targeting the CD40-CD154 Signaling Pathway for Treatment of Autoimmune Arthritis. *Cells* (2019) 8(8). doi: 10.3390/cells8080927
251. Gierut A, Perlman H, Pope RM. Innate Immunity and Rheumatoid Arthritis. *Rheum Dis Clin North Am* (2010) 36(2):271–96. doi: 10.1016/j.rdc.2010.03.004
252. Haubruck PSC, Liu Y, Moradi B, Blaker C, Clarke E, Little CB. Evaluating the Role and Origin of Pro-Inflammatory Macrophage Subsets as Part of the Cellular Immune Response During the Onset and Development of Posttraumatic Osteoarthritis in Mice. In: *ORS 2021 Annual Meeting* (2020). Virtual.
253. Pottie P, Presle N, Terlain B, Netter P, Mainard D, Berenbaum F. Obesity and Osteoarthritis: More Complex Than Predicted! *Ann Rheum Dis* (2006) 65 (11):1403–5. doi: 10.1136/ard.2006.061994
254. Datta P, Zhang Y, Parousis A, Sharma A, Rossomacha E, Endisha H, et al. High-Fat Diet-Induced Acceleration of Osteoarthritis is Associated With a Distinct and Sustained Plasma Metabolite Signature. *Sci Rep* (2017) 7 (1):8205. doi: 10.1038/s41598-017-07963-6
255. Larrañaga-Vera A, Lamuedra A, Pérez-Baos S, Prieto-Potin I, Peña L, Herrero-Beaumont G, et al. Increased Synovial Lipodystrophy Induced by High Fat Diet Aggravates Synovitis in Experimental Osteoarthritis. *Arthritis Res Ther* (2017) 19(1):264. doi: 10.1186/s13075-017-1473-z
256. Harasymowicz NS, Choi Y-R, Wu C-L, Iannucci L, Tang R, Guilak F. Intergenerational Transmission of Diet-Induced Obesity, Metabolic Imbalance, and Osteoarthritis in Mice. *Arthritis Rheumatol* (2020) 72 (4):632–44. doi: 10.1002/art.41147
257. Shen J, Abu-Amer Y, O'Keefe RJ, McAlinden A. Inflammation and Epigenetic Regulation in Osteoarthritis. *Connective Tissue Res* (2017) 58 (1):49–63. doi: 10.1080/03008207.2016.1208655
258. Raman S, FitzGerald U, Murphy JM. Interplay of Inflammatory Mediators With Epigenetics and Cartilage Modifications in Osteoarthritis. *Front Bioeng Biotechnol* (2018) 6:22. doi: 10.3389/fbioe.2018.00022
259. Hoeksema MA, de Winther MP. Epigenetic Regulation of Monocyte and Macrophage Function. *Antioxid Redox Signal* (2016) 25(14):758–74. doi: 10.1089/ars.2016.6695
260. Kapellos TS, Iqbal AJ. Epigenetic Control of Macrophage Polarisation and Soluble Mediator Gene Expression During Inflammation. *Mediators Inflammation* (2016) 2016:6591703. doi: 10.1155/2016/6591703
261. Logie C, Stunnenberg HG. Epigenetic Memory: A Macrophage Perspective. *Semin Immunol* (2016) 28(4):359–67. doi: 10.1016/j.smim.2016.06.003
262. Chen S, Yang J, Wei Y, Wei X. Epigenetic Regulation of Macrophages: From Homeostasis Maintenance to Host Defense. *Cell Mol Immunol* (2020) 17 (1):36–49. doi: 10.1038/s41423-019-0315-0
263. Soucie EL, Weng Z, Geirsdóttir L, Molawi K, Maurizio J, Fenouil R, et al. Lineage-Specific Enhancers Activate Self-Renewal Genes in Macrophages and Embryonic Stem Cells. *Science* (2016) 351(6274):aad5510. doi: 10.1126/science.aad5510
264. Heinz S, Benner C, Spann N, Bertolino E, Lin YC, Laslo P, et al. Simple Combinations of Lineage-Determining Transcription Factors Prime Cis-Regulatory Elements Required for Macrophage and B Cell Identities. *Mol Cell* (2010) 38(4):576–89. doi: 10.1016/j.molcel.2010.05.004
265. Kruidenier L, Chung CW, Cheng Z, Liddle J, Che K, Joberty G, et al. A Selective Jumonji H3K27 Demethylase Inhibitor Modulates the Proinflammatory Macrophage Response. *Nature* (2012) 488(7411):404–8. doi: 10.1038/nature11262
266. Sohn DH, Sokolove J, Sharpe O, Erhart JC, Chandra PE, Lahey LJ, et al. Plasma Proteins Present in Osteoarthritic Synovial Fluid can Stimulate Cytokine Production *via* Toll-Like Receptor 4. *Arthritis Res Ther* (2012) 14(1):R7–R. doi: 10.1186/ar3555
267. Rhoads JP, Major AS, Rathmell JC. Fine Tuning of Immunometabolism for the Treatment of Rheumatic Diseases. *Nat Rev Rheumatol* (2017) 13(5):313–20. doi: 10.1038/nrrheum.2017.54
268. Hong YH, Kong EJ. (18f)Fluoro-Deoxy-D-Glucose Uptake of Knee Joints in the Aspect of Age-Related Osteoarthritis: A Case-Control Study. *BMC Musculoskelet Disord* (2013) 14:141. doi: 10.1186/1471-2474-14-141
269. Courties A, Gualillo O, Berenbaum F, Sellam J. Metabolic Stress-Induced Joint Inflammation and Osteoarthritis. *Osteoarthritis Cartilage* (2015) 23 (11):1955–65. doi: 10.1016/j.joca.2015.05.016

270. Netea MG, Domínguez-Andrés J, Barreiro LB, Chavakis T, Divangahi M, Fuchs E, et al. Defining Trained Immunity and its Role in Health and Disease. *Nat Rev Immunol* (2020) 20(6):375–88. doi: 10.1038/s41577-020-0285-6
271. Blaker CL, Zaki S, Little CB, Clarke EC. Long-Term Effect of a Single Subcritical Knee Injury: Increasing the Risk of Anterior Cruciate Ligament Rupture and Osteoarthritis. *Am J Sports Med* (2021) 49(2):391–403. doi: 10.1177/0363546520977505
272. Wang X, Oo WM, Linklater JM. What is the Role of Imaging in the Clinical Diagnosis of Osteoarthritis and Disease Management? *Rheumatol (Oxford)* (2018) 57(suppl_4):iv51–60. doi: 10.1093/rheumatology/kex501
273. Glyn-Jones S, Palmer AJ, Agricola R, Price AJ, Vincent TL, Weinans H, et al. Osteoarthritis. *Lancet* (2015) 386(9991):376–87. doi: 10.1016/S0140-6736(14)60802-3
274. Shi J, Zhao W, Ying H, Du J, Chen J, Chen S, et al. The Relationship of Platelet to Lymphocyte Ratio and Neutrophil to Monocyte Ratio to Radiographic Grades of Knee Osteoarthritis. *Z Rheumatol* (2018) 77(6):533–7. doi: 10.1007/s00393-017-0348-7
275. Gao K, Zhu W, Liu W, Ma D, Li H, Yu W, et al. Diagnostic Value of the Blood Monocyte-Lymphocyte Ratio in Knee Osteoarthritis. *J Int Med Res* (2019) 47(9):4413–21. doi: 10.1177/0300060519860686
276. Soyocak A, Kurt H, Ozgen M, Turgut Cosan D, Colak E, Gunes HV. miRNA-146a, miRNA-155 and JNK Expression Levels in Peripheral Blood Mononuclear Cells According to Grade of Knee Osteoarthritis. *Gene* (2017) 627:207–11. doi: 10.1016/j.gene.2017.06.027
277. Taganov KD, Boldin MP, Chang KJ, Baltimore D. NF-kappaB-Dependent Induction of microRNA miR-146, an Inhibitor Targeted to Signaling Proteins of Innate Immune Responses. *Proc Natl Acad Sci U.S.A.* (2006) 103(33):12481–6. doi: 10.1073/pnas.0605298103
278. Ceppi M, Pereira PM, Dunand-Sauthier I, Barras E, Reith W, Santos MA, et al. MicroRNA-155 Modulates the Interleukin-1 Signaling Pathway in Activated Human Monocyte-Derived Dendritic Cells. *Proc Natl Acad Sci U.S.A.* (2009) 106(8):2735–40. doi: 10.1073/pnas.0811073106
279. Shi T, Shen X, Gao G. Gene Expression Profiles of Peripheral Blood Monocytes in Osteoarthritis and Analysis of Differentially Expressed Genes. *BioMed Res Int* (2019) 2019:4291689. doi: 10.1155/2019/4291689
280. Loukov D, Karampatos S, Maly MR, Bowdish DME. Monocyte Activation is Elevated in Women With Knee-Osteoarthritis and Associated With Inflammation, BMI and Pain. *Osteoarthritis Cartilage* (2018) 26(2):255–63. doi: 10.1016/j.joca.2017.10.018
281. Kriegova E, Manukyan G, Mikulkova Z, Gabcova G, Kudelka M, Gajdos P, et al. Gender-Related Differences Observed Among Immune Cells in Synovial Fluid in Knee Osteoarthritis. *Osteoarthritis Cartilage* (2018) 26(9):1247–56. doi: 10.1016/j.joca.2018.04.016
282. Liu B, Zhang M, Zhao J, Zheng M, Yang H. Imbalance of M1/M2 Macrophages is Linked to Severity Level of Knee Osteoarthritis. *Exp Ther Med* (2018) 16(6):5009–14. doi: 10.3892/etm.2018.6852
283. Allen PI, Conzemius MG, Evans RB, Kiefer K. Correlation Between Synovial Fluid Cytokine Concentrations and Limb Function in Normal Dogs and in Dogs With Lameness From Spontaneous Osteoarthritis. *Vet Surg* (2019) 48(5):770–9. doi: 10.1111/vsu.13212
284. Monibi F, Roller BL, Stoker A, Garner B, Bal S, Cook JL. Identification of Synovial Fluid Biomarkers for Knee Osteoarthritis and Correlation With Radiographic Assessment. *J Knee Surg* (2016) 29(3):242–7. doi: 10.1055/s-0035-1549022
285. Cuellar VG, Cuellar JM, Kirsch T, Strauss EJ. Correlation of Synovial Fluid Biomarkers With Cartilage Pathology and Associated Outcomes in Knee Arthroscopy. *Arthroscopy* (2016) 32(3):475–85. doi: 10.1016/j.arthro.2015.08.033
286. MacFarlane LA, Yang H, Collins JE, Jarraya M, Guermazi A, Mandl LA, et al. Association of Changes in Effusion-Synovitis With Progression of Cartilage Damage Over Eighteen Months in Patients With Osteoarthritis and Meniscal Tear. *Arthritis Rheumatol* (2019) 71(1):73–81. doi: 10.1002/art.40660
287. Haraden CA, Huebner JL, Hsueh MF, Li YJ, Kraus VB. Synovial Fluid Biomarkers Associated With Osteoarthritis Severity Reflect Macrophage and Neutrophil Related Inflammation. *Arthritis Res Ther* (2019) 21(1):146. doi: 10.1186/s13075-019-1923-x
288. Hsueh MF, Zhang X, Wellman SS, Bolognesi MP, Kraus VB. Synergistic Roles of Macrophages and Neutrophils in Osteoarthritis Progression. *Arthritis Rheumatol* (2021) 73(1):89–99. doi: 10.1002/art.41486
289. Jayadev C, Hulley P, Swales C, Snelling S, Collins G, Taylor P, et al. Synovial Fluid Fingerprinting in End-Stage Knee Osteoarthritis: A Novel Biomarker Concept. *Bone Joint Res* (2020) 9(9):623–32. doi: 10.1302/2046-3758.99.BJR-2019-0192.R1
290. Shih L, Guler N, Syed D, Hopkinson W, McComas KN, Walborn A, et al. Postoperative Changes in the Systemic Inflammatory Milieu in Older Surgical Patients. *Clin Appl Thromb Hemost* (2018) 24(4):583–8. doi: 10.1177/1076029617747412
291. Ghouri A, Conaghan PG. Update on Novel Pharmacological Therapies for Osteoarthritis. *Ther Adv Musculoskelet Dis* (2019) 11:1759720X19864492. doi: 10.1177/1759720X19864492
292. Furman BD, Mangiapani DS, Zeitler E, Bailey KN, Horne PH, Huebner JL, et al. Targeting Pro-Inflammatory Cytokines Following Joint Injury: Acute Intra-Articular Inhibition of Interleukin-1 Following Knee Injury Prevents Post-Traumatic Arthritis. *Arthritis Res Ther* (2014) 16(3):R134. doi: 10.1186/ar4591
293. Kimmerling KA, Furman BD, Mangiapani DS, Moverman MA, Sinclair SM, Huebner JL, et al. Sustained Intra-Articular Delivery of IL-1RA From a Thermally-Responsive Elastin-Like Polypeptide as a Therapy for Post-Traumatic Arthritis. *Eur Cell Mater* (2015) 29:124–39; discussion 39-40. doi: 10.22203/ecm.v029a10
294. Olson SA, Furman BD, Kraus VB, Huebner JL, Guilak F. Therapeutic Opportunities to Prevent Post-Traumatic Arthritis: Lessons From the Natural History of Arthritis After Articular Fracture. *J Orthop Res* (2015) 33(9):1266–77. doi: 10.1002/jor.22940
295. Kraus VB, Birmingham J, Stabler TV, Feng S, Taylor DC, Moorman CT, et al. 3rdEffects of Intraarticular IL1-Ra for Acute Anterior Cruciate Ligament Knee Injury: A Randomized Controlled Pilot Trial (NCT00332254). *Osteoarthritis Cartilage* (2012) 20(4):271–8. doi: 10.1016/j.joca.2011.12.009
296. Schieker M, Conaghan PG, Mindeholm L, Praestgaard J, Solomon DH, Scotti C, et al. Effects of Interleukin-1β Inhibition on Incident Hip and Knee Replacement : Exploratory Analyses From a Randomized, Double-Blind, Placebo-Controlled Trial. *Ann Intern Med* (2020) 173(7):509–15. doi: 10.7326/m20-0527
297. Mei J, Sun J, Wu J, Zheng X. Liraglutide Suppresses TNF-Alpha-Induced Degradation of Extracellular Matrix in Human Chondrocytes: A Therapeutic Implication in Osteoarthritis. *Am J Transl Res* (2019) 11(8):4800–8.
298. Utomo L, van Osch GJ, Bayon Y, Verhaar JA, Bastiaansen-Jenniskens YM. Guiding Synovial Inflammation by Macrophage Phenotype Modulation: An *In Vitro* Study Towards a Therapy for Osteoarthritis. *Osteoarthritis Cartilage* (2016) 24(9):1629–38. doi: 10.1016/j.joca.2016.04.013
299. Sieker JT, Ayturk UM, Proffen BL, Weissenberger MH, Kiapour AM, Murray MM. Immediate Administration of Intraarticular Triamcinolone Acetonide After Joint Injury Modulates Molecular Outcomes Associated With Early Synovitis. *Arthritis Rheumatol* (2016) 68(7):1637–47. doi: 10.1002/art.39631
300. Shu CC, Zaki S, Ravi V, Schiavinato A, Smith MM, Little CB. The Relationship Between Synovial Inflammation, Structural Pathology, and Pain in Post-Traumatic Osteoarthritis: Differential Effect of Stem Cell and Hyaluronan Treatment. *Arthritis Res Ther* (2020) 22(1):29. doi: 10.1186/s13075-020-2117-2
301. Xie JW, Wang Y, Xiao K, Xu H, Luo ZY, Li L, et al. Alpha Defensin-1 Attenuates Surgically Induced Osteoarthritis in Association With Promoting M1 to M2 Macrophage Polarization. *Osteoarthritis Cartilage* (2021) 4. doi: 10.1016/j.joca.2021.04.006
302. Thomas AC, Hubbard-Turner T, Wikstrom EA, Palmieri-Smith RM. Epidemiology of Posttraumatic Osteoarthritis. *J Athl Train* (2017) 52(6):491–6. doi: 10.4085/1062-6050-51.5.08
303. Snoeker B, Turkiewicz A, Magnusson K, Frobell R, Yu D, Peat G, et al. Risk of Knee Osteoarthritis After Different Types of Knee Injuries in Young Adults: A Population-Based Cohort Study. *Br J Sports Med* (2020) 54(12):725–30. doi: 10.1136/bjsports-2019-100959
304. Cook AE, Cook JL, Stoker AM. Metabolic Responses of Meniscus to IL-1beta. *J Knee Surg* (2018) 31(9):834–40. doi: 10.1055/s-0037-1615821
305. Favero M, Belluzzi E, Trisolino G, Goldring MB, Goldring SR, Cigolotti A, et al. Inflammatory Molecules Produced by Meniscus and Synovium in Early and End-Stage Osteoarthritis: A Coculture Study. *J Cell Physiol* (2019) 234(7):11176–87. doi: 10.1002/jcp.27766

306. Tsuchida AI, Beekhuizen M, t Hart MC, Radstake TR, Dhert WJ, Saris DB, et al. Cytokine Profiles in the Joint Depend on Pathology, But are Different Between Synovial Fluid, Cartilage Tissue and Cultured Chondrocytes. *Arthritis Res Ther* (2014) 16(5):441. doi: 10.1186/s13075-014-0441-0
307. Zaki S, Blaker CL, Little CB. OA Foundations - Experimental Models of Osteoarthritis. *Osteoarthritis Cartilage* (2021) 3. doi: 10.1016/j.joca.2021.03.024
308. Cucchiarini M, de Girolamo L, Filardo G, Oliveira JM, Orth P, Pape D, et al. Basic Science of Osteoarthritis. *J Exp Orthopaedics* (2016) 3(1):22. doi: 10.1186/s40634-016-0060-6
309. Little CB, Hunter DJ. Post-Traumatic Osteoarthritis: From Mouse Models to Clinical Trials. *Nat Rev Rheumatol* (2013) 9(8):485–97. doi: 10.1038/nrrheum.2013.72
310. Zaki S, Smith MM, Little CB. Pathology-Pain Relationships in Different Osteoarthritis Animal Model Phenotypes: It Matters What You Measure, When You Measure, and How You Got There. *Osteoarthritis Cartilage* (2021) 29(10):1448–61. doi: 10.1016/j.joca.2021.03.023
311. Zaki S, Smith MM, Smith SM, Little CB. Differential Patterns of Pathology in and Interaction Between Joint Tissues in Long-Term Osteoarthritis With Different Initiating Causes: Phenotype Matters. *Osteoarthritis Cartilage* (2020) 28(7):953–65. doi: 10.1016/j.joca.2020.04.009
312. Soul J, Barter MJ, Little CB, Young DA. OATargets: A Knowledge Base of Genes Associated With Osteoarthritis Joint Damage in Animals. *Ann Rheum Dis* (2020) 80(3):376–83. doi: 10.1136/annrheumdis-2020-218344

Conflict of Interest: The authors declare that the research was conducted in the absence of any commercial or financial relationships that could be construed as a potential conflict of interest.

Publisher's Note: All claims expressed in this article are solely those of the authors and do not necessarily represent those of their affiliated organizations, or those of the publisher, the editors and the reviewers. Any product that may be evaluated in this article, or claim that may be made by its manufacturer, is not guaranteed or endorsed by the publisher.

frontiers in Immunology

ORIGINAL RESEARCH
published: 09 November 2021
doi: 10.3389/fimmu.2021.765382

An Oxidative Stress-Related Gene Pair (*CCNB1/PKD1*), Competitive Endogenous RNAs, and Immune-Infiltration Patterns Potentially Regulate Intervertebral Disc Degeneration Development

*Shuai Cao[1], Hao Liu[1], Jiaxin Fan[2], Kai Yang[3], Baohui Yang[1], Jie Wang[1], Jie Li[1], Liesu Meng[4,5] and Haopeng Li[1]**

[1] Department of Orthopaedics, The Second Affiliated Hospital of Xi'an Jiaotong University, Xi'an, China, [2] Department of Neurology, The Second Affiliated Hospital of Xi'an Jiaotong University, Xi'an, China, [3] Department of Orthopaedic Surgery, Guangdong Provincial Key Laboratory of Orthopedics and Traumatology, First Affiliated Hospital of Sun Yat-sen University, Guangzhou, China, [4] National & Local Joint Engineering Research Center of Biodiagnostics and Biotherapy, The Second Affiliated Hospital of Xi'an Jiaotong University, Xi'an, China, [5] Key Laboratory of Environment and Genes Related to Diseases, Ministry of Education of China, Xi'an, China

OPEN ACCESS

Edited by:
Matthew William Grol, Western University, Canada

Reviewed by:
Cheryle Seguin, Western University, Canada
Shatovisha Dey, Christiana Care Health System, United States

***Correspondence:**
Haopeng Li
lihaopeng3993@163.com

Specialty section:
This article was submitted to Inflammation, a section of the journal Frontiers in Immunology

Received: *27 August 2021*
Accepted: *25 October 2021*
Published: *09 November 2021*

Citation:
Cao S, Liu H, Fan J, Yang K, Yang B, Wang J, Li J, Meng L and Li H (2021) An Oxidative Stress-Related Gene Pair (CCNB1/PKD1), Competitive Endogenous RNAs, and Immune-Infiltration Patterns Potentially Regulate Intervertebral Disc Degeneration Development. Front. Immunol. 12:765382. doi: 10.3389/fimmu.2021.765382

Oxidative stress (OS) irreversibly affects the pathogenesis of intervertebral disc degeneration (IDD). Certain non-coding RNAs act as competitive endogenous RNAs (ceRNAs) that regulate IDD progression. Analyzing the signatures of oxidative stress-related gene (OSRG) pairs and regulatory ceRNA mechanisms and immune-infiltration patterns associated with IDD may enable researchers to distinguish IDD and reveal the underlying mechanisms. In this study, OSRGs were downloaded and identified using the Gene Expression Omnibus database. Functional-enrichment analysis revealed the involvement of oxidative stress-related pathways and processes, and a ceRNA network was generated. Differentially expressed oxidative stress-related genes (De-OSRGs) were used to construct De-OSRG pairs, which were screened, and candidate De-OSRG pairs were identified. Immune cell-related gene pairs were selected *via* immune-infiltration analysis. A potential long non-coding RNA–microRNA–mRNA axis was determined, and clinical values were assessed. Eighteen De-OSRGs were identified that were primarily related to intricate signal-transduction pathways, apoptosis-related biological processes, and multiple kinase-related molecular functions. A ceRNA network consisting of 653 long non-coding RNA–microRNA links and 42 mRNA–miRNA links was constructed. Three candidate De-OSRG pairs were screened out from 13 De-OSRG pairs. The abundances of resting memory $CD4^+$ T cells, resting dendritic cells, and $CD8^+$ T cells differed between the control and IDD groups. $CD8^+$ T cell infiltration correlated negatively with cyclin B1 (*CCNB1*) expression and positively with protein kinase D1 (*PKD1*) expression. *CCNB1–PKD1* was the only pair that was differentially expressed in IDD, was correlated with $CD8^+$ T cells, and

displayed better predictive accuracy compared to individual genes. The *PKD1–miR-20b-5p–AP000797* and *CCNB1–miR-212-3p–AC079834* axes may regulate IDD. Our findings indicate that the OSRG pair *CCNB1–PKD1*, which regulates oxidative stress during IDD development, is a robust signature for identifying IDD. This OSRG pair and increased infiltration of $CD8^+$ T cells, which play important roles in IDD, were functionally associated. Thus, the OSRG pair *CCNB1–PKD1* is promising target for treating IDD.

Keywords: intervertebral disc degeneration, oxidative stress, gene pair, immune infiltration, competitive endogenous RNA, differential expression, cyclin B1, protein kinase D1

INTRODUCTION

Intervertebral disc degeneration (IDD) is a major factor inducing chronic lower back pain. Moreover, IDD frequently causes injury to the spinal cord and related nerves, which has important clinical implications when the contours change or contents leak (1). Severe health-related disabilities and enormous economic losses caused by IDD have drawn global attention (2, 3). The intervertebral disc, which lacks vasculature, comprises the interior nucleus pulposus (NP), outer annulus fibrosus, and thin cartilaginous endplates (4). Multiple risk factors, such as heredity, age, smoking, circadian rhythms, and high mechanical compression, contribute to the nutrient insufficiency and imbalanced acid–base homeostasis observed in NP cells (2, 5). Because of the early initiation of degenerative changes and absence of apparent symptoms, most patients with IDD are identified at an advanced stage, invasive surgery as the only treatment option, which has a poor prognosis. Thus, novel approaches that enable rapid detection of IDD pathogenesis and early diagnoses are urgently needed.

According to prevailing concepts, IDD pathogenesis centers on autophagy, apoptosis, inflammation, and metabolism (6–9). However, increasing evidence has shown that oxidative stress, caused by excessive accumulation of reactive oxygen species (ROS), plays a crucial role in driving IDD initiation and progression (10, 11). ROS, such as superoxide anions, hydrogen peroxide, and singlet oxygen, are byproducts of cellular oxidative metabolism (12). The physiological equilibrium is disturbed once the rate of ROS production exceeds that of its elimination within NP cells. Subsequently, ROS-driven oxidative stress causes time-dependent damage to DNA and proteins, which is compounded by coexisting cellular damage. The levels of some oxidation products of ROS or substances that participate in ROS metabolism (such as malondialdehyde, peroxynitrite, and glutathione) are elevated in patients with IDD (13, 14). Nevertheless, the precise underlying mechanisms and potential markers of oxidative stress-related genes (OSRGs) in IDD remain unclear.

In recent decades, non-coding RNAs, including microRNAs (miRNAs) and long non-coding RNAs (lncRNAs), have gained attention. Various non-coding RNAs have been identified as effective prognostic or diagnostic molecular signatures, particularly in the field of oncology (15, 16). Over 80% of transcripts in the human genome are not translated into proteins and remain as non-coding sequences (17). Among these, transcripts longer than 200 nucleotides are recognized as lncRNAs (18), whereas those with 18–22 nucleotides are classified as miRNAs (19). With the rapid evolution of sequencing technologies, a growing number of lncRNAs, such as *ANPODRT* (20), *FAM83H-AS1* (21), and *TRPC7-AS1* (22), has been considered as essential regulators of gene expression in IDD at the transcriptional, post-transcriptional, and epigenetic levels. According to the competing-endogenous RNA (ceRNA) hypothesis, regulatory lncRNAs interact with miRNAs by serving as decoys for specific miRNAs, resulting in changes in the expression of target mRNAs (23, 24). To date, relatively few studies have focused on oxidative stress-associated ceRNA networks. An in-depth understanding of ceRNA crosstalk may reveal the mechanisms underlying IDD pathogenesis.

Additionally, some components of NP cells are gradually exposed to the body's immune system during IDD development, thereby triggering a series of auto-immune responses (25). The activities of various infiltrating immune cells, such as macrophages (26) and $CD8^+$ T cells (27), which are present in this inflammatory microenvironment, contribute to the exacerbation of IDD. The mechanism(s) underlying oxidative stress and its association with immune privilege in human IDD remain unclear. Therefore, studies are needed to clarify the underlying immunological mechanisms and develop novel immunotherapeutic targets for IDD.

In this study, we investigated differentially expressed oxidative stress-related genes (De-OSRGs) using publicly available Gene Expression Omnibus (GEO) microarray sets and OSRGs associated with IDD. Simple batch-correction methods often do not fully eliminate batch effects. Hence, we constructed De-OSRG pairs by merging different datasets and establishing and annotating a ceRNA network based on the De-OSRGs. Moreover, machine-learning algorithms were used to screen for candidate De-OSRG pairs. Their associations with immune-infiltration features were further investigated to determine the optimal oxidative stress-related signature. Based

Abbreviations: BP, biological process; CCNB1, cyclin B1; ceRNA, competitive endogenous RNA; CI, confidence interval; DElncRNA, differentially expressed long non-coding RNA; DEmiRNA, differentially expressed microRNA; DEmRNA, differentially expressed messenger RNA; De-OSRG, differentially expressed oxidative stress-related gene; De-OSRGP, differentially expressed oxidative stress-related gene pair; GEO, Gene Expression Omnibus; GO, Gene Ontology; IDD, intervertebral disc degeneration; KEGG, Kyoto Encyclopedia of Genes and Genomes; LASSO, least absolute shrinkage and selection operator; lncRNA, long non-coding RNA; MAPK, mitogen-activated protein kinase; MF, molecular function; miRNA, microRNA; mRNA, messenger RNA; NP, nucleus pulposus; OS, oxidative stress; OSRG, oxidative stress-related gene; OSRGP, oxidative stress-related gene pair; PKD1, protein kinase D1; ROC, receiver operating characteristic; ROS, reactive oxygen species; SVM, support vector machine.

on the results, a receiver operating characteristic (ROC) curve, which evaluates distinguishing performers in IDD, was developed, and potential regulatory mechanisms were identified.

MATERIALS AND METHODS

Data Acquisition and Preprocessing

The gene-expression profiles of IDD, including GSE116726 (miRNA set), GSE56081 (lncRNA and mRNA sets), GSE70362 (mRNA set), and GSE15227 (mRNA and external validation sets), were retrieved (**Supplementary Table S1**) and collected using the GEO database (URL: **Supplementary Table S2**). The GSE116726 set consists of three controls (none female and three males) and three patients with IDD (none female and three males) from China, whose average age was 56 years. Five controls (one female and four males; average age 40.8 years) and five patients with IDD (two female and three males; average age 36.8 years) from China comprised the GSE56081 set. Fourteen controls (seven female and seven males; average age 48.9 years) and ten patients (three female and seven males; average age 74.8 years) with IDD from Ireland made up the GSE70362 set. The GSE15227 set consisted of twelve controls and three patients with IDD from the USA. However, information of sex and age in the GSE152227 set was not reported. The details of the clinical information in each data set are shown in **Supplementary Table S3**. All 1399 OSRGs obtained from the GeneCards database (URL: **Supplementary Table S2**) are listed in **Supplementary Table S4**. Consistent with the Thompson grading system (28), NP samples were divided into two categories: a control group that comprised grades I–III and IDD group that comprised grades IV–V. We preprocessed the raw data using the following methods: i) merging GSE56081, GSE70362, and OSRGs into a dataset (merged dataset) to obtain a sample size that was sufficient for mRNA analysis; and (ii) performing batch normalization using the "sva" package of R to maintain the homogeneity of these sets. The flowchart and details of data processing are shown in **Figure 1**. Public access and publication guidelines approved by the GEO database were strictly followed when obtaining public data. Approval from the ethics committee of the Second Affiliated Hospital of Xi'an Jiaotong University was not required for this study.

Identifying De-OSRGs

First, we performed expression validation using the "limma" package in R software to identify differentially expressed mRNAs, miRNAs, and lncRNAs (DEmRNAs, DEmiRNAs, and DElncRNAs, respectively) between the IDD and control groups in the expanded datasets (GSE116726 and GSE56081, respectively). To visualize the differences, volcano maps and clustering heat maps were established using the "ggplot2" and "pheatmap" packages in R. To ensure the reliability of the data, we performed online database predictions for the DElncRNAs to obtain target mRNAs. Briefly, miRDB, miRTarBase, and TargetScan (URL: **Supplementary Table S2**) were used to predict miRNA–mRNA interactions, and miRcode (URL: **Supplementary Table S2**) was utilized to predict lncRNA–miRNA interactions. Genes that overlapped between the DEmRNAs and target mRNAs were regarded as De-OSRGs. A P value of <0.05 and fold-change in expression of >1.5 were used as the screening threshold.

In addition, a ceRNA network was constructed with the De-OSRGs and their target DEmiRNAs, along with target DElncRNAs, and visualized using Cytoscape software (v3.8.0) (29).

Functional Annotation of the ceRNA Network

To systematically annotate the potential functions and pathways of the De-OSRGs, Kyoto Encyclopedia of Genes and Genomes (KEGG) and Gene Ontology (GO) analyses were conducted using the "enrichplot", "clusterProfile", "ggplot2", and "org.Hs.eg.db" packages in R (30). GO terms, consisting of molecular functions (MFs) and biological processes (BPs), were used. Statistical significance was set at $P < 0.05$.

Computation of De-OSRG Pairs

Using the identified De-OSRGs, we calculated De-OSRG pairs according to the computation rules described by Zhang et al. (15). Briefly, if $Expr_{OSRGa} < Expr_{OSRGb}$, then OSRGP = 1; otherwise, OSRGP = 0, where $Expr_{OSRGa}$ denotes the expression level of OSRG a, and $Expr_{OSRGb}$ denotes the expression level of OSRG b. Thus, each OSRG pair was considered to be comprised of 0s and 1s. Following these pair-comparison rules, the numerical OSRG pair levels of each dataset were computed separately.

Screening for Crucial De-OSRG Pairs and Candidate Signatures

The least-absolute shrinkage and selection operator (LASSO) regression and support vector machine (SVM) machine-learning algorithms can be used to reduce the number of feature variables (31). The former algorithm preserves a variable by finding the best penalty parameter, λ, when the classification error is minimal, whereas the latter algorithm searches for the best optimal hyperplane that classifies different groups (in our case, IDD and control patients). We integrated overlapping gene pairs, which were screened *via* LASSO regression and SVM, by considering them as candidate OSRG pair signatures for further analysis.

Estimating Immune-Infiltration Patterns

CIBERSORT, a computer analysis tool, is widely used to evaluate the abundance of immune cells and assess the proportions of various immune cells using RNA-sequencing-based expression values (32). Herein, the candidate signatures were subjected to immune-infiltration analysis using the "CIBERSORT", "parallel", "preprocessCore", and "e1071" packages in R. Based on previous findings (31), we selected 22 immune cell subsets for analysis (32). A histogram was used to visualize the distributions of infiltrating immune cells in each subject. A correlation heatmap was drawn to reveal correlations between infiltrating immune cells using the "corrplot" package in R. Furthermore, a violin diagram was generated to visualize differences between the IDD and normal groups. The filtering threshold was set at $P < 0.05$.

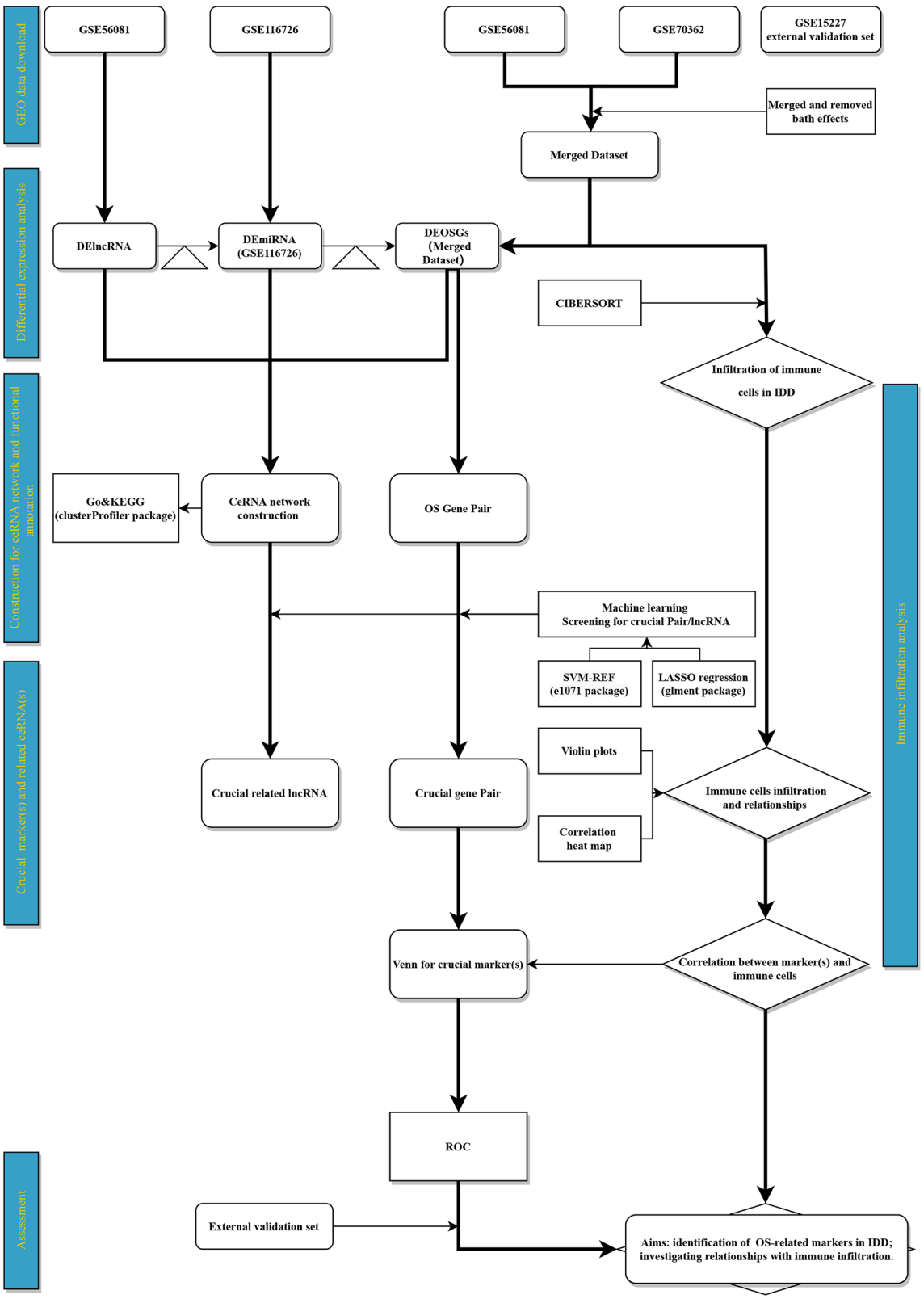

FIGURE 1 | Flowchart. Triangle represents target-gene prediction (first triangle, lncRNA target prediction; second triangle, miRNA target prediction).

Correlation Analysis Between Infiltrating Immune Cells and Candidate OSRGs

Spearman correlation analysis between infiltrating immune cells and candidate OSRGs was performed using the "limma" package in R and visualized using the "ggplot2", "tidyverse", and "ggsci" packages in R.

Screening for Key ceRNAs With Crucial De-OSRG Pairs

We screened ceRNAs with crucial gene pairs *via* LASSO regression and SVM. These ceRNAs were further analyzed.

Performance Evaluations

De-OSRG pairs-based ROC curve analysis was performed using the "pROC" package in R to distinguish IDD (33). We merged GSE56081 with GSE70362 as a training set and used GSE15227 as a validation set. The ROC curve, based on logistic regression, was evaluated for its efficacy in identifying IDD. In addition, we compared the areas under the receiver operating curves (AUCs) of separate genes and gene pairs, as well as the associated specificities, sensitivities, and 95% confidence intervals (CIs). The AUC was calculated separately to evaluate the performance/distinguishing ability of separate genes and gene pairs. Moreover, the external validation dataset was used to assess the De-OSRG pairs that distinguished IDD *via* ROCs.

Statistical Analysis

All statistical analyses were performed using R software (v3.6.2, R Core Team, The R Project for Statistical Computing, Vienna, Austria) and MedCalc statistical software (v19.0.4, MedCalc, Inc., Oostende, Belgium). GraphPad Prism (v8.0.1, GraphPad, Inc., La Jolla, CA, USA), Cytoscape (v3.8.0), and R software were used to generate graphics. All R packages used for analysis are listed in **Supplementary Table S5**. Upregulated expression was defined as a $\log_2$ fold-change of >0, whereas downregulated expression was defined as a $\log_2$ fold-change of <0. Statistical significance for each test was set at $P < 0.05$.

RESULTS

Identification of 18 De-OSRGs and Construction of a ceRNA Network

We identified 1428 DElncRNAs and 1176 DEmiRNAs using GSE56081 and GSE116726, respectively (**Figures 2A, B**). In addition, 69 DEmRNAs were extracted from the expanded dataset (**Figure 2C**). Based on online database predictions, 207 target miRNAs were predicted for 1428 DElncRNAs. Furthermore, 18 target miRNAs were obtained from miRNAs that overlapped between the 1176 DEmiRNAs and 207 miRNAs predicted by DElncRNAs. Eighteen De-OSRGs were associated with 69 DEmRNAs from the expanded dataset, along with 8612 predicted target mRNAs for miRNAs. Among these were 16 and 2 up- and downregulated De-OSRGs, respectively. The ceRNA network was comprised of 18 De-OSRGs, 211 target DElncRNAs, and 18 target DEmiRNAs (**Figure 2D**).

Functional Annotation

GO annotation indicated that the 18 De-OSRGs mainly participated in oxidative stress-associated and apoptosis-related BPs, such as cellular response to oxidative stress and regulation of neuronal apoptotic processes (**Figure 2E** and **Supplementary Table S6**). MF annotation showed that the MFs were primarily associated with kinase-related functions, including mitogen-activated protein kinase (MAPK) binding, kinase-regulator activity, transmembrane receptor-tyrosine kinase activity, and protein kinase-activator activity (**Figure 2F** and **Supplementary Table S6**). Furthermore, Kyoto Encyclopedia of Genes and Genomes enrichment analysis suggested that the 18 De-OSRGs were principally involved in the MAPK signaling pathway, phosphoinositide 3-kinase-protein kinase B signaling pathway, relaxin signaling pathway, FoxO signaling pathway, and cellular senescence, indicating that these genes play important roles in oxidative stress (**Figure 2G** and **Supplementary Table S7**).

Screening for Candidate Signatures of De-OSRG Pairs

Although batch normalization was performed, the expression heatmap of the 18 De-OSRGs showed gaps within the groups (**Figure 3A**). Hence, of the 18 De-OSRGs, 13 were established using filter values of 0.1–0.9 (**Figure 3B**). LASSO regression analysis (seed = 14) was used to select five gene pairs (**Figure 3C**). SVM analysis identified three gene pairs (seed = 14; **Figure 3D**) that intersected with the LASSO regression results (**Figure 3E**). We considered these three gene pairs, which included the following five OSRGs: cyclin B1 (CCNB1), protein kinase D1 (PKD1), cytochrome c oxidase assembly homolog 15, vascular endothelial growth factor C, and interferon regulatory factor 1, as candidate IDD signatures for further immune-infiltration analysis.

Immune Cell Infiltration

The violin diagram and histogram of immune cell infiltration clearly revealed abundant immune cells in IDD. The violin diagram indicated that resting memory $CD4^+$ T cells and resting dendritic cells showed less infiltration in the IDD group, whereas $CD8^+$ T cells showed more infiltration (**Figures 4A, B**). The correlation heatmap related to cell-type abundances indicated significant negative correlations between $CD8^+$ T cells and resting memory $CD4^+$ T cells and activated dendritic cells, and a positive correlation between $CD8^+$ T cells and neutrophils. Resting memory $CD4^+$ T cells showed a significant positive correlation with monocytes. Follicular helper T cells correlated positively with activated NK cells. Memory B cells correlated negatively with follicular helper T cells and plasma cells (**Figure 4C**). Immune infiltration analysis is predictive of specific infiltrating immune cell based on gene expression signatures.

Correlation Analysis Between Infiltrating Immune Cells and Candidate De-OSRG Pairs

To select optimal OSRG pairs and clarify the associations between immune cell infiltration and OSRGs, we performed correlation analyses between infiltrating immune cells and the

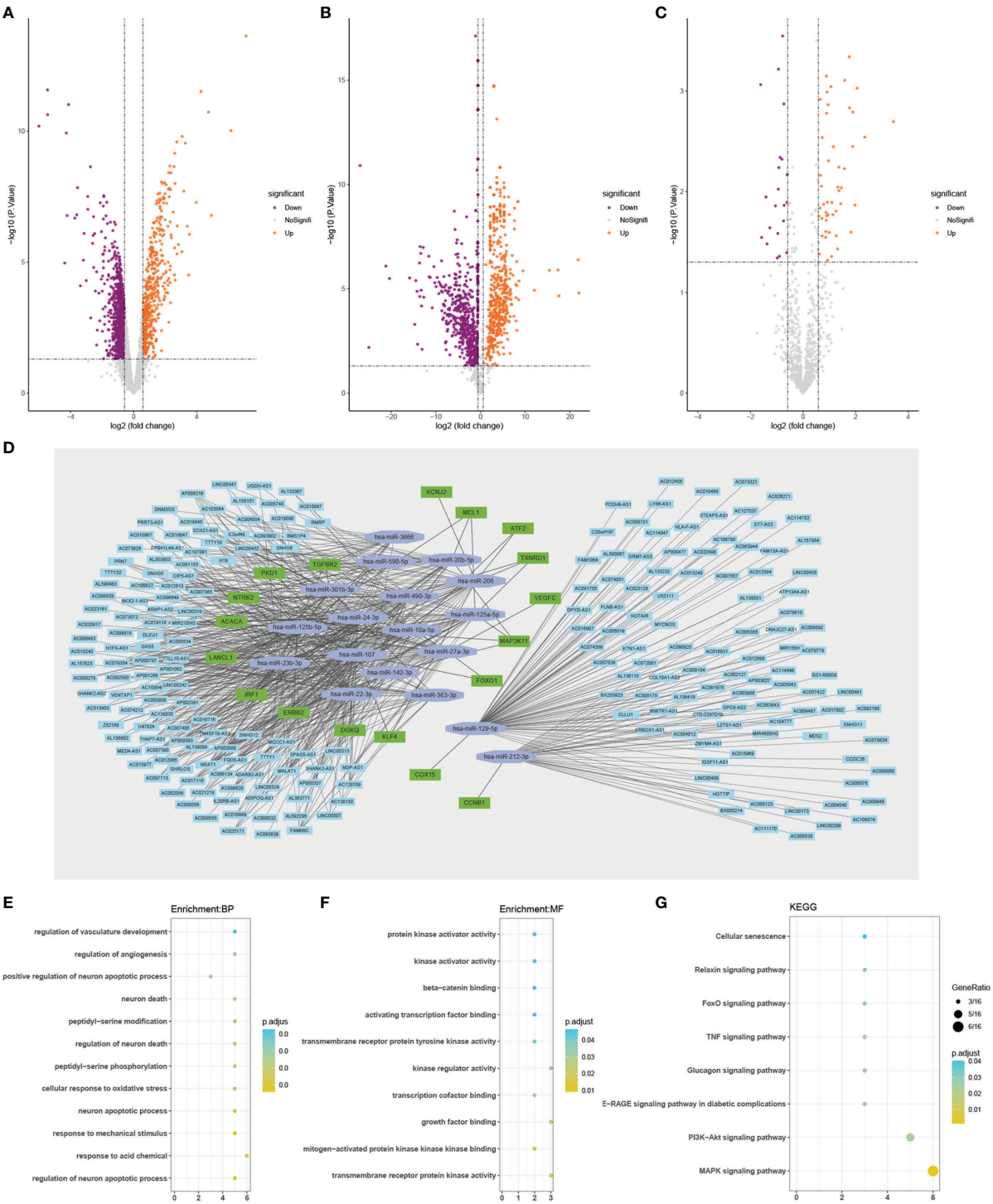

FIGURE 2 | Volcano plots of DEGs **(A–C)**. **(A)** Volcano plot of De–lncRNAs. **(B)** Volcano plot of De-miRNAs. **(C)** Volcano plot of De-mRNAs. Orange represents up-regulated differentially expressed genes, while purple represents down-regulated differentially expressed genes. The ceRNA network analyses of 18 DEOSRGs, and their function annotation by GO and KEGG **(D–G)**. **(D)** The ceRNA network analysis graph. GO enrichment analysis of 18 DEOSRGs **(E, F)**. **(E)** BP, biological process; **(F)** MF, molecular function. **(G)** KEGG pathway enrichment analysis of 18 DEOSRGs. De-lncRNAs, differentially expressed long noncoding RNAs; De–miRNAs, differentially expressed microRNAs; De-mRNAs, differentially expressed mRNAs; De–OSRGs, differentially expressed oxidative stress-related genes. GO, Gene Ontology; KEGG, Kyoto Encyclopedia of Genes and Genomes.

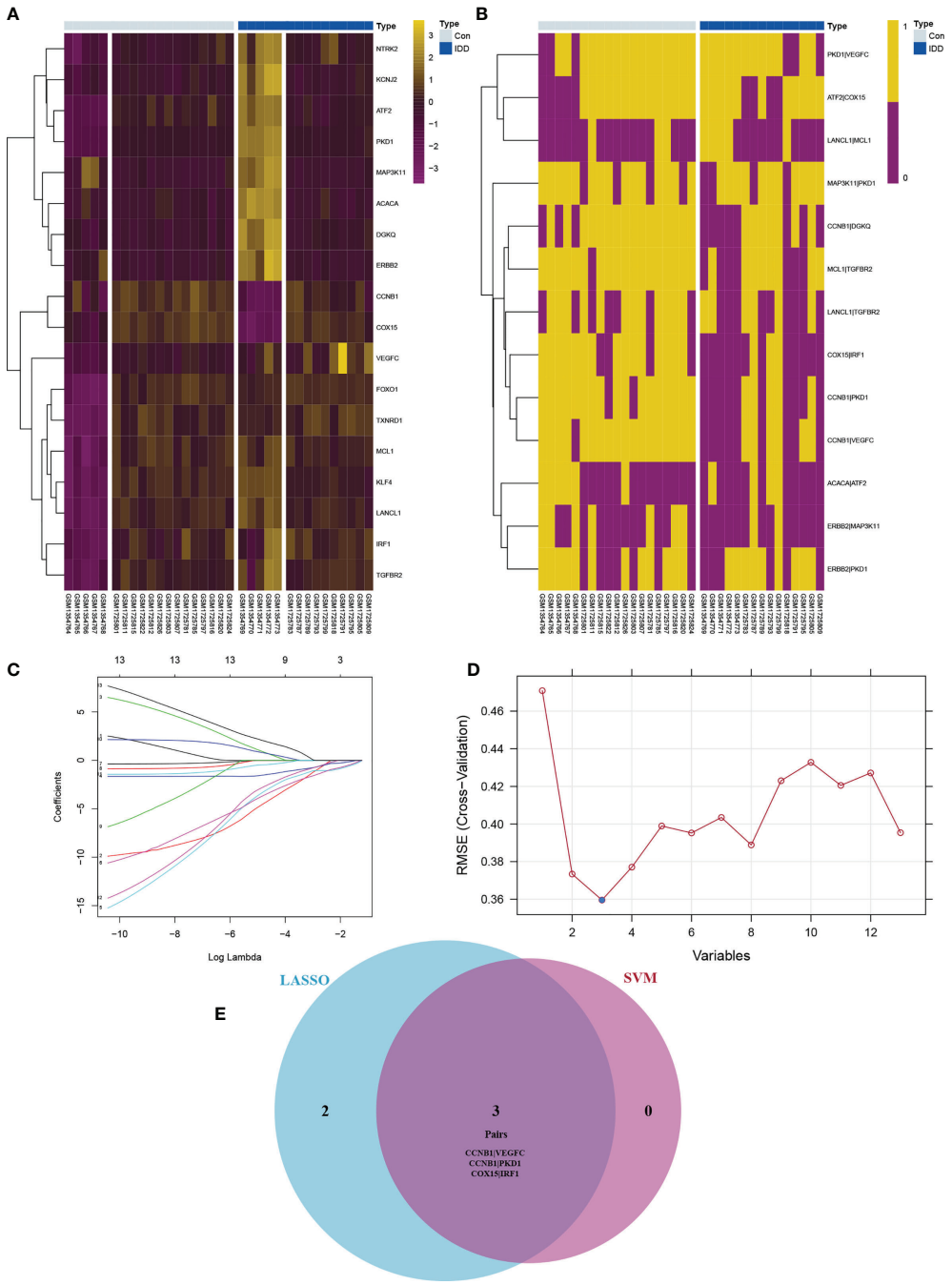

FIGURE 3 | The expression profile for De-OSRGs **(A)** and De-OSRGPs **(B)**. The difference between OSRGs heat map and OSRGPs heat map **(A, B)**: although the batch correction is used, the gap between different datasets can be clearly shown in panel **(A)** The screening process of key OSRGPs for IDD. **(C)** LASSO regression to screen for candidate signatures. **(D)** SVM to screen for candidate signatures. **(E)** Venn diagram demonstrating the intersection of candidate signatures screened by LASSO regression and SVM. OSRGs, oxidative stress-related genes; OSRGPs, oxidative stress-related gene pairs; IDD, intervertebral disc degeneration; LASSO, least absolute shrinkage and selection operator; SVM, support vector machine.

three candidate De-OSRG pairs. Correlation analysis showed that three of the five candidate De-OSRG pairs were prominently linked with various infiltrating immune cells (**Figures 5A–C**). Furthermore, significant differences were observed only between the numbers of $CD8^+$ T cells, resting memory $CD4^+$ T cells, and resting dendritic cells in the IDD and control groups. Interestingly, only the *CCNB1–PKD1* pair correlated with $CD8^+$ T cells simultaneously. Specifically, *CCNB1* correlated negatively with $CD8^+$ T cells (r = -0.630, P = 0.012; **Figure 5A**), and *PKD1* correlated positively with $CD8^+$ T cells

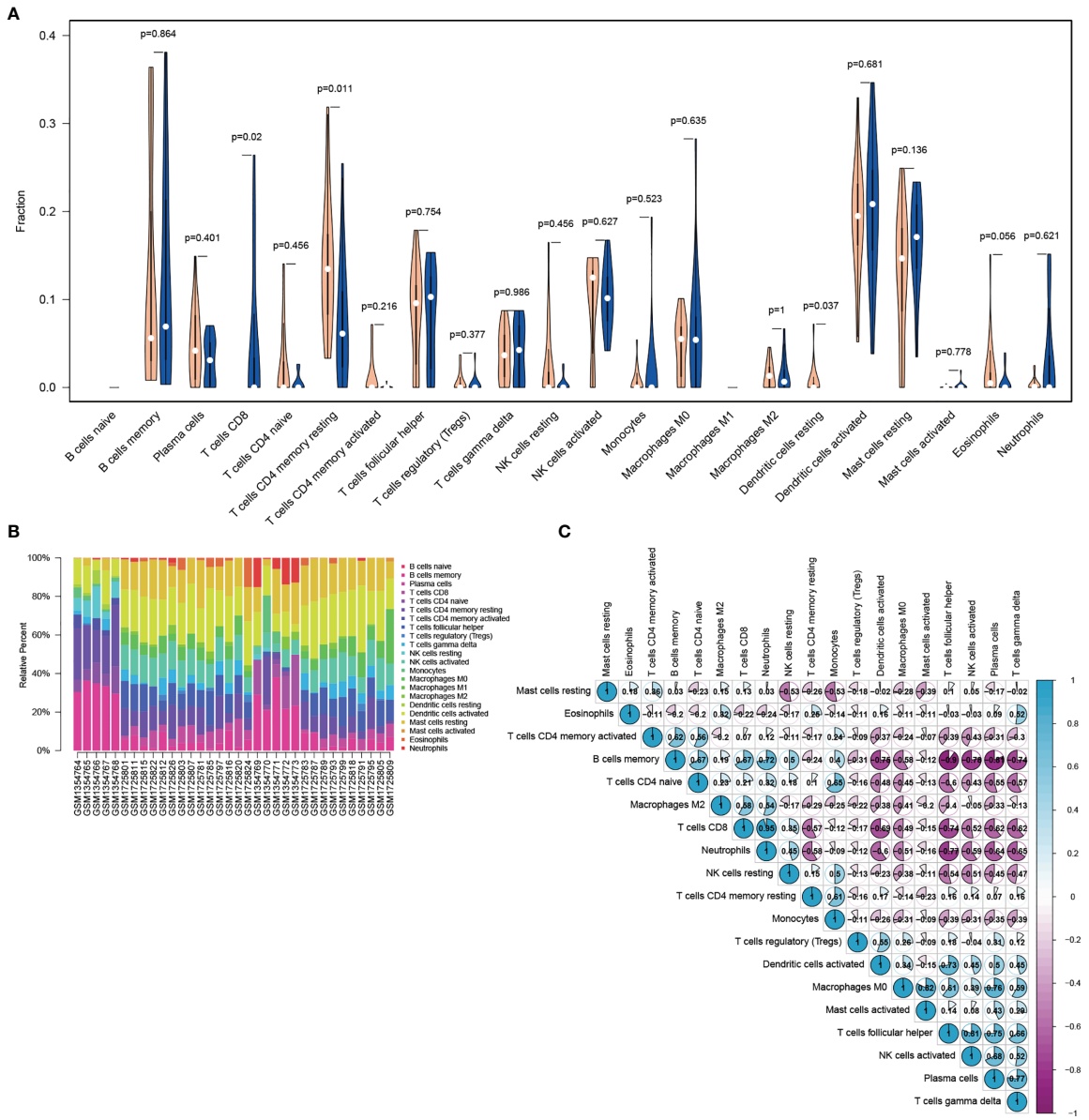

FIGURE 4 | Visualization of immune cell infiltration analysis. **(A)** Violin diagram of the abundance of infiltration by 22 immune cell subsets between IDD and control groups. Blue and orange colors represent IDD and control groups, respectively. **(B)** Histogram of the distribution of infiltrating immune cells in each individual. Columns represent IDD individuals. **(C)** Correlation heatmap of 22 immune cell subsets. Blue represents positive correlation, whereas purple represents negative correlation. The color and number in each circle indicate the correlation index between the two immune cell subsets. IDD, intervertebral disc degeneration.

(r = 0.817, P < 0.001; **Figure 5B**). Therefore, we focused on the *CCNB1–PKD1* pair in further analysis (**Figure 5D**). Correlation analysis between infiltrating immune cell and candidate De-OSRG pairs was based on the gene expression signatures.

Exploring Potential Regulatory Axes for the CCNB1–PKD1 Pair

Focusing on the *CCNB1–PKD1*–ceRNA network axis (**Figure 6A**) evaluated using LASSO regression (seed = 25) and SVM analyses, key lncRNAs associated with these genes were revealed (seed = 25) (**Figures 6B–E**, respectively): lncRNA *AC079834* for *CCNB1* and lncRNA *AP000797* for *PKD1*. The parameters and results for screening the key lncRNA (ceRNA), which competes with *CCNB1* to bind miR-212-3p, are shown in **Supplementary Table S8**. The parameters and results for screening the key lncRNA (ceRNA), which competes with *PKD1* to bind miR-20b-5p, are shown in **Supplementary Table S9**. The *CCNB1–miR-212-3p–AC079834* and *PKD1–miR-20b-5p–AP000797* axes were identified as potential regulatory ceRNA axes. These findings indicate that the

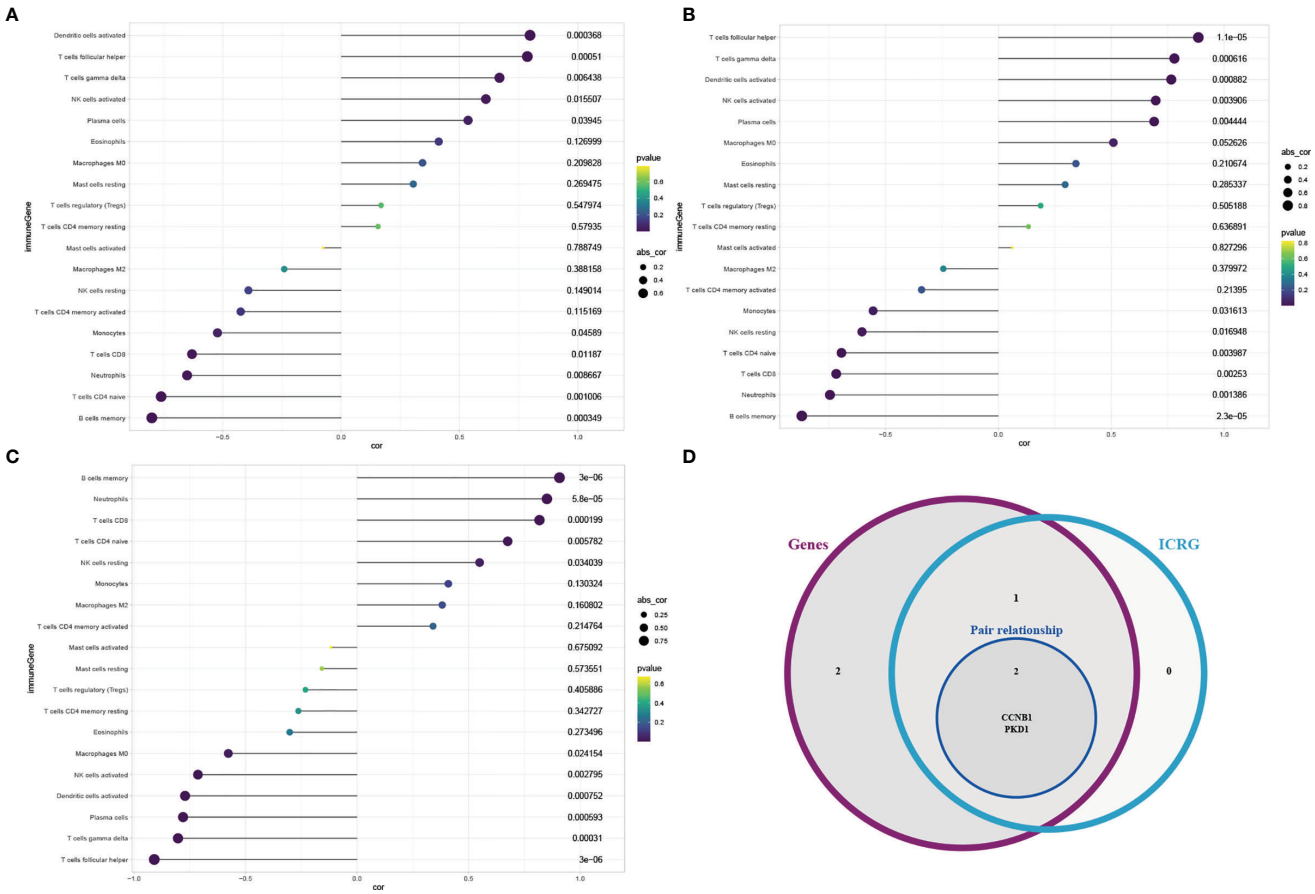

FIGURE 5 | Correlation analysis between infiltrating immune cell subtypes with the candidate De-OSRGs. Spearman correlation analysis between immune cell subtypes and *CCNB1* **(A)** /*PKD1* **(B)** /*COX15* **(C)**. Venn diagram **(D)** showing the key gene pair shared by the immune cell-related genes (ICRG) and candidate De-OSRGs.

CCNB1–PKD1 pair modulates oxidative stress through these axes during IDD initiation and development (**Figures 6F, G**). In summary, low *CCNB1* expression and high *PKD1* expression correlated negatively and positively, respectively, with increased $CD8^+$ T cell infiltration (**Figure 6H**).

Potential Discriminating Validity of CCNB1/PKD1 for IDD

After exploring the key gene pair (*CCNB1–PKD1*) and genes (*PKD1* and *CCNB1*), their distinguishing abilities were compared by using AUCs to evaluate the performance in differentiating the IDD and control cohorts based on ROC analysis. The AUCs of ROC curve analyses of the gene pair and genes were used to evaluate *CCNB1–PKD1* pair (AUC [95%CI] = 0.828 [0.660,0.935]), *PKD1* (AUC [95%CI] = 0.793 [0.620,0.912]), and *CCNB1* (AUC [95%CI] = 0.733 [0.554,0.870]) (**Figures 7A–C**). Compared to *CCNB1* and *PKD1*, the *CCNB1–PKD1* pair demonstrated the best distinguishing ability with the highest AUC value for effectively differentiating IDD from control samples. We next validated the gene pair (*CCNB1–PKD1*), *PKD1*, and *CCNB1* in the validation set. The AUCs [95%CI] for *CCNB1–PKD1*, *PKD1* and *CCNB1*, were 0.917 [0.658,0.996], 0.889 [0.623,0.990], and 0.528 [0.261,0.783]. Based on these results for the external validation dataset, this gene pair has excellent discriminating ability (**Figures 7D–E**). In the training and validation cohorts, the sensitivities and specificities of the *CCNB1–PKD1* pair were better than or equal to those of *PKD1* and *CCNB1* alone. The results of ROC curve analysis, including the AUCs, sensitivities, and specificities, are shown in **Supplementary Table S10**.

DISCUSSION

Although many treatments that are relatively effective for alleviating IDD progression have been developed, IDD diagnosis remains largely dependent on imaging and clinical symptoms, which render early IDD diagnosis and timely intervention difficult. Thus, identifying a potentially precise diagnostic signature and therapeutic targets may lead to new approaches for patients with IDD. A large volume of data indicates that oxidative stress promotes IDD development and

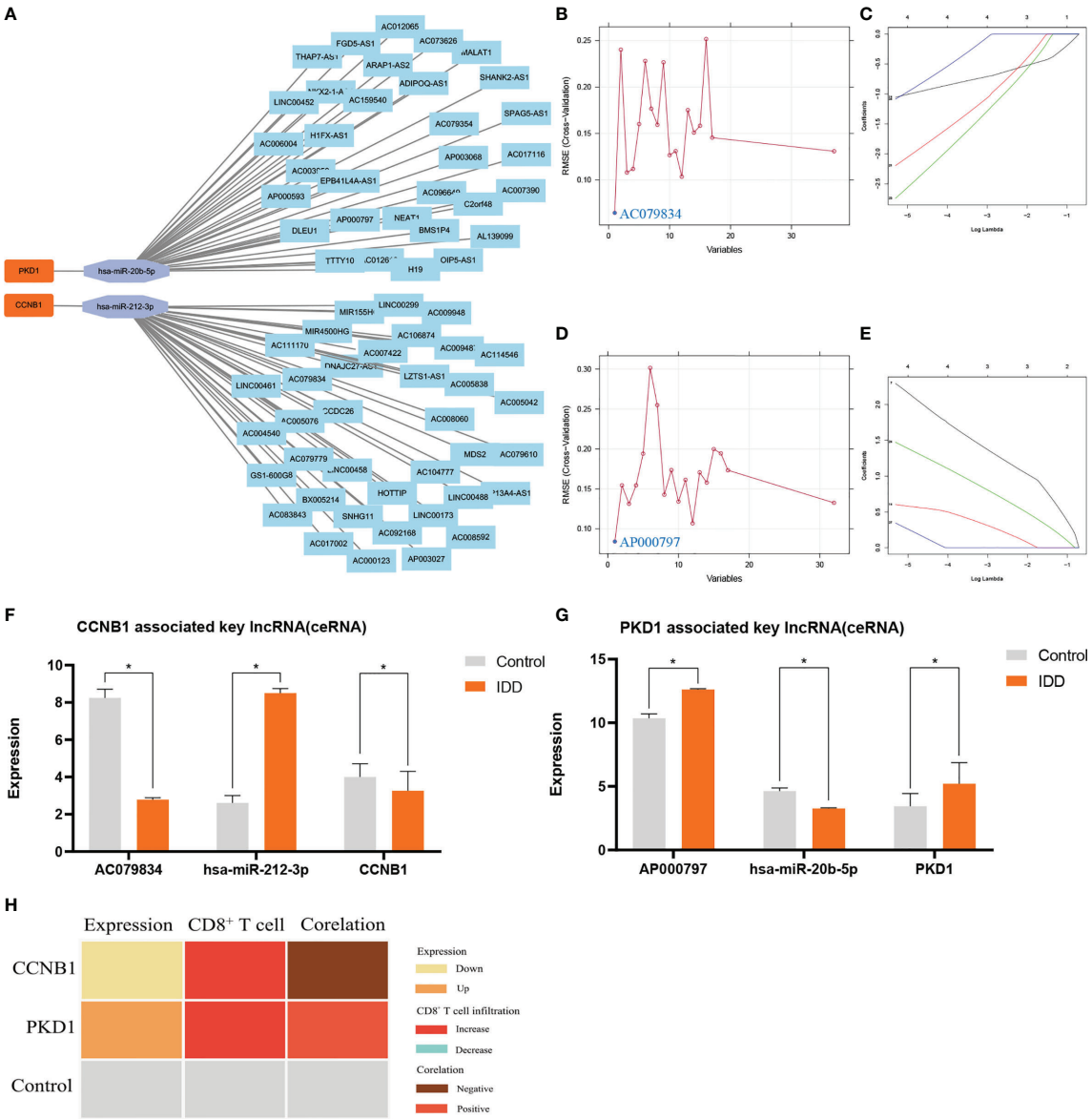

FIGURE 6 | |The 69lncRNAs–2miRNAs–2mRNAs (*CCNB1/PKD1* pair) ceRNA co-expression network was constructed **(A)** and was used to screen the key ceRNAs (lncRNAs) by SVM **(B, D)** and Lasso **(C, E)**. Panels **(B, C)**, venn result for SVM **(B)** and LASSO **(C)** is *AC079834*. LncRNA *AC079834* was selected in SVM and LASSO, and was used for building axis (*CCNB1–miR-212-3p–AC079834*). Panels **(D, E)**, venn result for SVM **(D)** and LASSO **(E)** is *AP000797*. LncRNA *AP000797* was selected in SVM and LASSO, and was used for building axis (*PKD1–miR-20b-5p–AP000797*). Parameters and results in detail are shown in **Supplementary Tables S9, S10**.The expression profile for *CCNB1–miR-212-3p–AC079834* axis **(F)** and *PKD1–miR-20b-5p–AP000797* axis **(G)**. The low expression of *CCNB1* is negatively correlated with increased $CD8^+$ T cells infiltration; the high expression of *PKD1* is positively correlated with increased $CD8^+$ T cells infiltration **(H)**. * represents $p < 0.05$.

that immune cells play vital roles in IDD progression. In this study, we evaluated a potential oxidative stress-related signature for IDD and predicted the mechanisms regulating its function and relationships with infiltrating immune cells.

We identified 18 significant De-OSRGs by analyzing GEO databases and assembled them into 13 gene pairs. Kyoto Encyclopedia of Genes and Genomes enrichment suggested that the 18 De-OSRGs were mainly enriched in MAPK signaling, phosphoinositide 3-kinase–protein kinase B signaling, FoxO signaling, and cellular senescence. Most of these pathways mediate intricate signal-transduction cascades associated with inflammation triggered by OS (34–37). In terms of cellular senescence, oxidative stress-induced injury continually disrupts the integrity of genes and proteins, leading to the gradual aging of organisms (38). GO annotation demonstrated enrichment of apoptosis-related BPs and multiple kinase-related MFs. As previously reported, IDD is a chronic, perplexing process that affects apoptosis and various kinase-mediated pathways (39–41).

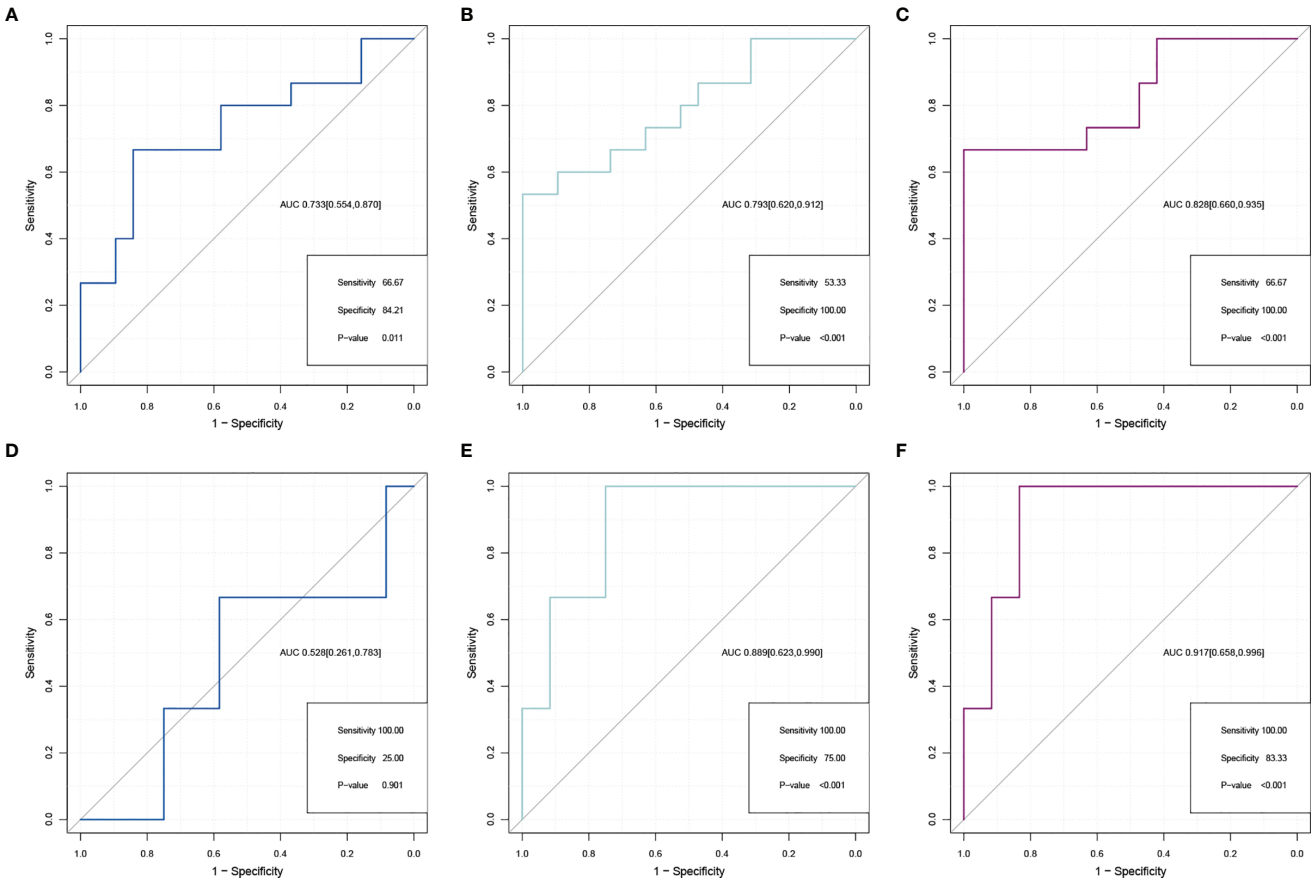

FIGURE 7 | Comparison of ROC analysis between gene pair and separate gene in predicting IDD in the expanded dataset **(A–C)** and external validation dataset **(D–F)**. ROCs for *CCNB1* **(A, D)**, *PKD1* **(B, E)**, and *CCNB1–PKD1* pairs **(C, F)**.

In contrast to traditional concepts, pairwise gene comparisons and integration strategies offer substantial advantages. Calculating the OSRG pair signature was specifically based on the relative ranking of OSRG expression levels. These calculations enabled pairwise weight comparison that did not require data normalization and overcame the batch effects associated with assorted platforms (**Figures 3A, B**). Moreover, pairwise gene comparisons have become accessible based on studies that included multiple datasets (14), offering a tremendous advantage over current orthopedic practices. Our results showed that discrimination based on the *CCNB1–PKD1* gene pair was significantly better than that using individual genes, suggesting that the integration strategy was reliable and robust.

CCNB1, a member of the cyclin family of proteins, integrates with a cell cycle-dependent Ser/Thr kinase to stimulate the production of the maturation-promoting factor, which plays an indispensable role in mitosis (42). Previous *in vivo* data demonstrated that *CCNB1* is responsible for cellular proliferation and differentiation and that its abolition inhibited proliferation and promoted apoptosis in gonocytes and spermatogonia (43). Meng et al. (44) revealed that CCNB1 is an important regulator of G2/M phase of NP cells. Once G2/M phase was arrested, NP cell proliferation was blocked. Several lines of evidence have indicated that CCNB1 is useful as a diagnostic or prognostic biomarker in rhabdomyosarcoma, hepatocellular carcinoma, and meningioma (42, 45, 46). Based on these findings, CCNB1 protein may participate in IDD development by regulating NP cell proliferation.

PKD1 encodes a serine/threonine kinase that belongs to the PKD family within the Ca^{2+}/calmodulin-dependent protein kinase superfamily (47). PKD1, when activated by hormones, oxidative stress, and/or growth factors, participates in cell proliferation, migration, motility, apoptosis, membrane trafficking, epidermal-to-mesenchymal transition, and angiogenesis (48, 49). Data from previous knockout studies indicated that *PKD1* orchestrates a battery of intracellular signaling pathways, such as cyclic AMP production, autophagy inhibition, G-protein coupled receptor signaling, MAPK signaling, nuclear factor-kappa B signaling, and cell–extracellular matrix interactions (50, 51). Although these signaling pathways have been reported to be distinctly linked to various diseases, the exact role of PKD1 remains unclear, particularly in neoplasia. For example, it was reported that PKD1

was highly expressed in skin and pancreatic cancers where it acted as a tumor-promoting factor (52, 53). Normally, PKD1 promotes mouse fibroblast and human endothelial cell proliferation (54, 55). In contrast, PKD1 functions as a tumor suppressor in invasive breast and gastric cancers (56, 57). This dual role of PKD1 depends on the degree of inflammation, microenvironmental factors, and tissue type or phenotype (58). Considering that PKD1 typically participates in proliferation, PKD1 may regulate NP cell proliferation during IDD. Previous evidence, as well as our current results, indicate that under oxidative stress conditions, the *CCNB1–PKD1* pair participates in IDD by regulating NP cell proliferation or apoptosis *via* a signaling pathway(s), such as the MAPK, nuclear factor-kappa B, and/or calcium-ion pathways. Although both *CCNB1* and *PKD1* may promote IDD, further verification *via* experimentation and clinical studies is needed to support this hypothesis.

Considering the predictive role of the *CCNB1–PKD1* signature in IDD, we further clarified the regulatory ceRNA mechanism associated with this pair. Comprehensive analysis through online database predictions and expression validation with GEO datasets (conducted in this study) revealed two regulatory ceRNA axes as potentially associated with *CCNB1* and *PKD1* modulation by oxidative stress in NP cells: the *CCNB1–miR-212-3p–AC079834* and *PKD1*–miR-20b-5p–*AP000797* axes. Specifically, *AC079834* acts as a ceRNA sponge for *miR-212-3p*, which inhibits its binding to *CCNB1* mRNA. Similarly, *PKD1* mRNA binding to miR-20b-5p is prone to interference by *AP000797*, which sponges miR-20b-5p. There was no *CCNB1* related reports linked to ceRNA in IDD in the literature. In terms of *PKD1*, only Qu et al. (59) identified an IDD-associated miRNA, *hsa-miR-140*, which was regulated by three lncRNAs: *KCNQ1* opposite strand/antisense transcript 1, OIP5 antisense RNA 1 and UGDH antisense RNA 1. Of the 3 lncRNAs, the latter two could target several overlapping co-expressed genes, including forkhead box F1 and polycystin 1, transient receptor potential channel interacting (*PKD1*). However, these findings were not validated experimentally. Increasing evidence suggests that lncRNAs and miRNAs regulate pathophysiologic BPs linked to IDD, such as oxidative stress and apoptosis (20).

MiR-212-3p acts as an important regulator of various cancers by modulating cell proliferation, angiogenesis, and tumor invasion (60). *MiR-212-3p* expression is decreased in patients with bladder cancer. Our results indicate that *miR-212-3p* upregulation promoted *CCNB1* downregulation, whereas downregulating *AC079834* upregulated *miR-212-3p*, thereby accelerating IDD development by reversing the former process. Previously, *miR-20b-5p* was reported as upregulated and could be used as a biomarker for diagnosing breast cancer (61). Our results also showed that *miR-20b-5p* downregulation induced *PKD1* upregulation, which was attenuated by *AP000797*. However, the functional roles of the two regulatory axes regarding oxidative stress in IDD must be validated in experimental studies.

In addition to the abovementioned regulatory mechanisms, the pattern of immune infiltration is another critical concern. Our immune-infiltration analysis of the three De-OSRG pairs (consisting of five OSRGs) showed that resting memory $CD4^+$ T cell and resting dendritic cell infiltration was decreased in IDD, whereas $CD8^+$ T cell infiltration was increased. Notably, only the *CCNB1–PKD1* pair was synchronously associated with $CD8^+$ T cells. During the degenerative process, substantial amounts of inflammatory cytokines and chemokines secreted by NP cells drive the activation and recruitment of immunocytes (including T cells and B cells) to further enhance the inflammatory cascade (62). For example, Shamji et al. reported that interleukin-17 released by Th17 lymphocytes was substantially expressed in degenerated and herniated human intervertebral disc tissues, which induced macrophage recruitment (63). North et al. revealed that T cells, including $CD4^+$ and $CD8^+$ T cells, were closely associated with NP extrusion (64). Another study showed that painful human intervertebral discs were highly infiltrated by regulatory T cells (65). Recent data showed that macrophages and $CD8^+$ T cells were more prone to apoptosis in rat IDD models than in normal rats (27). These findings partially clarify the function of $CD8^+$ T cells in IDD. Consistent with the results of these studies, our results suggest that an increase in $CD8^+$ T cells plays a role in immune infiltration, NP cell damage, and apoptosis during IDD pathogenesis. We conducted experiments to predict the role of $CD8^+$ T cells in human IDD. However, the correlation between the *CCNB1–PKD1* pair and $CD8^+$ T cells should be further investigated. In addition, the functional relevance of this pair in regulation of $CD8^+$ T cells and associated signaling in other diseases were also explored. For example, autosomal dominant polycystic kidney disease is presumably the direct consequence of mutations in *PKD1* or *PKD2*. Kleczko et al. (66) confirmed an increase in renal T cells associated with autosomal dominant polycystic kidney disease severity, specific activation of $CD8^+$ T cells, and a functional role for these cells in inhibiting cystogenesis. Craven et al. (67) reported that *PKD1* was more frequently mutated in a group enriched in both $CD8^+$ T cells and CD4 memory-activated T cells in triple-negative breast cancer. Li et al. (68) reported that four cyclin family genes, including *CCNB1*, were notably elevated in the early TNM stages in colon cancer and significantly correlated with overall survival. Moreover, they also found that the expression of *CCNB1* was positively correlated with tumor-killing immune cells, such as $CD8^+$ T cells, which may prolong the survival time of patients with colon cancer. Zou et al. (69) reported that upregulated *CCNB1* was associated with poorer prognosis in patients with hepatocellular carcinoma. Notably, through immune infiltration analysis, they found that the expression level of *CCNB1* was positively correlated with the infiltrating levels of $CD8^+$ T cells. Kao et al. (70) identified *CCNB1* as a shared human epithelial tumor-associated antigen recognized by T cells, such as $CD8^+$ T cells. Latner et al. (71) elucidated that the expression of cell cycle regulatory genes, such as *CCNB1*, was enhanced in virus-specific memory $CD8^+$ T cells. Moreover, *CCNB1* elicits T cell-dependent antibody responses not only in patients with cancer and premalignant disease, but also in healthy individuals (72, 73).

The current study had some limitations. For example, although we merged multiple datasets to increase the sample

size, the reliability of our findings must be confirmed using additional datasets and clinical samples, although more samples may not be readily obtainable. Moreover, as our study involved retrospective analysis, the potential diagnostic values and exact functions of *CCNB1* and *PKD1* should be verified in *in vivo* and *in vitro* experiments. Additionally, the lack of *in situ* localization/validation of the data limits the generality of the current findings. Further experimental verification is needed to determine whether $CD8^+$ T cell infiltration causes IDD or whether infiltration occurs after oxidative stress.

In conclusion, our results suggest that the *CCNB1–PKD1* gene pair is a robust, oxidative stress-related signature for identifying IDD. This gene pair may modulate oxidative stress, which leads to IDD, by regulating the *CCNB1–miR-212-3p–AC079834* and *PKD1–miR-20b-5p–AP000797* axes. The *CCNB1*–PKD1 signature was closely associated with $CD8^+$ T-cell infiltration. This *CCNB1–PKD1* signature provides a novel perspective on the immune microenvironment in IDD and is a promising immune target in patients with IDD. In our further studies, we will analyze the relationship between immunity, oxidative stress, and metabolism in IDD.

DATA AVAILABILITY STATEMENT

The original contributions presented in the study are included in the article/**Supplementary Material**. Further inquiries can be directed to the corresponding author.

ETHICS STATEMENT

The studies involving human participants were reviewed and approved by The Second Affiliated Hospital of Xi'an Jiaotong University. Written informed consent for participation was not required for this study in accordance with the national legislation and the institutional requirements.

AUTHOR CONTRIBUTIONS

SC and HPL collected the data and drafted the manuscript. SC and KY analyzed the data. HPL designed the study. All authors contributed to the article and approved the submitted version.

FUNDING

This work was supported by the Social Development Science and Technology Project in Shaanxi Province (grant number 2021SF-172).

SUPPLEMENTARY MATERIAL

The Supplementary Material for this article can be found online at: https://www.frontiersin.org/articles/10.3389/fimmu.2021.765382/full#supplementary-material

REFERENCES

1. Jeffery ND, Levine JM, Olby NJ, Stein VM. Intervertebral Disk Degeneration in Dogs: Consequences, Diagnosis, Treatment, and Future Directions. *J Vet Internal Med* (2013) 27(6):1318–33. doi: 10.1111/jvim.12183
2. Roh EJ, Darai A, Kyung JW, Choi H, Kwon SY, Bhujel B, et al. Genetic Therapy for Intervertebral Disc Degeneration. *Int J Mol Sci* (2021) 22(4):1579. doi: 10.3390/ijms22041579
3. Lyu FJ, Cui H, Pan H, Mc Cheung K, Cao X, Iatridis JC, et al. Painful Intervertebral Disc Degeneration and Inflammation: From Laboratory Evidence to Clinical Interventions. *Bone Res* (2021) 9(1):7. doi: 10.1038/s41413-020-00125-x
4. Dowdell J, Erwin M, Choma T, Vaccaro A, Iatridis J, Cho SK. Intervertebral Disk Degeneration and Repair. *Neurosurgery* (2018) 83(5):1084. doi: 10.1093/neuros/nyy437
5. Chao-Yang G, Peng C, Hai-Hong Z. Roles of NLRP3 Inflammasome in Intervertebral Disc Degeneration. *Osteoarthritis Cartilage* (2021) 29(6):793–801. doi: 10.1016/j.joca.2021.02.204
6. Cao S, Li J, Yang K, Li H. Major ceRNA Regulation and Key Metabolic Signature Analysis of Intervertebral Disc Degeneration. *BMC Musculoskeletal Disord* (2021) 22(1):249. doi: 10.1186/s12891-021-04109-8
7. Gong CY, Zhang HH. Autophagy as a Potential Therapeutic Target in Intervertebral Disc Degeneration. *Life Sci* (2021) 273:119266. doi: 10.1016/j.lfs.2021.119266
8. Yao M, Zhang J, Li Z, Bai X, Ma J, Li Y. Liraglutide Protects Nucleus Pulposus Cells Against High-Glucose Induced Apoptosis by Activating PI3K/Akt/mTOR/Caspase-3 and PI3K/Akt/Gsk3β/Caspase-3 Signaling Pathways. *Front Med (Lausanne)* (2021) 8:630962. doi: 10.3389/fmed.2021.630962
9. Xie C, Ma H, Shi Y, Li J, Wu H, Wang B, et al. Cardamonin Protects Nucleus Pulposus Cells Against IL-1β-Induced Inflammation and Catabolism via Nrf2/NF-κb Axis. *Food Funct* (2021) 12(6):2703–14. doi: 10.1039/d0fo03353g
10. Suzuki S, Fujita N, Hosogane N, Watanabe K, Ishii K, Toyama Y, et al. Excessive Reactive Oxygen Species are Therapeutic Targets for Intervertebral Disc Degeneration. *Arthritis Res Ther* (2015) 17:316. doi: 10.1186/s13075-015-0834-8
11. Dimozi A, Mavrogonatou E, Sklirou A, Kletsas D. Oxidative Stress Inhibits the Proliferation, Induces Premature Senescence and Promotes a Catabolic Phenotype in Human Nucleus Pulposus Intervertebral Disc Cells. *Eur Cell Mater* (2015) 30:89–102; discussion 103. doi: 10.22203/eCM.v030a07
12. Wu Z, Wang L, Wen Z, Yao J. Integrated Analysis Identifies Oxidative Stress Genes Associated With Progression and Prognosis in Gastric Cancer. *Sci Rep* (2021) 11(1):3292. doi: 10.1038/s41598-021-82976-w
13. León Fernández OS, Pantoja M, Díaz Soto MT, Dranguet J, García Insua M, Viebhan-Hánsler R, et al. Ozone Oxidative Post-Conditioning Reduces Oxidative Protein Damage in Patients With Disc Hernia. *Neurol Res* (2012) 34(1):59–67. doi: 10.1179/1743132811Y.0000000060
14. Poveda L, Hottiger M, Boos N, Wuertz K. Peroxynitrite Induces Gene Expression in Intervertebral Disc Cells. *Spine (Phila Pa 1976)* (2009) 34(11):1127–33. doi: 10.1097/BRS.0b013e31819f2330
15. Zhang B, Nie X, Miao X, Wang S, Li J, Wang S. Development and Verification of an Immune-Related Gene Pairs Prognostic Signature in Ovarian Cancer. *J Cell Mol Med* (2021) 25(6):2918–30. doi: 10.1111/jcmm.16327
16. Juarez-Flores A, Zamudio GS, José MV. Novel Gene Signatures for Stage Classification of the Squamous Cell Carcinoma of the Lung. *Sci Rep* (2021) 11(1):4835. doi: 10.1038/s41598-021-83668-1
17. Djebali S, Davis CA, Merkel A, Dobin A, Lassmann T, Mortazavi A, et al. Landscape of Transcription in Human Cells. *Nature* (2012) 489(7414):101–8. doi: 10.1038/nature11233
18. Zhao K, Zhang Y, Yuan H, Zhao M, Zhao D. Long Noncoding RNA LINC00958 Accelerates the Proliferation and Matrix Degradation of the

Nucleus Pulposus by Regulating miR-203/Smad3. *Aging* (2019) 11 (23):10814–25. doi: 10.18632/aging.102436
19. Zhan S, Wang K, Xiang Q, Song Y, Li S, Liang H, et al. lncRNA HOTAIR Upregulates Autophagy to Promote Apoptosis and Senescence of Nucleus Pulposus Cells. *J Cell Physiol* (2020) 235(3):2195–208. doi: 10.1002/jcp.29129
20. Kang L, Tian Y, Guo X, Chu X, Xue Y. Long Noncoding RNA ANPODRT Overexpression Protects Nucleus Pulposus Cells From Oxidative Stress and Apoptosis by Activating Keap1-Nrf2 Signaling. *Oxid Med Cell Longev* (2021) 2021:6645005. doi: 10.1155/2021/6645005
21. Jiang X, Chen D. LncRNA FAM83H-AS1 Maintains Intervertebral Disc Tissue Homeostasis and Attenuates Inflammation-Related Pain *via* Promoting Nucleus Pulposus Cell Growth Through miR-22-3p Inhibition. *Ann Transl Med* (2020) 8(22):1518. doi: 10.21037/atm-20-7056
22. Wang X, Li D, Wu H, Liu F, Liu F, Zhang Q, et al. LncRNA TRPC7-AS1 Regulates Nucleus Pulposus Cellular Senescence and ECM Synthesis *via* Competing With HPN for miR-4769-5p Binding. *Mech Ageing Dev* (2020) 190:111293. doi: 10.1016/j.mad.2020.111293
23. Batista PJ, Chang HY. Long Noncoding RNAs: Cellular Address Codes in Development and Disease. *Cell* (2013) 152(6):1298–307. doi: 10.1016/j.cell.2013.02.012
24. Salmena L, Poliseno L, Tay Y, Kats L, Pandolfi PP. A ceRNA Hypothesis: The Rosetta Stone of a Hidden RNA Language? *Cell* (2011) 146(3):353–8. doi: 10.1016/j.cell.2011.07.014
25. Capossela S, Schläfli P, Bertolo A, Janner T, Stadler BM, Pötzel T, et al. Degenerated Human Intervertebral Discs Contain Autoantibodies Against Extracellular Matrix Proteins. *Eur Cell Mater* (2014) 27:251–63; discussion 263. doi: 10.22203/eCM.v027a18
26. Silva AJ, Ferreira JR, Cunha C, Corte-Real JV, Bessa-Gonçalves M, Barbosa MA, et al. Macrophages Down-Regulate Gene Expression of Intervertebral Disc Degenerative Markers Under a Pro-Inflammatory Microenvironment. *Front Immunol* (2019) 10:1508. doi: 10.3389/fimmu.2019.01508
27. Li N, Gao Q, Zhou W, Lv X, Yang X, Liu X. MicroRNA-129-5p Affects Immune Privilege and Apoptosis of Nucleus Pulposus Cells *via* Regulating FADD in Intervertebral Disc Degeneration. *Cell Cycle* (2020) 19(8):933–48. doi: 10.1080/15384101.2020.1732515
28. Gruber HE, Hoelscher GL, Ingram JA, Hanley EN Jr. Genome-Wide Analysis of Pain-, Nerve- and Neurotrophin -Related Gene Expression in the Degenerating Human Annulus. *Mol Pain* (2012) 8:63. doi: 10.1186/1744-8069-8-63
29. Shannon P, Markiel A, Ozier O, Baliga NS, Wang JT, Ramage D, et al. Cytoscape: A Software Environment for Integrated Models of Biomolecular Interaction Networks. *Genome Res* (2003) 13(11):2498–504. doi: 10.1101/gr.1239303
30. Yu G, Wang LG, Han Y, He QY. Clusterprofiler: An R Package for Comparing Biological Themes Among Gene Clusters. *Omics* (2012) 16(5):284–7. doi: 10.1089/omi.2011.0118
31. Deng YJ, Ren EH, Yuan WH, Zhang GZ, Wu ZL, Xie QQ. GRB10 and E2F3 as Diagnostic Markers of Osteoarthritis and Their Correlation With Immune Infiltration. *Diagn (Basel)* (2020) 10(3):171. doi: 10.3390/diagnostics10030171
32. Cao J, Wu L, Lei X, Shi K, Shi L. A Signature of 13 Autophagyrelated Gene Pairs Predicts Prognosis in Hepatocellular Carcinoma. *Bioengineered* (2021) 12(1):697–707. doi: 10.1080/21655979.2021.1880084
33. Feng LH, Dong H, Lau WY, Yu H, Zhu YY, Zhao Y, et al. Novel Microvascular Invasion-Based Prognostic Nomograms to Predict Survival Outcomes in Patients After R0 Resection for Hepatocellular Carcinoma. *J Cancer Res Clin Oncol* (2017) 143(2):293–303. doi: 10.1007/s00432-016-2286-1
34. Ge J, Zhou Q, Cheng X, Qian J, Yan Q, Wu C, et al. The Protein Tyrosine Kinase Inhibitor, Genistein, Delays Intervertebral Disc Degeneration in Rats by Inhibiting the P38 Pathway-Mediated Inflammatory Response. *Aging (Albany NY)* (2020) 12(3):2246–60. doi: 10.18632/aging.102743
35. Qi W, Ren D, Wang P, Song Z, Wu H, Yao S, et al. Upregulation of Sirt1 by Tyrosol Suppresses Apoptosis and Inflammation and Modulates Extracellular Matrix Remodeling in Interleukin-1β-Stimulated Human Nucleus Pulposus Cells Through Activation of PI3K/Akt Pathway. *Int Immunopharmacol* (2020) 88:106904. doi: 10.1016/j.intimp.2020.106904
36. Farhan M, Wang H, Gaur U, Little PJ, Xu J, Zheng W. FOXO Signaling Pathways as Therapeutic Targets in Cancer. *Int J Biol Sci* (2017) 13(7):815–27. doi: 10.7150/ijbs.20052
37. Hussain T, Tan B, Yin Y, Blachier F, Tossou MC, Rahu N. Oxidative Stress and Inflammation: What Polyphenols Can Do for Us? *Oxid Med Cell Longev* (2016) 2016:7432797. doi: 10.1155/2016/7432797
38. Barbouti A, Vasileiou PVS, Evangelou K, Vlasis KG, Papoudou-Bai A, Gorgoulis VG, et al. Implications of Oxidative Stress and Cellular Senescence in Age-Related Thymus Involution. *Oxid Med Cell Longev* (2020) 2020:7986071. doi: 10.1155/2020/7986071
39. Chen D, Xia D, Pan Z, Xu D, Zhou Y, Wu Y, et al. Metformin Protects Against Apoptosis and Senescence in Nucleus Pulposus Cells and Ameliorates Disc Degeneration *In Vivo*. *Cell Death Dis* (2016) 7(10):e2441. doi: 10.1038/cddis.2016.334
40. Miao D, Zhang L. Leptin Modulates the Expression of Catabolic Genes in Rat Nucleus Pulposus Cells Through the Mitogen-Activated Protein Kinase and Janus Kinase 2/Signal Transducer and Activator of Transcription 3 Pathways. *Mol Med Rep* (2015) 12(2):1761–8. doi: 10.3892/mmr.2015.3646
41. Wu YD, Guo ZG, Deng WJ, Wang JG. SD0006 Promotes Nucleus Pulposus Cell Proliferation *via* the P38mapk/HDAC4 Pathway. *Eur Rev Med Pharmacol Sci* (2020) 24(21):10966–74. doi: 10.26355/eurrev_202011_23580
42. Li Q, Zhang L, Jiang J, Zhang Y, Wang X, Zhang Q, et al. CDK1 and CCNB1 as Potential Diagnostic Markers of Rhabdomyosarcoma: Validation Following Bioinformatics Analysis. *BMC Med Genomics* (2019) 12(1):198. doi: 10.1186/s12920-019-0645-x
43. Tang JX, Li J, Cheng JM, Hu B, Sun TC, Li XY, et al. Requirement for CCNB1 in Mouse Spermatogenesis. *Cell Death Dis* (2017) 8(10):e3142. doi: 10.1038/cddis.2017.555
44. Meng X, Zhu Y, Tao L, Zhao S, Qiu S. MicroRNA-125b-1-3p Mediates Intervertebral Disc Degeneration in Rats by Targeting Teashirt Zinc Finger Homeobox 3. *Exp Ther Med* (2018) 15(3):2627–33. doi: 10.3892/etm.2018.5715
45. Li N, Li L, Chen Y. The Identification of Core Gene Expression Signature in Hepatocellular Carcinoma. *Oxid Med Cell Longev* (2018) 2018:3478305. doi: 10.1155/2018/3478305
46. Bie L, Zhao G, Ju Y, Zhang B. Integrative Genomic Analysis Identifies CCNB1 and CDC2 as Candidate Genes Associated With Meningioma Recurrence. *Cancer Genet* (2011) 204(10):536–40. doi: 10.1016/j.cancergen.2011.08.019
47. Rozengurt E, Rey O, Waldron RT. Protein Kinase D Signaling. *J Biol Chem* (2005) 280(14):13205–8. doi: 10.1074/jbc.R500002200
48. Roy A, Ye J, Deng F, Wang QJ. Protein Kinase D Signaling in Cancer: A Friend or Foe? *Biochim Biophys Acta Rev Cancer* (2017) 1868(1):283–94. doi: 10.1016/j.bbcan.2017.05.008
49. Steinberg SF. Regulation of Protein Kinase D1 Activity. *Mol Pharmacol* (2012) 81(3):284–91. doi: 10.1124/mol.111.075986
50. Peintner L, Venkatraman A, Waeldin A, Hofherr A, Busch T, Voronov A, et al. Loss of PKD1/polycystin-1 Impairs Lysosomal Activity in a CAPN (Calpain)-Dependent Manner. *Autophagy* (2020) 17(9):2384–400. doi: 10.1080/15548627.2020.1826716
51. Fedeles SV, Gallagher AR, Somlo S. Polycystin-1: A Master Regulator of Intersecting Cystic Pathways. *Trends Mol Med* (2014) 20(5):251–60. doi: 10.1016/j.molmed.2014.01.004
52. Rashel M, Alston N, Ghazizadeh S. Protein Kinase D1 has a Key Role in Wound Healing and Skin Carcinogenesis. *J Invest Dermatol* (2014) 134 (4):902–9. doi: 10.1038/jid.2013.474
53. Liou GY, Döppler H, Braun UB, Panayiotou R, Scotti Buzhardt M, Radisky DC, et al. Protein Kinase D1 Drives Pancreatic Acinar Cell Reprogramming and Progression to Intraepithelial Neoplasia. *Nat Commun* (2015) 6:6200. doi: 10.1038/ncomms7200
54. Zhukova E, Sinnett-Smith J, Rozengurt E. Protein Kinase D Potentiates DNA Synthesis and Cell Proliferation Induced by Bombesin, Vasopressin, or Phorbol Esters in Swiss 3T3 Cells. *J Biol Chem* (2001) 276(43):40298–305. doi: 10.1074/jbc.M106512200
55. Wong C, Jin ZG. Protein Kinase C-Dependent Protein Kinase D Activation Modulates ERK Signal Pathway and Endothelial Cell Proliferation by Vascular Endothelial Growth Factor. *J Biol Chem* (2005) 280(39):33262–9. doi: 10.1074/jbc.M503198200
56. Eiseler T, Döppler H, Yan IK, Goodison S, Storz P. Protein Kinase D1 Regulates Matrix Metalloproteinase Expression and Inhibits Breast Cancer Cell Invasion. *Breast Cancer Res* (2009) 11(1):R13. doi: 10.1186/bcr2232

57. Kim M, Jang HR, Kim JH, Noh SM, Song KS, Cho JS, et al. Epigenetic Inactivation of Protein Kinase D1 in Gastric Cancer and its Role in Gastric Cancer Cell Migration and Invasion. *Carcinogenesis* (2008) 29(3):629–37. doi: 10.1093/carcin/bgm291
58. Youssef I, Ricort JM. Deciphering the Role of Protein Kinase D1 (PKD1) in Cellular Proliferation. *Mol Cancer Res* (2019) 17(10):1961–74. doi: 10.1158/1541-7786.MCR-19-0125
59. Qu Z, Quan Z, Zhang Q, Wang Z, Song Q, Zhuang X, et al. Comprehensive Evaluation of Differential lncRNA and Gene Expression in Patients With Intervertebral Disc Degeneration. *Mol Med Rep* (2018) 18(2):1504–12. doi: 10.3892/mmr.2018.9128
60. Li X, Zou ZZ, Wen M, Xie YZ, Peng KJ, Luo T, et al. ZLM-7 Inhibits the Occurrence and Angiogenesis of Breast Cancer Through miR-212-3p/Sp1/VEGFA Signal Axis. *Mol Med* (2020) 26(1):109. doi: 10.1186/s10020-020-00239-2
61. Zhang H, Zou X, Wu L, Zhang S, Wang T, Liu P, et al. Identification of a 7-microRNA Signature in Plasma as Promising Biomarker for Nasopharyngeal Carcinoma Detection. *Cancer Med* (2020) 9(3):1230–41. doi: 10.1002/cam4.2676
62. Risbud MV, Shapiro IM. Role of Cytokines in Intervertebral Disc Degeneration: Pain and Disc Content. *Nat Rev Rheumatol* (2014) 10(1):44–56. doi: 10.1038/nrrheum.2013.160
63. Shamji MF, Setton LA, Jarvis W, So S, Chen J, Jing L, et al. Proinflammatory Cytokine Expression Profile in Degenerated and Herniated Human Intervertebral Disc Tissues. *Arthritis Rheum* (2010) 62(7):1974–82. doi: 10.1002/art.27444
64. Gorth DJ, Shapiro IM, Risbud MV. Transgenic Mice Overexpressing Human TNF-α Experience Early Onset Spontaneous Intervertebral Disc Herniation in the Absence of Overt Degeneration. *Cell Death Dis* (2018) 10(1):7. doi: 10.1038/s41419-018-1246-x
65. Kepler CK, Markova DZ, Dibra F, Yadla S, Vaccaro AR, Risbud MV, et al. Expression and Relationship of Proinflammatory Chemokine RANTES/CCL5 and Cytokine IL-1β in Painful Human Intervertebral Discs. *Spine (Phila Pa 1976)* (2013) 38(11):873–80. doi: 10.1097/BRS.0b013e318285ae08
66. Kleczko EK, Marsh KH, Tyler LC, Furgeson SB, Bullock BL, Altmann CJ, et al. CD8(+) T Cells Modulate Autosomal Dominant Polycystic Kidney Disease Progression. *Kidney Int* (2018) 94(6):1127–40. doi: 10.1016/j.kint.2018.06.025
67. Craven KE, Gökmen-Polar Y, Badve SS. CIBERSORT Analysis of TCGA and METABRIC Identifies Subgroups With Better Outcomes in Triple Negative Breast Cancer. *Sci Rep* (2021) 11(1):4691. doi: 10.1038/s41598-021-83913-7
68. Li J, Zhou L, Liu Y, Yang L, Jiang D, Li K, et al. Comprehensive Analysis of Cyclin Family Gene Expression in Colon Cancer. *Front Oncol* (2021) 11:674394. doi: 10.3389/fonc.2021.674394
69. Zou Y, Ruan S, Jin L, Chen Z, Han H, Zhang Y, et al. CDK1, CCNB1, and CCNB2 are Prognostic Biomarkers and Correlated With Immune Infiltration in Hepatocellular Carcinoma. *Med Sci Monit* (2020) 26:e925289. doi: 10.12659/MSM.925289
70. Kao H, Marto JA, Hoffmann TK, Shabanowitz J, Finkelstein SD, Whiteside TL, et al. Identification of Cyclin B1 as a Shared Human Epithelial Tumor-Associated Antigen Recognized by T Cells. *J Exp Med* (2001) 194(9):1313–23. doi: 10.1084/jem.194.9.1313
71. Latner DR, Kaech SM, Ahmed R. Enhanced Expression of Cell Cycle Regulatory Genes in Virus-Specific Memory CD8+ T Cells. *J Virol* (2004) 78(20):10953–9. doi: 10.1128/JVI.78.20.10953-10959.2004
72. Suzuki H, Graziano DF, McKolanis J, Finn OJ. T Cell-Dependent Antibody Responses Against Aberrantly Expressed Cyclin B1 Protein in Patients With Cancer and Premalignant Disease. *Clin Cancer Res* (2005) 11(4):1521–6. doi: 10.1158/1078-0432.CCR-04-0538
73. Vella LA, Yu M, Fuhrmann SR, El-Amine M, Epperson DE, Finn OJ. Healthy Individuals Have T-Cell and Antibody Responses to the Tumor Antigen Cyclin B1 That When Elicited in Mice Protect From Cancer. *Proc Natl Acad Sci USA* (2009) 106(33):14010–5. doi: 10.1073/pnas.0903225106

Conflict of Interest: The authors declare that the research was conducted in the absence of any commercial or financial relationships that could be construed as a potential conflict of interest.

Publisher's Note: All claims expressed in this article are solely those of the authors and do not necessarily represent those of their affiliated organizations, or those of the publisher, the editors and the reviewers. Any product that may be evaluated in this article, or claim that may be made by its manufacturer, is not guaranteed or endorsed by the publisher.

frontiers in Immunology

ORIGINAL RESEARCH
published: 26 November 2021
doi: 10.3389/fimmu.2021.774177

Increased Ratio of $CD14^{++}CD80^{+}$ Cells/$CD14^{++}CD163^{+}$ Cells in the Infrapatellar Fat Pad of End-Stage Arthropathy Patients

Shuhe Ma[1], Kosaku Murakami[2], Rintaro Saito[1], Hiromu Ito[3,4], Koichi Murata[5], Kohei Nishitani[3], Motomu Hashimoto[5,6], Masao Tanaka[5], Masahi Taniguchi[1], Koji Kitagori[1], Shuji Akizuki[1], Ran Nakashima[1], Hajime Yoshifuji[1], Koichiro Ohmura[1], Akio Morinobu[1] and Tsuneyo Mimori[1,7]*

[1] Department of Rheumatology and Clinical Immunology, Kyoto University Graduate School of Medicine, Kyoto, Japan, [2] Center for Cancer Immunotherapy and Immunobiology, Kyoto University Graduate School of Medicine, Kyoto, Japan, [3] Department of Orthopaedic Surgery, Kyoto University Graduate School of Medicine, Kyoto, Japan, [4] Department of Orthopaedic Surgery, Kurashiki Central Hospital, Okayama, Japan, [5] Department for Advanced Medicine for Rheumatic Disease, Kyoto University Graduate School of Medicine, Kyoto, Japan, [6] Department of Clinical Immunology, Osaka City University Graduate School of Medicine, Osaka, Japan, [7] Ijinkai Takeda General Hospital, Kyoto, Japan

OPEN ACCESS

Edited by:
Matthew William Grol,
Western University, Canada

Reviewed by:
Berta Cillero-Pastor,
Maastricht University, Netherlands
Alexander Knights,
University of Michigan, United States

***Correspondence:**
Kosaku Murakami
kosaku@kuhp.kyoto-u.ac.jp

Specialty section:
This article was submitted to Inflammation, a section of the journal Frontiers in Immunology

Received: 11 September 2021
Accepted: 08 November 2021
Published: 26 November 2021

Citation:
Ma S, Murakami K, Saito R, Ito H, Murata K, Nishitani K, Hashimoto M, Tanaka M, Taniguchi M, Kitagori K, Akizuki S, Nakashima R, Yoshifuji H, Ohmura K, Morinobu A and Mimori T (2021) Increased Ratio of $CD14^{++}CD80^{+}$ Cells/$CD14^{++}CD163^{+}$ Cells in the Infrapatellar Fat Pad of End-Stage Arthropathy Patients. Front. Immunol. 12:774177. doi: 10.3389/fimmu.2021.774177

Objectives: This study sought to identify the ratio of M1/M2 cells in the infrapatellar fat pads (IFP) and subcutaneous fat tissues (SC) of osteoarthritis (OA) and rheumatoid arthritis (RA) patients. The clinical features of OA and RA patients treated with or without biological disease-modifying anti-rheumatic drugs (bDMARDs) were also assessed.

Methods: IFP and SC were collected from patients with OA and RA who are undergoing total knee arthroplasty (TKA). CD14-positive cells were then isolated from these samples. Flow cytometry was used to determine the number of $CD14^{++}CD80^{+}$ cells and $CD14^{++}CD163^{+}$ cells. The expression levels of lipid transcription factors, such as sterol regulatory element-binding protein 1 (SREBP1) and liver X receptor alpha (LXRA), and inflammatory cytokines were also evaluated.

Results: Twenty OA patients and 22 RA patients were enrolled in this study. Ten of the RA patients (45.4%) received bDAMRDs before TKA. On average, a fivefold increase in the number of CD14-positive cells and lower expression levels of *SREBP1C* and *LXRA* were observed in OA IFP relative to OA SC; however, these results were not obtained from the RA samples. The median ratio of $CD14^{++}CD80^{+}$ cells/$CD14^{++}CD163^{+}$ cells of OA IFP was 0.87 (0.76–1.09, interquartile range), which is higher to that of OA SC with a lower ratio ($p = 0.05835$).

Conclusions: The quantity and quality of CD14-positive cells differed between IFP and SC in arthropathy patients. To our knowledge, this is the first study to characterize the ratio of M1/M2 cells in the IFP and SC of end-stage OA and RA patients. The increased ratio of $CD14^{++}CD80^{+}$ cells/$CD14^{++}CD163^{+}$ cells in the IFP from patients with OA and RA treated with bDMARDs indicated that inflammation was localized in the IFP. As adipose tissue-derived innate immune cells were revealed as one of the targets for regulating

inflammation, further analysis of these cells in the IFP may reveal new therapeutic strategies for inflammatory joint diseases.

Keywords: osteoarthritis, rheumatoid arthritis, monocytes/macrophage, inflammation, infrapatellar fat pad (Hoffa's)

INTRODUCTION

Osteoarthritis (OA) and rheumatoid arthritis (RA) affects millions of people worldwide, with one in three people over the age of 65 having OA (1), and every five out of a thousand people suffer from RA (2). OA and RA are characterized by joint pain; however, in some cases, they are characterized by deformity owing to inadequate therapeutic strategies. The progression of OA can be seen as multiple reasons, such as mechanical stress to the cartilage (3, 4), subchondral bone remodeling (5), biochemical cascades (6), and inflammation (5, 6). On the other hand, RA is an autoimmune disease that causes inflammation in the synovial tissue (3, 7). Disease-modifying anti-rheumatic drugs (DMARDs), such as biological DMARDs (bDMARDs), are used to treat RA (8); however, currently, no disease-modifying therapeutics is available for OA patients. Thus, elderly patients with OA or RA sometimes opt for total knee arthroplasty (TKA) to restore joint function.

Adipose tissue participates in inflammatory processes because it is a source of cytokines, chemokines, and adipokines (9). The infrapatellar fat pad (IFP or Hoffa's fat pad) is an adipose tissue depot located within the knee joint and is surrounded by synovium, cartilage, and bone (10). The anatomical location of the IFP is displayed in **Figure 1A** (11). As described by Jiang et al., the IFP is sandwiched between the patellar retinacula and the patellar tendon anteriorly and the trochlear surface of the femur posteriorly on the horizontal perspective. In contrast, on the vertical perspective, the IFP is located between the patella, femoral condyle, and intercondylar notch (12). Functionally, the IFP is involved in shock absorption, lubrication, and synovial fluid secretion. Furthermore, it is an important site for inflammation in patients with pain due to OA. Notably, serious inflammation in the IFP is often associated with severe pain in such patients (12, 13). In this study, subcutaneous fat tissue (SC) is defined as fat tissues located under the epidermis and dermis but not found in the IFP tissues located in the lesion parts of the knees.

Adipose tissue comprises the stromal vascular fraction (SVF) and adipocytes, and adipose tissue macrophages and monocytes can be collected from the SVF (10). Adipose tissue macrophages (ATMs) in the IFP demonstrate aspects of both pro- and anti-inflammatory phenotypes *in vitro*, with most cells expressing the M2 marker, CD206, but secreting interleukin-6 (IL-6), tumor necrosis factor-alpha (TNF-α), and relatively low amounts of interleukin-10 (IL-10), similar to M1 cells (13–16). ATMs have been revealed to play important roles in both physiological processes and pathological mechanisms in adipose tissue—for instance, the proportion of ATM in lean mice was estimated to be less than 10% of all adipose tissues; however, in leptin-deficient mice, this proportion increased to over 50% (17). Unlike ATMs that are distributed throughout uninflamed adipose tissue and provide limited inflammatory activity in the lean state (18), ATMs in obese adipose tissue surround and consume dead adipocytes and exhibit a pro-inflammatory phenotype (19, 20). Furthermore, bigger amounts of TNF-α and IL-6 are secreted by ATMs in obese people (9), and a twofold increase in the release of IL-6 was observed in the IFP compared to the SC in patients with OA (21). However, the differentiation

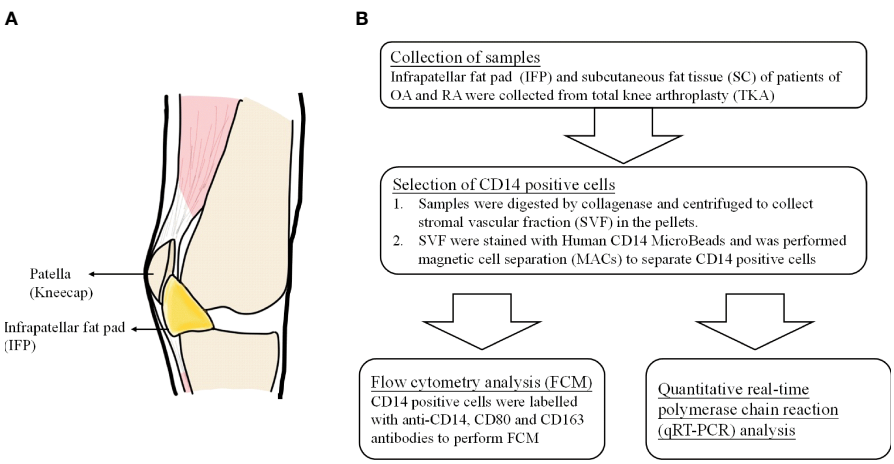

FIGURE 1 | **(A)** The anatomical location of infrapatellar fat pads. **(B)** Flow chart of the experimental method.

patterns of M1 and M2 cells in the IFP of arthropathy patients have not been studied.

To our knowledge, this is the first study to reveal the differentiation pattern of $CD14^{++}CD80^{+}$ cells and $CD14^{++}CD163^{+}$ cells in the IFP and SC of OA and RA patients. Furthermore, as IFP and SC are adipose tissues in the knee joints (**Figure 1A**) and IFP is considered to have a great potential to participate in inflammatory response (13), qRT-PCR was performed to identify the lipid transcription factors related to inflammation to clarify the signature expression pattern of these genes in the IFP and SC of arthropathy patients.

MATERIALS AND METHODS

Sample Collection From Patients With OA and RA

Patient Information

This study was approved by the Kyoto University Graduate School and Faculty of Medicine Ethics Committee (approval number G0502-1). Samples of the IFP and the SC were collected during TKA of patients with OA and RA admitted at Kyoto University Hospital from February 2018 to April 2020.

SVF Collection and Human CD14 Magnetic Cell Separation

Briefly, 2 g of fat tissue from each sample was digested in 5 ml of collagenase medium [0.1 mg collagenase IA (#C2674, Sigma Japan) in 1 ml RPMI medium (#52400, Gibco)] at 37°C for at least 1 h with rotation. The digested tissue was mashed through a 70-μm cell strainer with 2 ml syringe plungers and centrifuged at 18°C 620 × *g* for 3 min. The obtained pellets, labeled as the SVF, were washed twice in phosphate-buffered saline (PBS) *via* centrifugation at 18°C 620 × *g* for 3 min. Thereafter, they were rewashed in a magnetic cell separation (MACs) buffer solution of 0.5 M ethylenediaminetetraacetic acid (EDTA) in PBS containing 0.1% bovine serum albumin (BSA) *via* centrifugation at 18°C 300 × g for 10 min and subjected to MACs with human CD14 MicroBeads (#130-050-201, Miltenyi Biotec).

Flow Cytometry Analysis

Staining Strategy

CD14-positive cells were labeled with anti-CD14, anti-CD80, and anti-CD163 antibodies in 0.1% BSA and 0.5 M EDTA in PBS, with isotype and unstained controls. The following conjugated antibodies were used: anti-human CD14 (HCD14, APC, BioLegend), anti-human CD80 (2D10, PE, BioLegend), and anti-human CD163 (RM3/1, PerCP/Cyanine5.5, BioLegend). The following isotype controls were used: mouse IgG1, κ isotype control (FC) antibody (MOPC-21, APC, BioLegend); mouse IgG1, κ isotype control antibody (MOPC-21, PE, BioLegend); and mouse IgG1, κ isotype control antibody (MOPC-21, PerCP/Cyanine5.5, BioLegend). After washing, the cells were analyzed with a LSRFortessor cytometer (BD), and data were analyzed using FlowJo 10.4 software.

Gating Strategy

The gating strategy and fluorescence minus one are presented in **Supplementary Figures S1**, **S2**. Representative APC-FSC two-parameter dot plots of gate 1 among unstained, isotype control, and fully stained samples were presented. Cells gathered in neither unstained nor isotype controls in fully stained samples were allotted to gate 2. In gate 2, representative two-parameter dot plots of PE-APC and PerCP/Cyanine5.5-APC of samples stained by isotypes and antibodies were presented. Compared with the isotype control, positive plots were counted as "$CD14^{+}$, $CD80^{+}$" and "$CD14^{+}$, $CD163^{+}$" to calculate the proportions of $CD14^{++}CD80^{+}$ cells and $CD14^{++}CD163^{+}$ cells in CD14-positive cells.

Quantitative Real-Time Polymerase Chain Reaction

Total RNA was isolated with Isogen (#315-02504, Nippon Gene) and RNeasy Mini Kit (#74104, Qiagen). After DNAse treatment (#M6101, Promega), cDNA was prepared using an iScript cDNA Synthesis Kit (#1708890, BIO-RAD) according to the protocol of the manufacturer. qPCR was performed using TB Green Premix Ex Taq GC (#RR071A, TaKaRa) in a 7500 Real Time PCR System (Applied Biosystems). The following qPCR conditions were employed: one cycle for the initial denaturation stage at 95°C for 30 s, 70 cycles for the PCR stage with denaturation at 95°C for 10 s, and annealing at 60°C for 34 s; the melt curve stage was set according to the instructions for Takara TB Green for the 7500 Real-Time PCR System. The cell counts of the operation samples used in RNA extraction and qPCR are displayed in **Supplementary Table S1**. The sequences of the primers are listed in **Supplementary Table S2** (22–25).

Statistical Analyses

Patient information is presented as median values with interquartile ranges (IQR). For qPCR, the $2^{-\Delta\Delta CT}$ method was used to quantify the data. As the collected data did not follow normal distribution, Mann–Whitney *U*-test was utilized for statistics to describe differences between the groups. Furthermore, as sample sizes were the same within the same patients or the same SVF, paired-sample Wilcoxon signed-rank test was utilized to perform a more rigorous analysis. The statistical data were calculated using Origin 9.0 software (Originlab).

RESULTS

The IFP of Arthropathy Patients Has a Higher Proportion of CD14+ Cells Than the SC

The patients included in this study were arthropathy patients who underwent TKA. These patients were divided into OA, RA treated without bDMARDs, and RA treated with bDMARDs groups, as shown in **Table 1**. Twenty OA patients (group A) [15 females; median (IQR) age, 77.4 (74.7–81.3) years], 12 RA

TABLE 1 | Patient characteristics.

Patient groups	Group A	Group B	Group C		*p*-values between groups		
	OA	RA without bDMARDs	RA with bDMARDs		A and B	B and C	A and C
Total patients (*n*)	20	12	10	Age (years)	**0.0033**	0.6628	**0.0040**
Female patients (%)	75%	75%	100%	Height (cm)	0.3658	0.1855	0.9741
Age (years)	77.4 (74.7–81.3)	67.6 (66.5–70.5)	68.2 (46.5–76.0)	Body weight/total (kg)	**0.0023**	**0.0358**	0.5661
Height (cm)	153.3 (149.7–160.7)	158.3 (154.3–162.0)	153.8 (152.0–156.7)	Body weight/F (kg)	**0.0087**	**0.0101**	0.8244
Body weight/total (kg)	63.5 (55.4–70.3)	51.8 (47.8–55.4)	59.8 (56.6–63.7)	Body weight/M (kg)	0.0736	Not assessed	Not assessed
Body weight/F (kg)	60.9 (52.8–68.1)	48.8 (45.4–53.3)	59.8 (56.6–63.7)	BMI >24.99	Not assessed	Not assessed	0.3929
Body weight/M (kg)	70.4 (70.2–75.8)	60.1 (55.1–63.6)	Not applicable	CRP (mg/dl)	0.1717	0.5942	0.4574
BMI (kg/m^2)	26.1 (24.3–28.0)	19.9 (19.5–23.6)		ESR (mm/h)	0.1327	0.5278	0.4539
% of Obesity	65.0%	8.3%	70.0%	TC (mg/dl)	0.7958	0.1273	0.0926
CRP (mg/dl)	0.0 (0.0–0.13)	0.1 (0.0–1.6)	0.05 (0.0–0.4)	HDL (mg/dl)	0.9892	0.3053	0.1498
ESR (mm/h)	23.0 (10.8–30.3)	27.0 (18.5–50.5)	26.5 (6.0–44.0)	Disease duration (years)		0.2702	
TC (mg/dl)	193.0 (185.8–224.0)	197.0 (173.8–225.5)	221.5 (209.0–234.0)	% of RF positive		0.2530	
HDL (mg/dl)	63.0 (57.3–73.8)	62.0 (51.0–76.0)	77.0 (64.0–83.0)	% of ACPA positive		0.1273	
Disease duration (years)		11.7 (5.6–19.2)	15.1 (12.0–22.5)	% MTX use		0.4003	
% of RF positive		78.6	100	MTX dose (mg/week)		0.4205	
% of ACPA positive		71.4	100	% PSL use		1.0000	
% MTX use		42.9	66.7	PSL dose (mg/day)		0.7277	
MTX dose (mg/week)		0 (0–8.5)	6.0 (0–11.0)	TJC		0.0659	
% PSL use		28.6	33.3	SJC		0.8313	
PSL dose (mg/day)		0 (0–2.5)	0 (0–4.5)	PtGA VAS (cm)		0.8847	
TJC		2.0 (1.0–2.0)	1.0 (0–2.0)	PhGA VAS (cm)		0.2461	
SJC		1.0 (1.0–2.0)	1.0 (1.0–2.0)	CRP (mg/dl)		0.0755	
PtGA VAS (cm)		3.6 (2.1–6.9)	4.0 (1.9–6.7)	SDAI		0.2043	
PhGA VAS (cm)		3.3 (1.9–3.9)	2.0 (1.2–3.6)				
SDAI		11.5 (8.0–15.7)	10.7 (6.2–11.3)				

Data are presented as medians and interquartile ranges. Statistics between groups were assessed using Mann–Whitney U-tests or Fisher's exact tests. Bold values indicates significance. OA, osteoarthritis; RA, rheumatoid arthritis; bDMARDs, biological disease-modifying anti-rheumatic drugs (tocilizumab, n = 4; etanercept, n = 3; golimumab, n = 2; sarilumab, n = 1); F, female; M, male; BMI, body mass index; CRP, C-reactive protein; ESR, erythrocyte sedimentation rate; TC, total cholesterol; HDL, high-density lipoprotein; RF, rheumatoid factor; ACPA, anti-citrullinated protein antibodies; MTX, methotrexate; PSL, prednisolone; TJC, tender joint count; SJC, swollen joint count; PtGA, patient's global assessment; VAS, visual analog scale; PhGA, physician's global assessment; SDAI, simplified disease activity index.

patients who were not treated with bDMARDs (group B) [9 females; 67.6 (66.5–70.5) years], and 10 RA patients who were treated with bDMARDs (group C) [10 females; 68.2 (46.5–76.0) years] were included in the study. Information regarding C-reactive protein (CRP), erythrocyte sedimentation rate, total cholesterol, high-density lipoprotein, rheumatoid factor, anti-citrullinated protein antibodies, tender joint count, swollen joint count, patient's and physician's global assessment visual analog scale, and simplified disease activity index and the use of methotrexate (MTX) and prednisolone were described. OA patients who opted for surgery tended to be older, with a significance found between OA and both RA groups. The median body weight (kg) of patients who underwent surgery in these groups was 63.5, 51.8, and 59.8 kg, respectively, with a significance found between the group of RA patients who were not treated with bDMARDs and the other two groups. To gain more insights on whether gender is a factor in this significance, female and male patients were divided within each group. As shown in **Table 1**, female body weight had the same significance as that found for total patients, revealing a bias in body weight between genders. As the body mass index (BMI) of all members of the "RA without bDMARDs treatment" group

was below 25 kg/m^2, the *p*-values of the overweight population between this group and the other two groups could not be calculated.

CD14-positive cells from IFP and SC were assessed. The strategies to obtain CD14-positive cells and a schematic for flow cytometry and qPCR are displayed in **Figure 1B**. The amount of CD14-positive cells per gram of IFP was compared to that of SC for the same patients in each group (**Figure 2**). In the OA group, the amount of CD14-positive cells ($\times 10^5$) in the IFP of median (IQR) was 2.57 (0.96–4.13); however, this amount decreased to 0.28 (0.067–0.55) in the SC, with a *p*-value less than 0.0001 depicting significance. In RA patients who were not treated with bDMARDs, the number of CD14-positive cells ($\times 10^5$) in the IFP was 1.64 (0.61–4.84); however, this number decreased to 0.42 (0.20–0.58) in the SC, with significance found (p = 0.00792). In RA patients treated with bDMARDs, the number of CD14-positive cells ($\times 10^5$) in the IFP was 1.89 (0.69–2.49); however, this number decreased to 0.39 (0.13–1.74) in the SC. Statistics on the mean (standard deviation, SD) of CD14-positive cells per gram of fat tissue in each group are displayed in **Supplementary Figure S3A**.

CD14^{++}CD80^{+} and CD14^{++}CD163^{+} Cell Ratio Increased by 1.36-Fold in OA IFP

CD14-positive cells from the IFP and SC of all three groups were assessed. CD14^{++}CD80^{+} cells and CD14^{++}CD163^{+} cells were considered as M1 and M2 macrophages. As described in **Figure 3A**, the ratio [median (IQR)] of CD14^{++}CD80^{+} cells/CD14^{++}CD163^{+} cells of OA IFP was 0.87 (0.76–1.09); this ratio was higher to that of OA SC with a lower degree (p = 0.05835). In the group of RA patients who were not treated with bDMARDs, the ratio of CD14^{++}CD80^{+}/CD14^{++}CD163^{+} from both the IFP and SC was as high as 0.79 (0.65–0.90) and 0.86 (0.43–0.98) (**Figure 3B**). The RA bDMARDs group also had an increased ratio from 0.65 (0.44–0.86) in the SC to 0.94 (0.82–1.12) in the IFP (**Figure 3C**). **Figure 3D** shows that both diseases even had differentiation of CD14^{++}CD80^{+} cells and CD14^{++}CD163^{+} cells in the IFP. Statistics on the mean (SD) of M1/M2 ratio as well as their proportions in CD14-positive cells in each group are shown in **Supplementary Figures S3B, C**. The cell numbers in each group are presented in **Table 2**. However, the M1/M2 ratio was 0.59 (0.31–1.11) and was found to be biased to the M2 phenotype in peripheral blood mononuclear cell from RA patients (26).

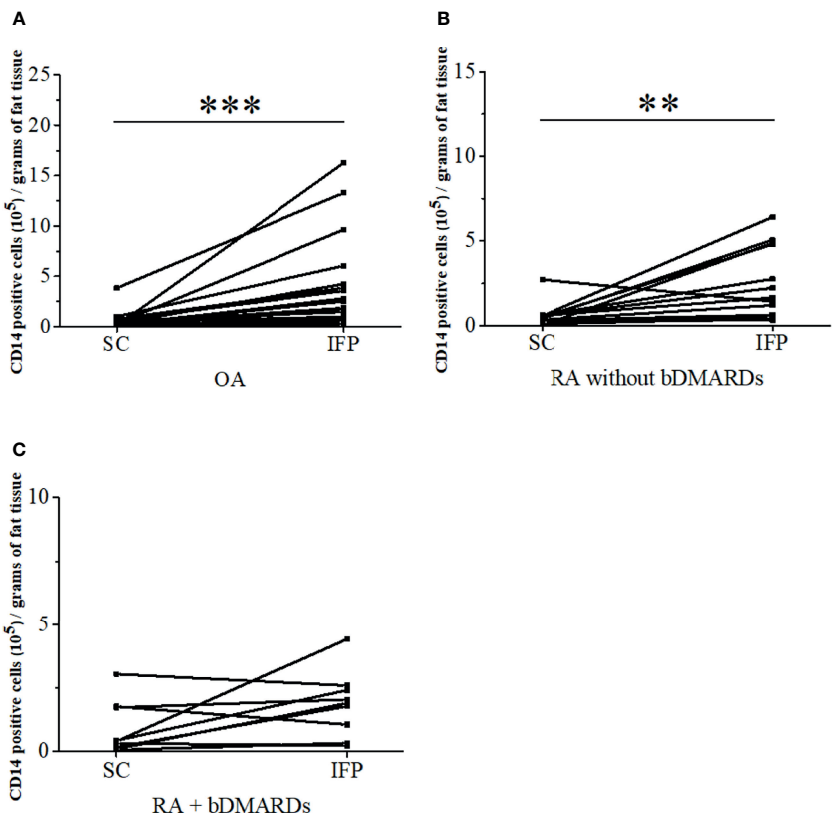

FIGURE 2 | The infrapatellar fat pads (IFP) of arthropathy patients has a higher proportion of CD14-positive cells than the subcutaneous fat tissues. CD14-positive cells per gram of SC or IFP in the osteoarthritis (OA) **(A)**, rheumatoid arthritis (RA) without bDMARDs **(B)**, and RA with bDMARDs **(C)**. Samples were obtained during total knee arthroplasty, digested in collagenase medium to obtain the stromal vascular fraction, and stained with human CD14 antibody to separate adipose-tissue-resident CD14-positive cells. $^{**}p < 0.01$ and $^{***}p < 0.001$, as determined by the paired-sample Wilcoxon signed-rank test to identify differences between SC and IFP OA. n = 20; RA without bDMARDs, n = 12; RA with bDMARDs, n = 10.

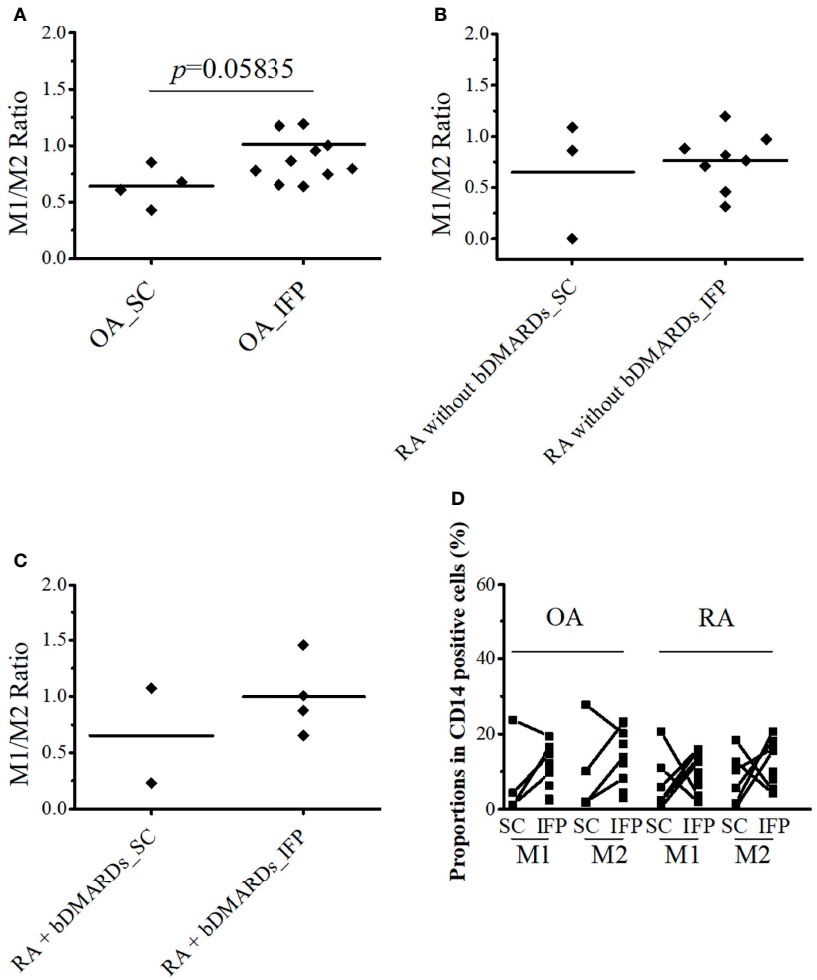

FIGURE 3 | $CD14^{++}CD80^{+}$ and $CD14^{++}CD163^{+}$ cell ratio increases by 1.36-fold in osteoarthritis (OA) infrapatellar fat pads (IFP). **(A–C)** Ratio of $CD14^{++}CD80^{+}/CD14^{+}{}^{+}CD163^{+}$ cells in the infrapatellar fat pads (IFP) and subcutaneous fat tissues (SC) from the OA, rheumatoid arthritis (RA) without bDMARDs, and RA treated with bDMARDs groups. To calculate ratios and proportions, adipose-resident CD14-positive cells were stained with anti-human CD80, CD163, and CD14 antibodies and evaluated using flow cytometry. **(D)** Proportions of $CD14^{++}CD80^{+}$ and $CD14^{++}CD163^{+}$ cells in the SC and IFP tissues of OA and RA patients (SC OA, $n = 4$; SC RA, $n = 6$; IFP OA, $n = 11$; IFP RA, $n = 13$). The x-axis displays samples from IFP and SC grouped by OA and RA, and the y-axis displays the proportions of $CD14^{++}CD80^{+}$ cells or $CD14^{++}CD163^{+}$ cells in CD14-positive cells. Lines connecting the dots between SC and IFP indicate samples from the same patients. Gating strategies for obtaining $CD14^{++}CD80^{+}$ cells and $CD14^{++}CD163^{+}$ cells as well as fluorescence minus one are presented in **Supplementary Figures S1** and **S2**. Statistics were calculated by the paired-sample Wilcoxon signed-rank test between $CD14^{++}CD80^{+}$ and $CD14^{++}CD163^{+}$ cells from the same patients. The Mann–Whitney *U*-test was used for analysis between different groups.

TABLE 2 | $CD14^{++}CD80^{+}$ cells and $CD14^{++}CD163^{+}$ cells from the IFP and SC in each disease group.

	IFP		SC	
	$CD14^{++}CD80^{+}$	**$CD14^{++}CD163^{+}$**	**$CD14^{++}CD80^{+}$**	**$CD14^{++}CD163^{+}$**
OA	9.3×10^4 (7.7×10^4)	1.1×10^5 (1.1×10^5)	3.9×10^3 (4.7×10^3)	5.4×10^3 (5.5×10^3)
	$N = 11$		$N = 4$	
RA without bDMARDs	3.2×10^4 (2.8×10^4)	4.4×10^4 (3.3×10^4)	4.9×10^3 (4.7×10^3)	4.8×10^3 (4.6×10^3)
	$N = 8$		$N = 3$	
RA with bDMARDs	5.7×10^4 (4.0×10^4)	7.4×10^4 (6.3×10^4)	672 (76)	1,646 (948)
	$N = 4$		$N = 2$	

Cell numbers were determined using flow cytometry and are displayed as mean (SD).
IFP, infrapatellar fat pad; SC, subcutaneous fat tissue.

The Expression of Lipid Transcription Factors Related to Inflammation Significantly Decreases in the IFP

As IFP and SC are fat tissues, and IFP is found in an environment related to inflammation, lipid transcription factors related to inflammation, such as SREBPs and LXRs, were of interest in this study. The expression levels of these genes and the inflammatory cytokines produced by CD14-positive cells from the IFP and SC were quantified by qRT-PCR (**Figures 4**, **5**). Statistics on mean (SD) of the expression levels of these genes in CD14-positive cells in each group are presented in **Supplementary Figure S4**. The samples analyzed by qRT-PCR were magnetically sorted CD14-positive cells in the SVF from each SC and IFP sample. Lines connecting the dots from the SC to IFP indicated samples from the same patients. Consequently, as described in the left panel of **Figure 4A**, the relative expression level [median (IQR)] of

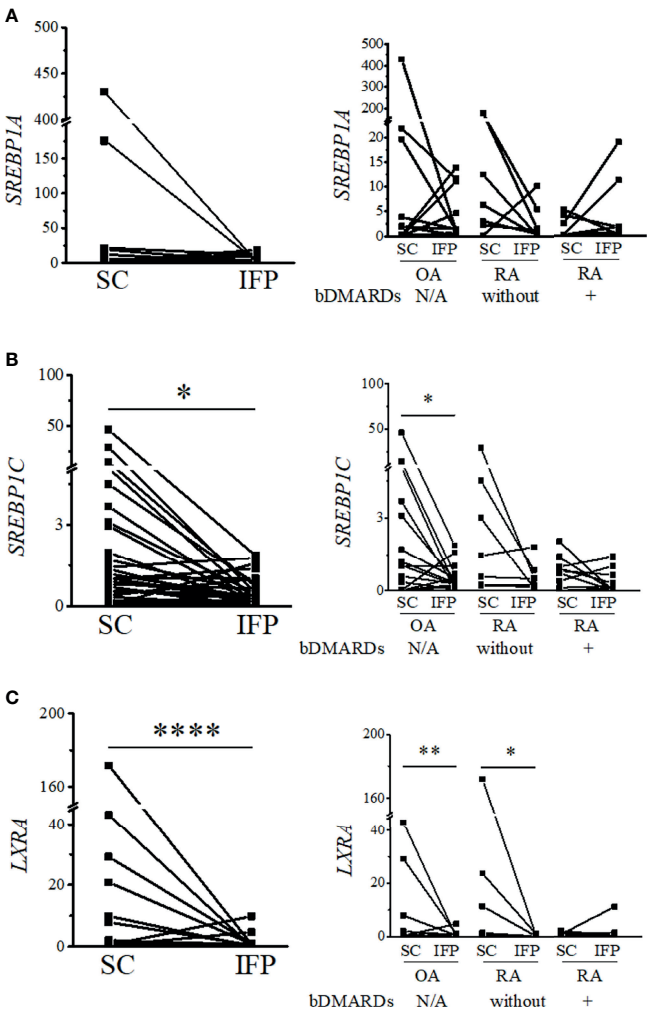

FIGURE 4 | Expression levels of lipid transcription factors related to inflammation decrease in the infrapatellar fat pads (IFP). Expression levels of SREBP1A **(A)**, SREBP1C **(B)**, and LXRA **(C)** in the IFP and subcutaneous fat tissues (SC) from osteoarthritis (OA) and rheumatoid arthritis (RA) patients. The panels to the left contain results comparing the expression levels between SC and IFP without division by diseases. The panels to the right contain results comparing the expression levels of SC and IFP in patients with OA, RA treated with bDMARDs, and RA without bDMARDs treatment. Lines connecting the dots from SC to IFP indicate samples from the same patients. The samples were labeled and separated into CD14-positive cells from the stromal vascular fraction of the IFP and SC from each patient. The median (interquartile range, IQR) expression levels of *SREBP1A*, *SREBP1C*, and *LXRA* in the SC from all patients were 0.31 (0–5.25), 0.98 (0.22–2.98), and 0.69 (0.34–2.12); these expression levels changed to 1.1 (0.09–4.81), 0.30 (0.16–0.71), and 0.039 (0.0085–0.50) in the IFP. The median (IQR) expression levels of *SREBP1C* and *LXRA* in the SC from OA patients were 1.03 (0.03–3.69) and 0.69 (0.34–2.14); these expression levels changed to 0.31 (0.23–0.71) and 0.039 (0.018–0.50) in the IFP. The median (IQR) expression levels of *LXRA* in the SC and IFP from RA patients who were not treated with bDMARDs were 1.04 (0.065–20.89) and 0.017 (0.0067–0.81). Significant differences are displayed in each figure. OA, $n = 15$; RA without bDMARDs, $n = 7$; RA with bDMARDs, $n = 9$, respectively. The $2^{-\Delta\Delta CT}$ method was used to quantify the qPCR data. *GAPDH* was used as the reference gene. The average *GAPDH* Ct values from all SC samples were used to normalize the Ct values. The Y-axes indicate the relative expression levels of mRNA, which were normalized by *GAPDH*. *$p < 0.05$, **$p < 0.01$, and ****$p < 0.0001$, as determined using the Mann–Whitney *U*-test for differences between the IFP and SC groups and the paired-sample Wilcoxon signed-rank test for differences between IFP and SC within the OA, RA without bDMARDs, and RA with bDMARDs groups.

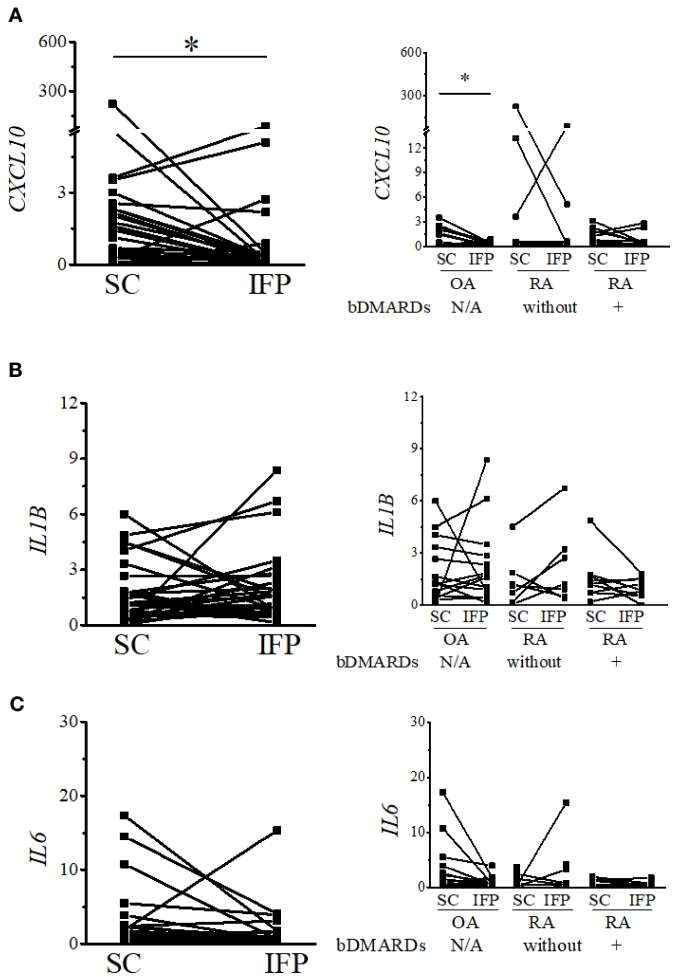

FIGURE 5 | Expression levels of inflammatory cytokines decrease in the IFP. Expression levels of CXCL10 **(A)**, IL1B **(B)**, and IL6 **(C)** in the infrapatellar fat pads (IFP) and subcutaneous fat tissues (SC) from osteoarthritis (OA) and rheumatoid arthritis (RA) patients. The panels to the left contain results comparing the expression levels between SC and IFP without division by diseases. The panels to the right contain results comparing the expression levels of SC and IFP in patients with OA, RA treated with bDMARDs, and RA who were not treated by bDMARDs. Lines connecting the dots from SC to IFP indicate samples from the same patients. The samples were labeled and separated into CD14-positive cells from the stromal vascular fraction of the IFP and SC of each patient. The median (interquartile range) expression levels of *CXCL10* in the SC and IFP from patients were 1.13 (0.23–2.33) and 0.33 (0.10–0.55); the expression level in the SC was 0.98 (0.07–2.33) and changed to 0.17 (0.05–0.42) in the IFP of OA patients. Significant differences are displayed in each figure. OA, $n = 15$; RA without bDMARDs, $n = 7$; RA with bDMARDs, $n = 9$, respectively. The $2^{-\Delta\Delta CT}$ method was used to quantify the qPCR data. *GAPDH* was used as the reference gene. The average *GAPDH* Ct values from all SC samples were used to normalize the Ct values. The Y-axes indicate the relative expression levels of mRNA, which were normalized by *GAPDH*. *$p < 0.05$, as determined using the Mann–Whitney *U*-tests for differences between the IFP and SC groups and the paired-sample Wilcoxon signed-rank test for differences between the IFP and SC within the OA, RA without bDMARDs, and RA with bDMARDs groups. Data for the sample whose *CXCL10* $2^{-\Delta\Delta CT}$ value was 69.2-fold higher than the average were removed from the plot.

SREBP1A in the CD14-positive cells of SC in all patients was 0.31 (0–5.25); however, in the IFP, this value changed to 1.1 (0.09–4.81), without any significance. As displayed in the left panels of **Figures 4B, C**, **5A**, the respective expression levels of *SREBP1C*, *LXRA*, and *CXCL10* in the CD14-positive cells of SC from whole patients were 0.98 (0.22–2.98), 0.69 (0.34–2.12), and 1.13 (0.23–2.33); however, these levels respectively decreased to 0.30 (0.16–0.71), 0.039 (0.0085–0.50), and 0.33 (0.10–0.55) in the IFP, with *p*-values less than 0.05 depicting significance. These differences were also apparent in patients with OA, with 1.03 (0.03–3.69), 0.69 (0.34–2.14), and 0.98 (0.07–2.33) in the SC, which decreased to 0.31 (0.23–0.71), 0.039 (0.018–0.50), and 0.17 (0.05–0.42) in the IFP, with *p*-values less than 0.05 depicting significance, as shown in the right panels of **Figures 4B, C**, **5A**. In addition, the expression levels of *LXRA* in the RA without bDMARDs treatment group were 1.04 (0.065–20.89) and 0.017 (0.0067–0.81) in the SC and IFP, respectively, which indicated significance. No significant relationship was found between *IL1B* and *IL6* within or among each group (**Figures 5B, C**).

Inflammation Status Is Influenced by BMI and Age in Arthropathy Patients

The impact of BMI and age on CD14-positive cells, the ratio of $CD14^{++}CD80^{+}$ cells/$CD14^{++}CD163^{+}$ cells, and the gene expression levels in each disease are highlighted in **Table 3**. Some of the results were not covered in the analysis among whole samples—for instance, in OA patients whose BMI was >25, *IL6* expression was significantly lower in the IFP than the SC; however, in OA patients whose BMI was <25 and in the whole group, this significance disappeared. Furthermore, some results in the whole group showed bias to a certain group in BMI—for example, in the RA without bDMARDs treatment group with BMI >25, *CXCL10* expression was significantly lower in the IFP than SC, while in the RA with bDMARDs treatment group with BMI <25, *LXRA* expression was significantly lower in the IFP than SC. Moreover, patients with BMI >25 in both the OA and RA with bDMARDs treatment groups tended to have higher proportions of CD14-positive cells in the fat tissue. To determine whether age impacts these results, the patients were divided into age groups below or above 75 (**Table 3**), which is indicated as senior people, or were divided into age groups below or above the median age (**Supplementary Table S3**). In **Table 3**, significant differences of CD14-positive cells per gram of fat tissues were found in OA patients who were over 75 years old as well as in the group of RA patients who were not treated by bDMARDs and under 75 years old. On the other hand, the expression levels of *LXRA* and *SREBP1C* had significant differences between SC and IFP in patients under 75 years old of both OA and RA who were not treated by bDMARDs groups. However, in the age groups divided into below or above median age in each disease, the significance of *LXRA* in RA patients who were not treated by bDMARDs was missing (**Supplementary Table S3**), which illustrated the accuracy of age classification in **Table 3**. Overall, inflammation was found to be influenced by BMI and age in arthropathy patients.

DISCUSSION

In the present study, samples obtained from patients with OA and RA who underwent knee surgery revealed that the number of CD14-positive cells per gram of IFP was significantly higher than that of the SC. The ratios of $CD14^{++}CD80^{+}$ cells/$CD14^{++}CD163^{+}$ cells increased between IFP and SC within the OA group and the RA treated with bDMARDs group (p = 0.05835 and 0.8170, respectively). In addition, the expression levels of lipid transcription factors related to inflammation were significantly lower in OA IFP than OA SC.

The IFP is demonstrated as an active inflammatory site in arthritis (27). Although the IFP is an adipose tissue, its characteristics differ from other "classic" adipose tissues, such as SC (21). Thus, we compared the features of IFP to those of SC to assess the varying differentiation pattern of macrophages in the IFP in the inflammatory environment. In our study, an average increase of fivefold was found for the number of CD14-positive cells in the IFP relative to that in the SC (**Figure 2**). Therefore, SC and IFP

TABLE 3 | Impact of body mass index (BMI) and age category of osteoarthritis (OA) and rheumatoid arthritis (RA) patients on the related gene expression.

		CD14-positive cells (105)/grams of fat tissue	M1/M2 ratio	*SREBP1A*	*SREBP1C*	*LXRA*	*CXCL10*	*IL1B*	*IL6*
BMI <25	OA	**0.0156**	Not assessed	0.6250	0.7500	0.5000	1.0000	0.2500	0.8750
		N = 7	*N* = 1			*N* = 4			
	RA without bDMARDs	**0.0068**	1.0000	0.1563	0.15623	**0.0313**	1.0000	0.5625	0.6875
		N = 12	*N* = 3			*N* = 6			
	RA with bDMARDs	0.2500	Not assessed			Not assessed			
		N = 3	*N* = 0			*N* = 2			
BMI ≥25	OA	**4.88E-04**	0.0952	0.6953	0.1094	0.0977	0.0098	0.2402	**0.0420**
		N = 13	*N* = 3			*N* = 11			
	RA without bDMARDs	Not assessed	Not assessed			Not assessed			
		N = 1	*N* = 0			*N* = 1			
	RA with bDMARDs	**0.0156**	1.0000	0.4375	0.5625	0.4375	**0.0313**	0.8438	0.3125
		N = 7	*N* = 2			*N* = 6			
Age <75	OA	0.0625	0.1143	0.6875	**0.0313**	**0.0313**	0.0938	0.5625	0.5625
		N = 6	*N* = 4			*N* = 6			
	RA without bDMARDs	**0.0195**	0.8333	0.2188	0.2188	**0.0313**	0.5625	0.5625	0.8438
		N = 11	*N* = 3			*N* = 6			
	RA with bDMARDs	0.4375	Not assessed	1.0000	0.3125	0.0625	0.3125	0.6250	0.1875
		N = 6	*N* = 1			*N* = 5			
Age ≥75	OA	**1.22E-04**	Not assessed	0.5703	0.4961	0.0742	0.1953	0.7344	0.0742
		N = 14	*N* = 0			*N* = 9			
	RA without bDMARDs	0.33333	Not assessed			Not assessed			
		N = 2	*N* = 0			*N* = 1			
	RA with bDMARDs	0.1250	Not assessed	0.5000	0.7500	1.0000	0.2500	0.7500	1.0000
		N = 4	*N* = 1			*N* = 3			

The impact of BMI and age in the OA and RA without bDMARDs and RA with bDMARDs groups. The patients were classified into groups with BMI below or over 25 or into age groups below or over 75 years old. The statistics of CD14-positive cells and the gene expression levels in each group were determined by paired-sample Wilcoxon signed-rank test, while the statistics for the M1/M2 ratio in each group were determined using Mann–Whitney U-tests. Data are expressed as p-values between subcutaneous fat tissue and infrapatellar fat pad. Data in bold font indicate significance.

were categorized as "inflammation-low tissue" and "inflammation-high tissue", respectively. Furthermore, the ratio of $CD14^{++}CD80^{+}$ cells/$CD14^{++}CD163^{+}$ cells and the expression levels of the genes related to lipid regulation and inflammation were compared to investigate the role of adipose-tissue-resident innate immune cells in the pathological process of arthropathy diseases. However, more samples are needed for this analysis. Furthermore, in addition to staining cells with anti-CD14, CD80, and CD163 antibodies, the quantification of CD68, inducible nitric oxide synthase, and arginase-1 in the adipose-tissue-resident CD14-positive cells by qRT-PCR might provide more reliable results.

As different groups of arthropathy patients have varying characteristics, a comparison between the groups was not performed. The number of CD14-positive cells and ratios of $CD14^{++}CD80^{+}$ cells/$CD14^{++}CD163^{+}$ cells were increased in the IFP in both the OA group and the RA treated with bDMARDs group. The CRP results based on blood tests (in **Table 1**) revealed a lower inflammation level in the OA [0.0 (0.0–0.13)] and RA treated with bDMARDs [0.05 (0.0–0.4)] groups than the RA without bDMARDs treatment [0.2 (0.0–1.7)] group. Such findings indicate that both OA and RA treated with bDMARDs patients had a lower inflammation level in their blood. However, a higher ratio of $CD14^{++}CD80^{+}$ cells/$CD14^{++}CD163^{+}$ cells appeared in the IFP of these patients, implying inflammation localization in the IFP. The expression levels of *LXRA* and *SREBP1* displayed different patterns between the IFP and SC in OA and RA patients, and the effects of concurrent or historical administration of MTX could serve as one of the reasons; this is because MTX was revealed to inhibit the amounts of inflammatory signals *via* the JAK1-STAT3 and JAK2-STAT5 transcriptional pathways in human macrophage cell lines (28, 29). In the right panel of **Figure 5A**, the expression levels of *CXCL10* in CD14-positive cells significantly decreased from the SC to IFP in OA; however, in both RA groups, this significance disappeared. As *CXCL10* responds to TNF-α, IFN-α/β/γ, IL-1β, or LPS (30), anti-TNF inhibitors, such as etanercept and golimumab used as bDMARDs (31), can alter *CXCL10* expression. The lower expression of *LXRA* in the IFP can be considered as an inhibitory effect of cytokines (32). The ratios of $CD14^{++}CD80^{+}$ cells/$CD14^{++}CD163^{+}$ cells in the IFP were relatively higher than those in the SC, which indicated that the IFP was in an inflammatory state. The *p*-value was displayed to show importance, but as the tendency is strong, if more samples can be obtained in the future, the interpretive power is supposed to increase.

To understand the mechanism of LXR downregulation in the IFP, besides inflammatory response genes, the expression levels of genes encoding enzymes involved in unsaturated fatty acid biosynthesis (*e.g.*, *SCD2*, *FADS1*, *ACOX3*, and *ELOVL5*) and the concentrations of omega-3 fatty acids (*e.g.*, docosahexaenoic acid and eicosatetraenoic acid) and omega-7 fatty acids (*e.g.*, 9Z-palmitoleic acid) need to be evaluated (33). Based on the theory that lipid transcription factors participate in the inflammation process, these results would be the first step to see the panorama of "localized lipid immunization."

This study revealed that, in the IFP of arthropathy patients, abundant CD14-positive cell stores and the ratio of $CD14^{++}CD80^{+}$ cells/$CD14^{++}CD163^{+}$ cells were elevated, implying the localization of inflammation in the IFP. Therefore, targeting adipose-tissue-resident innate immune cells in the IFP can be considered as a new therapeutic strategy for inflammatory arthritis.

DATA AVAILABILITY STATEMENT

The original contributions presented in the study are included in the article/**Supplementary Material**. Further inquiries can be directed to the corresponding author.

ETHICS STATEMENT

The studies involving human participants were reviewed and approved by the Kyoto University Graduate School and Faculty of Medicine Ethics Committee (approval number G0502-1). The patients/participants provided their written informed consent to participate in this study.

AUTHOR CONTRIBUTIONS

SM and KosM were responsible for the study design. SM, RS, and MTani collected samples during total knee arthroplasty. SM and RS carried out the experiments. HI, KoiM, and KN performed the surgery. SM wrote the first draft of the manuscript. MH, MTana, KK, SA, RN, HY, KO, AM, and TM supervised the draft of the manuscript. All authors contributed to the article and approved the submitted version.

FUNDING

This work was supported by Nagahama City, Shiga, Japan; Toyooka City, Hyogo, Japan; and five pharmaceutical companies (Mitsubishi Tanabe Pharma Co., Chugai Pharmaceutical Co. Ltd., UCB Japan Co. Ltd., AYUMI Pharmaceutical Co., and Asahi Kasei Pharma Co.). The KURAMA cohort study is supported by grants from Daiichi Sankyo Co. Ltd. This study was conducted as an investigator-initiated study. The companies had no role in the design of the study, the collection or analysis of the data, the writing of the manuscript, or the decision to submit the manuscript for publication.

ACKNOWLEDGMENTS

The authors would like to specially thank Atsuko Tamamoto for collecting samples in March of 2020 and Editage (www.editage.com) for English language editing.

SUPPLEMENTARY MATERIAL

The Supplementary Material for this article can be found online at: https://www.frontiersin.org/articles/10.3389/fimmu.2021.774177/full#supplementary-material

REFERENCES

1. Hawker GA. Osteoarthritis is a Serious Disease. *Clin Exp Rheumatol* (2019) 37 Suppl;120:3–6.
2. Aletaha D, Smolen JS. Diagnosis and Management of Rheumatoid Arthritis: A Review. *JAMA* (2018) 320:1360–72. doi: 10.1001/jama.2018.13103
3. Penatti A, Facciotti F, De Matteis R, Larghi P, Paroni M, Murgo A, et al. Differences in Serum and Synovial CD4+ T Cells and Cytokine Profiles to Stratify Patients With Inflammatory Osteoarthritis and Rheumatoid Arthritis. *Arthritis Res Ther* (2017) 19:103. doi: 10.1186/s13075-017-1305-1
4. Harasymowicz NS, Clement ND, Azfer A, Burnett R, Salter DM, Simpson AHWR. Regional Differences Between Perisynovial and Infrapatellar Adipose Tissue Depots and Their Response to Class II and Class III Obesity in Patients With Osteoarthritis. *Arthritis Rheumatol* (2017) 69:1396–406. doi: 10.1002/art.40102
5. Kapoor M, Martel-Pelletier J, Lajeunesse D, Pelletier JP, Fahmi H. Role of Proinflammatory Cytokines in the Pathophysiology of Osteoarthritis. *Nat Rev Rheumatol* (2011) 7:33–42. doi: 10.1038/nrrheum.2010.196
6. Woodell-May JE, Sommerfeld SD. Role of Inflammation and the Immune System in the Progression of Osteoarthritis. *J Orthop Res* (2020) 38:253–7. doi: 10.1002/jor.24457
7. Torices S, Julia A, Muñoz P, Varela I, Balsa A, Marsal S, et al. A Functional Variant of TLR10 Modifies the Activity of NFkB and may Help Predict a Worse Prognosis in Patients With Rheumatoid Arthritis. *Arthritis Res Ther* (2016) 18:221. doi: 10.1186/s13075-016-1113-z
8. Smolen JS, Landewé R, Bijlsma J, Burmester G, Chatzidionysiou K, Dougados M, et al. EULAR Recommendations for the Management of Rheumatoid Arthritis With Synthetic and Biological Disease-Modifying Antirheumatic Drugs: 2016 Update. *Ann Rheum Dis* (2017) 76:960–77. doi: 10.1136/annrheumdis-2016-210715
9. Wang T, He C. Pro-Inflammatory Cytokines: The Link Between Obesity and Osteoarthritis. *Cytokine Growth Factor Rev* (2018) 44:38–50. doi: 10.1016/j.cytogfr.2018.10.002
10. de Jong AJ, Klein-Wieringa IR, Andersen SN, Kwekkeboom JC, Herb-van Toorn L, de Lange-Brokaar BJE, et al. Lack of High BMI-Related Features in Adipocytes and Inflammatory Cells in the Infrapatellar Fat Pad (IFP). *Arthritis Res Ther* (2017) 19:186. doi: 10.1186/s13075-017-1395-9
11. Roemer FW, Jarraya M, Felson DT, Hayashi D, Crema MD, Loeuille D, et al. Magnetic Resonance Imaging of Hoffa's Fat Pad and Relevance for Osteoarthritis Research: A Narrative Review. *Osteoarthritis Cartilage* (2016) 24:383–97. doi: 10.1016/j.joca.2015.09.018
12. Jiang LF, Fang JH, Wu LD. Role of Infrapatellar Fat Pad in Pathological Process of Knee Osteoarthritis: Future Applications in Treatment. *World J Clin Cases* (2019) 7:2134–42. doi: 10.12998/wjcc.v7.i16.2134
13. Ioan-Facsinay A, Kloppenburg M. An Emerging Player in Knee Osteoarthritis: The Infrapatellar Fat Pad. *Arthritis Res Ther* (2013) 15:225. doi: 10.1186/ar4422
14. Cassetta L, Cassol E, Poli G. Macrophage Polarization in Health and Disease. *ScientificWorldJournal* (2011) 11:2391–402. doi: 10.1100/2011/213962
15. Sica A, Mantovani A. Macrophage Plasticity and Polarization: *In Vivo* Veritas. *J Clin Invest* (2012) 122:787–95. doi: 10.1172/JCI59643
16. Kontny E, Prochorec-Sobieszek M. Articular Adipose Tissue Resident Macrophages in Rheumatoid Arthritis Patients: Potential Contribution to Local Abnormalities. *Rheumatol (Oxford)* (2013) 52:2158–67. doi: 10.1093/rheumatology/ket287
17. Weisberg SP, McCann D, Desai M, Rosenbaum M, Leibel RL, Ferrante AW. Obesity is Associated With Macrophage Accumulation in Adipose Tissue. *J Clin Invest* (2003) 112:1796–808. doi: 10.1172/JCI19246
18. Boutens L, Stienstra R. Adipose Tissue Macrophages: Going Off Track During Obesity. *Diabetologia* (2016) 59:879–94. doi: 10.1007/s00125-016-3904-9
19. Murano I, Rutkowski JM, Wang QA, Cho YR, Scherer PE, Cinti S. Time Course of Histomorphological Changes in Adipose Tissue Upon Acute Lipoatrophy. *Nutr Metab Cardiovasc Dis* (2013) 23:723–31. doi: 10.1016/j.numecd.2012.03.005
20. Gericke M, Weyer U, Braune J, Bechmann I, Eilers J. A Method for Long-Term Live Imaging of Tissue Macrophages in Adipose Tissue Explants. *Am J Physiol Endocrinol Metab* (2015) 308:E1023–33. doi: 10.1152/ajpendo.00075.2015
21. Distel E, Cadoudal T, Durant S, Poignard A, Chevalier X, Benelli C. The Infrapatellar Fat Pad in Knee Osteoarthritis: An Important Source of Interleukin-6 and its Soluble Receptor. *Arthritis Rheumatol* (2009) 60:3374–7. doi: 10.1002/art.24881
22. Vandesompele J, De Preter K, Pattyn F, Poppe B, Van Roy N, De Paepe A, et al. Accurate Normalization of Real-Time Quantitative RT-PCR Data by Geometric Averaging of Multiple Internal Control Genes. *Genome Biol* (2002) 3:RESEARCH0034. doi: 10.1186/gb-2002-3-7-research0034
23. Ko HL, Wang YS, Fong WL, Chi MS, Chi KH, Kao SJ. Apolipoprotein C1 (APOC1) as a Novel Diagnostic and Prognostic Biomarker for Lung Cancer: A Marker Phase I Trial. *Thorac Cancer* (2014) 5:500–8. doi: 10.1111/1759-7714.12117
24. Greenblatt MB, Sargent JL, Farina G, Tsang K, Lafyatis R, Glimcher LH, et al. Interspecies Comparison of Human and Murine Scleroderma Reveals IL-13 and CCL2 as Disease Subset-Specific Targets. *Am J Pathol* (2012) 180:1080–94. doi: 10.1016/j.ajpath.2011.11.024
25. Singh R, Yadav V, Kumar S, Saini N. MicroRNA-195 Inhibits Proliferation, Invasion and Metastasis in Breast Cancer Cells by Targeting FASN, HMGCR, ACACA and CYP27B1. *Sci Rep* (2015) 5:17454. doi: 10.1038/srep17454
26. Fukui S, Iwamoto N, Takatani A, Igawa T, Shimizu T, Umeda M, et al. M1 and M2 Monocytes in Rheumatoid Arthritis: A Contribution of Imbalance of M1/M2 Monocytes to Osteoclastogenesis. *Front Immunol* (2017) 8:1958. doi: 10.3389/fimmu.2017.01958
27. Plebanczyk M, Radzikowska A, Burakowski T, Janicka I, Musialowicz U, Kornatka A, et al. Different Secretory Activity of Articular and Subcutaneous Adipose Tissues From Rheumatoid Arthritis and Osteoarthritis Patients. *Inflammation* (2019) 42(1):375–86. doi: 10.1007/s10753-018-0901-9
28. Thomas S, Fisher KH, Snowden JA, Danson SJ, Brown S, Zeidler MP. Methotrexate Is a JAK/STAT Pathway Inhibitor. *PloS One* (2015) 10: e0130078. doi: 10.1371/journal.pone.0130078
29. Gremese E, Alivernini S, Tolusso B, Zeidler MP, Ferraccioli G. JAK Inhibition by Methotrexate (and csDMARDs) may Explain Clinical Efficacy as Monotherapy and Combination Therapy. *J Leukoc Biol* (2019) 106:1063–8. doi: 10.1002/JLB.5RU0519-145R
30. Groom JR, Luster AD. CXCR3 Ligands: Redundant, Collaborative and Antagonistic Functions. *Immunol Cell Biol* (2011) 89:207–15. doi: 10.1038/icb.2010.158
31. Degboé Y, Rauwel B, Baron M, Boyer JF, Ruyssen-Witrand A, Constantin A, et al. Polarization of Rheumatoid Macrophages by TNF Targeting Through an IL-10/STAT3 Mechanism. *Front Immunol* (2019) 10:3. doi: 10.3389/fimmu.2019.00003
32. Laragione T, Gulko PS. Liver X Receptor Regulates Rheumatoid Arthritis Fibroblast-Like Synoviocyte Invasiveness, Matrix Metalloproteinase 2 Activation, Interleukin-6 and CXCL10. *Mol Med* (2012) 18:1009–17. doi: 10.2119/molmed.2012.00173
33. Oishi Y, Spann NJ, Link VM, Muse ED, Strid T, Edillor C, et al. SREBP1 Contributes to Resolution of Pro-Inflammatory TLR4 Signaling by Reprogramming Fatty Acid Metabolism. *Cell Metab* (2017) 25:412–27. doi: 10.1016/j.cmet.2016.11.009

Conflict of Interest: The authors declare that the research was conducted in the absence of any commercial or financial relationships that could be construed as a potential conflict of interest.

frontiers in Immunology

ORIGINAL RESEARCH
published: 09 December 2021
doi: 10.3389/fimmu.2021.791907

YAP/TAZ: Key Players for Rheumatoid Arthritis Severity by Driving Fibroblast Like Synoviocytes Phenotype and Fibro-Inflammatory Response

*Robin Caire[1], Estelle Audoux[2], Guillaume Courbon[1], Eva Michaud[2], Claudie Petit[3], Elisa Dalix[1], Marwa Chafchafi[1], Mireille Thomas[1], Arnaud Vanden-Bossche[1], Laurent Navarro[3], Marie-Thérèse Linossier[1], Sylvie Peyroche[1], Alain Guignandon[1], Laurence Vico[1], Stephane Paul[2,4] and Hubert Marotte[1,4,5]**

[1] INSERM, U1059-SAINBIOSE, Université de Lyon, Saint-Etienne, France, [2] CIRI (Centre International de Recherche en Infectiologie), Equipe GIMAP (Team 15), INSERM, U1111, CNRS, ENS, UCBL1, Université Jean Monnet, Université de Lyon, Saint-Etienne, France, [3] INSERM, U1059-SAINBIOSE, Mines Saint-Etienne, Université de Lyon, Saint-Etienne, France, [4] CIC INSERM, 1408, Université de Lyon, Saint-Etienne, France, [5] Department of Rheumatology, Hôpital Nord, University Hospital Saint-Etienne, Saint-Etienne, France

OPEN ACCESS

Edited by:
Gurpreet S Baht,
Duke University, United States

Reviewed by:
Gabriel Courties,
INSERM U1183 Cellules Souches, Plasticité Cellulaire, Médecine Régénératrice Et Immunothérapies, France
Aline Bozec,
University of Erlangen Nuremberg, Germany

***Correspondence:**
Hubert Marotte
hubert.marotte@chu-st-etienne.fr

Specialty section:
This article was submitted to Inflammation, a section of the journal Frontiers in Immunology

Received: 09 October 2021
Accepted: 18 November 2021
Published: 09 December 2021

Citation:
Caire R, Audoux E, Courbon G, Michaud E, Petit C, Dalix E, Chafchafi M, Thomas M, Vanden-Bossche A, Navarro L, Linossier M-T, Peyroche S, Guignandon A, Vico L, Paul S and Marotte H (2021) YAP/TAZ: Key Players for Rheumatoid Arthritis Severity by Driving Fibroblast Like Synoviocytes Phenotype and Fibro-Inflammatory Response. Front. Immunol. 12:791907. doi: 10.3389/fimmu.2021.791907

Objective: The role of YAP/TAZ, two transcriptional co-activators involved in several cancers, was investigated in rheumatoid arthritis (RA).

Methods: Fibroblast like synoviocytes (FLS) from patients with RA or osteoarthritis were cultured in 2D or into 3D synovial organoids. Arthritis rat model (n=28) and colitis mouse model (n=21) were used. YAP/TAZ transcriptional activity was inhibited by verteporfin (VP). Multiple techniques were used to assess gene and/or protein expression and/or localization, cell phenotype (invasion, proliferation, apoptosis), bone erosion, and synovial stiffness.

Results: YAP/TAZ were transcriptionally active in arthritis (19-fold increase for CTGF expression, a YAP target gene, in RA *vs.* OA organoids; $p<0.05$). Stiff support of culture or pro-inflammatory cytokines further enhanced YAP/TAZ transcriptional activity in RA FLS. Inhibiting YAP/TAZ transcriptional activity with VP restored a common phenotype in RA FLS with a decrease in apoptosis resistance, proliferation, invasion, and inflammatory response. Consequently, VP blunted hyperplasic lining layer formation in RA synovial organoids. *In vivo*, VP treatment strongly reduced arthritis severity (mean arthritic index at 3.1 in arthritic group *vs.* 2.0 in VP treated group; $p<0.01$) by restoring synovial homeostasis and decreasing systemic inflammation. YAP/TAZ transcriptional activity also enhanced synovial membrane stiffening *in vivo*, thus creating a vicious loop with the maintenance of YAP/TAZ activation over time in FLS. YAP/TAZ inhibition was also effective in another inflammatory model of mouse colitis.

Conclusion: Our work reveals that YAP/TAZ were critical factors during arthritis. Thus, their transcriptional inhibition could be relevant to treat inflammatory related diseases.

Keywords: YAP, mechanotransduction, inflammation, rheumatoid arthritis, inflammatory bowel disease

INTRODUCTION

Yes-associated protein (YAP) and transcriptional co-activator with PDZ-binding motif (TAZ) are two transcriptional co-activators sharing strong structure similarities (1). They are activated in several cancer cells (2, 3). Upon specific *stimuli*, YAP/TAZ are translocated to the nucleus to induce transcription by interacting mainly with transcriptional enhanced associate domains (TEAD) (4). YAP/TAZ are partly regulated by the Hippo pathway, which leads to their retention in the cytoplasm (5). YAP/TAZ were first linked to tissue size homeostasis as they promote overgrowth when hyperactivated (6). In chronic inflammatory diseases, tissue resident cells could acquire tumor-like features and participate in inflammation development and tissue destruction (7–9). There are some emerging evidence that YAP transcriptional activity could promote chronic inflammatory diseases, especially in inflammatory bowel disease (IBD) (10–13).

Rheumatoid arthritis (RA) is the most common immune disorder characterized by joint inflammation and destruction (14). In RA, fibroblast-like synoviocytes (FLS), resident cells of the synovial tissue, acquire an aggressive phenotype including hyperproliferation, apoptosis resistance and invasion ability [partly linked to the secretion of matrix metalloproteinases (MMPs) such as MMP-2 and MMP-13 (15, 16)] persisting even after the inflammation has been suppressed (7). FLS are also key actors in initiating and maintaining the recruitment of immune cells (17, 18). The mechanisms involved in RA FLS phenotype are still unclear, with some contributions from c-Jun, a member of the activator protein 1 (AP-1) (19), nuclear factor κB (NF-κB) pathway (20), p53 or B-cell lymphoma 2 (Bcl-2) family members involved in apoptosis regulation (20, 21), and/or epigenetic alterations (22). Recently, epigenetic modifications of the Hippo pathway were also reported in RA FLS (23). Inhibition of YAP activity with verteporfin (VP), which blocks the binding between YAP/TAZ and TEAD (24), decreased RA FLS invasion and MMP-13 expression thus improving arthritis in mice (23). In addition to the involvement of YAP/TAZ in joint resident cells, TAZ was also described to increase the balance between IL-17 producing CD4+ T helper lymphocyte (Th17) and T regulatory lymphocyte (Tregs), stimulating the transcription of retinoic acid receptor-related orphan receptor-γ (RORγT) and leading to an increase of Th17 differentiation (25), which are the main source of IL-17. In RA, Th17 cells are major pro-inflammatory actors, and consequently, inhibition of YAP/TAZ could prevent systemic inflammation during arthritis.

YAP/TAZ are also major mechanotransduction actors converting cell mechanical *stimuli* (such as stiffening of the surrounding environment) into transcriptional responses for cell phenotype adaptation, independently of the Hippo pathway (26, 27). Interestingly, inflammation is commonly associated with increased cellular tension, through actin stress fibers (SF) formation (28). Inflammation can also trigger stiffening process in tissues through extracellular matrix (ECM) remodeling including stiff ECM component synthesis such as tenascin-C and periostin, which are two stiffening markers (29, 30). Furthermore, chronic inflammation has been linked to aberrant mechanotransduction responses that activate YAP/TAZ signaling and promote aberrant cell phenotype (29). However, such mechanisms remained unexplored in arthritis.

Thus, despite the recent evidence of YAP involvement in arthritis, several critical aspects are still lacking. First, YAP activity in RA FLS *in vitro* or *in vivo* was not highlighted. Second, it is still unknown how YAP activity may be modulated in FLS during arthritis. Third, in addition to the role of YAP in FLS invasion, the role of YAP in several other arthritis mechanisms such as FLS survival, global pro-inflammatory response, and synovial tissue remodeling is still to be determined. Here, we demonstrated strong YAP/TAZ transcriptional activity in RA FLS, enhanced by inflammation and mechanotransduction events that, in turn, regulated critical cellular responses involved in RA.

MATERIAL AND METHODS

Cell Culture

RA FLS were obtained during surgery procedure as previously described (18). All RA patients gave a written consent after oral information (IRB # 2014-A01688-39). FLS were cultured in Dulbecco's modified Eagle's medium (DMEM, Sigma, St. Louis, MO, US) with 10% fetal bovine serum (FBS), 1% glutamine and 2% penicillin and on classic support substrate (2 GPa) until their use for experiments. For HEK293 cells, the same culture medium was used without glutamine but with non-essential amino acid solution at 1%. HEK293 $YAP^{-/-}$ were generated using specific CRISPR cas-9 and homology direct repair plasmid targeting YAP sequence (Santa Cruz Biotechnology, Dallas, TX, US), CRISPR clones generation was done following manufacturer instructions, and validated by western blot. For soft substrate culture (2 kPa), well plates (Cell guidance system, Cambridge, UK) or dishes (ExCellness, Lausanne, Switzerland) were used. Plates were coated with fibronectin (1:100, Sigma) for 2 hours at 37°C. TNF at 10 ng/ml and IL-17 at 50 ng/ml (R&D system, Minneapolis, MN, US) were used (except when specified in the Figures legend). Verteporfin (VP, Sigma) was used at 10 μM. For all VP experiments, cells were kept in relative darkness with blue light during manutention avoiding any aspecific activation of VP (due to its photosensitivity). For all experiments (except when

specified) FLS were plated at low cell density (2,000 cells/cm^2). HEK293 were grown on classic substrates coated with fibronectin at 100,000 cells/cm^2.

siRNA Transfection Technique

RA FLS were cultivated in classic medium antibiotic free for 24 hours and transfected at 80% confluency, before transfection FLS were rinsed using siRNA transfection medium (Santa Cruz Biotechnology, Dallas, TX, USA). RA FLS were transfected by adding YAP siRNA or control siRNA (Santa Cruz Biotechnology) at 7.5 µg/ml in siRNA transfection reagent (Santa Cruz Biotechnology; diluted 6/100 in transfection medium) for 6 hours at 37°C in a CO_2 incubator. DMEM containing 20% FBS and 2% PS was added to the wells overnight (achieving a ½ dilution of the added medium). Medium was then replaced with or without TNF and IL-17 for 48 hours before extraction. On soft substrate, RA FLS siRNA transfection was noneffective due to bovine fetal serum retention in the gel.

Western Blot

Protein extraction was performed with Allprep RNA/protein kit (Qiagen Inc, Hilden, Germany). Proteins (5 µg) were denatured and separated for 2 hours at 90 Volts before being transferred onto PVDF membranes (Thermo Fisher Scientific). The membrane was blocked and incubated with primary antibody overnight at 4°C. Then membrane was incubated with a horseradish peroxidase-conjugated secondary antibody (1:5000; Thermo Fisher Scientific, 31460) for 1 hour at RT. Immunoreactive protein bands were visualized with Clarity™ Western ECL Substrate (BioRad, Hercules, CA, US). Blots were stripped using a mild antibody stripping solution (200 mM glycine, 3.5 mM SDS, 1% Tween 20) and reprobed. Western blot (WB) was performed using the following primary antibodies diluted at 1:1,000: YAP/TAZ (8418, Cell Signaling Technology, Leiden, The Netherlands), CYR61 (14479, Cell Signaling Technology) MMP-13 (ab39012, Abcam, Cambridge, UK), NF-κB p65 (8242, Cell Signaling Technology), phospho NF-κB p65 ser536 (3031, Cell Signaling Technology) and 1:5,000: β-Actin (4970, Cell Signaling Technology).

LDH Cytotoxicity Assay

RA FLS with density at 50,000 cells/well in 100 µL of medium were plated in triplicate wells in a 96-well tissue culture plate. A complete medium control without cells were included to determine LDH background activity, additional cells were plated in triplicate wells for measurement of spontaneous LDH activity control (medium) and maximum LDH activity controls (1X lysis buffer). The cells were treated with VP at different concentrations for 24 hours at 37°C, 5% CO_2 and then the released of LDH in the supernatants was measuring using an LDH cytotoxicity assay kit (Thermo Fischer Scientific #88954).

Flow Cytometry

FLS grown on soft dishes at 2 kPa (ExCellness) for 72 hours coated with fibronectin with various *stimuli* for 48 hours were collected by trypsination. RA FLS were incubated in 1X annexin V binding buffer with Annexin V detection kit (ab14155, Abcam) or permeabilized and fixed before 1h labeling with ki67 antibody. Data were acquired using a FACSCanto II cytometer and analyzed with the BD FACS Diva software 6.1.3 (BD Nova Biosciences, UK).

Invasion Assay

RA FLS invasion abilities were assessed using BioCoat™ Growth Factor reduced Matrigel Invasion Chamber (Corning, Corning, NY, US). FLS were seeded in the upper chamber at 50,000 cells per insert in DMEM containing 1% glutamine, 1% PS and 0.1% BSA. DMEM containing 20% FBS, 1% glutamine, 1% PS and 0.1% BSA was added to the wells. The invasion chambers were then incubated for 48 hours with or without TNF, IL-17, and VP (which were added in the insert chamber and in the wells at the same concentrations). After incubation, noninvading cells were removed from the upper surface of the membrane, inserts were fixed in 4% PFA for 20 minutes at RT, and then stained with hematoxylin and eosin (H&E). Membranes of insert were imaged at x100 magnification and invading cells were counted. Results are represented by the mean of two inserts for each condition, and the mean of three images at x100 counting per insert.

Organoids Culture and Processing

Synovial organoids assembly protocol was adapted from previous publication (31). Briefly, cells from OA or RA patients were used and mixed with Matrigel (Corning) at 4.10^6 cells/ml of Matrigel, 22 µl droplets (representing approximatively 90,000 cells) were added to 96-well U-shaped very low attachment surface plates (Corning). Gelation was then allowed for 45 minutes at 37°C in a CO_2 incubator. Then specific medium was added: DMEM supplemented with 10% FBS, 1% glutamine1% nonessential amino acids, 1% penicillin-streptomycin (PS), 0.1mM ascorbic acid, and ITS solution. Organoids were maintained for 21 days in culture media. VP with or without TNF and IL-17 were used at the same concentration as for cell culture. At day 21, organoids were fixed with glyoxal/ethanol solution for 1 hour at RT (PFA fixation being deleterious). Organoids were then embedded in paraffin, cut at 6µm and stained with H&E. Other organoids were embedded in a gelatin-sucrose solution and frozen in an isopentane bath at -50°C for 2 minutes before storage at -80°C. Thick cryosections (30µm) were then used for immunofluorescence labeling.

Animals

General Information for Animal Experiments

Animals were tattooed and randomized into groups of equal weight. Experiments were performed after at least two weeks of acclimatization. All animal experiments were conducted by at least two independent experimenters, one of whom was blinded to the group allocation. There were no inclusion or exclusion criteria during animal experiments. No data exclusion was performed except if samples were impossible to use due to low quality (for example low RNA quality due to degradation). All animal studies were performed in accordance with the European Community legislation and approved by the Ethical Committee for Animal Experiments of Saint-Etienne University, agreement

number: 2019032816186046 for rat AIA model and 2019032010448893 for DSS mice.

Animal Care

All animals were housed at 2 or 3 per cage in the PLEXAN facility with 12/12h light/dark cycles and *ad libitum* water and food access. In accordance with these guidelines, regulations, and 3Rs principles, specific enrichments were used to improve animal wellfare. Anticipated endpoints were predefined and never reached. No specific pain medication was used since it interferes with inflammatory response.

AIA Rats for mRNA Kinetics

For rat mRNA kinetics analysis, samples from our previous work were used with the same protocol (32), rats were killed at different time points (n=5 for each time point) after arthritis induction (at day 6, 8, 10, 12, 17, and 24) with five control animals for each time point.

Adjuvant-Induced Arthritis Rat

The arthritis (rat AIA n=21) was induced by 1.5 mg of *Mycobacterium butyricum* (Difco Laboratories, Detroit, MI, US) injection in 6-weeks old Lewis female rats (Charles River Laboratories, L'arbresle, France) as previously described (32). Control (non-AIA n=7) rats received vehicle injection without *Mycobacterium butyricum*. In the preventive group, daily intraperitoneal (IP) injections of VP (Tocris biosciences, Bristol, UK) at 20 mg/kg/days started at day 6 (before arthritis onset); whereas in the curative VP treatment group, daily IP injections of VP at 40 mg/kg/days started at day 12 (after arthritis onset). For all groups, IP injections started at day 6 (with or without VP) and were performed with 600 µL of vehicle containing 10% DMSO. All rats were followed as previously described (31). Rats were sacrificed at day 17, ankle and spleen were stored at -80°C for further analysis. At necropsy, the right ankle was frozen and stored for mRNA analysis. A synovial biopsy was performed on the left ankle, then the fragment of synovial membrane was fixed in 4% PFA for 20 minutes and stored in 10% ethanol solution at 4°C before AFM measurements. After synovial fragment collection, left ankles were fixed with 4% PFA solution for 48 hours at 4°C. Microcomputed tomography analysis was conducted prior to decalcification in 0.5 M EDTA. Spleens were sectioned into two pieces, one for mRNA analysis and the second was fixed in 4% PFA. Spleens and decalcified ankles were next cryoprotected, then embedded and frozen at -80°C. Sections were performed using Microm HM 560 cryostat (Thermo Fisher Scientific).

Dextran Sulfate Sodium Induced Colitis Mice

Eight-weeks old female Balb/cByJ mice (Charles River Laboratories) were treated with an IP injection of VP at 40 mg/kg/day (100 µL, in 10% DMSO) or 10% DMSO one day prior to the beginning of DSS (MP Biomedicals) treatment. The latter was administered at 1.5% in drinking water, fresh solutions were prepared and changed every day for 11 days (n=14). Control mice received only drinking water and an injection of 10% DMSO (n=7). For all groups, daily IP injections were continued during DSS treatment until mice were sacrificed at day 11. Disease activity index scoring comprised several scales evaluating physiological and behavioral parameters including percentage of weight loss, stool consistency, evidences of intestinal leakage with the presence of blood in stool, animal general aspect and animal pain behavior. Scoring and weighing were performed each day. After death, intestinal tracts of mice were dissected and cut into pieces with each containing a Peyer's patch. Two pieces were snap frozen for further mRNA analysis and two other pieces were placed in 4% PFA at 4°C for 48 hours, embedded and frozen in the same process than rat AIA ankles.

RNA Extraction and RT-qPCR

For animal tissues (spleen, gut and ankle) and synovial organoids lysis was performed in TRI Reagent (Sigma). To obtain enough RNA, 3 synovial organoids were pooled for lysis. RNA was purified with RNeasy plus (Qiagen Inc.). For cell culture, RNA was extracted using Allprep RNA/protein kit (Qiagen Inc.). Quality and quantity of RNA were assessed by Experion RNA analysis (BioRad) and QuantIT RiboGreen RNA assay (Thermo Fisher Scientifc), respectively. Complementary DNA (cDNA) was synthesized using the iscript cDNA synthesis kit (Biorad). Quantitative RT polymerase chain reaction (PCR) was conducted on CFX96 RealTime System (BioRad) with LightCycler FastStart DNA Master plus SYBRgreen I (Roche Diagnostics, Basel, Switzerland). The results were normalized to the housekeeping gene expression hypoxanthine-guanine phosphoribosyltransferase (HPRT).

Immunofluorescence

This technique was done on frozen sections (organoids, spleen and ankle of rats, and mice gut) or on RA FLS and HEK293 cells fixed with 4% PFA at RT for 20 minutes. For RORγT (Biorbyt, San Francisco, CA, US) labelling on spleen and gut, citrate antigen retrieval was performed. Before labelling, sections or cells were rehydrated, permeabilized in 0.3% Triton X-100, then blocked in 1% BSA 5% goat serum and 0.1% Triton solution for 60 minutes at RT, and probed with the primary antibody diluted in the blocking solution overnight at 4°C. The following primary antibodies were used: YAP (63.7 sc-101199, Santa Cruz Biotechnology; 1:100), YAP (D8H1X, Cell Signaling Technology; 1:100), Ki67 (NB-110-89717, Novus Biologicals, Abingdon, UK; 1:100), c-Jun (9165, Cell Signaling Technology, 1:200), and tenascin-C (ab215369, Abcam, 1:100). After washing, sections or cells were incubated with secondary antibodies, goat anti-rabbit rhodamine coupled antibody (31686, Thermo Fisher; 1:300) and/or goat anti-mouse 488 (A11034, Thermo Fisher) for 75 minutes at RT, all diluted at 1:400. Slides or cells were counterstained with DAPI alone (10 minutes at 37°C) or coupled with phalloidin (R415, Thermo Fisher; or ab176753, Abcam) for 1 hour at 37°C. Isotypic controls were always performed using rabbit IgG isotype control (31235, Thermo Fisher) and mouse IgG isotype control (31903, Thermo Fisher), diluted at the same concentration as the primary antibody.

Image Acquisition, Analysis, and Quantification

Images were acquired using a confocal laser microscope (LSM) 800 airyscan (Zeiss, Oberkochen, Germany) equipped with Zen

software. This microscope was used in epifluorescence, classic confocal or airyscan confocal mode depending on the needs. Comparison between groups for image analysis and quantification were performed using the exact same settings from antibodies labelling to image processing.

Immunofluorescence Images Quantification

Ki-67 and YAP labelling on RA FLS were evaluated by automatically defining nuclear region of interest (ROI) area based on DAPI staining, ROI nuclear mask was then added on YAP and Ki67 images. Positive cells for YAP or Ki67 labelling in the nucleus were then counted and divided by the total number of nuclei (DAPI). This quantification was performed on large acquisition tiles at x100 magnification, representing approximately 50 to 200 cells per well. C-Jun labelling on frozen sections of organoid was quantified by measuring mean intensity in DAPI ROI in the synovial lining layer divided by the same measurement in the stroma.

Organoid Synovial Hyperplasia

This quantification was performed on H&E paraffin sections. Each organoid assessment was the result of two organoid slices. Images were binarized and a synovial lining layer area was automatically selected. Organoid perimeters were also measured. Hyperplasia criteria was the result of synovial lining layer area divided by synovial organoid perimeter.

Peyer's Patches Area

This quantification was performed on H&E frozen intestinal sections. Area of Peyer's patches was evaluated by manual ROI drawing based on histology. For each mouse, result was the mean of two distinct Peyer's patches (one from the beginning and one from the end of the intestinal tract).

Microcomputed Tomography

Rat AIA ankles were scanned *ex vivo* with vivaCT40 (Scanco, Brüttisellen, Switzerland) at 55 kVp (peak kilovoltage) and reconstructed under a resolution of 12.5 µm. Quantification and 3-D imaging were performed after reconstruction. Reconstruction was performed under 0.5/2/307 (Gauss sigma/ Gauss support/lower threshold).

AFM Measurement

AFM measurements were performed using standard force mode on a Veeco Multimode AFM equipped with Nanoscope IIIa controller and Picoforce extension. Briefly, we glued a 50-µm polystyrene microsphere (Alpha Nanotech, Morrisville, NC, US) on a 0.1 N/m rigidity cantilever (Bruker MLCT-Bio, E triangular) and this cantilever was used for all measurements. Rat synovial samples were dissected under binocular microscope from the same area. A nano-indentation was performed in force mode by recording two force curves on three independent areas twice for each sample. The acquired force curves were exported in ASCII format with nanoscope V614r1 software, and then the data were processed using a proper Matlab® code. The code includes the fitting of the contact area from the force curves with a Hertz contact model in order to extract Young's elastic modulus (rigidity in kPa).

Statistical Analysis

Data were represented as single values, with mean and standard deviation or median and interquartile range, accordingly to normality. Some parameters were expressed as percentage of the mean of control values. Two comparisons were done with Mann-Whitney test or unpaired Student t-test. Multiple comparisons were performed by ANOVA or Kruskal-Wallis test, *post hoc* comparisons were corrected with the false discovery rate method of Benjamini and Hochberg (q-values). Results were considered significantly different when $p<0.05$ or $q<0.05$. All statistical analyses were performed on GraphPad Prism 8.2.0 software.or.

RESULTS

High YAP/TAZ Transcriptional Activity During Arthritis

To investigate YAP/TAZ activity during arthritis, FLS from RA patients were used and compared to FLS from osteoarthritis (OA) patients as controls. As YAP/TAZ transcriptional activity was reported activated by substrate stiffness (such as classic culture dishes), YAP/TAZ activity was compared between RA and OA FLS using a synovial organoid model. This model recapitulated features of the synovial membrane *in vivo* and was closer to physiological conditions than 2D cell culture. Compared to OA organoids, RA synovial organoids displayed higher expression of YAP and its target genes: connective tissue growth factor (CTGF) and cysteine-rich angiogenic inducer 61 (CYR61; **Figure 1A**). The high *in vitro* YAP/TAZ transcriptional activity was then confirmed *in vivo* using the adjuvant-induced arthritis (AIA) rat model (32). In this model, the mRNA level of YAP increased in the ankle of AIA rats on days 6, 8 and 10 after induction (before arthritis onset), followed by an increased expression of its target genes, including E2F transcription factor 1 (E2F1), hexokinase 2 (HK2), ankyrin repeat domain-containing protein 1 (Ankrd1), CTGF and CYR61 on days 10 and 12 after induction (at the arthritis onset; **Figure 1B**).

Increased YAP/TAZ Transcriptional Activity in RA FLS by Inflammation and Mechanical Priming

Then, to explore the mechanisms involved in YAP/TAZ transcriptional activity in RA FLS, we first focused on inflammation effect. TNF and IL-17, two pro-inflammatory cytokines strongly involved in RA, were used to mimic the *in vivo* inflammatory environment of RA (33, 34). To avoid substrate stiffness-induced YAP activity, RA FLS were grown on soft substrate (2kPa). Nevertheless, classic support stiffness (2GPa) was kept as reference. TNF or IL-17 increased YAP nuclear localization at 48 hours in RA FLS with a synergistic effect (**Figures 2A, B**). Consistently, CYR61 protein level trended to increase upon cytokines treatment in RA FLS (**Figures 2C, D**),

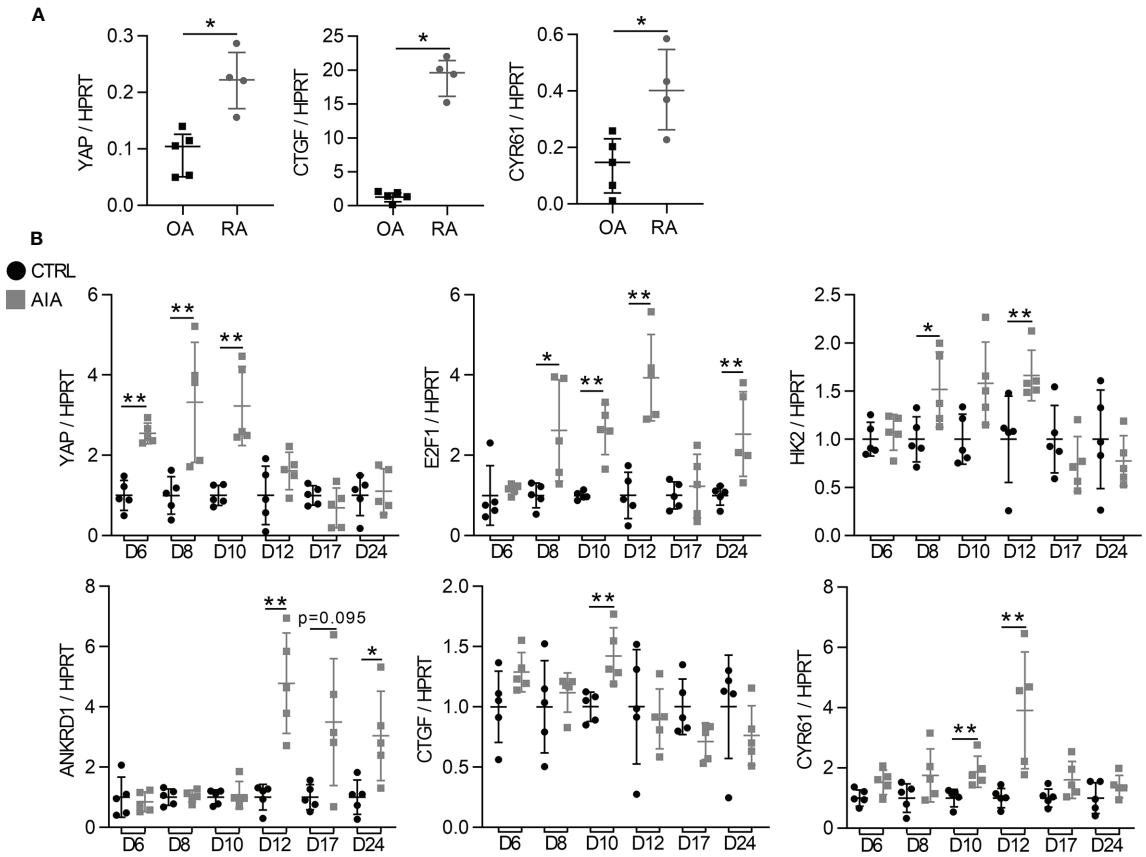

FIGURE 1 | High YAP/TAZ transcriptional activity during arthritis **(A)** RT-qPCR quantification of YAP, CTGF and CYR61 expression normalized to HPRT expression in synovial organoids at 21 days of culture. Organoids (n=12 to 15) were formed with FLS from one rheumatoid arthritis (RA) and one osteoarthritis (OA) patient. Each point represents three organoids that were mixed for RNA extraction. **(B)** RT-qPCR results of mRNA from the ankle of adjuvant induced arthritis (AIA) and control (CT) rats. Results were normalized to HPRT expression and expressed as fold change vs. CT at each day. Rats were sacrificed at different times (n=5) with an arthritis onset observed at day 10. Data were presented as individual values with median and interquartile range. Mann-Whitney tests were used. D, day post induction; YAP, yes-associated protein; HPRT, hypoxanthine phosphoribosyltransferase; CTGF, connective tissue growth factor; CYR61, cysteine-rich angiogenic inducer 61; E2F1, E2F transcription factor1; HK2, hexokinase2; ANKRD1, ankyrin repeat domain-containing protein1; *p < 0.05; **p < 0.01.

whereas the mRNA expression of YAP target genes was not significantly enhanced at 48 hours (**Figures 2E, H**). After TNF and IL-17 stimulation, YAP total protein was unchanged in RA FLS, while total TAZ protein trended to decrease (**Figures 2I, J**).

Despite absence of inflammation or substrate stiffness, YAP remained nuclear in some RA FLS (**Figures 2A, B**). Consequently, mechanical priming of FLS by stiff environment associated with a possible persistent YAP activation was explored, since this concept was already reported in mesenchymal stem cells (35). For this purpose, RA FLS were grown on stiff substrate (classic culture substrate 2 GPa) up to passage (P) 3, P4, or P5, then switched to soft substrate for 72 hours after each of these passages (P4, P5 or P6, respectively; **Supplementary Figure 1A**). YAP nuclear localization was higher at P5 than P4 (**Supplementary Figures 1B, C**) with higher ANKRD1 expression at P6 compared to P5 (**Supplementary Figure 1D**). Thus, time spent by RA FLS on stiff substrate enhanced YAP activity when assessed on a soft substrate suggesting that mechanical stiffening could promote YAP autonomous activity in FLS. Notably, inflammation and mechanical *stimuli* activated different YAP target genes when applied separately but had synergistic effects when applied together by increasing YAP target genes expression (**Supplementary Figures 1D, E**). Taken together, these results indicated that inflammation and mechanical stiffening were inducers of YAP/TAZ transcriptional activity in RA FLS.

Reduction of RA FLS Aggressive Phenotype by YAP/TAZ Inhibition

Since YAP/TAZ transcriptional activity was high in RA FLS, its inhibition with VP was explored to restore a normal phenotype in control or inflammatory conditions. First, VP treatment had no effect on YAP nuclear translocation (**Figure 2B**), but reduced YAP target genes levels (**Figures 2C–H**) blocking YAP transcriptional activity, as did a YAP siRNA on CYR61 expression (**Supplementary Figure 2A**). VP did not affect cell mortality (**Figure 3A**). However, apoptotic annexin V positive cells were increased by the combination of VP with TNF and IL-

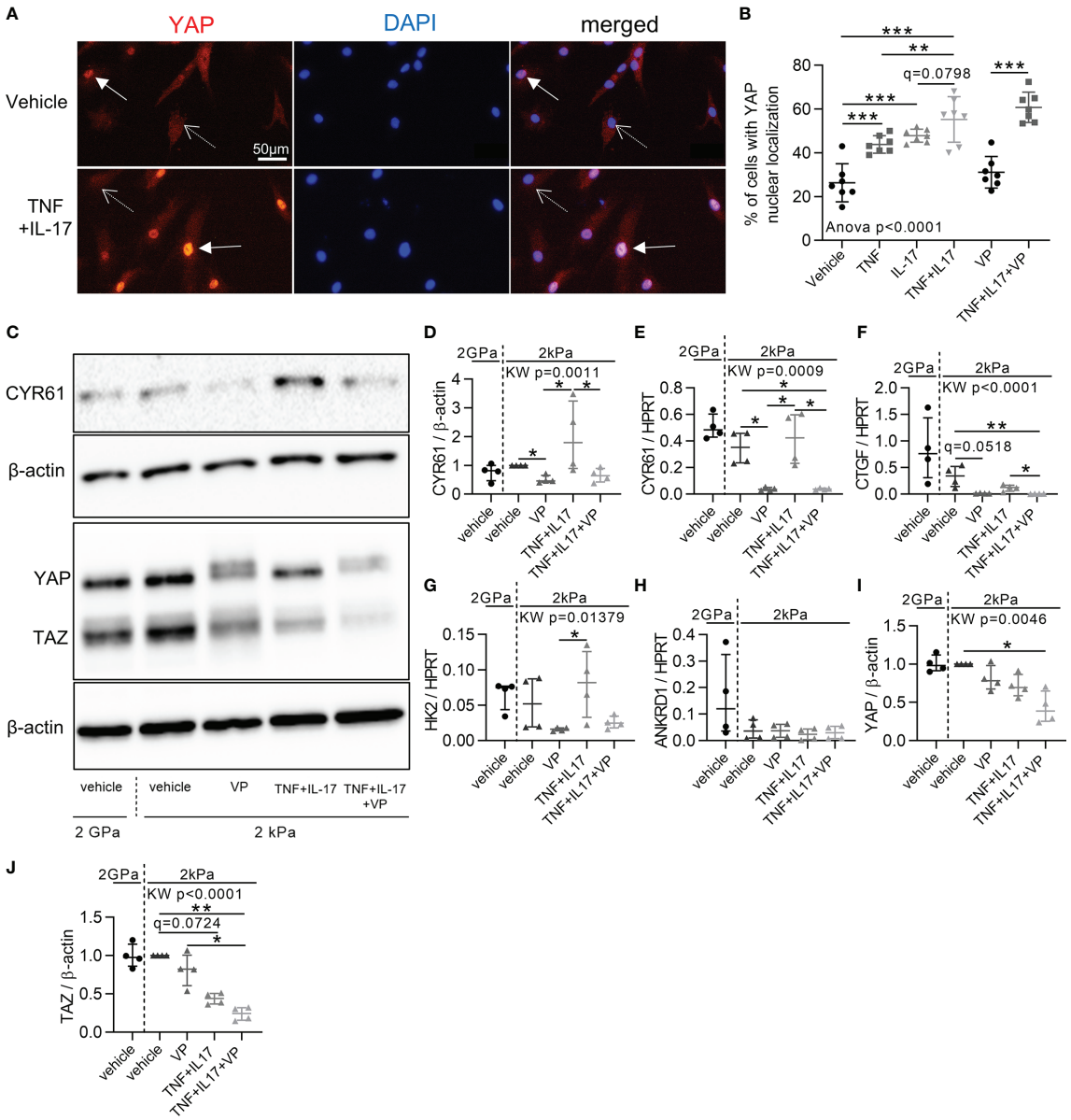

FIGURE 2 | Increased YAP/TAZ transcriptional activity in RA FLS by inflammation. RA FLS (n=4 patients) were cultured on soft (2 kPa) or classic stiff (2 GPa) substrates as indicated with VP, TNF, IL-17 alone or in combination for 48 hours. **(A)** Epifluorescence representative images of YAP (immunofluorescence, orange), DAPI (nucleus, blue), and merged images of RA FLS in 2kPa conditions. Arrows: positive YAP nuclear localization; dotted arrows: negative YAP nuclear localization. **(B)** Corresponding quantification for FLS from one RA patient (n=7). Experiments were repeated for FLS for three others RA patients showing the same pattern. **(C)** Representative western blot results of total YAP-TAZ, CYR61, and β-actin with their quantifications normalized to the 2 kPa group for each patient and to β-actin **(D, I, J)**. **(E–H)** RT-qPCR quantifications of CYR61, CTGF, HK2 and Ankrd1 expression normalized to HPRT expression. Data were presented as individual values with mean ± SD **(B)** or median and interquartile range **(D–J)**. ANOVA or Kruskal Wallis (KW) test with FDR corrected (q-value) for multiple comparisons *post hoc* tests between soft conditions (2kPa): *q < 0.05; **q < 0.01; ***q < 0.001. Verteporfin (VP), 10 µM; tumor necrosis factor (TNF), 10 ng/ml; Interleukin-17 (IL-17), 50 ng/ml; TAZ, transcriptional co-activator with PDZ-binding motif.

17 (**Figures 3B, C**). Consistently, the number of Ki-67 positive (proliferating) RA FLS was decreased by VP treatment in the presence of TNF and IL-17 assessed by two independent methods: immunofluorescence (**Figures 3D, E**) or flow cytometry (**Figure 3F**). At molecular level, changes in the proliferation/apoptosis balance were associated with decrease of Bcl2 expression in VP treated groups with or without inflammatory conditions (**Figure 3G**) and in YAP siRNA RA FLS with inflammatory conditions (**Supplementary Figure 2B**). Furthermore, VP strongly reduced the phospho(p)-NF-κB (phosphorylation on serine 536, active form involved in survival response)/total NF-κB ratio with or without TNF and

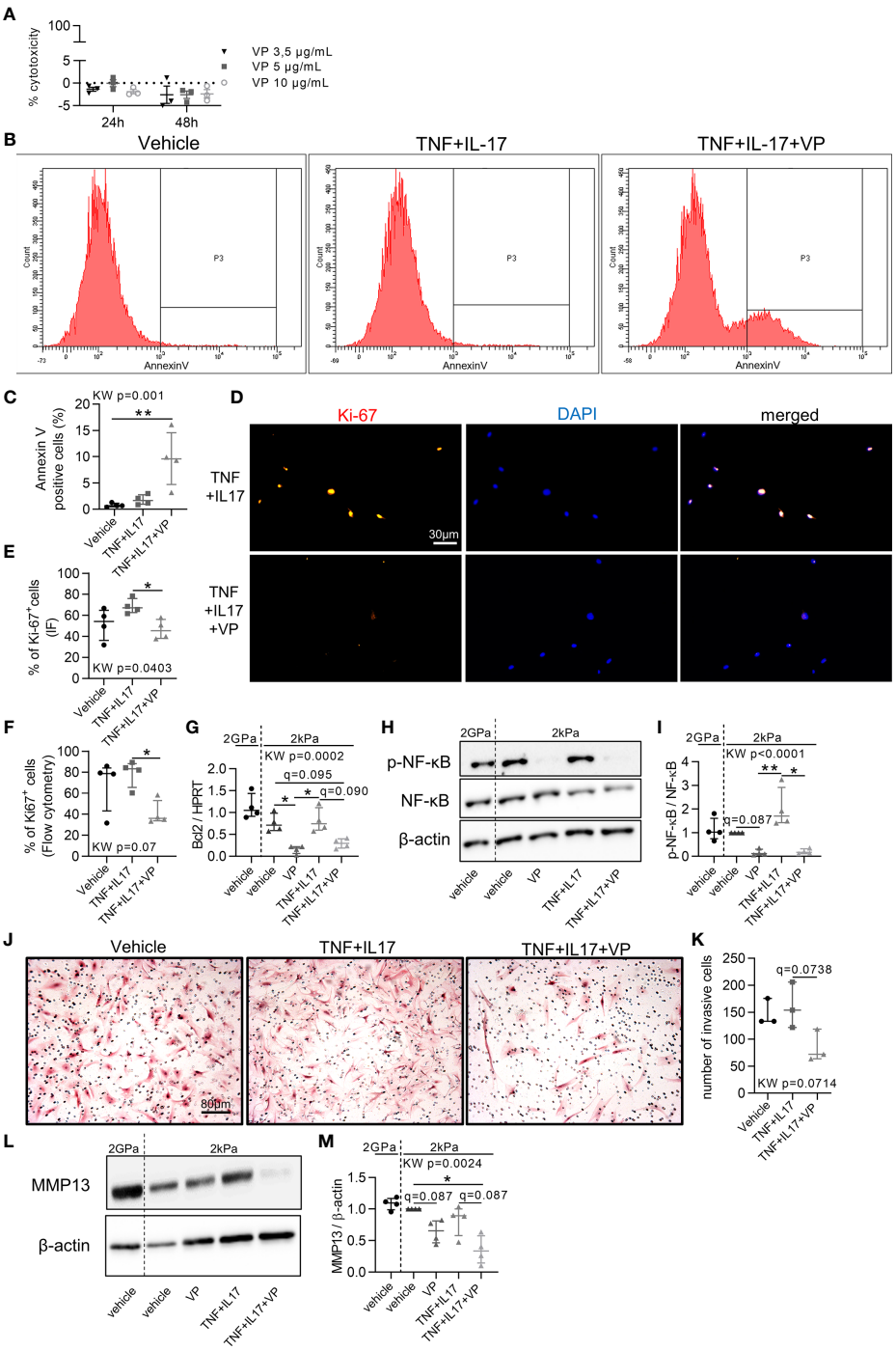

FIGURE 3 | Blocking the aggressive phenotype of RA FLS by YAP/TAZ inhibition. RA FLS (n=4 patients, except when specified) were cultured on soft (2 kPa) or classic stiff (2 GPa) substrate and treated with VP, TNF, IL-17 for 48 hours. **(A)** Lactate dehydrogenase cytotoxicity assay for RA FLS (n=1 patient) in triplicate. Positive control was set at 100%. **(B, C)** Flow cytometry representative histograms **(B)** showing the number of annexin V negative (left) and positive cells (right) with corresponding quantification **(C)**. **(D, E)** Representative epifluorescence images **(D)** of Ki-67 (orange), DAPI (blue), and merged with corresponding quantification **(E)** and flow cytometry quantification **(F)**. **(G)** RT-qPCR quantification of Bcl2 expression normalized by HPRT expression. **(H, L)** Representative western blot results of phospho(p)-NF-κB p65 (serine536: active form), total NF-κB p65, β-actin **(H)**; and MMP-13 **(L)** with their quantification normalized by the 2kPa group for each patient and β-actin **(I, M)**. **(J, K)** Representative images of invasion transwell assay stained with hematoxylin and eosin (H&E) at x10 magnification **(J)** with quantification **(K)** performed in duplicate for RA FLS (n=3 patients). Data were presented as individual values with median and interquartile range. For statistical analysis, please see Figure legend 2. VP, 10 µM (except other mention); TNF, 10 ng/ml; IL-17, 50 ng/ml; p, phospho; NF-κB, nuclear factor-κB; MMP, matrix metalloproteinase.

IL-17 treatment (**Figures 3H, I**). YAP siRNA reduced p-NF-κB/β-actin, but not the p-NF-κB/NF-κB ratio (**Supplementary Figures 2C–F**). Finally, VP trended to decrease the invasion ability of RA FLS even in pro-inflammatory conditions (**Figures 3J, K**) and MMP-13 protein level when TNF and IL-17 were co-administered with VP in RA FLS (**Figures 3L, M**). So, blocking YAP transcriptional activity strongly reduced aggressive RA FLS phenotype.

Prevention and Reversal of Synovial Hyperplasia in a Synovial Organoid Model by YAP/TAZ Inhibition

YAP has been described to promote synovial hyperplasia following cartilage injury in mouse model (36). Here, YAP inhibition was explored to prevent and to reverse synovial hyperplasia in RA. To mimic such synovial hyperplasia, we used the synovial organoid model. After 21 days of culture, RA FLS were able to form a thick lining layer, which trended to be thicker than those formed by osteoarthritic (OA) FLS independently of any inflammatory *stimuli* (**Figures 4A, B**). Since RA FLS organoids were already hyperplasic without any *stimuli*, TNF and IL-17 did not increase further synovial hyperplasia (**Figures 4C, D**). VP treatment from the start of organoid formation prevented hyperplasia in basal and inflammatory conditions (**Figures 4C, D**). In addition, VP treatment starting at day 14 (when synovial hyperplasia was already observed) also inhibited hyperplasia formation, suggesting its potential effect to reverse synovial hyperplasia, consistent with a curative approach (**Figures 4C, D**). To explore signaling pathways involved in hyperplasia formation, c-Jun subcellular localization was investigated. Nuclear localization of c-Jun in FLS was higher at the "lining layer" site compared to the "stroma" site and VP treatment suppressed this difference suggesting that YAP/TAZ have a role in the regulation of c-Jun in this context (**Figures 4E, F**).

Prevention and Reduction of Arthritis Severity in Rat AIA Model by YAP/TAZ Inhibition

To assess the involvement of YAP/TAZ in arthritis onset and severity, VP was delivered in AIA rats to explore preventive and curative approaches. Preventive VP injection from days 6 to 16 (starting before arthritis onset) induced a delay in arthritis onset, with a strong reduction in arthritis severity and ankles circumference compared to AIA vehicle rats (**Figures 5A, B**). Curative VP injection from days 12 to 16 (starting after arthritis onset) completely blocked arthritis progression and reduced arthritis severity with a decrease of both ankles circumference and arthritic index (**Figures 5A, B**). Thus, VP curative approach allowed regression of arthritis clinical signs. The reduction of arthritis severity was directly linked with a reduction of synovial hyperplasia observed in both VP groups at day 17 (**Figures 5C, D**), confirming our previous *in vitro* data and reinforcing the key role of YAP/TAZ activity for hyperplasia formation and maintenance. Bone volume per tissue volume (BV/TV) was decreased in AIA rats, corresponding to bone erosion, and linked with FLS invasion (**Figures 5E, F**). Strikingly, this bone loss was avoided in the preventive VP treatment, but not in the curative approach. In the preventive approach, the bone protection was associated with a reduction of MMP2 expression compared to the AIA group (**Figure 5G**), thus corroborating the reduced invasion ability of FLS under VP treatment. CYR61 expression was reduced in both VP injection protocol (**Figure 5H**), confirming VP effect on YAP/TAZ transcriptional activity.

Decreased Inflammatory Markers *In Vivo* and *In Vitro* Induced by YAP/TAZ Inhibition

Then, anti-inflammatory effect of systemic YAP/TAZ inhibition with both VP approaches was evaluated. RORγT labelling was detected in the marginal zone of spleen from AIA rats and strongly reduced in both VP groups (**Supplementary Figure 3A**). In the spleen, IL17 mRNA was reduced in the preventive VP group, with a similar trend in the curative VP group (**Supplementary Figure 3B**). In the ankle, IL17 mRNA was reduced only in the preventive VP group (**Supplementary Figure 3C**). No differences in IL10 expression (**Supplementary Figure 3D**) were observed in the spleen, suggesting that VP had no effect on Tregs. Unexpectedly, TNF expression was lower in spleen of VP treated animals, with no change in the ankle (**Supplementary Figures 3E, F**), whereas no change in IL6 expression was observed (**Supplementary Figures 3G, H**). Consequently, the effect of VP in reducing IL-6 or TNF expression by RA FLS was then investigated *in vitro*. TNF and IL-17 treatment increased both IL6 and TNF expressions in RA FLS (**Supplementary Figures 3I, J**). However, VP trended to inhibit both TNF and IL6 expression in RA FLS treated with or without TNF and IL-17 (**Supplementary Figure 3I, J**). To conclude, inhibiting YAP/TAZ transcriptional activity with VP in arthritis has immunomodulatory systemic effect by acting on both immune and non-immune cell types.

Regulation of Mechanical Changes in the Synovial Membrane During Arthritis Through YAP/TAZ Transcriptional Activity

Since YAP/TAZ activity was crucial during arthritis and YAP/TAZ activity could be regulated by mechanical changes in tissues, synovial mechanical properties during arthritis were investigated. In synovial membrane of AIA rats (**Figure 6A**), SF formations were observed. Strikingly SF formation was absent with VP treatments, suggesting that YAP could contribute to increase FLS tension. Consequently, the involvement of YAP in controlling the expression of ECM stiffness-related components was explored by focusing on tenascin-C and periostin (29). A strong tenascin-C (**Figure 6A**) and periostin (not shown) labelling was observed in the sublining area of the synovial membrane in non-treated AIA rats, but not in control and VP treated animals. Furthermore, tenascin-C expression was increased before and after arthritis onset, whereas periostin expression trended to increase only after arthritis onset in AIA rats ankles (**Figures 6B, C**). The decrease in tenascin-C and periostin was confirmed at the mRNA level in preventive VP approach (**Figures 6D, E**). The same pattern was observed *in*

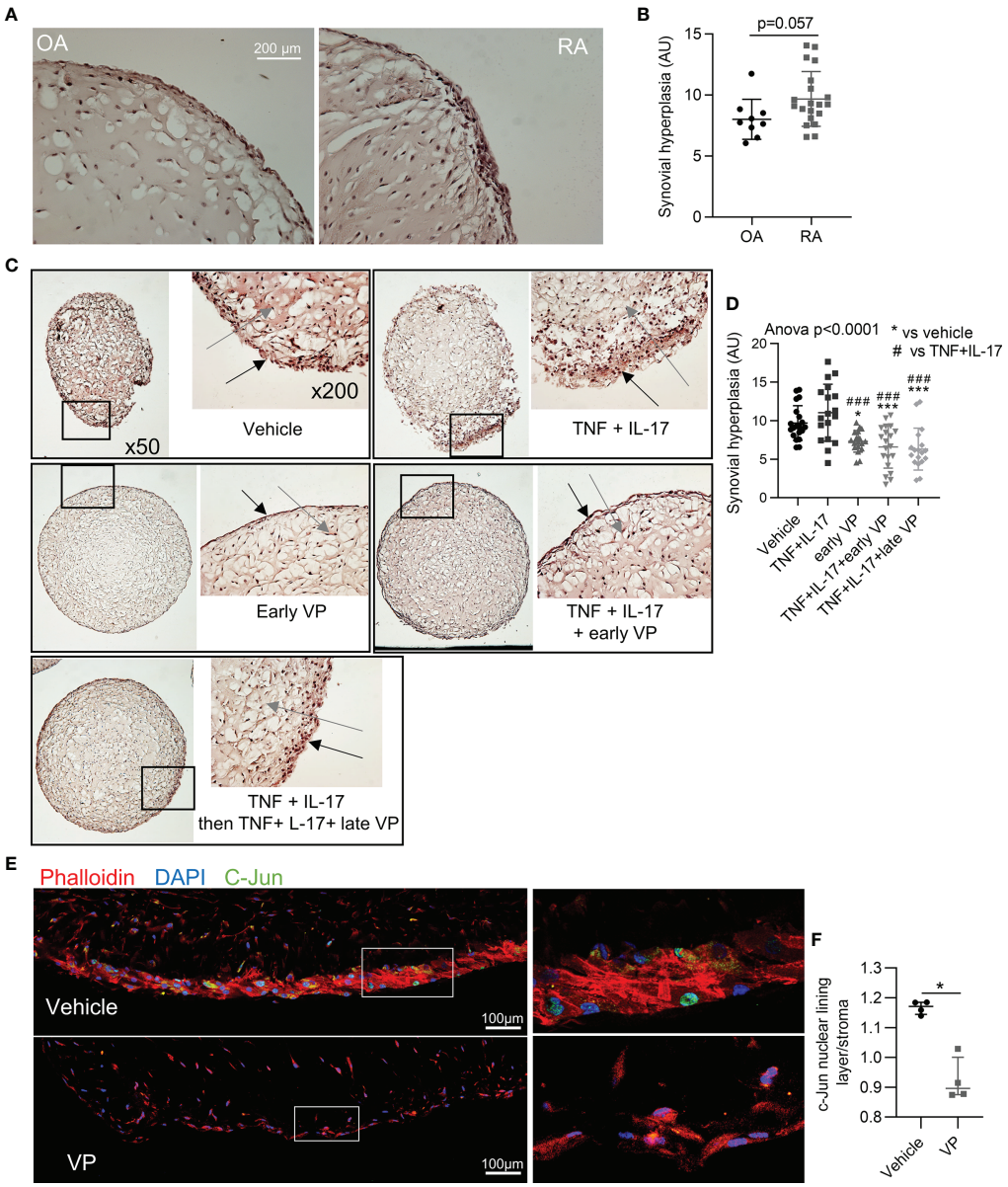

FIGURE 4 | Prevention and reversal of synovial hyperplasia in a synovial organoid model by YAP/TAZ inhibition. **(A, B)** Representative images at x200 magnification after H&E staining of synovial organoids **(A)** with quantification **(B)** of synovial hyperplasia in organoids (n=9 for OA and 20 for RA) from RA (4 patients) and OA (3 patients) FLS. **(C)** Representative images at x50 and x200 magnification after H&E staining sections of synovial organoids with RA FLS from the same patient; black arrows: synovial lining layer, grey arrows: synovial stroma. **(D)** Corresponding quantification of synovial hyperplasia in organoids (n=15 to 20 per group) from RA FLS (n=4 patients). * comparisons vs. vehicle, # comparisons vs. TNF+IL-17. **(E)** Representative confocal tiles images at x630 for c-Jun (green), phalloidin (actin, red), and DAPI (nucleus, blue) on RA organoid with corresponding zoom (right). **(F)** Ratio of nuclear c-Jun for cells in lining layer and nuclear c-Jun for cells in the stroma (organoids n=4 from FLS of one RA patient). Data were presented as individual values with mean ± SD **(B, D)** or median with interquartile range **(F)**. T-test **(B)**, ANOVA test with FDR *post hoc* test corrected (q-value) for multiple comparisons **(D)** or Mann-Whitney **(F)**. *q or $p < 0.05$; $^{\#\#\#}q < 0.001$). VP, 10 µM; TNF, 10 ng/ml; IL-17, 50 ng/ml; AU, arbitrary units.

vitro for VP treated RA FLS (**Figures 6F, G**). To further confirmed that these two genes are specifically regulated by YAP transcriptional activity, YAP deficient ($YAP^{-/-}$) HEK293 cells obtained with CRISPR-cas9 technique were used. Both tenascin-C and periostin expression were strongly reduced in $YAP^{-/-}$ HEK293 (**Figures 6H, I**). Additionally, using chromatin immunoprecipitation followed by next-generation sequencing (ChIP-seq) data from another report (37), three YAP/TAZ/TEAD4 peaks were found at active enhancer sites of tenascin-C gene (37). Together these results indicated that tenascin-C and periostin were YAP direct target genes. Next, to explore whether these changes in cytoskeletal and ECM composition could

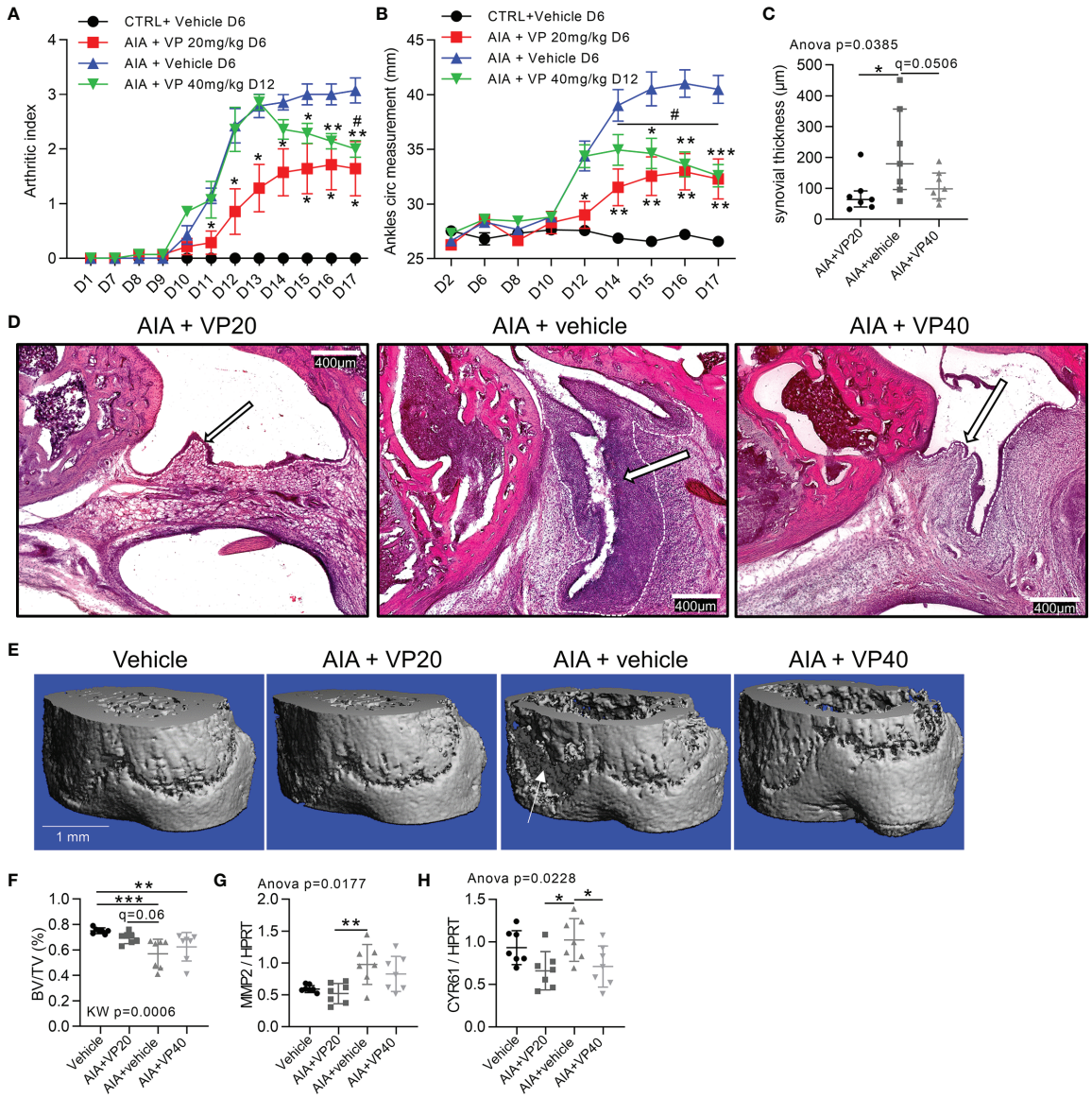

FIGURE 5 | Prevention and reduction of arthritis severity in rat AIA model by YAP inhibition. Day 0 corresponded to AIA induction. Control or arthritic (AIA) rats were IP injected with vehicle containing 10% DMSO, treated AIA rats received 20 µg/kg/day of VP from day 6 (VP20) as a preventive approach or 40 µg/kg/day VP from day 12 (VP40) as a curative approach. **(A, B)** Arthritic index and ankles circumference measurements. Two-way ANOVA with FDR *post hoc* test corrected for multiple comparison (*), and paired t-test between days 14 and 17 (#) for VP40 group. **(C, D)** Quantification of synovial hyperplasia **(C)** with representative tiles images at x100 magnification **(D)**, H&E staining; arrows: synovial lining layer; dotted lines: limit between synovial lining layer and synovial stroma. **(E, F)** Representative 3-D reconstruction of micro-computed tomography scan for distal tibia epiphysis **(E)** with corresponding quantification **(F)** of BV/TV (bone volume/tissue volume); arrow: bone erosion. G-H: RT-qPCR quantification of MMP2 **(G)** and CYR61 **(H)** expression normalized to HPRT expression. Data were presented as individual values with mean ± SEM **(A, B)** or mean ± SD **(C, F–H)**. Kruskal Wallis **(F)** or ANOVA test with FDR *post hoc* test corrected (q-value) for multiple comparisons. * or # $q < 0.05$; **$q < 0.01$; ***$q < 0.001$.

influence synovial stiffness, the Young's modulus, also known as the sample stiffness, was assessed in the rat AIA model. Synovial stiffening during arthritis was strongly increased in AIA rats. Furthermore, no synovial membrane stiffening was observed in both preventive and curative VP approaches (**Figures 6J, K**). These results showed that YAP transcriptional activity mediated pro-fibrotic responses and synovial stiffening in arthritis.

Prevention of Colitis in a Mouse Model by YAP/TAZ Inhibition Through Similar Mechanisms Observed in Arthritis

To extend our results in another inflammatory environment, we focused on colitis. Indeed, YAP/TAZ activity has already been described in IBD. VP decreased disease severity in a mouse colitis model (11). In this context, we focused on another colitis model,

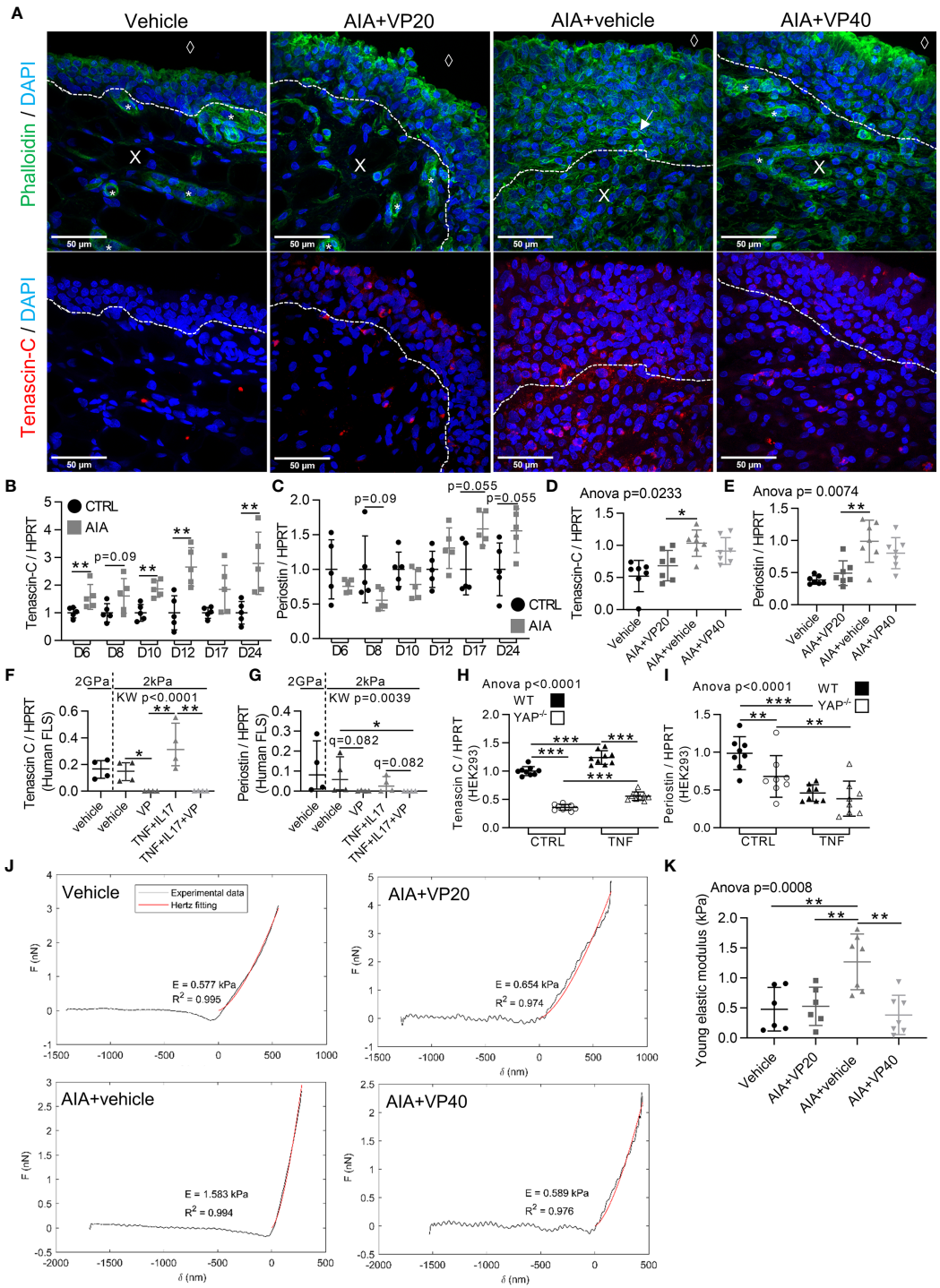

FIGURE 6 | Increased stiffness of synovial tissue during arthritis under the control of YAP/TAZ. Samples used for *in vivo* experiments were described in **Figures 1** and **4**. RA FLS (n=4 patients) were used as described in **Figure 2**. HEK293 results are representative of three independent experiments (n=9 per group). **(A)** Representative confocal tiled images of tenascin-C (red), counterstained with DAPI (blue) and phalloidin (green) in synovial membrane of rat AIA model; dotted lines: limit between synovial lining layer and synovial stroma; X: stromal compartment; diamond: synovial fluid compartment; star: blood vessels; arrow: actin stress fiber. **(B–I)** RT-qPCR results for tenascin-C and periostin in AIA and control rats ankle with different kinetics **(B, C)** VP AIA treated rats ankle **(D, E)**; RA FLS **(F, G)** or HEK293 WT and YAP$^{-/-}$ cells **(H, I)**. **(J)** Representative punctual nanoindentation curves for rat synovial membrane using AFM. Increased slope corresponded, when fitted with Hertz model (red), to an increased Young's modulus (indicated as **E**) **(K)** Corresponding quantification of Young's modulus (kPa). Data were presented as individual values with mean ± SD **(D, E, H, I, K)** or median and interquartile range **(B, C, F, G)** with Kruskal Wallis or ANOVA test with FDR *post hoc* test corrected (q-value) for multiple comparisons *q < 0.05; **q < 0.01; ***q < 0.001. TNF, 10ng/ml.

the dextran sulfate sodium (DSS) induced colitis mouse model and confirmed VP efficacy with a reduction of colitis severity (**Supplementary Figure 4A**). As previously shown for FLS or synovial tissue, VP also trended to downregulate CYR61 expression at the gut level (**Supplementary Figure 4B**). Histologically, intestinal *villi* appeared less damaged in the VP group, and the area of Peyer's patches, a witness of intestinal inflammation was reduced by VP treatment (**Supplementary Figures 4C–E**). VP treatment decreased gut TNF expression with no change for IL6 (**Supplementary Figures 4F, G**), thus reflecting the immunomodulatory effect of VP described in arthritis. However, no difference in IL17 expression during colitis was observed in the gut (**Supplementary Figure 4H**). MMP2 expression was also reduced under VP treatment with a similar trend for MMP13 (**Supplementary Figures 4I, J**). Finally, tenascin-C expression also trended to increase in DSS treated mice, whereas this was not the case in VP treated mice (**Supplementary Figure 4K**), suggesting that tissue stiffening could also occurred through YAP during colitis.

DISCUSSION

YAP/TAZ have been shown to be active in an increasing number of inflammatory related diseases especially in IBD (10–13, 25), but also in cancers where inflammation is also involved (2). Thus, we demonstrated that pro-inflammatory cytokines enhanced YAP/TAZ nuclear translocation and transcriptional activity, and this confirmed the relevance of YAP/TAZ targeting for therapeutic purpose in our arthritis and colitis models, but also possibly in other inflammatory diseases. Our study provided new and deeper *in vitro* and *in vivo* evidence on YAP/TAZ involvement during arthritis. Here, we focused mainly on YAP/TAZ-TEAD transcriptional activity which was targeted by VP (4, 24). This high transcriptional activity impacted the RA FLS phenotype and could be directly connected with YAP target genes function including Bcl-2 and NF-κB modulation for apoptosis/proliferation regulation or tenascin-C for tissue stiffening. CYR61 and CTGF were highly expressed in our arthritic models, whereas YAP transcriptional activity inhibition strongly reduced their expression. Both CYR61 and CTGF were already extensively considered in arthritis (without previously reported link with YAP activity) and involved in RA pathophysiology and critical for FLS aggressive phenotype (38–42). Furthermore, inhibiting YAP-TEAD interaction also blocked some of the c-Jun/AP-1 transcriptional activity (37, 43). The inhibition of c-Jun nuclear localization by VP treatment in the lining layer of our RA organoid model reinforced the AP-1 modulation by YAP.

YAP was not only a responder to inflammation, since its blocking decreased pro-inflammatory response, as highlighted *in vitro* and *in vivo*. Several studies have also demonstrated that YAP transcriptional activity could increase the expression of pro-inflammatory cytokines such as IL-6 (10), but also key inflammatory mediators for immune cells recruitment such as CCL2 and IL-8 (44, 45). In our model, since VP strongly changed resident cells phenotype *in vivo*, including the expression of pro-inflammatory cytokines, it could possibly prevent the inflammatory process by inhibiting immune cell recruitment which could be mediated by FLS activity (17, 18). Consequently, healing of tissue resident cells could prevent inflammation runaway, thus being a possible mechanism in our *in vivo* models for the anti-inflammatory effect of VP. Thus, to better understand the specific role of YAP in different cell types (FLS and immune cells) for arthritis onset and severity, lineage specific KO of YAP could be performed in the future.

YAP/TAZ are also well-known to be activated by mechanotransduction events, like mechanical stress, actin dynamics process (26, 27, 45), and ECM stiffness (27). To avoid, mechanic YAP/TAZ activation, our *in vitro* 2D investigations were performed on soft substrate or in 3D with synovial organoid model. These approaches allowed us to described modulations of YAP independently of the non-physiological stiffness of classic culture dishes (2GPa). Despite that mechanical stiffness could be a methodological bias to study YAP/TAZ *in vitro*, mechanical changes are often found in pathological conditions *in vivo*, especially during inflammatory processes. In chronic inflammatory processes, the mechanical change in tissue allows YAP/TAZ activation (29). Here, we found that YAP/TAZ were indeed responders to mechanotransduction events, but they also strongly modulated mechanical properties of synovial tissue. VP treatment prevented the formation of actin stress fibers in both synovial organoid model and synovial membrane of AIA rats, suggesting that YAP is essential to respond to the tensive signal induced by inflammation. We also unraveled that YAP drove tenascin-C expression probably contributing to the stiffening process observed in synovial membrane of AIA rats. Strikingly, in addition to the role of tenascin-C in ECM stiffness, it has also been reported to be highly expressed in RA patients and to modulate chronic inflammation in models of RA (46), reinforcing again the concept to target YAP during RA. It appears clearly that mechanical changes are closely related to inflammatory processes. Thus, our study suggested that YAP could be the missing link between those two processes by converting inflammatory *stimuli* into cellular and tissue mechanical remodeling.

Overall, we reported a new potential signaling loop, where YAP/TAZ drove cellular tension and ECM stiffness through a strong change in ECM composition in response to inflammation, thus creating a stiffer micro-environment. It could in turn maintains YAP activity over time even when inflammation has stopped, since RA FLS could be mechanically primed. Such a vicious loop could explain the phenotype of RA FLS, which kept aggressive features even if they were in a normal environment (eg. non-inflammatory), and the synovial hyperplasia persistence in RA patients treated with anti-inflammatory drugs (47). Since targeting YAP/TAZ modulated the mechanical environment of cells, their modulation could effectively restore the mechanical properties of tissues. Interestingly, T lymphocytes responses could be potentiated by stiffness *in vitro* (48), meaning that restoring rigidity of the tissue with VP could decrease inflammation through mechanotransduction in T lymphocytes

such as Th17. Additionally, this "self-maintained" YAP activity due to inflammation was probably also present in other inflammatory conditions such as IBD in which intestinal fibrosis has been described (49).

To conclude, our work shed light on YAP/TAZ role in arthritis, which could be also relevant for a broad range of inflammatory related events including cancer and inflammatory disorders research and therapy.

DATA AVAILABILITY STATEMENT

The datasets generated and analyzed during the current study are available from the corresponding author on reasonable request.

ETHICS STATEMENT

The animal study was reviewed and approved by The Ethical Committee for Animal Experiments of Saint-Etienne University, agreement number: 2019032816186046 for rat AIA model and 2019032010448893 for DSS mice.

AUTHOR CONTRIBUTIONS

RC and HM designed the study. RC performed most of the experiments and contributed to all of them. EA performed WB techniques and contributed to mRNA and protein extraction. GC contributed to AIA rat mRNA kinetics and RA cell harvesting. MC contributed to the organoid model experiments. CP and LN contributed to AFM experiments. EM contributed to DSS mice experiments. MT contributed to RT-qPCR experiments. HM and AV-B contributed to rat AIA model handling. M-TL designed the mRNA primers. RC, EA, MC, EM, CP and HM analysed the results. SyP gave technical support for cell culture experiments. RC, HM, AG, LV, GC, EA and StP wrote the paper. All authors contributed to the article and approved the submitted version.

FUNDING

This study received funding from Novartis DREAMER grant. The funder was not involved in the study design, collection, analysis, interpretation of data, the writing of this article or the decision to submit it for publication.

ACKNOWLEDGMENTS

We thank the members of the SAINBIOSE unit for feedback and support. We thank the hematology team and Carmen Aanei at the Saint-Etienne hospital for access to flow cytometer and technical advice. We thank Stephane Avril and Jerôme Molimard from the Ecole des Mines in Saint-Etienne for their support in the AFM experiment. We thank Myriam Normand from the Sainbiose unit for providing advice on statistical analysis. We thank Remi Philippot from Saint-Etienne hospital for access to human synovial samples. We thank Donata Iandolo, Maura Strigini, and Luc Malaval from the SAINBIOSE unit for correction of the manuscript.

SUPPLEMENTARY MATERIAL

The Supplementary Material for this article can be found online at: https://www.frontiersin.org/articles/10.3389/fimmu.2021.791907/full#supplementary-material

Supplementary Figure 1 | Increased YAP activation in RA FLS by the time spent on stiff substrate. **(A)** Schematic representation of RA FLS culture experiment. FLS were passed on soft support at passage (P) 4 or P5 or P6 following immunofluorescence (IF) or RT-qPCR analysis; time spent by FLS on stiff support was increased at each passage (P6>P5>P4). **(B)** Epifluorescence representative images of YAP (IF technique, red), on RA FLS at x10 magnification at P4 and P5 (luminosity and contrast were enhanced identically for each images for clarity purpose); for all conditions, cells were cultured on soft (2 kPa) 96-well culture dishes coated with fibronectin. **(C)** Corresponding quantification of the percentage of cells with YAP nuclear localization for FLS from one RA patient (n=7 P4, n=8 P5), experiment was repeated for one other RA patient showing the same pattern. **(D, E)** qPCR quantification of ANKRD1 **(D)** or CYR61 **(E)** for FLS from one RA patient (n=6 P5 and n=4 P6) on soft (2 kPa) or stiff (2 GPa) support; results were normalized to HPRT. T-test and Mann-Whitney test *$p < 0.05$; **$p < 0.01$; ***$p < 0.001$. Data are presented as individual values with mean ± SD **(C)** or median and interquartile range **(D, E)**.

Supplementary Figure 2 | YAP inhibition with siRNA on RA FLS. FLS from RA patient were grown on stiff (2 GPa) substrate coated with fibronectin for 72 hours. Following YAP or control siRNA transfection, FLS were treated with TNF and IL-17 for 48 hours. **(A, B)** RT-qPCR quantification of CYR61 **(A)** and Bcl2 **(B)**; results were normalized to HPRT. **(C)** Representative WB results of total YAP-TAZ, phospho-NF-κB p65 (serine536 = active form), total NF-κB p65, and β-actin. **(D-F)** WB quantification results for phospho-NF-κB / β-actin **(D)**, NF-κB / β-actin **(E)**, phospho-NF-κB / NF-κB **(D)** of four replicates for one arthritic patient. Mann-Whitney tests: *$p < 0.05$. Data are presented as individual values with median and interquartile range. TNF: 10 ng/ml, IL-17: 50 ng/ml.

Supplementary Figure 3 | YAP inhibition decreases inflammatory markers in vivo and in vitro. Samples used for in vivo experiments came from the animal protocols described in Figure 4 (AIA rats). **(A)** Representative airyscan confocal tiled images for RORγt (immunofluorescence technique, red), counterstained with DAPI (blue), 10-µm thick cryosections of rat spleen, right image: corresponding cropped image of merged in the marginal zone (MZ). **(B-J)** RT-qPCR quantification in spleen and ankle as indicated for AIA rats experiments **(B-H)** and RA FLS **(I, J)**. Results were normalized to HPRT. Kruskal Wallis (KW) or ANOVA test with FDR post hoc tests corrected (q-value) for multiple comparisons. *$q < 0.05$; **$q < 0.01$; ***$q < 0.001$. Data are presented as individual values with mean ± SD **(B-D, F-H)** or median and interquartile range **(E, I-J)**. MZ, marginal zone; GC, germinal center; arrows: RORγt positive cells located in the marginal zone.

Supplementary Figure 4 | Prevention of colitis in a mouse model by YAP/TAZ inhibition through similar mechanisms observed in arthritis. All animals received IP injection each day from day -1 to day 10; control (vehicle) or DSS mice (1.5% DSS in water) were injected with vehicle containing 10% DMSO, treated DSS mice were injected with 40 mg/kg/day of VP. **(A)** Disease activity index (DAI) represents the severity of the disease by evaluating percentage weight loss, general aspect of the mice like pain behavior and feces aspect; two-way ANOVA test with FDR post hoc test corrected (q-value) for multiple comparison; #: DSS vs. vehicle and *: DSS vs VP. **(B)** RT-qPCR quantification on intestinal tract; results are normalized to HPRT. **(C, D)** Representative brightfield tiled images at x200 magnification of 10-µm thick

paraffin transverse sections of intestinal tract, H&E staining. **(C)** DSS, **(D)** DSS+VP; dotted line represents Peyer's patches limit; black arrows: intestinal villi. **(E)** Corresponding quantification of Peyer's patches area in DSS and DSS+VP group; results represent the mean of 3 sections per Peyer's patches in duplicate for each mouse, Mann-Whitney test. **(F-J)** RT-qPCR quantification on intestinal tract for TNF **(F)**, IL6 **(G)** IL17 **(H)**, MMP13 **(I)**, MMP2 **(J)**, and tenascin-C **(K)**; results are normalized to HPRT. Kruskal Wallis (KW) or ANOVA test with FDR post hoc test corrected (q-value) for multiple comparisons. # or *q < 0.05; **q < 0.01; ***q < 0.001. Data are presented as individual values with median and interquartile range **(B)** or mean ± SD **(A, E, F-K)**.

REFERENCES

1. Hilman D, Gat U. The Evolutionary History of YAP and the Hippo/YAP Pathway. *Mol Biol Evol* (2011) 28:2403–17. doi: 10.1093/molbev/msr065
2. Zanconato F, Cordenonsi M, Piccolo S. YAP/TAZ at the Roots of Cancer. *Cancer Cell* (2016) 29:783–803. doi: 10.1016/j.ccell.2016.05.005
3. Moroishi T, Hansen CG, Guan K-L. The Emerging Roles of YAP and TAZ in Cancer. *Nat Rev Cancer* (2015) 15:73–9. doi: 10.1038/nrc3876
4. Vassilev A, Kaneko KJ, Shu H, Zhao Y, DePamphilis ML. TEAD/TEF Transcription Factors Utilize the Activation Domain of YAP65, a Src/Yes-Associated Protein Localized in the Cytoplasm. *Genes Dev* (2001) 15:1229–41. doi: 10.1101/gad.888601
5. Huang J, Wu S, Barrera J, Matthews K, Pan D. The Hippo Signaling Pathway Coordinately Regulates Cell Proliferation and Apoptosis by Inactivating Yorkie, the Drosophila Homolog of YAP. *Cell* (2005) 122:421–34. doi: 10.1016/j.cell.2005.06.007
6. Dong J, Feldmann G, Huang J, Wu S, Zhang N, Comerford SA, et al. Elucidation of a Universal Size-Control Mechanism in Drosophila and Mammals. *Cell* (2007) 130:1120–33. doi: 10.1016/j.cell.2007.07.019
7. Bottini N, Firestein GS. Duality of Fibroblast-Like Synoviocytes in RA: Passive Responders and Imprinted Aggressors. *Nat Rev Rheumatol* (2013) 9:24–33. doi: 10.1038/nrrheum.2012.190
8. Curciarello R, Canziani KE, Docena GH, Muglia CI. Contribution of Non-Immune Cells to Activation and Modulation of the Intestinal Inflammation. *Front Immunol* (2019) 10:647. doi: 10.3389/fimmu.2019.00647
9. de Bruyn M, Vandooren J, Ugarte-Berzal E, Arijs I, Vermeire S, Opdenakker G. The Molecular Biology of Matrix Metalloproteinases and Tissue Inhibitors of Metalloproteinases in Inflammatory Bowel Diseases. *Crit Rev Biochem Mol Biol* (2016) 51:295–358. doi: 10.1080/10409238.2016.1199535
10. Taniguchi K, Wu L-W, Grivennikov SI, de Jong PR, Lian I, Yu F-X, et al. A Gp130-Src-YAP Module Links Inflammation to Epithelial Regeneration. *Nature* (2015) 519:57–62. doi: 10.1038/nature14228
11. Yu M, Luo Y, Cong Z, Mu Y, Qiu Y, Zhong M. MicroRNA-590-5p Inhibits Intestinal Inflammation by Targeting YAP. *J Crohns Colitis* (2018) 12:993–1004. doi: 10.1093/ecco-jcc/jjy046
12. Zhou X, Li W, Wang S, Zhang P, Wang Q, Xiao J, et al. YAP Aggravates Inflammatory Bowel Disease by Regulating M1/M2 Macrophage Polarization and Gut Microbial Homeostasis. *Cell Rep* (2019) 27:1176–1189.e5. doi: 10.1016/j.celrep.2019.03.028
13. Kim H-B, Kim M, Park Y-S, Park I, Kim T, Yang S-Y, et al. Prostaglandin E2 Activates YAP and a Positive-Signaling Loop to Promote Colon Regeneration After Colitis But Also Carcinogenesis in Mice. *Gastroenterology* (2017) 152:616–30. doi: 10.1053/j.gastro.2016.11.005
14. McInnes IB, Schett G. The Pathogenesis of Rheumatoid Arthritis. *N Engl J Med* (2011) 365:2205–19. doi: 10.1056/NEJMra1004965
15. Ahmed S, Marotte H, Kwan K, Ruth JH, Campbell PL, Rabquer BJ, et al. Epigallocatechin-3-Gallate Inhibits IL-6 Synthesis and Suppresses Transsignaling by Enhancing Soluble Gp130 Production. *Proc Natl Acad Sci USA* (2008) 105:14692–7. doi: 10.1073/pnas.0802675105
16. Burrage PS, Mix KS, Brinckerhoff CE. Matrix Metalloproteinases: Role in Arthritis. *Front Biosci* (2006) 11:529–43. doi: 10.2741/1817
17. Imamura F, Aono H, Hasunuma T, Sumida T, Tateishi H, Maruo S, et al. Monoclonal Expansion of Synoviocytes in Rheumatoid Arthritis. *Arthritis Rheum* (1998) 41:1979–86. doi: 10.1002/1529-0131(199811)41:11<1979::AID-ART13>3.0.CO;2-C
18. Hong S-S, Marotte H, Courbon G, Firestein GS, Boulanger P, Miossec P. PUMA Gene Delivery to Synoviocytes Reduces Inflammation and Degeneration of Arthritic Joints. *Nat Commun* (2017) 8:146. doi: 10.1038/s41467-017-00142-1
19. Han Z, Boyle DL, Chang L, Bennett B, Karin M, Yang L, et al. C-Jun N-Terminal Kinase Is Required for Metalloproteinase Expression and Joint Destruction in Inflammatory Arthritis. *J Clin Invest* (2001) 108:73–81. doi: 10.1172/JCI12466
20. Ahmed S, Silverman MD, Marotte H, Kwan K, Matuszczak N, Koch AE. Down-Regulation of Myeloid Cell Leukemia 1 by Epigallocatechin-3-Gallate Sensitizes Rheumatoid Arthritis Synovial Fibroblasts to Tumor Necrosis Factor Alpha-Induced Apoptosis. *Arthritis Rheum* (2009) 60:1282–93. doi: 10.1002/art.24488
21. Matsumoto S, Müller-Ladner U, Gay RE, Nishioka K, Gay S. Ultrastructural Demonstration of Apoptosis, Fas and Bcl-2 Expression of Rheumatoid Synovial Fibroblasts. *J Rheumatol* (1996) 23:1345–52.
22. Karouzakis E, Gay RE, Gay S, Neidhart M. Epigenetic Control in Rheumatoid Arthritis Synovial Fibroblasts. *Nat Rev Rheumatol* (2009) 5:266–72. doi: 10.1038/nrrheum.2009.55
23. Bottini A, Wu DJ, Ai R, Le Roux M, Bartok B, Bombardieri M, et al. PTPN14 Phosphatase and YAP Promote Tgfβ Signalling in Rheumatoid Synoviocytes. *Ann Rheum Dis* (2019) 78:600–9. doi: 10.1136/annrheumdis-2018-213799
24. Liu-Chittenden Y, Huang B, Shim JS, Chen Q, Lee S-J, Anders RA, et al. Genetic and Pharmacological Disruption of the TEAD-YAP Complex Suppresses the Oncogenic Activity of YAP. *Genes Dev* (2012) 26:1300–5. doi: 10.1101/gad.192856.112
25. Geng J, Yu S, Zhao H, Sun X, Li X, Wang P, et al. The Transcriptional Coactivator TAZ Regulates Reciprocal Differentiation of TH17 Cells and Treg Cells. *Nat Immunol* (2017) 18:800–12. doi: 10.1038/ni.3748
26. Aragona M, Panciera T, Manfrin A, Giulitti S, Michielin F, Elvassore N, et al. A Mechanical Checkpoint Controls Multicellular Growth Through YAP/TAZ Regulation by Actin-Processing Factors. *Cell* (2013) 154:1047–59. doi: 10.1016/j.cell.2013.07.042
27. Dupont S, Morsut L, Aragona M, Enzo E, Giulitti S, Cordenonsi M, et al. Role of YAP/TAZ in Mechanotransduction. *Nature* (2011) 474:179–83. doi: 10.1038/nature10137
28. Wójciak-Stothard B, Entwistle A, Garg R, Ridley AJ. Regulation of TNF-Alpha-Induced Reorganization of the Actin Cytoskeleton and Cell-Cell Junctions by Rho, Rac, and Cdc42 in Human Endothelial Cells. *J Cell Physiol* (1998) 176:150–65. doi: 10.1002/(SICI)1097-4652(199807)176:1<150::AID-JCP17>3.0.CO;2-B
29. Nowell CS, Odermatt PD, Azzolin L, Hohnel S, Wagner EF, Fantner GE, et al. Chronic Inflammation Imposes Aberrant Cell Fate in Regenerating Epithelia Through Mechanotransduction. *Nat Cell Biol* (2016) 18:168–80. doi: 10.1038/ncb3290
30. Tavares S, Vieira AF, Taubenberger AV, Araújo M, Martins NP, Brás-Pereira C, et al. Actin Stress Fiber Organization Promotes Cell Stiffening and Proliferation of Pre-Invasive Breast Cancer Cells. *Nat Commun* (2017) 8:15237. doi: 10.1038/ncomms15237
31. Kiener HP, Lee DM, Agarwal SK, Brenner MB. Cadherin-11 Induces Rheumatoid Arthritis Fibroblast-Like Synoviocytes to Form Lining Layers *in Vitro*. *Am J Pathol* (2006) 168:1486–99. doi: 10.2353/ajpath.2006.050999
32. Courbon G, Lamarque R, Gerbaix M, Caire R, Linossier M-T, Laroche N, et al. Early Sclerostin Expression Explains Bone Formation Inhibition Before Arthritis Onset in the Rat Adjuvant-Induced Arthritis Model. *Sci Rep* (2018) 8:3492. doi: 10.1038/s41598-018-21886-w
33. Noack M, Miossec P. Selected Cytokine Pathways in Rheumatoid Arthritis. *Semin Immunopathol* (2017) 39:365–83. doi: 10.1007/s00281-017-0619-z
34. Chabaud M, Durand JM, Buchs N, Fossiez F, Page G, Frappart L, et al. Human Interleukin-17: A T Cell-Derived Proinflammatory Cytokine Produced by the Rheumatoid Synovium. *Arthritis Rheum* (1999) 42:963–70. doi: 10.1002/1529-0131(199905)42:5<963::AID-ANR15>3.0.CO;2-E
35. Li CX, Talele NP, Boo S, Koehler A, Knee-Walden E, Balestrini JL, et al. MicroRNA-21 Preserves the Fibrotic Mechanical Memory of Mesenchymal Stem Cells. *Nat Mater* (2017) 16:379–89. doi: 10.1038/nmat4780
36. Roelofs AJ, Zupan J, Riemen AHK, Kania K, Ansboro S, White N, et al. Joint Morphogenetic Cells in the Adult Mammalian Synovium. *Nat Commun* (2017) 8:15040. doi: 10.1038/ncomms15040

37. Zanconato F, Forcato M, Battilana G, Azzolin L, Quaranta E, Bodega B, et al. Genome-Wide Association Between YAP/TAZ/TEAD and AP-1 at Enhancers Drives Oncogenic Growth. *Nat Cell Biol* (2015) 17:1218–27. doi: 10.1038/ncb3216
38. Zhang Q, Wu J, Cao Q, Xiao L, Wang L, He D, et al. A Critical Role of Cyr61 in Interleukin-17-Dependent Proliferation of Fibroblast-Like Synoviocytes in Rheumatoid Arthritis. *Arthritis Rheum* (2009) 60:3602–12. doi: 10.1002/art.24999
39. Huang T-L, Mu N, Gu J-T, Shu Z, Zhang K, Zhao J-K, et al. DDR2-CYR61-MMP1 Signaling Pathway Promotes Bone Erosion in Rheumatoid Arthritis Through Regulating Migration and Invasion of Fibroblast-Like Synoviocytes. *J Bone Miner Res* (2017) 32:407–18. doi: 10.1002/jbmr.2993
40. Lin J, Zhou Z, Huo R, Xiao L, Ouyang G, Wang L, et al. Cyr61 Induces IL-6 Production by Fibroblast-Like Synoviocytes Promoting Th17 Differentiation in Rheumatoid Arthritis. *J Immunol* (2012) 188:5776–84. doi: 10.4049/jimmunol.1103201
41. Liu S-C, Chuang S-M, Hsu C-J, Tsai C-H, Wang S-W, Tang C-H. CTGF Increases Vascular Endothelial Growth Factor-Dependent Angiogenesis in Human Synovial Fibroblasts by Increasing miR-210 Expression. *Cell Death Dis* (2014) 5:e1485. doi: 10.1038/cddis.2014.453
42. Miyashita T, Morimoto S, Fujishiro M, Hayakawa K, Suzuki S, Ikeda K, et al. Inhibition of Each Module of Connective Tissue Growth Factor as a Potential Therapeutic Target for Rheumatoid Arthritis. *Autoimmunity* (2016) 49:109–14. doi: 10.3109/08916934.2015.1113405
43. Liu X, Li H, Rajurkar M, Li Q, Cotton JL, Ou J, et al. Tead and AP1 Coordinate Transcription and Motility. *Cell Rep* (2016) 14:1169–80. doi: 10.1016/j.celrep.2015.12.104
44. Wang L, Luo J-Y, Li B, Tian XY, Chen L-J, Huang Y, et al. Integrin-YAP/TAZ-JNK Cascade Mediates Atheroprotective Effect of Unidirectional Shear Flow. *Nature* (2016) 540:579–82. doi: 10.1038/nature20602
45. Hoffman LM, Smith MA, Jensen CC, Yoshigi M, Blankman E, Ullman KS, et al. Mechanical Stress Triggers Nuclear Remodeling and the Formation of Transmembrane Actin Nuclear Lines With Associated Nuclear Pore Complexes. *Mol Biol Cell* (2020) 31:1774–87. doi: 10.1091/mbc.E19-01-0027
46. Aungier SR, Cartwright AJ, Schwenzer A, Marshall JL, Dyson MR, Slavny P, et al. Targeting Early Changes in the Synovial Microenvironment: A New Class of Immunomodulatory Therapy? *Ann Rheum Dis* (2019) 78:186–91. doi: 10.1136/annrheumdis-2018-214294
47. Ramírez J, Celis R, Usategui A, Ruiz-Esquide V, Faré R, Cuervo A, et al. Immunopathologic Characterization of Ultrasound-Defined Synovitis in Rheumatoid Arthritis Patients in Clinical Remission. *Arthritis Res Ther* (2016) 18:74. doi: 10.1186/s13075-016-0970-9
48. Saitakis M, Dogniaux S, Goudot C, Bufi N, Asnacios S, Maurin M, et al. Different TCR-Induced T Lymphocyte Responses Are Potentiated by Stiffness With Variable Sensitivity. *Elife* (2017) 6:e23190. doi: 10.7554/eLife.23190
49. Latella G, Di Gregorio J, Flati V, Rieder F, Lawrance IC. Mechanisms of Initiation and Progression of Intestinal Fibrosis in IBD. *Scand J Gastroenterol* (2015) 50:53–65. doi: 10.3109/00365521.2014.968863

Conflict of Interest: The authors declare that the research was conducted in the absence of any commercial or financial relationships that could be construed as a potential conflict of interest.

Publisher's Note: All claims expressed in this article are solely those of the authors and do not necessarily represent those of their affiliated organizations, or those of the publisher, the editors and the reviewers. Any product that may be evaluated in this article, or claim that may be made by its manufacturer, is not guaranteed or endorsed by the publisher.

frontiers in Immunology

ORIGINAL RESEARCH
published: 20 January 2022
doi: 10.3389/fimmu.2021.794792

Investigating Molecular Signatures Underlying Trapeziometacarpal Osteoarthritis Through the Evaluation of Systemic Cytokine Expression

Anusha Ratneswaran[1,2,3], *Jason S. Rockel*[2,3], *Daniel Antflek*[1,3], *John J. Matelski*[4], *Konstantin Shestopaloff*[2,3], *Mohit Kapoor*[2,3,5] *and Heather Baltzer*[1,3,6*]

[1] Hand Program, Schroeder Arthritis Institute, University Health Network, Toronto, ON, Canada, [2] Division of Orthopedics, Osteoarthritis Research Program, Schroeder Arthritis Institute, University Health Network, Toronto, ON, Canada, [3] Krembil Research Institute, University Health Network, Toronto, ON, Canada, [4] Biostatistics Research Unit, University Health Network, Toronto, ON, Canada, [5] Department of Surgery and Laboratory Medicine and Pathobiology, University of Toronto, Toronto, ON, Canada, [6] Division of Plastic and Reconstructive Surgery, University of Toronto, Toronto, ON, Canada

Purpose: Non-operative management of trapeziometacarpal osteoarthritis (TMOA) demonstrates only short-term symptomatic alleviation, and no approved disease modifying drugs exist to treat this condition. A key issue in these patients is that radiographic disease severity can be discordant with patient reported pain, illustrating the need to identify molecular mediators of disease. This study characterizes the biochemical profile of TMOA patients to elucidate molecular mechanisms driving TMOA progression.

Methods: Plasma from patients with symptomatic TMOA undergoing surgical (n=39) or non-surgical management (n=44) with 1-year post-surgical follow-up were compared using a targeted panel of 27 cytokines. Radiographic (Eaton-Littler), anthropometric, longitudinal pain (VAS, TASD, quick DASH) and functional (key pinch, grip strength) data were used to evaluate relationships between structure, pain, and systemic cytokine expression. Principal Component Analysis was used to identify clusters of patients.

Results: Patients undergoing surgery had greater BMI as well as higher baseline quick DASH, TASD scores. Systemically, these patients could only be distinguished by differing levels of Interleukin-7 (IL-7), with an adjusted odds ratio of 0.22 for surgery for those with increased levels of this cytokine. Interestingly, PCA analysis of all patients (regardless of surgical status) identified a subset of patients with an "inflammatory" phenotype, as defined by a unique molecular signature consisting of thirteen cytokines.

Conclusion: Overall, this study demonstrated that circulating cytokines are capable of distinguishing TMOA disease severity, and identified IL-7 as a target capable of differentiating disease severity with higher levels associated with a decreased likelihood of TMOA needing surgical intervention. It also identified a cluster of patients who segregate based on a molecular signature of select cytokines.

Keywords: inflammation, osteoarthritis, trapeziometacarpal osteoarthritis, cytokine, molecular factors

OPEN ACCESS

Edited by:
Gurpreet S. Baht,
Duke University, United States

Reviewed by:
Federico Díaz-Gonzalez,
University of La Laguna, Spain
Eric Gracey,
Ghent University, Belgium

****Correspondence:***
Heather Baltzer
Heather.Baltzer@uhn.ca

Specialty section:
This article was submitted to Inflammation, a section of the journal Frontiers in Immunology

Received: *14 October 2021*
Accepted: *31 December 2021*
Published: *20 January 2022*

Citation:
Ratneswaran A, Rockel JS, Antflek D, Matelski JJ, Shestopaloff K, Kapoor M and Baltzer H (2022) Investigating Molecular Signatures Underlying Trapeziometacarpal Osteoarthritis Through the Evaluation of Systemic Cytokine Expression. Front. Immunol. 12:794792. doi: 10.3389/fimmu.2021.794792

INTRODUCTION

Osteoarthritis at the base of the thumb (Trapeziometacarpal Osteoarthritis [TMOA]), is a prevalent and painful condition (1). The etiology of TMOA is unknown, and pain is the main reason individuals seek medical attention (2). Though studies examining the occurrence of this specific condition are lacking, it is estimated that TMOA has a lifetime prevalence of approximately 10% (3, 4). This is highly variable between radiographic TMOA which has an estimated prevalence of 12-50%, and symptomatic TMOA which affects 1-16% of individuals (5). This joint site, in particular, is understudied compared to other osteoarthritic locations such as the knee. Historically, the TM joint has been grouped together with other hand joints in OA studies despite evidence supporting it as distinctly affected (6).

Risk factors for TMOA include age, obesity, heritability, repetitive occupational thumb use, ethnicity, and radial subluxation at the base of the thumb (in males) (1, 7–9). Preventative measures need further investigation, and subsequent meta-analyses. Currently, there are no pharmacological treatments which reduce the progression of TMOA, and early-stage non-operative management has typically shown only short-term symptomatic benefits (10–13). Patients who do not respond to non-operative therapy may opt to receive surgical intervention, often with lengthy recovery periods.

Radiographic TMOA severity is often discordant with patient reported pain and functional assessments (14–16). These inconsistencies illustrate the need for objective markers linking disease severity to clinical measures in order to detect the disease early, predict which patients are more likely to develop severe or rapidly progressing disease, evaluate treatment response, and develop probable treatment targets (17, 18). Yet, there are also no validated prognostic or diagnostic biomarkers of TMOA (19). While their current utility may be limited, a sensitive diagnostic tool which is able to identify TMOA early, and predict prognosis could benefit patients by reducing exposure to risk factors and helping start preventative strategies and therapies early as more efficacious regimes are identified. Identification of an objective marker or effective therapeutic target is contingent on a strong understanding of molecular mechanisms underlying disease progression. Profiling potential molecular or secretory signatures in a TMOA patient population can contribute to understanding their role within a disease-specific context and build a foundation for identifying these markers.

Cytokines are secreted signalling molecules that reflect active processes within the joint such as inflammation, cartilage synthesis and destruction, and bone remodeling, thereby having the ability to translate the intrinsic state of the joint proximally, or even systemically. Tissue damage and low level chronic inflammation in OA generates cytokines, which can alter joint tissue homeostasis directly [through the involvement in OA pathophysiology such as Interleukin(IL)-1B, IL-4, IL-6, IL-10, IL-13, TNFa] or indirectly through processes such as angiogenesis, chemotaxis, and inflammation (20, 21). A limitation which must be acknowledged is that it is largely unknown whether systemic levels of cytokines could reflect pathological processes in such a small joint. However, it has been reported that systemic cytokines are correlated to bone resorption in temporomandibular joint OA (22). Furthermore, CMC (TM) joints disproportionately impact the concentration of systemic OA biomarkers while joint size does not determine the contribution to systemic biomarker concentration (23). This suggests that these OA in these small joints can impact systemic molecular profiles.

In this study, we sought to determine molecular indicators which could classify TMOA patients based on clinical, biological and anthropometric factors. We evaluated whether circulating cytokines can distinguish symptomatic disease severity by comparing patients undergoing non-surgical management to those undergoing surgery (trapeziectomy), and provide a basis for communicating active processes occurring within the joint. We show that the cytokine IL-7 is capable of discriminating disease severity between these two groups. We also discovered that regardless of surgical status patients can be sub-classified into separate groups based on a distinct molecular signature of thirteen inflammatory cytokines indicating there may be different molecular phenotypes within this population.

MATERIALS AND METHODS

Study Population

Symptomatic TMOA patients receiving non-surgical management (splinting, education, physiotherapy or standard operative intervention (trapeziectomy with/without ligament reconstruction and tendon interposition), followed the pipeline in **Supplementary Figure 1** (approved study #16-5759). Indications for surgery included: persistent pain that limits normal hand function as assessed by patient report and clinical parameters including limited range of motion, deformity, grip and pinch strengths; failure of non-surgical measures; and capacity to give informed consent. Treatment program was based on surgeon recommendation with patient involvement in decision making. Patients were excluded from the study if they had post-traumatic, crystalline arthritis or corticosteroid injections within the past three months. Patients with steroid injections were excluded due to the possible effects on systemic cytokines. They were excluded in both the surgical group and non-surgical group.

Plasma was collected at baseline (pre-treatment) for surgical and non-surgical patients, and post-surgical time points of 6 weeks, 3 months, 6 months and 1 year. Clinical characteristics (age, sex, BMI, and painful joint count were self-reported by the participant. Functional measures (key pinch, grip strength), were conducted in triplicate using a dedicated Jamar pinch-gauge and dynamometer (Sammons Preston) using the average to produce a final value. Participants were asked to indicate the overall intensity of their thumb pain from 0-100 using an electronic Visual Analogue Scale(VAS) as well as symptoms and function using the shortened Disability of the Arm, Shoulder and Hand-quick DASH, and Trapeziometacarpal Arthrosis Symptom and

Disability Questionnaire- TASD) (24–27). The quick DASH is an abbreviated version of the DASH questionnaire that includes 11 of the original 30 items and is used to assess symptoms and function in the upper extremities. Responses for each item are indicated on a 5-point Likert scale ranging from no disability (1 point) to extreme disability (5 points). A summative score out of 100 (where 100 indicates greatest disability) was obtained by summing the value of responses, dividing by the number of completed items, subtracting 1, and then multiplying that value by 25 (28). The TASD also uses a 5-point Likert scale and has 12 items to assess thumb-specific symptoms and disability. Scoring for this measure is identical to that of the quick DASH. Radiographic severity for each patient was assessed by a blinded reviewer using the Eaton-Littler classification system (29). Painful joint count was collected using a homunculus form and has been previously used in studies of osteoarthritis (30–33). In brief: total joint count was derived from homunculus data and represented a value out of a maximum 28 points. The neck, upper back, mid back, lower back, shoulders, elbows, wrists, hips, knees, ankles and mid-feet were valued at 1 point when marked. In each hand, metacarpophalangeal joints, proximal interphalangeal joints, and distal interphalangeal joints were grouped and valued at 1 point if one or more of those joints were marked (for maximum of 3 points per hand). In each foot, metatarsophalangeal joints and interphalangeal joints were grouped and valued at 1 point if one or more of those joints were marked (for a maximum of 2 points per foot).

Cytokine Quantification

Expression of inflammatory cytokines was measured using the Bio-rad Bio-Plex Pro Human Cytokine 27-Plex Assay kit, read on a Luminex 200 system and analyzed using Luminex xPotent Software as per product specifications. The evaluated cytokines consisted of: basic fibroblast growth factor (bFGF), eotaxin, granulocyte colony-stimulating factor (G-CSF), granulocyte macrophage colony-stimulating factor (GM-CSF), interferon gamma (IFNg), interleukin-1 receptor antagonist (IL-1RA), Interleukins (IL-1b, IL-2, IL-4, IL-5, IL-6, IL-7, IL-8, IL-9, IL-10, IL-12p70, IL-13, IL-15, IL-17a, interferon gamma inducible protein 10 (IP-10), monocyte chemoattractant protein 1 (MCP-1), macrophage inflammatory protein (MIP-1a, MIP-1b), platelet derived growth factor bb (PDGF-bb), regulated on activation normal T-cell expressed and secreted, tumor necrosis factor alpha (TNFa), vascular endothelial growth factor (VEGF). Plasma samples were measured at baseline (pre-treatment), from either non-surgically managed (n=44) or surgical (n=39) patients, or post-surgically at 6-weeks (n=31), 3 months (n=24), 6 months (n=22) or 1 year (n=17). Samples from the different groups and time-points were randomly allocated to plates, and the experiment was conducted using de-identified samples run in duplicate. Cytokine concentration was calculated based on standard curve as per product manual.

Statistical Analyses

Statistical analyses were performed using R version 3.6.2. Clinical variables (age, sex, BMI, quick DASH, TASD, TASD- subscales symptoms and disability, key pinch strength, grip strength, and painful joint count) were analyzed using bivariate methods (**Table 1**). Cytokine concentrations were log (x+1) transformed, mean-centered and scaled by their respective standard deviation in order to mitigate the influence of extreme values and to facilitate interpretation of model coefficients. Principal Component Analysis (PCA) was performed on transformed cytokine data, and used for data visualization and cluster generation (34). Cytokines which had greater than 70% of values below the lower limit of detection were excluded. Wilcoxon tests were performed to examine differences in cytokine levels between treatment groups, sexes, and clusters. Adjusted associations between each cytokine at baseline and each clinical outcome at baseline (adjusting for age, sex, BMI and painful joint count) were assessed using Generalized Linear Models. Additionally, associations between

TABLE 1 | Baseline Patient Characteristics.

		Non-Surgical Management	Surgery	p-value
n		44	39	
Age [mean (SD)]		62.80 (10.24)	60.07 (8.11)	0.185
Sex (%)	FEMALE	31 (70.5)	27 (69.2)	1
	MALE	13 (29.5)	12 (30.8)	
BMI [median (IQR)]		25.18 [22.86, 28.27]	28.29 [24.38, 32.86]	**0.01**
Quick DASH [mean (SD)]		35.52 (18.20)	55.54 (18.93)	**<0.001**
VAS [median (IQR)]		75.50 [61.00, 90.00]	76.00 [70.00, 85.00]	0.913
TASD [mean (SD)]		42.28 (17.81)	61.27 (17.18)	**<0.001**
TASD Subscale Symptom [mean (SD)]		41.72 (18.64)	62.27 (16.16)	**<0.001**
TASD Subscale Disability [median (IQR)]		40.00 [30.00, 56.25]	60.00 [50.00, 75.00]	**<0.001**
XRAY grade (%)	1	0 (0.0)	1 (2.9)	0.103
	2	9 (22.0)	11 (31.4)	
	3	22 (53.7)	10 (28.6)	
	4	10 (24.4)	13 (37.1)	
Key Pinch Strength [mean (SD)]		5.48 (2.43)	4.80 (2.32)	0.208
Maximum Grip Strength [mean (SD)]		25.09 (10.66)	21.42 (11.40)	0.136
Total Joint Count [median (IQR)]		9.00 [5.00, 13.00]	8.00 [4.00, 12.00]	0.731

BMI, Body Mass Index; QDASH, quick Disability of Arm; Shoulder and Hand score; VAS, Visual Analogue Scale; TASD, Trapeziometacarpal Arthrosis Symptom and Disability Questionnaire; X-Ray Grade, Eaton- Littler classification 1-4 (most severe); Joint Count, painful joints as indicated by patient homunculus.
Bold values indicate statistically significant values.

baseline cytokines and change scores in the outcomes (baseline vs 6 months and baseline vs 12 months), as well as associations between change scores in the cytokines (baseline vs 6 months and baseline vs 12 months) and outcomes (at 6 and 12 months respectively), were similarly assessed (using GLM framework). P-values were adjusted using the method of Benjamin and Hochberg to maintain a false discovery rate of 0.1 (35).

RESULTS

Patients Undergoing Surgery Have More Disability, Higher Pain and BMI

Patient anthropometric data, reported outcome measures, and functional assessments are reported in **Table 1**. There were no significant differences in age or sex between the surgical and non-surgically managed group. Approximately 70% of the study population was female, nearly evenly distributed between surgical and non-surgical treatment modalities. No statistical differences were detected in VAS patient reported pain, radiographic disease severity, key pinch strength, grip strength or total number of painful joints between groups.

Patients undergoing surgery had significantly higher BMI than those undertaking non-surgical treatment (28.29 [24.38,32.86] vs 25.18 [22.86, 28.27], p=0.010). The surgical group also reported more severe pain and disability, as indicated by quick DASH scores (55.54± 18.93 vs 35.52± 18.20, p<0.001), and TASD total scores (61.27± 17.18 vs 42.28 ± 17.81, p<0.001), which was reflected in both of the TASD sub-scales of symptoms (62.27±16.16 vs 41.72±18.64, p<0.001), and disability (60.00 [50.00, 70.00] vs 40.00 [30.00, 56.25], p<0.001).

IL-7 Can Discriminate Between Surgical and Non-Surgical Patients

Biochemical profiling using targeted panel cytokine screening was used to examine whether there were systemic differences in the plasma of surgical compared to non-surgically managed patients (**Figure 1**). The levels of IL-7 (q<0.00001) were significantly different between the two groups. Patients with higher relative levels of IL-7 had a decreased likelihood of going into surgery with an adjusted odds ratio of 0.220 (q<0.05) (**Table 2**). None of the other cytokines tested were effective at discriminating surgical status. Data for cytokine screening in pg/ml, as well as baseline demographic and clinical measures can be accessed in **Supplementary Table 6**.

As females comprised more than two-thirds of the study population, we investigated whether there were differences in biochemical profiles between sexes. There were no differences in cytokine expression between sexes after correcting for false discovery rate (**Supplementary Figure 2**). Associations between radiographic severity, patient reported outcome

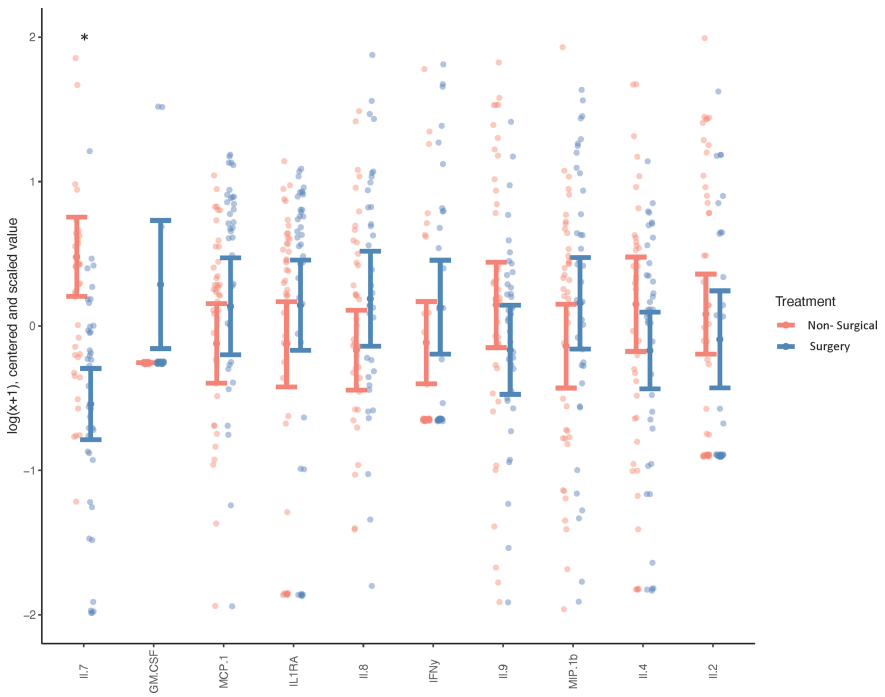

FIGURE 1 | Systemic Cytokine Expression in Surgical vs Non-surgically Managed Patients. Differences in circulating cytokines in the plasma of non-surgically managed (n=44) or surgically managed (n=39) patients at baseline. Wilcoxon test, *p < 0.0001, q < 0.0001, less than 5% of values below lower limit of detection. Adjusted for age, sex, BMI and painful joint count, the y-axis depicts cytokine concentrations (which were log[x+1] transformed, mean-centred and scaled by their respective standard deviation, while cytokines are labelled on the x-axis.

TABLE 2 | Cytokine Odds Ratio For Surgical vs. Non-surgical Management.

Cytokine	Adjusted Odds Ratio	lower 0.025	upper 0.975	p-value	q-value
IL-7	0.22	0.084	0.464	0.00044	**0.011433**
Eotaxin	1.636	0.982	2.865	0.06851	0.596163
MCP-1	1.54	0.948	2.616	0.090862	0.596163
IL-8	1.55	0.949	2.664	0.091717	0.596163
MIP-1a	1.441	0.88	2.43	0.153451	0.712417
MIP-1b	1.371	0.853	2.269	0.201402	0.712417

Adjusted (age, sex, BMI, painful joint count) odds ratio describing likelihood of undergoing surgical treatment with increased levels of cytokine expression in non-surgically managed (n=44) or surgically managed (n=39) patients at baseline.
Bold values indicate statistically significant values.

measures, functional assays and cytokine expression in surgical and non-surgically managed patients were evaluated. After adjusting for clinical factors (age, sex, BMI, painful joint count), there were few significant associations between functional tests and cytokine expression but not among other measures (**Supplementary Tables 1–4**).

Identification of a Unique Molecular Signature in TMOA Patients

Due to the minimal associations found between cytokine expression and clinical outcome measures, we sought to determine whether there were endogenous differences between patients that could explain the heterogeneity seen within surgical and non-surgical patient groups. Using Principal Component Analysis (PCA), we conducted an unbiased examination of cytokine expression in all patients and observed that patients segregated into two clusters, regardless of surgical status, age, sex, joint count or BMI (**Figure 2**). Two patient clusters emerged based on a unique molecular signature consisting of 13 cytokines: G-CSF, IL-17a, MCP-1, IL-6, IL-1b, IL-10, IL-12p70, Il-13, IL-2, TNFa, B-FGF, IP-10 and IFNγ. (q<0.02). The difference in each of these cytokines between the two clusters is visualized in **Figure 3**, where relative increase or decrease is seen in the latter. A summary of these cytokines and brief examination of their role within the context of OA can be found in **Supplementary Table 5**.

DISCUSSION

Currently there are no validated biomarkers of TMOA, and as such, there are limited options available to patients during early-

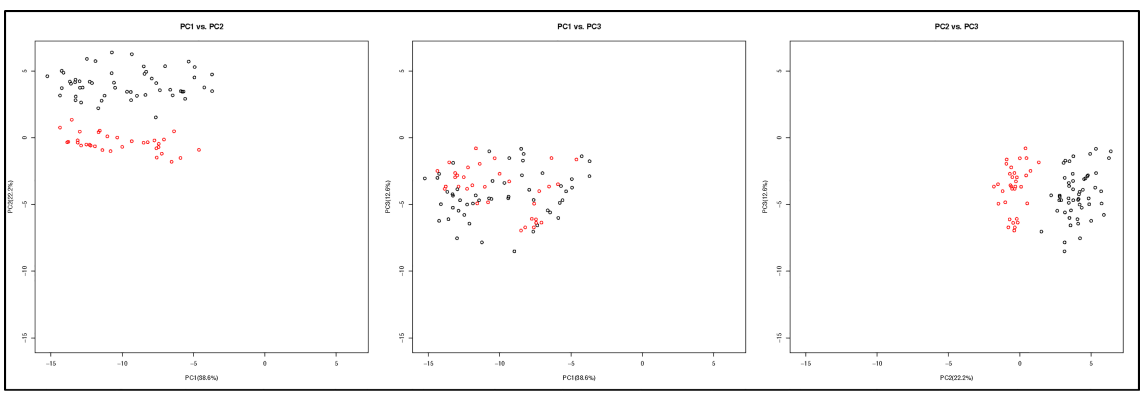

Cytokine	p-value	Cytokine	p-value	Cytokine	p-value
G-CSF	<0.001	IL-10	<0.001	bFGF	0.010
Il-17a	<0.001	IL-12p70	<0.001	IP-10	0.022
MCP-1	<0.001	IL-13	<0.001	IFNγ	0.047
IL-6	<0.001	IL-2	0.002		
IL-1B	<0.001	TNF-a	0.004		

FIGURE 2 | Cluster Analysis of TMOA Patients Indicates Presence of Sub-Groups. Principal component analysis (n=83) of cytokine expression of patients at baseline timepoint indicates a two sub-groups of patients. Wilcoxon tests performed between the two clusters indicates 13 cytokines which are differentially expressed ($p < 0.05$, $q < 0.1$).

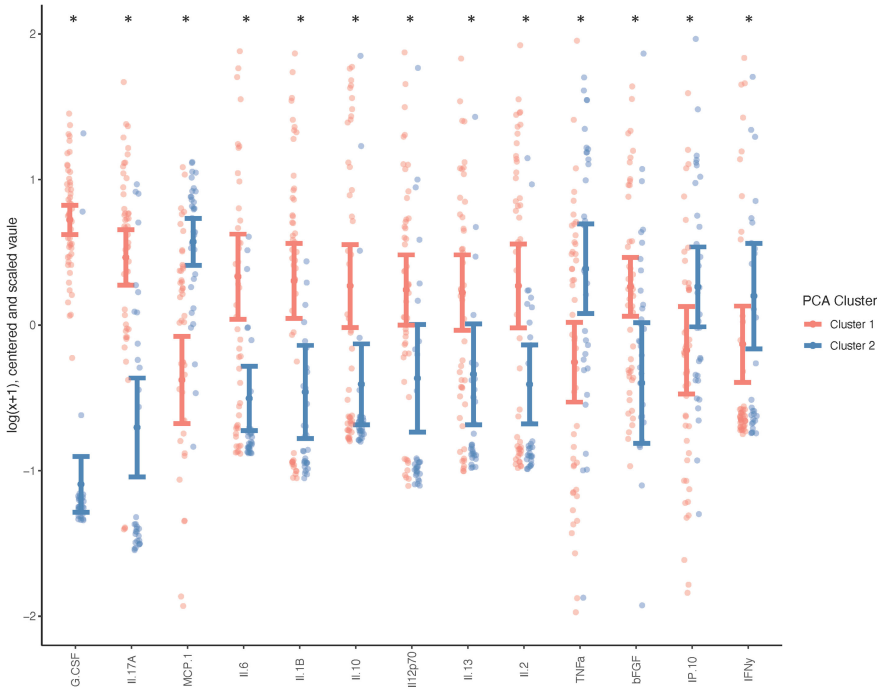

FIGURE 3 | Systemic Cytokine Differences between Patient Clusters. Wilcoxon test was performed on cytokines indicated as differently expressed between clusters (n=50 cluster 1, n=33 cluster 2), and adjusted for age, sex, BMI and total joint count (*$p < 0.05$, $q < 0.1$) and graph indicates the direction of differential expression between the two clusters.

stage disease when prognosis is largely unknown. A plasma biomarker, which is able to distinguish disease severity, is a feasible, minimally invasive option that could enable clinicians to make prognosis driven treatment recommendations as more efficacious therapies become available. In order to be able to identify biomarkers for TMOA, characterizing molecular profiles of the disease are required to foster an understanding of the complex regulatory environment. In this study, we used cytokine multiplex assays paired with matched patient clinical information to show that IL-7 is a molecular indicator, which could potentially differentiate between patients who are stably non-surgically managed, and those with advanced disease needing surgery. We also discovered that patients with TMOA can self-segregate into groups that are defined by a specific molecular signature indicating that phenotypes related to biological differences in TMOA may exist.

In order to create a comprehensive clinical picture of our study population, we compared patients undergoing non-surgical management to those undergoing trapeziectomy +\- tendon interposition. We found that although demographic and clinical measures were similarly distributed between groups, BMI and patient reported pain and function scores (TASD, quick DASH) were significantly different. Few studies have compared surgical and non-surgical management directly, though in these studies similar clinical characteristics (such as age and radiographic disease severity) are observed between the two patient groups (36, 37). These observations support literature describing radiographic severity and pain (the primary indication for surgery) as discordant. In fact, the decision to perform surgery for TMOA has been reported as largely subjective (38). Additionally, psychological factors such as illness perception and pain catastrophizing account for 42% of patient pre-treatment pain levels, whereas patient characteristics including radiographic disease severity only accounts for only 6%, leaving more than half of pain levels to unknown contributing factors (39). Biochemical factors such as cytokines may also be an important contributing factor that could be objectively measured allowing for comparisons within and between patients.

Cytokines that are able to distinguish disease severity could aid in defining mechanisms and finding molecular indicators capable of diagnosis and prognosis. Our adjusted analysis demonstrated that circulating IL-7 in plasma can distinguish between patients undergoing surgical or non-surgical management, despite similar radiographic disease severity, hand function measures and number of painful joints. This indicates that systemic levels of IL-7 could distinguish symptomatic disease severity in individuals with OA in multiple joints. Further, increased circulating IL-7 is associated with a significant decrease in likelihood of being symptomatic and requiring surgery (OR=0.220). Overall, this indicates the need to further study circulating IL-7 in TMOA patient

populations in order to determine if it could be used as a blood-based biomarker to monitor patients at risk for TMOA progression, to intervene with more aggressive treatment or preventative measures as they become available, or to plan for surgery. It is important to note that though our study accounted for the number of painful joints as a proxy for symptomatic OA in multiple joints, it does not account for the severity of OA in these joints which could be a significant contributing factor to circulating cytokine levels.

IL-7 is a growth factor involved in the development of B and T cells, but is also produced by variety of cell types including chondrocytes (20, 40). In a Han Chinese population, polymorphisms in the IL-7 gene are associated with increased risk of developing OA (41). In knee OA, IL-7 in synovial fluid was demonstrated to correlate positively with patient age, but was depressed in patients with severe osteoarthritis affecting multiple knee compartments (42). Increased local levels of IL-7 are typically considered pro-inflammatory and part of the senescence associated secretory phenotype (43, 44). *In-vitro*, IL-7 works to promote articular cartilage destruction through the up-regulation of cartilage destructive protease MMP-13 (40). Recent data from the Osteoarthritis Initiative cohort also indicates that significantly decreased levels of IL-7 are present in accelerated hand OA which progresses from minimal radiographic disease to end-stage over the course of 48 months (accepted abstract) (45). If indeed, IL-7 could be validated as a prognostic biomarker for TMOA then it may help to identify individuals who progress through this condition at different rates. Prognostic biomarkers can also be useful in facilitating understanding of disease pathogenesis, differentiating phenotypes within a heterogenous OA population, and comparing treatment outcomes during clinical trials where imaging outcomes may not reflect active disease (46). It is important to note none of the other 26 cytokines evaluated were capable of this measure after adjusting for painful joint count, age, sex and BMI, indicating the specificity of IL-7 as a molecular indicator of TMOA disease severity even when measured systemically.

Associations (MIP1a, MIP1b, Il-2 and bFGF) were observed in the relationship between the change in cytokine expression over time and some clinical outcome measures after adjusting for age, sex, BMI and painful joint count. Though these relationships were not consistently statistically significant across time points or outcome measures, some understanding may be drawn from current literature. MIP1a (CCL3) has previously been suggested as an early predictor of surgical outcome in non-union fracture therapy, implicated in likelihood of total-knee arthroplasty revisions, and as part of the senescence-associated secretory phenotype prediction of adverse post-surgical outcomes (47, 48). Both CCL3 and CCL4 (MIP1a, MIP1b) are elevated in revision total knee arthroplasty (TKA) patients compared to primary TKA patients, indicating their potential as predictors for post-surgical outcome (49). Whereas elevation of synovial fluid FGF2 (bFGF) reflects clinical response after joint distraction (50). However, within the literature the differences among source tissue and biofluids, as well as types and timing of measurements make it difficult to draw conclusions.

The heterogeneity in outcome measures within our non-surgically and surgically managed patient groups and the potential for treatment decisions to be influenced by patient and surgeon bias, prompted us to perform an unbiased examination of cytokine expression through Principal Component Analysis. It was observed that the data self-segregated into two visually discernable groups which differed based on the expression of unique combination of 13 cytokines; a molecular signature. This molecular signature consists of G-CSF, IL-17a, IL-6, IL-10, IL-1b, IL-12p70, IL-2, IL-13, MCP-1, B-FGF, IP-10, TNFa, and IFNy. In Cluster 1 G-CSF, IL-17a, IL-1b, IL-6, IL-10, IL-12p70, IL-13, IL-2 and B-FGF are elevated whereas in Cluster 2 MCP-1,TNFa, IP-10 and IFNy are elevated. These clusters cannot be attributed to difference in age, BMI, surgical status, patient reported outcome measures, or functional performance. The divergence of patients based solely on differing expression profiles of cytokines suggests that these subgroups may be indicative of endogenous phenotypes. The observed heterogeneity can also help inform that pharmacological therapies, prognostic, or diagnostic tools may have to be targeted to specific subpopulations to be successful.

Recent OA research has focused on understanding molecular and clinical phenotypes of this disease, of which there may be many (51). Common clinical phenotypes include chronic pain, mechanical overload, metabolic syndrome, bone and cartilage metabolism, minimal joint disease, and inflammatory phenotypes, while the senescence associated secretory phenotype is a distinct and well characterized molecular endotype (52). To our knowledge, this is the first study to show different molecular phenotypes in TMOA. The implication of an inflammation driven phenotype may signify that a subset of these patients may be more responsive to therapies precisely targeting these pathways, and understanding these pathological mechanisms will be crucial to developing effective therapies.

Limitations of the current study include a lack of a healthy comparator group, and decreased patient numbers during follow-up time points which may have impacted our ability to detect post-surgical differences in cytokine expression. The lack of a healthy patient group could indicate that the endogenous phenotypes we see within the TMOA population, could be true of the general population or other specific populations. Investigation of a healthy cohort would yield a valuable comparison to our molecular clusters, as well as surgical and non-surgical groups. In the current study we have not investigated a healthy control group due to the substantial (decades) age difference between the groups. Inclusion of a healthy control group could influence the interpretation of results by permitting the evaluation of the dispersion of circulating IL-7 levels between healthy, stably managed non-surgical as well as surgical patients. Hypothetically, if IL-7 levels were observed as similar between healthy controls and non-surgical TMOA patients, this could indicate that the relative decrease in IL-7 levels may be associated with mechanisms or pathways involved in more symptomatic TMOA. However, if levels of IL-7 in a healthy comparator were similar to those in the

surgical group (or in-between groups), it could indicate that relatively different levels between groups is the result of a factor external to those considered within the current study.

One source of bias in our study, may be the patient's decision to have surgery which could be based on a myriad of factors including their perception of surgery, convenience, time off work, and external support among others. Additionally, more precise imaging methods or analysis techniques such as quantifying osteophyte size, synovitis with ultrasound or MRI may more closely relate pain to structural damage than gross radiographic scores (53). In addition, though we present IL-7 as a cytokine capable of distinguishing between surgical and non-surgical TMOA patients, it should be noted that systemic cytokines are reflective of multiple active processes occurring concurrently throughout the body and not necessarily attributable to a specific process in a specific joint. It is also considered that the correlation between increased levels of this cytokine to decreased symptoms and likelihood of surgery may be an association and may not be due to causation, such as having a physiological role mediating this disease. Rather, it is possible that the association between these variables could be explained by factors which were not measured in the current study. Establishing a causative physiological role for the association observed would require additional interventional or experimental studies. Lastly, the cytokine expression and unique molecular signature discovered in this study will need to be validated in external cohorts to determine whether these results are applicable and reproducible in other TMOA populations.

TMOA, when symptomatic, has serious implications for hand function impacting vocational and avocational activities. Systemic IL-7 can distinguish between patients with disease severe enough to undergo surgery and less symptomatic patients. Elevated levels of IL-7 is associated with decreased likelihood to undergo surgery. This observation, if validated in other populations, could have the potential to provide an effective objective method to monitor patient response to non-surgical intervention. Interestingly, regardless of clinical variables, TMOA patients also segregate into two sub-groups based on the expression of a combination of 13 cytokines indicating that there may be endogenous phenotypes in TMOA that could be precisely targeted for more effective treatment.

DATA AVAILABILITY STATEMENT

The raw data supporting the conclusions of this article will be made available by the authors, without undue reservation.

ETHICS STATEMENT

The studies involving human participants were reviewed and approved by University Health Network Research Ethics Board. The patients/participants provided their written informed consent to participate in this study.

AUTHOR CONTRIBUTIONS

AR, JR, MK, and HB contributed to conception and design of the study. DA was responsible for clinical data collection. KS and JM performed the statistical analysis. AR wrote the the manuscript. All authors contributed to manuscript revision, read, and approved the submitted version.

FUNDING

This study was supported in part by grants to HB by the American Foundation for Surgery of the Hand Clinical Grant (#1407) and the Education Foundation of the Canadian Society of Plastic Surgeons. MK was supported in part by funding from the Canada Research Chairs Program (#950-232237), Canada Foundation for Innovation (#35171), Tony and Shari Fell Platinum Chair in Arthritis Research and Schroeder Arthritis Institute *via* the University Health Network Foundation (Toronto). AR is the recipient of the Canadian Institute of Health Research Postdoctoral Fellowship Award and the Krembil Research Institute Postdoctoral Fellowship Award.

ACKNOWLEDGMENTS

We would like to acknowledge Kim Perry and Amanda Weston at the Arthritis Program for patient sample and data collection, and biobanking. Dr. Mohit Kapoor for sharing lab space and providing study materials and Dr. Steven McCabe, Dr. Herb von Schroeder, Dr. Ryan Paul, Dr. Andrea Chan, Dr. Michelle Zec, and Dr. Ryan Wolek for performing trapeziectomy surgeries at Toronto Western Hospital and providing patient samples.

SUPPLEMENTARY MATERIAL

The Supplementary Material for this article can be found online at: https://www.frontiersin.org/articles/10.3389/fimmu.2021.794792/full#supplementary-material

Supplementary Figure 1 | Patient Pipeline. Patients followed the pipeline in the schematic above. In brief: patients undergoing non-surgical or surgical treatment for trapeziometacarpal osteoarthritis were recruited to the study and followed for 52 weeks. Patient reported outcome measures (PROM), key pinch strength and grip strength (clinical tests), as well as blood, urine and tissues (surgical group only) were collected.

Supplementary Figure 2 | Differences in Cytokine Expression Between Sexes in TMOA Patients.There were no differences in systemic cytokine expression between male or female patients at baseline after correcting for false discovery rate. (n=58 females: 31 nonsurgical/ 28 surgical, 25 males: 13 non-surgical/ 12 surgical, Wilcoxon Test $q > 0.1$).

Supplementary Table 1 | Radiographic Scores do not correlate with systemic cytokine expression. After adjusting for age, sex, BMI, and painful joint count, there were no significant associations between radiographic severity as determined by Eaton-Littler scores and systemic cytokine expression in surgical or non-

surgical patient groups at baseline (n=44 non-surgical,39 surgical, Wilcoxon Test, q > 0.1).

Supplementary Table 2 | PROM are not associated with systemic cytokine expression. After adjusting for age, sex, BMI, and painful joint count, there were no significant associations between Patient Reported Outcome Measures and systemic cytokine expression in surgical or non-surgical patient groups at baseline (n=44 non-surgical, 39 surgical, Wilcoxon Test, q > 0.1), in either the quick DASH, VAS, or TASD (total, symptomatic or disability scores).

Supplementary Table 3 | Clinical Function is not associated with systemic cytokine expression. After adjusting for age, sex, BMI, and painful joint count, there were no significant associations between clinical function and systemic cytokine expression in surgical or non-surgical patient groups at baseline (n=44 non-surgical, 39 surgical, Wilcoxon Test, q > 0.1), in key pinch strength.

Supplementary Table 4 | Associations between clinical outcomes and cytokine expression over time. After adjusting for age, sex, BMI and painful joint count there were few significant associations between change in cytokine expression over time and clinical outcome, (n= 44 surgical baseline, n=20-22 6 months, n=16-17 one-year, *p < 0.05, q < 0.1, bolded). BL-6M and BL-1Y describe the change in expression from Baseline to 6 Months, or Baseline to 1 Year.

Supplementary Table 5 | Roles and OA context of cytokines which differentiate patient subgroups. The traditional role of each cytokine or chemokine, as well as well as its associations within OA literature are described.

Supplementary Table 6 | Baseline Data. Baseline data for surgical and non-surgical patients, including clinical characteristics, PROM, functional scores and baseline cytokine measurements (pg/ml) are reported.

REFERENCES

1. Hunter DJ, Zhang Y, Sokolove J, Niu J, Aliabadi P, Felson DT. Trapeziometacarpal Subluxation Predisposes to Incident Trapeziometacarpal Osteoarthritis (OA): The Framingham Study. *Osteoarthritis Cartilage* (2005) 13(11):953–7. doi: 10.1016/j.joca.2005.06.007
2. Aebischer B, Elsig S, Taeymans J. Effectiveness of Physical and Occupational Therapy on Pain, Function and Quality of Life in Patients With Trapeziometacarpal Osteoarthritis - A Systematic Review and Meta-Analysis. *Handb Ther* (2016) 21(1):5–15. doi: 10.1177/1758998315614037
3. Oo WM, Deveza LA, Duong V, Fu K, Linklater JM, Riordan EA, et al. Musculoskeletal Ultrasound in Symptomatic Thumb-Base Osteoarthritis: Clinical, Functional, Radiological and Muscle Strength Associations. *BMC Musculoskelet Disord* (2019) 20(1):220. doi: 10.1186/s12891-019-2610-4
4. Moriatis Wolf J, Turkiewicz A, Atroshi I, Englund M. Prevalence of Doctor-Diagnosed Thumb Carpometacarpal Joint Osteoarthritis: An Analysis of Swedish Health Care. *Arthritis Care Res (Hoboken)* (2014) 66(6):961–5. doi: 10.1002/acr.22250
5. Hamasaki T, Lalonde L, Harris P, Bureau NJ, Gaudreault N, Ziegler D, et al. Efficacy of Treatments and Pain Management for Trapeziometacarpal (Thumb Base) Osteoarthritis: Protocol for a Systematic Review. *BMJ Open* (2015) 5(10):e008904. doi: 10.1136/bmjopen-2015-008904
6. Kloppenburg M, van Beest S, Kroon FPB. Thumb Base Osteoarthritis: A Hand Osteoarthritis Subset Requiring a Distinct Approach. *Best Pract Res Clin Rheumatol* (2017) 31(5):649–60. doi: 10.1016/j.berh.2018.08.007
7. Leung GJ, Rainsford KD, Kean WF. Osteoarthritis of the Hand I: Aetiology and Pathogenesis, Risk Factors, Investigation and Diagnosis. *J Pharm Pharmacol* (2014) 66(3):339–46. doi: 10.1111/jphp.12196
8. Fontana L, Neel S, Claise JM, Ughetto S, Catilina P. Osteoarthritis of the Thumb Carpometacarpal Joint in Women and Occupational Risk Factors: A Case-Control Study. *J Handb Surg Am* (2007) 32(4):459–65. doi: 10.1016/j.jhsa.2007.01.014
9. Cho HJ, Morey V, Kang JY, Kim KW, Kim TK. Prevalence and Risk Factors of Spine, Shoulder, Hand, Hip, and Knee Osteoarthritis in Community-Dwelling Koreans Older Than Age 65 Years. *Clin Orthop Relat Res* (2015) 473(10):3307–14. doi: 10.1007/s11999-015-4450-3
10. Heyworth BE, Lee JH, Kim PD, Lipton CB, Strauch RJ, Rosenwasser MP. Hylan Versus Corticosteroid Versus Placebo for Treatment of Basal Joint Arthritis: A Prospective, Randomized, Double-Blinded Clinical Trial. *J Handb Surg Am* (2008) 33(1):40–8. doi: 10.1016/j.jhsa.2007.10.009
11. Gomes Carreira AC, Jones A, Natour J. Assessment of the Effectiveness of a Functional Splint for Osteoarthritis of the Trapeziometacarpal Joint on the Dominant Hand: A Randomized Controlled Study. *J Rehabil Med* (2010) 42 (5):469–74. doi: 10.2340/16501977-0542
12. Day CS, Gelberman R, Patel AA, Vogt MT, Ditsios K, Boyer MI. Basal Joint Osteoarthritis of the Thumb: A Prospective Trial of Steroid Injection and Splinting. *J Handb Surg Am* (2004) 29(2):247–51. doi: 10.1016/j.jhsa.2003.12.002
13. Spaans AJ, van Minnen LP, Kon M, Schuurman AH, Schreuders AR, Vermeulen GM. Conservative Treatment of Thumb Base Osteoarthritis: A Systematic Review. *J Handb Surg Am* (2015) 40(1):16–21.e11-16. doi: 10.1016/j.jhsa.2014.08.047
14. Hoffler CE2nd, Matzon JL, Lutsky KF, Kim N, Beredjiklian PK. Radiographic Stage Does Not Correlate With Symptom Severity in Thumb Basilar Joint Osteoarthritis. *J Am Acad Orthop Surg* (2015) 23(12):778–82. doi: 10.5435/JAAOS-D-15-00329
15. Dahaghin S, Bierma-Zeinstra SM, Ginai AZ, Pols HA, Hazes JM, Koes BW. Prevalence and Pattern of Radiographic Hand Osteoarthritis and Association With Pain and Disability (The Rotterdam Study). *Ann Rheum Dis* (2005) 64 (5):682–7. doi: 10.1136/ard.2004.023564
16. Marshall M, van der Windt D, Nicholls E, Myers H, Dziedzic K. Radiographic Thumb Osteoarthritis: Frequency, Patterns and Associations With Pain and Clinical Assessment Findings in a Community-Dwelling Population. *Rheumatol (Oxf)* (2011) 50(4):735–9. doi: 10.1093/rheumatology/keq371
17. Lotz M, Martel-Pelletier J, Christiansen C, Brandi ML, Bruyere O, Chapurlat R, et al. Value of Biomarkers in Osteoarthritis: Current Status and Perspectives. *Ann Rheum Dis* (2013) 72(11):1756–63. doi: 10.1136/annrheumdis-2013-203726
18. Hunter DJ, Nevitt M, Losina E, Kraus V. Biomarkers for Osteoarthritis: Current Position and Steps Towards Further Validation. *Best Pract Res Clin Rheumatol* (2014) 28(1):61–71. doi: 10.1016/j.berh.2014.01.007
19. Marshall M, Watt FE, Vincent TL, Dziedzic K. Hand Osteoarthritis: Clinical Phenotypes, Molecular Mechanisms and Disease Management. *Nat Rev Rheumatol* (2018) 14(11):641–56. doi: 10.1038/s41584-018-0095-4
20. Mabey T, Honsawek S. Cytokines as Biochemical Markers for Knee Osteoarthritis. *World J Orthop* (2015) 6(1):95–105. doi: 10.5312/wjo.v6.i1.95
21. Miller RE, Miller RJ, Malfait AM. Osteoarthritis Joint Pain: The Cytokine Connection. *Cytokine* (2014) 70(2):185–93. doi: 10.1016/j.cyto.2014.06.019
22. Cevidanes LH, Walker D, Schilling J, Sugai J, Giannobile W, Paniagua B, et al. 3D Osteoarthritic Changes in TMJ Condylar Morphology Correlates With Specific Systemic and Local Biomarkers of Disease. *Osteoarthritis Cartilage* (2014) 22(10):1657–67. doi: 10.1016/j.joca.2014.06.014
23. Kraus VB, Kepler TB, Stabler T, Renner J, Jordan J. First Qualification Study of Serum Biomarkers as Indicators of Total Body Burden of Osteoarthritis. *PloS One* (2010) 5(3):e9739. doi: 10.1371/journal.pone.0009739
24. Rannou F, Dimet J, Boutron I, Baron G, Fayad F, Mace Y, et al. Splint for Base-of-Thumb Osteoarthritis: A Randomized Trial. *Ann Intern Med* (2009) 150 (10):661–9. doi: 10.7326/0003-4819-150-10-200905190-00003
25. Beaton DE, Wright JG, Katz JNUpper Extremity Collaborative G. Development of the QuickDASH: Comparison of Three Item-Reduction Approaches. *J Bone Joint Surg Am* (2005) 87(5):1038–46. doi: 10.2106/JBJS.D.02060
26. Becker SJ, Teunis T, Ring D, Vranceanu AM. The Trapeziometacarpal Arthrosis Symptoms and Disability Questionnaire: Development and Preliminary Validation. *Handb (N Y)* (2016) 11(2):197–205. doi: 10.1177/1558944715627239
27. Price DD, Patel R, Robinson ME, Staud R. Characteristics of Electronic Visual Analogue and Numerical Scales for Ratings of Experimental Pain in Healthy Subjects and Fibromyalgia Patients. *Pain* (2008) 140(1):158–66. doi: 10.1016/j.pain.2008.07.028

28. Gummesson C, Ward MM, Atroshi I. The Shortened Disabilities of the Arm, Shoulder and Hand Questionnaire (QuickDASH): Validity and Reliability Based on Responses Within the Full-Length DASH. *BMC Musculoskelet Disord* (2006) 7:44. doi: 10.1186/1471-2474-7-44
29. Cook GS, Lalonde DH. MOC-PSSM CME Article: Management of Thumb Carpometacarpal Joint Arthritis. *Plast Reconstr Surg* (2008) 121(1 Suppl):1–9. doi: 10.1097/01.prs.0000294708.70340.8c
30. Bellamy N, Klestov A, Muirden K, Kuhnert P, Do KA, O'Gorman L, et al. Perceptual Variation in Categorizing Individual Peripheral Joints for the Presence or Absence of Osteoarthritis Using a Standard Homunculus: Observations Based on an Australian Twin Registry Study of Osteoarthritis. *Inflammopharmacology* (1999) 7(1):37–46. doi: 10.1007/s10787-999-0024-x
31. Carlesso LC, Niu J, Segal NA, Frey-Law LA, Lewis CE, Nevitt MC, et al. The Effect of Widespread Pain on Knee Pain Worsening, Incident Knee Osteoarthritis (OA), and Incident Knee Pain: The Multicenter OA (MOST) Study. *J Rheumatol* (2017) 44(4):493–8. doi: 10.3899/jrheum.160853
32. Kim C, Linsenmeyer KD, Vlad SC, Guermazi A, Clancy MM, Niu J, et al. Prevalence of Radiographic and Symptomatic Hip Osteoarthritis in an Urban United States Community: The Framingham Osteoarthritis Study. *Arthritis Rheumatol* (2014) 66(11):3013–7. doi: 10.1002/art.38795
33. Perruccio AV, Power JD, Evans HM, Mahomed SR, Gandhi R, Mahomed NN, et al. Multiple Joint Involvement in Total Knee Replacement for Osteoarthritis: Effects on Patient-Reported Outcomes. *Arthritis Care Res (Hoboken)* (2012) 64(6):838–46. doi: 10.1002/acr.21629
34. Heard BJ, Fritzler MJ, Wiley JP, McAllister J, Martin L, El-Gabalawy H, et al. Intraarticular and Systemic Inflammatory Profiles may Identify Patients With Osteoarthritis. *J Rheumatol* (2013) 40(8):1379–87. doi: 10.3899/jrheum.121204
35. Yoav Benjamini YH. Controlling the False Discovery Rate: A Practical and Powerful Approach to Multiple Testing. *J R Stat Society: Ser B (Methodol)* (1995) 57(1):289–300. doi: 10.1111/j.2517-6161.1995.tb02031.x
36. Nayar S, Glasser R, Deune E, Ingari J, LaPorte D. Equivalent PROMIS Scores After Nonoperative or Operative Treatment of Trapeziometacarpal Osteoarthritis. *Arch Bone Joint Surg* (2019) 8(3):383–90. doi: 10.22038/abjs.2019.41772.2128
37. Marks M, Audige L, Reissner L, Herren DB, Schindele S, Vliet Vlieland TP. Determinants of Patient Satisfaction After Surgery or Corticosteroid Injection for Trapeziometacarpal Osteoarthritis: Results of a Prospective Cohort Study. *Arch Orthop Trauma Surg* (2015) 135(1):141–7. doi: 10.1007/s00402-014-2119-0
38. Ottenhoff JSE, Teunis T, Janssen SJ, Mink van der Molen AB, Ring D. Variation in Offer of Operative Treatment to Patients With Trapeziometacarpal Osteoarthritis. *J Handb Surg Am* (2020) 45(2):123–130 e121. doi: 10.1016/j.jhsa.2019.10.017
39. Hoogendam L, van der Oest MJW, Tsehaie J, Wouters RM, Vermeulen GM, Slijper HP, et al. Psychological Factors are More Strongly Associated With Pain Than Radiographic Severity in non-Invasively Treated First Carpometacarpal Osteoarthritis. *Disabil Rehabil* (2021) 43(13):1897–902. doi: 10.1080/09638288.2019.1685602
40. Long D, Blake S, Song XY, Lark M, Loeser RF. Human Articular Chondrocytes Produce IL-7 and Respond to IL-7 With Increased Production of Matrix Metalloproteinase-13. *Arthritis Res Ther* (2008) 10(1):R23. doi: 10.1186/ar2376
41. Zhang HX, Wang YG, Lu SY, Lu XX, Liu J. Identification of IL-7 as a Candidate Disease Mediator in Osteoarthritis in Chinese Han Population: A Case-Control Study. *Rheumatol (Oxf)* (2016) 55(9):1681–5. doi: 10.1093/rheumatology/kew220
42. Rubenhagen R, Schuttrumpf JP, Sturmer KM, Frosch KH. Interleukin-7 Levels in Synovial Fluid Increase With Age and MMP-1 Levels Decrease With Progression of Osteoarthritis. *Acta Orthop* (2012) 83(1):59–64. doi: 10.3109/17453674.2011.645195
43. Malemud CJ. Anticytokine Therapy for Osteoarthritis: Evidence to Date. *Drugs Aging* (2010) 27(2):95–115. doi: 10.2165/11319950-000000000-00000
44. Greene MA, Loeser RF. Aging-Related Inflammation in Osteoarthritis. *Osteoarthritis Cartilage* (2015) 23(11):1966–71. doi: 10.1016/j.joca.2015.01.008
45. Driban MBR JB, Eaton CB, Haugen IK, Harkey MS, Lo GH, Schäfer L, et al. Serum Measures of Metabolism and Inflammation Among Adults Prior to Incident Accelerated Hand Osteoarthritis: Data From the Osteoarthritis Initiative. *Osteoarthritis Cartilage* (2019) 27(S103). doi: 10.1016/j.joca.2019.02.152
46. Attur M, Krasnokutsky-Samuels S, Samuels J, Abramson SB. Prognostic Biomarkers in Osteoarthritis. *Curr Opin Rheumatol* (2013) 25(1):136–44. doi: 10.1097/BOR.0b013e32835a9381
47. Haubruck P, Solte A, Heller R, Daniel V, Tanner M, Moghaddam A, et al. Chemokine Analysis as a Novel Diagnostic Modality in the Early Prediction of the Outcome of non-Union Therapy: A Matched Pair Analysis. *J Orthop Surg Res* (2018) 13(1):249. doi: 10.1186/s13018-018-0961-4
48. Schafer MJ, Zhang X, Kumar A, Atkinson EJ, Zhu Y, Jachim S, et al. The Senescence-Associated Secretome as an Indicator of Age and Medical Risk. *JCI Insight* (2020) 5(12). doi: 10.1172/jci.insight.133668
49. Paish HL, Baldock TE, Gillespie CS, Del Carpio Pons A, Mann DA, Deehan DJ, et al. Chronic, Active Inflammation in Patients With Failed Total Knee Replacements Undergoing Revision Surgery. *J Orthop Res* (2019) 37(11):2316–24. doi: 10.1002/jor.24398
50. Watt FE, Hamid B, Garriga C, Judge A, Hrusecka R, Custers RJH, et al. The Molecular Profile of Synovial Fluid Changes Upon Joint Distraction and is Associated With Clinical Response in Knee Osteoarthritis. *Osteoarthritis Cartilage* (2020) 28(3):324–33. doi: 10.1016/j.joca.2019.12.005
51. Mobasheri A, van Spil WE, Budd E, Uzieliene I, Bernotiene E, Bay-Jensen AC, et al. Molecular Taxonomy of Osteoarthritis for Patient Stratification, Disease Management and Drug Development: Biochemical Markers Associated With Emerging Clinical Phenotypes and Molecular Endotypes. *Curr Opin Rheumatol* (2019) 31(1):80–9. doi: 10.1097/BOR.0000000000000567
52. Mobasheri A, Saarakkala S, Finnila M, Karsdal MA, Bay-Jensen AC, van Spil WE. Recent Advances in Understanding the Phenotypes of Osteoarthritis. *F1000Res* (2019) 8. doi: 10.12688/f1000research.20575.1
53. Kroon FPB, van Beest S, Ermurat S, Kortekaas MC, Bloem JL, Reijnierse M, et al. In Thumb Base Osteoarthritis Structural Damage is More Strongly Associated With Pain Than Synovitis. *Osteoarthritis Cartilage* (2018) 26(9):1196–202. doi: 10.1016/j.joca.2018.04.009

Conflict of Interest: The authors declare that the research was conducted in the absence of any commercial or financial relationships that could be construed as a potential conflict of interest.

frontiers in Immunology

ORIGINAL RESEARCH
published: 11 February 2022
doi: 10.3389/fimmu.2022.820843

Dental and Orthopaedic Implant Loosening: Overlap in Gene Expression Regulation

*Sabine Schluessel[1], Eliza S. Hartmann[1], Miriam I. Koehler[1], Felicitas Beck[1], Julia I. Redeker[1], Maximilian M. Saller[1], Elif Akova[1], Stefan Krebs[2], Boris M. Holzapfel[1] and Susanne Mayer-Wagner[1]**

[1] Department of Orthopaedics and Trauma Surgery, Musculoskeletal University Center Munich (MUM), University Hospital, Ludwig Maximilian University (LMU) Munich, Munich, Germany, [2] Gene Center, Laboratory for Functional Genome Analysis, University Hospital, Ludwig Maximilian University (LMU) Munich, Munich, Germany

OPEN ACCESS

Edited by:
Gurpreet S. Baht, Duke University, United States

Reviewed by:
Maria-Bernadette Madel, Baylor College of Medicine, United States
Maria Helena Fernandes, University of Porto, Portugal

***Correspondence:**
Susanne Mayer-Wagner
susanne.mayer@med.uni-muenchen.de

Specialty section:
This article was submitted to Inflammation, a section of the journal Frontiers in Immunology

Received: *23 November 2021*
Accepted: *17 January 2022*
Published: *11 February 2022*

Citation:
Schluessel S, Hartmann ES, Koehler MI, Beck F, Redeker JI, Saller MM, Akova E, Krebs S, Holzapfel BM and Mayer-Wagner S (2022) Dental and Orthopaedic Implant Loosening: Overlap in Gene Expression Regulation. Front. Immunol. 13:820843. doi: 10.3389/fimmu.2022.820843

Objectives: Endoprosthetic loosening still plays a major role in orthopaedic and dental surgery and includes various cellular immune processes within peri-implant tissues. Although the dental and orthopaedic processes vary in certain parts, the clinical question arises whether there are common immune regulators of implant loosening. Analyzing the key gene expressions common to both processes reveals the mechanisms of osteoclastogenesis within periprosthetic tissues of orthopaedic and dental origin.

Methods: Donor peripheral blood mononuclear cells (PBMCs) and intraoperatively obtained periprosthetic fibroblast-like cells (PPFs) were (co-)cultured with [± macrophage-colony stimulating factor (MCSF) and Receptor Activator of NF-κB ligand (RANKL)] in transwell and monolayer culture systems and examined for osteoclastogenic regulations [MCSF, RANKL, osteoprotegerin (OPG), and tumor necrosis factor alpha (TNFα)] as well as the ability of bone resorption. Sequencing analysis compared dental and orthopaedic (co-)cultures.

Results: Monolayer co-cultures of both origins expressed high levels of OPG, resulting in inhibition of osteolysis shown by resorption assay on dentin. The high OPG-expression, low RANKL/OPG ratios and a resulting inhibition of osteolysis were displayed by dental and orthopaedic PPFs in monolayer even in the presence of MCSF and RANKL, acting as osteoprotective and immunoregulatory cells. The osteoprotective function was only observed in monolayer cultures of dental and orthopaedic periprosthetic cells and downregulated in the transwell system. In transwell co-cultures of PBMCs/PPFs profound changes of gene expression, with a significant decrease of OPG (20-fold dental versus 100 fold orthopaedic), were identified. Within transwell cultures, which offer more *in vivo* like conditions, RANKL/OPG ratios displayed similar high levels to the original periprosthetic tissue. For dental and orthopaedic implant loosening, overlapping findings in principal component and heatmap analysis were identified.

Conclusions: Thus, periprosthetic osteoclastogenesis may be a correlating immune process in orthopaedic and dental implant failure leading to comparable reactions with regard to osteoclast formation. The transwell cultures system may provide an *in vivo* like model for the exploration of orthopaedic and dental implant loosening.

Keywords: dental and orthopaedic implant failure, osteoclastogenic regulation, periprosthetic tissue, immune reaction, RNA-sequencing, immune osteoclastic cells

1 BACKGROUND

The initial triggers of orthopaedic and dental implant loosening differ at first glance significantly also due to the aberrant microbiological environment. However, in both conditions the formation of a fibrous peri-implant tissue is initiated. Although it might be assumed that fundamentally different loosening processes and immune regulations occur in orthopaedic and dental implants, similar cytokines are involved in cascades of both processes, which lead to the formation and activation of osteoclasts. Both peri-implant tissues of loosened endoprostheses consist mainly of macrophages and periprosthetic fibroblast-like-cells (PPFs) (1).

PPFs in orthopaedic peri-implant tissues express TNFα, a cytokine that is an important signaling metabolite for local and systemic inflammatory reactions (2, 3). When MCSF is added *in vitro*, TNFα-expressing PPFs cause increased osteoclast formation and thus might contribute to endoprosthetic loosening (2, 3). TNFα is also highly expressed in peri-implant tissues of loosened dental implants (4). In gingival fibroblasts, TNFα leads to the release of prostaglandin E2 (PGE2) (5). PGE2, a signal protein of bone resorption, has been detected in orthopaedic and dental peri-implant tissues (6, 7). PGE2 synthesizing cyclooxygenase-2 (COX-2) is expressed in PPFs and stimulated by titanium particles (8). PGE2 induces an increased expression of Receptor Activator of NF-κB ligand (RANKL) in PPFs (9). RANKL has a strong impact on the regulation of bone formation and resorption. RANKL activates osteoclasts by binding to the RANK receptor of osteoclast precursor cells, thereby inducing their differentiation into osteoclasts. RANKL expression of PPFs thus directly induces osteoclast formation in orthopaedic and dental peri-implant tissues (10–12).

The opponent Osteoprotegerin (OPG) acts as decoy receptor for RANKL and inhibits osteoclast differentiation. In periodontitis, an increased RANKL/OPG Ratio (up-regulation of RANKL and down-regulation of OPG) is described (13).

PPFs also express matrix metalloproteinases (MMPs), which are found in elevated concentrations in orthopaedic and dental peri-implant tissues (14, 15). MMP13 degrades bone due to its substrate specificity for collagen type 1 (16). The increased expression of MMPs leads to collagen degradation in peri-implantation tissues. In addition, MMPs are found in periosteoclastic cells (15) and in subosteoclastic resorption lagoons of osteoclasts, thereby contributing to further bone loss (17). Due to their expression patterns, PPFs in peri-implant tissue assume similar functions to so-called "aggressive" fibroblasts in rheumatoid arthritis (18).

Osteocalcin (OCN), an extracellular matrix protein, is synthesized by mature osteoblasts and is able to influence bone mineralization and remodeling (19). Cathepsin K (CTSK), a cysteine protease, is mainly expressed by osteoclasts and is involved in collagen cleavage in the extracellular matrix (20). Increased levels of OCN and CTSK were found in peri-implant crevicular fluid and might indicate a higher bone turnover in implants (20, 21). Mandelin et al. showed that interface tissue fibroblasts are also able to secrete CTSK (10).

Tartrate-resistant-acid-phosphatase (TRAP) is an osteoclast-specific marker closely linked to bone resorption. In early phases of orthopaedic implant loosening increased TRAP levels are described, while late phases correlate with decreased amounts of TRAP (22).

These examples indicate that similar cytokines, prostaglandins and MMPs are involved in orthopaedic and dental peri-implant tissues that contribute to the formation and activation of osteoclasts.

Whether the processes in oral and orthopaedic peri-implant tissues might be closer related, and an overreaction of the immune system has a high impact on marginal bone loss and failure of dental and orthopaedic implants is discussed by Albrektsson et al. (23). The foreign body reaction might play an important part in oral as well as orthopaedic implants.

In order to examine the overlying immune effects with regards to osteoclast formation of dental and orthopaedic periprosthetic tissues, a common model of co-cultures, containing of peripheral blood mononuclear cells (PBMCs) and PPFs, was used (24, 25).

As *in vitro* cell studies often lack the complex three-dimensional component, a multilayer transwell (TW) culture system was applied. TW cultures have the advantage to provide an optimal medium supply from two sides improving intercellular connections and direct cell-cell contacts (26).

Abbreviations: COX-2 Cyclooxygenase-2, CP Crossing Point, CTSK Cathepsin K, DIF Dental Interfaces, DMEM Dulbecco´s Minimal Essential Medium, EF1a Elongation factor 1alpha, Fig Figure, HE Hematoxylin and eosin, HKG Housekeeping gene, IF Interfaces (orthopaedics), MCSF Macrophage colony-stimulating factor, ML Monolayer, MMPs Matrix metallopeptidases, MNC multinucleated cell, OCN Osteocalcin, OPG Osteoprotegerin, PBMCs Peripheral blood mononuclear cells, PBS Phosphate buffered saline, PDLFs Periodontal ligaments fibroblasts, PGE2 Prostaglandin E2, PPFs Periprosthetic fibroblast-like cells, dPPFs Dental periprosthetic fibroblast-like cells, oPPFs Orthopaedic periprosthetic fibroblast-like cells, RANK Receptor activator of NF-κB, RANKL Receptor activator of NF-κB ligand, RT Room temperature, TNFα Tumor necrosis factor alpha, TRAP Tartrate resistant acid phosphatase, TW Transwell, α-MEM α-Minimal Essential Medium.

TW cultures have been described to increase the number of cells in fibroblast cultures (27) and changes expression patterns of co-cultured orthopaedic PPFs (28). The effect of transwell cultures to modify the expression of major mediators of osteoclastogenesis was proven for PPF cells from orthopaedic implants (28).

To our knowledge, there have not been any studies comparing periprosthetic tissues of dental and orthopaedic cells. The hypothesis of overlapping peri-implant tissue reactions in dental and orthopaedic implant failure was investigated within this study using a co-culture model of periprosthetic fibroblast like cells from orthopaedic and dental implants and examining their effect on immune cells like PBMCs in terms of osteoclastogenesis and bone loss.

2 MATERIAL & METHODS

2.1 Patients

Peri-implant tissues were collected from eight patients (six female, two male; mean age 64, age range: 45 to 76 years) undergoing dental implant revision due to aseptic peri-implantitis. The diagnosis was conducted by the attending implantologist using the established criteria of the Sixth European Workshop on Periodontology (29, 30). Patients with allergies to components of the endoprosthetic material, early implant failure (<12 months), disorders of bone metabolism, rheumatoid arthritis or other inflammatory arthritis were excluded. Tissue samples were immediately incubated in the operating room in Dulbecco´s Modified Eagle Medium (DMEM; Biochrom, Berlin, Germany) with 60 IU/ml penicillin, 60 µg/ml streptomycin (Biochrom, Berlin, Germany) and 0.25 µg/ml Amphotericin B (Sigma–Aldrich Co., St. Louis, MO, USA). The study was approved by the medical ethics committee of the Ludwig-Maximilians-University Munich, Germany. Based on the design of the study using disposable material no patient consent was required. The experiment was carried out three times.

2.2 Isolation of Fibroblast-Like-Cells

Following the protocol of Hartmann et al. (31), collected tissue was washed with phosphate-buffered saline (PBS) (Biochrome, Berlin, Germany), cut into 2 mm sized pieces and digested with Dulbecco´s Minimal Essential Medium (DMEM, Biochrom, Berlin, Germany) containing 1mg/ml collagenase Type 1 (Sigma-Aldrich Co., St. Louis, MO, USA) for 30 min at 37°C. Next, a second digestion step with Versene (Invitrogen, Darmstadt, Germany) for 60 min at 37°C was conducted. After the digestion, the remnant was sterile-filtered using a 70 µm cell strainer (BD Bioscience, San Jose, USA) and centrifuged for 5 min at 1500 rpm. The pellet was resuspended in DMEM supplemented with 10% fetal bovine serum (FBS; PAA Laboratories, Cölbe, Germany), 2 mM L-glutamine, 60 IU/mL penicillin, 60 µg/mL streptomycin (all Biochrom, Berlin, Germany), 0.075 µg/mL amphotericin B (Sigma-Aldrich Co., St. Louis, MO, USA), 5 ml non-essential amino acids (50x, Thermo Fisher, New York, NY, USA) and cultured in a T75 culture flask (Nunc, Roskilde, Denmark) at a density of 3.5 x 10^3/cm^2 at 37°C and 5% CO_2. During the initial seven days, FBS was increased to 20%. The medium was changed twice a week. Cells were passaged at 80-90% confluence by using 0.05% trypsin (Biochrom Berlin, Germany) containing 0.02% ethylenediaminetetraacetic acid (EDTA, Biochrom Berlin, Germany).

Cultures of fibroblast-like cells were assessed histochemically for the absence of TRAP by using a TRAP detection kit (Sigma-Aldrich Co., St. Louis, MO, USA) to exclude the presence of TRAP positive cells, which would have falsified controls (2, 31, 32). Cell cultures were also tested for mycoplasma contamination in passage one performing PCR Mycoplasma Test Kit I/C (PromoCell, Heidelberg, Germany). The cells were used at passage three for the following monolayer and transwell culture experiments.

Additionally, primary tissues (n=8) were used for RNA isolation in order to compare the results to *in vivo* conditions (=baseline). Therefore, these tissues were directly placed in RNA later (Sigma-Aldrich Co., USA). The next day RNA later was removed and tissues stored at -80°C.

2.3 Isolation of PBMCs

Buffy coats (n = 4, male donors, blood group A (2 times), B and 0 respectively, all rhesus positive) were received from the German Red Cross Blood Donor Service at the university of Ulm, Germany. Buffy coats were processed on the same day following the established protocol (33).

2.4 Cell Culture Experiments

Cells were cultured following a protocol published by Koehler et al., 2019 on conventional 24-well monolayer (ML) plates for adherent cells (Nunc, Roskilde, Denmark) and on the membranes of 24-transwell (TW) plate inserts (pore size 0.4 µm, Nunc, Roskilde, Denmark). Cell culture experiments were performed in ten groups (please see **Table 1**). In both culture types a cell density of 1.2 x10^5 PPFs and 6x10^6 PBMCs per well was used. The PBMCs were seeded on day 0, followed by medium change on day 1 in order to remove non-adherent cells. On day 3, PPFs were added to co-cultures. The same medium was used for all groups containing α-Minimal Essential Medium (α-MEM, Biochrom, Berlin, Germany), 10% fetal bovine serum (FBS; PAA Laboratories, Cölbe, Germany), 2 mM L-glutamine, 60 IU/mL penicillin, 60 µg/mL streptomycin (all Biochrom, Berlin, Germany) and 0.075 µg/mL amphotericin B (Sigma-Aldrich Co., St. Louis, MO, USA). Cells were cultivated at 37°C and 5% CO2. The medium was changed three times a week.

In order to avoid bias by donor-specific cell characteristics, PPFs were separately co-cultivated with PBMCs of two different donors (donor of PBMCs =D). The stimulation of PBMCs (25 ng/ml MCSF (recombinant human MCSF, R&D Systems, Minneapolis, MN, USA) took place on day 0, 1 and 3 and with RANKL (recombinant human sRANK Ligand, Peprotech, Rocky Hill, NJ, USA) which started on day 6 with 10 ng/ml and was increased to 20ng/ml on day 8.

TABLE 1 | Cell culture groups.

Cell type		Cell culture	Stimulated with RANKL; MCSF
1	PPFs (negative osteoclastic control)	ML	–
2	PBMCs (positive osteoclastic control)	ML	+
3	PBMCs	ML	–
4	co-culture (PPFs and PBMCs)	ML	–
5	co-culture (PPFs and PBMCs) *	ML	+
6	PPFs (negative osteoclastic control)	TW	–
7	PBMCs (positive osteoclastic control)	TW	+
8	PBMCs	TW	–
9	co-culture (PPFs and PBMCs)	TW	–
10	co-culture (PPFs and PBMCs) *	TW	+

**Only performed on dentin chips; ML, monolayer; TW, transwel.*

2.5 Hoechst and TRAP Staining of Monolayer Cultures

The staining of TRAP was performed in conventional 24-well plates by using the commercial kit (Sigma-Aldrich Co., St Louis, MO, USA) on day 28 as recommended by the manufacturer. After rinsing, cell cultures were incubated with Hoechst Solution (Invitrogen, Darmstadt, Germany 1:1000 PBS) for 10 min at RT in the dark. The presence of multinucleated TRAP positive cells was detected by light microscope (Axiovert 40, Zeiss, Germany) and fluorescence microscope (BZ9000, Keyence, Japan).

2.6 Dentin Assay

In order to investigate osteoclastogenesis *via* bone resorption cells were cultivated on dentin chips as described by Koehler et al. (28). On day 29, the dentin chips were stained with Hoechst, as described. Afterwards, cells were removed by adding sodium hypochlorite (Merck, Darmstadt, Germany). After rinsing and cleaning in 80% ethanol, the slices were stained with 1% toluidine blue solution (Waldeck, Münster, Germany) for 10 seconds until they appeared in blue color. After rinsing the chips again with tap water, dentin chips surfaces were scanned for resorption lacunae (BioRevo Fluorescence Microscope, Keyence, Neu-Isenburg, Germany). The staining and dentin assay was carried out three times.

2.7 Quantitative Real-Time PCR (qRT-PCR) of Monolayer and Transwell Cultures

RNA was isolated from monolayer and transwell cultures on day 0, 13 and 20 following the protocol of Koehler et al. (28). For cDNA synthesis, 0.5 µg RNA was reversed-transcripted using QuantiTect Reverse Transcription Kit (Quiagen, Hilden, Germany). For qRT-PCR a Light Cycler (LightCycler 96 Real-Time PCR System, Roche Diagnostics, Mannheim, Germany) was used. Gene expression analysis of the following markers was implemented: *Elongation factor 1alpha (EF1a*, housekeeping gene), *CTSK*, *MCSF*, *TNFα*, *RANKL*, *RANK*, *OPG*, *OCN* and *TRAP*. Amplification reactions were performed using Light cycler® Fast Start Essential DNA Master Kit (Roche): 5 µL of FastStart Essential DNA Green Master Mix (Roche Diagnostics, Mannheim, Germany), 2.5 µl of 1:3 diluted cDNA and 0.3 µl (300 nM)/0.5 µl (500 nM) of primer were used, adding PCR grade water until reaching a total volume of 10 µl. Time, temperature and concentration of each primer are shown in **Table 2**. Reactions were performed in triplicates. For the relative quantification the 2^{-DCT} method was used, to provide comparison between gene expression levels of different genes. The 2^{-DCT} method was chosen to keep the comparability of expression levels of *RANKL* and *OPG*, which would have been lost using the 2^{-DDCT} method.

2.8 RNA-Sequencing and Analysis of Monolayer Cultures

Total RNA from monolayer cultures of PPFs, PBMCs, and co-cultures on day 0, 13 and 20 was isolated with the Trizol method. RNA-seq libraries were generated from 200 ng of total RNA using the mRNA SENSE kit (Lexogen, Vienna, Austria) according to the manufacturer's protocol. Multiplexed libraries were quality controlled on Agilent Bioanalyzer, pooled in equimolar amounts and sequenced in 100 bp single read mode on an Illumina HiSeq1500 instrument (Illumina, San Diego, CA, USA). Fastq files were demultiplexed according to the barcodes used for generation of each sample. Reads were aligned to the human genome (release GRCh38.101) using STAR (version 2.7.2b). Low gene expressions were filtered out by minimum 10 reads per gene cut off and 26,382 genes remained for further analysis. Normalization performed through variance stabilizing transformation (vst) for Principal Component Analysis (PCA). Top 50 differentially expressed genes defined through vst expression variance between each group. Significant differential gene expression was analyzed using DESeq2 (version 1.28.1) with 0.05 p-adjusted value cut off and 2 and -2 Log2FoldChange cut off for each group comparison. From 26,382 genes, 567 genes were differentially expressed between dental and orthopaedic co-cultures significantly. Furthermore, significant genes defined by the DESeq2 analysis of mono and co-cultures, independent from the derived location, were used to define significant Gene Ontology Biological Pathways by clusterProfiler (version 3.14) (35).

2.9 Statistical Analysis

Graph Pad Prism 8.3.0. for Windows (GraphPad Software, San Diego, CA, USA) was utilized to analyze the data. For

TABLE 2 | Primers for quantitative real-time PCR.

Gene	Primer Sequences (5´– 3´)	Primer Concentration (n)	Annealing Temperature (AT)	Amplification (95°C - AT - 72°C)	Ampli-con size (bp)
CTSK (31, 34)	TTCCCGCAGTAATGACACC TTTCCCCAGTTTTCTCCCC	500 nM	63°C	10 s - 10 s - 20 s	615
EF1a (28)	AGCGCCGGCTATGCCCCTG CTGAACCATCCAGGCCAAAT	300 nM	60°C	15 s - 60 s - 10 s	59
MCSF (28, 34)	CCGAGGAGGTGTCGGAGTAC AATTTGGCACGAGGTCTCCAT	300 nM	60°C	10 s - 10 s - 15 s	100
OCN	TGAGAGCCCTCACACTCCTC ACCTTTGCTGGACTCTGCAC	500 nM	60°C	10 s - 10 s - 15 s	209
OPG (28, 34)	CTGCGCGCTCGTGTTTC ACAGCTGATGAGAGGTTTCTTCGT	300 nM	60°C	30 s - 60 s - 15 s	100
RANK (31)	CCTGGACCAACTGTACCTTCCT ACCGCATCGGATTTCTCTGT	300 nM	60°C	10 s - 10 s - 15 s	67
RANKL (28, 34)	CATCCCATCTGGTTCCCATAA GCCCAACCCCGATCATG	300 nM	60°C	10 s - 10 s - 15 s	60
TNFα (28, 34)	CCCAGGGACCTCTCTCTAATC GCTTGAGGGTTTGCTACAACATG	300 nM	60°C	30 s - 60 s - 15 s	103
TRAP (31)	TAGCCGGAAACCATGACCACC GATGCCCACGCCATTCTCATC	500 nM	65°C	10 s - 10 s - 15 s	446

Forward and reverse primers for quantitative real-time PCR.

significance testing t-tests for unpaired samples were used. A p-value < 0.05 was considered significant.

3 RESULTS

General remark: Staining, Resorption Assay and RT-PCR results are only presented for dental cultures. The results of the orthopaedic cultures were already published 2019 by Koehler et al. (28). The Sequencing data shows the results for dental and orthopaedic monolayer cultures.

3.1 TRAP Staining Was Detected in Stimulated and Unstimulated PBMCs and in the Co-Culture Groups

TRAP staining enables the detection of multinucleated osteoclast like cells, but is no specific marker of osteoclastogenesis like bone resorption. All monocultures of PPFs showed TRAP negative, mononuclear, spindle-shaped cells. Mono- and co-cultures of PBMCs all contained TRAP positive multinucleated cells of various sizes with around 5 nuclei (**Figures 1A–C**). **Figure 1** shows PBMCs cultivated with (**Figure 1A**) and without

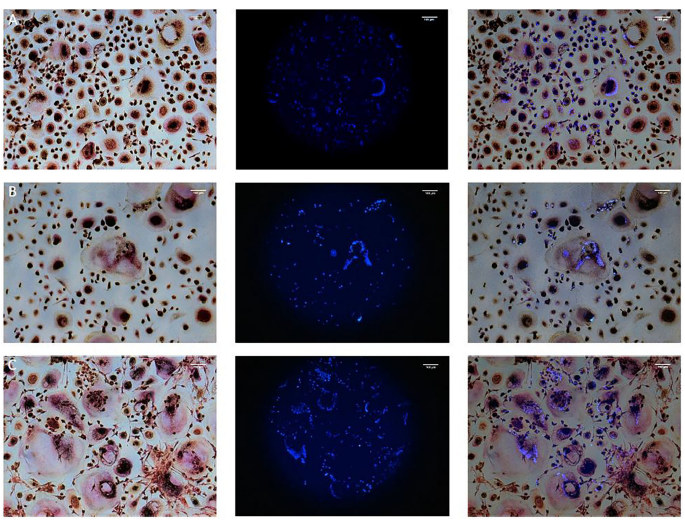

FIGURE 1 | TRAP and Hoechst staining on day 28. Monocultures of PBMCs cultivated with **(A)** and without **(B)** additional M-CSF/RANKL and **(C)** Co-cultures of PBMCs/PPFs. Different sizes of multiple TRAP positive multinucleated cells in **(C)** additionally surrounded by small spindle-shaped cells. Photos were taken via light microscope (left), a fluorescence filter (middle), and combined (right). Scale bar = 100 µm.

(**Figure 1B**) additional M-CSF/RANKL. Co-cultures of PBMCs/PPFs (**Figure 1C**) also showed multiple TRAP positive multinucleated cells. In this study, the experiments showed TRAP signals in stimulated and unstimulated PBMCs and in the co-culture group. The size of the multinucleated cells was the main difference between groups. Visually, co-culturing led to larger multinucleated cells, surrounded by spindle shaped fibroblast-like cells.

3.2 Only Stimulated PBMCs From Monolayer and Transwell Cultures Showed Resorption Activity on Dentin Chips

Resorption assay on dentin chips was used as gold standard to proof complete osteoclastogenesis on day 29. Positive controls of PBMCs cultivated with MCSF and RANKL from monolayer and transwell cultures showed both resorption activity on dentin chips. In general, resorption lacunae of these monolayer cultures were significantly larger than those of transwell PBMC monocultures (**Figures 2C, D**). All monocultures of unstimulated PBMCs did not show any sign of osteolysis, although they contained TRAP positive multinucleated cells.

No resorption lacunae were found on dentin chips of unstimulated PPF/PBMC co-cultures (monolayers and transwells). Stimulated PPF/PBMC co-cultures also showed no signs of osteolytic lacunae (**Figures 2A, B**). Monocultures of PPFs showed no resorption lacunae. (The presence of cells on the dentin chips was proven before with Hoechst staining *via* fluorescence filter. The presence of single nuclei indicated PPFs, while several nuclei in one space are typical for PBMCs (**Figures 1A–C**).

3.3 Quantitative Real Time PCR

Gene expressions of *MCSF*, *RANKL*, *RANK*, *OPG*, *TNFα*, *OCN*, *CTSK* and *TRAP* from PPF, PBMC and PPF/PBMC co-cultures were determined on day 0, 13 and 20 from monolayer and transwell plates.

3.3.1 Monolayer Co-Cultures Show High Levels of OPG

When compared to negative control (=monolayer PPF cultures), monolayer PPF/PBMC co-cultures showed mostly elevated expression levels for *RANKL* (**Figure 3A**, d13: $p<0.001$, d20: $p<0.001$), *RANK* (**Figure 3C**, d13: $p<0.001$, d20: $p<0.001$), *MCSF* (**Figure 3D**, d13: $p<0.001$, d20: $p=0.940$), *OCN* (**Figure 3E**, d13: $p= 0.0421$, d20: $p=0.0325$), CTSK (**Figure 3F**, d13: $p=0.0012$ d20: $p=0.1855$), *TRAP* (**Figure 3G**, d13: $p<0.001$, d20: $p<0.001$) and *TNFα* (**Figure 3H**, d13: $p<0.001$, d20: $p<0.001$). There was no significant difference of *OPG* expression measured (**Figure 3B** d13: $p=0.4663$, d20: $p=0.0901$) comparing monolayer PPF to monolayer PPF/PBMC co-cultures. The *RANKL*/*OPG* ratio of monolayer co-cultures stayed at the low level of monolayer PPF cultures at both time points (**Figure 4**).

3.3.2 Gene Expression of Transwell Co-Cultures Acts More Like Baseline Tissue

Transwell PPF/PBMC co-cultures showed significantly higher expressions for *RANKL* (**Figure 3A**, d13: $p<0.001$, d20: $p<0.001$), *RANK* (**Figure 3C**, d13: $p<0.001$, d20: $p<0.001$), *MCSF* (**Figure 3D**, d13: $p<0.001$, d20: $p<0.001$) and *OCN* (**Figure 3E**, d13: $p<0.001$, d20: $p<0.001$) in comparison to monolayer co-cultures.

For *OPG* (**Figure 3B**, d13: $p<0.001$, d20: $p<0.001$), *TRAP* (**Figure 3G** d13: $p= 0.2682$, d20: $p<0.001$) and *CTSK* (**Figure 3F**, d13: $p<0.001$, d20: $= 0.6833$) significantly lower expressions were

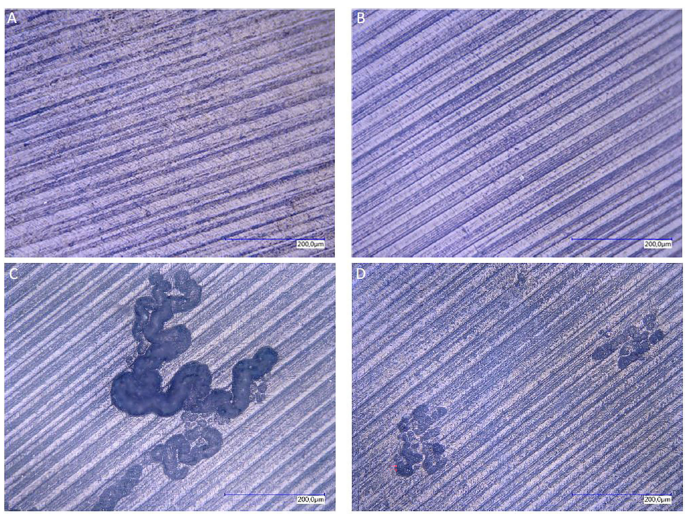

FIGURE 2 | Resorption lacunae on dentin after staining with toluidine blue. Resorption lacunae on dentin after staining with toluidine blue. Lack of resorption pits in monolayer PBMC/PPFs co-cultures **(A)**, even when cultivated in the presence of additional MCSF and RANKL **(B)**. PBMC monocultures stimulated with MCSF and RANKL, cultivated in monolayer **(C)** or on transwell membranes [and transferred on dentin **(D)**], showed traces of osteolysis.

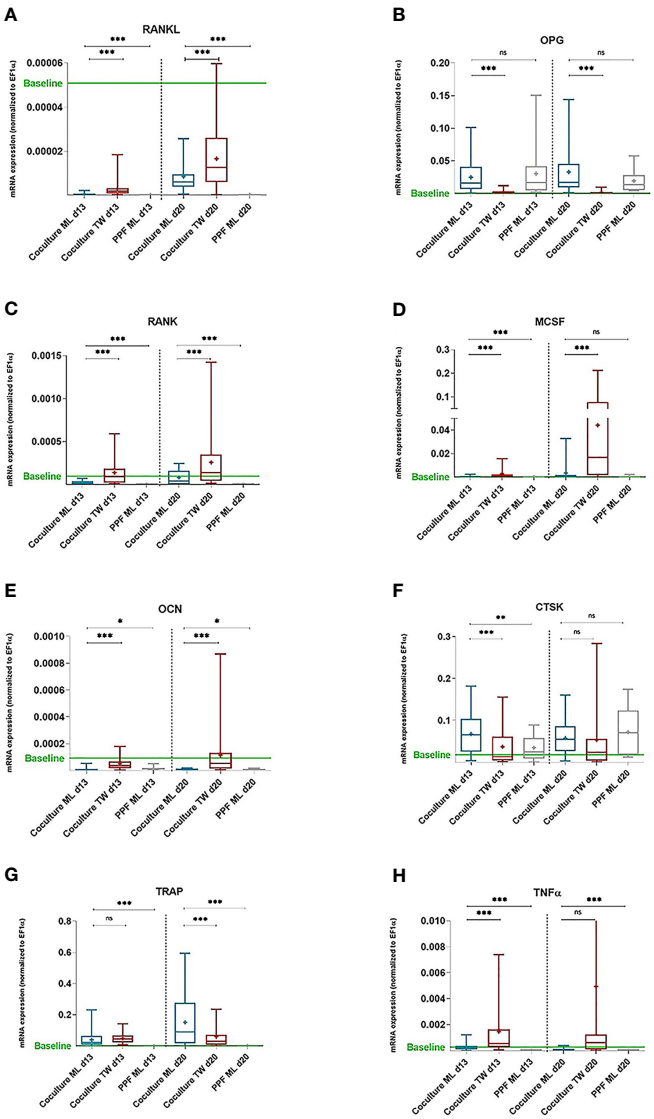

FIGURE 3 | mRNA expression of PPF monocultures and PBMC/PPF co-cultures (day 13 and 20). mRNA expression of PPF monocultures and PBMC/PPF co-cultures. Relative mRNA Relative mRNA expression **(A)** RANKL, **(B)** OPG, **(C)** RANK, **(D)** MCSF, **(E)** OCN, **(F)** CTSK, **(G)** TRAP and **(H)** TNFa (normalized to housekeeping gene EF1a) in co-cultures of PPF and PBMCs in monolayer (ML, n = 16) and transwell (TW, n = 16) as well as in monocultures of PPF in monolayer (n = 8) on day 13 and day 20. Bands inside the boxes indicate group medians,crosses indicate group means. End of whiskers represent minimum and maximum values. Baseline refers to relative mRNA expression of original periosteolytic tissue (n=8). p values are indicated with * ($p \leq 0.05$), ** ($p \leq 0.01$),*** ($p \leq 0.001$), ns, not significant.

observed in transwell co-cultures compared to monolayer co-cultures.

The indicated baseline refers to relative mRNA expression of original periosteolytic tissue for each gene. It is noticeable that transwell co-cultures act closer to baseline conditions than monolayers considering especially *RANKL*, *OPG*, *OCN* and *CTSK*.

Regarding *RANKL*/*OPG* ratios, transwell co-cultures showed a significant higher expression, when compared to monolayers (**Figure 4**, d13: p= 0.0304, d20: p= 0.0455), resulting in a more osteoclastogenic environment. **Figure 4** shows that *RANKL*/*OPG* ratios of transwell cultures on both time points are very close to baseline conditions (**Figure 4**, d13: p=ns, d20: p= ns).

Baseline tissue corresponds to *in vivo* conditions, as periprosthetic tissue samples were used.

3.3.3 Monocultures of PPFs in Transwell and Monolayer Show Similar Expression

Monocultures of PPFs showed about the same qPCR results in transwell as in monolayer cultures. In **Figure 3** only data from PPFs in monolayer cultures are shown to achieve a clearer graphical presentation.

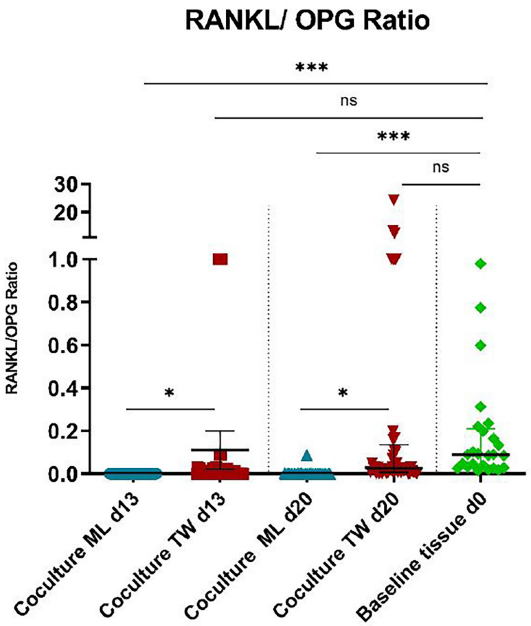

FIGURE 4 | RANKL/OPG ratios of PBMC/PPF co-cultures and baseline tissue (day 0). * ($p \leq 0.05$), *** ($p \leq 0.001$), ns, not significant.

3.4 RNA-Sequencing Data Analysis

3.4.1 RNA-Sequencing Data Analysis Shows Equivalent Results for Orthopaedic and Dental Monolayer Cultures

Sequencing data results from day 20 are shown in **Figure 5** for dental and orthopaedic co-cultures, dental and orthopaedic monocultures of PPFs, stimulated and unstimulated PBMC cultures. This data is equivalent to the result of the qPCR and is independent of donors (donor of PBMCs =D). Most striking was the upregulation of OPG in PPF-monocultures and PPF/PBMC-co-cultures. Furthermore, an upregulation of TNFα, TRAP and RANK in PBMC-monocultures and PPF/PBMC-co-cultures was observed. The higher OPG expression in monolayer was therefore mainly caused by PPFs, whereas PBMCs were responsible for most of the TNFα expression.

3.4.2 RNA-Sequencing Data: Top 50 Genes in Dental and Orthopaedic Monolayer Co-Cultures

Figure 6 shows the results of the RNA sequencing gene expression analysis of monolayers and co-cultures of dental and orthopaedic cell cultures all on day 20. There are 5 donors for orthopaedic cells and 4 donors for dental cells that are mono/co-cultured with PBMCs. The gene expression data were normalized by using the vst method. Even though the cells were derived from different origins, the PCA analysis showed similar gene expression patterns for each group: PBMCs, PPFs and co-cultures, with one single outlier: PPF2+ D4 co-culture (**Figure 6A**).

To validate the qPCR results, osteoclast differentiation regulator genes are filtered in each group from normalized gene expressions to check the variation. As an addition to the PCA clustering, osteoclast differentiation related genes also support the same clustering between each cell culture condition independent from the primary location of the cell. Furthermore, it shows the loss of *OPG* gene expression among the outlier PPF2+ D4 co-culture (**Figure 5**).

To understand how the osteoclast differentiation regulator gene expression varies between mono and co-culture in both dental and orthopaedic cell cultures, same genes are used from the qPCR results to filter DESeq2 analysis. Analysis performed in

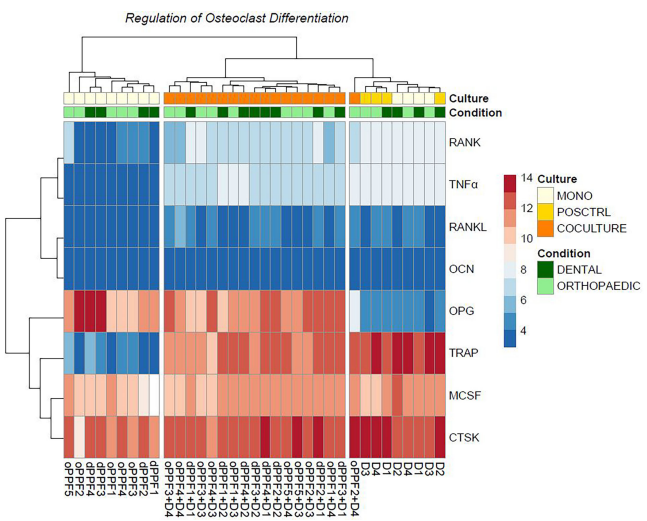

FIGURE 5 | Heatmap of dental cultures on day 20. Ns, not significant.

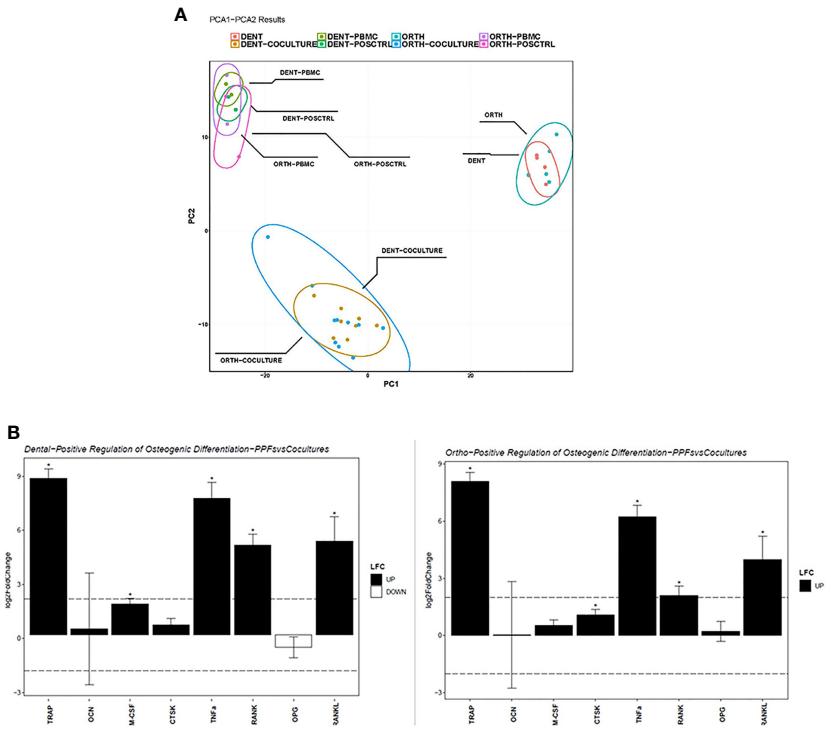

FIGURE 6 | Sequencing analysis of dental and orthopaedic cultures on day 20. **(A)** Principal component analysis for co-cultures (PPF + PBMC), dental PPF (dPPF), orthopaedic PPF (oPPF), PBMC and positive control; **(B)** Positive regulation of Osteogenic Differentiation for dental (left) and orthopaedic (right) Co-cultures and PBMCs. Asterisks (*) indicate a p-value < 0.05 LFC, log2 fold change.

between mono and co-cultured samples gene expression for both dental and orthopaedic samples separately (**Figure 6B**). It is observed that for both of the dental and orthopaedic cell cultures, *TRAP, TNFα, RANK* and *RANKL* genes are upregulated significantly through co-culture of PPFs and PBMCs. Significance determined in DESeq2 analysis by 2 as log fold change cutoff and 0.05 as p adjusted value cutoff. It shows that PBMCs increases the osteoclast differentiation related gene expression in both dental and orthopaedic PPFs. Although different donors were used for PBMCs and PPFs, there is a strong overlap in the expression patterns of dental and orthopaedic cultures.

Top 50 genes that are differentially expressed between mono- and co-cultures show, besides the genes which are verified both in qPCR and RNA sequencing, there are other regulators such as *MMP's* which are upregulated by co-cultures of PPFs and PBMCs (**Figure 7A**). MMP-13 and MMP-9 enhance osteoclastogenesis (36), whereas MMP-7 is accepted as one of the targets of RANKL to trigger osteolysis (37). The outlier PPF2+ D4 differs from the other co-cultured samples clearly observable in terms of gene expression.

Gene Ontology Biological Pathway analysis suggests that significant differentially expressed genes between mono- and co-cultured samples, independent from the driven location of the samples co-culturing PBMC and PPFs, show a suppression of several musculoskeletal related pathways, which are not directly connected to our experiments (**Figure 7B**). These results are however not supported yet by further data to prove the related gene expression results. It was observed on GO Pathways that pathways connected to immune responses might be activated within co-cultured samples (**Figure 7B**).

4 DISCUSSION

Comparing dental and orthopaedic implant loosening processes overlaps in cellular components and their gene expression patterns, which refer to the same triggers and result in similar mechanisms, influencing the induction of osteoclastogenesis within peri-implant tissues of both types, have been discussed. Especially the (immune) regulatory effects of dental and orthopaedic PPFs, which play a major role in implant loosening, have been described in literature (10, 11, 14, 18, 23, 24, 38–40).

Monolayer co-cultures of PPFs of orthopaedic and dental origin expressed high levels of OPG over time resulting in an inhibition of osteolysis, even in the presence of MCSF and RANKL as overserved for PPFs from orthopaedic origin in earlier studies from this group (28) and for PPFs with dental origin co-cultured with PBMCs within this study. The high OPG expression in monolayer results in a low RANKL/OPG ratio, not representing

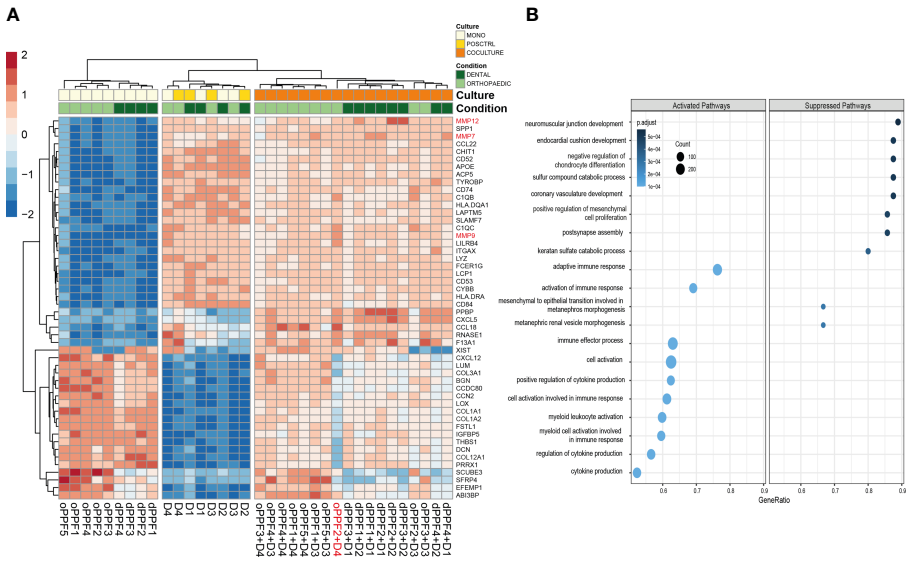

FIGURE 7 | Top 50 genes and Gene Ontology Biological Pathway analysis on day 20. RNA-Sequencing data for orthopaedic and dental monolayer cultures on day 20: Top 50 genes that are differentially expressed between mono- and co-cultures, D (Donor)=PBMC **(A)**; Gene Ontology Biological Pathway analysis for mono- and co-cultures. Size of the dots are defined by the Gene Counts, color of the dots represent p-adjusted value **(B)**.

the findings of original tissues where high RANKL/OPG ratios are usually described (11, 12, 31, 40). This effect, being due to the high OPG expression of PPFs in monolayer, can lead to a misinterpretation of results for dental and orthopaedic loosening, if monolayer cultures are used in evaluating processes of implant loosening. In monolayer cultures the immunomodulatory effect of PPFs is extremely efficiently blocking the osteoclastic activation of PBMCs due to an increase in OPG, with low RANKL, MCSF and TNFα expressions.

For transwell co-cultures, profound changes in gene expression, with a strong and significant decrease of OPG in PPFs of both origins (hundredfold in orthopaedic/twentyfold decrease in dental co-cultures) were observed. The RANKL/OPG ratios, which were rather low in monolayer co-cultures of both origins, were found to be significantly higher in transwell cultures and reached similar levels to original periprosthetic tissues. Several reviews state the importance of the RANKL/OPG pathway for the bone homeostasis, low levels of OPG lead to an activation of the osteoclastogenesis favoring bone resorption (41, 42). Elevated RANKL/OPG ratio were also found in peri-mucositis triggered by bacteria, peri-implantitis and gingival crevicular fluid of diseased peri-implant tissues (43–45). Increased RANKL/OPG ratios associated with bone resorption around dental implants were also shown in murine model (39). We hypothesized that the low OPG levels presented in the transwell co-culture system better reflect *in vivo* ratios of periprosthetic tissue than the increasing OPG expressions of the monolayer system. The transwell culture system allows improved cell-to-cell contacts favoring differentiation and intracellular signal pathways (46).

It has been shown that bone resorption cannot be equated with TRAP positivity and multinucleation in osteoclasts and PBMC cultures are capable of producing TRAP-positive cells without stimulation (3, 25, 28). In this study dentin chips were used as a gold standard for osteolysis. On dentin chips, all PBMC monocultures stimulated with MCSF/RANKL showed lacunae formation, whereas unstimulated PBMC cultures showed no lacunae formation. Cells from transwell cultures could be transferred to dentin chips after 21 days and showed about the same osteolytic activity as cells of monolayer cultures. Despite all similarities to original baseline tissue (corresponds to *in vivo* conditions), induction of osteoclastogenesis was absent in the co-cultures of the transwell system, where no resorption lacunae were found. Terminal osteoclastogenesis could not be induced by co-culturing dental PBMC/PPF due to similar reasons as described for orthopaedic co-cultures (28) and even an inhibition of osteoclastogenesis in stimulated co-cultures was observed.

Literature only shows complete differentiation of co-cultured fibroblasts and PBMCs in the presence of MCSF and RANKL, where the RANKL/OPG ratio had been higher in the first place, which might be an essential prerequisite. It may be postulated that the increased OPG expressed by orthopaedic and dental PPFs is sufficient to neutralize the elevated RANKL levels. Thus, dental and orthopaedic PPFs kept in monolayer can developed an osteoprotective effect that ultimately prevented active bone resorption (even when stimulated with MCSF and RANKL). This phenomenon of PPF inhibition of osteoclastogenesis occurred equally pronounced in co-cultures of dental or orthopaedic periprosthetic tissues within all donors. PPFs can significantly immunomodulate osteoclastic mechanisms and play an important role in dental and orthopaedic implant loosening. Comparing results from dental and orthopaedic gene expression pattern changes, many similar results were obtained for the groups of PBMCs, PPFs and co-cultures.

In our former study examining orthopaedic implant loosening, the same significant changes in gene expression of two major mediators of osteoclastogenesis were detected in transwell co-cultures compared to those in monolayer (28). The transwell co-cultures showed an extensive downregulation of OPG. We assumed, that the higher OPG expression in monolayer was mainly caused by PPFs, whereas PBMCs were responsible for most of the TNFα expression. The findings from this study make this assumption more reliable, as it can be shown that the origin of OPG is found in PPFs whereas PBMC seem to represent the origin of TNFα (**Figure 5**).

The role of TNFα might also play an important part, as TNFα is discussed as a direct mediator of osteoclastogenesis and a possible replacement for RANK-L. A RANK-L-independent formation of osteoclasts in the presence of MCSF and TNFα had been shown before in literature as described (28). Considering this alternative pathway, it may be assumed that expression of TNFα was insufficient in our studies to induce a RANK-L-independent osteoclast formation in the co-cultures. The *in vitro* conditions of transwell cultures mimic *in vivo* conditions to a certain content, but cannot reach the original tissue conditions. In the stimulated transwell co-cultures RANK-L and TNFα might have been insufficient to induce osteoclastogenesis.

In dental co-cultures the effects on gene expression obtained by transwell cultures are even more pronounced in some cases than in orthopaedic co-cultures. The expression of RANKL and MCSF increased significantly in transwell cultures of dental PPFs/PBMCs, whereas expression had only slightly increased in orthopaedic co-cultures (28). In transwells of dental origins, RANK was up-regulated in co-cultures compared to monolayer expression, whereas OPG as an opponent revealed an increased expression in monolayer co-cultures. This also corresponds to the findings of our previous study by Koehler et al. (28).

An overlap of expression within dental and orthopaedic co-cultures, PPFs and PBMCs was then further evaluated by RNA sequencing. The sequencing data reflected the results for the genes OPG, where PPF monocultures and PBMC/PPF co-cultures show rather high values in monolayer of all donors compared to PBMCs where low values for OPG are found in all donors. The OPG expression is therefore mainly driven by the PPFs of both origins. This further elucidates data from literature where PPF/PBMC co-cultures have been described to express high OPG levels (25, 38). According to sequencing and RT-PCR results RANK, TNFα and TRAP are upregulated in co-cultures and PBMCs of all donors compared to PPF monocultures. The RANK, TNFα and TRAP expression therefore seem mainly triggered by the PBMC input. When MCSF is added, TNFα-expressing PPFs cause increased osteoclast formation, the RANK receptor of osteoclast precursor cells is activated by RANKL, differentiation into osteoclasts increases their TRAP expression and thus contributes to endoprosthetic loosening. According to sequencing results the orthopaedic and dental samples show a strong overlap of processes. Dental and orthopaedic PPFs and their PBMC/PPF co-cultures showed broad agreement in principal component analysis and heat maps of differentially expressed genes. In particular, the upregulation of TRAP, TNFα and RANK associated with the downregulation of OPG leads to the osteoclastogenic differentiation in the co-cultures of both origins. This is, as to our knowledge, the first study showing the strong similarity between dental and orthopaedic peri-implant tissue cells, which supports the clinical thesis that similar immune responses play a crucial role in dental and orthopaedic implant loosening (23). Orthopaedic and dental implants represent foreign bodies to which the immunocompetent bone cells react and which, in case of mismatch, leads to bone resorption as evidenced by an increase in bone resorption markers. Therefore, the immune response by macrophages, foreign body giant cells, neutrophils etc. in orthopaedic and dental implant loosening might be similar and even might play a more decisive role than the biofilm theory. Albrektsson et al. hypothesized that bacterial pathogens arise only as a consequence to the foreign body reaction and thus, the immune response is the main reason for bone resorption (23). Considering osteoclasts as cells having an immune function besides the classical bone resorption activity, would furthermore open up the possibility for the hypothesis that degraded matrix components could leak out from the resorption lacuna, when the tight seal of this environment is loosened, and start a new resorption cycle (47).

In addition, recent studies using transcriptomic profiling show that periimplantitis is distinctly different from periodontitis in terms of molecular genetics. It has been shown that signaling pathways influencing the immune response are upregulated in peri-implantitis, whereas in periodontitis mainly bacterial response systems dominate (48, 49) and that higher RANKL/OPG ratios were measured, in particular, in peri-implant tissues (50). This reinforces our approach to compare dental and orthopaedic implants and suggests a common pathogenesis. To the best of our knowledge, this is the first study to have performed this direct comparison on a molecular level. On the one hand, this allows the transfer of scientific knowledge from one discipline to the other, although differences such as material, particle abrasion, biomechanics, etc. should be taken into account. On the other hand, understanding the primary pathogenesis opens up new therapy options in the field of regenerative medicine strategies such as platelet rich plasma, smart biomaterial-tissue interfaces or tissue-engineered Cell Sheets (51).

Especially the RANKL/OPG/RANK pathway, which is of interest in dental and orthopaedic implant osteolysis, needs to be further elucidated, as monolayer data here significantly deviate from transwell cultures, where more *in vivo* like results were obtained. Low OPG expression levels of periimplant tissues are stable, not dependent on time to revision surgery, endotoxin levels or other parameters (31). PPFs, which have been shown to express OPG, seem to play an important part in the remodelling of periprosthetic bone (52). Assuming that PPFs may be involved in osteoclastogenesis and bone resorption by the regulation of their expression leads to new understandings of implant loosening processes and might also change solution approaches.

Limitations of our study were the relatively small number of cases. However, sequencing data can prove that results in dental

and orthopaedic peri-implant tissue cultures showed coherence with significant results. Another limitation of the study is the fact that PBMCs might induce donor specific immune reactions, which could influence the study results. To exclude any bias by donor-specific characteristics, two PBMC donors were used for each experiment and PPFs of each patient were co-cultivated with PBMCs of each donor separately. As the Gene Ontology Biological pathway analysis showed, co-cultures tended to increase immune responses. This might also be regarded as an unspecific finding due to donor reactions.

Morphological characterization of PPFs in transwell cultures had been performed by our group (34). Detailed histomorphological characteristics were not performed in the current study due to a limited number of cells per donor. Hartmann et al. found conglomerates of PPFs in frozen sections of transwell cultures forming a polylayer structure (34). This coincides with findings of Sabater et al. (27), showing that cultivating fibroblasts in transwell systems lead to an increased number of cells and higher cell mass compared to cultures on standard well bottoms, despite the smaller surface of the transwell membranes.

In summary, periprosthetic osteoclastogenesis may be a correlating immune process in orthopaedic and dental implant failure leading to comparable (immune) reactions with regard to osteoclast activation. One of the main players in osteoclastogenesis, OPG, which was found to be upregulated in monolayer co-cultures of both origins, experienced profound changes in gene expression with a twenty- to hundredfold decrease in the transwell culture system. In transwell co-cultures, RANKL/OPG ratios were significantly higher, reaching levels similar to those in the original periprosthetic tissue. The transwell cultures system may provide an *in vivo* like model for the exploration of orthopaedic and dental implant loosening. This study provides more indications that similar loosening processes occur in dental and orthopaedic implant failure and offers the transwell system as culture model to gain insight into both processes. Further studies are necessary to investigate the similarities of dental and orthopaedic implant loosening and further elucidate the immune processes regarding osteoclast activation of implant failure.

DATA AVAILABILITY STATEMENT

The datasets presented in this article are not readily available because of DSGVO/GDPR restrictions. Requests to access the datasets should be directed to the corresponding author.

ETHICS STATEMENT

The studies involving human participants were reviewed and approved by LMU Ethic committee Munich. Written informed consent for participation was not required for this study in accordance with the national legislation and the institutional requirements.

AUTHOR CONTRIBUTIONS

SS, EH, MK, FB, JR, MS, EA, BH, SK, and SM-W: Study conception and design, analysis and interpretation of data, drafting of manuscript, and critical revision. SS, EH, MK, FB, JR, and SM-W: Acquisition of data. All authors have read and approved the final submitted manuscript.

FUNDING

This work was supported by the "Deutsche Forschungsgemeinschaft" (DFG- MA 5158/1-1).

ACKNOWLEDGMENTS

We thank Prof. Dr. Dr. Eberhard Fischer-Brandies and Dr. Robert Kirmeier for their sophisticated support providing dental peri-implant tissues. We also thank Brigitte Hackl and Baerbel Schmitt for their technical support and methodical advice. We also thank Dr. Alexander Crispin (LMU Institute for Medical Information Processing, Biometry, and Epidemiology) for his assistance with the statistical evaluation. This work was presented by Sabine M. S. Schluessel in partial fulfilment of the requirements for a MD degree, Ludwig-Maximilians-University, Medical School, Munich, Germany.

REFERENCES

1. Perry MJ, Mortuza FY, Ponsford FM, Elson CJ, Atkins RM. Analysis of Cell Types and Mediator Production From Tissues Around Loosening Joint Implants. *Br J Rheumatol* (1995) 34(12):1127–34. doi: 10.1093/rheumatology/34.12.1127
2. Sabokbar A, Itonaga I, Sun SG, Kudo O, Athanasou NA. Arthroplasty Membrane-Derived Fibroblasts Directly Induce Osteoclast Formation and Osteolysis in Aseptic Loosening. *J Orthop Res* (2005) 23(3):511–9. doi: 10.1016/j.orthres.2004.10.006
3. Sabokbar A, Kudo O, Athanasou NA. Two Distinct Cellular Mechanisms of Osteoclast Formation and Bone Resorption in Periprosthetic Osteolysis. *J Orthop Res* (2003) 21(1):73–80. doi: 10.1016/S0736-0266(02)00106-7
4. Konttinen YT, Lappalainen R, Laine P, Kitti U, Santavirta S, Teronen O. Immunohistochemical Evaluation of Inflammatory Mediators in Failing Implants. *Int J Periodontics Restorative Dent* (2006) 26(2):135–41.
5. Yucel-Lindberg T, Olsson T, Kawakami T. Signal Pathways Involved in the Regulation of Prostaglandin E Synthase-1 in Human Gingival Fibroblasts. *Cell Signal* (2006) 18(12):2131–42. doi: 10.1016/j.cellsig.2006.04.003
6. Jiranek WA, Machado M, Jasty M, Jevsevar D, Wolfe HJ, Goldring SR, et al. Production of Cytokines Around Loosened Cemented Acetabular Components. Analysis With Immunohistochemical Techniques and in Situ Hybridization. *J Bone Joint Surg Am* (1993) 75(6):863–79. doi: 10.2106/00004623-199306000-00007
7. Salcetti JM, Moriarty JD, Cooper LF, Smith FW, Collins JG, Socransky SS, et al. The Clinical, Microbial, and Host Response Characteristics of the Failing Implant. *Int J Oral Maxillofac Implants* (1997) 12(1):32–42.
8. Wei X, Zhang X, Flick LM, Drissi H, Schwarz EM, O'Keefe RJ. Titanium Particles Stimulate COX-2 Expression in Synovial Fibroblasts Through an Oxidative Stress-Induced, Calpain-Dependent, NF-kappaB Pathway. *Am J Physiol Cell Physiol* (2009) 297(2):C310–20. doi: 10.1152/ajpcell.00597.2008
9. Tsutsumi R, Xie C, Wei X, Zhang M, Zhang X, Flick LM, et al. PGE2 Signaling Through the EP4 Receptor on Fibroblasts Upregulates RANKL and

Stimulates Osteolysis. *J Bone Miner Res* (2009) 24(10):1753–62. doi: 10.1359/jbmr.090412
10. Mandelin J, Li TF, Hukkanen M, Liljestrom M, Salo J, Santavirta S, et al. Interface Tissue Fibroblasts From Loose Total Hip Replacement Prosthesis Produce Receptor Activator of Nuclear Factor-KappaB Ligand, Osteoprotegerin, and Cathepsin K. *J Rheumatol* (2005) 32(4):713–20.
11. Mandelin J, Li TF, Liljestrom M, Kroon ME, Hanemaaijer R, Santavirta S, et al. Imbalance of RANKL/RANK/OPG System in Interface Tissue in Loosening of Total Hip Replacement. *J Bone Joint Surg Br* (2003) 85 (8):1196–201. doi: 10.1302/0301-620X.85B8.13311
12. Crotti TN, Smith MD, Findlay DM, Zreiqat H, Ahern MJ, Weedon H, et al. Factors Regulating Osteoclast Formation in Human Tissues Adjacent to Peri-Implant Bone Loss: Expression of Receptor Activator NFkappaB, RANK Ligand and Osteoprotegerin. *Biomaterials* (2004) 25(4):565–73. doi: 10.1016/S0142-9612(03)00556-8
13. Belibasakis GN, Bostanci N. The RANKL-OPG System in Clinical Periodontology. *J Clin Periodontol* (2012) 39(3):239–48. doi: 10.1111/j.1600-051X.2011.01810.x
14. Bordin S, Flemmig TF, Verardi S. Role of Fibroblast Populations in Peri-Implantitis. *Int J Oral Maxillofac Implants* (2009) 24(2):197–204.
15. Wagner S, Gollwitzer H, Wernicke D, Langer R, Siebenrock KA, Hofstetter W. Interface Membrane Fibroblasts Around Aseptically Loosened Endoprostheses Express MMP-13. *J Orthop Res* (2008) 26(2):143–52. doi: 10.1002/jor.20494
16. Ma GF, Ali A, Verzijl N, Hanemaaijer R, TeKoppele J, Konttinen YT, et al. Increased Collagen Degradation Around Loosened Total Hip Replacement Implants. *Arthritis rheumatism* (2006) 54(9):2928–33. doi: 10.1002/art.22064
17. Delaisse JM, Andersen TL, Engsig MT, Henriksen K, Troen T, Blavier L. Matrix Metalloproteinases (MMP) and Cathepsin K Contribute Differently to Osteoclastic Activities. *Microsc Res Tech* (2003) 61(6):504–13. doi: 10.1002/jemt.10374
18. Pap T, Claus A, Ohtsu S, Hummel KM, Schwartz P, Drynda S, et al. Osteoclast-Independent Bone Resorption by Fibroblast-Like Cells. *Arthritis Res Ther* (2003) 5(3):R163–73. doi: 10.1186/ar752
19. Przekora A, Ginalska G. Enhanced Differentiation of Osteoblastic Cells on Novel Chitosan/β-1,3-Glucan/Bioceramic Scaffolds for Bone Tissue Regeneration. *BioMed Mater* (2015) 10(1):015009. doi: 10.1088/1748-6041/10/1/015009
20. Yamalik N, Günday S, Kilinc K, Karabulut E, Berker E, Tözüm TF, et al. Analysis of Cathepsin-K Levels in Biologic Fluids From Healthy or Diseased Natural Teeth and Dental Implants. *Int J Oral Maxillofac Implants* (2011) 26 (5):991–7.
21. Murata M, Tatsumi J, Kato Y, Suda S, Nunokawa Y, Kobayashi Y, et al. Osteocalcin, Deoxypyridinoline and Interleukin-1beta in Peri-Implant Crevicular Fluid of Patients With Peri-Implantitis. *Clin Oral Implants Res* (2002) 13(6):637–43. doi: 10.1034/j.1600-0501.2002.130610.x
22. Maier GS, Eberhardt C, Strauch M, Kafchitsas K, Kurth AA. Is Tartrate-Resistant Acid Phosphatase 5b a Potent Bio-Marker for Late Stage Aseptic Implant Loosening? *Int Orthop* (2014) 38(12):2597–600. doi: 10.1007/s00264-014-2471-2
23. Albrektsson T, Becker W, Coli P, Jemt T, Molne J, Sennerby L. Bone Loss Around Oral and Orthopedic Implants: An Immunologically Based Condition. *Clin Implant Dent Relat Res* (2019) 21(4):786–95. doi: 10.1111/cid.12793
24. Dickerson TJ, Suzuki E, Stanecki C, Shin HS, Qui H, Adamopoulos IE. Rheumatoid and Pyrophosphate Arthritis Synovial Fibroblasts Induce Osteoclastogenesis Independently of RANKL, TNF and IL-6. *J Autoimmun* (2012) 39(4):369–76. doi: 10.1016/j.jaut.2012.06.001
25. de Vries TJ, Schoenmaker T, Wattanaroonwong N, van den Hoonaard M, Nieuwenhuijse A, Beertsen W, et al. Gingival Fibroblasts Are Better at Inhibiting Osteoclast Formation Than Periodontal Ligament Fibroblasts. *J Cell Biochem* (2006) 98(2):370–82. doi: 10.1002/jcb.20795
26. Majety M, Pradel LP, Gies M, Ries CH. Fibroblasts Influence Survival and Therapeutic Response in a 3D Co-Culture Model. *PLoS One* (2015) 10(6): e0127948. doi: 10.1371/journal.pone.0127948
27. Sabater D, Fernández-López J-A, Remesar X, Alemany M. The Use of Transwells™ Improves the Rates of Differentiation and Growth of Cultured 3T3L1 Cells. *Anal Bioanal Chem* (2013) 405(16):5605–10. doi: 10.1007/s00216-013-6970-6
28. Koehler MI, Hartmann ES, Schluessel S, Beck F, Redeker JI, Schmitt B, et al. Impact of Periprosthetic Fibroblast-Like Cells on Osteoclastogenesis in Co-Culture With Peripheral Blood Mononuclear Cells Varies Depending on Culture System. *Int J Mol Sci* (2019) 20(10). doi: 10.3390/ijms20102583
29. Lindhe J, Meyle J. Peri-Implant Diseases: Consensus Report of the Sixth European Workshop on Periodontology. *J Clin Periodontol* (2008) 35(8 Suppl):282–5. doi: 10.1111/j.1600-051X.2008.01283.x
30. Sanz M, Chapple IL. Clinical Research on Peri-Implant Diseases: Consensus Report of Working Group 4. *J Clin Periodontol* (2012) 39(Suppl 12):202–6. doi: 10.1111/j.1600-051X.2011.01837.x
31. Hartmann ES, Kohler MI, Huber F, Redeker JI, Schmitt B, Schmitt-Sody M, et al. Factors Regulating Bone Remodeling Processes in Aseptic Implant Loosening. *J Orthop Res* (2017) 35(2):248–57. doi: 10.1002/jor.23274
32. Weinberg E, Zeldich E, Weinreb MM, Moses O, Nemcovsky C, Weinreb M. Prostaglandin E2 Inhibits the Proliferation of Human Gingival Fibroblasts via the EP2 Receptor and Epac. *J Cell Biochem* (2009) 108(1):207–15. doi: 10.1002/jcb.22242
33. Beck F, Hartmann ES, Koehler MI, Redeker JI, Schluessel S, Schmitt B, et al. Immobilization of Denosumab on Titanium Affects Osteoclastogenesis of Human Peripheral Blood Monocytes. *Int J Mol Sci* (2019) 20(5). doi: 10.3390/ijms20051002
34. Hartmann ES, Schluessel S, Köhler MI, Beck F, Redeker JI, Summer B, et al. Fibroblast-Like Cells Change Gene Expression of Bone Remodelling Markers in Transwell Cultures. *Eur J Med Res* (2020) 25(1):52. doi: 10.1186/s40001-020-00453-y
35. Yu G, Wang LG, Han Y, He QY. Clusterprofiler: An R Package for Comparing Biological Themes Among Gene Clusters. *Omics* (2012) 16(5):284–7. doi: 10.1089/omi.2011.0118
36. Pivetta E, Scapolan M, Pecolo M, Wassermann B, Abu-Rumeileh I, Balestreri L, et al. MMP-13 Stimulates Osteoclast Differentiation and Activation in Tumour Breast Bone Metastases. *Breast Cancer Res* (2011) 13(5):R105. doi: 10.1186/bcr3047
37. Kessenbrock K, Plaks V, Werb Z. Matrix Metalloproteinases: Regulators of the Tumor Microenvironment. *Cell* (2010) 141(1):52–67. doi: 10.1016/j.cell.2010.03.015
38. Bloemen V, Schoenmaker T, de Vries TJ, Everts V. Direct Cell-Cell Contact Between Periodontal Ligament Fibroblasts and Osteoclast Precursors Synergistically Increases the Expression of Genes Related to Osteoclastogenesis. *J Cell Physiol* (2010) 222(3):565–73. doi: 10.1002/jcp.21971
39. Deng S, Hu Y, Zhou J, Wang Y, Wang Y, Li S, et al. TLR4 Mediates Alveolar Bone Resorption in Experimental Peri-Implantitis Through Regulation of CD45(+) Cell Infiltration, RANKL/OPG Ratio, and Inflammatory Cytokine Production. *J Periodontol* (2020) 91(5):671–82. doi: 10.1002/JPER.18-0748
40. Koulouvaris P, Ly K, Ivashkiv LB, Bostrom MP, Nestor BJ, Sculco TP, et al. Expression Profiling Reveals Alternative Macrophage Activation and Impaired Osteogenesis in Periprosthetic Osteolysis. *J Orthop Res* (2008) 26 (1):106–16. doi: 10.1002/jor.20486
41. Kim JM, Lin C, Stavre Z, Greenblatt MB, Shim JH. Osteoblast-Osteoclast Communication and Bone Homeostasis. *Cells* (2020) 9(9). doi: 10.3390/cells9092073
42. Carrillo-López N, Martínez-Arias L, Fernández-Villabrille S, Ruiz-Torres MP, Dusso A, Cannata-Andía JB, et al. Role of the RANK/RANKL/OPG and Wnt/β-Catenin Systems in CKD Bone and Cardiovascular Disorders. *Calcif Tissue Int* (2021) 108(4):439–51. doi: 10.1007/s00223-020-00803-2
43. Shuto T, Wachi T, Shinohara Y, Nikawa H, Makihira S. Increase in Receptor Activator of Nuclear Factor κb Ligand/Osteoprotegerin Ratio in Peri-Implant Gingiva Exposed to Porphyromonas Gingivalis Lipopolysaccharide. *J Dent Sci* (2016) 11(1):8–16. doi: 10.1016/j.jds.2015.10.005
44. Theodoridis C, Doulkeridou C, Menexes G, Vouros I. Comparison of RANKL and OPG Levels in Peri-Implant Crevicular Fluid Between Healthy and Diseased Peri-Implant Tissues. A Systematic Review and Meta-Analysis. *Clin Oral Investig* (2021). doi: 10.1007/s00784-021-04061-w
45. Gürlek Ö, Gümüş P, Nile CJ, Lappin DF, Buduneli N. Biomarkers and Bacteria Around Implants and Natural Teeth in the Same Individuals. *J Periodontol* (2017) 88(8):752–61. doi: 10.1902/jop.2017.160751
46. Knight E, Przyborski S. Advances in 3D Cell Culture Technologies Enabling Tissue-Like Structures to Be Created In Vitro. *J Anat* (2015) 227(6):746–56. doi: 10.1111/joa.12257

47. Madel MB, Ibáñez L, Wakkach A, de Vries TJ, Teti A, Apparailly F, et al. Immune Function and Diversity of Osteoclasts in Normal and Pathological Conditions. *Front Immunol* (2019) 10:1408. doi: 10.3389/fimmu.2019.01408
48. Cho YD, Kim PJ, Kim HG, Seol YJ, Lee YM, Ryoo HM, et al. Transcriptome and Methylome Analysis of Periodontitis and Peri-Implantitis With Tobacco Use. *Gene* (2020) 727:144258. doi: 10.1016/j.gene.2019.144258
49. Becker ST, Beck-Broichsitter BE, Graetz C, Dörfer CE, Wiltfang J, Häsler R. Peri-Implantitis Versus Periodontitis: Functional Differences Indicated by Transcriptome Profiling. *Clin Implant Dent Relat Res* (2014) 16(3):401–11. doi: 10.1111/cid.12001
50. Liu Y, Liu Q, Li Z, Acharya A, Chen D, Chen Z, et al. Long Non-Coding RNA and mRNA Expression Profiles in Peri-Implantitis vs Periodontitis. *J Periodontal Res* (2019) 55:343–53. doi: 10.1111/jre.12718
51. Bijukumar DR, McGeehan C, Mathew MT. Regenerative Medicine Strategies in Biomedical Implants. *Curr Osteoporos Rep* (2018) 16(3):236–45. doi: 10.1007/s11914-018-0441-0
52. Koreny T, Tunyogi-Csapóy M, Gál I, Vermes C, Jacobs JJ, Glant TT. The Role of Fibroblasts and Fibroblast-Derived Factors in Periprosthetic Osteolysis. *Arthritis Rheum* (2006) 54(10):3221–32. doi: 10.1002/art.22134

Conflict of Interest: The authors declare that the research was conducted in the absence of any commercial or financial relationships that could be construed as a potential conflict of interest.

frontiers in Immunology

ORIGINAL RESEARCH
published: 04 March 2022
doi: 10.3389/fimmu.2022.818630

Pro Nerve Growth Factor and Its Receptor p75NTR Activate Inflammatory Responses in Synovial Fibroblasts: A Novel Targetable Mechanism in Arthritis

Luciapia Farina[1], Gaetana Minnone[1], Stefano Alivernini[2], Ivan Caiello[1], Lucy MacDonald[3], Marzia Soligo[4], Luigi Manni[4], Barbara Tolusso[2], Simona Coppola[5], Erika Zara[5], Libenzio Adrian Conti[6], Angela Aquilani[7], Silvia Magni-Manzoni[7], Mariola Kurowska-Stolarska[3], Elisa Gremese[2], Fabrizio De Benedetti[1,7] and Luisa Bracci-Laudiero[1,4]*

[1] Department of Immunology, Laboratory of ImmunoRheumatology, Bambino Gesù Children's Hospital, Istituto di Ricovero e Cura a Carattere Scientifico (IRCCS), Rome, Italy, [2] Division of Rheumatology, Fondazione Policlinico Universitario A. Gemelli Istituto di Ricovero e Cura a Carattere Scientifico (IRCCS), Università Cattolica del Sacro Cuore, Facoltà di Medicina e Chirurgia, Rome, Italy, [3] Inflammatory Arthritis Centre Versus Arthritis (RACE), Institute of Infection, Immunity and Inflammation, University of Glasgow, Glasgow, United Kingdom, [4] Institute of Translational Pharmacology (IFT-CNR), Consiglio Nazionale delle Ricerche, Rome, Italy, [5] National Centre for Rare Diseases, Istituto Superiore di Sanita', Rome, Italy, [6] Confocal Microscopy Core Facility, Research Center, Bambino Gesù Children's Hospital, Istituto di Ricovero e Cura a Carattere Scientifico (IRCCS), Rome, Italy, [7] Division of Rheumatology, Bambino Gesù Children's Hospital, Istituto di Ricovero e Cura a Carattere Scientifico (IRCCS), Rome, Italy

OPEN ACCESS

Edited by:
Matthew William Grol, Western University, Canada

Reviewed by:
Esmeralda Blaney Davidson, Rheumatology Research Radboudumc Nijmegen, Netherlands
Dai Lie, Sun Yat-sen Memorial Hospital, China

***Correspondence:**
Fabrizio De Benedetti
fabrizio.debenedetti@opbg.net

Specialty section:
This article was submitted to Inflammation, a section of the journal Frontiers in Immunology

Received: *19 November 2021*
Accepted: *14 February 2022*
Published: *04 March 2022*

Citation:
Farina L, Minnone G, Alivernini S, Caiello I, MacDonald L, Soligo M, Manni L, Tolusso B, Coppola S, Zara E, Conti LA, Aquilani A, Magni-Manzoni S, Kurowska-Stolarska M, Gremese E, De Benedetti F and Bracci-Laudiero L (2022) Pro Nerve Growth Factor and Its Receptor p75NTR Activate Inflammatory Responses in Synovial Fibroblasts: A Novel Targetable Mechanism in Arthritis. Front. Immunol. 13:818630. doi: 10.3389/fimmu.2022.818630

We have recently provided new evidence for a role of p75NTR receptor and its preferential ligand proNGF in amplifying inflammatory responses in synovial mononuclear cells of chronic arthritis patients. In the present study, to better investigate how activation of the p75NTR/proNGF axis impacts synovial inflammation, we have studied the effects of proNGF on fibroblast-like synoviocytes (FLS), which play a central role in modulating local immune responses and in activating pro-inflammatory pathways. Using single cell RNA sequencing in synovial tissues from active and treatment-naïve rheumatoid arthritis (RA) patients, we demonstrated that p75NTR and sortilin, which form a high affinity receptor complex for proNGF, are highly expressed in $PRG4^{pos}$ lining and $THY1^{pos}COL1A1^{pos}$ sublining fibroblast clusters in RA synovia but decreased in RA patients in sustained clinical remission. In *ex vivo* experiments we found that FLS from rheumatoid arthritis patients (RA-FLS) retained *in vitro* a markedly higher expression of p75NTR and sortilin than FLS from osteoarthritis patients (OA-FLS). Inflammatory stimuli further up-regulated p75NTR expression and induced endogenous production of proNGF in RA-FLS, leading to an autocrine activation of the proNGF/p75NTR pathway that results in an increased release of pro-inflammatory cytokines. Our data on the inhibition of p75NTR receptor, which reduced the release of IL-1β, IL-6 and TNF-α, further confirmed the key role of p75NTR activation in regulating inflammatory cytokine production. In a set of *ex vivo* experiments, we used RA-FLS and cultured them in the presence of synovial fluids obtained from arthritis patients that, as we demonstrated, are characterized by a high

concentration of proNGF. Our data show that the high levels of proNGF present in inflamed synovial fluids induced pro-inflammatory cytokine production by RA-FLS. The blocking of NGF binding to p75NTR using specific inhibitors led instead to the disruption of this pro-inflammatory loop, reducing activation of the p38 and JNK intracellular pathways and decreasing inflammatory cytokine production. Overall, our data demonstrate that an active proNGF/p75NTR axis promotes pro-inflammatory responses in synovial fibroblasts, thereby contributing to chronic synovial inflammation, and point to the possible use of p75NTR inhibitors as a novel therapeutic approach in chronic arthritis.

Keywords: synoviocytes, inflammation, p75NTR inhibition, arthritis, nerve growth factor

HIGHLIGHTS

Many chronic arthritis patients do not reach clinical remission (up to 50% for adult rheumatoid arthritis and 30% in juvenile idiopathic arthritis) with the available therapies. Identification of novel inflammatory mechanisms and biomarkers will help to identify new strategies for the treatment of arthritis patients. Our study focused on NGF and its receptor system. As a number of studies demonstrated, NGF directly modulates functions of immune cells and is involved in the regulation of the inflammatory response. Our working hypothesis was that the activation of NGF receptor pathways could play a role in the pathogenesis of arthritis. Our results demonstrated for the first time the involvement of proNGF, the immature form of NGF, and its specific receptor p75NTR, in activating pro-inflammatory responses in synovial fibroblasts, which play a central role in modulating joint inflammation. Our study demonstrated that inhibition of p75NTR/proNGF axis inhibits inflammatory response in rheumatoid arthritis synovial fibroblasts by reducing the production of cytokines that promote inflammation. These findings suggest that neutralization of p75NTR may represent a novel targetable pathway in chronic arthritis.

INTRODUCTION

The basal production of nerve growth factor (NGF), that regulates peripheral innervation of tissues and organs, is enhanced during inflammatory responses in epithelial, muscular and endothelial tissues (1). Inflammatory cytokines regulate NGF production in several cell types (1) including fibroblasts (2, 3) and, not surprisingly, a number of studies have shown that NGF levels correlate with the magnitude of the inflammatory response in several chronic inflammatory diseases (1). High levels of NGF are reported in serum and synovium of patients with chronic arthritis (4–6) as well as in animal models of the disease (7, 8).

At the time these studies on inflammatory diseases were performed it was not possible to discriminate between the relative concentrations of mature NGF and the immature proNGF forms.

NGF is synthesized as a precursor, proNGF (9), which is processed into the mature form either in the Golgi or in the extracellular space (9, 10). Studies in neurons have shown that the immature proNGF form is not an inactive precursor (11) but binds with high affinity to the p75NTR/sortilin receptor complex (12) inducing effects that differ from those induced by mature NGF, which binds preferentially to TrkA. ProNGF activates apopototic mechanism in neuronal cells while mature NGF, through TrkA, regulates neuronal survival and phenotype maintenance (11, 13, 14). *In vivo* studies on neurodegenerative diseases and on diabetes suggest that proNGF is even more abundant than mature NGF in brain and peripheral tissues (15–17). At present, very little is known about the relative concentrations of proNGF and mature NGF in inflammatory diseases and the specific effects of proNGF and mature NGF on inflammatory responses are not yet clear.

Previous data in animal models of inflammatory diseases such as experimental autoimmune encephalomyelitis and inflammatory bowel disease (18, 19), suggested that the administration of mature NGF induces an improvement in symptoms, without providing any mechanistic information. Using Toll-like receptor 2 and 4 ligands to activate monocytes, we have demonstrated that mature NGF, through binding to TrkA, reduces the production of pro-inflammatory cytokines and increases the production of the anti-inflammatory cytokines, IL-1RA and IL-10, activating an Akt dependent intracellular signaling pathway (20). This regulatory mechanism seems defective in patients with chronic arthritis: they are characterized by a marked decrease in TrkA expression in peripheral blood and synovial fluid mononuclear cells (MNC), resulting in a loss of the inhibitory effect of NGF on inflammatory cytokine release that it is instead observed in healthy donor MNC (20). Subsequent studies demonstrated that blood MNC of juvenile idiopathic arthritis (JIA) patients are characterized by a marked over-expression of p75NTR and sortilin, the proNGF high affinity receptor complex and a significant decrease of TrkA expression, while healthy donor blood MNC show a high TrkA and a low p75NTR expression (21). The altered p75NTR and TrkA ratio found in blood JIA MNC is even more evident in the MNC obtained from JIA synovial fluids. In inflamed synovial fluids the expression of p75NTR in the MNC is enhanced compared to the one of JIA blood MNC and correlates with clinical parameters: the more inflamed was the patient the highest was the expression of

p75NTR in synovial fluid MNC (21). This change in p75NTR and TrkA ratio in arthritis patient MNC, characterized by high p75NTR and low TrkA expression, results in an increased binding affinity for the proNGF form. In *ex vivo* experiment we demonstrated that administration of proNGF increases the release of inflammatory cytokines in synovial MNC from JIA patients (21). Since proNGF concentration is extremely high in the synovial fluids (SF) of inflamed synoviae (21), we hypothesized that activation of the p75NTR/proNGF axis may play an important role in synovial inflammation.

To better characterize how an active proNGF-p75NTR pathway can regulate inflammatory response in the synovia of arthritis patients we used single cell analysis to identify the p75NTR+ cell populations in the inflamed tissue and focused on fibroblast-like synoviocytes (FLS). FLS are considered major players in the pathogenesis of chronic arthritis producing cytokines that perpetuate inflammation and proteases that contribute to cartilage destruction (22).

Our data show that specific subsets of sublining FLS from RA patients overexpress p75NTR and actively express NGF. We also demonstrated in *ex vivo* experiments that inflammatory cytokines further enhanced both the expression of p75NTR and the release of proNGF in RA-FLS, creating a pro-inflammatory loop that sustains the inflammatory response. Inhibition of p75NTR activity significantly down-regulates pro-inflammatory cytokine production indicating p75NGF inhibition as a novel target for chronic arthritis treatment.

MATERIALS AND METHODS

Patient Samples and Cell Cultures

As a source of inflamed synovial fluids, synovial fluid (SF) was obtained from patients with juvenile idiopathic arthritis (JIA) followed at the Division of Rheumathology of Bambino Gesú Children's Hospital. The study was approved by the local ethical committee (ID#2333_OPBG_2020) and written consent was obtained from parents of children, as appropriate. Synovial tissues (total of 8) were obtained from treatment-naïve (n=4) and in sustained clinical and ultrasound remission (n=4) RA patients at the SYNGem Biopsy Unit of the Fondazione Policlinico Universitario A. Gemelli IRCCS, as approved by the Institutional Ethics Committee (ID#6334/15). The patients involved provided signed informed consent. Diagnosis of JIA and RA were based on the International League of Associations for Rheumatology classification criteria and on 2010 EULAR/ACR criteria (23). JIA patients (n= 18) had oligoarticular, extended oligoarticular, or polyarticular JIA. Ten were females. The median age at disease at sampling was 9.4 years (IQR 2.1–12.7) and the median disease duration at sampling was 2.8 years (IQR 1.9–8.7). All patients had active disease with overt arthritis at sampling. 11 patients were untreated, 7 were receiving traditional DMARDs. Patients receiving glucocorticoids were not included.

FLS from rheumatoid arthritis patients (RA-FLS) (n=8) and osteoarthritis patients (OA-FLS) (n=6) were purchased from CliniSciences (Abbiotec, Escondido, USA). Control skin fibroblasts (CTRL) were from American Type Culture Collection (ATCC). Cells were cultured in 10% fetal bovine serum (FBS) high-glucose Dulbecco's Modified Eagle Medium (complete DMEM) with or without the addition of different doses of human recombinant IL1-β or TNF-α (all from R&D systems, Minneapolis, MN), or LPS (Sigma Aldrich, St Louis, MO). For proNGF experiments, 200 ng/ml of a cleavage-resistant proNGF that has an R-to-G substitution at amino acid position 104 (Alomone Labs, Jerusalem, Israel) were used to stimulate cells cultured in AIMV Serum Free Medium (Life Technologies, Rockville, Maryland, USA). Supernatants were collected after 18 hours of incubation before IL-6 production reaches a plateau (24). For p75NTR inhibition, cells were pre-treated for 1 hour with LM11A-31 (25) (a kind gift of Dr. Frank Longo, Stanford University) or with anti-p75NTR antibodies (clone ME20.4 Millipore, Billerica, MA, USA). *Ex vivo* experiments were performed with RA-FLS cultured in complete DMEM with or without the addition of 30% v/v synovial fluid. Cells were pre-treated 1 hour at 37°C with or without LM11A-31 or the anti-IL-1β monoclonal antibody canakinumab (5 μg/ml). (26)

Single Cell-RNA Sequencing of Synovial Tissue

Methods for single-cell RNA sequencing (scRNAseq) of synovial tissue have already been described in detail (27). Briefly, synovial tissue biopsies were collected from naive to treatment RA patients (n=4) and from RA patients in sustained clinical and ultrasound remission (n=4) at the SYNGem Biopsy Unit of the Fondazione Policlinico Universitario A. Gemelli IRCCS using US-guided minimally invasive technique (28). High-quality total RNAs (RIN >8) were used to construct Illumina mRNA sequencing libraries. cDNA synthesis and amplification were performed by using SMART-seq v4 Ultra Low Input RNA Kit for Sequencing (cat. no. 634890, Takara) starting with 10 ng of total RNA, following the manufacturers protocol. 10 ng of amplified cDNAs were sheared prior to preparing the final libraries using the Bioruptor® Pico system (Diagenode, 24 cycles of 30 sec on and 30 sec off). Dual indexed Illumina sequencing libraries were prepared by SMARTer® ThruPLEX® DNA-seq 48D Kit (cat. no. R400406, Takara) following the kit protocol. The pooled libraries were sequenced at Glasgow Polyomics (Glasgow, UK) on a NovaSeq 6000 system using a read length of 100 bases in paired-end mode. The reads were mapped with STAR (version 020201) with default parameter against the Human genome version GRCh38, release 91. The read count matrix was constructed with featureCounts (Version 1.6.4) using default parameters. All differential expression analysis was performed in R using the DESeq2 package. All genes with an adjusted p value < 0.05 and a log fold change of > +/- 1,5 were considered significantly differentially expressed. All raw and processed data were deposited at EMBL-EBI and are available with the accession number E-MTAB-8322.

RNA Extraction and Real-Time PCR Analysis

After RNA extraction using Trizol Reagent (Thermo Fisher Scientific, MA), cDNAs were retro-transcribed using the

Superscript Vilo kit (Invitrogen, CA). Real-time PCRs were performed using TaqMan Universal PCR Master Mix and gene expression assays from Applied Biosystems (CA, USA). TrkA, p75NTR, NGF, sortilin mRNA expressions were tested using Assays on Demand reagents (TrkA Hs01021011_m1; p75NTR Hs00182120_m1; NGF Hs00171458_m1; sortilin Hs00361760_m1). TaqMan Endogenous Control human HPRT Hs 02800695_m1 and GAPDH Hs 99999905_m1 (Applied Biosystems) were used as housekeeping genes. Normalized gene expression levels were calculated as

$2^{-\Delta Ct}$ [ΔCt = Ct (gene of interest) – Ct (housekeeping gene)] and results were expressed in arbitrary units (A.U.). Fold changes were calculated using the $2^{-\Delta\Delta Ct}$ equation [ΔΔCt = ΔCt (treated sample) – ΔCt (untreated sample)] (29).

Cytokine and NGF-proNGF ELISA

Levels of IL-6, MCP1, IL-8 were analyzed using R&D Quantikine ELISA. Conditioned media and SF were assayed using ELISAs specific for human mature NGF or proNGF, as described (30).

Western Blot Analysis

After RIPA buffer lysis (Cell Signaling, Leiden, The Netherlands), protein concentration was measured with BCA Protein assay (Thermo Fisher Scientific). 30 μg protein extracts were resolved by 10% SDS PAGE, transferred to nitrocellulose membranes and probed with antibodies against: phospho-stress-activated protein kinase/c-Jun NH(2)-terminal kinase (SAPK/JNK) (Thr183/Tyr185, clone G9 MAB #9255), total SAPK/JNK (#9252), phospho-p38 Mitogen-Activated Protein Kinase (MAPK) (Thr180/Tyr182, clone 28B10 MAB #9216), total p38 MAPK (#9212) (all from Cell Signaling), p75NTR (clone 8211 MAB5264) (EMD Millipore), GAPDH (clone G9, MAB #32233) (Santa Cruz Biotechnology), and tubulin (Sigma Aldrich). Blots were developed by ECL system (Amersham Biosciences) according to the manufacturer's protocol.

Immunofluorescence Analysis

RA-FLS and OA-FLS were fixed in 4% paraformaldehyde, permeabilized with 0.5% Triton X-100 PBS, incubated for 1 hour at RT with 1% BSA, 5% goat serum (Abcam, Cambridge, UK) PBS and then with mouse anti-p75NTR antibody (Merck, Darmstadt, Germany, clone 8211) or rabbit anti-proNGF (Merck AB9040) and Alexa Fluor secondary antibodies (Invitrogen). Confocal imaging acquisition was performed on Olympus Fluoview FV1000 confocal microscope using a 40× (0.90 NA oil) objective.

Apoptosis Detection

Cells were incubated with or without LM11A-31 (10, 100 nM) for 1 hour at 37°C and then 30% v/v SF was added. After 18 hours apoptotic cells were stained using Annexin V-FITC Apoptosis Detection Kit (Sigma Aldrich). Cells were analyzed by flow cytometry (FACSCanto II, BD Biosciences CA, USA).

Statistical Analysis

Data are presented as mean ± standard error of the mean (SEM). Statistical analysis was performed using GraphPad Prism 5 Software (GraphPad Software, La Jolla, CA). Statistical significance is shown as *p<0.05 **p<0.01 and ***p<0.001.

RESULTS

p75NTR Expression Is Markedly Increased in Distinct Synovial Fibroblasts Clusters From RA

To determine which immune or stromal cells might be activated by the proNGF/p75NTR axis in synovial tissue, we investigated the expression of p75NTR, TrkA and SORT1 in previously published scRNAseq data sets referring to whole synovial tissues (total 118.622 cells) derived from treatment-naïve RA patients or from RA in sustained clinical and imaging remission (**Figure 1A**) (27). Among different synovial fibroblast clusters, in treatment-naïve RA synovial tissues, lining layer $PRG4^{pos}$ cluster and sublining $THY1^{pos}COL1A1^{pos}$ fibroblast cluster are enriched of p75NTR compared to other FLS clusters as well as to other resident and inflammatory synovial cells such as macrophages or T and B lymphocytes (**Figure 1B**). Moreover, as shown in **Supplementary Figure 1**, scRNAseq analysis revealed that, when compared to treatment-naïve RA, p75NTR and TrkA expression is significantly reduced in $THY1^{pos}COL1A1^{pos}$ fibroblast cluster in RA patients in sustained clinical and imaging remission. We also observed a significant reduction of SORT1 expression in lining layer ($PRG4^{pos}$ cluster) as well as in sublining layer fibroblasts ($THY1^{pos}COL1A1^{pos}$).

Expression of p75NTR and proNGF Release by RA Synovial Fibroblasts

Given the high *in vivo* expression of p75NTR in pathogenic synovial fibroblast clusters in RA synovium, we investigated whether its expression is maintained in RA-FLS *in vitro* and what is the biological effect of an active p75NTR pathway. We analysed p75NTR and sortilin expression also in OA-FLS because although OA is a degenerative non-autoimmune disease, it is characterized by some inflammation of the joints. To verify the basal expression of p75NTR in non-inflamed conditions we used skin fibroblasts (skin-FB) from healthy donors. As shown in **Figure 2A** p75NTR is expressed far more in RA-FLS than in either OA-FLS or skin-FB. Control skin fibroblast express higher levels of TrkA than RA-FLS. p75NTR mRNA expression data were confirmed by Western blot (**Supplementary Figure 2A**). Sortilin showed the same expression pattern as p75NTR (**Supplementary Figure 2B**).

In vitro stimulation with IL-1β marginally up-regulated p75NTR mRNA expression in OA-FLS (**Figure 2B**), while induced a marked dose-dependent increase in RA-FLS (**Figure 2B** and **Supplementary Figure 2C**). Immunofluorescence confirmed a higher basal expression of p75NTR and its enhancement after stimulation with IL-1β in RA-FLS, while only a slight increase was observed in OA-FLS using a maximal dose (10ng/ml) of IL-1β (**Figure 2C**). Other pro-inflammatory stimuli, such as TNF-α and LPS, also upregulate p75NTR expression in RA-FLS (**Figure 2D**).

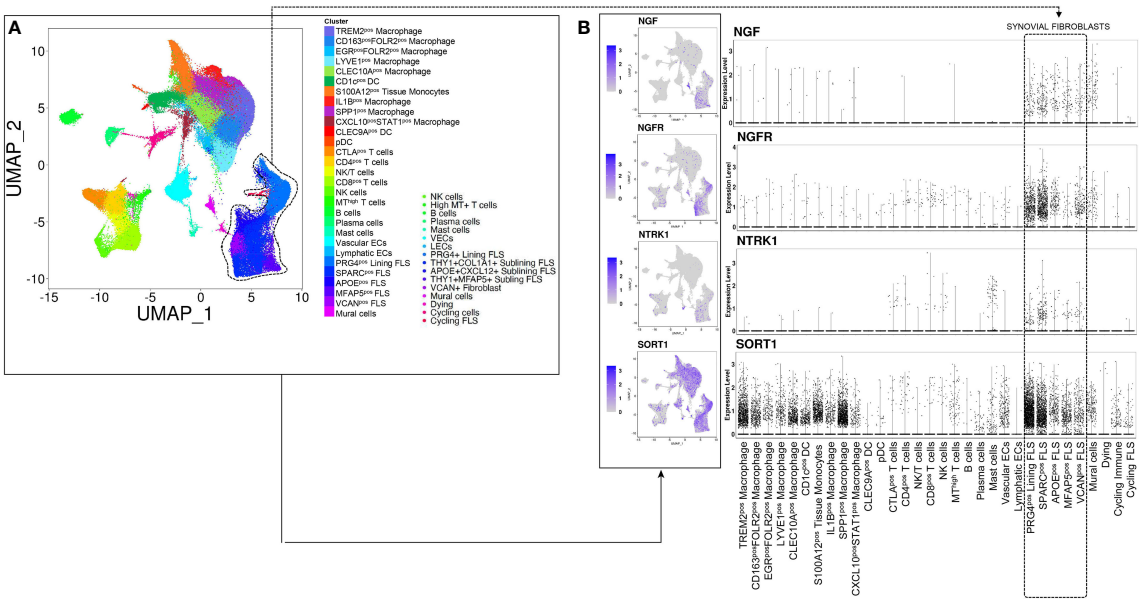

FIGURE 1 | NGF, p75NTR, TRKA and SORT1 are expressed in lining and sublining synovial fibroblasts clusters from treatment-naïve patients with rheumatoid arthritis. **(A)** UMAP (Uniform Manifold Approximation and Projection for Dimension Reduction) of synovial tissue cells from treatment-naïve Rheumatoid Arthritis patients (n = 4) (27) by scRNAseq. Each dot represents a cell and distinct cell clusters are identified according to the color legend. **(B)** UMAP and dot plots showing NGF, NGFR, NTRK1 and SORT1 gene expression in distinct inflammatory and stromal cells clusters. The violet color identifies cells expressing NGF, p75NTR, TrkA and sortilin.

Compared with OA-FLS and CTRL-FB, unstimulated RA-FLS express higher basal levels of NGF mRNA. In RA FLS the already high NGF mRNA levels were further increased in a dose-dependent manner by IL-1β (**Figure 3A** and **Supplementary Figure 2D**), as well as by TNF-α or LPS (**Figure 3B**). At a protein level, proNGF is the most abundant form of NGF secreted by unstimulated RA-FLS, consistently with our previous observation that proNGF, and not mature NGF, is the predominant NGF form in synovial fluids from inflamed joints of JIA and RA patients (21). Secretion of proNGF in RA-FLS is further enhanced by IL-1β, as well as by LPS or TNF–α (**Figure 3C**). Immunofluorescence showed that proNGF is higher in unstimulated RA-FLS, than in OA-FLS, and markedly increased in the cytoplasm of RA-FLS after IL-1β-stimulation (**Figure 3D**).

p75NTR Activation Enhances Inflammatory Cytokine Production by RA Synovial Fibroblasts

To understand the functional relevance of proNGF-p75NTR interaction, we stimulated RA-FLS with recombinant proNGF and analyzed the production of inflammatory cytokines. To avoid interference by NGF and/or proNGF present in bovine serum (31), cells were cultured in serum-free medium. The addition to RA-FLS of proNGF alone did not modify the release of IL-6 (**Figure 4A**). In contrast, the addition of proNGF together with sub-optimal concentrations of IL-1β significantly enhanced IL-6 release (**Figure 4A**). The synergy between IL-1β and proNGF was lost at higher IL-1β concentrations. Since IL-1β induces a dose-dependent increase in both p75NTR and proNGF expression in RA-FLS (**Supplementary Figures 2C, D**), the lack of effect of the exogenous proNGF addition at maximal IL-1β concentrations suggested the presence of a proNGF/p75NTR autocrine loop. Consistently with an autocrine loop, in RA-FLS stimulated with IL-1β, TNF-α or LPS without the addition of exogenous proNGF, the selective blocking of the binding site for proNGF on p75NTR, using a small non-peptide p75NTR ligand inhibitor (LM11A-31 (25), resulted in a significant decrease in inflammatory cytokine production (**Figures 4B–D** and **Supplementary Figures 3A–C**). Similarly, the blocking of p75NTR using a p75NTR-neutralizing antibody significantly decreased IL-6 production in RA-FLS stimulated with different inflammatory stimuli and without the addition of exogenous proNGF (**Figures 4E** and **Supplementary Figures 3D, E**). Moreover, when exogenous pro-NGF was added to IL-1β activated RA-FLS the LM11A-31 blocking of proNGF binding to p75NTR resulted in a more pronounced inhibition of IL-6 release than would be expected if only exogenous proNGF binding was blocked (**Supplementary Figure 4A**).

proNGF Present in Synovial Fluid Induces Inflammatory Cytokine Production From RA-FLS

The synovial fluids (SF) of JIA and RA patients are characterized by high concentrations of proNGF and markedly lower

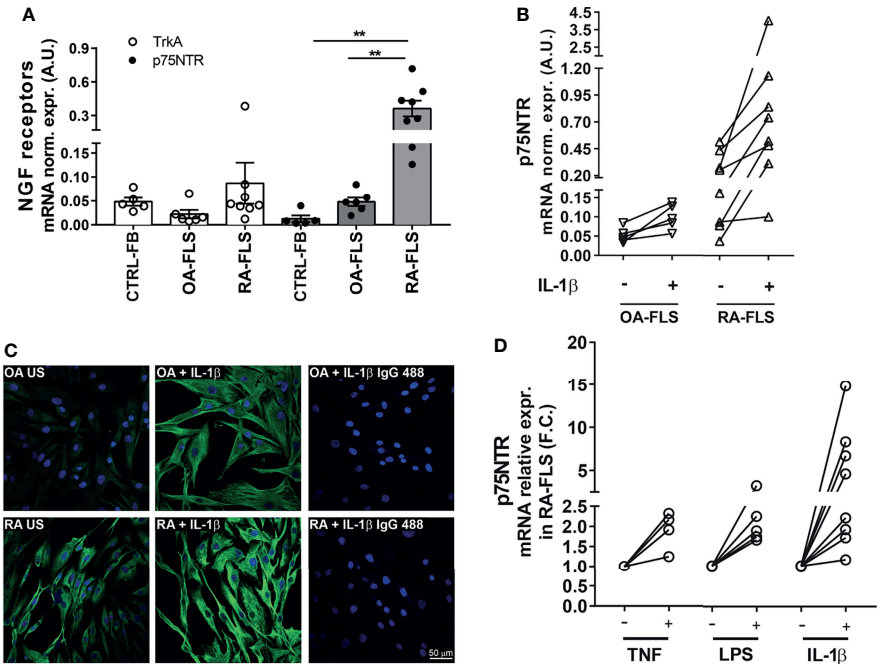

FIGURE 2 | NGF receptor levels in synovial fibroblasts from RA patients. **(A)** FLS from RA patients (RA-FLS) (n = 8) have lower TrkA and higher p75NTR mRNA expression levels than OA-FLS (n = 6), and skin fibroblasts (CTRL-FB) (n = 5). Results are reported in arbitrary units (A.U.) after normalization with *HPRT* expression. Data were analyzed using unpaired *t*-test (**p < 0.01). **(B)** 1 ng/ml IL-1β up-regulates p75NTR expression in RA-FLS (n = 8) compared to OA-FLS (n = 5). Results are reported in arbitrary units (A.U.) after normalization with *HPRT* expression. **(C)** Immunofluorescence analysis confirms higher basal levels of p75NTR in RA-FLS (Untreated, RA-US) than in OA-FLS (OA US). IL-1β (10 ng/ml) stimulation further enhances p75NTR in RA-FLS. Representative images of three independent experiments are shown. p75NTR immunofluorescence is shown in green, nuclei in dark blue. Scale bar 50μm. **(D)** Inflammatory stimuli, 100 ng/ml TNF-α (n = 4), 100 ng/ml LPS (n = 5), and 1 ng/ml IL-1β (n = 8), induce p75NTR expression in RA-FLS. Results are compared to unstimulated condition and calculated as Fold Change (F.C.).

concentrations of mature NGF (21). To investigate the role of these high proNGF synovial concentrations, we recapitulated pathological synovial conditions *in vitro* by culturing RA-FLS in a medium supplemented with 30% v/v of SF from patients with active arthritis. As shown in **Figure 5A** and **Supplementary Figure 4B**, we further confirm that SF from arthritis patients have much higher concentration of proNGF than of mature NGF. The addition of 30% SF led to a significant increase of IL-6 release by RA-FLS (**Figure 5B**). The addition of the p75NTR inhibitor LM11A-31, by blocking the binding of the proNGF present in SF to p75NTR (highly expressed in RA-FLS), resulted in a significant inhibition ($p<0.0001$) of IL-6 release induced by synovial fluid stimulation (**Figure 5C**). Since it is well known that IL-1β is a potent activator of RA-FLS (32, 33), as an internal control in these experiments we neutralized the IL-1β present in the inflamed synovial fluid by using canakinumab. We found that neutralization of p75NTR using LM11A-31 was as effective as IL-1β inhibition with canakinumab (**Figure 5D**).

The observed decrease in cytokine production, induced by LM11A-31 blocking of p75NTR activity, is not due to any toxic effect of the p75 inhibitor or decreased survival of RA-FLS: neither 30% v/v SF nor different LM11A-31 concentrations (the highest dose was 10-fold that used in the neutralization experiments) induced an increase in the percentage of apoptotic cells in RA-FLS (**Figure 5E**). To gain insights into the intracellular mechanisms regulated by p75NTR activation in RA-FLS, we focused on the p38 and JNK proteins, members of the MAPK pathways and key mediators of pro-inflammatory cytokine production in RA synovium (34). As shown in **Figure 6**, our data indicated that p75NTR activity modulates the pro-inflammatory signaling response. Indeed, RA-FLS cultured in 30%SF showed an increase in p38 and JNK phosphorylation. This effect is mediated by the proNGF present in inflamed SF, since p75NTR neutralization significantly reduced p38 and JNK phosphorylation. As previously observed in human FLS (35) and in an *in vivo* collagen-induced arthritis model (34), JNK was expressed only as 54 kDa isoform.

DISCUSSION

Despite currently available targeted therapies, many patients with RA or JIA do not achieve remission, instead accruing functional and structural damage, suggesting the imperative need of new therapeutic approaches based on novel mechanisms of action. Here, we provide the evidence for a novel pro-inflammatory role of p75NTR and its ligand proNGF in the amplification of synovial inflammatory responses.

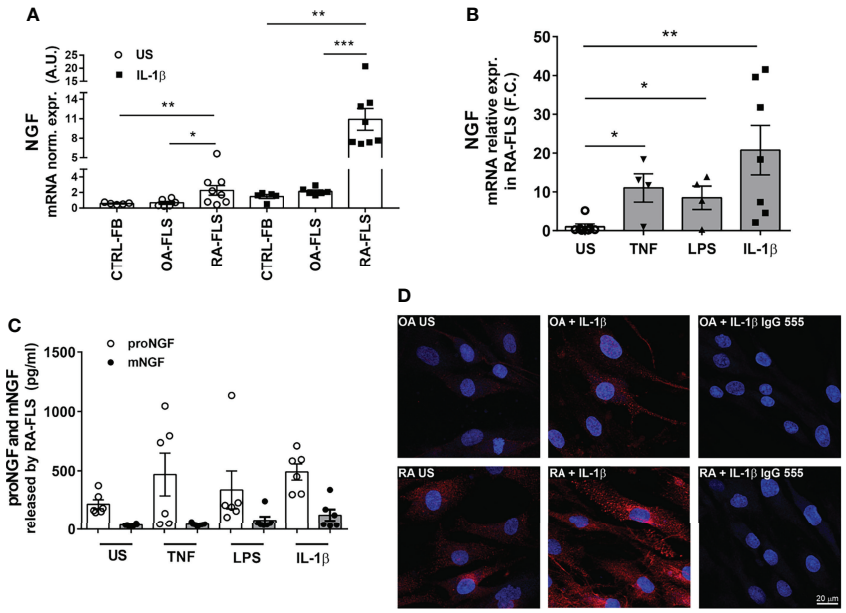

FIGURE 3 | Inflammatory stimuli enhance NGF expression in synovial fibroblasts from RA patients. **(A)** Stimulation with 1 ng/ml of IL-1β induces the expression of NGF in RA-FLS (n = 8), OA-FLS (n = 6) and skin-fibroblasts (CTRL-FB) (n = 5). Results are expressed as arbitrary units (A.U.) after normalization with *HPRT*. Data were analyzed using unpaired *t*-test (**p < 0.01). **(B)** Inflammatory stimuli enhance NGF mRNA expression in RA-FLS. Basal levels of NGF expression were measured in unstimulated (US) RA-FLS (n = 7) and in RA-FLS stimulated with 100 ng/ml TNF-α (n = 4), 100 ng/ml LPS (n = 4) and 1 ng/ml IL1-β (n = 7). Results are compared to unstimulated condition and calculated as Fold Change (F.C.). Data were analyzed using unpaired *t*-test (*p < 0.05, **p < 0.01, ***p < 0.0001). **(C)** Newly developed ELISAs that discriminate between proNGF and mNGF showed that proNGF is the most abundant form in conditioned media collected from RA-FLS. proNGF production is enhanced by inflammatory stimuli (100ng/ml TNF, 100 ng/ml LPS, 1 ng/ml IL-1β) in RA FLS (n = 6). **(D)** RA FLS show an increase in proNGF basal protein synthesis after stimulation with IL-1β (1 ng/ml). A dim immunofluorescence for proNGF was observed in OA-FLS after IL-1β stimulation. Representative images of three independent experiments are shown. proNGF immunofluorescence is shown in red, nuclear staining in dark blue. Scale bar 50µm.

We found that in RA synovium at disease onset two distinct clusters of FLS with specific tissue locations (sublining $THY1^{pos}COLA1^{pos}$ and lining $PGR4^{pos}$ FLS respectively), that drive inflammation and damage (36), show the highest expression levels of p75NTR and of its co-receptor sortilin when compared to other synovial tissue cells. Moreover, the comparative analysis of proNGF/p75NTR axis component expression, at single cell level, on synovial tissues from treatment-naïve and remission RA patients supports the notion that proNGF/p75NTR axis is actively involved in RA synovial inflammation, being significantly repressed once sustained remission is achieved. In *in vitro* studies we confirmed that RA-FLS have a markedly higher basal expression of p75NTR and sortilin than skin fibroblasts or OA-FLS, indicating the presence of a functional high-affinity proNGF receptor complex. Inflammatory stimuli, such as LPS and the classical pro-inflammatory cytokines as IL-1β and TNF-α, enhance the expression of p75NTR in RA-FLS, as it is seen in blood and synovial fluid-derived immune cells (21), indicating a strict relationship between inflammation and the overexpression of p75NTR. FLS isolated from patients with arthritis are thus characterized by a high p75NTR and a low TrkA expression that may favor the biological effects of proNGF and dampen the anti-inflammatory actions of mature NGF mediated through TrkA activation (20). In RA-FLS, in addition to the observed overexpression of a functional p75NTR receptor complex, we found that inflammatory stimuli, among which IL-1β is the most effective, also markedly enhanced the production of large amounts of proNGF, but not of mature NGF. These data are consistent with our previous findings of high levels of proNGF, but not of mature NGF, in synovial fluids from inflamed joints of JIA and RA patients (21). Constitutively high expressions of p75NTR and enhanced release of proNGF, as well as their up-regulation induced by IL-1β, TNF-α and LPS, are specific features of RA-FLS. OA-FLS show a much lower basal expression of p75NTR and of proNGF, which are only marginally up-regulated by IL-1β. A vast body of evidence shows that OA-FLS and RA-FLS are characterized by differences in the proportion (37) of fibroblast subsets with non-overlapping functions which play distinct roles in the pathogenesis of OA and RA: in RA there is a prevalence of immune effector fibroblasts that sustain inflammation through the production of chemokines and cytokines, and of bone effector fibroblasts that mediate joint damage through the production of matrix metalloproteinases (37–40). RA-FLS have a pro-inflammatory and aggressive phenotype (41) and a number of epigenetic changes have been suggested to account for these abnormalities (42). In this contest, p75NTR overexpression and proNGF overproduction may be part of this abnormal pro-inflammatory phenotype in RA-FLS and,

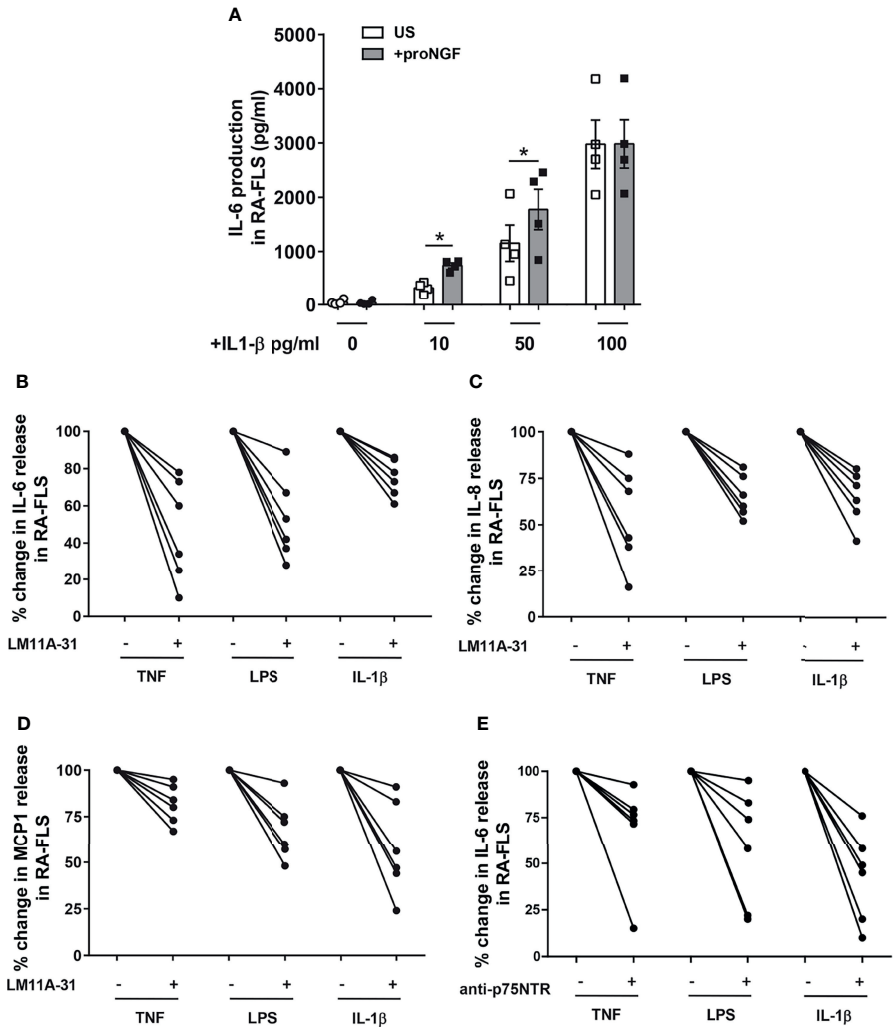

FIGURE 4 | proNGF increases the expression of inflammatory cytokines in synovial fibroblasts from RA patients. **(A)** The addition of exogenous proNGF (200ng/ml) together with IL-1β at suboptimal doses (10pg/ml and 50pg/ml) induces a synergic increase in IL-6 production not observed at higher concentration of IL-1β. The experiments (n = 4) were performed in serum free medium. Data were analyzed by paired *t*-test (*p < 0.05). **(B–D)** Inhibition of proNGF binding to p75NTR with LM11A-31 (10nM) decreases inflammatory mediators: IL-6 **(B)**, IL-8 **(C)** and MCP1 **(D)** production was significantly reduced in RA-FLS cells activated using 100 ng/ml TNF-α, 100 ng/ml LPS or 1 ng/ml IL-1β. RA-FLS were cultured for 18 hours in 10% FBS DMEM. The inhibitory effect of LM11A-31 on cytokine release is expressed as percentage decrease (% decrease) from activated cells. **(E)** To obtain a confirm of the effects of p75NTR blocking, p75NTR was neutralized using a specific anti-p75NTR antibody (2,5 μg/ml) and the release of IL-6 was measured in RA-FLS activated with 100 ng/ml TNF-α, 100 ng/ml LPS or 1ng/ml IL-1β. In this set of experiments (n = 6) cells were cultured in 10% FBS DMEM for 18 hours. The results are expressed as percentage decrease (% decrease) from activated cells.

possibly, of the underlying epigenetic changes. It is tempting to speculate that overproduction of proNGF and overexpression of p75NTR, leading to hyperactivation of this pathway, is, at least in part, responsible for the known prolonged and exaggerated responses of RA-FLS to cytokines (43). We therefore investigated the effects of an active proNGF/p75NTR axis in RA-FLS. The addition of proNGF to sub-optimal concentrations of IL-1β synergistically up-regulated inflammatory cytokine release. At higher concentrations of IL-1β, the effects of exogenously added proNGF became negligible, possibly because IL-1β is a strong inducer of proNGF, with high amounts of proNGF being released by IL-1β-activated RA-FLS.

To test the hypothesis of an active autocrine loop involving proNGF production and p75NTR expression in RA-FLS, we inhibited p75NTR using a neutralizing antibody or LM11A-31, a non-peptide ligand of p75NTR that selectively blocks the binding site of proNGF (44, 45). The blocking of the binding of the endogenously-produced proNGF to p75NTR in IL-1β-activated RA-FLS resulted in a marked decrease in inflammatory cytokine production, indicating the functional interaction of p75NTR and proNGF and the presence of a pro-inflammatory autocrine loop. Thus, RA-FLS activated by inflammatory cytokines overexpress p75NTR and, at the same time, release increased amounts of proNGF which, by binding to p75NTR, further up-regulates

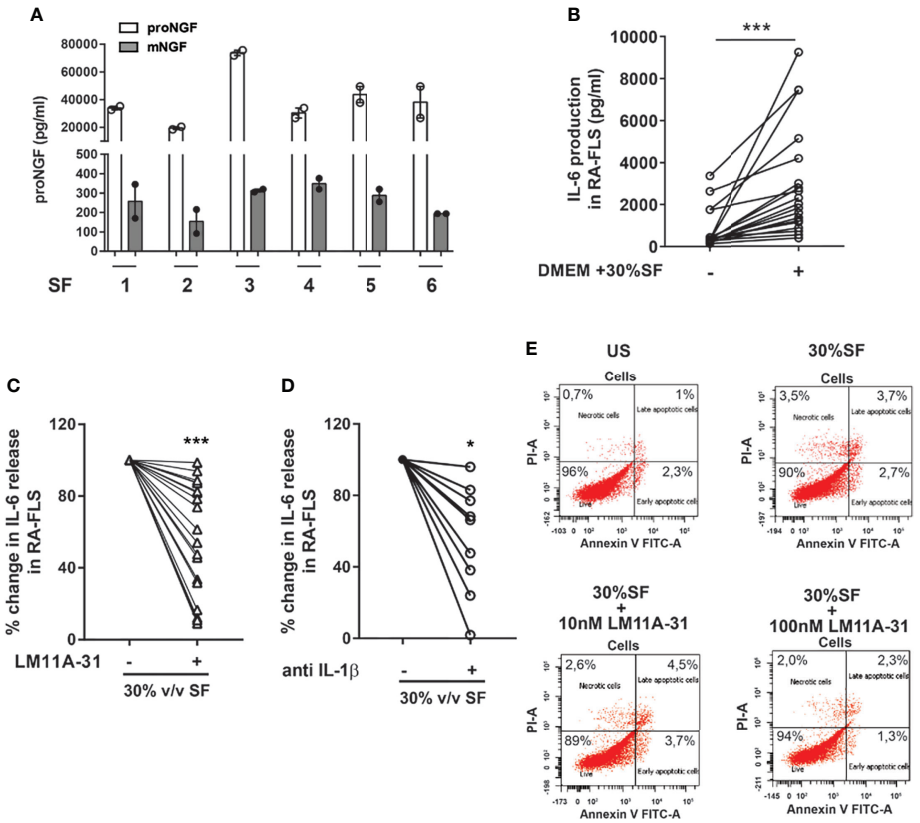

FIGURE 5 | proNGF present in synovial fluids increases the expression of inflammatory mediators in synovial fibroblasts from RA patients. **(A)** proNGF is by far the most abundant NGF form (100 to 200-fold that of mature NGF) detected in synovial fluids (SF) obtained from six active patients (1-6). **(B)** To recreate *ex vivo* inflamed synovia condition, 30% v/v synovial fluid was added to RA-FLS (n = 19) cultured in 10% FBS DMEM. Data were analyzed by paired *t*-test (***p < 0.001). **(C)** RA-FLS in 30% v/v synovial fluid were treated with 10 nM of LM11A-31 with LM11A-31 and IL-6 production was measured after 18 hours. The data represent the percentage of inhibition obtained in 19 independent experiments performed using seven different RA-FLS and synovial fluids obtained from different patients (n = 18). Data were analyzed by one sample *t*-test (***p < 0.001). **(D)** 30% v/v synovial fluid was added to RA-FLS cultured in 10% FBS DMEM with or without the addition of anti-IL1β (5μg/ml) (n = 9). IL-6 release was measured after 18 hours of incubation. Data were analyzed by one sample t-test (*p < 0.05). **(E)** The apoptosis rate of RA-FLS treated with 30% v/v of synovial fluids with or without the addition of LM11A-31 at two different doses (10nM used for all our experiment and a ten-fold higher dose 100 nM) was analyzed by Annexin V/PI staining. No modification in the percentage of apoptotic cells was observed following the addition of synovial fluid or after p75NTR inhibition with LM11A-3 with both the doses used. Representative scatterplots of three independent experiments are shown.

inflammatory cytokine production. Neutralization of p75NTR breaks this pro-inflammatory loop and significantly reduces inflammatory cytokine production as summarized in **Figure 7**.

In order to confirm these findings using a more physiological culture system (46), we recreated, at least partially, the pathological conditions of an inflamed synovium by culturing RA-FLS in media supplemented with 30% SF obtained from arthritis patients. Rather than using a chemically defined medium and only one stimulus, such as a single recombinant cytokine, this *ex vivo* model provides a means to activate FLS with the mixture of pro-inflammatory and anti-inflammatory mediators that are present in the SF of diseased joints. We found that the addition of SF to RA-FLS significantly increased the production of IL-6. This effect is mediated almost completely by the proNGF present in SF, as the inhibition of proNGF binding to p75NTR led to an 80% reduction in IL-6 production. As it is well known that IL-1β enhances the expression levels of various inflammatory factors in RA-FLS through the activation of NF-kB/ERK/STAT1 axis, p38 mitogen-activated protein kinase (MAPK) and JUNK signaling pathways (22, 32, 33, 47), we compared the effects of IL-1β and p75NTR neutralization on inflammatory cytokine production. We found that in RA-FLS the inhibition of p75NTR activation by LM11A-31 reduces the release of IL-6 to a similar extent as IL-1β inhibition by canakinumab. Although these data are limited to an *ex vivo* culture system, they nonetheless suggest that inhibition of p75NTR is, at least, as effective as the inhibition of a potent activator of pro-inflammatory response in RA-FLS as IL-1β.

In neurons, proNGF binding to p75NTR activates intracellular pathways that involve JNK and lead to cell death (48–50). Our results demonstrated that the effects of p75NTR activation or inhibition were not due to changes in cell viability of RA-FLS.

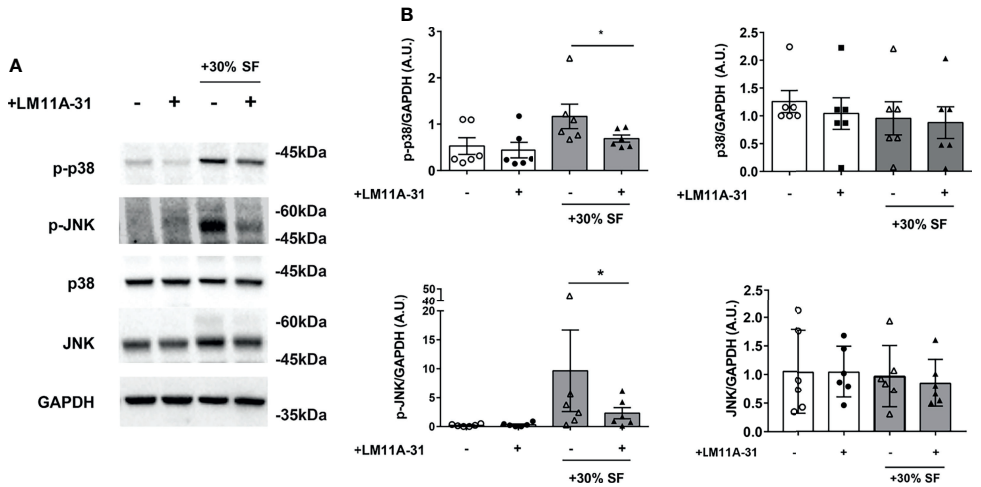

FIGURE 6 | Activation of p38 and JNK is reduced by LM11A-31 inhibition of p75NTR in RA FLS **(A)** RA-FLS were starved for 3 hours and incubated with 10% FBS-DMEM supplemented with 30% v/v synovial fluid and with or without LM11A-31 (10nM) for 18 hours. A reduction in the phosphorylation of p38 and JNK was observed after LM11A-31 inhibition of p75NTR activity. *GAPDH* was used as loading control. **(B)** Densitometric analysis was normalized to the corresponding band intensity of *GAPDH*. Data were analyzed by paired *t*-test (*p < 0.05) and represent mean ± SEM of 6 independent experiments. Results are expressed as arbitrary units (A.U.).

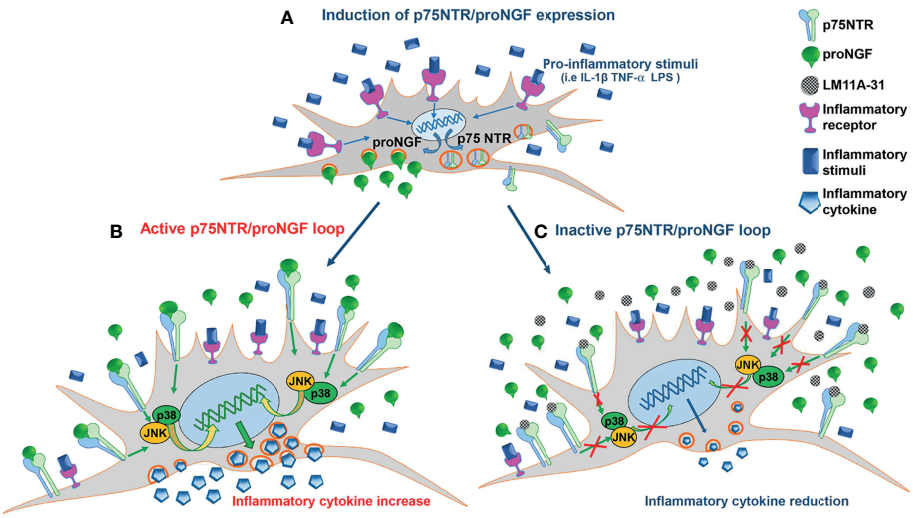

FIGURE 7 | The pro-inflammatory p75NTR/proNGF loop in RA-FLS. **(A)** Inflammatory stimuli activate an autocrine loop involving proNGF and p75NTR. Inflammatory stimuli strongly induce the contemporary expression of p75NTR, the specific proNGF receptor, and of its ligand, proNGF, in RA-FLS. The increased p75NTR expression results in a higher binding capacity of RA-FLS for proNGF, whose endogenous production is strongly induced by inflammatory stimuli. **(B)** The active p75NTR/proNGF axis enhances inflammatory cytokines production. The high amounts of endogenously-produced proNGF, released by activated RA-FLS, interact with the p75NTR receptors highly expressed on RA-FLS membrane. The activation of p75NTR intracellular pathways (i.e. p38 and JNK) results in an amplified production of inflammatory cytokines (i.e. IL-6). **(C)** Inhibition of the p75NTR/proNGF loop decreases inflammatory cytokines production. The blocking of p75NTR using LM11A-31, a small molecule that specifically blocks the binding site of p75NTR for proNGF, results in a net reduction of inflammatory cytokine production (i.e. IL-6). The endogenous proNGF released by active RA-FLS cannot bind to p75NTR and, consequently, does not activate p75NTR intracellular pathways that induce inflammatory cytokine production.

We also provide an initial characterization of the intracellular pathway activated by p75NTR in RA-FLS. We investigated the JNK and p38 MAPK-induced pathways that regulate pro-inflammatory cytokines and metalloproteinase expression, matrix degradation and joint destruction (34, 51). Activated RA-FLS are characterized by p38 and JNK phosphorylation. Inhibition of p75NTR by LM11A-31 effectively reduces phosphorylation of both MAPKs, demonstrating their

involvement in p75NTR signal transduction in RA-FLS. This observation is consistent with the known role of these MAPKs in mediating pro-inflammatory responses (48).

Preliminary data in other inflammatory conditions in mice indicate that the involvement of p75NTR in regulating inflammatory pathways may not be restricted to arthritis. In murine streptozotocin-induced diabetes, accumulation of proNGF and enhanced p75NTR expression are present in the retina. p75NTR-KO mice are protected from diabetes-induced retinal inflammation and show decreased TNF-α expression (52). Treatment of streptozotocin-treated mice with LM11A-31 significantly inhibits an increase in serum TNF-α and IL-1β (53). Similarly, in sepsis-induced neuroinflammation in mouse hippocampus, LM11A-31 treatment causes a decrease in IL-1β concentrations, associated with a reduction in JNK phosphorylation (53).

In conclusion, we demonstrate that *in vivo*, in the synovium of treatment-naïve RA patients, the clusters of FLS typically involved in joint inflammation and damage show a distinctive overexpression of p75NTR. Complementing this finding, we demonstrated *in vitro* that RA-FLS are characterized by a high expression of p75NTR and by a high production of proNGF that, together, promote an autocrine loop that enhances RA-FLS inflammatory responses. Altogether, our results suggest that an active proNGF/p75NTR axis contributes to the chronicity of synovial inflammation and that the proNGF/p75NTR pathway could represent a novel target in the treatment of chronic arthritis.

New approaches in arthritis based on novel mechanisms of actions and targets are needed since many patients do not reach remission and continue to accumulate damage, with significant social and economic costs. Thus, the demonstration of the novel pro-inflammatory role of p75NTR and its preferential ligand, proNGF, in the amplification of inflammatory responses and the preclinical studies with specific receptor inhibitors together will provide the rationale for targeting p75NTR in chronic arthritis and potentially in other chronic inflammatory diseases.

At present the safety of p75NTR inhibition with LM11A-31 is being investigated in a phase 2 trial (ClinicalTrials.gov Identifier: NCT03069014) to test its use in the treatment of Alzheimer's disease patients.

DATA AVAILABILITY STATEMENT

The original contributions presented in the study are publicly available. This data can be found here: www.ebi.ac.uk/arrayexpress/experiments/E-MTAB-8322/.

ETHICS STATEMENT

The studies involving human participants were reviewed and approved by Fondazione Policlinico Universitario A. Gemelli IRCCS, Institutional Ethics Committee (ID#6334/15) Bambino Gesú Children's Hospital IRCCS ethical committee (ID#2333_OPBG_2020). Written informed consent to participate in this study was provided by the participants' legal guardian/next of kin.

AUTHOR CONTRIBUTIONS

LF, GM, IC, LMD,MS, EZ, BT, and LC contributed to acquisition of data. LB-L, SA, BT, LM, EG, MK-S, AA, SM-M, and FDB contributed to analysis and interpretation of data. LB-L, LF, FDB, LM, MS, EG, SC, and SA drafted the article and revised it critically. All authors contributed to the article and approved the submitted version.

FUNDING

This research was supported by the Ministry for Economic Development (Call for the implementation of patent enhancement programs through the funding of Proof of Concept (PoC) projects of Italian Universities and Bodies Italian Public Research (EPR) Institutes and Scientific Institutes for Treatment and Inpatient Care (IRCCS)-Enhancement program "ELEVATOR-mEdicaL patEnts VAlorizaTiOn pRogram"), by Ricerca Corrente grants from the Italian Ministry of Health to FDB and LB-L and by Fondazione Bambino Gesu'grant to LB-L. Single-cell RNA sequencing data were funded by Ricerca Finalizzata Ministero della Salute (GR-2018-12366992) for SA and Research into Inflammatory Arthritis Centre Versus Arthritis (RACE 20298 & 22072) for MK-S. The grantors were not involved in the study design, or in the analysis and interpretation of the data.

ACKNOWLEDGMENTS

The authors wish to thank Dr Frank Longo (University of Stanford, CA, USA) for kindly providing the p75NTR inhibitor LM11-A31.

SUPPLEMENTARY MATERIAL

The Supplementary Material for this article can be found online at: https://www.frontiersin.org/articles/10.3389/fimmu.2022.818630/full#supplementary-material

Supplementary Figure 1 | Violin plots showing NGF, NGFR, NTRK1 and SORT1 gene expression in distinct stromal cells clusters from synovial tissue of naive to treatment RA (n=4) and RA in sustained clinical and ultrasound remission (n=4). Data are reported as mean (white dot).

Supplementary Figure 2 | (A) Western Blot for p75NTR confirmed protein overexpression of p75NTR in RA-FLS (n=3) compared to skin-FB (CTRL). **(B)** Sortilin expression in RA-FLS (n=8), OA-FLS (n=6) and CTRL-FB (n=5) showed the same expression pattern of p75NTR. **(C)** Increase of p75NTR expression in RA-FLS is dose–dependently induced by IL-1β. Results are compared to unstimulated condition and calculated as Fold Change (F.C.) and represent the mean ± SEM of 5 independent experiments. Differences between groups were analyzed using

unpaired *t*-test (*p<0.05, **p<0.01). **(D)** RA-FLS stimulated with different doses of IL-1β showed a dose-dependent increase of NGF mRNA. The data represent the mean ± SEM of 5 independent experiments. Results were compared to unstimulated condition and calculated as Fold Change (F.C.) using unpaired *t*-test (**p<0.01, ***p<0.001).

Supplementary Figure 3 | LM11A-31 (10nM) was used to inhibit proNGF binding to p75NTR in RA-FLS activated using 100 ng/ml TNF-α, 100 ng/ml LPS or 1 ng/ml IL-1β. The production of IL-6 **(A)**, IL-8 **(B)** and MCP1 **(C)** in RA-FLS cultured in 10% FBS DMEM was measured in the conditioned media after 18 hours of incubation. p75NTR was neutralized using a specific anti-p75NTR antibody (2,5 µg/ml) and the release of IL-6 was measured in RA-FLS activated with 100 ng/ml TNF-α **(D)**, 100 ng/ml LPS **(E)** or 1ng/ml IL-1β **(F)**. In this set of experiments (n=6) cells were cultured in 10% FBS DMEM for 18 hours. All the results are expressed as pg/ml.

Supplementary Figure 4 | (A) The addition of exogenous proNGF (200ng/ml) to RA-FLS, cultured in a chemically defined medium, enhances the production of IL-6 in RA-FLS activated with sub-optimal doses of IL-1β (IL-1β 10-50-100 pg/ml). The increase of IL-6 induced by exogenous proNGF (IL-1b+pNGF) is blocked by p75NTR inhibition with 10nM LM11A-31 (IL-1b+i31). IL-1β-activated RA-FLS show a similar IL-6 reduction when p75NTR was inhibited (IL-1b+i31). To interpret this data, it should be considered that LM11A-31 prevents the binding of the endogenously-produced proNGF to p75NTR, whose synthesis is strongly activated in RA-FLS by IL-1β stimulation (see **Figures 3A**–**C**, **Supplementary 2D**). The data represent the mean ± SEM, results were analyzed using paired *t*-test (*p<0.05). **(B)** Western Blot analysis showed that almost only proNGF forms were detectable in synovial fluids of patients (40 µg total protein). Very low protein levels of mature NGF were observed. 10% reducing gels were incubated with anti-NGF M20 antibody that recognizes both mNGF and proNGF forms.

REFERENCES

1. Minnone G, De Benedetti F, Bracci-Laudiero L. NGF and Its Receptors in the Regulation of Inflammatory Response. *Int J Mol Sci* (2017) 18. doi: 10.3390/ijms18051028
2. Hattori A, Iwasaki S, Murase K, Tsujimoto M, Sato M, Hayashi K, et al. Tumor Necrosis Factor Is Markedly Synergistic With Interleukin 1 and Interferon-Gamma in Stimulating the Production of Nerve Growth Factor in Fibroblasts. *FEBS Lett* (1994) 340:177–80. doi: 10.1016/0014-5793(94)80132-0
3. Takano S, Uchida K. Nerve Growth Factor Regulation by TNF-α and IL-1β in Synovial Macrophages and Fibroblasts in Osteoarthritic Mice. *J Immunol Res* (2016) 2016:5706359. doi: 10.1155/2016/5706359
4. Aloe L, Tuveri MA, Carcassi U, Levi-Montalcini R. Nerve Growth Factor in the Synovial Fluid of Patients With Chronic Arthritis. *Arthritis Rheum* (1992) 35:351–5. doi: 10.1002/art.1780350315
5. Falcini F, Matucci Cerinic M, Lombardi A, Generini S, Pignone A, Tirassa P, et al. Increased Circulating Nerve Growth Factor Is Directly Correlated With Disease Activity in Juvenile Chronic Arthritis. *Ann Rheum Dis* (1996) 55:745–8. doi: 10.1136/ard.55.10.745
6. Halliday DA, Zettler C, Rush RA, Scicchitano R, Mcneil JD. Elevated Nerve Growth Factor Levels in the Synovial Fluid of Patients With Inflammatory Joint Disease. *Neurochem Res* (1998) 23:919–22. doi: 10.1023/A:1022475432077
7. Aloe L, Probert L, Kollias G, Bracci-Laudiero L, Spillantini MG, Montalcini R. The Synovium of Transgenic Arthritic Mice Expressing Human Tumor Necrosis Factor Contains a High Level of Nerve Growth Factor. *Growth Factors* (1993) 9:149–55. doi: 10.3109/08977199309010830
8. Manni L, Lundeberg T, Tirassa P, Aloe L. Role of Cholecystokinin-8 in Nerve Growth Factor and Nerve Growth Factor mRNA Expression in Carrageenan-Induced Joint Inflammation in Adult Rats. *Rheumatol (Oxford)* (2002) 41:787–92. doi: 10.1093/rheumatology/41.7.787
9. Seidah NG, Benjannet S, Pareek S, Savaria D, Hamelin J, Goulet B, et al. Cellular Processing of the Nerve Growth Factor Precursor by the Mammalian Pro-Protein Convertases. *Biochem J* (1996) 314(Pt 3):951–60. doi: 10.1042/bj3140951
10. Bruno MA, Cuello AC. Activity-Dependent Release of Precursor Nerve Growth Factor, Conversion to Mature Nerve Growth Factor, and Its Degradation by a Protease Cascade. *Proc Natl Acad Sci USA* (2006) 103:6735–40. doi: 10.1073/pnas.0510645103
11. Lee R, Kermani P, Teng KK, Hempstead BL. Regulation of Cell Survival by Secreted Proneurotrophins. *Science* (2001) 294:1945–8. doi: 10.1126/science.1065057
12. Nykjaer A, Lee R, Teng KK, Jansen P, Madsen P, Nielsen MS, et al. Sortilin Is Essential for proNGF-Induced Neuronal Cell Death. *Nature* (2004) 427:843–8. doi: 10.1038/nature02319
13. D'onofrio M, Paoletti F, Arisi I, Brandi R, Malerba F, Fasulo L, et al. NGF and proNGF Regulate Functionally Distinct mRNAs in PC12 Cells: An Early Gene Expression Profiling. *PloS One* (2011) 6:e20839. doi: 10.1371/journal.pone.0020839
14. Soligo M, Albini M, Bertoli FL, Marzano V, Protto V, Bracci-Laudiero L, et al. Different Responses of PC12 cells to Different Pro-Nerve Growth Factor Protein Variants. *Neurochem Int* (2019) 129:104498. doi: 10.1016/j.neuint.2019.104498
15. Fahnestock M, Michalski B, Xu B, Coughlin MD. The Precursor Pro-Nerve Growth Factor Is the Predominant Form of Nerve Growth Factor in Brain and Is Increased in Alzheimer's Disease. *Mol Cell Neurosci* (2001) 18:210–20. doi: 10.1006/mcne.2001.1016
16. Bierl MA, Jones EE, Crutcher KA, Isaacson LG. 'Mature' Nerve Growth Factor Is a Minor Species in Most Peripheral Tissues. *Neurosci Lett* (2005) 380:133–7. doi: 10.1016/j.neulet.2005.01.029
17. Ali TK, Al-Gayyar MM, Matragoon S, Pillai BA, Abdelsaid MA, Nussbaum JJ, et al. Diabetes-Induced Peroxynitrite Impairs the Balance of Pro-Nerve Growth Factor and Nerve Growth Factor, and Causes Neurovascular Injury. *Diabetologia* (2011) 54:657–68. doi: 10.1007/s00125-010-1935-1
18. Reinshagen M, Rohm H, Steinkamp M, Lieb K, Geerling I, Von Herbay A, et al. Protective Role of Neurotrophins in Experimental Inflammation of the Rat Gut. *Gastroenterology* (2000) 119:368–76. doi: 10.1053/gast.2000.9307
19. Villoslada P, Hauser SL, Bartke I, Unger J, Heald N, Rosenberg D, et al. Human Nerve Growth Factor Protects Common Marmosets Against Autoimmune Encephalomyelitis by Switching the Balance of T Helper Cell Type 1 and 2 Cytokines Within the Central Nervous System. *J Exp Med* (2000) 191:1799–806. doi: 10.1084/jem.191.10.1799
20. Prencipe G, Minnone G, Strippoli R, De Pasquale L, Petrini S, Caiello I, et al. Nerve Growth Factor Downregulates Inflammatory Response in Human Monocytes Through TrkA. *J Immunol* (2014) 192:3345–54. doi: 10.4049/jimmunol.1300825
21. Minnone G, Soligo M, Caiello I, Prencipe G, Manni L, Marafon DP, et al. ProNGF-P75ntr Axis Plays a Proinflammatory Role in Inflamed Joints: A Novel Pathogenic Mechanism in Chronic Arthritis. *RMD Open* (2017) 3:e000441. doi: 10.1136/rmdopen-2017-000441
22. Bartok B, Firestein GS. Fibroblast-Like Synoviocytes: Key Effector Cells in Rheumatoid Arthritis. *Immunol Rev* (2010) 233:233–55. doi: 10.1111/j.0105-2896.2009.00859.x
23. Aletaha D, Neogi T, Silman AJ, Funovits J, Felson DT, Bingham CO, et al. 2010 Rheumatoid Arthritis Classification Criteria: An American College of Rheumatology/European League Against Rheumatism Collaborative Initiative. *Arthritis Rheum* (2010) 62:2569–81. doi: 10.1002/art.27584
24. Guerne PA, Zuraw BL, Vaughan JH, Carson DA, Lotz M. Synovium as a Source of Interleukin 6 *In Vitro*. Contribution to Local and Systemic Manifestations of Arthritis. *J Clin Invest* (1989) 83:585–92. doi: 10.1172/JCI113921
25. Massa SM, Xie Y, Yang T, Harrington AW, Kim ML, Yoon SO, et al. Small, Nonpeptide P75ntr Ligands Induce Survival Signaling and Inhibit proNGF-Induced Death. *J Neurosci* (2006) 26:5288–300. doi: 10.1523/JNEUROSCI.3547-05.2006
26. Cheleschi S, Cantarini L, Pascarelli NA, Collodel G, Lucherini OM, Galeazzi M, et al. Possible Chondroprotective Effect of Canakinumab: An *In Vitro* Study on Human Osteoarthritic Chondrocytes. *Cytokine* (2015) 71:165–72. doi: 10.1016/j.cyto.2014.10.023
27. Alivernini S, Macdonald L, Elmesmari A, Finlay S, Tolusso B, Gigante MR. Distinct Synovial Tissue Macrophage Subsets Regulate Inflammation and

Remission in Rheumatoid Arthritis. *Nat Med* (2020) 26:1295–306. doi: 10.1038/s41591-020-0939-8
28. Alivernini S, Tolusso B, Gessi M, Gigante MR, Mannocci A, Petricca L, et al. Inclusion of Synovial Tissue-Derived Characteristics in a Nomogram for the Prediction of Treatment Response in Treatment-Naive Rheumatoid Arthritis Patients. *Arthritis Rheumatol* (2021) 73:1601–13. doi: 10.1002/art.41726
29. Schmittgen TD, Livak KJ. Analyzing Real-Time PCR Data by the Comparative C(T) Method. *Nat Protoc* (2008) 3:1101–8. doi: 10.1038/nprot.2008.73
30. Soligo M, Protto V, Florenzano F, Bracci-Laudiero L, De Benedetti F, Chiaretti A, et al. The Mature/Pro Nerve Growth Factor Ratio Is Decreased in the Brain of Diabetic Rats: Analysis by ELISA Methods. *Brain Res* (2015) 1624:455–68. doi: 10.1016/j.brainres.2015.08.005
31. Brunner D, Frank J, Appl H, Schöffl H, Pfaller W, Gstraunthaler G. Serum-Free Cell Culture: The Serum-Free Media Interactive Online Database. *Altex* (2010) 27:53–62. doi: 10.14573/altex.2010.1.53
32. Mcinnes IB, Schett G. Cytokines in the Pathogenesis of Rheumatoid Arthritis. *Nat Rev Immunol* (2007) 7:429–42. doi: 10.1038/nri2094
33. Nygaard G, Firestein GS. Restoring Synovial Homeostasis in Rheumatoid Arthritis by Targeting Fibroblast-Like Synoviocytes. *Nat Rev Rheumatol* (2020) 16:316–33. doi: 10.1038/s41584-020-0413-5
34. Schett G, Tohidast-Akrad M, Smolen JS, Schmid BJ, Steiner CW, Bitzan P, et al. Activation, Differential Localization, and Regulation of the Stress-Activated Protein Kinases, Extracellular Signal-Regulated Kinase, C-JUN N-Terminal Kinase, and P38 Mitogen-Activated Protein Kinase, in Synovial Tissue and Cells in Rheumatoid Arthritis. *Arthritis Rheum* (2000) 43:2501–12. doi: 10.1002/1529-0131(200011)43:11<2501::AID-ANR18>3.0.CO;2-K
35. Inoue T, Hammaker D, Boyle DL, Firestein GS. Regulation of JNK by MKK-7 in Fibroblast-Like Synoviocytes. *Arthritis Rheum* (2006) 54:2127–35. doi: 10.1002/art.21919
36. Croft AP, Campos J, Jansen K, Turner JD, Marshall J, Attar M, et al. Distinct Fibroblast Subsets Drive Inflammation and Damage in Arthritis. *Nature* (2019) 570:246–51. doi: 10.1038/s41586-019-1263-7
37. Mizoguchi F, Slowikowski K, Wei K, Marshall JL, Rao DA, Chang SK, et al. Functionally Distinct Disease-Associated Fibroblast Subsets in Rheumatoid Arthritis. *Nat Commun* (2018) 9:789. doi: 10.1038/s41467-018-02892-y
38. Stephenson W, Donlin LT, Butler A. Single-Cell RNA-Seq of Rheumatoid Arthritis Synovial Tissue Using Low-Cost Microfluidic Instrumentation. *Nat Commun* (2018) 9:791. doi: 10.1038/s41467-017-02659-x
39. Zhang F, Wei K, Slowikowski K, Fonseka CY, Rao DA, Kelly S, et al. Defining Inflammatory Cell States in Rheumatoid Arthritis Joint Synovial Tissues by Integrating Single-Cell Transcriptomics and Mass Cytometry. *Nat Commun* (2019) 20:928–42. doi: 10.1038/s41590-019-0378-1
40. Cheng L, Wang Y, Wu R, Ding T, Xue H, Gao C, et al. New Insights From Single-Cell Sequencing Data: Synovial Fibroblasts and Synovial Macrophages in Rheumatoid Arthritis. *Front Immunol* (2021) 12:709178. doi: 10.3389/fimmu.2021.709178
41. Ai R, Laragione T, Hammaker D, Boyle DL, Wildberg A, Maeshima K, et al. Comprehensive Epigenetic Landscape of Rheumatoid Arthritis Fibroblast-Like Synoviocytes. *Nat Commun* (2018) 9:1921. doi: 10.1038/s41467-018-04310-9
42. Doody KM, Bottini N, Firestein GS. Epigenetic Alterations in Rheumatoid Arthritis Fibroblast-Like Synoviocytes. *Epigenomics* (2017) 9:479–92. doi: 10.2217/epi-2016-0151
43. Bottini N, Firestein GS. Duality of Fibroblast-Like Synoviocytes in RA: Passive Responders and Imprinted Aggressors. *Nat Rev Rheumatol* (2013) 9:24–33. doi: 10.1038/nrrheum.2012.190
44. Yang T, Knowles JK, Lu Q, Zhang H, Arancio O, Moore LA, et al. Small Molecule, Non-Peptide P75 Ligands Inhibit Abeta-Induced Neurodegeneration and Synaptic Impairment. *PloS One* (2008) 3:e3604. doi: 10.1371/journal.pone.0003604
45. Simmons DA, Knowles JK, Belichenko NP, Banerjee G, Finkle C, Massa SM, et al. A Small Molecule P75ntr Ligand, LM11A-31, Reverses Cholinergic Neurite Dystrophy in Alzheimer's Disease Mouse Models With Mid- to Late-Stage Disease Progression. *PloS One* (2014) 9:e102136. doi: 10.1371/journal.pone.0102136
46. Casnici C, Lattuada D, Tonna N, Crotta K, Storini C, Bianco F. Optimized "*In Vitro*" Culture Conditions for Human Rheumatoid Arthritis Synovial Fibroblasts. *Mediators Inflamm* (2014) 2014:702057. doi: 10.1155/2014/702057
47. Yang J, Wang J, Liang X, Zhao H, Lu J, Ma Q, et al. Il–1β Increases the Expression of Inflammatory Factors in Synovial Fluid–Derived Fibroblast–Like Synoviocytes *via* Activation of the NF–κb–Mediated ERK–STAT1 Signaling Pathway. *Mol Med Rep* (2019) 20:4993–5001. doi: 10.3892/mmr.2019.10759
48. Barr RK, Bogoyevitch MA. The C-Jun N-Terminal Protein Kinase Family of Mitogen-Activated Protein Kinases (JNK MAPKs). *Int J Biochem Cell Biol* (2001) 33:1047–63. doi: 10.1016/S1357-2725(01)00093-0
49. Fukushima A, Boyle DL, Corr M, Firestein GS. Kinetic Analysis of Synovial Signalling and Gene Expression in Animal Models of Arthritis. *Ann Rheum Dis* (2010) 69:918–23. doi: 10.1136/ard.2009.112201
50. Shanab AY, Mysona BA, Matragoon S, El-Remessy AB. Silencing P75(NTR) Prevents proNGF-Induced Endothelial Cell Death and Development of Acellular Capillaries in Rat Retina. *Mol Ther Methods Clin Dev* (2015) 2:15013. doi: 10.1038/mtm.2015.13
51. Thalhamer T, Mcgrath MA, Harnett MM. MAPKs and Their Relevance to Arthritis and Inflammation. *Rheumatol (Oxford)* (2008) 47:409–14. doi: 10.1093/rheumatology/kem297
52. Mysona BA, Al-Gayyar MM, Matragoon S, Abdelsaid MA, El-Azab MF, Saragovi HU, et al. Modulation of P75(NTR) Prevents Diabetes- and proNGF-Induced Retinal Inflammation and Blood-Retina Barrier Breakdown in Mice and Rats. *Diabetologia* (2013) 56:2329–39. doi: 10.1007/s00125-013-2998-6
53. Elshaer SL, Alwhaibi A, Mohamed R, Lemtalsi T, Coucha M, Longo FM, et al. Modulation of the P75 Neurotrophin Receptor Using LM11A-31 Prevents Diabetes-Induced Retinal Vascular Permeability in Mice *via* Inhibition of Inflammation and the RhoA Kinase Pathway. *Diabetologia* (2019) 62:1488–500. doi: 10.1007/s00125-019-4885-2

Conflict of Interest: FDB has received grants from Abbvie, Novimmune, Sobi, Novartis, Roche, Sanofi, all unconnected with the submitted work. LB-L and FDB are the inventors and OPBG and CNR are the owners of an issued European Patent EP2667895.

The remaining authors declare that the research was conducted in the absence of any commercial or financial relationships that could be construed as a potential conflict of interest.

frontiers in Immunology

ORIGINAL RESEARCH
published: 14 March 2022
doi: 10.3389/fimmu.2022.836837

Can CD200R1 Agonists Slow the Progression of Osteoarthritis Secondary to Injury?

Kathak Vachhani[1,2], *Aaron Prodeus*[2,3], *Sayaka Nakamura*[4,5], *Jason S. Rockel*[4,5], *Adam Hopfgartner*[2], *Mohit Kapoor*[4,5,6], *Jean Gariépy*[2,3], *Cari Whyne*[1,2,6] *and Diane Nam*[2,6]*

[1] Institute of Biomedical Engineering, University of Toronto, Toronto, ON, Canada, [2] Sunnybrook Research Institute, Toronto, ON, Canada, [3] Department of Medical Biophysics, University of Toronto, Toronto, ON, Canada, [4] Division of Orthopaedics, Osteoarthritis Research Program, Schroeder Arthritis Institute, University Health Network, Toronto, ON, Canada, [5] Krembil Research Institute, University Health Network, Toronto, ON, Canada, [6] Division of Orthopedic Surgery, Department of Surgery, University of Toronto, Toronto, ON, Canada

OPEN ACCESS

Edited by:
Gurpreet S. Baht,
Duke University, United States

Reviewed by:
Susanne Wijesinghe,
University of Birmingham,
United Kingdom
Dominika Nanus,
University of Birmingham,
United Kingdom

***Correspondence:**
Diane Nam
diane.nam@sunnybrook.ca

Specialty section:
This article was submitted to Inflammation, a section of the journal Frontiers in Immunology

Received: 16 December 2021
Accepted: 21 February 2022
Published: 14 March 2022

Citation:
Vachhani K, Prodeus A, Nakamura S, Rockel JS, Hopfgartner A, Kapoor M, Gariépy J, Whyne C and Nam D (2022) Can CD200R1 Agonists Slow the Progression of Osteoarthritis Secondary to Injury? Front. Immunol. 13:836837. doi: 10.3389/fimmu.2022.836837

Post-traumatic knee osteoarthritis is characterized by cartilage degeneration, subchondral bone remodeling, osteophyte formation, and synovial changes. Therapeutic targeting of inflammatory activity in the knee immediately post injury may alter the course of osteoarthritis development. This study aimed to determine whether CD200R1 agonists, namely the protein therapeutic CD200Fc or the synthetic DNA aptamer CCS13, both known to act as anti-inflammatory agents, are able to delay the pathogenesis of injury-associated knee osteoarthritis in a murine model. Ten week old male C57BL/6 mice were randomized and surgical destabilization of the medial meniscus (DMM) to induce knee arthritis or sham surgery as a control were performed. CCS13 was evaluated as a therapeutic treatment along with CD200Fc and a phosphate-buffered saline vehicle control. Oligonucleotides were injected intra-articularly beginning one week after surgery, with a total of six injections administered prior to sacrifice at 12 weeks post-surgery. Histopathological assessment was used as the primary outcome measure to assess cartilage and synovial changes, while μCT imaging was used to compare the changes to the subchondral bone between untreated and treated arthritic groups. We did not find any attenuation of cartilage degeneration or synovitis in DMM mice with CD200Fc or CCS13 at 12 weeks post-surgery, nor stereological differences in the properties of subchondral bone. The use of CD200R1 agonists to blunt the inflammatory response in the knee are insufficient to prevent disease progression in the mouse DMM model of OA without anatomical restoration of the normal joint biomechanics.

Keywords: osteoarthritis, DMM, CD200R1, mouse model, aptamer

INTRODUCTION

Post-traumatic knee osteoarthritis is a prevalent musculoskeletal disease leading to significant disability with enormous medical and socioeconomic consequences. It is characterized by articular cartilage degeneration, subchondral bone remodeling, osteophyte formation, and synovial changes, including inflammation.

Arthritic changes begin in the acute phase post-insult and progress ominously to symptomatic osteoarthritis (1, 2). With the goal of reducing the risk of osteoarthritis, surgery to optimize anatomic repair of the joint when possible is the primary management option in traumatic knee injuries. However, eligibility criteria for surgical repair are not well defined and depend on the nature of the injury and patient characteristics. Moreover, a large proportion of joint injuries are of lower severity and managed conservatively. The armamentarium of non-surgical treatments in such cases focuses on providing symptomatic relief and restoring joint mobility, critically leaving the need for arthritic management unmet (3). Therapeutics that can successfully halt the destructive inflammatory activity in the knee immediately after injury represents an ideal non-surgical option to alter the course of osteoarthritis development.

DNA aptamers are oligonucleotides that have shown promise in many applications as both therapeutic and imaging agents to treat patients with inflammatory diseases (4, 5). Aptamers can be developed against any biological targets and thus the resulting agents can be designed to specifically target or modulate key biological processes in humans and animals towards either dampening or augmenting inflammatory responses. Applications for these synthetic aptamers may be potentially found in reducing arthritis symptoms through specifically targeting clinically important immune molecules such as CD200R1, TNFα, and PD-1 (5).

CD200R1 is expressed on the surface of myeloid and lymphoid cells and delivers immune inhibitory signals to modulate inflammation when engaged with its ligand CD200 (6). As such signaling through the CD200R1 pathway plays a prominent role in limiting inflammation in a wide range of immune-related diseases and autoimmune disorders (including rheumatoid arthritis) by increasing the macrophage fusion interaction (formation of osteoclasts) to potentiate bone resorption (6). Our team recently developed a synthetic, pegylated aptamer (pegylated CCS13, referred to herein as CCS13) that acts as an agonist for the inhibitory immune checkpoint receptor CD200R1 (7). The consequence of the CCS13 aptamer binding to CD200R1 present on immune cells is to dampen the production of inflammatory cytokines, reducing the damaging immune responses that typically cause inflammation. This aptamer recognizes both human and mouse CD200R1 and thus can be evaluated in murine models of inflammation, including osteoarthritis.

The objective of this work was to determine whether the CD200R1 agonist aptamer CCS13 or a natural dimeric form of the CD200R1 ligand, namely, CD200Fc can delay the pathogenesis of injury-associated osteoarthritis in a murine model. It was hypothesized that this synthetic oligonucleotide may help reduce the progression of osteoarthritis pathologies including cartilage degeneration, synovitis, and bone remodeling (**Figure 1**).

METHODS

Animal Model

All animal experiments were approved by the Animal Care Committee at Krembil Research Institute. Ten week old male C57BL/6 mice were randomized to destabilization of the medial meniscus (DMM), or sham surgery as a control, as previously described (8). Briefly, right hind limbs were sterilized and a 3mm longitudinal incision was made from distal patella to proximal tibial plateau and the medial meniscotibial ligament was identified. For the DMM group, this ligament was transected, and the destabilization of meniscal tissue was confirmed by

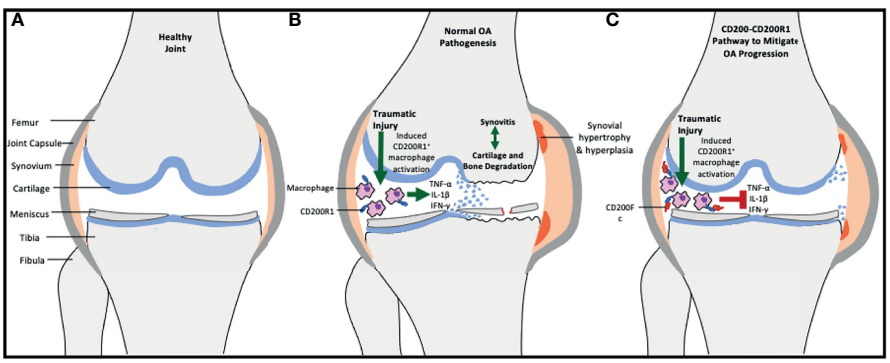

FIGURE 1 | Schematic showing the role of CD200-CD200R1 pathway in osteoarthritis development. **(A)** demonstrates the anatomic structure of a healthy, non-arthritic joint. **(B)** In case of knee traumatic injury, a vicious cycle of reparative processes through inflammatory activity and structural damage is induced, leading to osteoarthritic changes. CD200R1 expressing macrophages are important mediators of synovitis through secretion of pro-inflammatory cytokines. **(C)** By upregulating CD200 expression (via exogenous CD200Fc or CCS13 aptamer), the CD200R1 positive macrophages are inhibited *via* the binding of CD200 to the receptor sites, hence leading to downregulation of proinflammatory cytokines and disruption of the vicious cycle.

lifting the free end of the meniscus. Transection was not performed for sham surgery. The soft tissues and overlaying skin were sutured. Mice were allowed unrestricted access to food and water and were fully weight-bearing on both hind limbs post-surgery. There were six groups (n=8/group) in this study: DMM+PBS, DMM+CCS13, DMM+CD200Fc, SHAM+PBS, SHAM+CCS13, and SHAM+CD200Fc.

Treatment

CCS13 was evaluated as the therapeutic along with CD200Fc and phosphate-buffered saline (PBS; vehicle control). The formulation of CD200Fc and pegylated CCS13 (referred to as CCS13) is described elsewhere (7, 9). PBS or molarity-matched pegylated CCS13 (650 pmol) or CD200Fc (325 pmol) were administered *via* intra-articular injections, (3 microliters each) in the operated knee joints. Injections were started one week after surgery, with six injections administered over the course of the experimental period (**Figure 2**). All mice were sacrificed at 12 weeks post-surgery. Right hind limbs were harvested and immersed in 70% alcohol for fixing the tissue prior to imaging.

Micro-CT Based Stereology

Harvested limbs were vertically aligned and scanned at 10 μm isotropic voxel size using energy settings of 55 kV, 200 μA, and beam hardening correction factor of 1200 mg hydroxyapatite (mgHA) per cm^3 (μCT 100 scanner, Scanco Medical, Brüttisellen, Switzerland). Reconstructed scans were exported as DICOM images and processed in AmiraDEV 5.3.3 (Visualization Sciences Group, FEI). The scans were cropped to bind the proximal tibia extending from the tibial plateau to the proximal tibial growth plate in 3D view. Next, the subchondral trabecular bone was manually segmented from 2D slices in the coronal plane. The resulting 3D ROI was divided through the depression between the intercondylar tubercles into lateral and medial condyles for separate evaluation. Stereological measures of bone volume (BV), total volume (TV), bone volume fraction (BV/TV), bone mineral density (BMD), and bone mineral content (BMC) were computed using CT Analyser software (SkyScan, Kontich, Belgium).

Histology

After CT scanning, the limbs were stored in 70% alcohol until further processing. The specimens were fixed in TissuFix (Chaptec) overnight, decalcified in RDO Rapid Decalcifier (Apex Engineering) for 1.5 hours, refixed in TissuFix overnight, embedded in paraffin, and sectioned. Representative sections from the medial femur and tibia were stained with Safranin O Fast Green (Millipore Sigma) to analyze cartilage degradation (orange-red = proteoglycans, green = collagen/cytoplasm, black = nuclei) and Masson's trichrome (blue = collagen, red = cytoplasm, black = nuclei) to analyze synovitis from 0 (normal) to 3 (severe) using OARSI scoring recommendations for mice (10). The cartilage on the femoral condyle and tibial plateau was scored separately from 0 (normal) to 6 (erosion >75% of articular surface) using the OARSI scoring system. Synovitis was scored from 0 (no synovitis) to 3 (severe synovitis) considering collagen deposition, cell infiltration, tissue thickness and tissue invasion onto the cartilage surface.

Statistical Analysis

Mean values were compared for the primary outcome measures of synovitis and tibial plateau scores using one-way analysis of variance test (SPSS V18, IBM, IL, USA) between the six groups. One-way ANOVA and Student's T-test with Sidak correction was used to compare stereological measures between groups. Results are reported as mean ± standard deviation. For all analyses, $p<0.05$ was considered significant.

RESULTS

No mice were lost during the experimental period. Two animals, one from SHAM+CCS13 and the second from SHAM+PBS, were excluded from all analysis as the specimens were damaged during the harvest procedure.

Histology

Average OARSI scores from safranin O-stained sections as a measure of cartilage degradation in the DMM+PBS group were

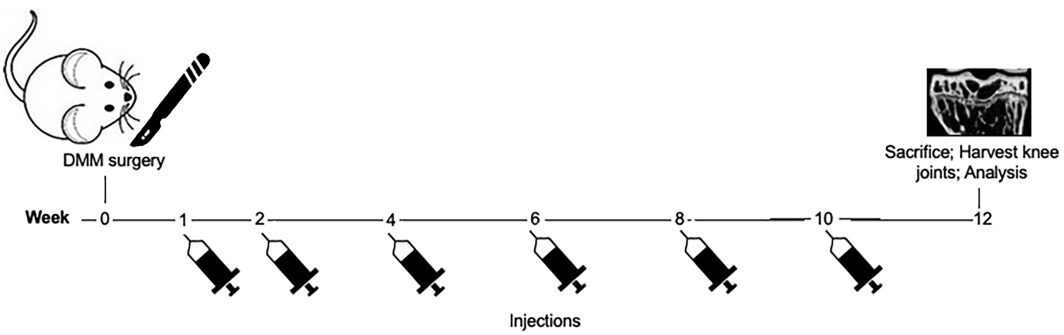

FIGURE 2 | Schematic showing the protocol for treatment following DMM surgery. Knee surgery (sham or destabilization of medial meniscus) was performed on day 0. Intra-articular injections of either PBS (control), CD200Fc, or CCS13 were given in the healing joint at weeks 1, 2, 4, 6, 8, and 10. All mice were sacrificed at week 12 and the healing knee joints were analyzed *via* histology and microCT imaging.

2.63 ± 1.19 for the femoral condyle and 3.38 ± 0.92 for the tibial plateau, which was indicative of moderate arthritis (**Figure 3**). These were significantly higher compared to average scores for SHAM+PBS group (healthy control; femoral condyle: 0.69 ± 0.59, p<0.01; tibial plateau: 1.19 ± 0.92, p<0.01). CCS13- treated DMM group had similar OARSI cartilage degeneration scores (femoral condyle:3.25 ± 1.16; tibial plateau: 3.75 ± 1.28) to the DMM+PBS group (femoral condyle:2.63 ± 1.19, p=0.31; tibial plateau: 3.38 ± 0.92, p=0.51). Moderate synovitis, as indicated by synovitis scores, was observed in all DMM groups (**Figure 3**). These data suggest that the dosing regimen of CCS13 in this does not attenuate mouse DMM-induced OA.

Bone Stereology

Figure 4A shows 3D models with coronal slices of knee joints at 12 weeks post-injury and **Figure 4B** shows means and standard deviations for stereological parameters at this timepoint. SHAM+CD200Fc had higher average total volume of subchondral bone compared to SHAM+PBS for lateral tibia (difference: 0.12 ± 0.04cm^3; p=0.07) and medial tibia (difference: 0.21 ± 0.05cm^3; p<0.01) indicating effect of CD200Fc injectable on bone tissue. For lateral tibia, DMM+PBS group had significantly higher average total volume compared to the SHAM+PBS group (difference: 0.14 ± 0.01cm^3, p=0.01), however, the two groups had similar bone volume (difference: 0.04 ± 0.02cm^3; p=0.09) and bone volume fraction (difference: -1.59 ± 0.95%, p=0.43). For medial tibia, DMM+PBS was similar to SHAM+PBS in bone properties. Compared to the DMM+PBS group, DMM+CCS13 had significantly higher bone volume (difference: 0.12 ± 0.03cm^3, p=0.01) and total volume (difference: 0.18 ± 0.05cm^3, p=0.02) but similar bone volume fraction (difference: 1.80 ± 2.43%, p=1). In comparison to SHAM+CD200Fc, DMM+CD200Fc group had significantly lower total volume (difference: -0.16 ± 0.04cm^3, p=0.01), higher bone volume fraction (difference: 7.32 ± 0.59%, p<0.01), and higher BMD (difference:13.69 ± 0.79mgHA/cm^3, p<0.01). No significant differences were seen between DMM+SHAM and DMM+CD200Fc or DMM+SHAM and DMM+CCS13 (**Figure 4B**).

DISCUSSION

To our knowledge, this is the first study to assess the therapeutic potential of the CD200-CD200R1 pathway in osteoarthritis. We evaluated the effect of upregulating CD200Fc and CD200Fc-based aptamer, CCS13, in a meniscal tear model. We utilized histopathology as the primary outcome measure to assess soft tissue changes, and μCT imaging to compare the changes in the subchondral bone between untreated and treated arthritic groups. Our analyses did not find any maintenance of cartilage tissue integrity in the disease state with the dose and intra-articular injection regimen of CD200Fc or CCS13 12 weeks post-injury. Similar to some previous studies, there were no stereological differences in the properties of subchondral bone between SHAM+PBS and DMM+PBS groups at 12 weeks as well as no differences between the DMM+PBS and the treated DMM groups at this timepoint (11, 12).

The search for therapeutic targets in osteoarthritis has failed to yield clinically translatable drugs that effectively attenuates disease progression in patients. An important shortcoming in previous works, which this study aimed to overcome, was targeting specific cytokines to dampen inflammation-induced damage. Osteoarthritis is complex and the strategy of targeting singular pro-inflammatory markers (most notably IL-1β) to tackle the disease, at least systemically, has been recognized as

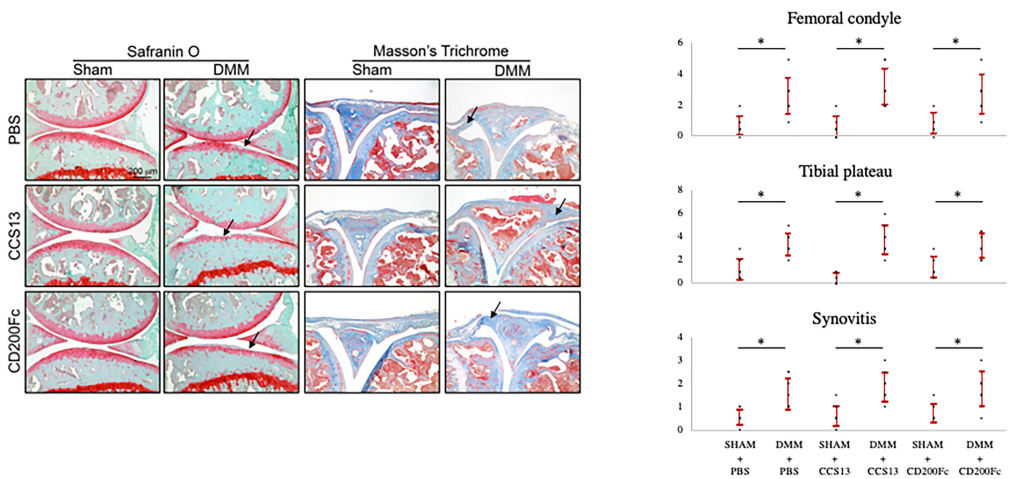

FIGURE 3 | Histology images and scores of representative stained knee sections. [1]The extent of cartilage loss in the femoral condyle and tibial plateau was scored separately using the OARSI scoring system: 0 [normal] to 6[erosion>75% of articular surface]. Synovitis was scored from 0 (normal) to 3 (severe). Safranin O-stained sections were used to score cartilage degeneration and Masson's trichrome-stained sections were used to measure synovitis. Black arrows indicate areas of cartilage degeneration and synovitis in Safranin O or Masson's Trichome-stained sections respectively. [2]Dots represent individual data points and error bar represents standard deviation. [3]Statistical analysis was conducted using one-way analysis of variance test to compare the six groups. *p < 0.05.

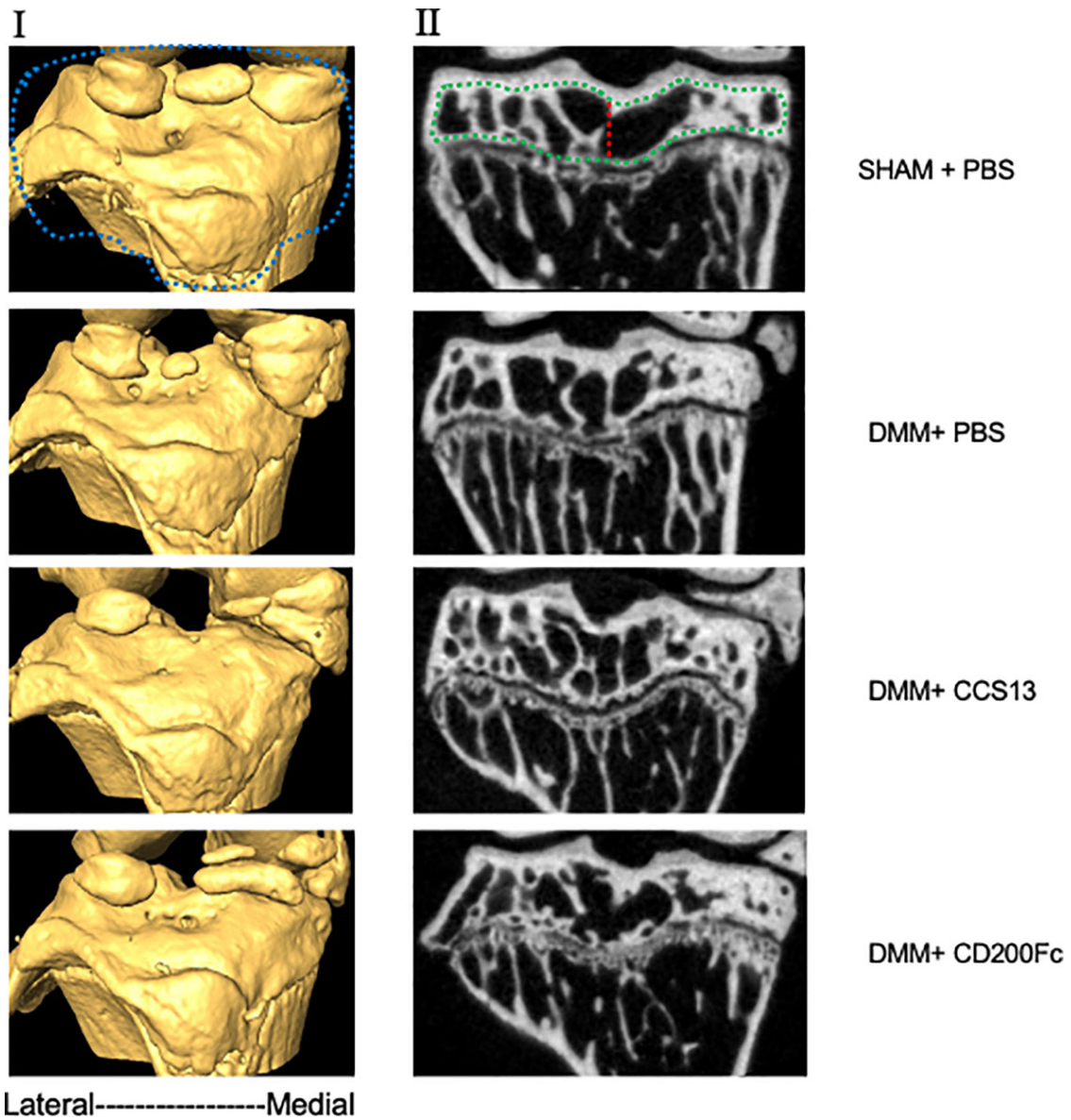

FIGURE 4 | MicroCT images of representative specimens (3D model in panel I and 2D coronal slices in panel II). Stereological analysis involved a series of cropping steps in order to isolate the region of interest. First, the epiphyseal region, demarcated by blue line, was crudely selected in the 3D reconstructed model. Next, the subchondral trabecular bone (green line) was segmented in 2D slices. Finally, the segmented slices were merged and divided into lateral and medial halves (red line) and analyzed separately.

ineffective (13). In contrast, upstream targets, like macrophages themselves, offers better opportunities to control cytokine release and cell signaling, and hence modulate the biochemical response in osteoarthritis (14, 15).

CD200Fc attenuates early arthritic changes in animal models of rheumatoid arthritis. In the collagen-induced rheumatoid arthritis model, CD200Fc treatment significantly lowers expression of pro-inflammatory cytokines (IL-1β and TNFα) and lowers disease severity at 10 days post disease induction (16, 17). Our study was based on positive findings in the rheumatoid models as the etiology of osteoarthritis is similarly driven, in part, by inflammatory activity. In osteoarthritis, the acute phase after an injury is marked by infiltration of monocytes and macrophages to respond to the cellular damage, followed by a sustained low-grade inflammation in response to, albeit also causing, cartilage thinning and bone surface erosion (17). As such, suppressing pro-inflammatory myeloid cells *via* the CD200-CD200R1 pathway presents an opportunity to break the cycle that causes joint destruction following injury.

The distinction between the pathophysiology of osteoarthritis and rheumatoid arthritis may explain why CD200 based treatment failed in the osteoarthritis model despite being successful in the rheumatoid model. Unlike rheumatoid arthritis, the process of osteoarthritis involves dysfunctional biomechanics due to loss of structural integrity in addition to the altered biochemical activity (18). When left unrepaired, abnormal joint loading translates to persistent micro-damage with joint use, which further aggravates tissue damage and immune response. Thus, anti-inflammatory treatment may be sufficient to break the autoimmune cycle in rheumatoid arthritis which has no inciting traumatic intra-articular internal derangements, but it may not be sufficient in arthritic conditions resulting from repetitive damage occurring with dysfunctional joint loading from injury. To assess the role of joint biomechanics in driving osteoarthritic changes, Heard et al. (19) used a sheep anterior cruciate ligament (ACL) tear model (19). Grafting was performed as the intervention to restore mechanical stability and disease burden in these animals was compared with sham surgery controls and healthy controls. Despite the repair, acute inflammation was noted at two weeks post-surgery and could not be rescued by surgical intervention. However, the levels of inflammatory cytokines were restored to that of healthy controls by 20 weeks, indicating that surgical management with repair of the tear to restore the normal joint stability can delay osteoarthritis by preventing ongoing micro-trauma.

The parameters for treatment were chosen to maximize the benefit from treatments while being mindful of the clinical translatability of the regimen. CD200R1 are found on macrophages and macrophages are highly expressed, albeit in a cyclic manner, during the entirety of osteoarthritis (15, 20). As such, we opted for repeated, local delivery of CD200R1 agonist to target the persistent inflammation driven by macrophages. The following paragraphs describe the rationale for the choices made with respect to the treatment regimen. We also highlight areas of improvement that may be considered in designing exploratory drug studies in osteoarthritis.

Treatment onset was one week after DMM surgery. As the joint space is 5-10ul in volumetric size, injecting 3ul of drug dose in a swollen, injured joint may incite further inflammation (21, 22). However, this treatment timing implied that the initial surge of macrophage activity, which occurs at day 0-1 post-injury, was not targeted. Whether starting the treatment earlier (to curb the acute pro-inflammatory activity) would have translated to a chronic delay in the development of arthritic changes is uncertain.

The maximal frequency for treatment doses was deemed to be one time per week. More frequent injections in an already damaged intra-articular region may negatively impact healing. From a clinical standpoint, high frequency of knee injections is not a feasible strategy due to cost and long-term adherence associated with the management of osteoarthritis. Modulating other aspects of the dosing regimen and timepoint of analysis may be considered in future exploration of CD200 based therapeutics for osteoarthritis. As well, utilizing larger animals with similar knee size as humans may represent a more relevant strategy when testing therapeutics requiring frequent (for instance, once a week) injections.

Only limited dosing regimens were explored in this study, as described above. Further work may consider different dosing regimens and their utilization in combination with surgical meniscal repair to assess the full potential of CD200R1 agonists in halting arthritic changes. An additional methodological limitation is that immunostaining with CD200R1 antibody was not performed in this study. Analyzing the expression of CD200R1-positive immune cells should be considered in future work particularly to better understand if alternate treatment regimens may be effective. Finally, the study design did not involve serial analysis at multiple time points. As such, temporary benefits, if any, in the acute phase following drug injection remain unknown. However, clinical translation of short-term gain that does not result in a long-term benefit or symptom delay is not relevant in the management of a chronic disease like osteoarthritis. Patients with a traumatic knee injury would benefit most from treatments that can delay osteoarthritis in the range of months to years.

Nearly 50% of patients with traumatic knee injury develop OA (23). There remains a significant need for strategies to reduce chronic post-traumatic inflammation that contributes to the degenerative process of osteoarthritis that afflicts millions of individuals. While the use of aptamer interventions to blunt the persistence of the inflammatory response may be effective, it appears that without anatomical restoration of the normal joint biomechanics, biochemical treatments alone are insufficient to prevent disease progression. Even with surgical treatment to correct traumatic joint injuries, while the onset of osteoarthritis may be delayed, it does not entirely prevent degenerative changes leading to symptomatic presentation. Therefore, in appreciating the significance of the synergistic role of biomechanics and biochemical activity in osteoarthritis, future work may be directed at exploring the CD200-CD200R1 pathway in the context of surgically repaired joints.

DATA AVAILABILITY STATEMENT

The raw data supporting the conclusions of this article will be made available by the authors, without undue reservation.

ETHICS STATEMENT

The animal study was reviewed and approved by Animal Care Committee at Krembil Research Institute.

AUTHOR CONTRIBUTIONS

KV: Methodology, Experiments, Formal Analysis, Manuscript Writing, and Editing. AP: Methodology, Experiments, Formal Analysis. SN: Methodology, Experiments, Formal Analysis. JR: Methodology, Formal Analysis, and Manuscript Review and Editing. AH: Manuscript Writing and Editing. MK: Methodology, Manuscript Review and Editing, Funding Acquisition, and

Supervision. JG: Funding Acquisition, Conceptualization, Methodology, Manuscript Review and Editing, and Supervision. CW: Funding Acquisition, Conceptualization, Methodology, Resource Provision, Manuscript Writing and Editing, and Supervision. DN: Funding Acquisition, Conceptualization, Methodology, Resource Provision, Manuscript Writing and Editing, Supervision, and Project Administration. All authors contributed to the article and approved the submitted version.

FUNDING

Support for this study was provided by FED DEV Ontario, CIHR operating grants 125862 and 148556 (JG) with matching from D5Pharma (in kind) and the Holland Bone and Joint Collaborative Research Innovation Fund (DN and CW). Animal studies in part were supported by the Tier 1 Canada Research Chair Award (MK).

REFERENCES

1. Muthuri SG, McWilliams DF, Doherty M, Zhang W. History of Knee Injuries and Knee Osteoarthritis: A Meta-Analysis of Observational Studies. *Osteoarthritis Cartilage* (2011) 19(11):1286–93. doi: 10.1016/j.joca.2011.07.015
2. Silverwood V, Blagojevic-Bucknall M, Jinks C, Jordan JL, Protheroe J, Jordan KP. Current Evidence on Risk Factors for Knee Osteoarthritis in Older Adults: A Systematic Review and Meta-Analysis. *Osteoarthritis Cartilage* (2015) 23(4):507–15. doi: 10.1016/j.joca.2014.11.019
3. Glyn-Jones S, Palmer AJ, Agricola R, Price AJ, Vincent TL, Weinans H, et al. Osteoarthritis. *Lancet* (2015) 386(9991):376–87. doi: 10.1016/S0140-6736(14)60802-3
4. Kaur H, Bruno JG, Kumar A, Sharma TK. Aptamers in the Therapeutics and Diagnostics Pipelines. *Theranostics* (2018) 8(15):4016. doi: 10.7150/thno.25958
5. Shatunova EA, Korolev MA, Omelchenko VO, Kurochkina YD, Davydova AS, Venyaminova AG, et al. Aptamers for Proteins Associated With Rheumatic Diseases: Progress, Challenges, and Prospects of Diagnostic and Therapeutic Applications. *Biomedicines* (2020) 8(11):527. doi: 10.3390/biomedicines8110527
6. Gorczynski RM. CD200: CD200R-Mediated Regulation of Immunity. *Int Scholarly Res Notices* (2012) 2012. doi: 10.5402/2012/682168
7. Prodeus A, Sparkes A, Fischer NW, Cydzik M, Huang E, Khatri I, et al. A Synthetic Cross-Species CD200R1 Agonist Suppresses Inflammatory Immune Responses In Vivo. *Mol Therapy-Nucleic Acids* (2018) 12:350–8. doi: 10.1016/j.omtn.2018.05.023
8. Glasson SS, Blanchet TJ, Morris EA. The Surgical Destabilization of the Medial Meniscus (DMM) Model of Osteoarthritis in the 129/SvEv Mouse. *Osteoarthritis Cartilage* (2007) 15(9):1061–9. doi: 10.1016/j.joca.2007.03.006
9. Prodeus A, Cydzik M, Abdul-Wahid A, Huang E, Khatri I, Gorczynski R, et al. Agonistic CD200R1 DNA Aptamers are Potent Immunosuppressants That Prolong Allogeneic Skin Graft Survival. *Mol Therapy-Nucleic Acids* (2014) 3:e190. doi: 10.1038/mtna.2014.41
10. Glasson SS, Chambers MG, Van Den Berg WB, Little CB. The OARSI Histopathology Initiative–Recommendations for Histological Assessments of Osteoarthritis in the Mouse. *Osteoarthritis Cartilage* (2010) 18:S17–23. doi: 10.1016/j.joca.2010.05.025
11. Botter SM, van Osch GJ, Clockaerts S, Waarsing JH, Weinans H, van Leeuwen JP. Osteoarthritis Induction Leads to Early and Temporal Subchondral Plate Porosity in the Tibial Plateau of Mice: An *In Vivo* Microfocal Computed Tomography Study. *Arthritis Rheumatism* (2011) 63(9):2690–9. doi: 10.1002/art.30307
12. Sambamurthy N, Zhou C, Nguyen V, Smalley R, Hankenson KD, Dodge GR, et al. Deficiency of the Pattern-Recognition Receptor CD14 Protects Against Joint Pathology and Functional Decline in a Murine Model of Osteoarthritis. *PloS One* (2018) 13(11):e0206217. doi: 10.1371/journal.pone.0206217
13. Vincent TL. IL-1 in Osteoarthritis: Time for a Critical Review of the Literature. *F1000Research* (2019) 8. doi: 10.12688/f1000research.18831.1
14. Kraus VB, McDaniel G, Huebner JL, Stabler TV, Pieper CF, Shipes SW, et al. Direct *In Vivo* Evidence of Activated Macrophages in Human Osteoarthritis. *Osteoarthritis Cartilage* (2016) 24(9):1613–21. doi: 10.1016/j.joca.2016.04.010
15. Zhang H, Cai D, Bai X. Macrophages Regulate the Progression of Osteoarthritis. *Osteoarthritis Cartilage* (2020) 28(5):555–61. doi: 10.1016/j.joca.2020.01.007
16. Šimelyte E, Criado G, Essex D, Uger RA, Feldmann M, Williams RO. CD200-FC, a Novel Antiarthritic Biologic Agent That Targets Proinflammatory Cytokine Expression in the Joints of Mice With Collagen-Induced Arthritis. *Arthritis Rheumatism* (2008) 58(4):1038–43. doi: 10.1002/art.23378
17. Lieberthal J, Sambamurthy N, Scanzello CR. Inflammation in Joint Injury and Post-Traumatic Osteoarthritis. *Osteoarthritis Cartilage* (2015) 23(11):1825–34. doi: 10.1016/j.joca.2015.08.015
18. Guilak F. Biomechanical Factors in Osteoarthritis. *Best Pract Res Clin Rheumatol* (2011) 25(6):815–23. doi: 10.1016/j.berh.2011.11.013
19. Heard BJ, Solbak NM, Achari Y, Chung M, Hart DA, Shrive NG, et al. Changes of Early Post-Traumatic Osteoarthritis in an Ovine Model of Simulated ACL Reconstruction are Associated With Transient Acute Post-Injury Synovial Inflammation and Tissue Catabolism. *Osteoarthritis Cartilage* (2013) 21(12):1942–9. doi: 10.1016/j.joca.2013.08.019
20. Wright GJ, Cherwinski H, Foster-Cuevas M, Brooke G, Puklavec MJ, Bigler M, et al. Characterization of the CD200 Receptor Family in Mice and Humans and Their Interactions With CD200. *J Immunol* (2003) 171(6):3034–46. doi: 10.4049/jimmunol.171.6.3034
21. Chen AL, Desai P, Adler EM, Di Cesare PE. Granulomatous Inflammation After Hylan GF 20 Viscosupplementation of the Knee: A Report of Six Cases. *JBJS* (2002) 84(7):1142–7. doi: 10.2106/00004623-200207000-00008
22. Charalambous CP, Tryfonidis M, Sadiq S, Hirst P, Paul A. Septic Arthritis Following Intra-Articular Steroid Injection of the Knee–a Survey of Current Practice Regarding Antiseptic Technique Used During Intra-Articular Steroid Injection of the Knee. *Clin Rheumatol* (2003) 22(6):386–90. doi: 10.1007/s10067-003-0757-7
23. Lohmander LS, Englund PM, Dahl LL, Roos EM. The Long-Term Consequence of Anterior Cruciate Ligament and Meniscus Injuries: Osteoarthritis. *Am J Sports Med* (2007) 35(10):1756–69. doi: 10.1177/0363546507307396

Conflict of Interest: The authors declare that the research was conducted in the absence of any commercial or financial relationships that could be construed as a potential conflict of interest.

Publisher's Note: All claims expressed in this article are solely those of the authors and do not necessarily represent those of their affiliated organizations, or those of the publisher, the editors and the reviewers. Any product that may be evaluated in this article, or claim that may be made by its manufacturer, is not guaranteed or endorsed by the publisher.

frontiers | Frontiers in Immunology

ORIGINAL RESEARCH
published: 22 April 2022
doi: 10.3389/fimmu.2022.789349

SOX4 and RELA Function as Transcriptional Partners to Regulate the Expression of TNF- Responsive Genes in Fibroblast-Like Synoviocytes

Kyle Jones[1,2], *Sergio Ramirez-Perez*[1,2], *Sean Niu*[1,2], *Umesh Gangishetti*[1,2], *Hicham Drissi*[1,2,3] *and Pallavi Bhattaram*[1,2*]

[1] Department of Orthopaedics, Emory University School of Medicine, Atlanta, GA, United States, [2] Department of Cell Biology, Emory University School of Medicine, Atlanta, GA, United States, [3] Department of Veterans Affairs, Atlanta VA Medical Center, Decatur, GA, United States

OPEN ACCESS

Edited by:
Matthew William Grol, Western University, Canada

Reviewed by:
Kyuho Kang, Chungbuk National University, South Korea
S. Amanda Ali, Henry Ford Health System, United States

***Correspondence:**
Pallavi Bhattaram
pallavi.bhattaram@emory.edu

Specialty section:
This article was submitted to Inflammation, a section of the journal Frontiers in Immunology

Received: *04 October 2021*
Accepted: *15 March 2022*
Published: *22 April 2022*

Citation:
Jones K, Ramirez-Perez S, Niu S, Gangishetti U, Drissi H and Bhattaram P (2022) SOX4 and RELA Function as Transcriptional Partners to Regulate the Expression of TNF- Responsive Genes in Fibroblast-Like Synoviocytes. Front. Immunol. 13:789349. doi: 10.3389/fimmu.2022.789349

SOX4 belongs to the group C of the SOX transcription factor family. It is a critical mediator of tumor necrosis factor alpha (TNF)-induced transformation of fibroblast-like s-ynoviocytes (FLS) in arthritis. In this study we investigated the genome wide association between the DNA binding and transcriptional activities of SOX4 and the NF-kappaB signaling transcription factor RELA/p65 downstream of TNF signaling. We used ChIP-seq assays in mouse FLS to compare the global DNA binding profiles of SOX4 and RELA. RNA-seq of TNF-induced wildtype and *SoxC*-knockout FLS was used to identify the SOX4-dependent and independent aspects of the TNF-regulated transcriptome. We found that SOX4 and RELA physically interact with each other on the chromatin. Interestingly, ChIP-seq assays revealed that 70.4% of SOX4 peak summits were within 50bp of the RELA peak summits suggesting that both proteins bind in close-proximity on regulatory sequences, enabling them to co-operatively regulate gene expression. By integrating the ChIP-seq results with RNA-seq from *SoxC*-knockout FLS we identified a set of TNF-responsive genes that are targets of the RELA-SOX4 transcriptional complex. These TNF-responsive and RELA-SOX4-depenedent genes included inflammation mediators, histone remodeling enzymes and components of the AP-1 signaling pathway. We also identified an autoregulatory mode of *SoxC* gene expression that involves a TNF-mediated switch from RELA binding to SOX4 binding in the 3' UTR of *Sox4* and *Sox11* genes. In conclusion, our results show that SOX4 and RELA together orchestrate a multimodal regulation of gene expression downstream of TNF signaling. Their interdependent activities play a pivotal role in the transformation of FLS in arthritis and in the inflammatory pathology of diverse tissues where RELA and SOX4 are co-expressed.

Keywords: NF-kappaB, SOX4 transcription factor, RelA/p65, synovial fibroblasts (FLS), TNF, rheumatoid arthritis

INTRODUCTION

Fibroblast-like synoviocytes (FLS) are cells that reside in the synovial lining of joints. During homeostasis, FLS maintain the composition of synovial fluid, produce joint lubricating and cartilage protecting proteins. However, during arthritic diseases they undergo epigenetic changes and transform into pathological cells (1). The transformed FLS are a major source of inflammatory cytokines and catabolic enzymes that promote joint degeneration in autoimmune forms of arthritis such as rheumatoid arthritis (RA), juvenile arthritis, and psoriatic arthritis (1, 2). Among the various signaling pathways that drive FLS transformation, NF-kappaB (NF-κB) signaling downstream of Tumor necrosis factor (TNF)-alpha plays a critical role in joint degeneration by driving a wide range of cellular and molecular changes leading to synovial hyperplasia, cartilage degeneration and bone loss (3, 4). Importantly, the genomic and transcriptomic responses of the FLS from TNF-driven arthritis mouse model are largely comparable to the responses FLS from human RA patients (5, 6). RELA/p65 is the transcription factor that mediates gene expression changes induced by the canonical NF-κB signaling pathway (7). Increase in RELA/p65 protein level and activity were reported in the inflamed synovium of osteoarthritis (OA) and RA patients (8, 9). While p50 is a critical co-factor of RELA for the activation of canonical pathway (10), RELA was also shown to interact with other partners such as p300 acetyl transferase, E2F transcription factor 1(E2F1), Activator Protein 1 (AP1) family in a context dependent manner to activate pro-inflammatory gene expression in a variety of tissues and cells (11–13). In a previous study we showed that, simultaneous conditional deletion of the *SoxC* family (SRY-related HMG-box; Group C) of genes in the FLS inhibits synovitis and articular cartilage degeneration in TNF-induced arthritis in mice (14). The goal of this study is to understand the mechanisms underlying the interaction between TNF and its major transcriptional mediator, RELA/p65 with the SOXC family transcription factors and to determine if SOXC proteins act as transcriptional partners of RELA to promote TNF-induced pathological behavior of the FLS.

SOX4, SOX11, and SOX12 form group C of the SOX family of transcription factors (15). Studies from mouse development, showed that *Sox4*, *Sox11* and *Sox12* are co-expressed in various types of progenitor cells, and act largely in redundancy to determine the behavior and survival of the progenitor cells (15, 16). The SOXC proteins possess a highly conserved DNA binding high mobility group (HMG)-box domain, which enables them to bind to similar SOX binding motifs on DNA. However, they possess divergent transactivation domains in their C-terminus, which confers the highest transactivation potential to SOX11, followed by SOX4. SOX12 possess the weakest transactivation domain (17). As a result, knockout of *Sox12* alone does not affect embryonic development (16, 18). We therefore focused on SOX4 and SOX11 in this study. SOX4 is recognized as a master regulator of cell proliferation and metastasis in several cancer types, while SOX11 recognized as a poor prognosis marker in lymphoma and breast cancer subtypes (19, 20). We previously identified that SOXC proteins, SOX4 and SOX11 play a critical role in inflammation-induced pathological behavior of FLS in osteoarthritis (OA) and RA (14). In addition, *Sox4* and *Sox11* overexpression causes articular cartilage degeneration associated with increased expression of ADAMTS4 and ADAMTS5 (21). At the molecular level, SOXC proteins are highly unstable. They are rapidly degraded under basal conditions but are robustly stabilized upon stimulation with proinflammatory cytokines such as TNF, IL-1 and IL-6 (14). In the current study we used genome wide approaches to uncover the interactions between SOX4 and RELA/p65, downstream of TNF signaling. We thus obtained an in depth understanding of the role and mechanisms underlying the activation of the TNF/SOXC molecular axis in FLS transformation.

MATERIALS AND METHODS

Mice and FLS Preparation

All animal experiments were approved and carried out in accordance with the guidelines by the institutional care and use committee (IACUC) at Emory University. FLS were prepared either from wild type or $Sox4^{fl/fl}11^{fl/fl}12^{fl/fl}$ ($SoxC^{fl/fl}$) mice according to a well-established protocol (5, 22). Briefly, fore limbs were separated at the radiocarpal joint while hind limbs were separated at the tibiotalar joint. Skin and nail were removed carefully, and phalanges were separated as to keep the interphalangeal and metacarpophalangeal joints intact. This was followed by a first Collagenase IV (Sigma-Aldrich, 2mg/mL for 30 min) digestion of the isolated joints to remove skin fibroblasts and other surface cells. A second digestion with Collagenase IV (1mg/mL for 2h) was carried out to digest the synovium covering the phalangeal joints. The digests were filtered in a 50-micron cell strainer to remove the undigested bones and debris. The resulting cell suspension containing >90% FLS were cultured in DMEM with 10% fetal bovine serum (Corning) and 1% penicillin/streptomycin for a period of 16h, followed by washing with PBS and changing cell culture medium to remove unattached and dead cells. Upon reaching confluency, the FLS were sub-cultured and utilized between passage 3.

RNA-seq

RNA-seq was performed in triplicates of independent preparations of FLS. $SoxC^{fl/fl}$ FLS at passage 3 were infected with AdCMV5eGFP (control) or AdCMV5Cre (SoxC-knockout) adenovirus (UI Viral Vector Core) at a concentration of 200 pfu/cell, for a period of 24h. FLS were treated with or without 10ng/mL recombinant human TNF (R&D Systems) for the last 16h. Total RNA was extracted and purified using Direct-zol RNA MicroPrep (Zymo Research). Only samples with an RNA integrity number (RIN) >8 were used. Libraries were generated from 250 ng RNA using TruSeq Stranded Total RNA Sample Prep Kit (Illumina). Paired-end 150-base sequence reads at a sequencing depth of 50 million reads per sample were obtained using Illumina HiSeq 2500 System (Novogene). FASTQ files were analyzed using Strand NGS 4.0 software and aligned to the mm10 mouse genome assembly. Quality of sequencing was ensured by plots for measuring per base sequence quality (Q30 = 99%). Duplicate reads were filtered, followed by quantification and normalization using DESeq method.

ChIP-seq

Chromatin was prepared and immunoprecipitated according to the following procedure. Triplicates of wild type mouse FLS containing 40 million cells per replicate were treated with or without 10ng/mL TNF for 16 h, followed by fixation with 1.5% paraformaldehyde. Chromatin was extracted and sheared into 100- to 500-bp fragments using a Bioruptor (Diagenode). 10 µg of antibodies against p65 (Active Motif) or SOX4 (Diagenode), coupled to 20 µl Dynabeads (Life Technologies) were used for immunoprecipitating chromatin from each replicate and DNA was purified by phenol/chloroform/isoamyl alcohol extraction and ethanol precipitation. DNA pooled from the triplicates was used for library preparation. Single-end 50-base sequence reads were obtained at a sequencing depth of 30 million reads per sample using Illumina HiSeq 2500 System and analyzed using ChIP-seq pipeline on Strand NGS 4.0 software. Quality of sequencing was ensured by plots for measuring per base sequence quality (Q30 = 97.8%). Reads were mapped to the mm10 mouse genome build. Peak calling and gene annotation was performed using MACS with an upstream padding distance of 50kb. *De novo* motif enrichment analysis was performed using MEME-ChIP suite (23).

Immunoprecipitation

Wildtype mouse FLS were treated with TNF (10ng/mL) for 16 h. Nuclear extracts were prepared from FLS using NE-PER™ Extraction Reagents (Thermo Scientific) protocol. Immunoprecipitation was carried out by conjugating 5 µg of p65 antibody (Active Motif) or rabbit non-immune IgG (Millipore) to 20 µl Dynabeads (Life Technologies). Cell extracts were added to the conjugated beads overnight and eluted protein was analyzed by western blotting using antibodies against SOX4 (Diagenode), p65 (Cell Signaling) or HDAC1(Cell signaling).

Luciferase Reporter Assays

ChIP-seq enhancer peak regions assigned to *Sox4*, *Sox11*, *Il15* and *Mapk1* were amplified from mouse genomic DNA and cloned into pBV- Luc, a luciferase reporter plasmid with a minimal promoter and very low basal activity (24). These reporter plasmids were co-transfected with 3X-FLAG SOX4 or 3X-FLAG SOX11 expression plasmids (14) into HEK293 cells using Viromer Red reagent (Origene). pSV2bgal plasmid was used as a control for transfection efficiency. Cells were treated with 10ng/mL recombinant TNF (R&D systems) for the last 16h of the 36h transfection period. Luciferase and β-galactosidase activities were assayed using the Dual-light combined reporter gene assay system (Applied Biosystems) using Synergy H1 Multi-Mode Plate Reader (Biotek). Reporter activities were normalized for transfection efficiency and reported as fold change in luciferase activity. Assays were performed as triplicates.

Statistical Analysis

Experiments were performed in triplicates. Differential gene expression in changes in RNA-seq were calculated by Audic Claverie and Benjamini Hochberg false discovery rate for multiple testing correction. p-value cut-off of was set at 0.05. Statistical significance in reporter assays was calculated by student's t-test.

RESULTS

SOX4 and RELA Are Transcriptional Partners

We previously showed that the transcription factor SOX4 plays a role in promoting FLS transformation and thereby TNF-induced arthritogenesis (14). To understand the mechanism underlying the role SOX4 in TNF-induced gene expression we investigated whether SOX4 and the canonical NF-κB signaling transcription factor RELA/p65 are part of the same transcriptional complex. We predicted a potential physical interaction between and SOX4 and RELA and tested it by a co-immunoprecipitation assay. We immunoprecipitated RELA from the nuclear extracts of wildtype mouse FLS that were treated with or without TNF (**Figure 1A**). As reported earlier the level of SOX4 protein was increased upon TNF-treatment. Interestingly, we found that SOX4 co-immunoprecipitated with RELA in mouse FLS both in the presence and absence of TNF. However, the interaction was higher under TNF-treated condition likely due to the expected increase in the nuclear localization of RELA. To determine whether SOX4 and RELA interaction occurs at the genome wide level and to identify the genes co-regulated by SOX4 and RELA, we developed an experimental design involving ChIP-seq and RNA-seq assays (**Table 1**). We first performed ChIP-seq using either SOX4 or RELA antibodies. We found that TNF treatment increased the number of SOX4 and RELA binding peaks by 3-fold. The enrichment of sequencing reads from the around the transcription start sites (**Figure 1B**) and box plots (**Figure 1C**) show increased binding of both SOX4 and RELA antibody on the chromatin from TNF-treated FLS in comparison with the untreated FLS. At the genomic level the SOX4 and RELA peaks were predominantly (50-60%) located upstream of TSS. About 20% percent of the peaks were located in the intronic regions. A small percentage (2-6%) of them were localized the 3' or 5' untranslated regions and even smaller percentage (>1%) of binding was detected in the coding sequence (**Figure 1D**, **Supplementary Tables S1**–**S4**). Based on the physical interaction between RELA and SOX4 we speculated that these proteins might bind in close proximity to each other at a genome wide level. We overlapped the peak summits identified from SOX4 and RELA ChIP-seq experiments under TNF-treated condition to find that 70.4% of the SOX4 peak summits were present within 50bp of a RELA peak summit which we labelled as Group 1. The peaks with SOX4 only or RELA only peaks were labeled as Groups 2 and 3, respectively (**Figure 1E**, **Supplementary Table S5**). The TSS profile plots and the read density heatmaps show that while read density for Group 1 peaks with SOX4-RELA co-binding is enriched in SOX4 and RELA ChIP-seq and as expected the Groups 2 and 3 peaks show a higher enrichment around TSS only in either SOX4 or RELA peaks respectively (**Figures 1F, G**). The genomic tracks for ChiP-seq peaks at representative examples of Groups 1, 2 and 3 further

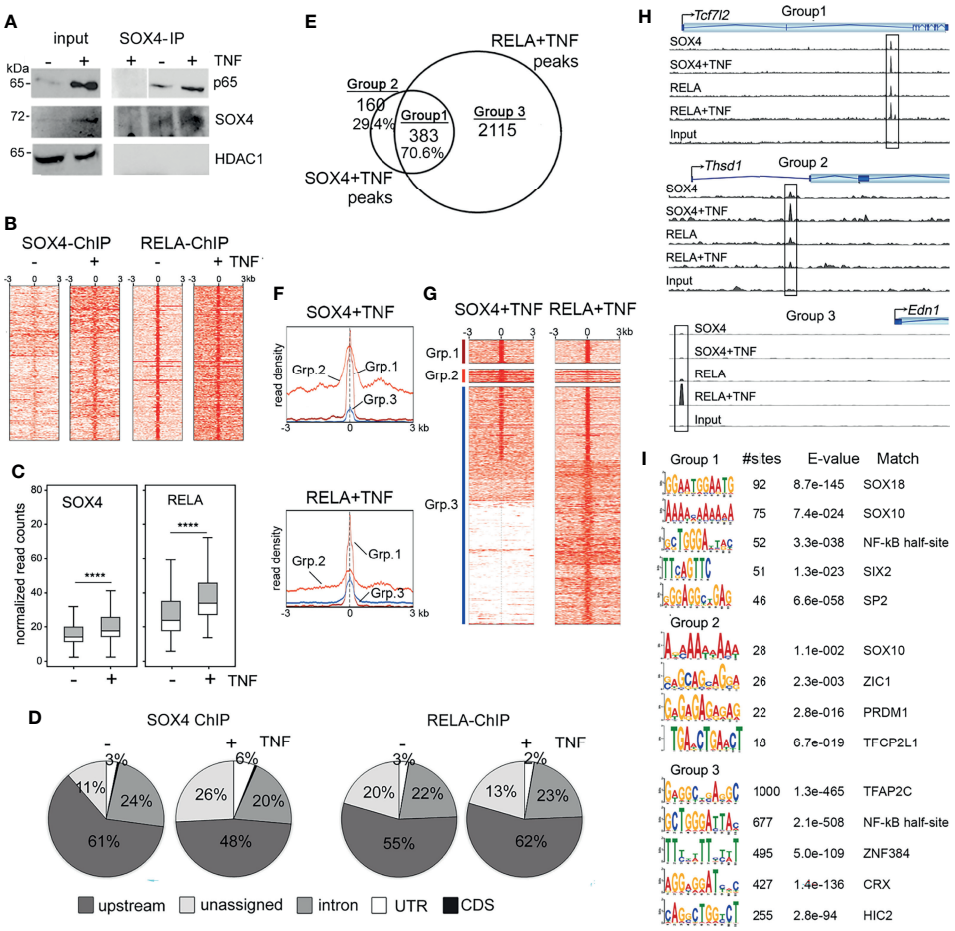

FIGURE 1 | SOX4 and RELA interact on the chromatin **(A)** Immunoprecipitation of nuclear extracts from wildtype FLS treated with or without 10ng/mL TNF for 16 h. Western blot showing lysates and immunoprecipitates detected with the indicated antibodies. **(B)** Heatmap of the read coverage density (more red means more reads at that location) around the transcription start site (TSS) in wildtype FLS treated with or without TNF. **(C)** Box plot representation of normalized read counts in of SOX4 and RELA ChIP-seq peaks. ****p-value < 0.0001 (pairwise t-test adjusted by the Benjamini-Hochberg method). **(D)** Genome wide distribution of SOX4 and RELA ChIP-seq peaks in wildtype FLS treated with or without TNF. **(E)** Venn diagram showing overlap between SOX4 and RELA ChIP-seq peaks that are located within 50bp of each other. **(F)** TSS profile plot and **(G)** Heatmap showing the pattern of binding at the overlapped locations identified by the Venn Diagram in **(F)**. The color bars on the left correspond to Venn Diagram grouping of peaks. **(H)** Genome tracks of SOX4 and RELA ChIP-seq peaks at the loci of representative examples of Group 1, 2 and 3 genes. **(I)** Enriched motifs in the RELA-SOX4 overlapping ChIP-seq peaks in TNF-treated FLS.

demonstrate the co-binding and differential binding of SOX4 and RELA (**Figure 1H**). *De novo* motif search by MEME-ChIP discovered SOX binding motifs as the most frequently identified motif in the SOX4-RELA overlapping peaks, followed by a partial NF-κB as reported for CyclinD1 and Il12β genes (25), SIX2 and SP2 binding motifs. Contrastingly motif analysis of the RELA only peaks did not indicate the enrichment of SOX motifs but were instead enriched with AP-2 and NF-kB binding motifs (**Figure 1I**). To determine the functional roles of the genes co-bound by SOX4 and RELA, we compiled a list of 600 genes that were assigned to the RELA-SOX4 overlapping peaks. Network analysis by Ingenuity Pathway Analysis (IPA) revealed a potential crosstalk between the SOX4 and NF-κB signaling regulated genes (**Supplementary Figure S1A**). At the functional level, the SOX4-RELA genes were predicted to regulate pain signaling pathways, xenobiotic stress and tryptophan metabolism, nitric oxide signaling as well as macrophage, fibroblasts, and endothelial cell activities in rheumatoid arthritis (**Supplementary Figure S1B**).

SOX4 Regulates the Expression of TNF-Responsive Transcriptome

We next investigated whether SOX4 is required for regulating the global TNF-responsive transcriptome by RNA-seq. We generated *SoxC* knockout FLS by infecting $SoxC^{fl/fl}$ with Cre recombinase-expressing adenovirus. Their corresponding controls were generated by infection with GFP-expressing adenovirus. We utilized total *SoxC* knockout background instead of a *Sox4* knockout background because the *SoxC* family genes (*Sox4, Sox11* and *Sox12*) are functionally redundant and possesses a

TABLE 1 | Conceptual design to study the molecular interactions between RELA and SOXC transcription factors.

Step1: ChIP-seq to identify TNF-induced DNA binding of SOX4 & RELA

Wild-type mouse FLS treated w or w/o TNF	
SOX4 antibody	RELA/p65 antibody
Identification of SOX4-RELA co-binding and independent DNA binding events	

Step 2: RNA-seq to identify the SOXC and TNF-induced transcriptome

$Sox4^{fl/fl}$ $11^{fl/fl}$ $12^{fl/fl}$ mouse FLS	
AdeCMV5eGFP (control)	AdeCMV5-Cre (SoxC-knockout)
w TNF and w/o TNF	w TNF and w/oTNF
Identification of the TNF-responsive SOXC-dependent gene expression	

Step 3: Classification of TNF-responsive SOXC-dependent genes based on SOX4 and RELA DNA binding

Integration of ChIP-seq and RNA-seq data			
Class-1	Class-2	Class-3	Class-4
RELA-SOX4 co-binding	RELA only binding	SOX4 only binding	RELA to SOX4 binding switch

highly identical HMG-box domain allowing them bind to the same SOX-binding sites on DNA (17). Therefore, deletion of *Sox4* alone may be compensated for by *Sox11* and *Sox12*. We defined TNF-responsive genes as those that were differentially expressed by ≥ 1.5-fold by TNF treatment in the AdeGFP-$SoxC^{fl/fl}$ FLS. Interestingly, 60% of the TNF-responsive genes remained unchanged or exhibited a reversed regulation in the AdeCre-$SoxC^{fl/fl}$ FLS indicating that the effect of TNF on FLS is significantly altered in the absence of *SoxC* genes (**Figure 2A**, **Supplementary Figure S2A** and **Supplementary Table S6**). Pathway analysis revealed that that the upregulated TNF-responsive transcriptome which was either SOXC-dependent and independent is predicted to play a role in inflammatory disease pathways, cell migration and tumorigenesis. Interestingly, the downregulated TNF-responsive genes that are SOXC-dependent were predicted to regulate organogenesis and cell survival (**Figure 2B**). We integrated the differential gene expression data with the ChIP-seq results to find that only a small proportion i.e., 17 of 638 *SoxC*-dependent TNF-responsive genes were assigned to RELA-SOX4 peaks and 66 genes were assigned to RELA only peaks (**Figure 2C**). The genes with RELA-SOX4 peaks regulated inflammation mediators such as interleukin-15 (*Il15*), chromatin remodeling factors such as histone deacetylase 4 (*Hdac4*), lysine acetyltransferase 6b (*Katb6*), SET-binding protein 1 (*Setbp1*) and nuclear receptor coactivator 1 *(Ncoa1*) and Activating protein-1 (AP-1) signaling components such as mitogen-activated protein kinase 1 (*Mapk1*/ERK2), mitogen-activated protein kinase 8 (*Map3k8*/MEKK) and JunB proto-oncogene (*Junb*/AP-1) (**Figure 2D**). To understand the clinical significance of the SOXC-dependent TNF-responsive genes we analyzed a published RNA-seq data set from freshly sorted CD45- Podoplanin+ FLS from the synovia from OA and RA patients (26). We found that the expression levels of SOX4, and *SOX11* remained unchanged between the highly inflammatory FLS from leukocyte rich RA patients than in OA patient FLS with low level of inflammation. However, the SoxC-dependent TNF-responsive genes were upregulated in the leukocyte rich RA FLS (**Supplementary Figure S2**). These data suggest that the SOXC/RELA molecular axis may play a critical role in the pathology of highly inflammatory forms of RA.

Using representative examples of SOX4-RELA co-bound genes, such as *Il15* and *Mapk1* we showed the extent of overlap between RELA and SOX4 peaks (**Figure 2E**). Their *SoxC*-dependance was demonstrated by showing that the knockout of *SoxC* genes prevented their TNF-induced upregulation, whereas the levels of *Sox4*, *Sox11* and *Sox12* remained unchanged (**Figure 2F** and **Supplementary Figure S3A**). The *SoxC*-dependent regulation of *Il15* (**Figure 2G**) and Mapk **(Supplementary Figure S3B**) were additionally demonstrated in a luciferase reporter assay, where SOX4 and SOX11 overexpression in the presence of TNF significantly increased the activity of a luciferase reporter gene encompassing the SOX4-RELA ChIP-seq peak. Mutation of the two SOXC binding sites in the *Il15* ChIP-seq peak sequence (position 52: AATCAA to AGATCGA and position 168: AAACAAT to AGACAGT) resulted in a loss of SOXC-dependent activation of the Il15-reporter in the absence and presence of TNF. Similarly, examples of genes assigned to RELA only peaks such as Sequestosome 1 (*Sqstm1)*, a ubiquitin binding protein that plays a role in autophagy and NF-κB inhibitor beta (*Nfkbib)*, critical intermediate in the canonical NF-κB signaling were upregulated by TNF only in the presence of *SoxC* genes, but the neighboring gene *Ccer* remained unchanged by TNF or *SoxC* knockout. *Mgatb4* remained unexpressed in the FLS (**Figures 2H, I**).

TNF Activates a 'RELA to SOX4 Regulatory Switch' to Maintain *Sox4* and *Sox11* Gene Expression

We previously showed that TNF increases SOX4 and SOX11 protein levels, at least in part by protein stabilization without

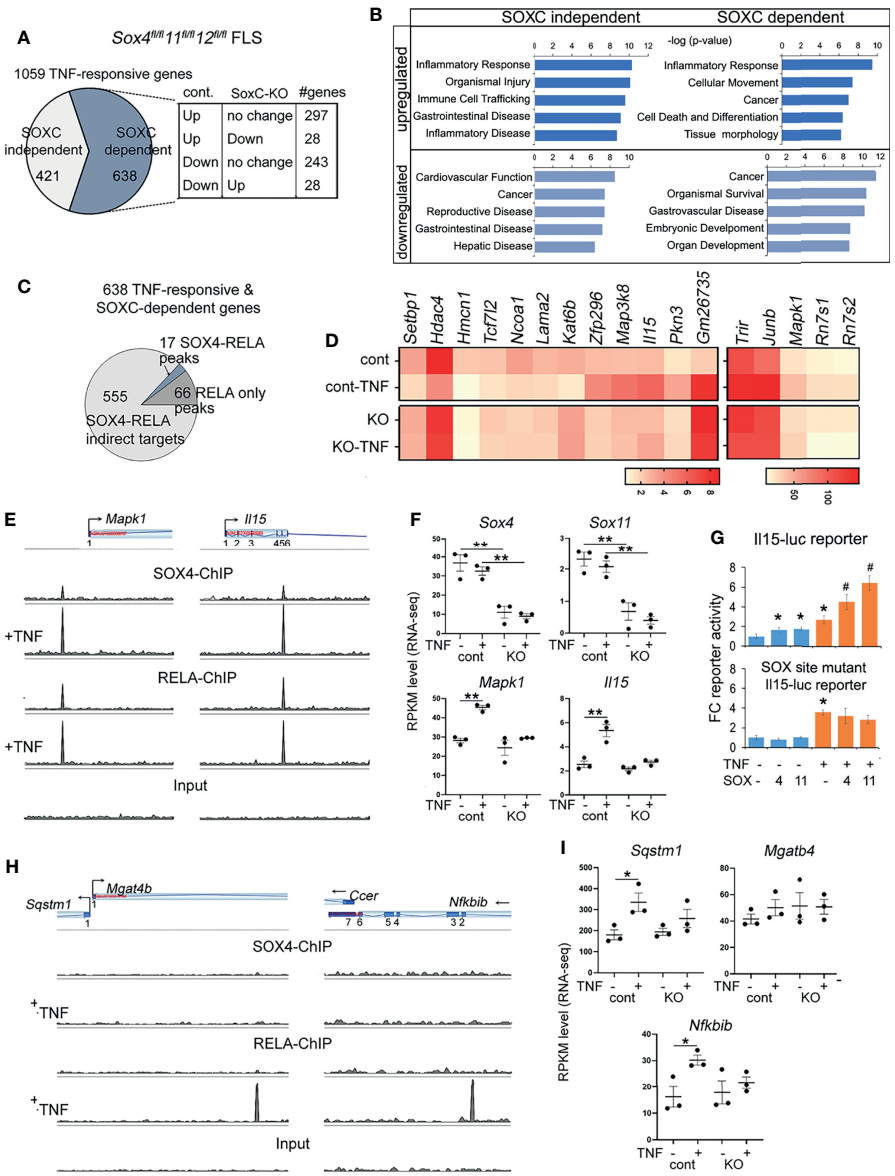

FIGURE 2 | Characterization of SOXC-dependent TNF-responsive genes. **(A)** Pie-chart showing the proportion of SOXC-dependent and SOXC-independent TNF-responsive genes identified from RNA-seq TNF-treated control and SoxC-KO FLS. Cont, *Sox4*$^{fl/fl}$*11*$^{fl/fl}$*12*$^{fl/fl}$ FLS infected with GFP adenovirus. SoxC-KO, *Sox4*$^{fl/fl}$*11*$^{fl/fl}$*12*$^{fl/fl}$ FLS infected with GFP adenovirus. The number genes upregulated, downregulated or unchanged by TNF treatment of control and SoxC-KO FLS are indicated in the box. **(B)** IPA pathway analysis of SOXC-dependent and independent TNF-responsive genes. **(C)** Pie chart showing the number of SOX4-RELA co-binding and RELA only bound genes among the SOXC-dependent TNF-responsive genes. **(D)** Heatmap of averaged and normalized RPKM values from RNA-seq of control and SoxC-KO FLS. **(E, H)** Genomic profiles of SOX4 and RELA ChIP-seq peaks. **(F, I)** Gene expression changes by RNA-seq in control and SoxC-KO FLS upon TNF treatment. **(G)** Fold-change *Il15* and SOX-site mutated *Il15* luciferase reporter activity in HEK293 cells transfected with SOX4 or SOX11 expression plasmids and treated with 10ng/mL TNF for 16h. *p-value < 0.05, **p-value < 0.001 by student's t-test compared to untreated condition. #p-value < 0.05 by student's t-test compared to SOX4 or SOX11 only conditions.

significantly effecting the mRNA levels (14). Here we addressed the additional mechanisms that might contribute to the TNF-mediated regulation of *Sox4* and *Sox11* expression. In ChIP-seq assays we found that the 3'UTR of *Sox4* and *Sox11* genes were bound by RELA under basal conditions, suggesting that RELA may function as an upstream regulator of *Sox4* and *Sox11* expression. Notably, the RELA binding was lost upon TNF-treatment and this loss corresponded with a gain in SOX4 binding to the same genomic region, suggesting a switch from RELA-mediated expression to an autoregulatory mode of expression (**Figures 3A, B**). We generated luciferase reporter constructs composing the ChIP-seq peak region in the 3' UTR

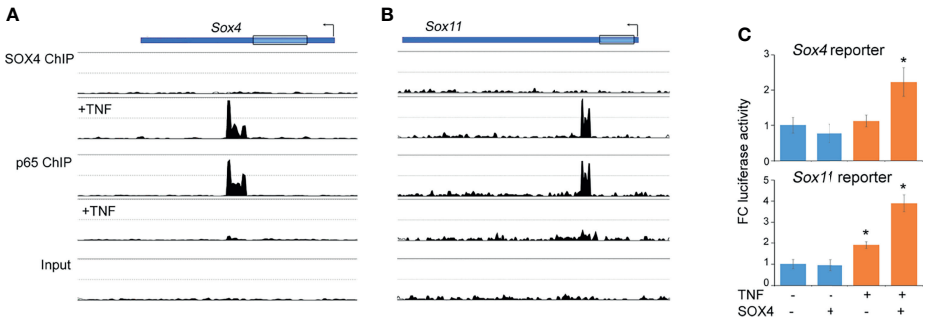

FIGURE 3 | Autoregulatory switch in the *Sox4* and *Sox11* gene expression. **(A, B)** Changes in the profiles of SOX4 and RELA ChIP-seq peaks in the Sox4 and Sox11 genomic locus upon TNF treatment. **(C)** Fold-change Sox4 and Sox11 luciferase reporter activity in HEK293 cells transfected with SOX4 expression plasmids and treated with 10ng/mL TNF for 16h. *p-value < 0.05 by student's t-test compared to untreated condition.

of *Sox4* and *Sox11* genes to find that a combination of TNF-treatment and transient over expression of SOX4 was necessary for increasing the reporter activity (**Figure 3C**). In consistence with our previous results, TNF-treatment did not result in the level of *Sox4* or *Sox11* expression (**Figure 2F**), indicating that a switch in RELA to SOX4 binding did not alter the overall gene expression, but rather helped in maintaining a consistent level of gene expression in the presence of inflammation.

DISCUSSION

In this study we utilized genome wide ChIP-seq and RNA-seq approaches to show that (1) The SOXC family member, SOX4 interacts with RELA in FLS. (2) The SOX4-RELA interaction is likely fortified by the proximity of SOX4 and RELA binding sites on the chromatin. (3) A significant subset of the TNF-responsive RELA target genes require *SoxC* genes for their optimal expression. (4) TNF activates an autoregulatory switch, which results in shift from RELA binding to SOX4 binding at the Sox4 and Sox11 regulatory regions.

SoxC genes regulate the expression of TNF target genes *via* multiple different modes of action (**Figure 4**); Class-1 includes SOX4-RELA direct target genes that require the binding of both SOX4 and RELA to their regulatory sequences. The Class-2 genes are RELA-direct targets that require only RELA to bind to their regulatory regions, while SOX4 may regulate the expression of one or more of the transcriptional co-factors or upstream regulators of NF-κB signaling. The Class-3 genes are indirect targets of both RELA and SOX4. They are neither bound by RELA or SOX4 and likely use a different transcription factor, whose expression or activity is controlled by RELA and SOX4. The Class-4 genes exhibit regulation *via* 'regulatory switch' in which TNF-induces a switch from RELA to SOX4 binding. The autoregulation of *Sox4* and *Sox11* is mediated by this regulatory switch.

We made an interesting finding that about three quarter of all SOX4 binding events induced by TNF (383 out of 584 peaks), were in proximity of a RELA binding event. However, RNA-seq results showed that most of the SOX4-RELA or RELA binding events did not lead to differential gene expression. This suggests that additional factors or stimuli are needed for their expression. Based on the *de novo* binding site predictions by MEME-ChIP, we speculate that these additional factors may include SIX2, SP-2 and AP family of transcription factors. The bulk of SOXC-dependent TNF-responsive transcriptome is constituted by Class-3 genes that are the indirect targets of SOX4 and RELA. Only a small subset of (16 out of 638 genes) belong to Class-1 that require RELA-SOX4 co-binding for their differential regulation.

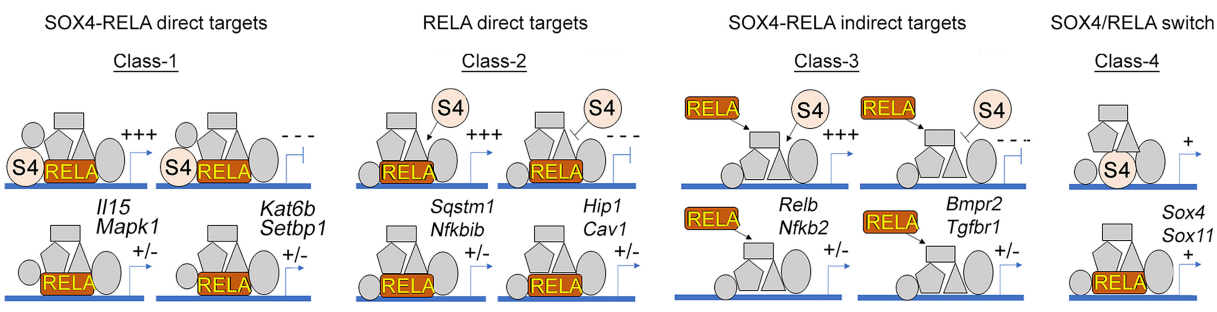

FIGURE 4 | Multimodal regulation of gene expression by RELA and SOX4. Illustration of the 4 different classes of SOXC-dependent and TNF-responsive genes and their predicted responses upon SoxC-knockout are indicated. Two representative examples of each class are indicated.

None-the-less the Class-1 genes possess the potential to induce drastic changes in the FLS transcriptome. For instance, the downregulation of histone methylation writer, *Kat6b* and upregulation of histone acetylation eraser, *Hdac4* could potentially remodel the chromatin landscape in the FLS. Overexpression of HDAC4 histone deacetylase correlates with decreased production of proinflammatory cytokines in FLS (27) and decreased expression of Runx2, MMP-13 and collagen X in chondrocytes (28). *HDAC4* was also found to be downregulated in RA synovium (29), which may explain why inflammatory mediator production is actively amplified in RA.

Similarly, differential expression of AP-1 signaling pathway components including *Mapk1* (ERK2), *Map3k8* (MEKK8) and *Junb* (AP1) is also expected to contribute to large-scale cellular and molecular changes. Regarding ERK2, Wang et al. reported that overexpression of this kinase was involved in maintaining cartilage homeostasis through modulating the TGF-β/SMAD axis *via* reducing the expression of *Col2a1*, Aggrecan, and *Sox9*, which are key molecules for cartilage homeostasis (30). The AP-1 subunit, JunB, has been proposed as a negative regulator of proliferation and production of cytokines in fibroblasts (31, 32). Thus, upregulation of *Mapk1* and *Junb* in *SoxC*-KO FLS could indicate a regulatory role for SOXC in inflammatory arthritis.

Our analysis of published RNA-seq data from freshly isolated FLS from leukocyte rich RA patient synovium and OA patient synovium (26) showed a differential regulation of SOXC and TNF-dependent genes, suggesting that the higher level of inflammation present in leukocyte rich RA activates the SOXC/RELA pathway. However, these data did not allow us to comment on the role of SOXC/RELA axis in OA patient FLS, since normal (non-arthritic) FLS were not included in this study. We previously showed that pro-inflammatory cytokines stabilize the protein level of SOX4 and SOX11 and promote inflammatory gene expression in both OA and RA FLS. Supporting this notion, other studies reported a role for SOX4 in promoting the inflammatory phenotype of both OA and RA FLS (33, 34). Taken together, these suggest that the SOXC/RELA axis is activated by inflammation, irrespective of the disease etiology and may thus contribute to the pathology of both OA and RA.

Studies from breast cancer cells showed that SOX4 is a downstream of Transforming growth factor beta (TGFβ) signaling and that SOX4 expression was required for TGFβ-mediated induction of a subset of SMAD3/SOX4-co-bound genes (35). Here we show that SOX4 is required for the induction of RELA/SOX4 co-bound genes, however these co-bound regions did not contain SMAD binding sites. Studies performed in chondrocytes have shown increased expression of ADAMTS-5 after TNF induction in a SOX4-dependent manner (21, 36). These data therefore put forth a notion that SOX4's choice of transcriptional partners is highly context dependent.

Autoregulation is a mechanism by which a transcription factor regulates its own expression. It is a common mechanism observed in several developmentally important transcription factors to ensure their abundance and activity is not repressed by other factors (37, 38). Several members of SOX family such as *SOX2* and *SOX9* (39, 40) that are master regulators of embryonic development exhibit autoregulation. We here show that *Sox4* autoregulates its own expression in addition to its group-member *Sox11 via* binding to a regulatory region in the 3' UTR. This finding suggests that SOX4 is critical factor in the regulation of inflammatory responses and hence acquired the property of autoregulation. Interestingly, it was reported that single nucleotide polymorphism (SNP) in the untranslated region (UTR) lead to osteoporosis susceptibility, suggesting an important role for the 3' UTR in the regulation of SOX4 gene expression in other diseases associated with inflammation (41).

A limitation of this study it presents a simplified view of the TNF/SOXC molecular axis. The functionally redundant activities of *Sox4*, *Sox11* and *Sox12* in TNF-induced arthritis and the diverse range of stimuli that can potentially activate the canonical NF-κB signaling in the FLS are suggestive of a role for multiple additional co-factors besides SOXC and RELA. The proposed Class 1 to 4 modes of interaction between RELA and SOXC proteins (**Figure 4**), especially the TNF-induced autoregulatory switch described in Class-4, requires additional follow up studies to completely unravel its biological significance. Another limitation is the lack of investigation on the role of *Sox12*, the third member of the *SoxC* gene family. Although SOX12 has the weakest transactivation domain among the SOXC proteins (17) it was shown to play a role in the inflammatory response of T cells (42, 43) and cancer cells (44–46). Thus, it may contribute to the transcriptional regulation of inflammation in the FLS, which needs to be determined in future studies. In addition, future investigations using a variety of *in vivo* arthritis models are required to further delineate the molecular and functional interactions of SOXC and RELA proteins during synovial inflammation.

In conclusion, we uncovered the molecular mechanism by which *SoxC* genes regulate the inflammatory responses in the FLS at the genomic level. Our data will serve as a resource for studies on RELA and SOX4 target genes in the FLS arthritic diseases. Together with our previous findings, we demonstrate a role of TNF/SOXC molecular axis in FLS during arthritis and suggest its role in the inflammatory pathology of other cell types where SOXC proteins play a vital role.

DATA AVAILABILITY STATEMENT

The original contributions presented in the study are publicly available. This data can be found here: NCBI, GSE197694.

ETHICS STATEMENT

The animal study was reviewed and approved by IACUC Emory University.

AUTHOR CONTRIBUTIONS

KJ, SR-P, SN, and UG contributed to the generation of the data, data analysis and critical reading of the manuscript. KJ, SR-P,

HD, and PB contributed to manuscript writing. PB and HD contributed to study design. All authors contributed to the article and approved the submitted version.

FUNDING

We thank the support from the National Institutes of Health/ National Institute of Arthritis, Musculoskeletal and Skin Disease grant (R01 AR070736) and Startup funds from the Department of Orthopaedics, Emory University School of Medicine to PB.

ACKNOWLEDGMENTS

We thank the support from Cleveland Clinic Lerner Research Institute, and the V. Lefebvre laboratory. We also thank V. Lefebvre for the *SoxC*$^{fl/fl}$ mice and SOX4 and SOX11 expression plasmids.

SUPPLEMENTARY MATERIAL

The Supplementary Material for this article can be found online at: https://www.frontiersin.org/articles/10.3389/fimmu.2022.789349/full#supplementary-material

REFERENCES

1. Nygaard G, Firestein GS. Restoring Synovial Homeostasis in Rheumatoid Arthritis by Targeting Fibroblast-Like Synoviocytes. *Nat Rev Rheumatol* (2020) 16:316–33. doi: 10.1038/s41584-020-0413-5
2. Pap T, Dankbar B, Wehmeyer C, Korb-Pap A, Sherwood J. Synovial Fibroblasts and Articular Tissue Remodelling: Role and Mechanisms. *Semin Cell Dev Biol* (2020) 101:140–5. doi: 10.1016/j.semcdb.2019.12.006
3. Simmonds RE, Foxwell BM. Signalling, Inflammation and Arthritis: NF-Kappab and its Relevance to Arthritis and Inflammation. *Rheumatol (Oxf)* (2008) 47:584–90. doi: 10.1093/rheumatology/kem298
4. Liu S, Ma H, Zhang H, Deng C, Xin P. Recent Advances on Signaling Pathways and Their Inhibitors in Rheumatoid Arthritis. *Clin Immunol* (2021) 230:108793. doi: 10.1016/j.clim.2021.108793
5. Ntougkos E, Chouvardas P, Roumelioti F, Ospelt C, Frank-Bertoncelj M, Filer A, et al. Genomic Responses of Mouse Synovial Fibroblasts During Tumor Necrosis Factor-Driven Arthritogenesis Greatly Mimic Those in Human Rheumatoid Arthritis. *Arthritis Rheumatol* (2017) 69:1588–600. doi: 10.1002/art.40128
6. Gangishetti U, Ramirez-Perez S, Jones K, Arif A, Drissi H, Bhattaram P. Chronic Exposure to TNF Reprograms Cell Signaling Pathways in Fibroblast-Like Synoviocytes by Establishing Long-Term Inflammatory Memory. *Sci Rep* (2020) 10:20297. doi: 10.1038/s41598-020-77380-9
7. Chawla M, Roy P, Basak S. Role of the NF-Kappab System in Context-Specific Tuning of the Inflammatory Gene Response. *Curr Opin Immunol* (2021) 68:21–7. doi: 10.1016/j.coi.2020.08.005
8. Ahmed AS, Gedin P, Hugo A, Bakalkin G, Kanar A, Hart DA, et al. Activation of NF-Kappab in Synovium Versus Cartilage From Patients With Advanced Knee Osteoarthritis: A Potential Contributor to Inflammatory Aspects of Disease Progression. *J Immunol* (2018) 201:1918–27. doi: 10.4049/jimmunol.1800486
9. Makarov SS. NF-Kappa B in Rheumatoid Arthritis: A Pivotal Regulator of Inflammation, Hyperplasia, and Tissue Destruction. *Arthritis Res* (2001) 3:200–6. doi: 10.1186/ar300
10. Chen FE, Huang DB, Chen YQ, Ghosh G. Crystal Structure of P50/P65 Heterodimer of Transcription Factor NF-Kappab Bound to DNA. *Nature* (1998) 391:410–3. doi: 10.1038/34956
11. Lim CA, Yao F, Wong JJ, George J, Xu H, Chiu KP, et al. Genome-Wide Mapping of RELA(P65) Binding Identifies E2F1 as a Transcriptional Activator Recruited by NF-Kappab Upon TLR4 Activation. *Mol Cell* (2007) 27:622–35. doi: 10.1016/j.molcel.2007.06.038
12. Zhao W, Wang L, Zhang M, Wang P, Zhang L, Yuan C, et al. NF-Kappab- and AP-1-Mediated DNA Looping Regulates Osteopontin Transcription in Endotoxin-Stimulated Murine Macrophages. *J Immunol* (2011) 186:3173–9. doi: 10.4049/jimmunol.1003626
13. Agalioti T, Lomvardas S, Parekh B, Yie J, Maniatis T, Thanos D. Ordered Recruitment of Chromatin Modifying and General Transcription Factors to the IFN-Beta Promoter. *Cell* (2000) 103:667–78. doi: 10.1016/S0092-8674(00)00169-0
14. Bhattaram P, Muschler G, Wixler V, Lefebvre V. Inflammatory Cytokines Stabilize SOXC Transcription Factors to Mediate the Transformation of Fibroblast-Like Synoviocytes in Arthritic Disease. *Arthritis Rheumatol* (2018) 70:371–82. doi: 10.1002/art.40386
15. Lefebvre V. Roles and Regulation of SOX Transcription Factors in Skeletogenesis. *Curr Top Dev Biol* (2019) 133:171–93. doi: 10.1016/bs.ctdb.2019.01.007
16. Bhattaram P, Penzo-Mendez A, Sock E, Colmenares C, Kaneko KJ, Vassilev A, et al. Organogenesis Relies on Soxc Transcription Factors for the Survival of Neural and Mesenchymal Progenitors. *Nat Commun* (2010) 1:9. doi: 10.1038/ncomms1008
17. Dy P, Penzo-Mendez A, Wang H, Pedraza CE, Macklin WB, Lefebvre V. The Three Soxc Proteins–Sox4, Sox11 and Sox12–Exhibit Overlapping Expression Patterns and Molecular Properties. *Nucleic Acids Res* (2008) 36:3101–17. doi: 10.1093/nar/gkn162
18. Bhattaram P, Penzo-Mendez A, Kato K, Bandyopadhyay K, Gadi A, Taketo MM, et al. SOXC Proteins Amplify Canonical WNT Signaling to Secure Nonchondrocytic Fates in Skeletogenesis. *J Cell Biol* (2014) 207:657–71. doi: 10.1083/jcb.201405098
19. Bhattaram P, Kato K, Lefebvre V. Progenitor Cell Fate, SOXC and WNT. *Oncotarget* (2015) 6:24596–7. doi: 10.18632/oncotarget.5237
20. Seok J, Gil M, Dayem AA, Saha SK, Cho SG. Multi-Omics Analysis of SOX4, SOX11, and SOX12 Expression and the Associated Pathways in Human Cancers. *J Pers Med* (2021) 11:823. doi: 10.3390/jpm11080823
21. Takahata Y, Nakamura E, Hata K, Wakabayashi M, Murakami T, Wakamori K, et al. Sox4 Is Involved in Osteoarthritic Cartilage Deterioration Through Induction of ADAMTS4 and ADAMTS5. *FASEB J* (2019) 33:619–30. doi: 10.1096/fj.201800259R
22. Armaka M, Gkretsi V, Kontoyiannis D, Kollias G. A Standardized Protocol for the Isolation and Culture of Normal and Arthritogenic Murine Synovial Fibroblasts. *Protocol Exchange* (2009) 1038:102. doi: 10.1038/nprot.2009.102
23. Ma W, Noble WS, Bailey TL. Motif-Based Analysis of Large Nucleotide Data Sets Using MEME-Chip. *Nat Protoc* (2014) 9:1428–50. doi: 10.1038/nprot.2014.083
24. He TC, Chan TA, Vogelstein B, Kinzler KW. Ppardelta is an APC-Regulated Target of Nonsteroidal Anti-Inflammatory Drugs. *Cell* (1999) 99:335–45. doi: 10.1016/S0092-8674(00)81664-5
25. Mulero MC, Wang VY, Huxford T, Ghosh G. Genome Reading by the NF-Kappab Transcription Factors. *Nucleic Acids Res* (2019) 47:9967–89. doi: 10.1093/nar/gkz739
26. Zhang F, Wei K, Slowikowski K, Fonseka CY, Rao DA, Kelly S, et al. Defining Inflammatory Cell States in Rheumatoid Arthritis Joint Synovial Tissues by Integrating Single-Cell Transcriptomics and Mass Cytometry. *Nat Immunol* (2019) 20:928–42. doi: 10.1038/s41590-019-0378-1
27. Shao L, Hou C. Mir-138 Activates NF-Kappab Signaling and PGRN to Promote Rheumatoid Arthritis *via* Regulating HDAC4. *Biochem Biophys Res Commun* (2019) 519:166–71. doi: 10.1016/j.bbrc.2019.08.092
28. Gu XD, Wei L, Li PC, Che XD, Zhao RP, Han PF, et al. Adenovirus-Mediated Transduction With Histone Deacetylase 4 Ameliorates Disease Progression in an Osteoarthritis Rat Model. *Int Immunopharmacol* (2019) 75:105752. doi: 10.1016/j.intimp.2019.105752
29. Kawabata T, Nishida K, Takasugi K, Ogawa H, Sada K, Kadota Y, et al. Increased Activity and Expression of Histone Deacetylase 1 in Relation to

Tumor Necrosis Factor-Alpha in Synovial Tissue of Rheumatoid Arthritis. *Arthritis Res Ther* (2010) 12:R133. doi: 10.1186/ar3071
30. Wang W, Zhu Y, Sun Z, Jin C, Wang X. Positive Feedback Regulation Between USP15 and ERK2 Inhibits Osteoarthritis Progression Through TGF-Beta/SMAD2 Signaling. *Arthritis Res Ther* (2021) 23:84. doi: 10.1186/s13075-021-02456-4
31. Passegue E, Wagner EF. Junb Suppresses Cell Proliferation by Transcriptional Activation of P16(INK4a) Expression. *EMBO J* (2000) 19:2969–79. doi: 10.1093/emboj/19.12.2969
32. Szabowski A, Maas-Szabowski N, Andrecht S, Kolbus A, Schorpp-Kistner M, Fusenig NE, et al. C-Jun and Junb Antagonistically Control Cytokine-Regulated Mesenchymal-Epidermal Interaction in Skin. *Cell* (2000) 103:745–55. doi: 10.1016/S0092-8674(00)00178-1
33. Ahmed EA, Ibrahim HM, Khalil HE. Pinocembrin Reduces Arthritic Symptoms in Mouse Model *via* Targeting Sox4 Signaling Molecules. *J Med Food* (2021) 24:282–91. doi: 10.1089/jmf.2020.4862
34. Ye X, Yin C, Huang X, Huang Y, Ding L, Jin M, et al. ROS/TGF-Beta Signal Mediated Accumulation of SOX4 in OA-FLS Promotes Cell Senescence. *Exp Gerontol* (2021) 156:111616. doi: 10.1016/j.exger.2021.111616
35. Vervoort SJ, Lourenco AR, Tufegdzic Vidakovic A, Mocholi E, Sandoval JL, Rueda OM, et al. SOX4 can Redirect TGF-Beta-Mediated SMAD3-Transcriptional Output in a Context-Dependent Manner to Promote Tumorigenesis. *Nucleic Acids Res* (2018) 46:9578–90. doi: 10.1093/nar/gky755
36. Xiong X, Liu L, Xu F, Wu X, Yin Z, Dong Y, et al. Feprazone Ameliorates TNF-Alpha-Induced Loss of Aggrecan *via* Inhibition of the SOX-4/ADAMTS-5 Signaling Pathway. *ACS Omega* (2021) 6:7638–45. doi: 10.1021/acsomega.0c06212
37. Kielbasa SM, Vingron M. Transcriptional Autoregulatory Loops are Highly Conserved in Vertebrate Evolution. *PloS One* (2008) 3:e3210. doi: 10.1371/journal.pone.0003210
38. Ngondo RP, Carbon P. Transcription Factor Abundance Controlled by an Auto-Regulatory Mechanism Involving a Transcription Start Site Switch. *Nucleic Acids Res* (2014) 42:2171–84. doi: 10.1093/nar/gkt1136
39. Chew JL, Loh YH, Zhang W, Chen X, Tam WL, Yeap LS, et al. Reciprocal Transcriptional Regulation of Pou5f1 and Sox2 *via* the Oct4/Sox2 Complex in Embryonic Stem Cells. *Mol Cell Biol* (2005) 25:6031–46. doi: 10.1128/MCB.25.14.6031-6046.2005
40. Mead TJ, Wang Q, Bhattaram P, Dy P, Afelik S, Jensen J, et al. A Far-Upstream (-70 Kb) Enhancer Mediates Sox9 Auto-Regulation in Somatic Tissues During Development and Adult Regeneration. *Nucleic Acids Res* (2013) 41:4459–69. doi: 10.1093/nar/gkt140
41. Li G, Gu Z, He Y, Wang C, Duan J. The Effect of SOX4 Gene 3'UTR Polymorphisms on Osteoporosis. *J Orthop Surg Res* (2021) 16:321. doi: 10.1186/s13018-021-02454-x
42. Suehiro KI, Suto A, Suga K, Furuya H, Iwata A, Iwamoto T, et al. Sox12 Enhances Fbw7-Mediated Ubiquitination and Degradation of GATA3 in Th2 Cells. *Cell Mol Immunol* (2021) 18:1729–38. doi: 10.1038/s41423-020-0384-0
43. Tanaka S, Suto A, Iwamoto T, Kageyama T, Tamachi T, Takatori H, et al. Sox12 Promotes T Reg Differentiation in the Periphery During Colitis. *J Exp Med* (2018) 215:2509–19. doi: 10.1084/jem.20172082
44. Zhang W, Yu F, Weng J, Zheng Y, Lin J, Qi T, et al. SOX12 Promotes Stem Cell-Like Phenotypes and Osteosarcoma Tumor Growth by Upregulating JAGGED1. *Stem Cells Int* (2021) 2021:9941733. doi: 10.1155/2021/9941733
45. Xu J, Zhang J, Li L, Mao J, You T, Li Y. SOX12 Expression Is Associated With Progression and Poor Prognosis in Human Breast Cancer. *Am J Transl Res* (2020) 12:8162–74.
46. Gao Y, Li L, Hou L, Niu B, Ru X, Zhang D. SOX12 Promotes the Growth of Multiple Myeloma Cells by Enhancing Wnt/Beta-Catenin Signaling. *Exp Cell Res* (2020) 388:111814. doi: 10.1016/j.yexcr.2020.111814

Conflict of Interest: The authors declare that the research was conducted in the absence of any commercial or financial relationships that could be construed as a potential conflict of interest.

Publisher's Note: All claims expressed in this article are solely those of the authors and do not necessarily represent those of their affiliated organizations, or those of the publisher, the editors and the reviewers. Any product that may be evaluated in this article, or claim that may be made by its manufacturer, is not guaranteed or endorsed by the publisher.

frontiers | Frontiers in Immunology

ORIGINAL RESEARCH
published: 24 May 2022
doi: 10.3389/fimmu.2022.890094

Sex-Differences and Associations Between Complement Activation and Synovial Vascularization in Patients with Late-Stage Knee Osteoarthritis

Emily U. Sodhi[1†], *Holly T. Philpott*[2,3†], *McKenzie M. Carter*[1,3], *Trevor B. Birmingham*[2,3] *and C. Thomas Appleton*[1,2,3,4*]

[1] Department of Physiology & Pharmacology, Schulich School of Medicine and Dentistry, Western University, London, ON, Canada, [2] Health & Rehabilitation Sciences, Faculty of Health Sciences, Western University, London, ON, Canada, [3] Bone & Joint Institute, Western University, London, ON, Canada, [4] Department of Medicine, Schulich School of Medicine, Western University, London, ON, Canada

OPEN ACCESS

Edited by:
Gurpreet S. Baht,
Duke University, United States

Reviewed by:
Xin Zhang,
Duke University, United States
Elisa Assirelli,
Rizzoli Orthopedic Institute (IRCCS), Italy
Elena Magrini,
University of Milan, Italy

***Correspondence:**
C. Thomas Appleton
tom.appleton@sjhc.london.on.ca

[†]These authors share first authorship

Specialty section:
This article was submitted to Inflammation, a section of the journal Frontiers in Immunology

Received: 05 March 2022
Accepted: 27 April 2022
Published: 24 May 2022

Citation:
Sodhi EU, Philpott HT, Carter MM, Birmingham TB and Appleton CT (2022) Sex-Differences and Associations Between Complement Activation and Synovial Vascularization in Patients with Late-Stage Knee Osteoarthritis. Front. Immunol. 13:890094. doi: 10.3389/fimmu.2022.890094

Purpose: Synovial inflammation in knee osteoarthritis (OA) causes disorganized synovial angiogenesis and complement activation in synovial fluid, but links between complement and synovial microvascular pathology have not been established. Since complement causes vascular pathology in other diseases and since sex-differences exist in complement activation and in OA, we investigated sex differences in synovial fluid complement factors, synovial tissue vascular pathology, and associations between complement and synovial vascular pathology in patients with late-stage knee OA.

Methods: Patients with symptomatic, late-stage radiographic knee OA undergoing total knee arthroplasty or high tibial osteotomy provided matched synovial fluid and tissue biopsies during surgery. Complement factors (C2, C5, adipsin, MBL, and CFI) and terminal complement complex (sC5b-C9) were measured in synovial fluid by multiplex or enzyme-linked immunosorbent assay, respectively. Features of synovial vascular pathology (vascularization, perivascular edema, and vasculopathy) were assessed by histopathology. Multivariate linear regression models were used to assess associations between synovial fluid complement factors and histopathological features of vascular pathology, with adjustment for age, sex, body mass index, and sex interaction. Sex-disaggregated comparisons were completed.

Results: Synovial fluid biomarker and histopathology data were included from 97 patients. Most synovial fluid complement factors and synovial tissue histopathological features were similar between sexes. Synovial fluid C5 trended to lower levels in males (-20.93 ng/mL [95%CI -42.08, 0.23] p=0.05). Median vasculopathy scores (0.42 [95%CI 0.07, 0.77] p=0.02) were higher in males. In the full cohort, C5 concentration was associated with lower vascularization scores (-0.005 [95%CI -0.010, -0.0001] p=0.04) while accounting for sex*C5 interaction. In sex-disaggregated analyses, increased C5 concentration was associated with lower vascularization scores (-0.005 [95%CI –0.009, -0.0001] p=0.04) in male patients, but not in female patients. Males had higher sC5b-C9

compared to females. Additionally, males with high C5 had a higher synovial fluid concentration of sC5b-C9 compared to males with low C5. No differences were found in females.

Conclusion: Higher synovial fluid C5 levels were associated with increased complement activation and decreased synovial vascularization in males but not in females with OA. Future studies should test whether synovial fluid complement activation suppresses synovial angiogenesis and identify mechanisms accounting for C5-related sex-differences in synovial fluid complement activation in patients with knee OA.

Keywords: complement, synovium, osteoarthritis, sex-differences, inflammation, histopathology, vascularization

1 INTRODUCTION

Synovial inflammation in knee osteoarthritis (OA) causes disorganized synovial angiogenesis and complement activation in synovial fluid, but links between complement and synovial microvascular pathology have not been established. The formation of new blood vessels by angiogenesis is stimulated during wound healing and dysregulated by chronic inflammation (1). In knee OA, chronic synovial inflammation (synovitis) is associated with increased joint pain and disease progression (2). Synovitis disrupts the homeostatic roles of synovial tissue including synovial fluid production (3), nourishing articular cartilage (3), clearance of tissue turnover products (3), and joint tissue regeneration (4). Synovial vascular pathology in OA demonstrates angiogenesis (vascularization) (5), thick-walled microvessels (vasculopathy) (6), and perivascular edema (7). The mechanisms driving synovial angiogenesis in knee OA are not well understood (5, 8). Scanzello et al. proposed that synovitis in OA resembles a chronic wound, where disorganized angiogenesis may be a sign of attempted wound healing (9). We considered that complement may be associated with synovial vascular pathology in this study since complement-driven inflammation also disturbs wound healing, including regulation of angiogenic processes (10).

Inflammation in OA primarily involves components of the innate immune system, including activation of the complement cascade (11, 12). Complement activation occurs through three activation pathways (alternative, classical, and lectin), which ultimately converge in a terminal effector pathway (10). Downstream inflammatory effects of complement activation include increased blood vessel permeability (13), histamine release from mast cells (13), smooth muscle contraction (14), synthesis of angiogenic factors (15, 16), regulation of apoptosis, and release of chemoattractants by immune cells (13, 17), all of which may exacerbate synovial inflammation within the knee joint.

Wang et al. reported that the synovium and synovial fluid of knee OA patients have higher gene expression of complement effectors and lower complement inhibitors compared to healthy individuals (18). Knockout of common and alternative complement pathway components also protected against the development of structural joint damage in multiple rodent models of knee OA, but synovial vascular outcomes were not assessed. To our knowledge, there are presently no published studies investigating relationships between complement and synovial vascular pathology in knee OA.

Female sex is a major OA risk factor (19). Females are 1.4 times more likely than males to be diagnosed with OA after age 65 (20), suffer from more severe symptoms (21), and have lower responses to current therapies than males (22). Interestingly, sex-differences in complement activation have also been identified. For example, serum samples from healthy females demonstrated lower alternative pathway activation and lower common/terminal pathway and mannose-binding lectin components compared to males (23). Accordingly, it is recommended that the effects of sex be evaluated in studies investigating complement-associated pathologies. Considering the well-recognized sex-differences in both knee OA epidemiology and complement activation, our objectives were to investigate sex differences in complement factors in synovial fluid, synovial tissue vascular pathology, and associations between complement factors and vascular pathology in patients with late-stage knee OA.

2 METHODS

2.1 Study Participants

Participants were recruited from the Western Ontario Registry for Early Osteoarthritis (WOREO) Knee Study, a prospective cohort designed to investigate clinical, biomechanical, and pathophysiological features of inflammation in patients with knee OA. The present study included 97 consecutively recruited patients with symptomatic, late-stage knee OA. Eligibility criteria included patients with Kellgren-Lawrence (KL) grades of 3 or 4 (24), frequent knee pain, and compromised function indicating surgical management by total knee arthroplasty or high tibial osteotomy. Patients without synovial histopathology and synovial fluid data were excluded. One patient reported currently taking hormone replacement therapy. A sample of n=85 was required to detect a Cohen's f^2 of 0.15 (moderate effect size) with 80% power and an $\alpha = 0.05$, indicating we were adequately powered for our primary analysis with the total cohort (n=97) (25). Knee radiographs were acquired at study enrollment. Participants provided written,

informed consent and the study was approved by Western University's Research Ethics Board for Health Sciences Research Involving Human Subjects (HSREB #109255). Demographic measures including age, sex, and body mass index (BMI) were collected. Patient-reported pain in the target (study) knee was measured using the Knee Osteoarthritis Outcome Score (KOOS) pain subscale, normalized to 100%, where 100 corresponds to no pain and 0 to the worst pain possible.

2.2 Synovial Fluid Collection and Complement Concentrations in Synovial Fluid

At the time of surgery, prior to knee joint arthrotomy, synovial fluid was aspirated to avoid contamination by blood. Synovial fluid samples were then centrifuged at 2800g and at 4°C for 15 minutes. Supernatants were aliquoted into cryovials for storage at -80°C until use. Synovial fluid samples with sufficient volume and minimal blood contamination were selected for multiplex analysis. Samples were treated with hyaluronidase (1 μg/mL) prior to assay with the Human Complement-2, Milliplex Multiplex Assay using Luminex (Millipore, USA), performed commercially at Eve Technologies, Calgary, AB, Canada, to measure the concentration of complement factors C5, C2, CFI, adipsin (factor D), and MBL (mannose-binding lectin) (ng/mL). We excluded the short-lived, unstable intermediates C4b and C5a in these *in vivo* samples as we did not use protease inhibitors at the time of synovial fluid processing and this assay does not measure the more stable glycosylated (des Arg) metabolite.

2.3 Synovial Fluid Concentrations of Terminal Complement Complex (sC5b-C9)

To assess levels of a stable complement activation product and ensure that lower C5 levels were not due to consumption due to rapid C5 cleavage/activation, synovial fluid samples from a subset of patients that had adequate synovial fluid volume were treated with hyaluronidase prior to measuring terminal complement complex (sC5b-C9) using an enzyme-linked immunosorbent assay (ELISA) kit according to manufacturer's protocol (Svar Life Science, Malmö, Sweden). We included samples from 16 male and 16 females patients, with n = 8 per quartile (highest/lowest) of C5 concentration. Absorbance reading at 620 nm (reference) was subtracted from the absorbance reading at 450 nm. Amount of sC5b-C9 (ng/mL) present in each sample was interpolated using a standard curve.

2.4 Synovial Tissue Histopathology

To standardize the location of tissue collection, all synovial tissue biopsies were obtained from the lateral suprapatellar recess at the time of surgery. After overnight fixation in 4% paraformaldehyde, synovial tissue samples were processed, and paraffin embedded. Serial sections (5 μm thickness) were mounted on glass slides, stained with hematoxylin and eosin, and 5 high powered fields (hpf) per patient at least 100μm apart were assessed. Six histopathological features were graded as described previously (7): perivascular edema, fibrosis, sub-synovial infiltrate, surface fibrin deposition, synovial lining thickness, and vascularization. A seventh feature, vasculopathy, was graded according to the number of thick-walled vessels (lumen diameter is smaller than vessel wall thickness) per high powered field (hpf) and was adapted from Philosophe et al. (2014) (26). Our primary analysis focused on measures of vascular pathology. Vascularization and perivascular edema were graded 0-3 (none-severe) (7). Vasculopathy was graded 0-3 as follows: Grade 0 = no thick-walled vessels per hpf; Grade 1 = <1/3 thick-walled vessels per hpf; Grade 2 = 1/3-2/3 thick-walled vessels per hpf; Grade 3 = >2/3 thick-walled vessels per hpf. The mean and median grades of all hpf per patient were calculated for each histopathological feature.

2.5 Synovial Tissue Immunofluorescence

To assess classical pathway activation in synovial tissue, we performed immunofluorescent detection for C1q. Slides were heated at 62°C for 30 minutes, cooled to room temperature, and then deparaffinized and rehydrated. For antigen retrieval, sections were immersed in 70°C Tris buffer (10 mM Tris, 1 mM EDTA, 10% glycerol pH 9) and allowed to cool to below 30°C. Sections were permeabilized by incubation in 0.2% Triton-X in 1x PBS for 10 minutes. Slides were rinsed with 1X phosphate buffered saline (PBS) and blocked with 5% bovine serum albumin blocking solution (1x PBS, 5.0% BSA, 0.1% Triton-X). Samples were incubated overnight at 4°C with anti-human C1q (1:100; ab268120; Abcam, Cambridge, UK). We included negative (no primary antibody) control sections. Goat anti-mouse conjugated to Alexa Fluor-647 (1:500; Jackson ImmunoResearch Laboratories) in 1X PBS was added to the slides for an hour at room temperature. Slides were mounted with Molecular Probes Prolong Gold Antifade Mountant with DAPI (Fisher Scientific, P36931).

Slides were imaged at 40X using a Leica Aperio VERSA 8 microscope scanner located at Molecular Pathology Core Facility, Robart's Research Institute. Immunofluorescence images were analyzed quantitatively using QuPath (v0.3.1) (27) pixel classifier tools to measure percent positive cells for C1q.

2.6 Statistical Analyses

All analyses were done using *Graphpad Prism 8* (GraphPad Software, San Diego, California USA) or Stata IC/15.1 (StataCorp LLC, College Station, TX, USA).

2.6.1 Descriptive Statistics

Descriptive statistics for patient's demographics and clinical characteristics were calculated as mean +/- standard deviation (range) and frequency (percentage of total) for continuous and categorical variables, respectively. Two-tailed independent student's t-tests were used to compare age, BMI, and KOOS pain between sexes. A Fisher's Exact test was used to compare proportions of KL grades between sexes. Statistical significance was set at $p<0.05$.

2.6.2 Sex-Based Analyses

Unpaired, two-tailed t-tests (or Mann-Whitney U tests in case of non-normally distributed data as assessed using QQ plots) were

conducted to assess differences in synovial fluid complement concentrations between sexes. Measures were reported as the difference in mean concentrations +/- 95% confidence intervals. To assess for relationships between synovial fluid levels of C5 and other measured complement components, we fitted a series of sex-disaggregated multivariate linear regression models with adjustment for age and BMI. Results were reported as unstandardized beta coefficients +/- 95% confidence intervals.

To assess sex-differences in complement activation, we used an unpaired, two-tailed t-test to test if terminal complement complex (sC5b-C9) was different between males and females. To determine if C5 concentration was indicative of complement activation, a two-way ANOVA with Tukey's post-hoc test was used to assess differences in synovial fluid sC5b-C9 (complement activation product) between patients from the highest and lowest quartiles of synovial fluid C5 levels for both sexes. Results were reported as mean difference +/- 95% confidence intervals.

To assess sex-differences in classical pathway activation, we used an unpaired, two-tailed t-test to measure any differences in percent positive synovial lining cells for C1q in males and females. To identify whether synovial lining C1q was indicative of complement activation, a two-way ANOVA with Tukey's post-hoc test was used to assess differences in percent positivity of synovial lining cells for C1q between patients from the highest and lowest quartiles of synovial fluid C5 levels for both sexes. Results were reported as mean difference +/- 95% confidence intervals.

2.6.3 Multivariate Linear Regression

A series of multivariate linear regression models were fitted to test the association between median synovial vascular pathology scores (predictor) and synovial fluid C5 concentration (outcome) while adjusting for age, sex, and BMI. To test whether the relationship between C5 and vascular pathology depended on sex, we included sex by C5 concentration interaction terms. As recommended by SAGER guidelines (28), sex-disaggregated analyses were then performed and the estimated marginal means and their respective 95% confidence intervals for C5 concentration and vascularization were reported separately for male and female sex. Unstandardized beta coefficients were reported in the regression model tables to represent change per 1 unit (ng/mL) increase in C5 concentration. To aid interpretation, we also reported the unstandardized beta coefficients per 100 units (ng/mL) increase in C5 concentration (Results text and Figure). Data were linear with normally distributed and homoscedastic residuals. Variance inflation factor (VIF) was used to assess multicollinearity, and all variables had a VIF of < 5.

3 RESULTS

A total of 126 patients with late-stage knee OA were screened for eligibility. Four (3.17%) were excluded because they did not have synovial biopsies available. Twenty-four (19.05%) were excluded due to having inadequate synovial fluid volumes (18; 14.29%) or blood contamination (6; 4.76%). One (0.79%) patient was excluded due to low bead counts during the multiplex assay. Therefore, a total of 97 patients with complete synovial fluid biomarker and histopathology data were included in this analysis. Demographics and clinical characteristics for the cohort are presented in **Table 1**. Male and female participants had similar mean and ranges of age, BMI, radiographic knee OA grade, and KOOS pain score.

3.1 Synovial Fluid Complement Factors

Synovial fluid concentrations of complement factors are reported for the total cohort and separated by sex in **Table 2**. The mean synovial fluid C5 concentration of the cohort was 268.96 ng/mL. Males trended toward lower synovial fluid C5 levels (-20.93 [95% CI -42.08, 0.23]) compared to females (**Table 2**; **Figure 1**). No clear sex differences were found in synovial fluid levels of adipsin (factor D), C2, CFI, or MBL.

3.2 Sex-Specific Associations Between C5 and Other Complement Factors in Synovial Fluid

In males, there was no evidence of associations between C5 and other complement factors C2, MBL, CFI, and adipsin (**Table 3**). In females, synovial fluid concentrations of C5 and C2 were positively associated (0.25 [95%CI 0.06 to 0.45]) (**Table 3**). No other complement factors were associated with C5 in females.

TABLE 1 | Demographic and clinical characteristics of participants (n=97).

	Total Cohort (n=97)	Males (n=52)	Females (n=45)	Difference between Males - Females Mean (95%CI) *p*
Age, mean ± SD (range)	67.20 ± 8.53 (44-85)	67.39 ± 8.79 (44-85)	66.98 ± 8.31 (53-82)	0.41 (-3.06, 3.87) *p*= 0.82
BMI, mean ± SD (range)	32.60 ± 5.64 (21.10-47.18)	31.93 ± 4.61 (24.20-47.18)	33.38 ± 6.61 (21.10-45.60)	-1.45 (-3.72, 0.83) *p*= 0.21
KL Grade, frequency (%)				
3	40 (41.24)	22 (42.31)	18 (40.00)	0.02 (-0.18, 0.22)
4	57 (58.76)	30 (57.69)	27 (60.00)	*p*= 0.84
KOOS Pain Score, mean ± SD (range)	47.20 ± 16.42 (0-89)	48.69 ± 14.87 (17-89)	45.47 ± 18.07 (0-83)	3.23 (-3.41, 9.87) *p*= 0.34

BMI, body mass index; CI, confidence interval; KL, Kellgren-Lawrence; KOOS, Knee Injury and Osteoarthritis Outcomes Score; MBL, Mannose-binding lectin; p, p-value; SD, standard deviation.

TABLE 2 | Synovial fluid complement concentrations: total cohort and disaggregated by sex.

	Total Cohort (n= 97) mean ± SD (range)	Males (n= 52) mean ± SD (range)	Females (n= 45) mean ± SD (range)	Difference between Males - Females Mean (95%CI) *p*
Adipsin (ng/mL)	10.67 ± 2.85 (2.72-18.94)	11.06 ± 3.16 (2.72-18.94)	10.22 ± 2.40 (3.59-13.91)	0.83 (-0.31, 1.98) *p*= 0.15
C2 (ng/mL)	311.23 ± 82.47 (112.61-592.12)	317.29 ± 88.33 (112.61-592.12)	304.24 ± 75.51 (131.75-445.15)	13.05 (-20.35, 46.45) *p*= 0.44
C5 (ng/mL)	268.96 ± 53.12 (94.80-432.95)	259.25 ± 55.59 (94.80-357.25)	280.17 ± 48.31 (198.01-432.95)	-20.93 (-42.08, 0.23) *p*= 0.05)
CFI (ng/mL)	73.52 ± 26.35 (8.04-140.03)	73.79 ± 27.84 (8.99-140.03)	73.21 ± 24.83 (8.04-116.70)	0.58 (-10.13, 11.29) *p*= 0.91
MBL* (ng/mL)	28.16 ± 20.28 (1.58-122.70)	28.39 ± 19.81 (1.58-77.01)	27.91 ± 21.03 (4.12-122.70)	-1.84 (-6.96, 7.53) *p*= 0.99

**MBL concentrations were not normally distributed, hence a Mann-Whitney U test measured differences in median MBL concentrations between sexes as opposed to means. C2, complement component 2; C5, complement component 5; CI, confidence interval; CF1, complement factor 1; MBL, mannose-binding lectin; p, p-value; SD, standard deviation.*

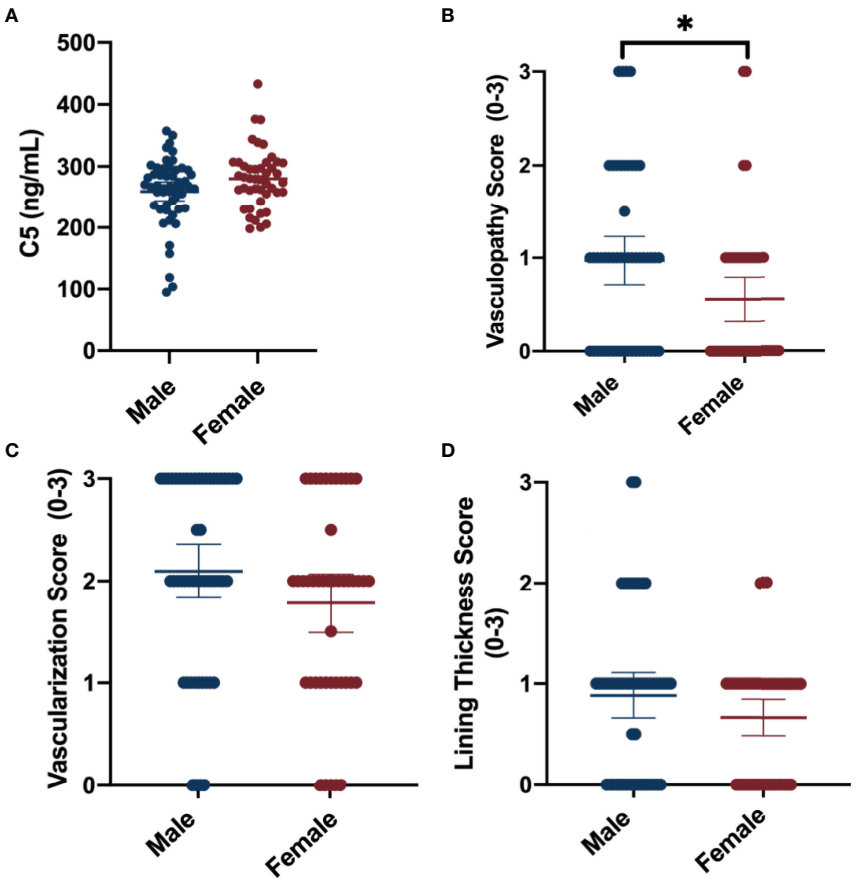

FIGURE 1 | Summary of sex -differences in complement and synovial vascular pathology. Data shown include means ± 95%CI and mean differences between sexes for **(A)** synovial fluid C5 concentrations (ng/mL), **(B)** median vasculopathy score, **(C)** median vascularization score, and **(D)** median synovial lining thickness score. Vascular pathologies were scored on a scale of 0 to 3 (none-severe). *P-value <0.05.

3.3 Sex-Differences in Synovial Vascular Pathology

The average of the median synovial histopathology scores of the total cohort, as well as the averages separated by sex, are shown in **Table 4**. Males had higher median vasculopathy score (0.42 [95%CI 0.07, 0.77]) compared to females, and demonstrated trends toward higher median vascularization (0.32 [95%CI -0.07, 0.70)] and lining thickness scores (0.22 [95%CI -0.07, 0.51]); however, the latter estimates lacked precision (**Figure 1**). No clear sex differences were detected between sexes for median perivascular edema, infiltrate, fibrosis, or fibrin deposition scores.

3.4 Synovial Fluid C5 Concentration is Associated with Synovial Tissue Vascularization in Males

Multivariate linear regression showed that synovial fluid C5 concentrations were inversely associated with median synovial vascularization, while adjusting for age, sex, and BMI (-0.003

TABLE 3 | Multivariate linear regression model estimates for C5 concentration with synovial fluid C2, MBL, adipsin, CFI concentration (ng/mL).

	*Adjusted β coefficient (95%CI) *p*
Male (n= 52)	
C2	0.11 (-0.07, 0.29) *p*= 0.25
MBL	0.30 (-0.51, 1.11) *p*= 0.46
CFI	-0.39 (-0.96, 0.18) *p*= 0.18
Adipsin	-3.57 (-8.72, 1.58) *p*= 0.17
Female (n= 45)	
C2	**0.25 (0.06, 0.45) *p*= 0.01**
MBL	0.20 (-0.50, 0.91) *p*= 0.56
CFI	-0.01 (-0.62, 0.60) *p*= 0.96
Adipsin	-0.21 (-6.41, 5.99) *p*= 0.95

**Adjusting for age and BMI.*
CI, confidence interval; p, p-value.
Regression model estimates with 95% CI excluding 0 are in bold.

[95%CI -0.006, 0.001]; **Supplementary Table 1**); however, the 95% confidence intervals included 0. As recommended by SAGER guidelines and the complement literature, we then assessed potential sex differences by fitting models including a sex by C5 concentration interaction term (**Table 5**) and performed sex-disaggregated analyses (**Table 6**).

Sex-specific predictive marginal means graphs are shown in **Figure 2** and represent the association between synovial fluid C5 concentration (at 100 ng/mL intervals) and median vascularization scores (at 1-unit intervals). Sex-disaggregated analyses suggest that for every 100ng/mL increase in C5 concentration, there was a 0.5-unit decrease (beta = -0.005 [95%CI, -0.009, -0.0001] per 1 ng/mL change) in median vascularization score in males (**Table 6** and **Figure 2A**). However, there was no evidence of a relationship between C5 concentration and vascularization identified in females (**Figure 2B**). In males but not females, similar but weaker trends of association were seen between synovial fluid C5 levels and increased synovial tissue perivascular edema and decreased vasculopathy in males; however, the 95%CIs were imprecise (**Table 6**). Representative synovial histopathology images for both sexes from the highest/lowest synovial fluid C5 quartile groups are shown in **Figure 2C**; lower vascularization was observed in males in the highest C5 quartile, but similar vascularization between highest and lowest C5 quartiles in females.

TABLE 5 | Multivariate linear regression model estimates for the association between vascular pathology and C5 synovial fluid concentration, including sex by C5 concentration interaction terms. (n= 97).

	Adjusted* β coefficient (95%CI) *p*
Model 1: Vascularization	
Sex	
Male	Reference
Female	-1.84 (-3.92, 0.23) *p*= 0.08
C5 concentration	**-0.005 (-0.010, -0.0001) *p*= 0.04**
Sex × C5 concentration	0.006 (-0.002, 0.014) *p*= 0.12
Model 2: Vasculopathy	
Sex	
Male	Reference
Female	-1.69 (-3.63, 0.25) *p*= 0.09
C5 concentration	-0.002 (-0.007, 0.002) *p*= 0.33
Sex × C5 concentration	0.005 (-0.002, 0.012) *p*= 0.19
Model 3: Perivascular edema	
Sex	
Male	Reference
Female	0.57 (-0.86, 2.01) *p*= 0.43
C5 concentration	0.003 (-0.001, 0.006) *p*= 0.12
Sex × C5 concentration	-0.002 (-0.007, 0.003) *p*= 0.42

**Adjusting for age and BMI.*
Bold values indicate significance at the 5% level.
CI, confidence interval; p, p-value.

TABLE 6 | Sex-disaggregated multivariate linear regression model estimates for C5 concentration and vascular pathology.

	*Adjusted β coefficient (95%CI) *p*
Male (n= 52)	
Model 1: Vascularization	
C5 concentration	**-0.005 (-0.009, -0.0001) *p*= 0.04**
Model 2: Vasculopathy	
C5 concentration	-0.002 (-0.007, 0.003) *p*= 0.36
Model 3: Perivascular edema	
C5 concentration	0.003 (-0.001, 0.006) *p*= 0.13
Female (n=45)	
Model 1: Vascularization	
C5 concentration	0.002 (-0.004, 0.008) *p*= 0.56
Model 2: Vasculopathy	
C5 concentration	0.003 (-0.002, 0.009) *p*= 0.19
Model 3: Perivascular edema	
C5 concentration	0.0002 (-0.004, 0.004) *p*= 0.94

**Adjusting for age and BMI.*
CI, confidence interval; p, p-value.
Regression model estimates with 95% CI excluding 0 are in bold.

TABLE 4 | Median synovial vascularization: total cohort and disaggregated by sex.

	Total Cohort (n= 97) mean ± SD (range)	Males (n= 52) mean ± SD (range)	Females (n= 45) mean ± SD (range)	Mean Difference (Males – Females) (n= 97) mean (95%CI) *p*
Median vascularization	1.95 ± 0.96 (0-3)	2.10 ± 0.95 (0-3)	1.78 ± 0.96 (0-3)	0.32 ± 0.19(-0.07, 0.70) *p*= 0.10
Median perivascular edema	0.55 ± 0.65 (0-3)	0.52 ± 0.66 (0-3)	0.58 ± 0.63 (0-3)	-0.06 ± 0.13 (-0.32, 0.20) *p*= 0.66
Median vasculopathy	0.78 ± 0.89 (0-3)	0.97 ± 0.93 (0-3)	0.56 ± 0.78 (0-3)	**0.42 ± 0.18 (0.07, 0.77) *p*= 0.02**
Median lining thickness	0.78 ± 0.72 (0-3)	0.89 ± 0.80 (0-3)	0.67 ± 0.60 (0-3)	0.22 ± 0.15 (-0.07, 0.51) *p*= 0.14
Median infiltrate	1.12 ± 0.85 (0-3)	1.09 ± 0.94 (0-3)	1.16 ± 0.74 (0-3)	-0.07 ± 0.17 (-0.41, 0.28) *p*= 0.69
Median fibrosis	1.24 ± 0.75 (0-3)	1.23 ± 0.70 (0-3)	1.24 ± 0.80 (0-3)	-0.01 ± 0.15 (-0.32, 0.29) *p*= 0.93
Median fibrin deposition	0.87 ± 0.34 (0-1)	0.83 ± 0.38 (0-1)	0.91 ± 0.29 (0-1)	-0.08 ± 0.07 (-0.22, 0.05) *p*= 0.23

CI, confidence interval; p, p-value; SD, standard deviation.
No scores above grade 1 (mild) were assigned for fibrin deposition.
Mean sex-differences in histopathology scores with 95% CI excluding 0 are in bold.

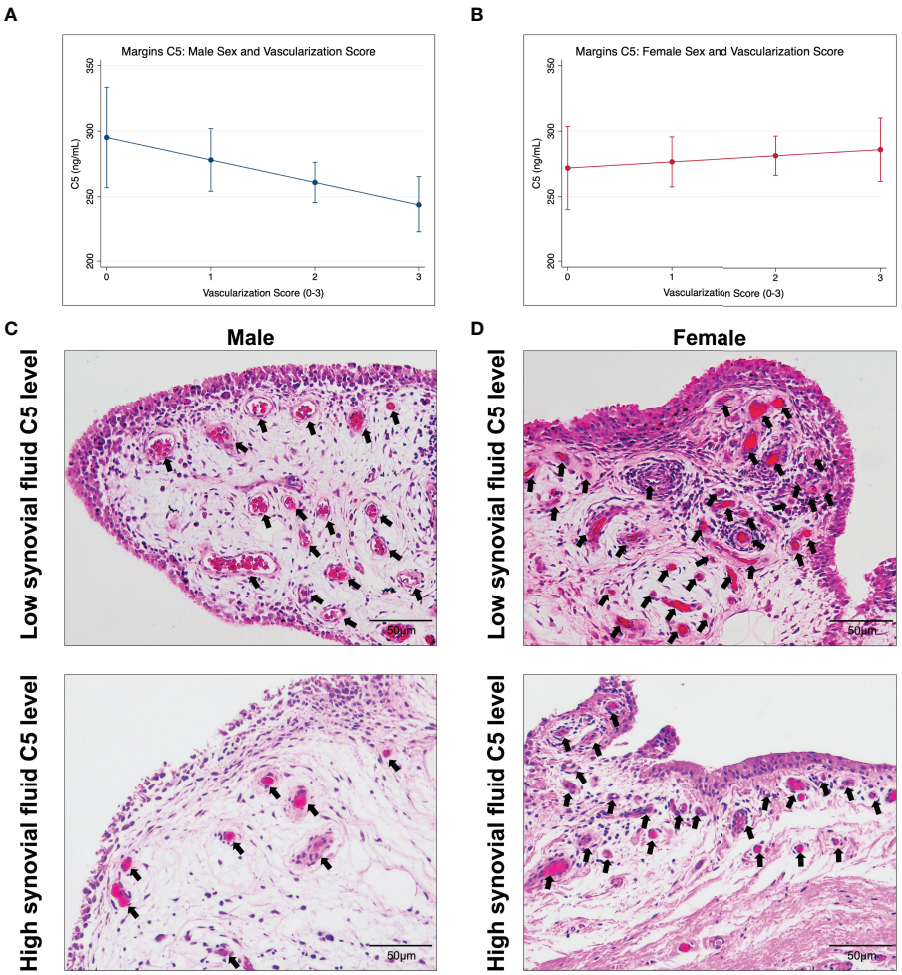

FIGURE 2 | Marginal effects for the association between synovial fluid C5 levels and median synovial vascularization by sex and representative synovial histopathology. Data shown are estimated marginal means ± 95% CIs for median vascularization score (0-3; none-severe) at C5 concentration (ng/mL) of 100, 200, 300, and 400 ng/mL by **(A)** male and **(B)** female sex. Histopathological images of synovium stained with hematoxylin and eosin, representing the C5 and vascularization trend in **(C)** males, and lack of trend in **(D)** females. **(C)** shows synovium from a male with low C5 concentration and high vascularization and from a male with high C5 and less vascularization (arrows). Scale bar 50 µm.

3.5 Sex-Differences in Synovial Fluid Complement Activation

We compared sC5b-9 levels in synovial fluid between subgroups of male and female patients in the highest and lowest synovial fluid C5 quartiles. Overall, males had higher synovial fluid sC5b-C9 levels (477.70 [95%CI 118.10, 837.30]) compared to females (**Figure 3A**). Similarly, comparing males and females from the highest synovial fluid C5 quartiles also demonstrated higher sC5b-C9 levels in males (858.5 ng/mL [95%CI 249.60, 1467.00]) than females (**Figure 3B**). When disaggregated by sex, synovial fluid sC5b-C9 concentrations were higher in males with high synovial fluid C5 (678.6 ng/mL [95%CI 69.73, 1287.00]) compared to males with low synovial fluid C5 concentrations (**Figure 3B**). In contrast, similar levels of synovial fluid sC5b-C9 were measured in females regardless of synovial fluid C5 levels.

To determine if classical complement pathway activation might differ between sexes, we measured C1q deposition in synovial lining. However, no differences between sexes, regardless of synovial fluid C5 level, were identified (**Figures 3C, D**).

4 DISCUSSION

Complement factor expression in joint tissues is associated with synovitis (18, 29), worse pain (30), and disease progression (27, 31). Genetic and pharmacologic inhibition of complement in mouse models of OA have shown protective effects against structural joint damage (18). Although complement activation is associated with vascular pathology in diseases such as retinopathy (32–34), no such associations have been

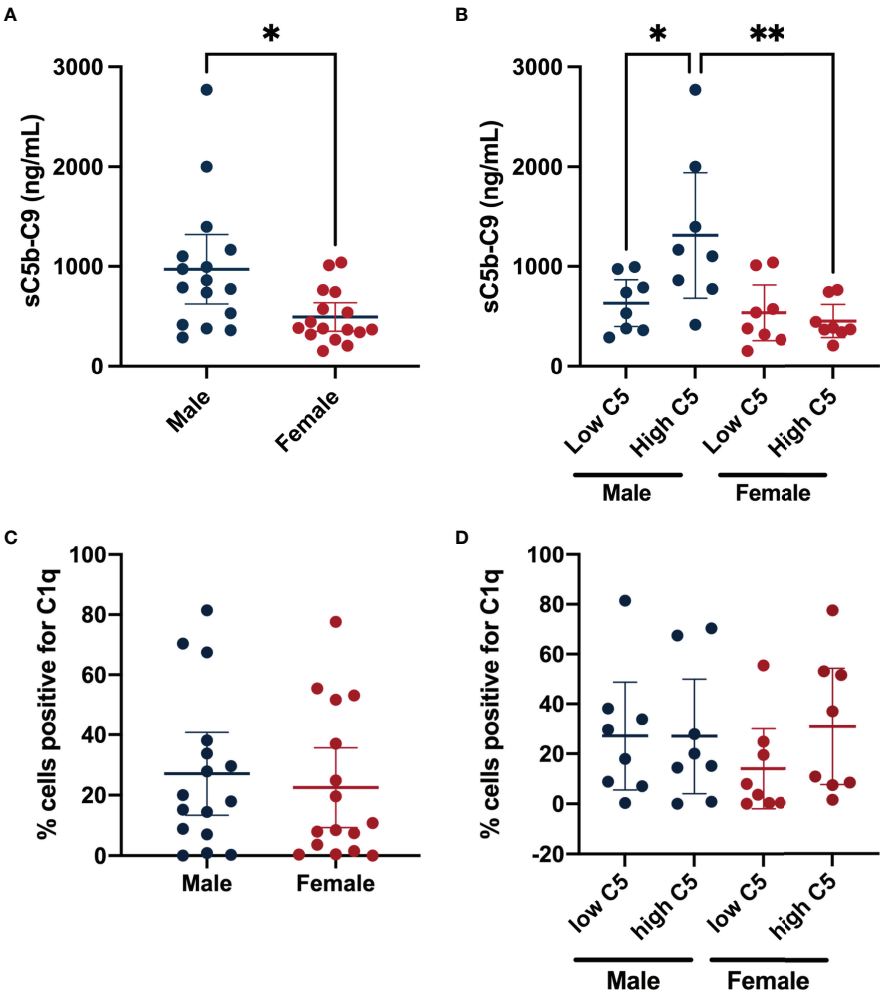

FIGURE 3 | Synovial fluid terminal complement complex sC5b-C9 levels and synovial lining C1q grouped by sex and synovial fluid C5 quartile. Data shown are mean sC5b-C9 concentrations (ng/mL) ± 95% CIs for **(A)** Male (n=16) and Female (n=16). **(B)** Represents sub-groups of males with low synovial fluid C5 concentrations (n= 8), males with high synovial fluid C5 concentrations (n= 8), females with low synovial fluid C5 concentrations (n= 8), and females with high synovial fluid C5 concentrations (n= 8). **(C)** Shows mean percent positive synovial lining cells for C1q ± 95% CIs for males (n=16) and females (n=16). **(D)** Shows the percent positive synovial lining cells for C1q of patients from the highest and lowest quartiles of synovial fluid C5 levels for both sexes. *P-value <0.05; **P-value <0.005 for between-group comparisons of synovial fluid sC5b-C9 concentrations.

determined for OA. Further, well-recognized sex-differences exist in complement activation (23) and OA outcomes (21, 35). In this study, we investigated whether complement levels are related to synovial vascular pathology, and whether sex-differences may interact with this relationship. We focused on late-stage knee OA where vascular pathology is likely greatest and matched synovial fluids and tissues are readily available. Our primary analysis included C5 because it is the first factor in the terminal effector pathway and C5 deletion protects against OA development in experimental mouse models (18), suggesting that higher C5 levels may be associated with worse OA outcomes. We found that males with higher total C5 complement have reduced synovial vascularization, but this association does not occur in females. Interestingly, males with higher synovial fluid C5 had increased terminal complement activation in synovial fluid, whereas higher C5 levels did not correspond to higher terminal complement activation in females. These findings raise some interesting questions that require further investigation.

Total C5 complement was inversely associated with vascularization, raising the hypothesis that complement signaling might inhibit synovial vascularization in OA. However, due to our cross-sectional design, we cannot confirm any causal mechanistic relationship. Indeed, the null hypothesis would indicate that the association is an epiphenomenon where pathophysiological OA conditions that lead to greater C5 levels and terminal complement activation in males also have an inhibitory effect on synovial vascularization through a

mechanism independent of complement. Notwithstanding, current knowledge from other diseases suggests that an epiphenomenon is less likely, since complement signaling regulates pathological angiogenesis in multiple diseases involving chronic inflammation. Our work therefore indicates that prospective interventional studies should be completed to test potential inhibitory effects of C5 activation on vascular pathology. If complement inhibits synovial vascularization, this has important implications for joint healing in knee OA. In particular, the synovium is critical to restore and maintain joint homeostasis and impairment of normal wound healing processes by interfering with synovial angiogenesis is one potential mechanism through which complement may lead to worse knee OA outcomes.

Previous studies have suggested that complement may be activated by numerous proteases secreted into the OA joint environment (18). Since multiple complement pathways converge on C5 to generate C5a and C5b activation fragments, which in turn activate C5a receptors and the terminal effector pathway (sC5b-9) respectively, synovial fluid total C5 levels therefore serve as a useful proxy indicator of the potential for complement activation in OA joints. Accordingly, we focused our primary analyses on C5 levels in synovial fluid and confirmed that higher levels of C5 in males are associated with higher sC5b-9, indicating greater complement activation. Further, continuous physiologic turnover of parent complement factors such as C5 *in vivo* leads to the generation of activation fragments that are proportional to the level of the parent factor in healthy and disease states. However, in some diseases such as in systemic lupus erythematosus, very rapid activation may exceed the rate of synthesis leading to consumption of the parent factor. Even though excessive complement activation to the point of consumption is very unlikely in OA, we conducted secondary analyses in sub-groups of patients with high or low total C5 levels and confirmed this is not the case. These secondary analyses were therefore critical in allowing us to determine that the inverse relationship between total C5 levels and synovial vascularization suggests the hypothesis that an anti-angiogenic role for complement may exist in males with knee OA, rather than a pro-angiogenic role.

Numerous studies have reported pro- or anti-angiogenic roles of complement signaling. Importantly, disease context and the pathological cell types involved may influence the divergent roles of complement (11). If we interpret our findings using the concept that OA resembles a chronic wound as proposed by others (9), OA-related angiogenesis may be driven by pro-angiogenic wound healing mechanisms that go awry due to innate-driven chronic inflammation interrupting normal healing (36). Indeed, some complement factors such as C1q may promote canonical angiogenesis in healthy and wounded tissue (37), whereas components of the C5-C5a axis may exert pro-angiogenic effects in healthy contexts but disrupt angiogenic processes in chronic wounds. Considering our findings of an inverse association between C5 complement and vascularization in males with OA, innate inflammation mechanisms including complement may interfere with wound healing-related angiogenesis. For example, in a model of experimental wound healing, mice deficient in C3, C5, and C5aR1 had better cutaneous wound healing compared to wild-type mice (38). This study also found that C5a-mediated immune cell activation delayed wound healing and angiogenesis (11, 38). Further, in a surgical model of post-traumatic knee OA, mice with C5-deficiency had less cartilage degradation and had lower expression of pro-inflammatory mediators compared to mice with normal C5 (18), although synovial vascularization was not assessed. Notably, all of these studies were completed using male mice. Considering our data in context with these findings, pathological complement activation may lead to increased inflammation and derangements in angiogenesis, with important implications in OA pathogenesis and synovial vascular pathology. Although complement activation can influence inflammatory processes such as immune cell recruitment, activation, metabolism, apoptosis, and interactions with the adaptive immune system (39), we did not identify any relationships between synovial fluid complement levels and other inflammatory features of synovial histopathology (*e.g.*, lining thickening, immune infiltrate, fibrin deposition). However, we cannot rule out complement-related changes in inflammatory mediators such as cytokines or inflammatory cell function, as these were not measured in this study. Future studies investigating how complement activation directly affects

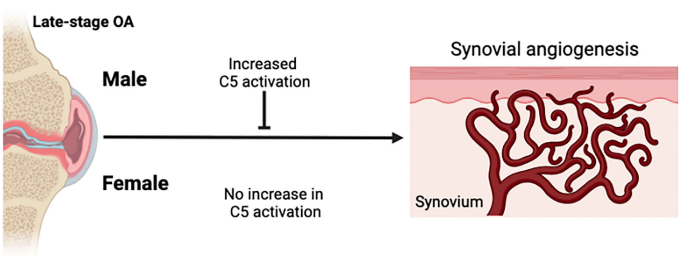

FIGURE 4 | Schematic summary of sex-differences in complement activation and synovial angiogenesis. Knee OA is associated with synovial tissue angiogenesis. In males with knee OA, complement activation was increased and associated with reduced synovial vascularization. In females with knee OA, complement activation was not increased and no association between complement activation and synovial vascularization was detected. Figure created in Biorender.com.

synovial vascular pathology and how this may impact clinical outcomes in knee OA patients is warranted, and such studies should investigate sex differences.

Our sex-specific analyses suggest that complement activation may play more of a role in synovial vascular pathology mechanisms in males than it does in females with knee OA (**Figure 4**). Males with higher C5 levels had higher levels of complement activation (sC5b-C9) compared to males with lower C5 levels and compared to females with high C5 levels. This suggested that females with knee OA do not activate terminal complement as effectively as males do, regardless of the level of C5 present in synovial fluid. Sex-specific regulation of synovial fluid complement activation at the level of C5 or subsequent steps in the cascade may be important in knee OA pathophysiology. Females with knee OA appear to have a reduced ability to activate complement and/or convert C5b intermediate to sC5b-C9 in synovial fluid. This finding corroborates previous studies demonstrating lower levels of terminal pathway components in the serum of healthy females compared to males (23), which has also been shown in mice (40) but has not previously been demonstrated in synovial fluid. Several candidate mechanisms may mediate sex differences in how complement influences disease processes, which should be explored in future studies. For example, CD59 may be expressed at higher levels in the synovium of female patients, which could prevent the conversion of the MAC complex after cleavage of C5 (41). Sex differences in the inflammatory cell composition and/or function of the synovium might differentially regulate complement activation between sexes or responses to complement signaling. Gaya da Costa et al. also showed that serum levels of C3 and properdin were lower in females compared to males, while the complement activator Factor D (adipsin) levels were significantly higher (23). Although we did not measure C3 levels in this study, we did not find any sex-differences in synovial fluid levels of adipsin, other complement factors, nor the complement inhibitor CFI, in patients with late-stage knee OA. The differences between our study and others are likely due to differences between complement expression in serum vs. synovial fluid since complement factor production by local joint tissues is dysregulated in OA; other differences in cohort demographic factors including age, BMI, or ethnicity may have also played a role. It is also notable that most murine studies are done using male mice alone, without comparative analyses in females, although this trend is starting to improve in the OA research field in recent years. Considering our findings that complement activation was not associated with vascularization in females, comparative analyses in both sexes remains an important gap in the literature and should be considered carefully in future studies, especially those examining complement roles in disease.

Upstream complement pathway activation was not assessed in this study but may influence downstream events. Synovial fluid levels of C5 trended to be higher in females than in males and were associated with C2 levels in females only. This suggested a potential sex-specific link between C5 levels and classical pathway activation in females, but we found no sex differences in C1q deposition in synovial tissues regardless of synovial fluid C5 levels. However, we cannot rule out a link between C1q and synovial vascularization since C1q has also been linked with angiogenesis through mechanisms that bypass downstream complement activation (37), and our analysis was limited to subgroups of patients based on total C5 level. In addition to playing a role in classical pathway activation (23, 42), mixed reports also suggest a role for C2 in lectin pathway activity. Gaya da Costa et al. did not find any association between C2 concentrations and lectin pathway activity in serum of healthy individuals (24), while a previous study showed that human serum deficient in C2 ablated lectin pathway activity (42). Although our study was focused on downstream effector pathway associations, upstream pathways should be investigated for sex differences in different disease contexts.

Our study is limited to cross-sectional relationships. Although we cannot conclude that causal relationships exist between complement and synovial vascular pathology, our findings raise the novel hypothesis that complement signaling inhibits synovial angiogenesis in knee OA and that sex differences modify these effects. The focus on late-stage knee OA also limits the generalizability of our findings to the context of early knee OA. Future studies should also assess longitudinal relationships since increased vascularization has been shown to be associated with increased KL grade at follow up (7). Nearly 15% of patients were excluded due to insufficient synovial fluid volumes at time of aspiration, which may have influenced our findings, although it remains uncertain whether this would lead to over-estimation, under-estimation, or no effect. Although our sample size was met for the primary analysis, larger samples are needed (*e.g.*, 70-80 per group) to be appropriately powered for the sex-disaggregated analyses. Synovial angiogenesis is a pathological feature in knee OA and associated with worse joint pain yet, it is not known whether disease-related or therapeutic reduction of synovial vascularization would be protective or lead to worse disease outcomes. Given the strong relationship between synovial vascularization and OA symptoms, the effects of reducing synovial angiogenesis on OA outcomes should be investigated.

This is the first study to describe an association between synovial fluid complement C5 levels and synovial tissue microvascular pathology in patients with knee OA. Importantly, we also identified sex differences in this association and in synovial fluid complement activation. Higher synovial fluid C5 levels were associated with greater terminal complement activation and decreased synovial vascularization in males, but neither occurred in female patients. These findings raise the hypothesis that sex differences in synovial fluid complement activation in knee OA may lead to differential effects on synovial microvascular pathology. Prospective studies are required to confirm whether complement directly or indirectly inhibits synovial angiogenesis or is merely an indicator of the inflammatory milieu within the joint. Our findings also serve as a compelling reminder to include sex-disaggregated analyses in OA research.

DATA AVAILABILITY STATEMENT

The original contributions presented in the study are included in the article/**Supplementary Material**. Further inquiries can be directed to the corresponding author.

ETHICS STATEMENT

The studies involving human participants were reviewed and approved by Western University Health Sciences Research Ethics Board. The patients/participants provided their written informed consent to participate in this study.

AUTHOR CONTRIBUTIONS

ES and HP contributed to study design, data collection and analysis, and drafted the manuscript. MC contributed to data analysis. TB and TA contributed to study design, data interpretation and critically revised the manuscript. All authors read and approved final manuscript.

FUNDING

This work was funded in part by grants from the Academic Medical Organization of Southwestern Ontario (AMOSO; INN17-004), the Canada Research Chairs program, and Western University's Bone and Joint Institute. HP is supported by Frederick Banting and Charles Best Doctoral Award from CIHR.

ACKNOWLEDGMENTS

We would like to acknowledge the WOREO Study team members and participants and Western University's Bone & Joint Institute.

SUPPLEMENTARY MATERIAL

The Supplementary Material for this article can be found online at: https://www.frontiersin.org/articles/10.3389/fimmu.2022.890094/full#supplementary-material

REFERENCES

1. Rodrigues M, Kosaric N, Bonham CA, Gurtner GC. Wound Healing: A Cellular Perspective. *Physiol Rev* (2019) 99:665–706. doi: 10.1152/physrev.00067.2017
2. Bonnet CS, Walsh DA. Osteoarthritis, Angiogenesis, and Inflammation. *Rheumatol (Oxford)* (2004) 44:7–16. doi: 10.1093/rheumatology/keh344
3. Bhattaram P, Chandrasekharan U. The Joint Synovium: A Critical Determinant of Articular Cartilage Fate in Inflammatory Joint Diseases. *Semin Cell Dev Biol* (2017) 62:86–93. doi: 10.1016/j.semcdb.2016.05.009
4. De Bari C. Are Mesenchymal Stem Cells in Rheumatoid Arthritis the Good or Bad Guys? *Arthritis Res Ther* (2015) 17:113. doi: 10.1186/s13075-015-0634-1
5. Haywood L, McWilliams DF, Pearson CI, Gill SE, Ganesan A, Wilson S, et al. Inflammation and Angiogenesis in Osteoarthritis. *Arthritis Rheumatism* (2003) 48:2173–2177. doi: 10.1002/art.11094
6. Haywood L, Walsh DA. Vasculature of the Normal and Arthritic Synovial Joint. *Histol Histopathol* (2001) 16:277–84. doi: 10.14670/HH-16.277
7. Minten MJM, Blom A, Snijders GF, Kloppenburg M, van den Hoogen FHJ, den Broeder AA, et al. Exploring Longitudinal Associations of Histologically Assessed Inflammation With Symptoms and Radiographic Damage in Knee Osteoarthritis: Combined Results of Three Prospective Cohort Studies. *Osteoarthritis Cartilage* (2019) 27:71–9. doi: 10.1016/j.joca.2018.10.014
8. Mapp PI, Walsh DA. Mechanisms and Targets of Angiogenesis and Nerve Growth in Osteoarthritis. *Nat Rev Rheumatol* (2012) 8:390–8. doi: 10.1038/nrrheum.2012.80
9. Scanzello CR, Plaas A, Crow MK. Innate Immune System Activation in Osteoarthritis: Is Osteoarthritis a Chronic Wound? *Curr Opin Rheumatol* (2008) 20:565–72. doi: 10.1097/BOR.0b013e32830aba34
10. Markiewski MM, Daugherity E, Reese B, Karbowniczek M. The Role of Complement in Angiogenesis. *Antibodies (Basel)* (2020) 9:67. doi: 10.3390/antib9040067
11. John T, Stahel PF, Morgan SJ, Schulze-Tanzil G. Impact of the Complement Cascade on Posttraumatic Cartilage Inflammation and Degradation. *Histol Histopathol* (2007) 22:781–90. doi: 10.14670/HH-22.781
12. Silawal S, Triebel J, Bertsch T, Schulze-Tanzil G. Osteoarthritis and the Complement Cascade. *Clin Med Insights Arthritis Musculoskelet Disord* (2018) 11:1179544117751430. doi: 10.1177/1179544117751430
13. Sarma JV, Ward PA. The Complement System. *Cell Tissue Res* (2011) 343:227–35. doi: 10.1007/s00441-010-1034-0
14. Drouin SM, Kildsgaard J, Haviland J, Zabner J, Jia HP, McCray PB, et al. Expression of the Complement Anaphylatoxin C3a and C5a Receptors on Bronchial Epithelial and Smooth Muscle Cells in Models of Sepsis and Asthma. *J Immunol* (2001) 166:2025–32. doi: 10.4049/jimmunol.166.3.2025
15. DiScipio RG, Khaldoyanidi SK, Moya-Castro R, Schraufstatter IU. Complement C3a Signaling Mediates Production of Angiogenic Factors in Mesenchymal Stem Cells. *J BioMed Sci Eng* (2013) 6:8a. doi: 10.4236/jbise.2013.68A1001
16. Markiewski MM, DeAngelis RA, Benencia F, Ricklin-Lichtsteiner SK, Koutoulaki A, Gerard C, et al. Modulation of the Antitumor Immune Response by Complement. *Nat Immunol* (2008) 9:1225–35. doi: 10.1038/ni.1655
17. Gaudenzio N, Sibilano R, Marichal T, Starkl P, Reber LL, Cenac N, et al. Different Activation Signals Induce Distinct Mast Cell Degranulation Strategies. *J Clin Invest* (2016) 126:3981–98. doi: 10.1172/JCI85538
18. Wang Q, Rozelle AL, Lepus CM, Scanzello CR, Song JJ, Larsen DM, et al. Identification of a Central Role for Complement in Osteoarthritis. *Nat Med* (2011) 17:1674–9. doi: 10.1038/nm.2543
19. Cho HJ, Chang CB, Kim KW, Park JH, Yoo JH, Koh IJ, et al. Gender and Prevalence of Knee Osteoarthritis Types in Elderly Koreans. *J Arthroplasty* (2011) 26:994–9. doi: 10.1016/j.arth.2011.01.007
20. Public Health Agency of Canada. *Aging and Chronic Diseases: A Profile of Canadian Seniors* (2020). Available at: https://www.canada.ca/en/public-health/services/publications/diseases-conditions/aging-chronic-diseases-profile-canadian-seniors-report.html (Accessed January 15, 2022).
21. Cho HJ, Chang CB, Yoo JH, Kim SJ, Kim TK. Gender Differences in the Correlation Between Symptom and Radiographic Severity in Patients With Knee Osteoarthritis. *Clin Orthop Relat Res* (2010) 468:1749–58. doi: 10.1007/s11999-010-1282-z
22. Leopold SS, Redd BB, Warme WJ, Wehrle PA, Pettis PD, Shott S. Corticosteroid Compared With Hyaluronic Acid Injections for the Treatment of Osteoarthritis of the Knee. A Prospective, Randomized Trial. *JB JS Open Access* (2003) 85:1197–203. doi: 10.2106/00004623-200307000-00003
23. Gaya da Costa M, Poppelaars F, van Kooten C, Mollnes TE, Tedesco F, Würzner R, et al. Age and Sex-Associated Changes of Complement Activity and Complement Levels in a Healthy Caucasian Population. *Front Immunol* (2018) 9:2664. doi: 10.3389/fimmu.2018.02664

24. Kellgren JH, Lawrence JS. Radiological Assessment of Osteo-Arthrosis. *Ann Rheum Dis* (1957) 16:494–502. doi: 10.1136/ard.16.4.494
25. Cohen J. *Statistical Power Analysis for the Behavioural Sciences*. New Jersey: Lawrence Erlbaum Associates, Inc (1988). 567 p.
26. Philosophe B, Malat GE, Soundararajan S, Barth RN, Manitpisikul W, Wilson NS, et al. Validation of the Maryland Aggregate Pathology Index (MAPI), a Pre-Implantation Scoring System That Predicts Graft Outcome. *Clin Transplant* (2014) 28:897–905. doi: 10.1111/ctr.12400
27. Ayral X, Pickering EH, Woodworth TG, Mackillop N, Dougados M. Synovitis: A Potential Predictive Factor of Structural Progression of Medial Tibiofemoral Knee Osteoarthritis - Results of a 1 Year Longitudinal Arthroscopic Study in 422 Patients. *Osteoarthritis Cartilage* (2005) 13:361–7. doi: 10.1016/j.joca.2005.01.005
28. Heidari S, Babor TF, De Castro P, Tort S, Curno M. Sex and Gender Equity in Research: Rationale for the SAGER Guidelines and Recommended Use. *Res Integr Peer Rev* (2016) 1:2. doi: 10.1186/s41073-016-0007-6
29. Assirelli E, Pulsatelli L, Dolzani P, Mariani E, Lisignoli G, Addimanda O, et al. Complement Expression and Activation in Osteoarthritis Joint Compartments. *Front Immunol* (2020) 11:535010. doi: 10.3389/fimmu.2020.535010
30. Baker K, Grainger A, Niu J, Clancy M, Guermazi A, Crema M, et al. Relation of Synovitis to Knee Pain Using Contrast-Enhanced Mris. *Ann Rheum Dis* (2010) 69:1779–83. doi: 10.1136/ard.2009.121426
31. Roemer FW, Guermazi A, Felson DT, Niu J, Nevitt MC, Crema MD, et al. Presence of MRI-Detected Joint Effusion and Synovitis Increases the Risk of Cartilage Loss in Knees Without Osteoarthritis at 30-Month Follow-Up. *Ann Rheum Dis* (2011) 70:1804–9. doi: 10.1136/ard.2011.150243
32. Geerlings MJ, de Jong EK, den Hollander AI. The Complement System in Age-Related Macular Degeneration: A Review of Rare Genetic Variants and Implications for Personalized Treatment. *Mol Immunol* (2017) 84:65–76. doi: 10.1016/j.molimm.2016.11.016
33. Klein RJ, Zeiss C, Chew EY, Tsai JY, Sackler RS, Haynes C, et al. Complement Factor H Polymorphism in Age-Related Macular Degeneration. *Science* (2005) 308:385–9. doi: 10.1126/science.1109557
34. Sweigard JH, Yanai R, Gaissert P, Saint-Geniez M, Kataoka K, Thanos A, et al. The Alternative Complement Pathway Regulates Pathological Angiogenesis in the Retina. *FASEB J* (2014) 28:3171–82. doi: 10.1096/fj.14-251041
35. Zhang Y, Jordan JM. Epidemiology of Osteoarthritis. *Clin Geriatr Med* (2010) 26:355–69. doi: 10.1016/j.cger.2010.03.001
36. Langer HF, Chung KJ, Orlova VV, Choi EY, Kaul S, Kruhlak MJ, et al. Complement-Mediated Inhibition of Neovascularization Reveals a Point of Convergence Between Innate Immunity and Angiogenesis. *Blood* (2010) 116:4395–403. doi: 10.1182/blood-2010-01-261503
37. Bossi F, Tripodo C, Rizzi L, Bulla R, Agostinis C, Guarnotta C, et al. C1q as a Unique Player in Angiogenesis With Therapeutic Implication in Wound Healing. *Proc Natl Acad Sci USA* (2014) 111:4209–14. doi: 10.1073/pnas.1311968111
38. Rafail S, Kourtzelis I, Foukas PG, Markiewski MM, DeAngelis RA, Guariento M, et al. Complement Deficiency Promotes Cutaneous Wound Healing in Mice. *J Immunol* (2015) 194:1285–91. doi: 10.4049/jimmunol.1402354
39. Merle NS, Noe R, Halbwachs-Mecarelli L, Fremeaux-Bacchi V, Roumenina LT. Complement System Part II: Role in Immunity. *Front Immunol* (2015) 6:257. doi: 10.3389/fimmu.2015.00257
40. Kotimaa J, Klar-Mohammad N, Gueler F, Schilders G, Jansen A, Rutjes H, et al. Sex Matters: Systemic Complement Activity of Female C57BL/6J and BALB/cJ Mice Is Limited by Serum Terminal Pathway Components. *Mol Immunol* (2016) 76:13–21. doi: 10.1016/j.molimm.2016.06.004
41. Farkas I, Baranyi L, Ishikawa Y, Okada N, Bohata C, Budai D, et al. Cd59 Blocks Not Only the Insertion of C9 Into MAC But Inhibits Ion Channel Formation by Homologous C5b-8 as Well as C5b-9. *J Physiol* (2002) 539(Pt 2):537–45. doi: 10.1113/jphysiol.2001.013381
42. Seelen MA, Roos A, Wieslander J, Mollnes TE, Sjöholm AG, Wurzner R, et al. Functional Analysis of the Classical, Alternative, and MBL Pathways of the Complement System: Standardization and Validation of a Simple Elisa. *J Immunol Methods* (2005) 296:187–98. doi: 10.1016/j.jim.2004.11.016

Conflict of Interest: The authors declare that the research was conducted in the absence of any commercial or financial relationships that could be construed as a potential conflict of interest.

Publisher's Note: All claims expressed in this article are solely those of the authors and do not necessarily represent those of their affiliated organizations, or those of the publisher, the editors and the reviewers. Any product that may be evaluated in this article, or claim that may be made by its manufacturer, is not guaranteed or endorsed by the publisher.

Frontiers in Immunology

Explores novel approaches and diagnoses to treat immune disorders.

The official journal of the International Union of Immunological Societies (IUIS) and the most cited in its field, leading the way for research across basic, translational and clinical immunology.

Discover the latest Research Topics

See more →

Frontiers

Avenue du Tribunal-Fédéral 34
1005 Lausanne, Switzerland
frontiersin.org

Contact us

+41 (0)21 510 17 00
frontiersin.org/about/contact